Design of Novel Functionalized Lipidic Mesophases and their Applications in Catalysis, Water Confinement and Cellular Oxygen Delivery

---

Dissertation

zur

Erlangung der naturwissenschaftlichen Doktorwürde
(Dr. sc. nat.)

vorgelegt der

Mathematisch-naturwissenschaftlichen Fakultät

der

Universität Zürich

von

Michael Duss

von

Entlebuch LU

Promotionskommission

Prof. Dr. Ehud M. Landau (Leitung der Dissertation)

Prof. Dr. Henning J. Jessen

Prof. Dr. Oliver Zerbe

Zürich, 2018

Abstract

The central goal of this dissertation is to evaluate the feasibility of lipidic cubic phase gels (LCPs) and their dispersed nanoparticles (cubosomes) as self-assembled nanoreactor scaffolds for heterogeneous catalysis, and to design and develop such systems. This novel approach exploits, among other things, the very large lipid/water interface of LCPs, thereby performing efficient aqueous chemistry that takes place in the structured aqueous channels of the mesophases. Since LCPs can be doped with guest lipids without losing their three-dimensional architecture, such materials have a large potential for designing tailor-made functional biomaterials. Finally, these materials can coexist with any amount of excess water, thereby making them ideal matrices for heterogeneous reactions. Thus, research in this direction is necessary and opens exciting new avenues to discoveries in materials science and technology.

Functionalization of LCPs and cubosomes was achieved using various approaches. Lipidic proline-derived organocatalysts were designed, synthesized, and incorporated into the mesophases, and the kinetics and stereochemistry of a model aldol reaction was investigated. The kinetics of the model aldol reactions are tunable by modifying the diameter of the aqueous channels. Similarly, lipidic Pt-catalyst were synthesized and used as additives in LCPs to hydrolyze phosphate-ester derived pesticides that are structurally related to chemical warfare agents such as sarin. Palladium nanoparticles (PdNPs), known to be synthesized in the aqueous compartment of LCPs at ambient conditions, were used to catalyze *Suzuki-Miyaura* cross coupling reactions. Interestingly, catalysis is only possible if the aqueous channels of the LCPs are being enlarged after PdNP synthesis. This allows for an “on demand” on/off switching of the *Suzuki-Miyaura* cross coupling. Additionally, attempts to immobilize enzymes electrostatically and *via* lipidic modification were made.

An additional goal of this thesis was to synthesize a small library of cyclopropanated lipids as building blocks of mesophases with novel properties. The mesophases of these compounds exhibit remarkable low temperature phase behavior, which was investigated in a joint project with the group of Prof. Raffaele Mezzenga at the ETH. Most importantly, confined water in LCPs of the doubly cyclopropanated lipid DCPML was shown to remain liquid down to -11 °C, rendering these materials interesting for various biochemical and biophysical investigations of systems that are unstable at ambient temperatures.

A third project was launched in collaboration with the group of Prof. Dr. Dr. med. Daniel Eberli at the University Hospital Zurich to develop cubosomes which enable controlled oxygen release and delivery to anoxic muscle cells. To this end, lipidic pyridone endoperoxides were synthesized and incorporated in cubosomes. Preliminary data indicate

that such host-guest cubosomes could affect cellular reactivity to hypoxia by providing oxygen to the cells.

Zusammenfassung

Das zentrale Ziel dieser Dissertation ist, die Evaluation der Machbarkeit lipidischer kubischen Phasen (LCPs) und deren dispergierten Nanopartikel (Cubosomes), als selbstassemblierte Nanoreaktor-Gerüste für die heterogene Katalyse zu prüfen und solche Systeme zu planen und zu entwickeln. Dieses neue Konzept nutzt, unter anderem, die grosse Lipid-Wasser-Oberfläche aus, um effiziente wässrige Synthesen in den strukturierten wässrigen Kanälen der Mesophasen durchzuführen. Da LCPs mit Additiv-Lipiden versehen werden können, ohne die dreidimensionale Architektur zu verlieren, haben diese Materialien grosses Potential, um massgeschneiderte, funktionale Biomaterialien herzustellen. Zudem sind LCPs in Anwesenheit von überschüssigem Wasser stabil, was aus diesen Materialien ideale Matrizen für heterogene Katalyse macht. Forschung in diese Richtung ist erforderlich und eröffnet neue, spannende Wege und Entdeckungen in Materialwissenschaften und Technik.

Die Funktionalisierung der LCPs und Cubosomes wurde auf verschiedenen Wegen erreicht. Lipidische prolinverwandte Organokatalysatoren wurden entworfen, synthetisiert und in die Mesophasen eingebaut um die Kinetik und die Stereochemie einer Model-Aldol-Reaktion zu untersuchen. Die Kinetik dieser Model-Aldol-Reaktion konnte durch Modifikation der Durchmesser der wässrigen Kanäle gesteuert werden.
Pt-Katalysatoren wurden hergestellt und, ähnlich wie zuvor, in die Mesophasen eingebaut um Phosphatester mit kampfstoffähnlicher Struktur wie z.B. Sarin, zu hydrolysieren und unschädlich zu machen. Palladium-Nanopartikel, die bekanntlich in den wässrigen Kanälen von LCPs unter Umgebungsbedingungen gebildet werden, wurden für die Katalyse von *Suzuki-Miyaura*-Kreuzkupplungen verwendet. Interessanterweise ist die Katalyse nur möglich, wenn die wässrigen Kanäle nach der Palladium-Nanopartikel-Synthese vergrössert werden. Dies ermöglicht, die Reaktion mit einem “Schalter“ bei Bedarf an- oder auszuschalten. Zusätzlich wurden Versuche gemacht, um Enzyme in den Mesophasen elektrostatisch oder via lipidische Modifikation zu immobilisieren.
Ein zusätzliches Ziel dieser Arbeit ist es, eine Serie von cyclopropylierten Lipiden als Bestandteile von Mesophasen mit neuen Eigenschaften zu synthetisieren. Die Mesophasen dieser Verbindungen zeigen aussergewöhnliche Eigenschaften bei tiefen Temperaturen. Diese Eigenschaften wurden in einem gemeinsamen Projekt mit der Gruppe von Prof. Raffaele Mezzenga an der ETH untersucht. Dabei wurde in den LCPs des

zweifachcyclopropylierten Lipids DCPML “confined water“ gefunden, also Wasser, das in sehr wenig Raum eingeengt ist und das trotz Temperaturen von bis -11 °C nicht einfriert. Dies macht diese Materialien interessant für biochemische und biophysikalische Untersuchungen von Systemen, welche bei Raumtemperatur nicht stabil sind.

Ein drittes Projekt wurde in Kollaboration mit der Gruppe von Prof. Dr. Dr. med. Daniel Eberli vom Universitätsspital Zürich gestartet, um Cubosomes zu entwickeln, die eine kontrollierte Abgabe und Zufuhr von Sauerstoff zu anoxischen Muskelzellen ermöglichen. Hierfür wurden lipidische Pyridonendoperoxide synthetisiert und in Cubosomes eingebaut. Erste Daten deuten darauf hin, dass diese Cubosomes die zelluläre Reaktivität dieser Zellen auf Hypoxia, durch die Sauerstoff-Zufuhr beeinflussen.

Table of Contents

Chapter 1

1.1 General Introduction

1.1.1 Lipids – prelude

Lipids are fascinating molecules, and they are the building blocks of lipidic mesophases which are the core of this thesis. Before structure, properties, preparation and applications of lipidic mesophases will be introduced and discussed, a short general overview of these mesophase building blocks will be provided.

Lipids are considered as biological substances that are insoluble in water due to their hydrophobic or amphiphilic nature. Natural lipids can be composed of two different biosynthetic subunits, which are ketoacyl and isoprene moieties.[1] They can be divided into eight groups:

- Fatty acids consist of a hydrocarbon chain and a carboxylic acid head group. These two moieties render fatty acids amphiphilic, though insoluble in water. The hydrocarbon chain length can vary from 4 to 24 carbons and can be either saturated or unsaturated.[2]
- Glycerolipids have a glycerol head group that can bear one to three fatty acid substituents attached via ester bonds. These lipids function as energy storage for mammals. Hydrolysis of the ester group is the initial step in fat digestion.[2]
- Phospholipids bear a phospho-glycerol head group. They play important roles in lipid bilayer of cells and in cell signaling.[3]
- Sterol lipids are important elements of membranes. Cholesterol is the most prominent representative of this class of lipids. Steroids are derived from a fused four ring framework and play important roles as hormones.[4]
- Saccharolipids are esters of fatty acids and a monosaccharide.
- Sphingolipids are a broad class of lipids derived from the amino acid serine and contain a phosphate group.
- Prenol lipids are isoprene derived lipids. They are synthesized via the mevalonic acid pathway.[5]
- Polyketides

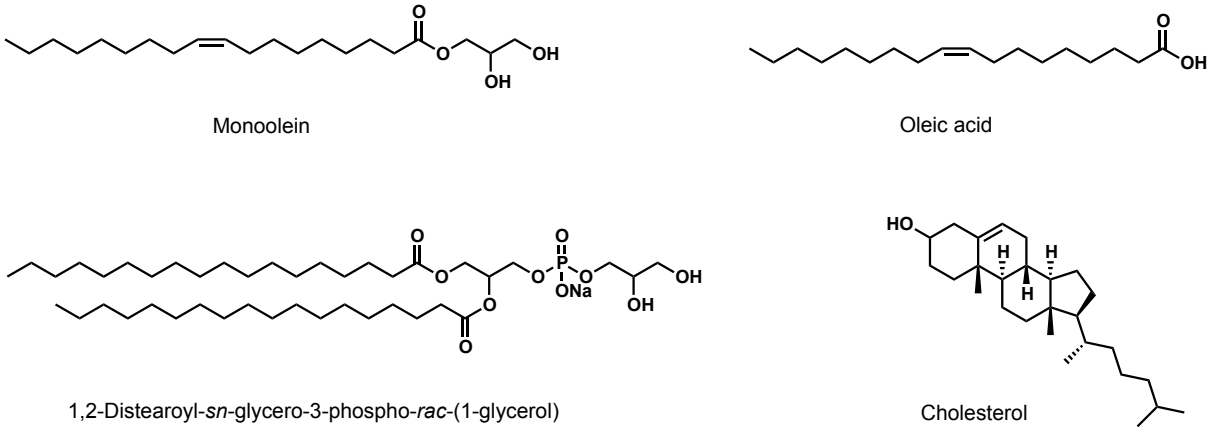

Figure 1: Structures of monoolein, a glycerolipid; oleic acid, a fatty acid; cholesterol, a sterol lipid; and 1,2-Distearoyl-*sn*-glycero-3-phospho-*rac*-(1-glycerol), a phospholipid.

The class of glycerolipids plays a central role in this thesis, with monoolein (MO) as their representative, responsible for the unique architecture of lipidic cubic phases discussed in the research herein. Examples of the classes of fatty acids, phospholipids and sterol lipids have been used as additives to modify the properties of the lipidic mesophase applied in this thesis. Thus, for example, the aqueous channel radii were enlarged to enable electrostatic interactions with enzymes.

Mammals transform carbohydrates, if an excess is available, to triglycerides. This process is called lipogenesis. Fatty acid synthases polymerize and reduce acetyl-CoA building blocks, whereas sterol and prenol lipids are built up from reactive isopentenyl pyrophosphates.[5] The metabolic process of lipid digestion is called ß-oxidation. After a sequence of dehydrogenation, hydration and oxygenation, a ß-keto acid is formed which is cleaved by thiolysis to generate acetyl-CoA.[2]

Historically, lipids were divided into two categories: solid and fluid greases. This definition was refined and a classification into oils, greases, tallow, waxes, resins, balsams and essential oils was introduced.[6] William Prout realized in 1827 that fats, together with carbohydrates and proteins are an essential part of human and animal's nutrition.[6] Triglycerides, phospholipids and cholesterol are among the most represented fats in food and are needed to enable the uptake of hydrophobic vitamins.[2] Mammals, humans included, cannot produce all the required lipids: linoleic acid and α-linolenic acid for example, are essential and need to be directly absorbed from diet.[2] Additionally, phospholipids, are a major element of biological membranes, like the cellular plasma membrane. Such membranes are responsible for the compartmentalization in cells by spatial separation of different organelles. Furthermore, lipids play an important role in cell signaling. Activation of G protein-coupled receptors occurs upon lipid signaling,[7–9] whereby several lipid classes are involved in cell signaling processes.[10]

1.1.2 Lipidic self-assembly

Hydrated lipids tend to aggregate and form self-assembled structures. The major driving force for amphiphilic self-assembly is the hydrophobic effect, which leads to the minimization of the interface between the hydrocarbon tails of the amphiphile and water molecules. The ensuing supramolecular structures can feature different phases, depending on molecular shape, concentration, temperature and pressure, whereas their complexity reaches from one-dimensional (lamellar *Lα*, micellar *L*) over two-dimensional (hexagonal, *H*) to more complex three-dimensional (cubic, *Q*) morphologies (Figure 2). This phenomenon is referred to as lipid polymorphism.[11,12] The ratio of the molecular volume, length of the lipidic chain and the head group area determines the packing parameter and as follows the curvature of the lipidic bilayer.[13]

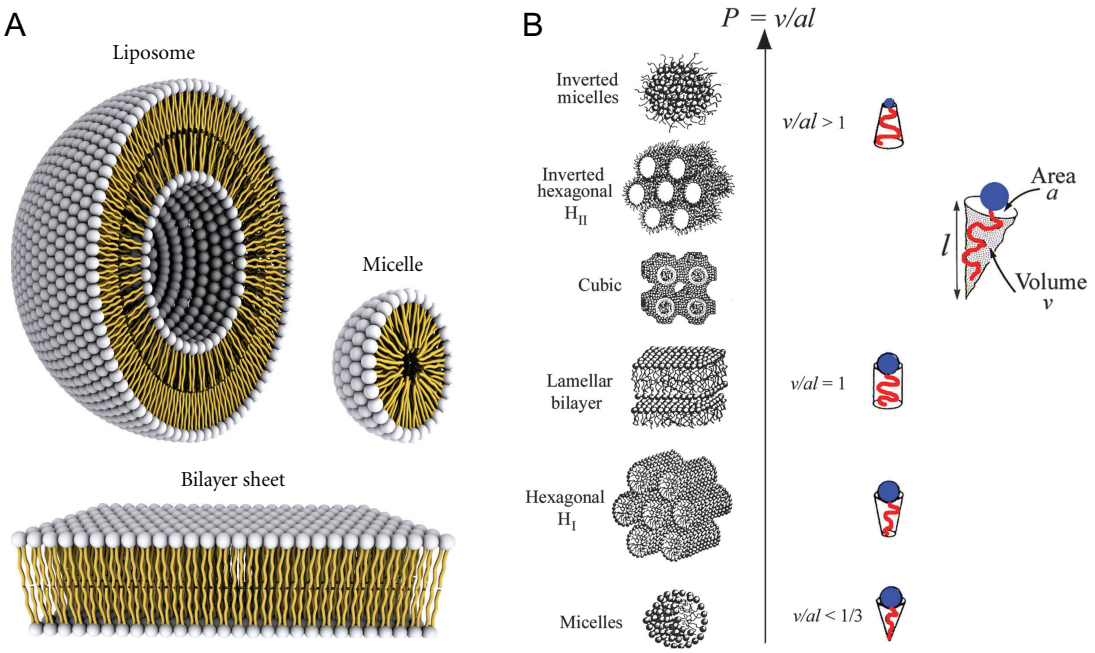

Figure 2: A) The profiles of a liposome, a micelle and a lipidic bilayer. Reprinted with permission from Ref. 12. B) Schematic illustration lipidic self-assembled structures, depending on the packing parameter P, which depends on the molecular volume (v), the area of the head group (a), and the length of the molecule (l). Reprinted with permission from Ref. 13.

1.1.3 Lipidic cubic phases

Lyotropic liquid crystals (LLCs) are liquid crystals that are located between the liquid and solid state of matter, and are often referred to as the “fourth state of matter”. Lipidic cubic phases (LCPs) are a special form of LLCs that form spontaneously upon mixing water and lipids, and possibly a small amount of additive, in a certain ratio given by the phase diagram (Figure 3).

They are gel-like and stable materials with a well-defined 3-dimensional nanostructure and exhibit two non-intercommunicating aqueous channel system. LCPs are thermodynamically stable in excess of water and show a combination of other useful properties: optical transparency, biocompatibility, deformability, and adhesivity to hydrophilic as well as hydrophobic surfaces. Another important property of LCPs for the realization of the project described herein is the ability to host a wide variety of guest lipids with a broad range of properties.[14–16] Guest lipids, often also referred to as additives, usually have an amphiphilic character or are hydrophobic since they otherwise would be dissolved in water and washed away. Such additives can be small or large, positively or negatively charged or neutral, and can bear any conceivable functional groups and moieties, such as chromophores, photo switches or catalysts.

Monoolein (MO) is the best-studied lipid that forms LCPs. It consists of a glycerol headgroup coupled through an ester bond to an oleyl chain (Figure 1). The phase behavior of the MO/water system and the structure and properties of the ensuing mesophases is well described in literature (Figure 3).[17] Such phase diagrams have been constructed by systematically varying temperature and hydration degree of this binary system. The phases and their transitions were identified using small angle X-ray scattering (SAXS), differential scanning calorimetry (DSC) and microscopy.[18–22]

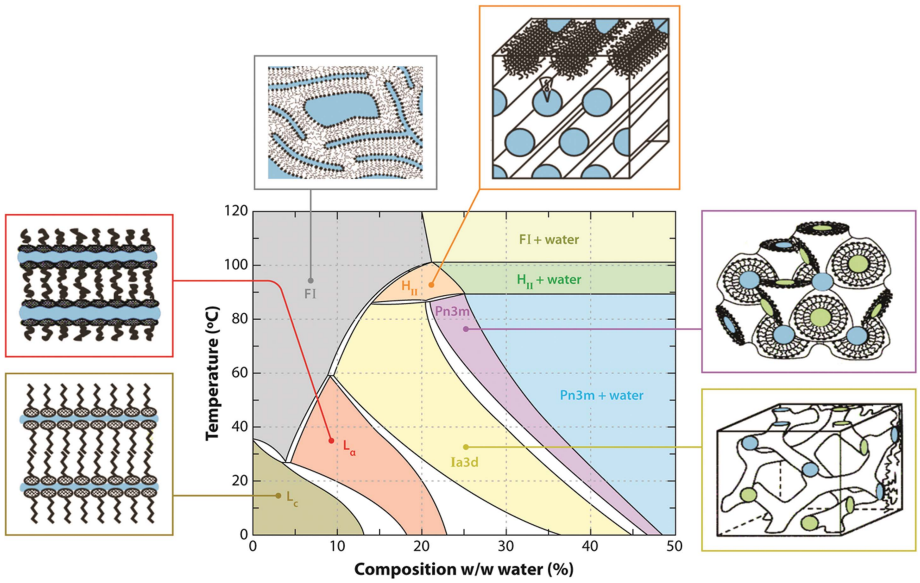

Figure 3: Binary phase diagram of monoolein and water with representation of the various phases. Abbreviations: *FI*, fluid isotropic phase; H_{II}, inverted hexagonal phase; L_α , lamellar liquid crystalline phase; L_c, lamellar crystal phase. Reprinted with permission from Ref. 17.

Upon hydration at room temperature, MO exhibits phase transitions from lamellar crystalline (L_c) to lamellar liquid crystalline (L_α) in which lipids can laterally diffuse due to the increased water content. Further increase of water gives rise to a reorganization of the lamellar phase

forming an *Ia3d* phase, a low-hydration bicontinuous cubic phase, which transforms to a higher-hydration bicontinuous cubic phase, denoted *Pn3m* phase. Upon further hydration, this phase does not dissolve, and is stable in excess of water. At low hydration and high temperatures, an isotropic fluid (*Fl*) is formed. Upon raising the temperature to 85°C at a water content greater than 15%, phase transition from a bicontinuous cubic (*Ia3d* or *Pn3m*) to the inverse hexagonal phase (H_{II}) takes place. This hexagonal phase, like the *Pn3m* cubic phase, is stable in excess water. The phenomenon of lipid polymorphism renders these materials interesting for application in diverse fields of science and technology.

3,7,11,15-Tetramethyl-1,2,3-hexadecanetriol, usually called phytantriol (PT), is a synthetic lipid that is often used as a cosmetic ingredient because of its positive effects on moisture retention in the skin and enhancing penetration of panthenol, vitamins and amino acids.[23] The mesophases of PT are, besides the ones of MO and monolinoleate, of the few that can be considered as safe to use in drug delivery applications.[23] The phase behavior of the PT and water system is very similar to the one of MO and water. Noteworthy is the fact that the PT phase diagram is based on a mixture of stereoisomers. A major difference, however, is the lower hydration degree and smaller lattice parameter of the *Pn3m* cubic phase at excess water conditions as compared to MO.[24] This is a disadvantage from our perspective, as in this project we plan to use LCPs as nanoreactors for catalysis. To that end, the chemical reactions in these systems should take place in the confined aqueous compartments, in which a maximal water proportion and aqueous channel diameter are certainly advantageous. Additionally, the lower hydration degree leads to a more viscous cubic phase. The absence of the ester group in PT is the main structural difference as compared to MO, resulting in PT being chemically much more stable than MO, since ester groups are prone to hydrolysis at strongly basic or acidic conditions. The same is true for *in vivo* applications in the presence of digestive enzymes.

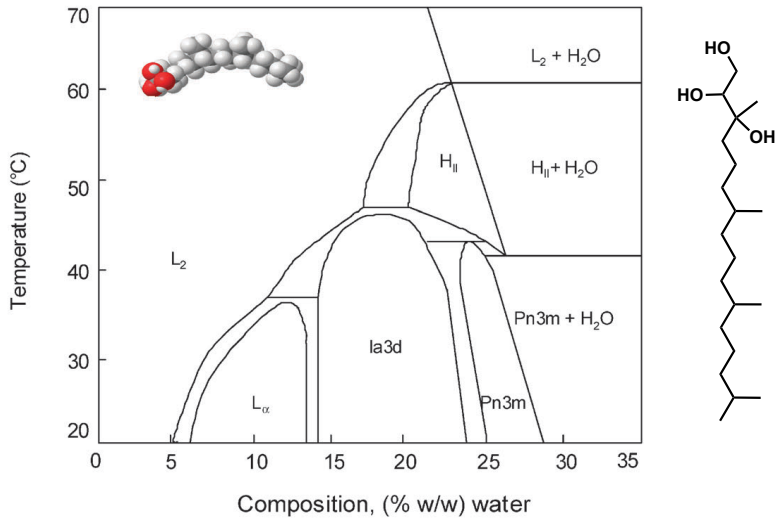

Figure 4: Phytantriol (PT) and water binary phase diagram and molecular structure of phytantriol. Abbreviations: L_2, inversed micellar phase; H_{II}, inverced hexagonal phase; L_α , lamellar liquid crystalline phase. Reprinted with permission from Ref. 23.

Bicontinuous cubic phases can adopt different defined space group geometries. The aqueous channels in the double gyroid cubic phase (*Ia3d*) possess a three-fold junction (Figure 5A), whereas the double diamond cubic phase (*Pn3m*) has a four-fold junction (Figure 5B), and the primitive cubic phase (*Im3m*) even a six-fold (Figure 5C).[19,25] Notably, the *Im3m* cubic phase is not present in the MO/water phase diagram (Figure 3), however it is formed with other lipids or if additives are applied to MO cubic phases.[26]

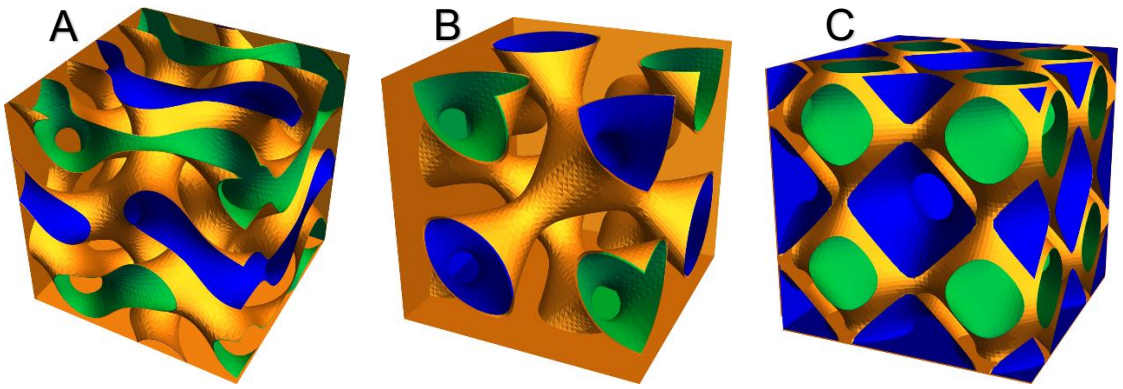

Figure 5: Topological Representation of the three bicontinuous cubic phases. Aqueous channels are colored in blue and green and the lipidic bilayer is colored yellow. A) *Ia3d* double gyroid cubic phase, B) *Pn3m* double diamond cubic phase, and C) *Im3m* primitive cubic phase.

Even though these cubic phases show different three-dimensional structures, they share several properties. They consist of a curved lipidic bilayer that forms an infinite periodic minimal surface with zero mean curvature that is encompassed by two identical, but non-intersecting water channel systems. Furthermore, lipids can diffuse laterally within its compartment whereas water can do so within the channels and to excess water reservoirs, if present.[27]

The geometrical models of the cubic phases can be used to calculate the aqueous channel radii. The water-lipid interface in the bicontinuous cubic phase is assumed to be parallel to the minimal surface.[28] The geometry and the lattice parameter *a* are determined by SAXS measurements and knowing the lipid volume fraction of the sample ϕ, the length of the lipid tail, *l,* can be calculated by solving the following cubic equation[29]:

$$\Phi = 2A_0\left(\frac{L_{lip}}{a}\right) + \frac{4}{3}\pi\chi\left(\frac{L_{lip}}{a}\right)^3 \qquad (1)$$

where A_0 is the area of the surface in the unit cell in which the lattice parameter is equal to unity, and χ is the Euler-Poincare characteristic. Depending on the specific cubic phase they have the following values: $A_0 = 3.091$ and $\chi = -8$ for *Ia3d;* $A_0 = 1.919$ and $\chi = -2$ for *Pn3m;* and $A_0 = 2.345$ and $\chi = -4$ for *Im3m*. For the radius of the aqueous channels, *r* the following equations are valid for the *Ia3d*, *Pn3m* and *Im3m* phases, respectively[20]:

$$r = 0.248a - L_{lip} \quad (2a)$$

$$r = 0.391a - L_{lip} \quad (2b)$$

$$r = 0.3055a - L_{lip} \quad (2c)$$

1.1.4 Cubosomes

In addition to their use as bulk gels, LCPs can be dispersed in water by ultra-sonication, forming nanoparticles that are denoted as cubosomes. Both LCPs and cubosomes exhibit a periodic, three-dimensional aqueous channel network and a very large lipid/water interfacial area (*ca.* 400 m^2 g^{-1} lipid).[30] Whereas bulk LCPs are malleable and can be attached to various surfaces due to their solid consistency and adhesive properties, cubosome nanoparticles dispersions have low viscosity and their appearance is comparable to the one of milk. Their typical particle size varies from 100 to 800 nm and can be determined by dynamic light scattering. The same method can be used to determine the polydispersity index of the particles. Cubosomes exhibit identical packing arrangement and phase identity to those of the parent gel LCP.[31] Because of their very large ratio of surface area to volume, cubosomes tend to aggregate to form thermodynamically stable bulk LCPs. To overcome this, their surfaces need to be kinetically stabilized.[32] Pluronics,[33] are the most frequently used stabilizers for such systems. In Figure 9, cryo-transmission electron microscopy image shows catalytic cubosomes that were used to catalyze aldol reactions (see Chapter 2). A more detailed description of cubosomes as drug delivery system will be provided in the introduction to Chapter 9. In this project, cubosomes were loaded with lipidic endoperoxides and delivered to anoxic cells which, upon controlled oxygen release might be supplied with the latter.

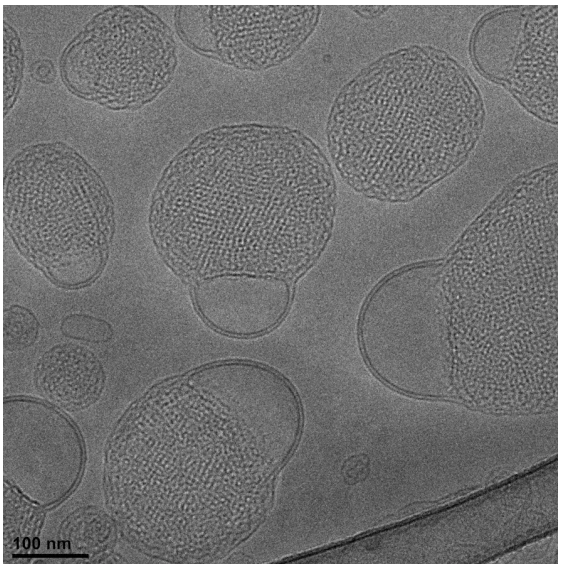

Figure 9: Cryo-transmission electron microscopy image of catalytic cubosomes with a *Pn3m* symmetry. Cubosomes need to be stabilized with a polymer, leading to a lamellar surrounding. Catalytic cubosomes will be described in Chapter 2.

1.1.5 Hexagonal phases

In the hexagonal phase, six cylinders consisting of a lipidic monolayer are packed in hexagonal symmetry. MO, for example shows an inverse hexagonal phase (H_{II}) in which the head groups of the lipids point inwards and the hydrophobic tails protrude to the external surface, thereby confining the aqueous channels.[34] MO shows the H_{II} phase at high temperatures of 70-100°C, which is typical for hydrated monoacylglycerols.[22] H_{II} phases are highly curved and thus the hydrophobic chains are densely packed. This is only possible at higher temperatures where hydrogen bonding between water and the lipid head groups are weaker as compared to lower temperatures. The weaker hydrogen bonding leads to a decrease in the hydration sphere that allows for an optimized packing. In contrast, normal hexagonal phases (H_I) are typically formed by detergents in water dispersions.

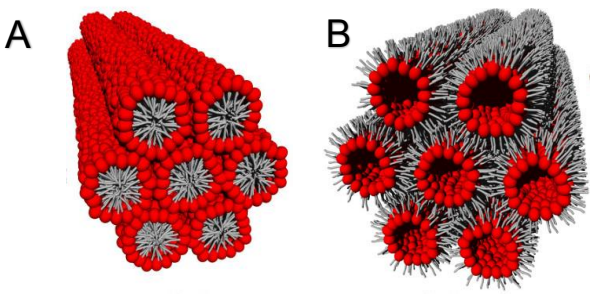

Figure 6: Schematic representation of A) normal (H_I), and B) inverse hexagonal phases (H_{II}) formed upon self-assembly of lipids in water at certain conditions. Polar head groups are shown in red, apolar chains are shown in grey. Reprinted with permission from Ref. 34.

1.1.6 Applications of LCPs

Due to their unique properties LCPs find applications in a very wide range of fundamental- and applied fields. Landau and Rosenbusch introduced LCPs for the solubilization, stabilization, and crystallization of membrane proteins. The implementation of this novel concept led to an explosion in solved membrane protein structures and had therefore a significant impact on structural biology and biomedicine.[14] The use of LCPs as drug delivery systems is a promising approach, thus research in this field is steadily expanding. LCPs with customized properties like negative or positive charged surfaces have been developed. The resulting electrostatic interactions with a charged drug allow for modified drug-release behavior.[35,36] The development of stimuli responsive lipidic materials has the potential to lift the drug delivery field to a higher level. Temperature has a major effect on the mesophase symmetry, which on the other hand affects the release of a drug. Temperature induced switching of the mesophase symmetry enables controlled drug release.[37,38] The use of pH-responsive LCPs exploits the changes in pH in different regions of the human body. Thus, phase transitions can be induced by protonation or deprotonation of pH sensitive additives. Negrini *et al*. for example, used a linoleic acid-based system to deliver phloroglucinol to the intestine. The low pH in the stomach induced a phase transition to a H_{II} phase leading to a reduced drug release, which was increased again in the intestine at higher pH (Figure 7).[39]

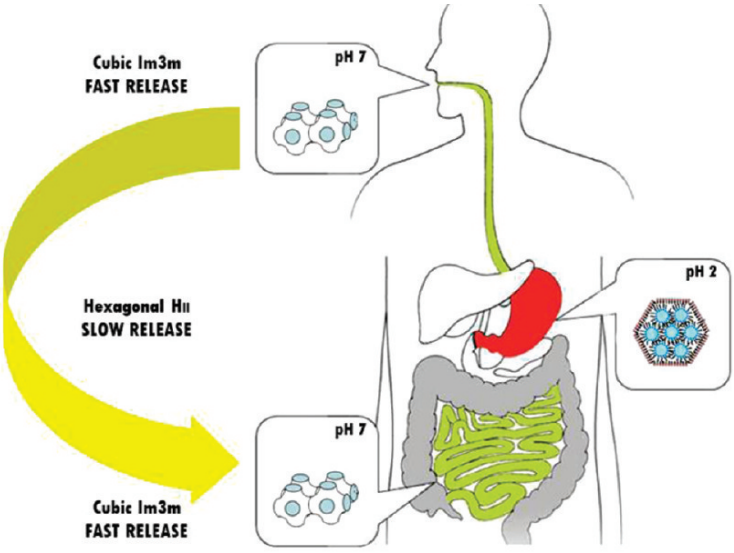

Figure 7: Schematic representation of the proposed pH-responsive drug delivery mechanism across the gastrointestinal tract. The lipidic nanoparticles have a cubic symmetry (Im3m) at pH 7, whereas the low pH in the stomach (pH 2), induces a phase transition to a reverse hexagonal phase (H_{II}). Due to the slower diffusion in H_{II} phases, the drug release is reduced. In the intestine at pH 7, the phase transition is inverted back to bicontinuous cubic (Im3m), enabling efficient release of the drug. Reprinted with permission from Ref. 39.

By adding photochromic compounds to LCPs, light responsive materials can be obtained. Aleandri *et al*. incorporated a lipidic photoswitch into dye-loaded mesophases. The light induced *trans-cis* isomerization of a lipidic azo-benzene derivative leads to disrupted lipid packing and therefore faster release of the dye.[40] Finally, electromagnetic energy can be applied as an external trigger. For example, magneto-responsive lipidic materials were used to macroscopically align lamellar and hexagonal phases, by incorporating magnetite nanoparticles to the system.[41] Apart from drug delivery systems, lyotropic liquid crystals have been used as biosensors and diagnostic platforms. Director distortion or crystallization based liquid crystal biosensors have been developed.[6,42] Crystallization based biosensors were used to monitor a birefringence signal that occurred upon crystallization of an enzymatic product in the LCP.[43] Finally, LCPs find application as food emulsifiers.[44]

1.1.7 Modification of aqueous channel diameters

The water channel diameter is of importance for the above-mentioned applications of lipidic mesophases such as drug delivery and release or membrane protein crystallization.[45] Therefore, several research groups have identified compounds which act as swelling agents when added to the LCP. Angelov *et al*. found that octyl glycoside can swell MO-based LCPs at excess water conditions.[46] Diglycerol monooleate and sucrose stearate have been shown to enlarge the channels of monolinolein systems, inducing a phase transition from a *Pn3m* to a *Im3m* cubic phase (Figure 8).[45,47] Engblom *et al*. showed that distearoylphosphatidylglycerol increases the aqueous channels of MO LCPs.[6] A very efficient swelling strategy was developed by Tyler *et al*. who used a two-step procedure to swell MO phases at 40°C by first adding cholesterol and then anionic lipids.[48]

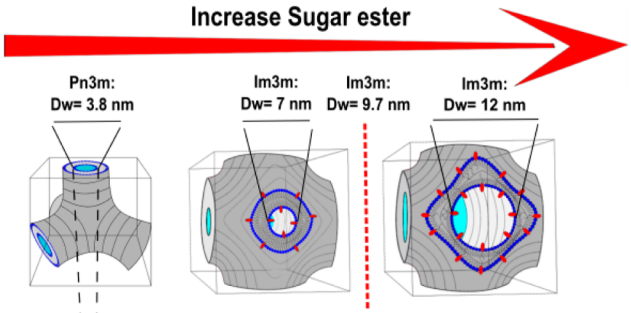

Figure 8: Illustration of aqueous channel swelling upon increasing the sugar ester concentration and phase transition from *Pn3m* to *Im3m* cubic phase. Reprinted with permission from Ref. 45.

To sum up, swelling of LCPs aqueous channels is a useful tool to tune the release of incorporated compounds or to affect protein crystallization.[49,50] The available know-how on

modifications of water channel diameter is significant for this thesis, as it allows us to control the kinetics of reactions carried out within LCPs or cubosomes.

1.1.8 Non-lipid based thermotropic and lyotropic liquid crystals

A brief introduction to the non-lipid based liquid crystals is provided here in order to complete the picture of the field of liquid crystals. These are often referred to as LCs in the literature. LCs revolutionized the area of display technology where they are being applied in televisions, cameras, mobile phones and laptops. Furthermore, LCs are used in materials science, nanoscience and in medicine.[51–53] Additionally, LCs are supramolecular models based on many noncovalent secondary interactions like hydrogen and halogen bonding or π-stacking and play therefore an important role from a fundamental research point of view.[54] Essentially, LCs can be divided into two groups, based on how their respective phase transitions are induced: lyotropic or thermotropic.[54] Thermotropic LCs are achieved by changing the temperature of a mesogen in its pure state, either by heating a crystalline solid of a mesogen or cooling an isotropic liquid (Figure 10). Upon heating, the mesogens lose their positional-, but not their orientational ordering, which upon further heating vanishes as well. In contrast, lyotropic LCs (LLCs) require a solvent and mesogens undergo phase transitions upon changing their concentration. Common LLCs display nematic, lamellar, columnar and cubic phases.

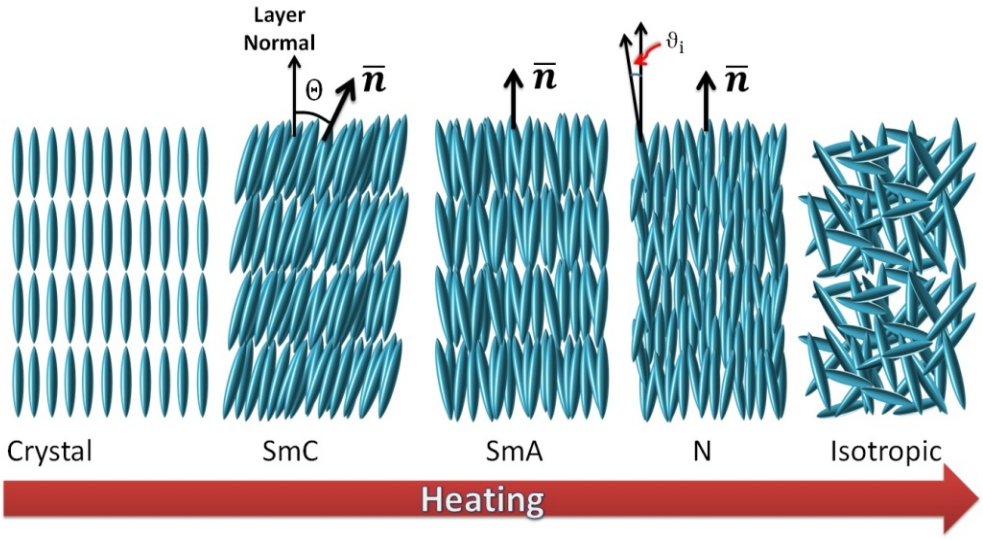

Figure 10: Schematic illustration of different liquid crystal phases observed upon heating from the solid state. In the smectic phases (SmC and SmA), positional and orientational ordering is mostly retained. Upon further heating, a phase transition to nematic (N) takes place, in which the positional ordering is lost and only orientational ordering is maintained, which upon further heating vanishes as well. Reprinted with permission from Ref. 54.

Metal complexes exhibiting thermotropic or lyotropic liquid crystalline behavior are referred to as metallomesogens. Luminescent metallomesogens are very attractive materials for OLEDs,[51,55] Pt-metallomesogens have been used as fluorescent probes for the detection of Hg^{2+}, Zn^{2+}, Cd^{2+} and Pd^{2+} and liquid crystalline metallofullerenes have been applied for bulk heterojunction solar cells.[56,57]

Whereas surfactant and lipid-based LLCs have been studied to a great extent, leading to in-depth knowledge of the self-assembly behavior, other LLC forming compound classes like chromonics are underexplored. LLCs in organic (or nonaqueous) media have rarely been studied.[58] Kölbel et al. reported rod-like rigid amphiphiles displaying lyotropic smectic and columnar liquid crystalline phases in glycerol.[59] The phase behavior of Gemini surfactants in a protic ionic liquid has revealed a reverse hexagonal phase.[60] Fullerene derivatives often show thermotropic LC behaviour, but when modified with bisphenyl groups bearing long alkyl chains, lyotropic hexagonal columnar phases were obtained.[61] A very promising approach is to transfer the chiral, nematic and photonic properties of cellulose nanocrystals to other materials, e.g. polymers or mesoporous silica.[62,63]

Research on thermotropic LCs has reached much higher levels of sophistication as compared to non-lipid-based LLCs. Thus, smart stimuli-responsive materials based on thermotropic LCs have been developed. Such tailor-made materials are in high-demand and have been used for almost every conceivable application. Several LCs displaying photostimulated isothermal phase transitions, based on different molecular switches have been reported.[54] Chiral nematic LCs that allow for helical chirality inversion upon photoswitching,[64] and metallomesogens showing different symmetries based on the coordinating metal have been developed.[65] These materials have potential applications in photonics, holographic optical data storage, self-healing materials, sensors and as polarizers.[54]

1.2 Rationale of this research

1.2.1 Lipidic material

As mentioned above, lipidic mesophases have been applied in a wide range of demanding purposes in different fields of science ranging from materials science, food science to nanomedicine. However, to the best of our knowledge, lipidic mesophases have not been functionalized and used as catalytic systems. Given the plethora of fascinating properties and characteristics of lipidic mesophases, particularly of the lipidic cubic phases, we embarked on a research program aimed at using such biomaterials as frameworks for the immobilization of catalysts in organic reactions. This novel approach exploits, among other things, the large lipid/water interface to perform efficient aqueous chemistry, taking place in the aqueous channels of the mesophases. Because lyotropic liquid crystals have a large potential for

designing tailor-made materials, research in this direction is necessary and will open exciting new avenues to discoveries in materials science. The next paragraph will introduce briefly the field of aqueous chemistry and its development over the past decades, since this thesis combines materials science of lipidic mesophases with aqueous chemistry.

1.2.2 Aqueous organic chemistry

Breslow's discovery of the positive effect of water on the reaction rate and selectivity of *Diels-Alder* reactions in the 1980s is commonly considered as the "Big Bang" in aqueous organic synthesis.[66] In this pioneering work, Rideout and Breslow showed that several Diels-Alder reactions can be significantly accelerated when water was used as the solvent (Scheme 1). The reaction of cyclopentadiene and butenone in 2,2,4-trimethylpentane was shown to be 700-fold slower as compared to the same reaction in water.[67] They rationalized that the hydrophobic effect was responsible for the strong rate enhancement. Later it has been shown that, in addition to the hydrophobic effect, also hydrogen bonding between water and the substrates in the transition states plays an important role, as water acts in a similar mode as Lewis-acids do.[68]

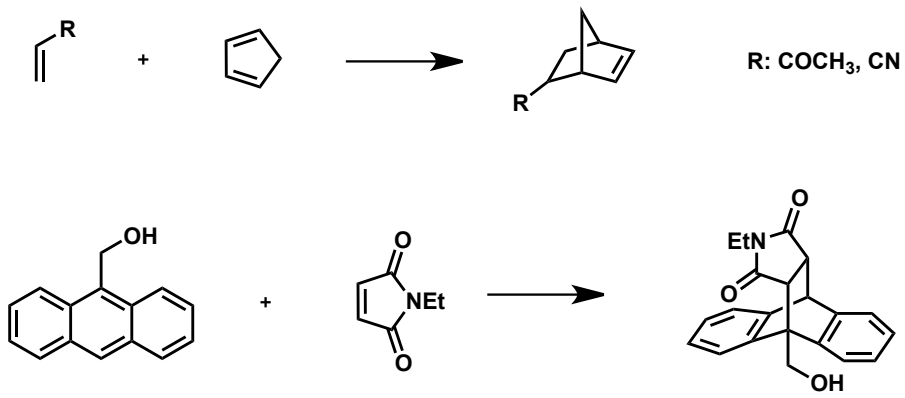

Scheme 1: Diels-Alder reaction of cyclopentadiene and butenon or acrylonitrile and of anthracene-9-carbinol and *N*-Ethylmaleimide, used by Rideout and Breslow to show the accelerative effect of water on these reactions. Adapted from Ref 67.

This work has initiated widespread interest in this field, and the repertoire of chemical transformations that can efficiently be carried out in water is ever growing. In addition to the *Diels-Alder* reaction, *Michael*-type additions, allylation reactions, cyclopropanation, cross coupling reactions, oxidations and reductions, as well as aldol-type reactions - to mention just a few examples - have been reinvented in aqueous medium.[66] However, the poor solubility of many small molecules in water and the negative effect of water on certain chemical transformation might be the main reason why water was not considered as a useful solvent

for organic reactions until recently. This is inconsistent with the fact that many very desirable synthetic targets, e.g. nucleotides, peptides and carbohydrates are well soluble in water.[66] Chemists have developed different strategies to circumvent the solubility problem of building blocks. The use of a cosolvent, often DMF, DMSO or alcohols is one method to increase the solubility, although it is controversial.[66,69] By varying the pH of a solution, charges can be added to ionizable compounds which can substantially increase the solubility of the solute.[66] A very efficient approach is the use of surfactants which leads to a compartmentalization of the reaction, which locally increases the concentration of reaction partners and therefore has beneficial impact on many reactions.[70–72] Finally, hydrophilic auxiliaries, for example some ethylene glycol-units, can be covalently attached to insoluble compounds which ideally can be cleaved afterwards.[66,73]

Generally, using water as a solvent is very desirable since it is environmentally sustainable, nontoxic and cheap. However, the mere use of water as a solvent does not automatically lead to “greener” processes, as was already pointed out by several authors.[69,74] The process needs to be evaluated in its entirety and factors such as substrate- and catalyst production, work-up and purification of products, as well as recycling of the catalyst need to be considered. Regarding these problems, our approach provides a number of promising features: The reaction takes place in water or buffer, and work-up comprises only freeze drying followed by purification by chromatography, if required. Furthermore, the modified LCPs and cubosomes can be reused without any catalyst recycling process, and no extraction or chromatographic process is necessary.

1.2.3 Catalyst immobilization

The immobilization of catalysts is beneficial for many reasons; the recovery and recycling of often tediously synthesized catalysts from homogeneous systems is challenging. Various heterogeneous systems have been developed to allow for easy catalyst recovery. Furthermore, the immobilization of a catalyst can have positive effects on its long-term stability, this is especially the case for enzymes.[75] In some cases, catalyst immobilization can even alter the outcome of the reaction, e.g. inverting the stereoselectivity of the products.[76] Other catalysts, like elemental metals, require an immobilization matrix and are not applicable otherwise. A widely used and established example is palladium on carbon that is used for hydrogenation reactions in academia and industry.

1.3 Objectives

With the introduction of lipidic cubic phase as immobilization matrices for catalysts in organic chemistry we plan to add a novel and versatile material to the list of catalyst immobilization platforms. Lipidic mesophases have a plethora of properties that make these materials suitable nanocatalysts. The large surface area of *ca.* 400 m^2 g^{-1} lipid[30] between the aqueous channels and the lipidic bilayer promises efficient catalysis. The diameter of the aqueous channels can be controlled and tuned, not only during the mesophase preparation process but also at later stages, even while catalysis is ongoing. This allows to modify the kinetics of the reactions carried out within these materials on-demand. Lipidic mesophases are formed upon self-assembly, therefore the production process is simpler as compared to many other immobilization materials, since only mixing of lipids and water followed by centrifugation and equilibration is needed. Cubosomes need to be sonicated, therefore an additional working step is required. Another advantage is the fact that these materials enable application in a dual mode: As bulk mesophases or as nanoparticle dispersions, depending on the set-up requirements. Finally, this approach is very general, and in principle many different catalyst types can be incorporated, ranging from organocatalysts, metal-compex catalysts, palladium nanoparticles and enzymes.

The goal of this thesis is to introduce lipidic cubic phases and cubosomes as a novel platform for catalysis, and to investigate the influence of these biomaterials on the chemical reactions carried out therein. This will be achieved as follows:

- Suitable model reactions, with the focus on organocatalyzed and metal-complex catalyzed reactions, will be chosen to provide an initial proof of principle.
- The respective catalysts will to be designed, synthesized and the catalyst-containing mesophases will be characterized by small angle X-ray scattering (SAXS) and dynamic light scattering (DLS).
- The effect of structural modifications of the catalysts on the catalytic performance will be investigated.
- These *in-meso* reactions will be investigated in terms of kinetics, stereochemistry, substrate scope and the influence of aqueous channel swelling on the reaction rates.
- Cubosomes and LCPs exhibit identical internal cubic symmetry, but their external features may vary significantly, as cubosomes are stabilized nanoparticles and have a larger outer surface as compared to bulk LCP. The impact of these differences on catalysis will be investigated.
- The scope of catalyst types will be expanded to palladium nanoparticles and enzymes.

Beside mesophase catalysis, which is the main project of this thesis, three additional subprojects have been carried out:

- Synthesis of enantiopure phytantriol and comparison of the ensuing LCPs with the one of commercially available phytantriol, which is a mixture of isomers.
- Synthesis of a small library of cyclopropanated lipids, their assembly into mesophases and their material investigation at sub-zero temperatures (Collaboration with the group of Prof. Dr. Raffaele Mezzenga from the Department of Health Sciences and Technology at the ETH) This is a continuation of an existing project.[77]
- Synthesis of lipidic endoperoxides and their incorporation into cubosomes in order to develop a nanocarrier that enables delivery of oxygen-releasing compounds to anoxic muscle cells followed by controlled oxygen release to increase the survival of transplanted tissue (Collaboration with the group of Prof. Dr. Dr. med. Daniel Eberli at the University Hospital Zurich)

Bibliography

(1) Fahy, E.; Subramaniam, S.; Murphy, R. C.; Nishijima, M.; Raetz, C. R. H.; Shimizu, T.; Spener, F.; van Meer, G.; Wakelam, M. J. O.; Dennis, E. A. Update of the LIPID MAPS Comprehensive Classification System for Lipids. *J. Lipid Res.* **2009**, *50*, 9-S14.

(2) Berg, J. M.; Tymoczko, J. L.; Stryer, L. *Stryer Biochemie*, 7th ed.; Springer-Verlag Berlin Heidelberg, 2013.

(3) Berridge, M. J.; Irvine, R. F. Inositol Phosphates and Cell Signalling. *Nature* **1989**, *341*, 197–205.

(4) Bach, D.; Wachtel, E. Phospholipid/cholesterol Model Membranes: Formation of Cholesterol Crystallites. *Biochim. Biophys. Acta - Biomembr.* **2003**, *1610*, 187–197.

(5) Kuzuyama, T.; Seto, H. Diversity of the Biosynthesis of the Isoprene Units. *Nat. Prod. Rep.* **2003**, *20*, 171–183.

(6) Fong, W.-K.; Negrini, R.; Vallooran, J. J.; Mezzenga, R.; Boyd, B. J. Lipids: Nutrition and Health. *J. Colloid Interface Sci.* **2016**, 484, 320–339.

(7) Malinauskas, T. Docking of Fatty Acids into the WIF Domain of the Human Wnt Inhibitory Factor-1. *Lipids* **2008**, *43*, 227–230.

(8) Malinauskas, T.; Aricescu, A. R.; Lu, W.; Siebold, C.; Jones, E. Y. Modular Mechanism of Wnt Signaling Inhibition by Wnt Inhibitory Factor 1. *Nat. Struct. Mol. Biol.* **2011**, *18*, 886–893.

(9) Dinasarapu, A. R.; Saunders, B.; Ozerlat, I.; Azam, K.; Subramaniam, S. Signaling Gateway Molecule Pages-a Data Model Perspective. *Bioinformatics* **2011**, *27*, 1736–1738.

(10) Eyster, K. M. The Membrane and Lipids as Integral Participants in Signal Transduction: Lipid Signal Transduction for the Non-Lipid Biochemist. *AJP Adv. Physiol. Educ.* **2007**, *31*, 5–16.

(11) Luzzati, V.; Tardieu, A.; Gulilk-Krzywicki. Polymorphism of Lipids. *Nature* **1968**, *219*, 862–863.

(12) Bitounis, D.; Fanciullino, R.; Iliadis, A.; Ciccolini, J. Optimizing Druggability through Liposomal Formulations: New Approaches to an Old Concept. *ISRN Pharm.* **2012**, *2012*, 1–11.

(13) Mouritsen, O. G. Lipidology and Lipidomics—quo Vadis? A New Era for the Physical Chemistry of Lipids. *Phys. Chem. Chem. Phys.* **2011**, *13*, 19195.

(14) Landau, E. M.; Rosenbusch, J. P. Lipidic Cubic Phases : A Novel Concept for the Crystallization of Membrane Proteins. *Proc. Natl. Acad. Sci.* **1996**, *93*, 14532–14535.

(15) Komisarski, M.; Osornio, Y. M.; Siegel, J. S.; Landau, E. M. Tailored Host-Guest Lipidic Cubic Phases: A Protocell Model Exhibiting Nucleic Acid Recognition. *Chem. - A Eur. J.* **2013**, *19*, 1262–1267.

(16) Lindblom, G.; Rilfors, L. Cubic Phases and Isotropic Structures Formed by Membrane Lipids — Possible Biological Relevance. *Biochim. Biophys. Acta* **1989**, *988*, 221–256.

(17) Cherezov, V.; Clogston, J.; Papiz, M. Z.; Caffrey, M. Room to Move: Crystallizing Membrane Proteins in Swollen Lipidic Mesophases. *J. Mol. Biol.* **2006**, *357*, 1605–1618.

(18) Lutton, E. S. Phase Behavior of Aqueous Systems of Monoglycerides. *J. Am. Oil Chem. Soc.* **1965**, *42*, 1068–1070.

(19) Hyde, S. T.; Andersson, S.; Ericsson, B.; Larsson, K. A Cubic Structure Consisting of a Lipid Bilayer Forming an Infinite Periodic Minimum Surface of the Gyroid Type in the Glycerolmonooleat-Water System. *Zeitschrift für Krist. - New Cryst. Struct.* **1984**, *168*, 213–219.

(20) Briggs, J.; Chung, H.; Caffrey, M. The Temperature-Composition Phase Diagram and Mesophase Structure Characterization of the Monoolein / Water System. *J. Phys. II Fr.* **1996**, *6*, 723–751.

(21) Cherezov, V.; Clogston, J.; Misquitta, Y.; Abdel-Gawad, W.; Caffrey, M. Membrane Protein Crystallization In Meso: Lipid Type-Tailoring of the Cubic Phase. *Biophys. J.* **2002**, *83*, 3393–3407.

(22) Qiu, H.; Caffrey, M. The Phase Diagram of the Monoolein/water System: Metastability and Equilibrium Aspects. *Biomaterials* **2000**, *21*, 223–234.

(23) Barauskas, J.; Landh, T. Phase Behavior of the Phytantriol/Water System. *Langmuir* **2003**, *19*, 9562–9565.

(24) Dong, Y. D.; Larson, I.; Hanley, T.; Boyd, B. J. Bulk and Dispersed Aqueous Phase Behavior of Phytantriol: Effect of Vitamin E Acetate and F127 Polymer on Liquid Crystal Nanostructure. *Langmuir* **2006**, *22*, 9512–9518.

(25) Hyde, S. T. Bicontinuous Structures in Lyotropic Liquid Crystals and Crystalline Hyperbolic Surfaces. *Curr. Opin. Solid State Mater. Sci.* **1996**, *1*, 653–662.

(26) Duss, M.; Salvati Manni, L.; Moser, L.; Handschin, S.; Mezzenga, R.; Jessen, H. J.; Landau, E. M. Lipidic Mesophases as Novel Nanoreactor Scaffolds for Organocatalysts: Heterogeneously Catalyzed Asymmetric Aldol Reactions in Confined Water. *ACS Appl. Mater. Interfaces* **2018**, *10*, 5114–5124.

(27) Lee, W. B.; Mezzenga, R.; Fredrickson, G. H. Self-Consistent Field Theory for Lipid-Based Liquid Crystals: Hydrogen Bonding Effect. *J. Chem. Phys.* **2008**, *128*.

(28) Schwarz, U. S.; Gompper, G. Bending Frustration of Lipid-Water Mesophases Based on Cubic Minimal Surfaces. *Langmuir* **2001**, *17*, 2084–2096.

(29) Turner, D. C.; Wang, Z.-G.; Gruner, S. M.; Mannock, D. a.; McElhaney, R. N. Structural Study of the Inverted Cubic Phases of Di-Dodecyl Alkyl-β-D-Glucopyranosyl-Rac-Glycerol. *J. Phys. II* **1992**, *2*, 2039–2063.

(30) Lawrence, M. J. Surfactant Systems: Their Use in Drug Delivery. *Chem. Soc. Rev.* **1994**, *23*, 417–424.

(31) Aleandri, S.; Bandera, D.; Mezzenga, R.; Landau, E. M. Biotinylated Cubosomes: A Versatile Tool for Active Targeting and Codelivery of Paclitaxel and a Fluorescein-Based Lipid Dye. *Langmuir* **2015**, *31*, 12770–12776.

(32) Chong, J. Y. T.; Mulet, X.; Waddington, L. J.; Boyd, B. J.; Drummond, C. J. Steric Stabilisation of Self-Assembled Cubic Lyotropic Liquid Crystalline Nanoparticles: High Throughput Evaluation of Triblock Polyethylene Oxide-Polypropylene Oxide-Polyethylene Oxide Copolymers. *Soft Matter* **2011**, *7*, 4768–4777.

(33) Kaasgaard, T.; Drummond, C. J. Ordered 2-D and 3-D Nanostructured Amphiphile Self-Assembly Materials Stable in Excess Solvent. *Phys. Chem. Chem. Phys.* **2006**, *8*, 4957–4975.

(34) Seddon, J. M. Structure of the Inverted Hexagonal (HII) Phase, and Non-Lamellar Phase Transitions of Lipids. *Biochim. Biophys. Acta* **1990**, *1031*, 1–69.

(35) Lynch, M. L.; Ofori-Boateng, A.; Hippe, A.; Kochvar, K.; Spicer, P. T. Enhanced Loading of Water-Soluble Actives into Bicontinuous Cubic Phase Liquid Crystals Using Cationic Surfactants. *J. Colloid Interface Sci.* **2003**, *260* , 404–413.

(36) Negrini, R.; Sánchez-Ferrer, A.; Mezzenga, R. Influence of Electrostatic Interactions on the Release of Charged Molecules from Lipid Cubic Phases. *Langmuir* **2014**, *30*, 4280–4288.

(37) Lee, K. W. Y.; Nguyen, T. H.; Hanley, T.; Boyd, B. J. Nanostructure of Liquid Crystalline Matrix Determines in Vitro Sustained Release and in Vivo Oral Absorption Kinetics for Hydrophilic Model Drugs. *Int. J. Pharm.* **2009**, *365*, 190–199.

(38) Phan, S.; Fong, W. K.; Kirby, N.; Hanley, T.; Boyd, B. J. Evaluating the Link between Self-Assembled Mesophase Structure and Drug Release. *Int. J. Pharm.* **2011**, *421*, 176–182.

(39) Negrini, R.; Mezzenga, R. pH-Responsive Lyotropic Liquid Crystals for Controlled Drug Delivery. *Langmuir* **2011**, *27*, 5296–5303.

(40) Aleandri, S.; Speziale, C.; Mezzenga, R.; Landau, E. M. Design of Light-Triggered Lyotropic Liquid Crystal Mesophases and Their Application as Molecular Switches in “On Demand” Release. *Langmuir* **2015**, *31*, 6981–6987.

(41) Vallooran, J. J.; Bolisetty, S.; Mezzenga, R. Macroscopic Alignment of Lyotropic Liquid Crystals Using Magnetic Nanoparticles. *Adv. Mater.* **2011**, *23*, 3932–3937.

(42) Fang, J.; Ma, W.; Selinger, J. V.; Shashidhar, R. Imaging Biological Cells Using Liquid Crystals. *Langmuir* **2003**, *19*, 2865–2869.

(43) Vallooran, J. J.; Handschin, S.; Pillai, S. M.; Vetter, B. N.; Rusch, S.; Beck, H. P.; Mezzenga, R. Lipidic

Cubic Phases as a Versatile Platform for the Rapid Detection of Biomarkers, Viruses, Bacteria, and Parasites. *Adv. Funct. Mater.* **2016**, *26*, 181–190.

(44) Mezzenga, R.; Schurtenberger, P.; Burbidge, A.; Michel, M. Understanding Foods as Soft Materials. *Nat. Mater.* **2005**, *4*, 729–740.

(45) Negrini, R.; Mezzenga, R. Diffusion, Molecular Separation, and Drug Delivery from Lipid Mesophases with Tunable Water Channels. *Langmuir* **2012**, *28*, 16455–16462.

(46) Angelov, B.; Angelova, A.; Ollivon, M.; Bourgaux, C.; Campitelli, A. Diamond-Type Lipid Cubic Phase with Large Water Channels. *J. Am. Chem. Soc.* **2003**, *125*, 7188–7189.

(47) Yaghmur, A.; De Campo, L.; Sagalowicz, L.; Leser, M. E.; Glatter, O. Control of the Internal Structure of MLO-Based Isasomes by the Addition of Diglycerol Monooleate and Soybean Phosphatidylcholine. *Langmuir* **2006**, *22*, 9919–9927.

(48) Tyler, A. I. I.; Barriga, H. M. G.; Parsons, E. S.; McCarthy, N. L. C.; Ces, O.; Law, R. V.; Seddon, J. M.; Brooks, N. J. Electrostatic Swelling of Bicontinuous Cubic Lipid Phases. *Soft Matter* **2015**, *11*, 3279–3286.

(49) Zabara, A.; Amar-Yuli, I.; Mezzenga, R. Tuning in-Meso-Crystallized Lysozyme Polymorphism by Lyotropic Liquid Crystal Symmetry. *Langmuir* **2011**, *27*, 6418–6425.

(50) Zabara, A.; Mezzenga, R. Plenty of Room to Crystallize: Swollen Lipidic Mesophases for Improved and Controlled in-Meso Protein Crystallization. *Soft Matter* **2012**, *8*, 6535.

(51) Wöhrle, T.; Wurzbach, I.; Kirres, J.; Kostidou, A.; Kapernaum, N.; Litterscheidt, J.; Haenle, J. C.; Staffeld, P.; Baro, A.; Giesselmann, F.; Laschat, S. Discotic Liquid Crystals. *Chem. Rev.* **2016**, *116*, 1139–1241.

(52) Bisoyi, H. K.; Kumar, S. Liquid-Crystal Nanoscience: An Emerging Avenue of Soft Self-Assembly. *Chem. Soc. Rev.* **2011**, *40*, 306–319.

(53) Woltman, S. J.; Jay, G. D.; Crawford, G. P. Liquid-Crystal Materials Find a New Order in Biomedical Applications. *Nat. Mater.* **2007**, *6*, 929–938.

(54) Bisoyi, H. K.; Li, Q. Light-Driven Liquid Crystalline Materials: From Photo-Induced Phase Transitions and Property Modulations to Applications. *Chem. Rev.* **2016**, *116*, 15089–15166.

(55) Kozhevnikov, V. N.; Donnio, B.; Bruce, D. W. Phosphorescent, Terdentate, Liquid-Crystalline Complexes of platinum(II): Stimulus-Dependent Emission. *Angew. Chemie - Int. Ed.* **2008**, *47*, 6286–6289.

(56) Cuerva, C.; Campo, J. A.; Ovejero, P.; Torres, M. R.; Oliveira, E.; Santos, S. M.; Lodeiro, C.; Cano, M. Columnar Discotic Pt(II) Metallomesogens as Luminescence Multifunctional Materials with Chemo and Thermosensor Abilities. *J. Mater. Chem. C* **2014**, *2*, 9167–9181.

(57) Toth, K.; Molloy, J. K.; Matta, M.; Heinrich, B.; Guillon, D.; Bergamini, G.; Zerbetto, F.; Donnio, B.; Ceroni, P.; Felder-Flesch, D. A Strongly Emitting Liquid-Crystalline Derivative of Y3N@C80: Bright and Long-Lived near-IR Luminescence from a Charge Transfer State. *Angew. Chemie - Int. Ed.* **2013**, *52*, 12303–12307.

(58) Masters, A. Chromonic Liquid Crystals: More Questions than Answers. *Liq. Cryst. Today* **2016**, *25*, 30–37.

(59) Kölbel, M.; Tschierske, C.; Diele, S. Formation of Thermotropic and Lyotropic Smectic and Columnar Liquid Crystalline Phases by a Novel Type of Rigid Rod-like Amphiphilic Molecule. *Chem. Commun.* **1998**,15, 1511–1512.

(60) Wang, X.; Chen, X.; Zhao, Y.; Yue, X.; Li, Q.; Li, Z. Nonaqueous Lyotropic Liquid-Crystalline Phases Formed by Gemini Surfactants in a Protic Ionic Liquid. *Langmuir* **2012**, *28*, 2476–2484.

(61) Sawamura, M.; Kawai, K.; Matsuo, Y.; Kanie, K.; Kato, T.; Nakamura, E. Stacking of Conical Molecules with a Fullerene Apex into Polar Columns in Crystals and Liquid Crystals. *Nature* **2002**, *419*, 702–705.

(62) Cheung, C. C. Y.; Giese, M.; Kelly, J. A.; Hamad, W. Y.; Maclachlan, M. J. Iridescent Chiral Nematic Cellulose Nanocrystal/polymer Composites Assembled in Organic Solvents. *ACS Macro Lett.* **2013**, *2*, 1016–1020.

(63) Wang, P. X.; Hamad, W. Y.; MacLachlan, M. J. Polymer and Mesoporous Silica Microspheres with Chiral Nematic Order from Cellulose Nanocrystals. *Angew. Chemie - Int. Ed.* **2016**, *55*, 12460–12464.

(64) Hayasaka, H.; Miyashita, T.; Nakayama, M.; Kuwada, K.; Akagi, K. Dynamic Photoswitching of Helical

Inversion in Liquid Crystals Containing Photoresponsive Axially Chiral Dopants. *J. Am. Chem. Soc.* **2012**, *134*, 3758–3765.

(65) Kawano, S. ichiro; Hamazaki, T.; Suzuki, A.; Kurahashi, K.; Tanaka, K. Metal-Ion-Induced Switch of Liquid-Crystalline Orientation of Metallomacrocycles. *Chem. - A Eur. J.* **2016**, *22*, 15674–15683.

(66) Lindström, U. M. Stereoselective Organic Reactions in Water. *Chem. Rev.* **2002**, *102*, 2751–2772.

(67) Rideout, D. C.; Breslow, R. Hydrophobic Acceleration of Diels-Alder Reactions. *J. Am. Chem. Soc.* **1980**, *102*, 7816–7817.

(68) Otto, S.; Blokzijl, W.; Engberts, J. B. F. N. Diels-Alder Reactions in Water. Effects of Hydrophobicity and Hydrogen Bonding. *J. Org. Chem.* **1994**, *59*, 5372–5376.

(69) Blackmond, D. G.; Armstrong, A.; Coombe, V.; Wells, A. Water in Organocatalytic Processes: Debunking the Myths. *Angew. Chem. Int. Ed. Engl.* **2007**, *46*, 3798–3800.

(70) Tascioglu, S. Micellar Solutions as Reaction Media. *Tetrahedron* **1996**, *52*, 11113-11152.

(71) La Sorella, G.; Strukul, G.; Scarso, A. Recent Advances in Catalysis in Micellar Media. *Green Chem.* **2015**, *17*, 644–683.

(72) Lipshutz, B. H.; Abela, A. R. Micellar Catalysis of Suzuki-Miyaura Cross-Couplings with Heteroaromatics in Water. *Org. Lett.* **2008**, *10*, 5329–5332.

(73) Benz, S.; Nötzli, S.; Siegel, J. S.; Eberli, D.; Jessen, H. J. Controlled Oxygen Release from Pyridone Endoperoxides Promotes Cell Survival under Anoxic Conditions. *J. Med. Chem.* **2013**, *56*, 10171–10182.

(74) Mlynarski, J.; Baś, S. Catalytic Asymmetric Aldol Reactions in Aqueous Media--a 5 Year Update. *Chem. Soc. Rev.* **2014**, *43*, 577–587.

(75) Hanefeld, U.; Gardossi, L.; Magner, E. Understanding Enzyme Immobilisation. *Chem. Soc. Rev.* **2009**, *38*, 453–468.

(76) Yeh, C.; Sun, Y.; Huang, S.; Tsai, Y. Alternating Chiral Selectivity of Aldol Reactions under the Confined Space of Mesoporous Silica. *Chem. Commun.* **2015**, *51*, 17116–17119.

(77) Salvati Manni, L.; Zabara, A.; Osornio, Y. M.; Schöppe, J.; Batyuk, A.; Plückthun, A.; Siegel, J. S.; Mezzenga, R.; Landau, E. M. Phase Behavior of a Designed Cyclopropyl Analogue of Monoolein: Implications for Low-Temperature Membrane Protein Crystallization. *Angew. Chem. Int. Ed. Engl.* **2014**, 1–6.

Chapter 2

Lipidic mesophases as novel nanoreactor scaffolds for organocatalysts: Heterogeneously catalyzed asymmetric aldol reactions in confined water

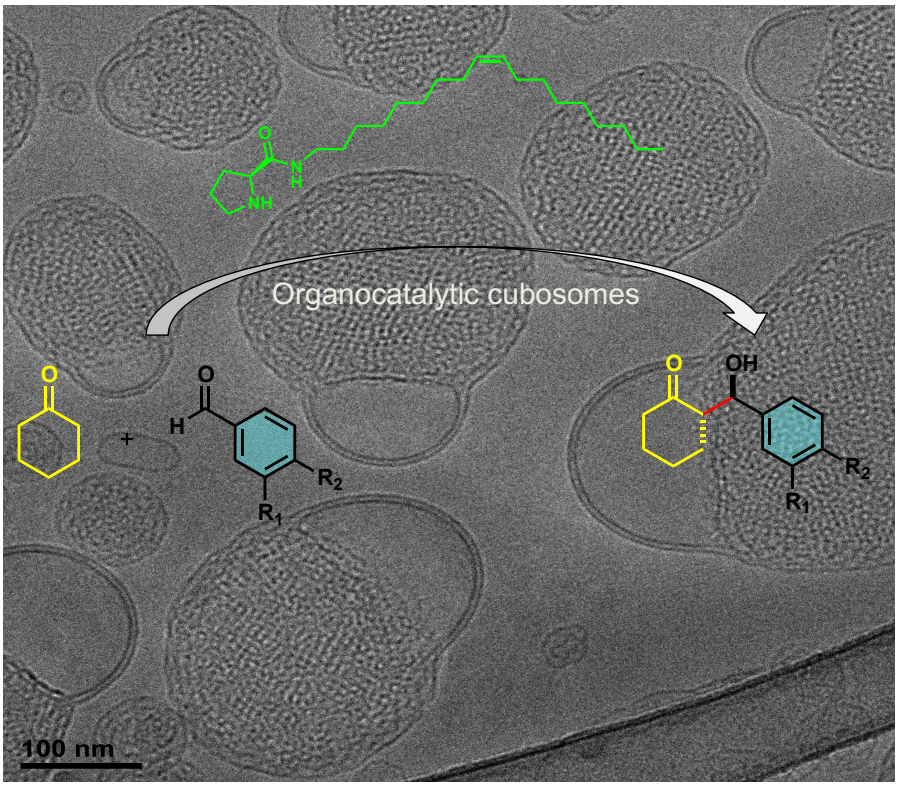

2.1 Introduction

Nature has evolved enzymes to catalyze a plethora of reactions very efficiently and highly stereoselectively in aqueous environment and under mild conditions. Organocatalysis relies on small organic molecules to mimic nature´s sophistication without having to synthesize large protein assemblies. However, the recovery and recycling of potentially valuable catalysts from homogeneous systems is challenging. Various heterogeneous systems have been developed to allow easy catalyst recovery. Thus, organocatalysts have been immobilized on mesoporous silica[1], on polymer supports[2], on crystalline metal-organic frameworks[3], on covalent organic frameworks[4] or on cloth[5].

In addition to these solid supported systems, the applicability of lipidic self-assembly in micellar and vesicular catalysis is a large research field, as the use of surfactants is an efficient approach to conduct chemical reactions in water. Numerous processes have been developed that are competitive or even superior, in terms of yield, selectivity and catalyst recycling to their equivalents in organic solvents.[6] Furthermore, in some examples the reaction was conducted under energy-saving conditions.[7] Vesicles have been widely used to study enzymatic reactions. Their tunable size and lipid composition render them not only attractive membrane model systems, but also a platform for other catalysts.[8–11] König *et al.* for example, used vesicles to catalyze hydrolytic cleavage of organophosphates with amphiphilic zinc complexes.[12,13] In contrast to liposomal and micellar systems, only a few examples of chemical reactions carried out using lipidic mesophases are known. Mezzenga *et al.* studied enzyme kinetics of horseradish peroxidase (HRP) in different mesophase types.[14,15] Watzke *et al.* showed that a *Maillard* reaction was more efficient in lipidic cubic phase (LCP) medium than in bulk water.[16]

LCPs, are liquid crystalline biomaterials that form spontaneously upon mixing water and lipid molecules in a well-defined composition and temperature range given by the phase diagram.[17] The driving force for such amphiphilic self-assembly is the hydrophobic effect, which leads to the minimization of the interface between hydrocarbon tails of the amphiphile and water. LCPs are gel-like, stable biomaterials whose nanostructure depends on the specific lipid molecular structure. The latter is packed into a spatially curved lipid bilayer encompassing two identical but non-intercommunicating aqueous channel systems. Significantly, LCPs can be doped with various additive molecules, thereby functionalizing them by design.[18] These complex biomaterials find application in a wide range of fundamental and applied fields such as drug delivery,[19,20] membrane biology,[21,22] biodevices,[23] and food emulsifiers.[24] LCPs are thermodynamically stable in excess of water and show a combination of useful properties: optical transparency, biocompatibility, deformability, and adhesivity to hydrophilic as well as hydrophobic surfaces, which allows their application on practically any surface.

Monoolein (MO, Figure 1) is the best-studied and most widely used lipid that forms LCPs. In addition to their use as gels, LCPs can be dispersed in water by ultra-sonication, forming

nanoparticles that are denoted as cubosomes. The surface of cubosomes needs to be stabilized, typically with a polymeric additive, in order to prevent reassembly of the nanoparticles into the thermodynamically stable bulk LCP.[25] Both LCPs and cubosomes exhibit a periodic, three-dimensional aqueous channel network and a very large lipid/water interfacial area (*ca.* 400 m^2 g^{-1} lipid).[26]

Whereas the above-mentioned examples have used LCPs merely as reaction medium, our approach entails the judicious modification of LCPs and cubosomes by design, thereby forming host-guest molecular systems that are intrinsically catalytically active. MO as the host lipid is responsible for the molecular architecture and properties of the biomaterial whose specific geometries can be used to host the guest lipid catalyst. The latter is "semi-immobilized" in the bilayer, and orientated at the large interface between the aqueous and the lipidic compartments, exposing its catalytic site towards the aqueous subphase. Such "semi-immobilization" denotes the free lateral diffusion of the catalyst within the curved lipidic bilayer. Figure 1 illustrates the concept of these designed catalytic mesophases.

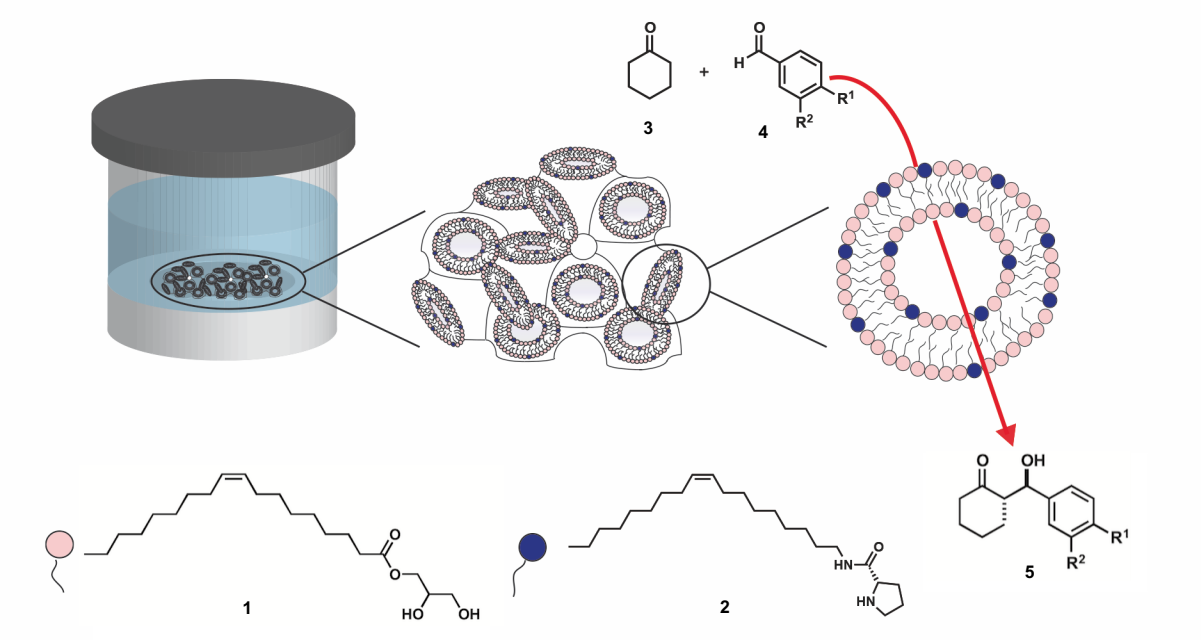

Figure 1: Schematic representation of the experimental set up (upper left), structure of the host guest LCP (upper middle), and the principle of catalytic LCPs (upper right). The LCP, composed of host MO lipids (pink), guest lipid-modified organocatalyst (dark blue) and water, is placed in a specially designed holder and overlaid with an aqueous solution (upper left). The reaction, catalyzed by the blue lipidic catalysts, takes place at the lipid-water interface of the catalytic mesophase.

In addition to the large surface area of LCPs, these biomaterials offer several additional features which facilitate their application as efficient matrices for heterogeneous catalysis: The aqueous pores communicate freely with the overlay bulk water, thus avoiding the need for substrate diffusion across membranes. Mesophases can be used as bulk LCPs or in dispersed form as cubosomes, as both are thermodynamically stable in excess water. Thus,

depending on the requirements, either an adhesive gel or dispersion can be employed. Furthermore, both experimental set-ups allow simple catalyst recycling. Preparation of the mesophase is simple and fast and the lattice parameters as well as the geometry can be tuned at will by either using specific additives, or by controlling environmental parameters such as hydration, temperature,[17] pH,[20,27] or ionic strength[28] of the aqueous medium. A fundamental requirement for the broad applicability of such mesophases as nanoreactor scaffolds in organic chemistry is their ability to host a wide variety of guest lipids with a broad range of properties,[18,27,29] allowing to conduct different catalytic reactions.

In this study, we report the first organocatalytic reaction conducted in designed host-guest LCPs and cubosomes as new class of self-assembled nanoreactor scaffolds, and analyze their effect on catalysis. The organocatalyzed aldol reaction between water-soluble aldehydes and cyclohexanone was chosen as a model reaction, as this reaction is one of the most important carbon-carbon bond forming reactions for the generation of β-hydroxycarbonyl moieties,[30–32] being responsible for the biosynthesis of carbohydrates, keto acids and some amino acids.[33] Enzymes catalyze these reactions very efficiently and highly stereoselectively in water under mild conditions. These are all very desirable attributes for chemical processes. However, although enzymes have been applied in synthesis, they usually suffer of limited up-scale compatibility.[34] The use of organocatalysts in order to mimic nature is therefore a very elegant approach. One of the first organocatalysts that was introduced was proline.[35] However, in contrast to enzymes, proline-catalyzed aldol reactions are usually carried out in polar organic solvents such as DMF or DMSO, and addition of large amounts of water led to decrease in reaction rate and stereoselectivity.[36–38] This drawback could be overcome if a proline-derived catalyst, instead of proline itself is applied.[39–41]

2.2 Results and discussion

2.2.1 First generation lipidic aldol organocatalysts

It has been shown that aldol reactions in water catalyzed by proline-derivatives with free carboxylic acid are usually slow and their enantio- and diastereo-selectivity is poor. However, if the reaction occurs in confined space and the catalytic system provides a molecular environment comparable to a hydrophobic pocket of an enzyme, good results can be obtained.[42] We hypothesized that a similar situation would be achieved in the confined aqueous channels of the LCPs. Therefore catalysts **9** and **13** were synthesized according to previously reported procedures.[18] Catalyst **9** has been synthesized with two different methods: By a *Steglich*-esterification and by esterification using oleylchloride as the activated carboxylic acid species (Scheme 1, top panel). The product was obtained by both approaches in low yield, probably due the lowered nucleophilicity of the secondary alcohol and rather short reaction times. Additionally, the amide derivative was also synthesized, since ester tend to hydrolyze (Scheme 1, bottom panel). The Boc-protecting group of **8** and **12** was cleaved under acidic conditions using TFA in CH_2Cl_2.

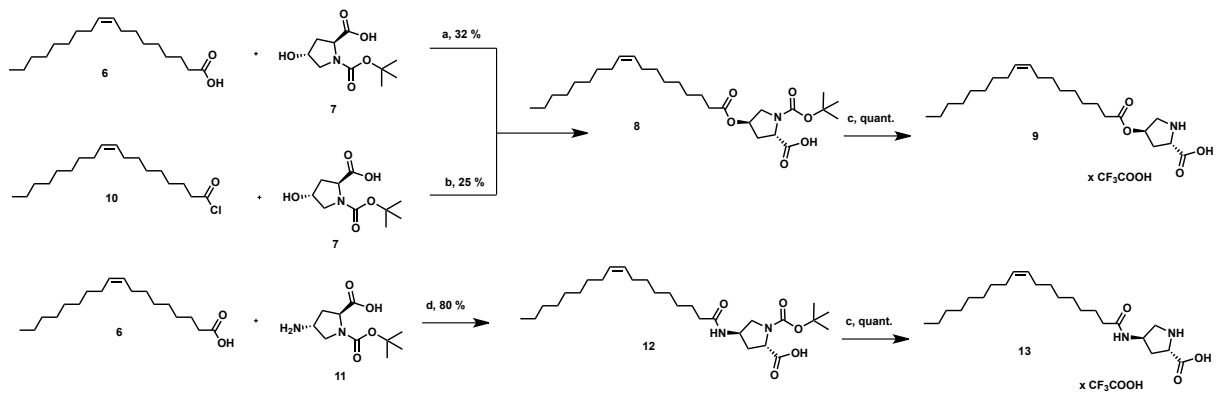

Scheme 1: Syntheses of lipidic catalysts **9** and **13** Conditions: a) Oleic acid, DCC (1.1 eq), DMAP (0.1 eq) CH_2Cl_2 / DMF 4:1, r.t. b) DIPEA, CH_2Cl_2, 0°C c) TFA / CH_2Cl_2 (1:4), 0°C, d) EDC (1.1 eq), DMAP (0.1 eq) CH_2Cl_2 / DMF 4:1, r.t..

The amide as well as the ester derivative (**9** and **13**) could be incorporated into MO-based LCPs at a content of up to 10 % (w/w) of the lipid. These LCPs were subsequently used to perform the very first catalysis experiments with LCPs. As a model aldol reaction 4-nitro-benzaldehyde (**14**) and cyclohexanone (**3**) was used (Scheme 2).

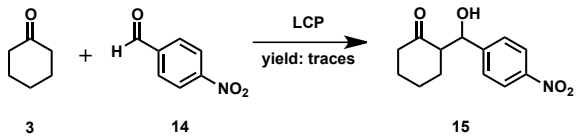

Scheme 2: First LCP catalysis experiment using 4-nitro-benzaldehyde **14** and cyclohexanone (**3**) as the substrate pair. Conditions: 4 days at room temperature with 30 mol % catalyst and 2 eq cyclohexanone.

The reaction was very sluggish and after four days, only traces of product were detected. Thus, the choice of both the catalyst and the substrates was not ideal, and needed to be optimized. As already mentioned, better results can be expected if the proline carboxylic acid is derivatized, for example to an amide. The aldol reaction of 4-nitro-benzaldehyde and cyclohexanone is the benchmark aldol reaction in literature, however, for our system it is not suitable due to the low solubility in water. Less lipophilic substrates will probably lead to better reaction rates since they do not accumulate in the lipidic compartments of the LCP.

2.2.2 Second generation lipidic aldol organocatalyst

2.2.2.1 Synthesis of lipidic prolineamido-glycoside catalyst

In order to implement the gained insights from the first experiments, a new, LCP compatible organocatalyst was designed. Catalyst **24**, reported by Tsutsui's *et al*. catalyzes aldol reactions of carbohydrates efficiently,[43,44] and served as inspiration. The carbohydrate moiety possesses several advantages. Firstly, the hydroxyl groups stabilize the transition state of the aldol reaction.[43] Secondly, the sugar acts as a linker between the lipidic chain and the catalytically active proline moiety, pushing the proline further into the aqueous channel of the mesophase, which might lead to easier contact between catalyst and substrates. Thirdly, carbohydrate-derived lipids are known to swell the aqueous channels of mesophases.[45–47] Furthermore, the primary alcohol of the carbohydrate moiety offers a good synthetis opportunity to install the lipidic chain.

The starting point of the synthesis was the commercially available *N*-Acetyl-*D*-glucoseamine (**16**), which was treated with MeOH/Dowex to methylate the anomeric position and obtain an anomeric mixture of α- and ß-methyl glucoside.[48] The ratio of the two anomers was determined by ^{1}H-NMR to be 2:1 and they could easily be separated by column

chromatography to obtain pure **17**. After cleaving the acetyl protecting group with barium oxide, the free amine **18** was coupled to Boc-*L*-proline (**19**) using DCC/DMAP to obtain Boc-protected proline glycoside **20**. Attempts to improve the yield of this step failed. The oleic chain was installed at the carbohydrate moiety by selective oxidation of the primary alcohol to the aldehyde[49] and subsequent reductive amination using oleyl amine and $NaCNBH_3$ to **22**, which was treated with TFA to obtain catalyst **23**. The unlipidated catalyst **24**, to be used as reference catalyst, was synthesized directly from Boc-protected proline glucosamine **20** (Scheme 3).

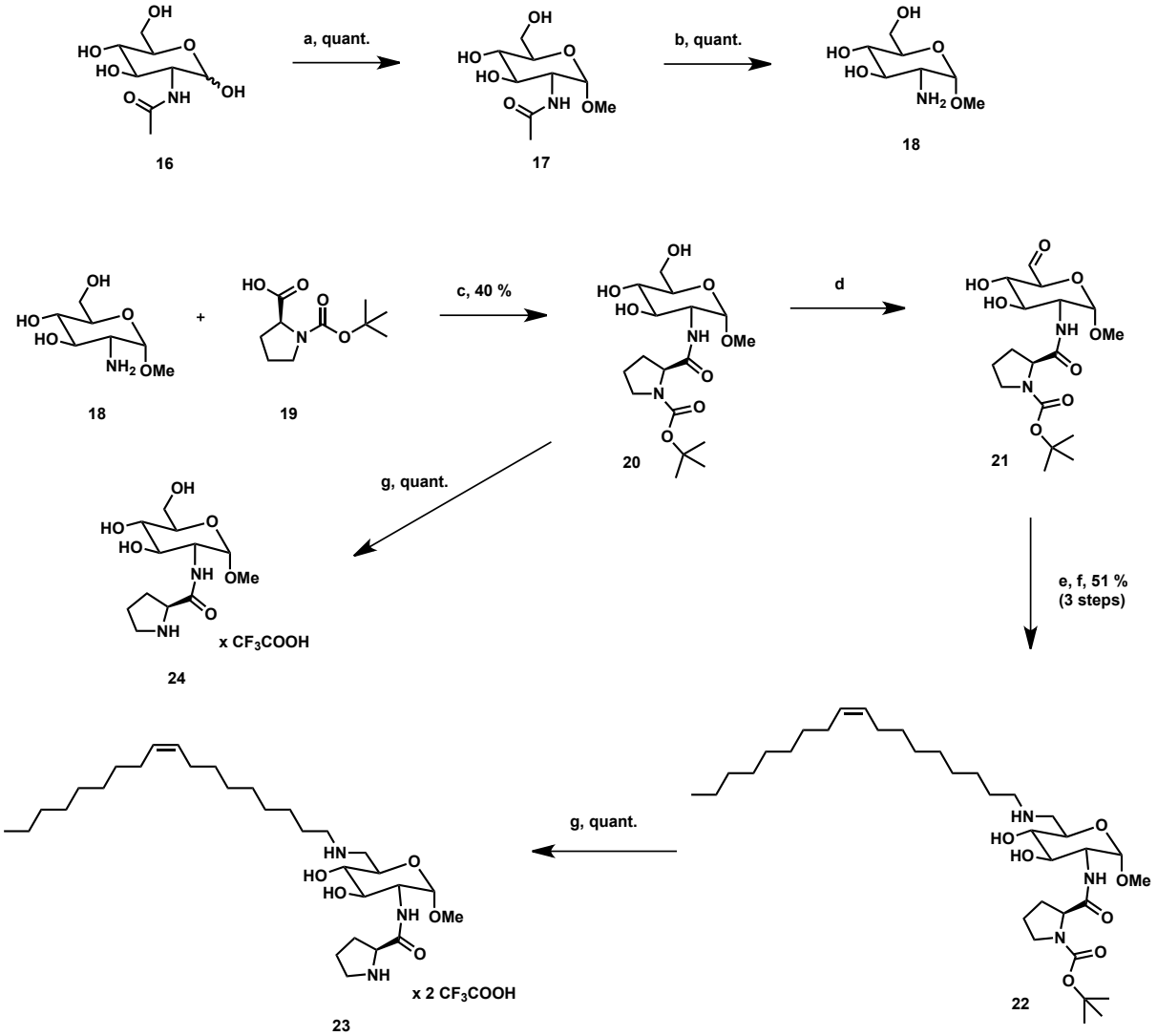

Scheme 3: Synthesis of lipidic aldol organocatalyst **23** and its unlipidated version **24**. Conditions: a) MeOH, Dowex, reflux; b) BaO, H_2O, reflux; c) Boc-*L*-Proline (1 eq) DCC (1 eq), DMAP (1 eq), DMF, r.t.; d) TEMPO, TCC, DMF, 0°C; e) Oleylamine (1 eq) MeOH, r.t., 1h; f) $NaCNBH_3$ (1.3 eq), MeOH, r.t., g) TFA, DCM, 0 °C.

2.2.2.2 Substrate screening with reference catalyst 24

In order to find suitable, i.e. robust and water-soluble aldol substrates for mesophase catalysis, a screening of various aromatic and non-aromatic candidates was performed. The results are summarized in Table 1.

Table 1: Screening of different aldol substrate pairs using reference catalyst **24**.

Entry	Donor	Acceptor	Outcome	Remarks
1			Reaction completed	Works only freshly distilled
4			Reaction completed	-
5			No product formation	-
6			No product formation	-
7			No product formation	-
8		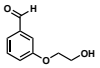	57 % conversion	Reaction time: 3 d
9		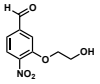	Reaction completed	-
10		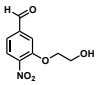	Reaction completed	-
11		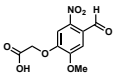	No reaction	Reaction time: 5 d
12			Reaction completed	-
13			Reaction completed	-
14		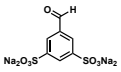	No product formation	-
15		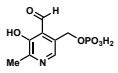	No product formation	-
16			No product formation	-
17			Traces of product formed	-
18			Traces of product formed	Reaction time: 3 d, mainly aldehyde dimer detected
19		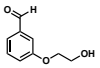	65 % conversion	-
20			No reaction	Reaction time: 3d

21		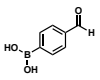	No reaction	pH 12 (not soluble at neutral pH)
22			No reaction	Reaction time: 3d
23			No reaction	Reaction time: 3d, at 40°C
24			Traces of product formed	Reaction time: 2d, mainly aldehyde dimer detected
25			No reaction	Reaction time: 5d
26			Reaction completed	-
27			28 % conversion	Reaction time: 8d

Conditions: Reactions carried out at room temperatures with 30 mol % catalyst **24** and 2 eq of donor. Monitored by ^{1}H-NMR.

Even though the substrate screening was restricted to water-soluble compounds only, several suitable substrate pairs, aromatic and non-aromatic, have been found. 2,2-dimethyl-1,3-dioxan-5-one (DDO) and 2,3-*O*-isopropylidene-glyceraldehyde (IGA) was found to be a good substrate pair to start with, since both are highly water-soluble and showed good results in the screening (Table 1, entry 1). Furthermore, studying carbohydrate syntheses with this new system would distinguish our work from many other reported aldol studies.[1,4,39,50–54]

2.2.2.3 LCP catalysis with substrates DDO and IGA and catalyst 23

For initial experiments, LCPs including catalyst **23** was placed at the bottom of an NMR tube and the substrate solution was added on top. Product formation was detected by ^{1}H-NMR and ESI-MS, and the reaction was completed after four days. Because of the specific geometry used, the surface area between the bulk water and the LCP in a NMR tube is not very large (0.13 cm^2). We thus designed special metal holders with significantly larger surface area (3.14 cm^2) to be used in further experiments. Since stirring is not possible, the reaction mixture had to be gently shaken. With this improved set-up, the reaction rate could be significantly accelerated; the reaction was completed after *ca.* 36 hours. However, during further investigations it has been shown that the initial results were hard to reproduce. One problem was the erratic decomposition, i.e. deprotection of the hydroxyl groups of the substrates, which occurred despite buffering the system at pH 7.4. Furthermore, the reaction rates varied substantially, from 36 hours to several days to complete the reaction, while in some cases the reaction did not even start. Catalyst deactivation after incorporation into the LCP is another scenario that cannot be excluded, although no experimental evidence was encountered.

Despite these drawbacks, these initial results proved the feasibility of this project; to use LCPs as a novel platform for catalysis. However, the choice of substrates and lipidic catalyst was still not ideal, and needed to be further optimized to obtain detailed information on how LCPs influence catalysis in terms of kinetics and stereochemistry.

2.2.3 Third generation lipidic aldol organocatlaysts

2.2.3.1 Design and syntheses of the catalysts, preparation of catalytic LCPs and comparison of their performances in LCPs

Even small amounts of added guest catalysts can affect significantly the structural and dynamic properties of the ensuing host mesophases.[18,27,29,55] The size of the aqueous channels, the curvature of the bilayer and the geometry of the LCP can be controlled by judicious modifications of the lipidic chains and head group region of the additive. To that end, six different proline-derived lipidic catalysts were designed and synthesized (Scheme 4). Modifications were introduced at the lipidic chain and at the linker that connects the proline headgroup to the lipidic chain(s), thereby obtaining catalysts with one (**2, 23** and **26**) or two (**27**, **28** and **29**) lipidic chains, saturated (**26** and **27**) and unsaturated (**2**, **23**, **28** and **29**), as well as catalysts in which the proline is linked to the lipids via an amide (**2, cn** and **10**), an amine (**7** and **8**) or an amide with a carbohydrate as a spacer (**9**).

Starting from Boc-*L*-proline (**19**) catalysts **2, 26** and **29** were obtained after EDC/DMAP coupling with the corresponding amines and Boc-deprotection. The same procedure was applied for catalyst **27**, before the corresponding amide was reduced using $LiAlH_4$.[56] Catalyst **7** was obtained after reduction of **29**. Dioleylamine (**31**) was synthesized in two steps: oleyl alcohol (**30**) was converted to the corresponding bromoalkene,[57] and subsequent alkylation of oleylamine afforded dioleylamine (**31**) (Scheme 4, box).[58] Starting from Boc-protected **24**, catalyst **9** was obtained after selective oxidation of the primary alcohol to the aldehyde using TEMPO,[49] and subsequent reductive amination using oleylamine and $NaCNBH_3$ before the Boc-protection group was cleaved with trifluoroacetic acid (TFA). To evaluate the catalytic results, water-soluble compound **24** (synthesized according to the literature)[59] was used as a reference catalyst, thereby providing a comparison between the model reaction carried out in our heterogeneous lipidic systems and a model reaction under homogeneous conditions.

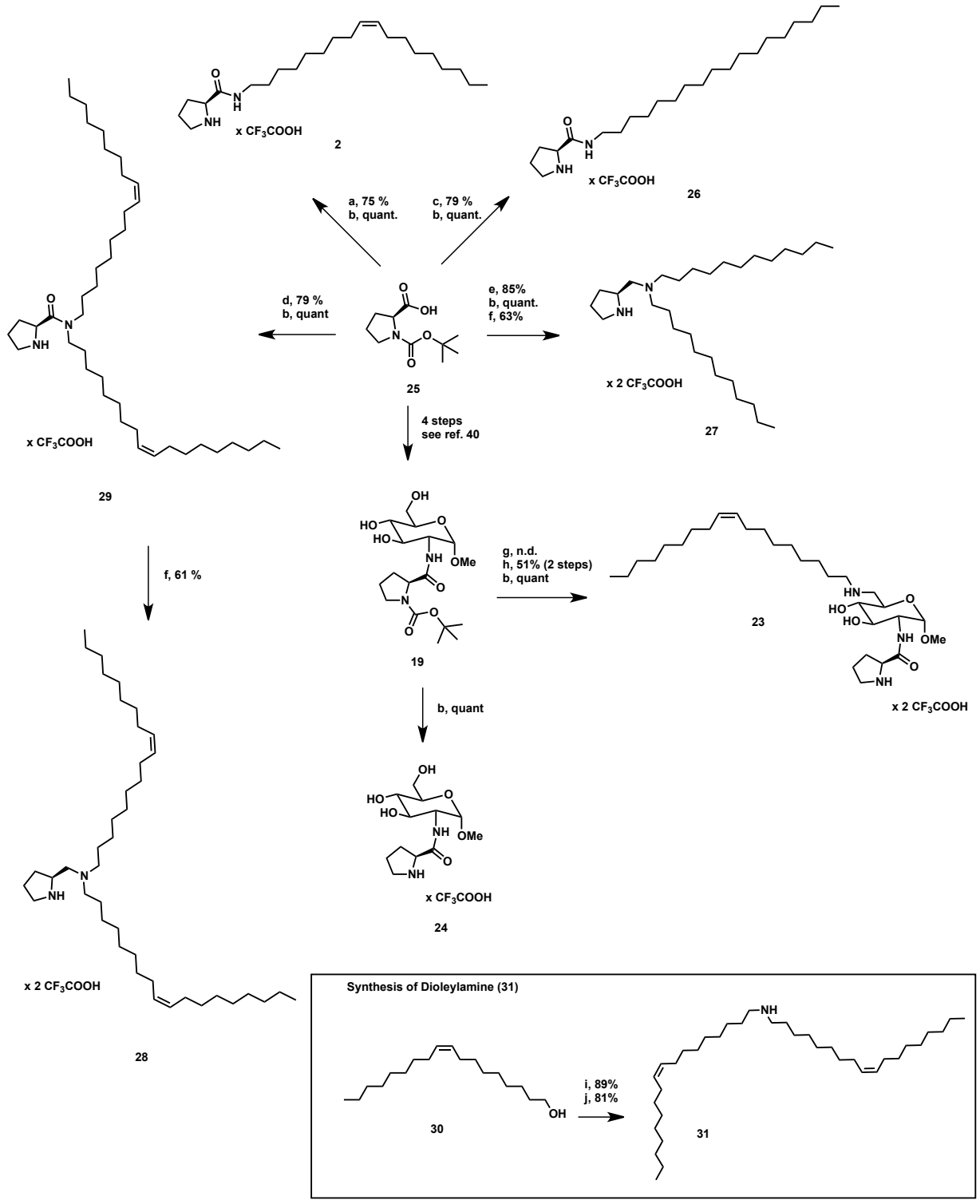

Scheme 4: Syntheses of lipidic catalysts **2**, **23**, **26**, **27**, **28**, **29** and water-soluble reference catalyst **11**. Conditions: a) Oleylamine, EDC (1.1 eq), DMAP (0.1 eq) CH_2Cl_2 / DMF 4:1, r.t. b) CH_2Cl_2 / TFA 4:1, 0°C c) Stearylamine (1.1 eq), EDC (1.1 eq), DMAP (0.1 eq) CH_2Cl_2 / DMF 4:1, r.t. d) Dioleylamine (1.1 eq), EDC (1.1 eq), DMAP (0.1 eq) CH_2Cl_2 / DMF 4:1, r.t. e) Didodecylamine (1.1 eq), EDC (1.1 eq), DMAP (0.1 eq) CH_2Cl_2 / DMF 4:1, r.t. f) $LiAlH_4$, THF, 0°C 2 h then reflux 20 h g) TEMPO, TCC, DMF, 0°C h) Oleylamine (1 eq), MeOH, r.t. 1h then $NaCNBH_3$ (1.3 eq). i) $P(Ph)_3$ (1.1 eq), CBr_4 (1.1 eq.), DCM, 0°C, j) Oleylamine (1 eq), K_2CO_3 (0.3 eq), DMSO, 80°C.

With this range of catalysts in hand, the effects of molecular modifications of the catalyst additive on the synthetic performance of the designed host-guest LCPs were investigated. In the literature, the aldol reaction between water-insoluble 4-nitrobenzaldehyde and cyclohexanone is used as a model- and benchmark reaction for catalytic systems based on proline derivatives.[30,37,39,52] However, for catalysis in LCPs and cubosomes, water-soluble substrates are required to facilitate diffusion of substrate from the bulk water into the pores of the mesophase material. To this end, water-soluble aldehyde **4a** was synthesized (see paragraph 2.4.2 for procedure). An ethylene glycol unit was installed to increase water solubility (ca. 30 mmol/L or 6 g/L, and a ClogP value of -0.625 compared to 0.309 for 4-nitrobenzaldehyde (derived from ChemDraw Ultra, version 13)). The aldol reaction of aldehyde **4a** and cyclohexanone (**3**) serves as model reaction to study catalysis in LCPs and cubosomes. The conversions and the diastereomeric ratios were obtain from an ^{1}H-NMR. A section of a spectrum from a reaction control is depicted in Figure 2. Catalytic mesophases were prepared such that the lipid-modified catalyst is laterally immobilized in the bilayer, exposing the catalytic moiety towards the aqueous compartment. The phase identity and lattice parameters of the mesophases were established by small angle x-ray scattering (SAXS). The catalytic performance of these designed LCPs was compared with those of the water-soluble catalyst **24** and of the lipidic catalyst **2** without LCP, which forms polydisperse micellar particles. Table 2 summarizes the results of the catalyst screening on the model aldol reaction of aldehyde **4a** and cyclohexanone (**3**).

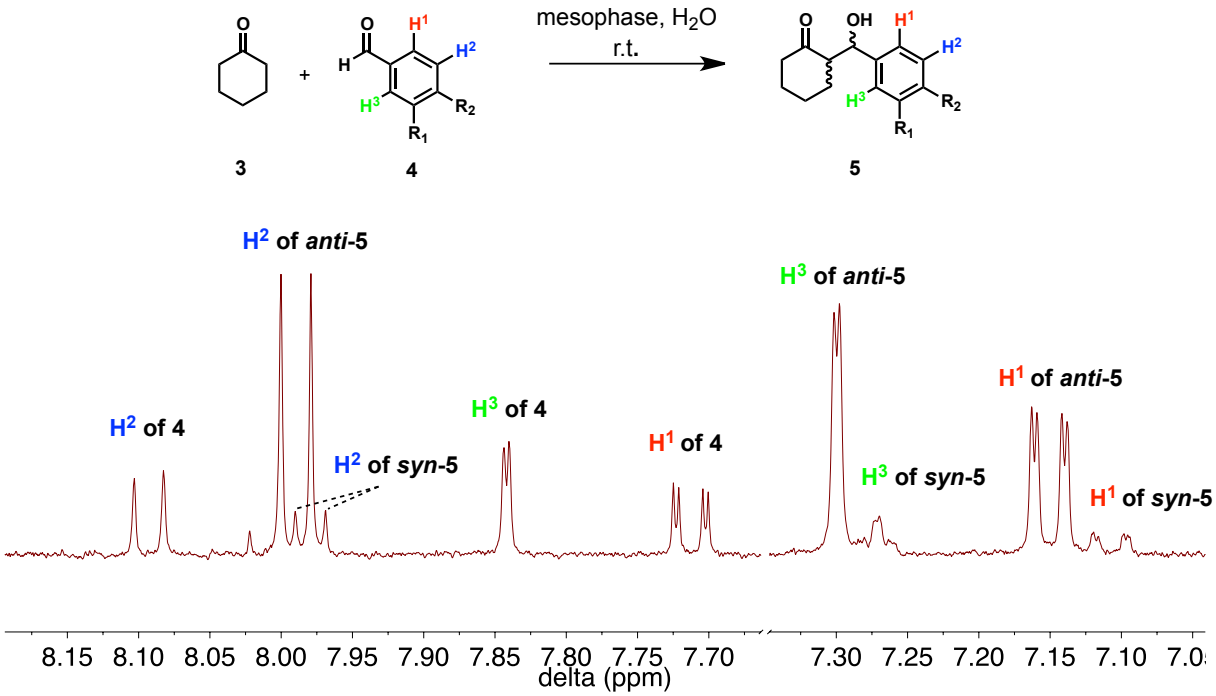

Figure 2: Section of a ^{1}H-NMR spectrum from a reaction control sample. Conversion and d.r. could easily be determined, no side product was formed.

Catalysts **2**, **23** and **29** with an amide bond between the proline and the lipidic chain deliver higher yields as compared to the tertiary amine catalysts **27** and **28**. Mase *et al*. reported that tertiary amine and amide catalysts bearing decanyl chains show similar catalytic activity in an aqueous emulsion.[39] This fact indicates that the difference in activity between LCPs that contain catalyst **28** and **29,** whose structures differ only in the mode of linking of the lipidic chains to the head group, is due to different embedding into the lipidic bilayer. This phenomenon can be rationalized by considering that the amide moiety is more polar than the tertiary amine, thereby enhancing the accessibility for the water-soluble substrates at the lipid-water interface, whereas the tertiary amine derivatives are likely incorporated deeper in the lipidic bilayer. The aqueous channel diameters were calculated from the fully hydration lines of the respective LCPs containing the lipid-modified catalysts (**2**, **23**, **27**, **28**, **29**), which were determined by SAXS.

Table 2: Comparison of the catalytic efficiencies of the various LCP and non-LCP conditions used for the model aldol reaction of aldehyde **4a** with cyclohexanone (**3**).

Entry	Catalyst	Time [h]	Conv. [%]	Water channel diameter [nm]	SAXS spectra q = [Å^{-1}]
1	**2**	48	81	4.73	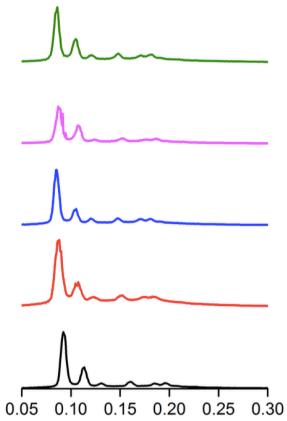
2	**28**	48	71	4.63	
3	**27**	48	42	4.70	
4	**23**	48	75	5.11	
5	**29**	48	78	4.29	
6[a]	**2**	4h	98	-	
7	**24**	48	65	-	
8[b]	-	72	0	-	

Conditions: Reactions were carried out in special, home built metal holders (see experimental section) at room temperature with PBS buffer (1X) at pH 7.4, 2 eq of ketone, 30 mol % of catalyst. Holders were shaken at 330 rpm during the reaction to ensure optimal mixing. Conversions were determined by ^{1}H-NMR integrals. [a] Catalyst **2** was dispersed by sonication in PBS 1X without addition of MO. [b] Catalyst-free LCPs were used. Aqueous channel diameters were calculated from SAXS parameters as shown in the experimental section.

The data shown in Table 2 indicate that the lipidic structure of the catalyst and the aqueous channel size have a strong effect on the performance of the system. LCPs containing catalyst **23** with the carbohydrate-prolinamide head group exhibit the largest lattice parameter with an aqueous channel diameter of 5.11 nm. As the larger aqueous pores enable faster diffusion of water-soluble species, and the sugar moiety acts as an additional hydrophilic linker which ensures that the catalytic site is well exposed to water soluble substrates, we expected this catalyst to show superior performance. This was, however, not the case (cf. Table 2): the best result in terms of yield was obtained using catalyst **2**, which has a very simple structure that can be obtained within two synthetic steps. This indicates that already the simpler amide derivatives are well exposed to the aqueous compartments to catalytically transform the substrates. In order to compare the LCP-based catalysis with a homogeneously catalysed one, the aldol reaction was conducted with catalyst **24** (Table 2, entry 7). The model reaction with this water-soluble catalyst was rather sluggish, yielding 65 % conversion after 48 h, which did not increase significantly even after 60 h. In contrast, a dispersion of catalyst **2** in 1X PBS converted the substrates very efficiently to the products (Table 2, entry 6): Within 4 h,

98 % of the starting material was consumed and transformed to the products. This is probably due to the catalyst's higher accessibility for the substrate as compared to the confined geometry in LCPs, in which the substrates need to diffuse from the overlay solution into the catalytic sites within the mesophase, and products need to diffuse out. However, a drawback of the dispersion set-up is the difficult recovery of the catalyst, which is much simpler and more efficient in the case of LCP-based catalysis. As expected, the control experiment with pure MO-water LCP, i.e. without catalyst did not show any catalytic activity (Table 2, entry 8). Catalyst **26** did not form LCPs with the required catalyst loading

2.2.3.2 Controlling catalytic activity by tuning the LCPs

To study the impact of the unit cell size, and related aqueous channel diameter on the reaction rate, three types of MO-based LCPs were tested (Table 3): PBS-hydrated LCP (LCP A, aq. channel diameter of 4.73 nm), HEPES-hydrated LCP (LCP B, aq. channel diameter of 4.65 nm), and HEPES-hydrated LCP which has been additionally doped with the strong swelling agent cholesterol (LCP C, aq. channel diameter of 5.71 nm).[60] All LCPs contained 5% w/w catalyst **2** (relative to the total weight of the LCP), which was chosen for this study as it exhibited the best performance in the screening experiments (Table 2). The amount of LCP was varied to adjust the catalyst loading to 7.5, 15 and 30 mol % of catalyst **2**, and their catalytic efficiency compared using the model aldol reaction of aldehyde **4a** and cyclohexanone (**3**). The catalyst loading refers to the mol % of catalyst with respect to the aldehyde used. The results are summarized in table 2.

Comparison of the catalytic efficiency of LCP C (Table 2, entries 7-9) with that of LCP B (Table 2, entries 4-6) indicates that a combination of buffer, additives (e.g. cholesterol) and aqueous channel size affect the catalytic conversion rate: LCP C, with the largest aqueous channel diameter of 5.71 nm, allows higher conversion at all catalyst loadings compared with LCP B with an aqueous channel diameter of 4.65 nm. These systems can be directly compared, as in both regimes the model reaction runs in HEPES buffer and the only difference is the added swelling agent cholesterol in LCP C. In contrast, the model reaction with LCP A takes place in PBS buffer. Experiments with water-soluble catalyst **24** revealed that the effects of the buffer on the model reaction are not negligible: it was shown that the conversion of the reaction in PBS buffer is significantly higher as compared to the identical reaction in HEPES buffer (65 % vs. 41 % after 48 h). Interestingly, this tendency was reversed when the model reaction was carried out in LCPs. The conversion of the model aldol reaction with HEPES-containing LCP B (table 2, entries 4-6) and LCP C (Table 2, entries 7-9) was higher than with PBS-containing LCP A (Table 3, entries 1-3) after 48 h. In case of LCP C, this finding can be rationalized by the larger aqueous channels determined by SAXS

(diameter of 5.71 nm). In the case of LCPs A and B, these are however comparable (4.73 vs. 4.65 nm).

The reaction progress in these three media, LCP A, B and C with catalyst loading of 30 mol % (Table 3, entries 1, 4 and 7) are depicted in Figure 3. The highest conversion of 95 % after 48 h was obtained using medium C with 30 mol % catalyst loading (Table 3, entry 7), followed by medium C with 15 mol % catalyst loading (Table 3, entry 8) and medium B with 30 mol % catalyst loading (Table 3, entry 4), both with 85 % conversion after 48 h. The experiments using medium A (Table 3, entry 1-3) show lowest conversion. Remarkably, medium C with 15 mol % catalyst loading (Table 3, entry 8) is more efficient than medium A with 30 mol % catalyst loading (Table 3, entry 1) and equally efficient as medium B with 30 mol % catalyst loading (Table 3, entry 4) despite the lower catalyst loading. The reaction progress of these three entries is shown in Figure 3.

Table 3: Comparison of the catalytic efficiencies of LCPs with different aqueous channel diameters as function of increasing catalyst loading. The model aldol reaction of cyclohexanone (**3**) with aldehyde **4a** in different LCPs at varied catalyst loadings was investigated.

Entry	Medium	Cat.-ldg. [mol %]	Conv.[b] [%]	Aq channel diameter [a] [nm]	SAXS spectra q = [Å^{-1}]
1		30	81		
2	A	15	72	4.73	
3		7.5	63		
4		30	85		
5	B	15	75	4.65	
6		7.5	67		
7		30	95		
8	C	15	85	5.71	
9		7.5	71		

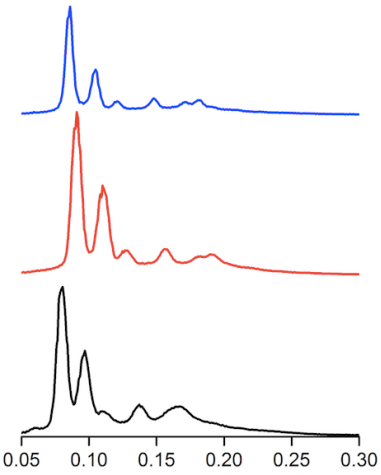

Conditions: Reactions were carried out in special, home built metal holders (see experimental part) at room temperature with PBS buffer pH 7.4, 2 eq of ketone. The holders were shaken at 330 rpm during the reaction to ensure optimal mixing. [a] Determined by SAXS. [b] Determined by ^{1}H-NMR. Medium legend: A) PBS 1X. B) HEPES 25 mM. C) HEPES 25 mM, cholesterol doped LCP.

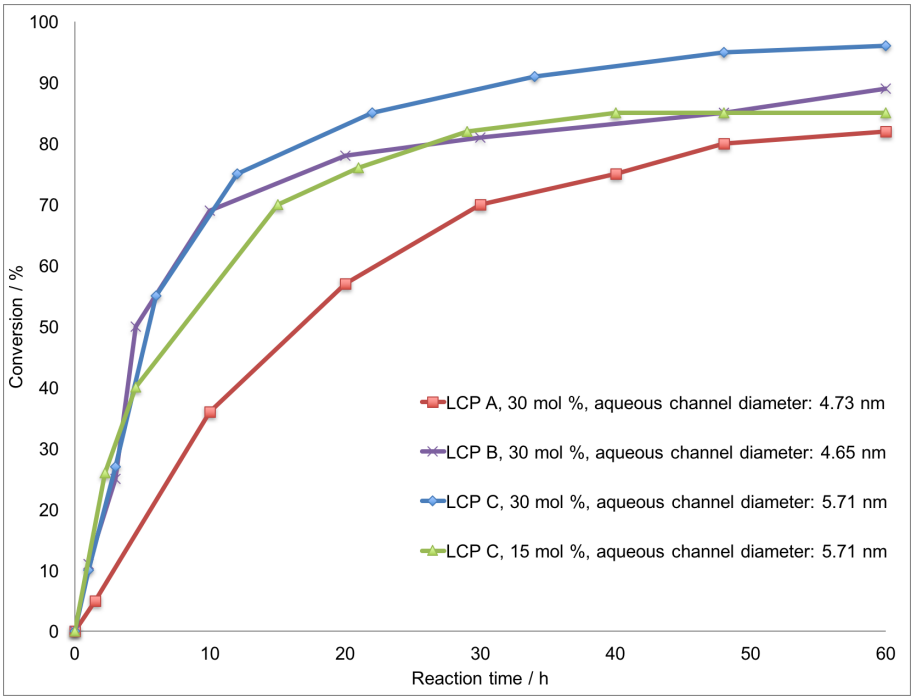

Figure 3: Progress of the aldol reaction of cyclohexanone **3** with aldehyde **4a in** different LCP systems (determined by ^{1}H-NMR). Comparison of the four LCP media A, B and C with 30 mol % cat. loading and medium C with 15 mol % cat. loading.

Phytantriol-based LCPs

In addition to the above described MO-based LCP systems, also phytantriol (PT) LCPs have been investigated. PT shows a similar phase diagram like MO (see introduction, page 5). The lower degree of hydration and smaller lattice parameter of the *Pn3m* cubic phase at excess water conditions, as compared to MO, is the major difference between these systems.[61] This is a disadvantage from our perspective since diffusion of the substrate into the LCPs aqueous channels is slowed down, as can be seen in Figure 4. Commercial PT is a mixture of stereoisomers. In order to obtain LCPs that are composed of homochiral lipids, *S,S*-PT and *R,R*-PT have been synthesized. The synthesis of these PTs and attempts towards chiral recognition of small molecules with these homochiral PT-LCPs are described in Chapter 7. Preliminary data indicate that the phase diagrams of enantiopure PTs differs from commercial PT, which consists of four stereoisomers. Therefore, we prepared *S,S*-PT, *R,R*-PT and racemic-PT based catalytic LCPs containing catalyst **2** with 40 mol % to perform our model aldol reaction and compare the kinetics (Figure 4) and stereochemistry. We proposed that the chiral surfaces of these LCPs influence the preorganization of the substrates and thus affect the stereochemical outcome of the reaction. However, neither the reaction rates nor the stereochemistry was found to be significantly different for one of the three PT-LCPs, as shown in Figure 4.

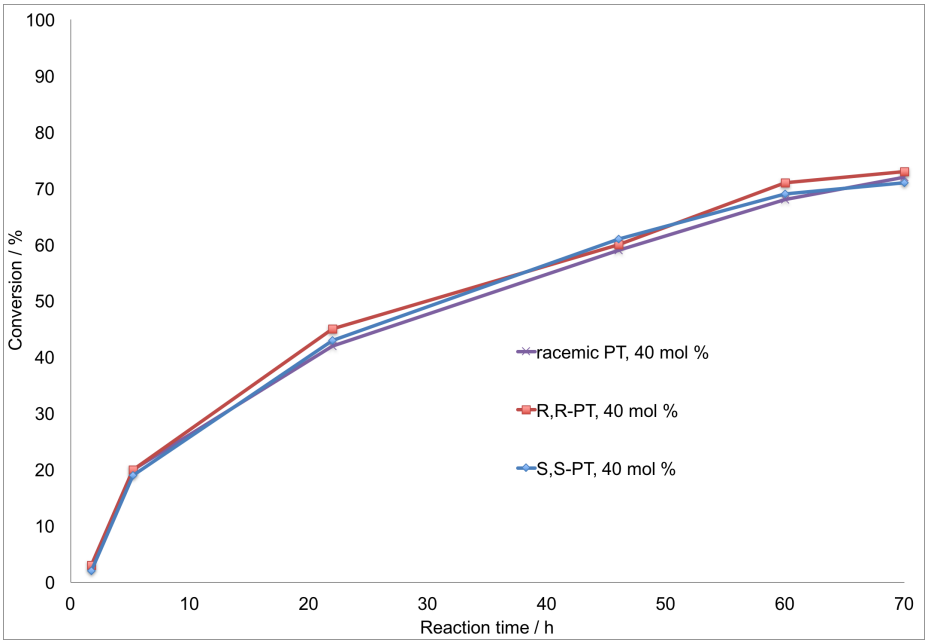

Figure 4: Progress of the aldol reaction of cyclohexanone **3** with aldehyde **4a** in three different phytantriol LCP systems with catalyst **2** (determined by ^{1}H-NMR). Comparison of LCP media consisting of racemic PT, *S,S*-PT and *R,R*-PT with 40 mol % cat. loading.

In summary, the reaction rate is strongly dependent on the type of LCP. By changing parameters such as buffers or by using additives, catalytic LCPs can be modified such that the kinetics of the reactions performed therein can be tuned. Additionally, the influence of the

buffer (HEPES vs. PBS) on the reaction rate needs to be taken into account. In a reference system with water-soluble catalyst **24**, the model reaction was found to proceed faster in PBS than in HEPES buffer.

The isolated yields were between 50 and 91%. Catalytic LCPs delivered the product even at a low catalyst loading of 7.5 mol % and with only two equivalents of cyclohexanone (**3**), which is low as compared to examples in literature where often 5 equivalents[50,52] or more were used.[51]

2.2.3.3 Cubosomes

Whereas bulk LCPs are malleable and can be attached to various surfaces due to their solid consistency and adhesive properties, they can alternatively be dispersed to form cubosome nanoparticles. The latter exhibit identical packing arrangement and phase identity to those of the parent gel LCP, but their viscosity is much lower.[62] Because of their very large ratio of surface area to volume, cubosomes tend to aggregate to form thermodynamically stable bulk LCPs. To overcome this, their surfaces need to be kinetically stabilized.[63] Pluronics,[64] are the most frequently used stabilizers for such systems. The most efficient stabilizer was found to be Pluronic F108 (PF 108),[63] which was consequently used in this study. Such self-assembled fluid dispersions thus allow running reactions in classical reaction flasks using stirring, and therefore potentially increase reaction rates. These two options of reaction media, bulk LCP and cubosomes offer a high degree of flexibility in the choice of the experimental set-up. Furthermore, this study delivers information about the differences and similarities in performance in terms of reaction rate.

2.2.3.4 Cubosome preparation and characterization

Cubosomes were prepared by mixing MO with the appropriate amount of catalyst. Subsequently, the lipid mixture was hydrated with a PF 108-containing buffer solution (cf. experimental section for more detail). The total lipid and PF 108 concentrations were 33.0 and 1.65 mg/mL, respectively.

Three types of cubosomes were investigated: Cubosomes A were hydrated with PBS 1X and adopted a Pn3m cubic phase, cubosomes B, hydrated with HEPES 25 mM buffer exhibited an Im3m cubic phase and cubosomes C, which are hydrated with HEPES 25 mM buffer and contain cholesterol (15 % w/w) as swelling agent form coexistence of Pn3m and Im3m cubic phase. The hydrodynamic diameter of the cubosomes was determined by dynamic light scattering (DLS) and varied from 133 - 177 nm, and no significant change in the particle size before and after the aldol reaction of cyclohexanone (**3**) and water-soluble aldehyde **4a** was

observed. Thus, the influence of mesophase geometry on the kinetics of the catalytic reaction conducted in these media was investigated.

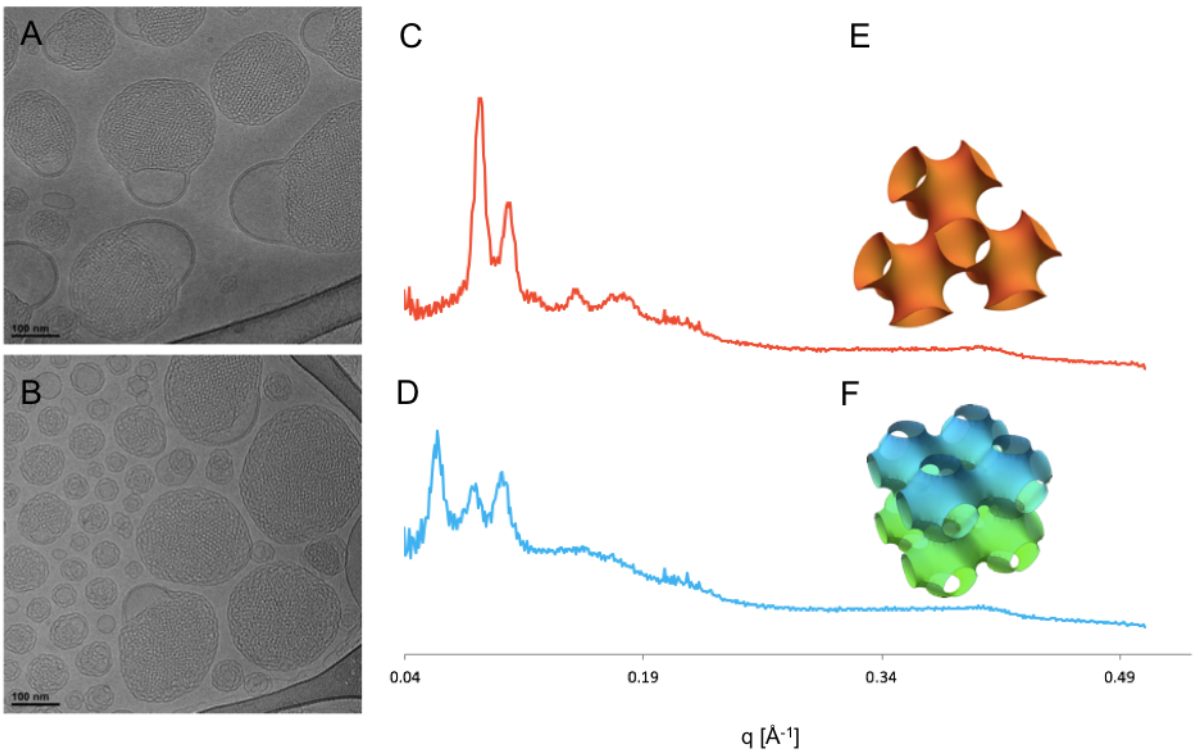

Figure 5: Representative cryo-TEM images of cubosomes dispersed in PBS 1X (A) and HEPES (B) buffers, respectively. SAXS pattern of cubosomes dispersed in PBS (C, orange, Pn3m) and HEPES (D, blue, Im3m) buffers, respectively. The sketches of the repeating units for the Pn3m (inset in top panel) and the Im3m symmetries (inset in bottom panel) were obtained as level surfaces of the nodal approximations reported in[65].

Results of the catalytic experiments are summarized in table 3. As in the LCP case, the best results were obtained with cubosomes C with a catalyst loading of 30 mol % (Table 4, entry 7). The conversion exceeded 80 % in less than 10 h of reaction time (Figure 6), with complete conversion being achieved after 48 h. With a catalyst loading of 15 mol %, the conversion similarly exceeded 80 % in less than 10 h, while after 48 h 86 % conversion was obtained. The conversion of cubosomes C with 15 mol % catalyst (Table 4, entry 8) was comparable to the cubosomes A with 30 mol % (Table 4, entry 1) and with cubosomes B with 30 mol % (Table 4, entry 4). Cubosomes B with 30 mol % (Table 4, entry 4), exceeded 80 % of conversion in less than 10 h of reaction time (Figure 6), and after 48 h, conversion was 90 % (Table 4, entry 4). The isolated yields ranged between 65 and 94%. Catalytic cubosomes delivered the product even at a low catalyst loading of 7.5 mol %.

Table 4: Comparison of the catalytic efficiencies of cubosomes with different geometries as function of increasing catalyst loading. The model aldol reaction of cyclohexanone (**3**) with aldehyde **4a** was investigated

Entry	Cubosomes	Space group[a]	Size [nm]	PDI	Cat.-ldg. [mol %]	Conv.[b] [%]
1					30	85
2	A	Pn3m	174 ± 2	0.17	15	73
3					7.5	48
4					30	90
5	B	Im3m	177 ± 2	0.19	15	71
6					7.5	60
7					30	100
8	C	Pn3m/Im3m	133 ± 1	0.17	15	86
9					7.5	65

Conditions: Reactions carried out at room temperature with PBS buffer pH 7.4, 2 eq of ketone. Reaction time 48 h [a] Determined by SAXS. [b] Determined by ^{1}H-NMR. Cubosome type legend: A) PBS 1X. B) HEPES 25 mM. C) HEPES 25 mM, cholesterol doped LCP. All dispersions were stabilized with 1.65 mg/mL PF-108.

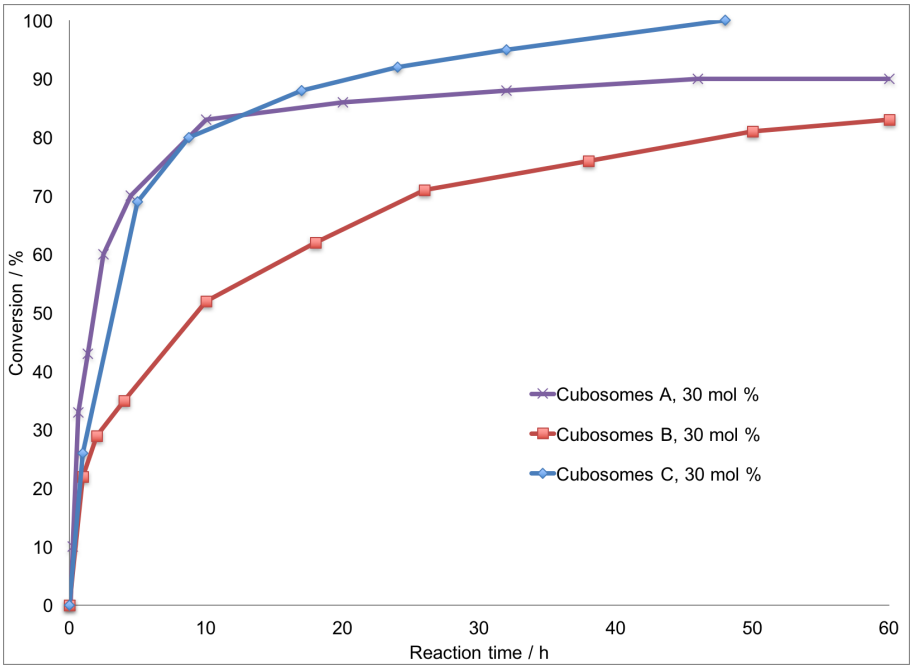

Figure 6: Progress of the model aldol reaction of cyclohexanone (**3**) with aldehyde **4a** carried out in cubosomes A, B and C (determined by ^{1}H-NMR).

LCP experiments were carried out in special, home-built metal holders with an interfacial area between the overlay bulk water and the LCP surface ("outer interfacial area") of ca. 0.0003 m^2 per 100 mg LCP (see experimental section for pictures of our set-up). In contrast, assuming spherical geometry and monodisperse cubosome particle size of 200 nm, the interfacial area between the latter and bulk water is ca. 3 m^2 per 100 mg, which is 4 orders of magnitude

larger. Based on these considerations one would expect the cubosomes to be catalytically much more efficient than bulk LCPs. Interestingly, this is not the case, and the reaction rates of the model aldol reaction in LCPs and cubosomes are comparable (after 48 h). Possible explanation for this effect is the stabilization mechanism of cubosomes. As was demonstrated by Larsson *et al.*[66] and Demurtas *et al,*[67] cubosomes exhibit a perfect bicontinuous cubic phase geometry at the inner part, while at the outside lamellar attachments are present, which can be seen in Figure 5A and 5B. Consequently, the aqueous pores are not directly accessible from bulk water as the lamellar structure at the outside forms a barrier for the substrates to diffuse to the catalytic sites inside the cubosomes. Comparison of the conversion rate of the catalytic LCPs vs. cubosomes at various time points (Figure 6) shows significantly faster initial reaction rates in the cubosome systems. It seems thus that there is an advantage of the large outer interfacial area of cubosomes at the beginning of the reaction, despite the lamellar attachments which function to some extent as a barrier. Figure 7 illustrates this finding. We can conclude that the outer interfacial area has only a minor impact on the overall conversion rate, and diffusion inside the aqueous channels, once the substrates have entered, is rate limiting. This interpretation is supported by the fact that mesophases with different water channel diameters show different conversion rates (for example Table 3, entry 4 and 7).

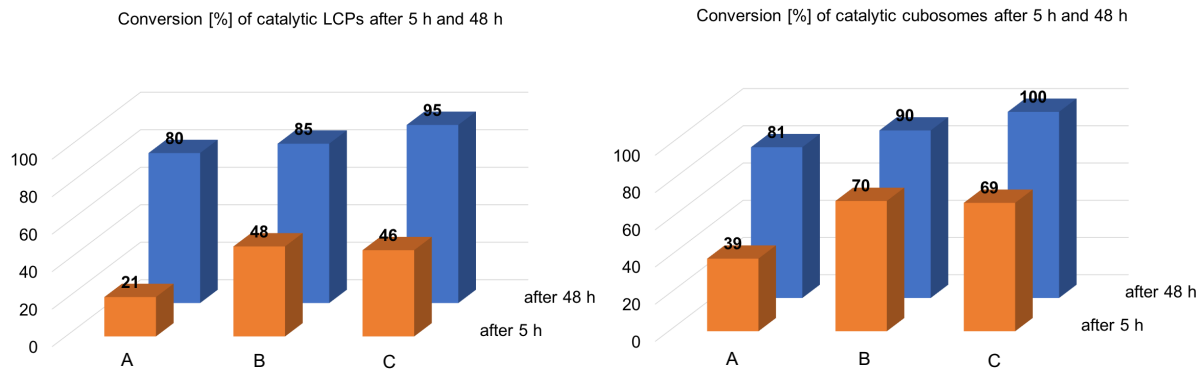

Figure 7: Comparison of the conversion rate of the model aldol reaction of cyclohexanone (**3**) with aldehyde **4a** after 5 and 48 h (orange and blue, respectively) of catalytic LCPs (left) and cubosomes (right).

2.2.3.5 Stereochemistry and substrate scope

Following the demonstration of the applicability of catalytic cubosomes and LCPs as novel nanoreactor scaffolds for organocatalysis, we set out to investigate the stereochemistry and substrate scope of such reactions, which was extended by two unactivated aldehydes: benzaldehyde (**4b**) and 3-(2-hydroxyethoxy) benzaldehyde (**4c**). The experiments described

above (Table 2 - 4) showed good diastereoselectivity (up to 87:13, table 4, entries 1 - 14) but only moderate enantioselectivity (67-89 % e.r.). Comparable low enantioselectivities were also obtained when conditions known from literature[39] Table 5, entries 21 and 22) were applied and buffer was used instead of water. The low enantioselectivity might be a result of the relative high buffer concentrations (HEPES 25 mM, PBS 1X). As was shown in the literature,[39] higher enantioselectivities can be obtained when trifluoroacetic acid (TFA) is used as an additive. To that end, a TFA-salt of the catalyst was formed. At higher buffer concentrations, there is a stronger salt competition, leading to the loss of the TFA salts of the catalysts. However, reducing the buffer concentrations led indeed to significantly better enantioselectivities (Table 5, entries 15 - 20), while the performance of catalysts **27** and **28** was significantly reduced. Catalyst **29** delivered similar results to **2**. Lowering the pH resulted in significant decrease in reaction rates, and using water instead of buffer led to much less stable mesophases. The best conditions were obtained using PBS 0.1X buffer, resulting in e.r.'s up to 93 %, which is comparable to examples of prolinederivative-catalyzed asymmetric aldol reactions between nitro-benzaldehydes and cyclohexanone (**3**) in aqueous systems.[39,51,53,54,68,69] This system decreased the reaction rate as compared to the more concentrated buffer conditions (Table 5). There is no significant difference in terms of e.r. if the catalyst loading is changed (Table 5, entries 1 - 3). The enantiomers were assigned indirectly, by comparing the aldol products synthesized with catalytic mesophases and literature known reference catalysts by NMR and HPLC chiral stationary phase.

Table 5: Aldol reactions of cyclohexanone (**3**) with aldehydes **4a**, **4b** and **4c** performed in catalytic mesophases.

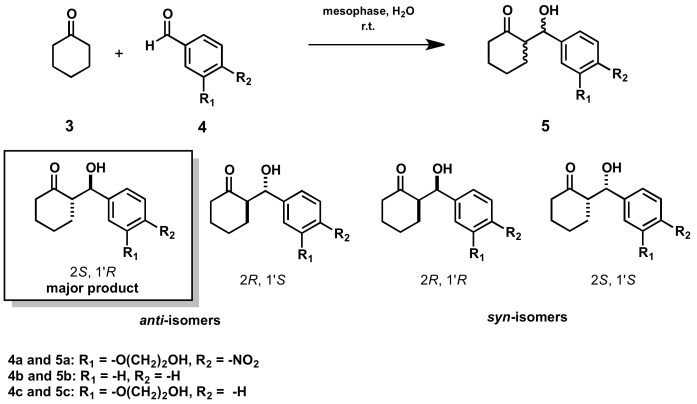

Entry	Cat.	Medium	Aldehyde	Time	e.r.[a] (%)	*anti* / *syn*[b]	Conv.[a] [%]
1	**2**	A	4a	48	78	81 / 19	81
2[c]	**2**	A	4a	48	75	81 / 19	72
3[d]	**2**	A	4a	48	77.5	82 / 18	63
4	**2**	A	4a	20	84	86 / 14	57
5	**27**	A	4a	48	71	73 / 27	42
6	**28**	A	4a	48	68	77 / 23	71
7	**23**	A	4a	48	72	87 / 13	75
8	**2**	B	4a	60	73	85 / 15	83
9	**2**	B	4b[e]	72	77	66 / 34	42
10	**2**	B	4c[e]	96	89	71 / 29	35
11	**2**	C	4a	20	71	86 / 14	78
12	**2**	D	4a	48	67	85 / 15	90
13	**2**	E	4a	48	73	87 / 13	95
14	**2**	F	4a	48	70	82 / 18	100
15	**2**	G	4a	60	93	80 / 20	62
16	**2**	G	4a	48	92	88 / 12	39
17	**23**	G	4a	96	72	82 / 18	79
18	**29**	G	4a	60	92	86 / 14	35
19	**2**	G	4b[e]	72	92	90 / 10	8
20	**2**	H	4a	60	91	90 / 10	55
21	**2**	H	4a	60	91	90 / 10	60
22	**2**	I	4a	4	69	77 / 23	98
23	**2**	J	4a	4	80	79 / 21	99
24	**24**	K	4a	48	70	76 / 14	65

Conditions: Reactions were carried out at room temperature, 2 eq of ketone, 30 mol % of catalyst. [a] Determined by chiral-phase HPLC analysis for *anti*-product [b] Determined by ^{1}H-NMR. [c] 15 mol % of catalyst. [d] 7.5 mol % of catalyst. [e] 3 eq of ketone, 40 mol % catalyst Medium legend: A) PBS 1X LCP. B) PBS 1X cubosomes (Cubosomes A). C) HEPES 25 mM LCP. D) HEPES 25 mM cubosomes (Cubosomes B). E) HEPES 25 mM, cholesterol doped LCP. F) HEPES 25 mM, cholesterol doped cubosomes (Cubosomes C). G) PBS 0.1X LCP. H) PBS 0.1X cubosomes (Cubosomes D). I) Dispersion of **2** in PBS. J) Dispersion of **2** in HEPES 25 mM. K) Solution of **24** in PBS 1X.

2.2.4 Recycling

Catalytic LCPs as well as catalytic cubosomes can be reused up to five times without loss of activity. This is consistent with similar conclusions drawn on *in-meso* enzymatic reactions run over multiple cycles.[70] In the case of the catalytic LCPs, the aqueous phase containing the crude product can be decanted, and the LCP rinsed with the corresponding buffer. Subsequently, a new substrate solution can be added as an overlay to the LCP. To recycle catalytic cubosomes, the dispersion is filtered, a new stabilizer solution is added, and the sonication process is repeated.

2.2.5 Synthesis of various substrates and nornicotine reference catalyst

Many of the substrates used in this chapter had to be synthesized first, either because they were not commercially available or their supply was too expensive. Substrates **34** and **37** were not commercially available in satisfying quality. The syntheses will be briefly discussed.

2.2.5.1 Carbohydrate derived substrates

2,3-*O*-isopropylidene-glyceraldehyde (**34**) was synthesized in two synthetic steps from *D*-mannitol (**32**) according to a reported procedure (Scheme 4A). To that end, *D*-mannitol (**32**) was diketalized using 2,2-dimethoxypropane under basic conditions and $SnCl_2$ as a *Lewis* acid to obtain diacetonide **33**. In a second step, the carbon-carbon bond between the vicinal diols of **33** was oxidatively cleaved using $NaIO_4$ to obtain the final product **34**.[71] 2,2-dimethyl-1,3-dioxan-5-one (**37**) was obtained in two similar synthetic steps (Scheme 4B). Tris(hydroxymethyl)aminomethane was protected with 2,2-dimethoxypropane under acidic conditions. The amino alcohol **36** was subsequently transformed to ketone **37** by oxidative cleavage with $NaIO_4$.[72] Glyceraldehyde-3-phosphate (**39**) was synthesized from D-fructose-6-phosphate (**38**) in one step after treatment with periodic acid (Scheme 4C).[73]

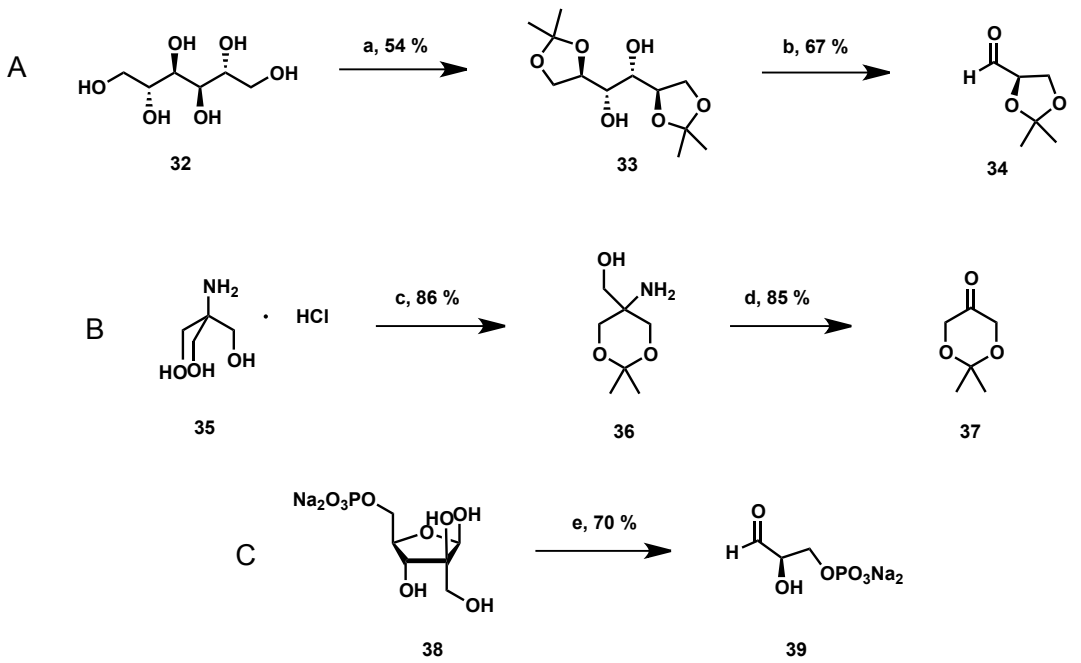

Scheme 4: Syntheses of 2,3-*O*-isopropylidene-glyceraldehyde (**34**), 2,2-dimethyl-1,3-dioxan-5-one (**37**) and glyceraldehyde-3-phosphate (**39**). Conditions: a) $SnCl_2$, pyridine, glyme, reflux. b) $NaIO_4$, CH_2Cl_2, 0°C. c) *p*TSA, DMF, r.t. d) $NaIO_4$, KH_2PO_4, H_2O, 0°C. e) H_5IO_6, H_2O, 0°C.

2.2.5.2 Synthesis of aromatic aldehyde 4a

Since aldol reactions with substrates **34** and **37** turned out to be very difficult, a more stable alternative was needed. 4-nitrobenzaldehyde, together with cyclohexanone is used as benchmark aldol reaction in literature. However, 4-nitrobenzaldehyde is hardly soluble in water. Therefore, aldehyde **4a** was designed, which bears an ethylene glycol unit that renders the compound water-soluble (Scheme 5). Furthermore, the hydroxyl moiety could be phosphorylated to further increase the hydrophilicity.

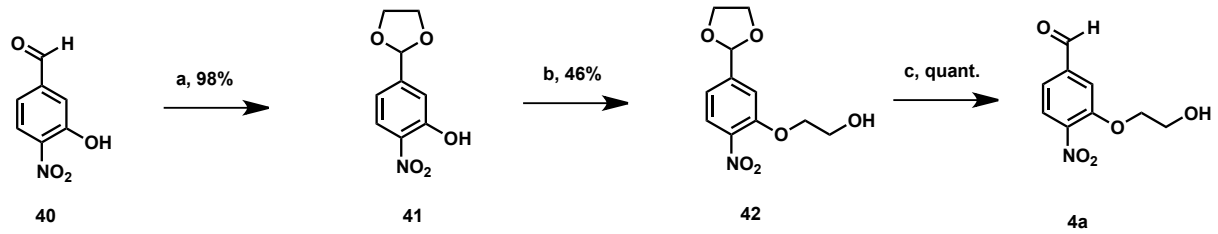

Scheme 5: Synthetic route to water-soluble aldehyde **4a**. Conditions: a) Ethylene glycol, *p*TsOH, toluene, reflux. b) Ethylene glycol, PPh_3, DIAD, THF, 55 °C. c) *p*TsOH, acetone/water 9:1, 55°C.

Compound **40** is an ideal starting material for the planned synthesis because the ethylene glycol moiety can be installed at the phenol group using a *Mitsunobu* reaction[74] once the aldehyde was protected. Acetal **42** was then deprotected using *p*TsOH.

2.2.5.3 Towards intramolecular aldol reactions in LCPs

Diffusion of the substrates from bulk water into the aqueous channels where the catalyst is located is one of the rate determining steps for chemical reactions carried out in mesophases. It would be interesting to compare the kinetics of an intermolecular with an intramolecular aldol reaction in mesophases, in which only one substrate molecule needs to diffuse into the water channel system to get in contact with the catalyst. In contrast to organocatalytic, intermolecular aldol reactions, its intramolecular version is much less well developed and, to the best of our knowledge, no organocatalytic, intramolecular aldol reactions in aqueous medium have been reported. One of few targets is the isochroman-1-one heterocyclic unit. *Fronert* and co-workers[75] addressed this topic using proline and proline derived catalysts in organic solvents (Scheme 6).

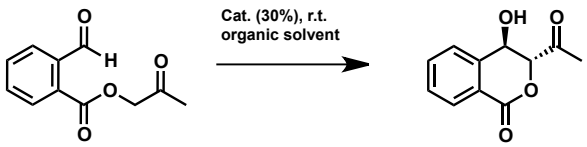

43 44

Scheme 6: Intramolecular aldol reaction of **43** forming isochroman-1-one derivative **44**.[75]

Having this substrate as a starting point in mind, two new water-soluble and activated analogues **52** and **53** have been designed (Scheme 7). The synthesis of 2-formyl-5-nitrobenzoic acid **47** was developed by *Zhang et al*.[76] This compound was also used in the previously described substrate screening for intermolecular aldol reactions, albeit no product was formed (Table 1, entry 20).

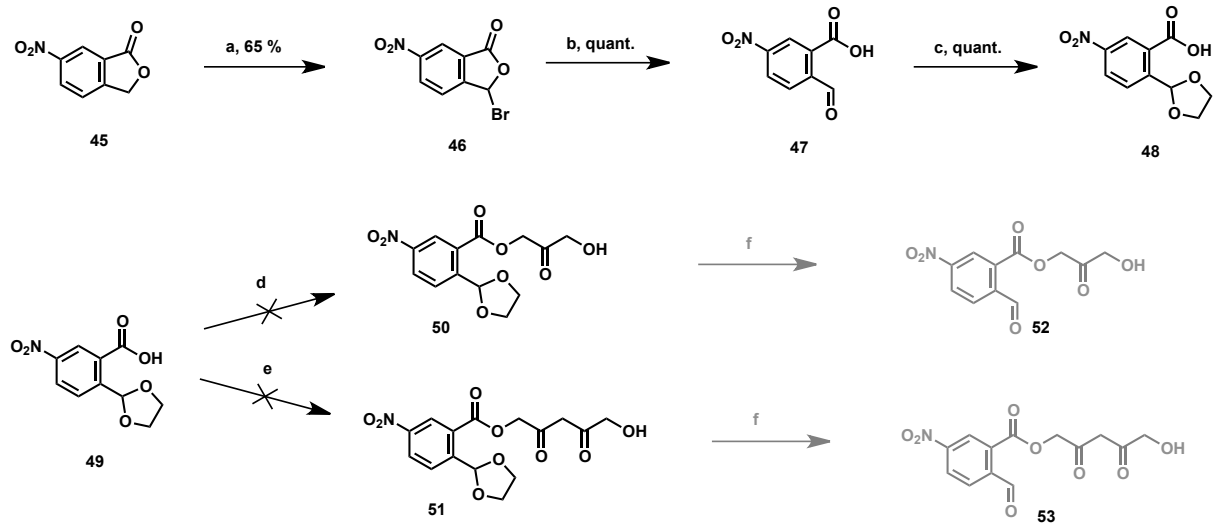

Scheme 7: Synthesis of 2-formyl-5-nitrobenzoic acid **47** and attempts to synthesize substrates **52** and **53**, which would enable intramolecular aldol reactions. Conditions: a) NBS, AIBN, benzene, reflux. b) H_2O, reflux. c) Ethylene glycol, *p*TsOH, toluene, reflux. d) Dihydroxy acetone, EDC, DMAP, DMF, r.t. e) 1,5-dihydroxypentane-2,4-dione EDC, DMAP, DMF, r.t..

The esterification of 2-formyl-5-nitrobenzoic acid was found to be much more challenging than expected (Scheme 7). The coupling with dihydroxy aceton using DCC/DMAP and EDC/DMAP did not work, neither in DMF nor in CH_2Cl_2 as the solvent. Dihydroxy aceton is commercially available in dimeric form. In order to obtain the monomer, an aqueous solution has to be prepared and stored for a few hours, before it is lyophilized and can be used. Remaining water from the lyophilisation could be an explanation for the failed esterification experiments.

2.2.5.4 Nornicotine reference catalyst

In order to have a second water-soluble reference catalyst in hand, nornicotine was synthesized and the resolution of the enantiomers was carried out according to a reported procedure. The synthesis started with a *Steglich* esterification of commercially available 5-bromo-nicotinic acid (**54**) with ethanol, followed by base catalyzed condensation with *N*-vinylpyrrolidone. After acid catalyzed hydrolysis, decarboxylation and cyclization, imine **56** was obtained, which was reduced by $NaBH_4$ to 5-bromonornicotine (**57**). The chiral resolution of this racemic mixture was achieved by treatment with the chiral organic acid 3,3,3-trifluoro-2-methoxy-2-phenylpropanoic acid (MTPA) and subsequent crystallization.[77] Both nornicotine enantiomers were obtained after treating of bromo-nornicotine using *n*-BuLi and water at -78 °C.

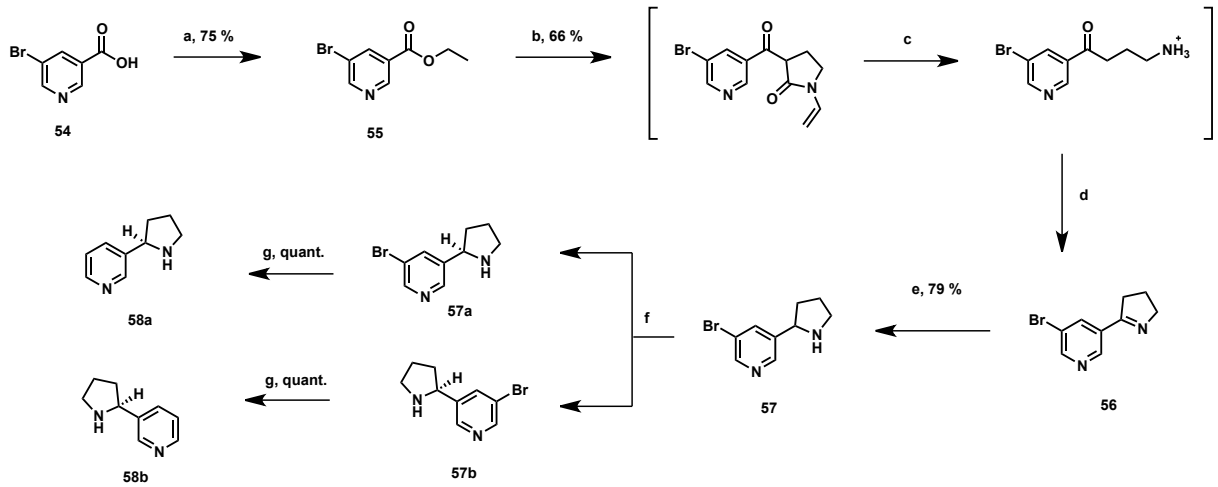

Scheme 8: Synthesis of *R*- and *S*-nornicotine **58a** and **58b** by chiral resolution by crystallization of the MTPA salts of bromo-nornicotine **53** and subsequent debromination. Conditions: a) EtOH (1 eq), DCC (1 eq), DMAP (0.1 eq); b) NaH (1.33 eq), Vinylpyrrolidone (1.1 eq), THF, reflux. c) H_2O, conc. HCl; d) NaOH 10%; e) $NaBH_4$ (2.3 eq), MeOH/AcOH 5:1, -40°C. e) $NaBH_4$, methanol/acetic acid (8:2), -40°C. f) Crystallisation with the corresponding MTPA salt. g) *n*BuLi, THF, -78 °C.

2.3 Conclusions

Host-guest lipidic mesophases were established as novel nanoreactor scaffolds for heterogeneous organocatalysis. Five proline-based lipidated catalysts were designed, synthesized and laterally immobilized into LCPs and cubosomes. The resulting catalytic lipidic mesophases were tested for a model asymmetric aldol reaction in confined aqueous buffers with three different aldehydes. The influence of the chemical structure of the catalysts on the phase identity and on the lattice parameter of the lipidic mesophases was established and correlated with the performance of various catalyst-mesophase systems. Both LCPs and cubosomes constitute efficient catalytic systems with good diastereo - and enantioselectivity. These readily prepared, biocompatible, sustainable and benign systems can be recycled at least five times without loss of activity. The novel catalytic lipidic mesophase systems present two modes of use with distinct features: Whereas gel-like bulk LCP is malleable and can adhere to any surface, fluid cubosome dispersions can be used in a classical reaction flasks. Significantly, the reaction rate of the model aldol reaction could be controlled by modifying catalytic LCPs and cubosomes using cholesterol as an additive. The approach presented herein is general, and in principle various types of (organo)catalysts may be used, including lipidic metal complexes. However, the system has also limitations, as it is restricted to aqueous chemistry, and the reactions need to be run at rather low concentrations of water-soluble substrates, in order not to disrupt the self-assembled lipidic structure of the mesophase. In conclusion, while catalysis in homogeneous systems has been developed to high sophistication, and immobilized catalysts on surfaces have been studied in great detail, the use of lipidic cubic phases as nanoreactor scaffolds for catalysts is novel. This remarkable and highly versatile mesophase material allows the tuning of various physical and chemical parameters, such as channel size, hydration, phase geometry interface charge, thereby providing exciting new avenues to be explored in catalysis in confined space.

2.4 Outlook

The reaction rates of the studied aldol reaction with both catalytic LCPs and cubosomes might be increased by applying massive swelling of the aqueous channels, according to a reported procedure.[78] Furthermore, the substrate scope needs to be extended to render catalytic LCP and cubosomes a more general tool for aqueous chemistry. Therefore, the attempts to synthesize carbohydrates need to be optimized. The same is true for the intramolecular aldol reaction. The stereochemistry of our model aldol reaction is moderate, however there is room to improve. Our system in its present form does not allow to catalyze water-insoluble compounds, as they accumulate in the lipidic compartment of the mesophases which destabilizes them. This problem is being addressed by developing catalytic LCPs made of polymerizable lipids. Since the polymerizable acroyl moieties in of these lipids are situated just the headgroup, enrichment of hydrophobic compounds in the lipidic compartment might be reduced (see Chapter 6).

2.5 Experimental section

General Information

1-Monooleoyl-sn-glycerol C18:1 (monoolein, MO) was purchased from Nu-Chek Prep, Inc. (MN, USA), and phosphate buffer solution (PBS (1X) pH 7.4) was purchased from Invitrogen. Phytantriol was purchased from DSM. N-(3- dimethylaminopropyl)-N′-ethylcarbodiimide hydrochloride (EDC) was purchased from TCI, and all other reagents and solvents were purchased from Sigma Aldrich. All chemicals and solvents were used as received, unless otherwise stated. Reactions were carried out under an inert atmosphere of argon in dry solvents. Dichloromethane was degassed with argon and purified by passage through activated alumina solvent column (MC Brown solvent system) prior to use. Column chromatography was performed using silica gel Merck 60 (particle size 0.040–0.063 mm). Analytical thin- layer chromatography (TLC) was performed using Merck pre-coated silica gel plates 60 F_{254}; visualization by UV absorption and/or by dipping in a solution of $KMnO_4$ (1 g), K_2CO_3 (2 g) in H_2O (100 mL) and subsequent heating. ^{1}H-NMR spectra were recorded on a Bruker AV2-500 (500MHz) spectrometer. Chemical shifts are given in parts per million (ppm) relative to the internal standard TMS (δ = 0 ppm). Coupling constants J are expressed in Hz and multiplicities are abbreviated as follows: s (singlet), br (broad), d (doublet), t (triplet), q (quadruplet), quint (quintet), m (multiplet). ^{13}C-NMR chemical shifts are reported relative to the solvent residual peaks: $CDCl_3$ = 77.00 ppm. Mass spectra were recorded by the Mass Spectroscopy Service of UZH on Finnigan MAT95 MS, BrukerLC MS and Finnigan TSQ700 MS machines.

2.5.1 Synthesis

2.5.1.1 General procedures

Amide coupling:

To a stirred solution of BOC-*L*-proline (500 mg, 2.32 mmol, 1 eq) in 50 mL of a mixture of dry CH_2Cl_2 and dry DMF (1:1) was added EDC (466 mg mg, 3.00 mmol, 1.3 eq) and DMAP (28 mg, 0.232 mmol, 0.1 eq) at 0 °C under an inert atmosphere. The solution was stirred for 1 h at 0 °C and then the corresponding amine (3.48 mmol) was added dropwise over a period of 10 min. The reaction mixture was stirred for 14 h at room temperature and then CH_2Cl_2 (50 mL) was added, the mixture was washed with a saturated solution of $NaHCO_3$. The organic phase was separated and the aqueous phase was extracted with CH_2Cl_2 (50 mL). The combined organic phases were washed with brine and dried over $MgSO_4$. The solvent was removed and the crude product was purified by column chromatography. The solvent was evaporated to afford the corresponding products.

Boc-deprotection:

Boc-protected catalysts (0.43 mmol) were dissolved in CH_2Cl_2 (10 mL), cooled to 0°C and trifluoro acetic acid (TFA) (3 mL) was added slowly. The solution was stirred for 3 h at 0°C while the reaction was monitored by TLC. Upon completion of the reaction, the solvent was evaporated *in vacuo*. In order to remove residual TFA, CH_2Cl_2 (3 x 3 mL) was added and evaporated.

Amide reduction:

The corresponding amide (1.1 mmol, 1 eq) was dissolved in THF (10 mL) and slowly added to a suspension of $LiAlH_4$ (141 mg, 3.7 mmol, 3.4 eq) in THF (10 mL) at 0°C. The reaction mixture was then heated up to reflux for 20 h. After cooling down to 0°C, saturated Na_2SO_4 solution was added and the mixture was filtrated. After removal of the solvent in *vacuo*, the crude product was purified by column chromatography. The tertiary amine was then treated with CH_2Cl_2/TFA (3:1) to obtain the product as TFA salts.

Aldol reaction using catalytic lipidic cubic phases (LCPs)

Previously prepared LCP (containing 0.0071 mmol, 66 mg MO and corresponding buffer, LCP preparation as described on page 15) was put on homemade metal holders (Figure 8) and the plastic container for the aqueous phase was attached. Subsequently, a solution of the desired aldehyde **4a**, **4b** or **4c** (0.0235 mmol, 1 eq) and cyclohexanone (**3**) (4.6 mg, 0.047 mmol, 2 eq) in 2 mL of the desired buffer at pH 7.4 (PBS 1X, HEPES 25 mM, PBS 0.1X) was carefully poured on top of the catalytic LCP. The reaction set-up was gently shaken on a

laboratory shaker. The reaction was monitored by ^{1}H-NMR. After completion of the reaction, the aqueous phase was removed and the LCP rinsed with 2 mL of corresponding buffer. The aqueous phases were extracted with EtOAc (5 x 3 mL). The combined organic phases were washed with brine and dried over $MgSO_4$. The solvent was removed and the crude product was purified by column chromatography (silica gel, cyclohexane/EtOAc) to obtain the aldol products.

Figure 8: Homemade metal holders for aldol reactions catalyzed by LCPs. Left: Empty metal holder with indentation for LCP, plastic container for the aqueous overlay and cap. Centre: LCP loaded metal holder. Left: Prepared set-up for aldol reactions catalyzed by LCPs.

Aldol reaction using catalytic cubosomes

Aldehyde **4a**, **4b** or **4c** (0.0235 mmol, 1 eq) and cyclohexanone (**3**) (4.6 mg, 0.047 mmol, 2 eq) were added to previously prepared cubosomes (0.0071 mmol catalyst, 66 mg MO, and 2 mL of the corresponding buffer, cubosome preparation as described on page 15) and the reaction mixture was stirred. The reaction was monitored by ^{1}H-NMR. After completion of the reaction, the cubosome were separated from the aqueous phase by centrifugation with vivacon 500 filter and the lipidic part was rinsed with 2 mL of the corresponding buffer. The aqueous phases were extracted with EtOAc (5 x 3 mL). The combined organic phases were washed with brine and dried over $MgSO_4$. The solvent was removed and the crude product was purified by column chromatography (silica gel, cyclohexane/EtOAc) to obtain the aldol products.

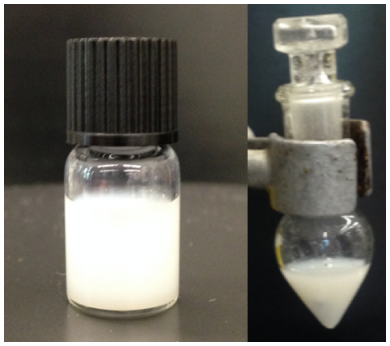

Figure 9: Set up for aldol reaction using catalytic cubosomes.

2.5.1.2 First generation catalysts

Synthesis of 8 ((2*S*,4*R*)-1-(*tert*-butoxycarbonyl)-4-(oleoyloxy)pyrrolidine-2-carboxylic acid)[18]

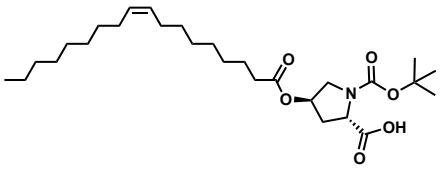

A) To a solution of oleic acid (**6**) 90% (271 mg, 0.865 mmol, 1 eq) in DCM (5 ml), DMAP (106 mg, 0.865 mmol, 1 eq), DCC (217 mg, 0.95 mmol, 1.1 eq) and (2*S*,4*R*)-1-(*tert*-butoxycarbonyl)-4-hydroxypyrrolidine-2-carboxylic acid (**7**) (200 mg, 0.865 mmol, 1 eq) was added. The suspension was allowed to stir for 2 days at room temperature at which time it was filtrated, and after addition of DCM (5 mL), washed with brine (2x). The organic phase was dried over $MgSO_4$ and the solvents evaporated. The crude product was purified by column chromatography (hexane/EtOAc 1:1, 1% acetic acid) to afford the product as a yellow oil (123 mg, 0.25 mmol, 32%).

B) To a stirred solution (2*S*,4*R*)-1-(*tert*-butoxycarbonyl)-4-hydroxypyrrolidine-2-carboxylic acid (**7**) (200 mg, 0.86 mmol, 1.0 eq), DIPEA (0.86 mL) in anhydrous CH_2Cl_2 (10 mL) was cooled to 0 °C and treated dropwise with a solution of oleyl chloride (**10**) (361 mg, 1.2 mmol, 1.4 eq) in DCM (5 mL). The ice bath was removed and the reaction mixture was stirred until no more starting material was observed by TLC. The reaction mixture was poured into brine and extracted three times with CH_2Cl_2. The combined organic phases were washed with brine, dried over $MgSO_4$ and concentrated under reduced pressure. The residue was purified by column chromatography on silica gel to obtain the product as a yellow oil (107 mg, 0.22 mmol, 25 %).
Analytical data were identical with the values reported in literature.[18]

Synthesis of catalyst 9 ((2*S*,4*R*)-4-(oleoyloxy)pyrrolidine-2-carboxylic acid)[18]

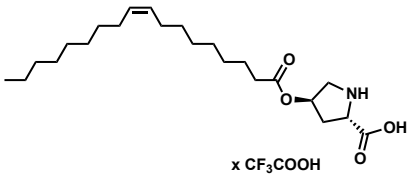

Catalyst **9** was obtained after Boc-deprotection of **8** according to the general procedure as a yellow oil in quantitative yield.
Analytical data were identical with the values reported in literature.[18]

Synthesis of 12 ((2*S*,4*R*)-1-(*tert*-butoxycarbonyl)-4-oleamidopyrrolidine-2-carboxylic acid)[18]

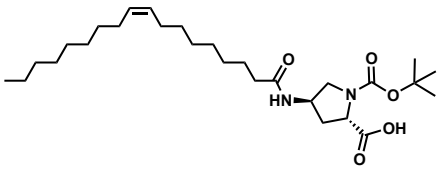

To a solution of oleic acid (**6**) 90% (271 mg, 0.865 mmol, 1 eq) in DCM (5 ml), DMAP (11 mg, 0.087 mmol, 0.1 eq), EDC (182 mg, 0.95 mmol, 1.1 eq) and (2*S*,4*R*)-4-amino-1-(*tert*-butoxycarbonyl)pyrrolidine-2-carboxylic acid (**11**) (200 mg, 0.865 mmol, 1 eq) was added. The suspension was allowed to stir for 10 h at room temperature at which time it was filtrated, and after addition of DCM (5 mL), washed with brine (2 x 5 mL). The organic phase was dried over $MgSO_4$ and the solvents evaporated. The crude product was purified by FC (hexane/EtOAc 1:1, 1% acetic acid) to obtain the desired product as a slightly yellow oil (330 mg, 0.692 mmol, 80 %).
Analytical data were identical with the values reported in literature.[18]

Synthesis of catalyst 13 ((2*S*,4*R*)-4-oleamidopyrrolidine-2-carboxylic acid)[18]

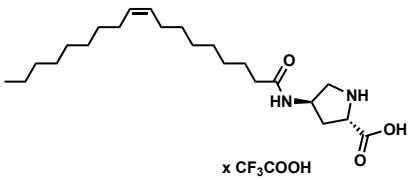

Catalyst **13** was obtained after Boc-deprotection of **12** according to the general procedure as a yellow oil in quantitative yield.Analytical data were identical with the values reported in literature.[18]

2.5.1.3 Second and third generation catalysts

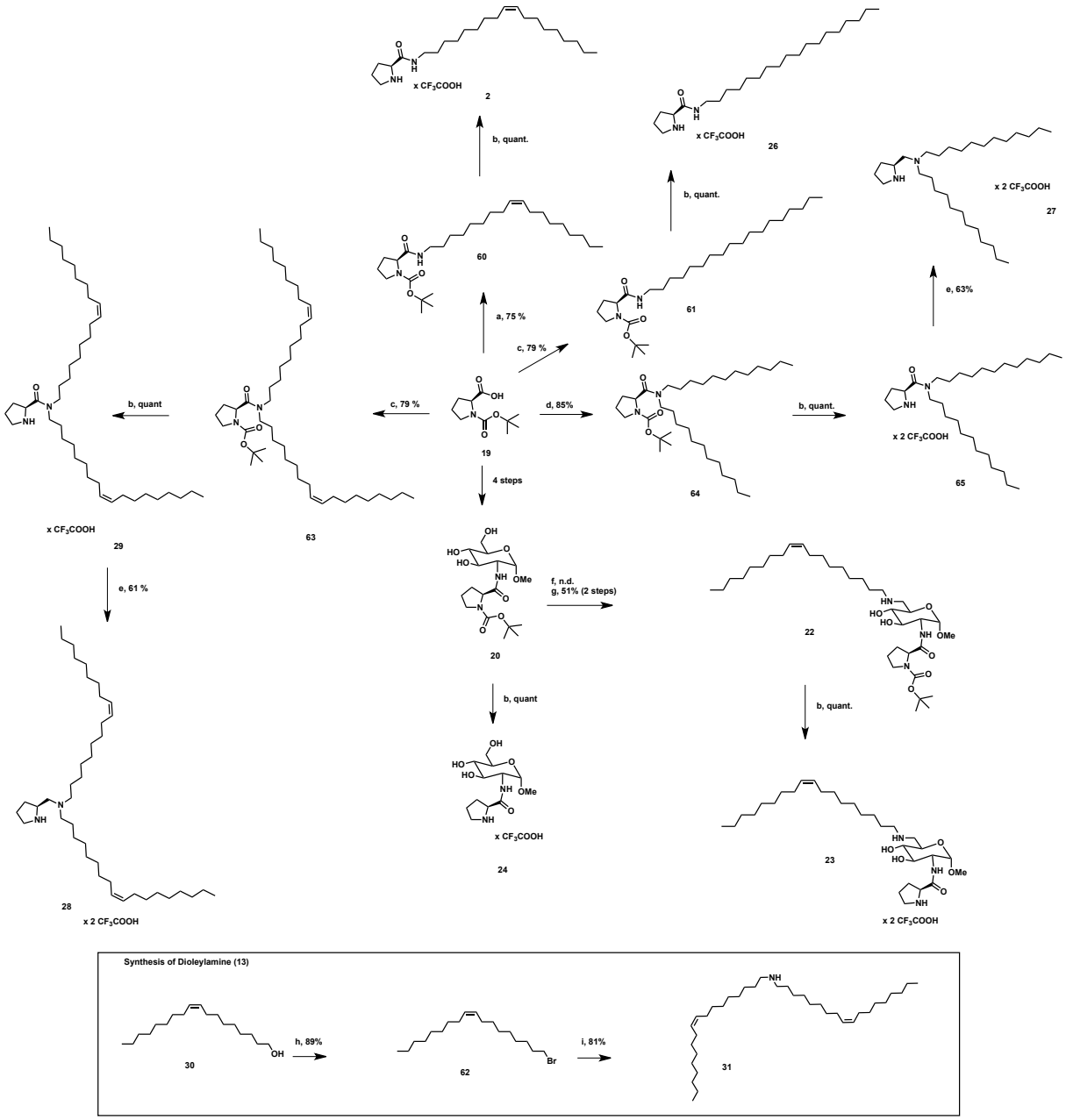

Scheme 9: Overview of the syntheses of lipidic catalysts **2**, **23**, **26**, **27**, **28**, **29** and water-soluble reference catalyst 11. Conditions: a) Oleylamine, EDC (1.1 eq), DMAP (0.1 eq) CH_2Cl_2 / DMF 4:1, r.t. b) CH_2Cl_2 / TFA 4:1, 0°C c) Stearylamine (1.1 eq), EDC (1.1 eq), DMAP (0.1 eq) CH_2Cl_2 / DMF 4:1, r.t. d) Dioleylamine (1.1 eq), EDC (1.1 eq), DMAP (0.1 eq) CH_2Cl_2 / DMF 4:1, r.t. e) Didodecylamine (1.1 eq), EDC (1.1 eq), DMAP (0.1 eq) CH_2Cl_2 / DMF 4:1, r.t. f) $LiAlH_4$, THF, 0°C 2 h then reflux 20 h. g) TEMPO, TCC, DMF, 0°C h) Oleylamine (1 eq), MeOH, r.t. 1h then $NaCNBH_3$ (1.3 eq). i) $P(Ph)_3$ (1.1 eq.), CBr_4 (1.1 eq), DCM, 0°C. j) Oleylamine (1 eq), K_2CO_3 (0.3 eq), DMSO, 80°C.

Synthesis of 17 (*N*-((3*R*,4*R*,5*S*,6*R*)-4,5-dihydroxy-6-(hydroxymethyl)-2-methoxytetrahydro-2*H*-pyran-3-yl)acetamide)[59]

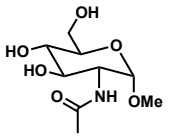

N-Acetyl-*D*-glucosamine (**16**) (1.0 g, 4.5 mmol, 1 eq) was dissolved in MeOH (25 mL) before Dowex 50W X8, 50-100 mesh (0.2 g) was added. The reaction mixture was refluxed for 20 h, filtrated, the solvent evaporated *in vacuo* to give crude product (α/β mixture of anomers 2:1). The crude product was purified by flash chromatography (EtOAc/MeOH 8:2-6:4) to obtain the title compound as colorless solid (800 mg, 3.38 mmol, 75 % α-anomer)
Analytical data were identical with the values reported in literature.[59]

Synthesis of (18) ((2*R*,3*S*,4*R*,5*R*,6*S*)-5-amino-2-(hydroxymethyl)-6-methoxytetrahydro-2*H*-pyran-3,4-diol)[59]

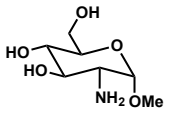

N-Acetyl-*D*-methoxyglucoseamine (**17**) (1.0 g, 3.95 mmol, 1 eq) was dissolved in H_2O (30 mL) and the pH was adjusted to 13 by adding BaO. The reaction mixture was stirred at reflux for 12 h. The reaction mixture was cooled to room temperature before the white precipitate was filtered off. Subsequently, the water was removed by lyophilisation and the desired product was obtained as a colorless solid in quantitative yield.
Analytical data were identical with the values reported in literature.[59]

Synthesis of 20 ((*S*)-*tert*-butyl 2-(((2*S*,3*R*,4*R*,5*S*,6*R*)-4,5-dihydroxy-6-(hydroxymethyl)-2-methoxytetrahydro-2*H*-pyran-3-yl)carbamoyl)pyrrolidine-1-carboxylate)

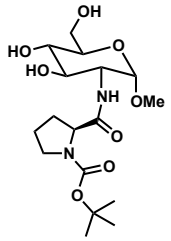

Boc-*L*-proline (**19**) (2.13 g, 10 mmol, 1 eq), DCC (2.04 g, 10 mmol, 1 eq) and DMAP (0.12 g, 1 mmol, 0.1 eq) in DMF (125 mL) was stirred at 0°C for 1 h. To this mixture, **18** (1.9 g, 10 mmol, 1 eq) was added. After an additional hour at 0 C°, the ice bath was removed und the mixture was stirred for 30 h at room temperature. The mixture was filtrated and the solvent evaporated. Purification by flash chromatography (EtOAc/MeoH 9:1-8:2) delivered pure the product as a yellow, sticky solid (1.56 g, 4 mmol, 40 %).
Analytical data were identical with the values reported in literature.[59]

Synthesis of 24 ((*S*)-*N*-((2*S*,3*R*,4*R*,5*S*,6*R*)-4,5-dihydroxy-6-(hydroxymethyl)-2-methoxytetrahydro-2*H*-pyran-3-yl)pyrrolidine-2-carboxamide)

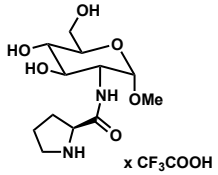

Reference catalyst **24** was obtained after Boc-deprotection of **20** according to the general procedure as a yellow oil in quantitative yield.
Analytical data were identical with the values reported in literature.[59]

Synthesis of 22 ((*S*)-*tert*-butyl 2-(((2*S*,3*R*,4*R*,5*S*,6*R*)-4,5-dihydroxy-2-methoxy-6-(((*Z*)-octadec-9-en-1-ylamino)methyl)tetrahydro-2*H*-pyran-3-yl)carbamoyl)pyrrolidine-1-carboxylate)[49,79]

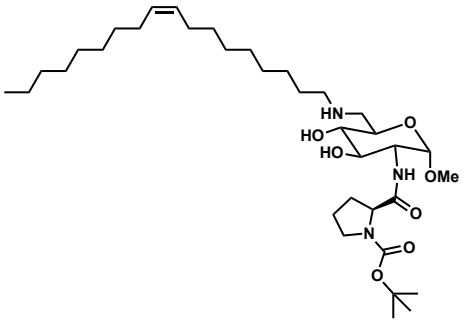

To a stirred solution of the proline carbohydrate **20** (300 mg, 0.77 mmol, 1 eq) in DMF (130 mL), $NaHCO_3$ (1.93 g, 94.4 mmol and TEMPO (3 mg, 0.02 mmol, 0.26 eq) was added. After cooling to 0°C, TCC (111 mg, 0.483 mmol, 0.63 eq) was added. The reaction mixture was stirred for 7 h at 0°C, the white precipitate was filtered off and solvent was removed under vacuum. The remaining yellow oil was immediately used for the next step (since the aldehyde is prone to decomposition). Crude aldehyde was dissolved in MeOH (70 mL) and oleylamine (227 mg, 0.847 mmol, 1.1 eq) was added and stirred at room temperature. The reaction was monitored by TLC. After 2 h, the imine formation was completed. Subsequently, $NaCNBH_3$ (53.2 mg, 0.847 mmol 1.1 eq) was added and the reaction mixture was stirred at reflux for 5 h. After cooling the reaction mixture to room temperature, EtOAc (100 mL) was added and the organic layer was washed with brine, dried over $MgSO_4$ and concentrated under *vacuo.* The crude product was purified by flash chromatography (EtOAc/ MeOH). The product was obtained as sticky and slightly yellow solid (251 mg, 0.393 mmol, 51%). ^{1}H NMR (500 MHz, Chloroform-*d*) δ 5.37 – 5.23 (m, 2H), 4.56 (d, *J* = 3.1 Hz, 1H), 4.26 – 4.13 (m, 1H), 4.09 – 3.92 (m, 1H), 3.69 – 3.54 (m, 2H), 3.53 – 3.34 (m, 2H), 3.29 (s, 3H), 3.18 – 3.00 (m, 1H), 2.98 – 2.91 (m, 2H), 2.79 – 2.63 (m, 1H), 2.24 – 1.75 (m, 8H), 1.59 – 1.48 (m, 2H), 1.40 (s, 9H), 1.32 – 1.12 (m, 20H), 0.81 (t, *J* = 6.7 Hz, 3H). ^{13}C NMR (126 MHz, $CDCl_3$) δ 174.12, 171.30, 130.14, 129.94, 98.83, 80.71, 73.84, 68.38, 61.29, 60.56, 55.63, 53.77, 50.85, 49.75, 47.36, 46.79, 32.09, 29.95, 29.89, 29.71, 29.66, 29.55, 29.50, 29.44, 28.52 (3C), 27.40, 22.86, 14.30. HRMS (ESI $[M + H]^+$) m/z: calcd for ($C_{35}H_{66}N_3O_7$) 640.48953, found 640.48947.

Synthesis of catalyst 23 ((*S*)-*N*-((2*S*,3*R*,4*R*,5*S*,6*R*)-4,5-dihydroxy-2-methoxy-6-(((*Z*)-octadec-9-en-1-ylamino)methyl)tetrahydro-2*H*-pyran-3-yl)pyrrolidine-2-carboxamide)

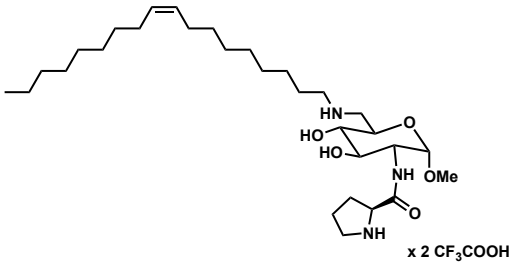

Catalyst **23** was obtained after Boc-deprotection of **22** according to the general procedure as a yellow oil in quantitative yield. ^{1}H NMR (500 MHz, DMSO-d_6) δ 8.80 – 8.51 (m, 2H), 5.43 – 5.26 (m, 2H), 4.63 (d, *J* = 3.3 Hz, 1H), 4.21 (s br, 1H), 3.81 – 3.66 (m, 2H), 3.50 (t, *J* = 9.6 Hz, 1H), 3.33 (s, 3H), 3.31 – 3.16 (m, 3H), 3.12 (t, *J* = 9.2 Hz, 2H), 3.08 – 3.00 (m, 1H), 2.97 – 2.89 (m, 2H), 2.33 – 2.23 (m, 1H), 2.02 – 1.81 (m, 8H), 1.68 – 1.52 (m, *2*H), 1.34 – 1.18 (m, 20H), 0.85 (t, *J* = 6.6 Hz, 3H). ^{13}C NMR (126 MHz, DMSO-d_6) δ 168.64, 129.64, 129.59, 98.09, 72.26, 69.97, 67.96, 55.23, 53.87, 48.05, 47.49, 45.80, 31.28, 29.85, 29.14, 29.08, 29.04, 28.82, 28.68 (2C), 28.58, 28.55, 28.48, 26.62, 26.56, 25.93, 25.08, 23.50, 22.09, 13.94. HRMS (ESI [M + H]$^+$) m/z: calcd for ($C_{30}H_{58}N_3O_5$) 540.43710, found 540.43743.

Synthesis of 60 ((*S*,*Z*)-*tert*-butyl 2-(octadec-9-en-1-ylcarbamoyl)pyrrolidine-1-carboxylate

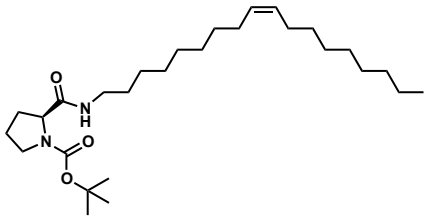

Boc-protected compound **60** was synthesized according to the general procedure for the amide coupling. The crude product was purified by column chromatography (silica gel, cyclohexane/EtOAc 4:1). The product was obtained as a slightly yellow oil (784 mg, 1.74 mmol, 75 %). ^{1}H NMR (500 MHz, DMSO-d_6) δ 7.78 (s), 7.69 (s), 5.39 – 5.28 (m, 2H), 4.04 – 3.95 (m, 1H), 3.40 – 3.33 (m, 1H), 3.30 – 3.23 (m, 1H), 3.10 – 2.92 (m, 2H), 2.12 – 1.90 (m, 4H), 1.85 – 1.67 (m, 3H), 1.44 – 1.17 (m, 34H), 0.85 (t, *J* = 6.8 Hz, 3H). ^{13}C NMR (126 MHz, DMSO) δ 172.13, 153.29, 129.59, 78.21, 59.82, 46.41, 38.39, 31.24, 31.06, 29.24, 29.09, 29.06, 28.97 (2C), 28.92, 28.79, 28.73, 28.65, 28.55 (2C), 28.10, 27.97 (2C), 26.53, 26.34, 23.11, 22.06, 13.90. HRMS (ESI [M + Na]$^+$) m/z: calcd for ($C_{28}H_{52}N_2O_3Na$) 487.38701, found 487.38674.

Synthesis of catalyst 2, ((*S*,*Z*)-*N*-(octadec-9-en-1-yl)pyrrolidine-2-carboxamide (TFA salt)

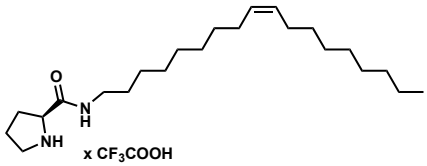

Catalyst **2** was obtained after Boc-deprotection of **60** according to the general procedure as a yellow oil in quantitative yield. ^{1}H NMR (500 MHz, DMSO-d_6) δ 8.52 (s, 1H), 5.37 – 5.28 (m, 2H), 4.16 – 4.09 (m, 1H), 3.29 – 3.03 (m, 4H), 2.31 – 2.24 (m, 1H), 2.01 – 1.75 (m, 6H), 1.45 – 1.38 (m, 2H), 1.32 – 1.19 (m, 22H), 0.85 (t, *J* = 7.0 Hz, 3H). ^{13}C NMR (126 MHz, DMSO) δ 167.81, 129.60, 59.01, 45.56, 40.00, 38.85, 31.32, 29.65, 29.17, 29.12, 29.08, 29.04, 28.89, 28.87, 28.79, 28.72, 28.62, 26.63, 26.59, 26.30, 23.56, 22.12, 13.92. HRMS (ESI [M + H]$^{+}$) m/z: calcd for ($C_{23}H_{45}ON_2$) 365.35264, found 365.35290.

Synthesis of 61 (*S*)-*tert*-butyl 2-(octadecylcarbamoyl)pyrrolidine-1-carboxylate

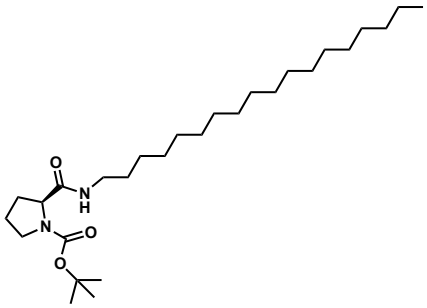

The title compound was synthesized according to the general procedure for the amide coupling. The crude product was purified by column chromatography (silica gel, EtOAc). The solvent was evaporated to afford a slightly yellow oil (670 mg, 1.83 mmol 79%). ^{1}H NMR (500 MHz, Chloroform-*d*) δ 6.86 (s), 5.99 (s), 4.51 (t, *J* = 5.0 Hz), 4.44 – 4.32 (m), 4.18 (s, 1H), 3.56 – 3.00 (m, 4H), 2.41 – 1.70 (m, 4H), 1.66 – 1.58 (m, 4H), 1.56 – 1.49 (m, 1H), 1.39 (s, 9H), 1.32 – 0.97 (m, 30H), 0.81 (t, *J* = 6.9 Hz, 3H). ^{13}C NMR (126 MHz, Chloroform-*d*) δ 172.39, 171.78, 157.67, 156.90, 80.23, 48.87, 47.04, 39.32, 33.96, 31.87, 29.64 (4C), 29.60 (4C), 29.54, 29.48, 29.30, 29.24, 28.33, 26.82, 25.62, 24.94, 22.63, 14.06. HRMS (ESI [M + H]$^{+}$) m/z: calcd for ($C_{28}H_{55}O_3N_2$) 467.42072, found 467.42136.

Synthesis of catalyst 26 ((*S*)-*N*-octadecylpyrrolidine-2-carboxamide)

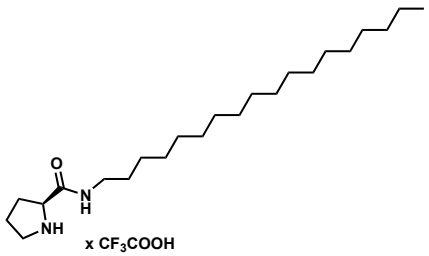

Catalyst **26** was obtained after Boc-deprotection of **56** according to the general procedure as a yellow oil in quantitative yield. ^{1}H NMR (500 MHz, Chloroform-*d*) δ 7.80(s, 1H), 3.40 – 3.09 (m, 4H), 3.05 (t, *J* = 7.2 Hz, 1H), 2.42 – 2.31 (m, 1H), 2.03 – 1.92 (m, 2H), 1.91 – 1.76 (m, 3H), 1.72 – 1.63 (m, 2H), 1.60 – 1.34 (m, 6H), 1.18 (s, 32H), 0.81 (t, *J* = 6.9 Hz, 3H). ^{13}C NMR (126 MHz, Chloroform-*d*) δ 168.28, 59.44, 50.00, 46.50, 41.11, 40.34, 39.46, 33.36, 33.29, 31.91, 30.38, 29.69, 29.65, 29.59, 29.50, 29.35, 29.28, 29.21, 29.11, 28.36, 25.32, 24.72, 22.68, 14.10. HRMS (ESI $[M + H]^+$) m/z: calcd for ($C_{23}H_{47}ON_2$) 367.36829, found 367.36849.

Synthesis of 31 ((*Z*)-di((*Z*)-octadec-9-en-1-yl)amine)[58]

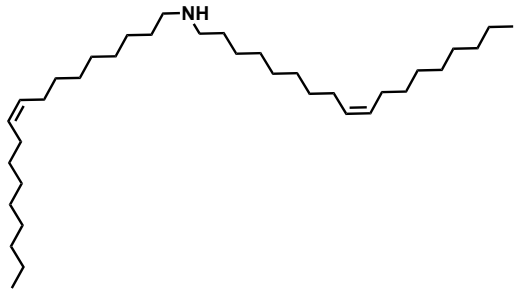

To a stirred mixture of oleylamine (800 mg, 3.0 mmol) in DMSO (20 mL) and K_2CO_3 (150 mg, 1.10 mmol), oleylbromide **62** (100 mg, 3.0 mmol) was added and the reaction mixture was heated to 80°C for 20 h. After cooling to room temperature, the mixture was filtered and water was added (50 mL). The mixture was extracted with CH_2Cl_2 (3 x 50 mL), and the combined organic phases were washed with brine and dried over $MgSO_4$. The solvent was removed and the crude product was purified by column chromatography (silica gel, cyclohexane/EtOAc 1:1) to afford the product as a slightly yellow oil (141 mg, 0.273 mmol, 81%). ^{1}H NMR (500 MHz, $CDCl_3$) δ 5.32 – 5.24 (m, 4H), 2.51 (t, *J* = 7.3 Hz, 4H), 1.97 – 1.86 (m, 4H), 1.44 – 1.36 (m, 8H), 1.32 – 1.13 (m, 44H), 0.81 (t, *J* = 6.8 Hz, 6H). ^{13}C NMR (125 MHz, $CDCl_3$) δ 129.91 (2C), 129.83 (2C), 50.20 (2C), 32.60 (2C), 31.90 (2C), 30.24 (2C), 29.77 (2C), 29.69 (2C), 29.65, 29.57 (2C), 29.52 (2C), 29.50 (2C), 29.31 (2C), 29.25, 29.17, 29.10, 27.43 (2C), 27.20 (2C),

22.68 (2C), 14.10 (2C). HRMS (ESI [M + H]$^+$) m/z: calcd for ($C_{36}H_{72}N$) 518.56593, found 518.56610.

Synthesis of 62 ((*Z*)-1-bromooctadec-9-ene)[57]

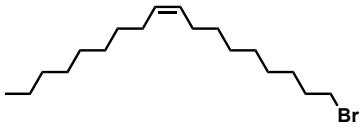

Oleyl alcohol (2.0 g, 7.4 mmol, 1 eq) and triphenylphosphine (2.1 g, 8.2 mmol, 1.1 eq) were dissolved in CH_2Cl_2 (40 mL) and cooled to 0°C. Subsequently, tetrabromomethane (2.72 g, 8.2 mmol, 1.1 eq) was added in portions. The reaction mixture was stirred for 2 h at 0°C before the solvent was evaporated and the crude product was purified by column chromatography (silica gel, cyclohexane/EtOAc 4:1) to afford the product as a colourless liquid (2.4 g, 6.6 mmol, 89 %). ^{1}H NMR (500 MHz, $CDCl_3$) δ 5.33 – 5.25 (m, 2H), 3.34 (t, *J* = 6.9 Hz, 2H), 1.98 – 1.87 (m, 4H), 1.78 (quint, *J* = 7.0 Hz, 2H), 1.39 – 1.32 (m, 2H), 1.30 – 1.14 (m, 20H), 0.81 (t, *J* = 6.8 Hz, 3H). ^{13}C NMR (126 MHz, $CDCl_3$) δ 129.99, 129.74, 34.00, 32.83, 31.91, 29.77, 29.70, 29.53, 29.33 (3C), 29.17, 28.74, 28.17, 27.22, 27.16, 22.69, 14.11. HRMS (EI [M]$^+$) m/z: calcd for ($C_{18}H_{35}Br$) 330.19167, found 330.19126.

Synthesis 63 of ((*S*)-*tert*-butyl 2-(di((*Z*)-octadec-9-en-1-yl)carbamoyl)pyrrolidine-1-carboxylate)

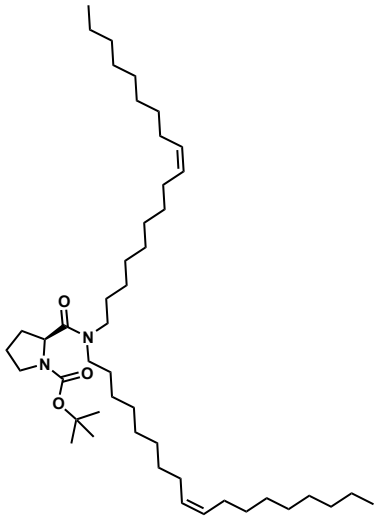

The title compound was synthesized according to the general procedure for the amide coupling. The crude product was purified by column chromatography (silica gel, EtOAc). The solvent was evaporated to afford a slightly yellow oil (262 mg, 0.367 mmol, 79 %). ^{1}H NMR

(500 MHz, $CDCl_3$) δ 5.32 -5.23 (m, 4H), 4.51 – 4.32 (m, 1H), 3.60 – 3.47 (m, 1H), 3.44 – 3.05 (m, 9H), 2.15 – 1.87 (m, 10H), 1.81 – 1.72 (m, 2H), 1.63 – 1.14 (m, 55H) 0.81 (t, *J* = 6.8 Hz, 6H). ^{13}C NMR (126 MHz, $CDCl_3$) δ 172.17, 153.90, 130.05, 129.92, 129.78, 129.64, 79.50, 56.43, 47.81 (2C), 46.96, 46.85, 46.79, 46.53, 32.59, 31.89 (2C), 31.37, 30.36, 29.76 (2C), 29.72, 29.65 (2C), 29.51 (2C), 29.41, 29.31 (3C), 29.18, 28.51 (4C), 27.69, 27.20 (2C), 27.00 (2C), 24.20, 23.33, 22.67 (2C), 14.10 (2C). HRMS (ESI $[M + H]^+$) m/z: calcd for ($C_{46}H_{87}O_3N_2$) 715.67112, found 715.67138.

Synthesis of catalyst 29 ((*S*)-*N*,*N*-di((*Z*)-octadec-9-en-1-yl)pyrrolidine-2-carboxamide)

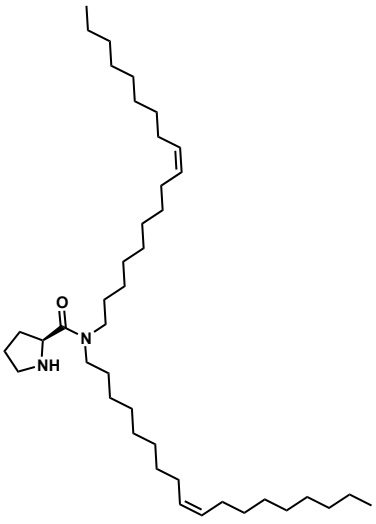

x CF_3COOH

Catalyst **10** was obtained after Boc-deprotection of **63** according to the general procedure as a yellow oil in quantitative yield. ^1H NMR (500 MHz, $CDCl_3$) δ 5.35 – 5.22 (m, 4H), 4.74 (s (br), 1H), 3.55 – 3.29 (m, 3H), 3.23 – 3.07 (m, 3H), 2.50 – 2.42 (m, 1H), 2.16 – 2.07 (m, 1H), 2.00 – 1.86 (m, 8H), 1.85 – 1.77 (m, 1H), 1.60 – 1.41 (m, 4H), 1.32 – 1.14 (m, 45H), 0.81 (t, *J* = 6.8 Hz, 6H). ^{13}C NMR (126 MHz, $CDCl_3$) δ 167.91, 130.00 (2C), 129.70 (2C), 57.98, 47.41, 46.81, 46.39, 32.60, 31.89 (2C), 30.31, 29.75 (2C), 29.71, 29.68, 29.65, 29.51 (2C), 29.43, 29.34, 29.31 (3C), 29.25, 29.23, 29.20, 29.15, 28.55, 27.21 (2C), 27.17, 27.15, 26.86, 26.73. 25.17, 22.67 (2C), 14.09 (2C). HRMS (ESI $[M + H]^+$) m/z: calcd for ($C_{41}H_{79}ON_2$) 615.61869 found 615.61827

Synthesis of catalyst 28 ((*Z*)-*N*-((*Z*)-octadec-9-en-1-yl)-*N*-((*S*)-pyrrolidin-2-ylmethyl)octadec-9-en-1-amine)

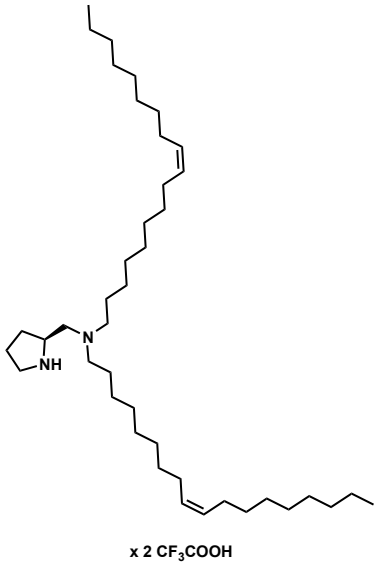

x 2 CF_3COOH

Catalyst **28** was synthesized according to the general procedure for the amide reduction from catalyst **29**. The crude product was purified by column chromatography (silica gel, cyclohexane/EtOAc 2:1) to afford the product as a slightly yellow oil (59.7 mg, 0.100 mmol, 61 %). ^{1}H NMR (500 MHz, $CDCl_3$) δ 5.44 – 5.15 (m, 4H), 3.61 – 3.38 (m, 1H), 3.15 – 2.92 (m, 3H), 2.47 – 2.21 (m, 4H), 2.02 – 1.72 (m, 8H), 1.55 – 1.01 (m, 53H), 0.81 (t, *J* = 6.8 Hz, 6H). ^{13}C NMR (126 MHz, $CDCl_3$) δ 129.93 (2C), 129.81 (2C), 56.11, 54.17, 44.79, 32.61 (2C), 31.90 (2C), 29.85 - 29.45 (17C), 29.31 (2C), 29.18, 28.84, 27.45, 27.21 (2C), 26.84, 24.11, 22.68 (2C), 14.11 (2C). HRMS (ESI $[M + H]^+$) m/z: calcd for ($C_{41}H_{81}N_2$) 601.63943, found 601.63925.

Synthesis of 64 ((*S*)-*tert*-butyl 2-(didodecylcarbamoyl)pyrrolidine-1-carboxylate

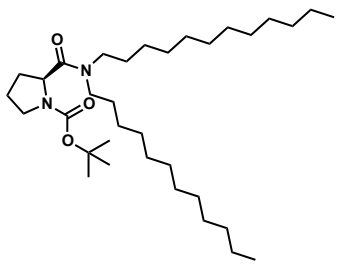

The title compound was synthesized according to the general procedure for the amide coupling. The crude product was purified by column chromatography (silica gel, cyclohexane/EtOAc 4:1). The solvent was evaporated to afford a slightly yellow oil (1.02 g, 1.85 mmol, 83 %). ^{1}H NMR (500 MHz, $CDCl_3$) δ 4.59 – 4.41 (m, 1H), 3.66 – 3.54 (m, 1H),

3.50 – 3.13 (m, 5H), 2.21 – 1.97 (m, 2H), 1.89 – 1.77 (m, 2H), 1.70 – 1.37 (m, 11H), 1.35 – 1.19 (m, 38H), 0.88 (td, *J* = 6.9, 2.1 Hz, 6H). ^{13}C NMR (125 MHz, $CDCl_3$) δ 172.17, 153.91, 79.52, 56.43, 56.09, 47.81, 46.86, 46.81, 46.53, 31.90 (2C), 31.36, 30.37, 29.61 (2C), 29.59, 29.58 (2C), 29.54 (2C), 29.32 (2C), 28.51 (3C), 27.90, 27.68, 27.02, 26.97, 24.20, 23.33, 22.67 (2C), 14.10 (2C). HRMS (ESI [M + H]$^+$) m/z: calcd for ($C_{34}H_{67}O_3N_2$) 551.51462, found 551.51505.

Synthesis of 65 ((*S*)-*N*,*N*-didodecylpyrrolidine-2-carboxamide)[54]

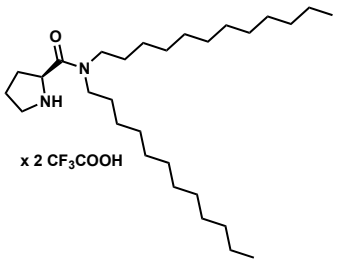

Catalyst 60 was obtained after Boc-deprotection of **59** according to the general procedure as a yellow oil in quantitative yield.
Analytical data according to Arivalagan *et al*.[54]

Synthesis of catalyst 27 ((*S*)-*N*-dodecyl-*N*-(pyrrolidin-2-ylmethyl)dodecan-1-amine)[56]

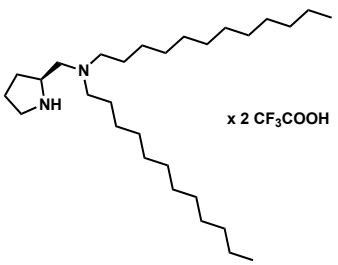

Catalyst **27** was synthesized according to the general procedure for the amide reduction from **60**. The crude product was purified by column chromatography (silica gel, cyclohexane/EtOAc 2:1) to afford the product as a slightly yellow oil (292 mg, 0.670 mmol, 63 %). ^{1}H NMR (500 MHz, $CDCl_3$) δ 3.60 (quint, *J* = 6.9 Hz, 1H), 3.29 – 3.12 (m, 2H), 2.60 – 2.25 (m, 6H), 2.19 – 1.52 (m, 1H), 1.48 – 1.09 (m, 6H), 0.81 (t, *J* = 6.9 Hz, 1H). ^{13}C NMR (126 MHz, $CDCl_3$) δ 60.34, 55.99, 54.16, 54.10, 45.29, 31.85 (2C), 29.55 (2C), 29.53 (2C), 29.42 (2C), 29.34 (2C), 29.30, 29.28 (2C), 29.05 (2C), 26.64 (2C), 23.73, 23.15, 22.64 (2C), 14.06 (2C). HRMS (ESI [M + H]$^+$) m/z: calcd for ($C_{29}H_{61}N_2$) 437.48293, found 437.48325.

2.5.1.4 Synthesis of substrates

Synthesis of 33 ((1*S*,2*S*)-1,2-bis((*R*)-2,2-dimethyl-1,3-dioxolan-4-yl)ethane-1,2-diol)[71]

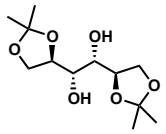

To a mixture of *D*-Mannitol (**32**) (20 g, 0.11 mol, 1 eq), 2,2-dimethoxypropane (32 ml, 0.26 mol, 2.4 eq) and glyme (50 mL), tin(II) chloride (20 mg, 0.1 mmol) was added and the mixture was heated to reflux until a clear solution was obtained (ca. 1 h). The solution was refluxed for another 30 min before cooling to room temperature. Pyridine (24 µl, 0.3 mmol) was added. The solvent was removed *in vacuo* the crude product was purified by flash chromatography (ethylacetate/cyclohexane 1:1 - pure ethylacetate) to obtain the desired product as colorless solid (15.7 g, 60 mmol, 54 %).
Analytical data were identical with the values reported in literature.[71]

Synthesis of 34 ((*R*)-2,2-dimethyl-1,3-dioxolane-4-carbaldehyde)[71]

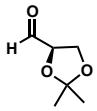

Diacetonide **33** (1 g, 4 mmol, 1.0 eq) was dissolved in CH_2Cl_2 (15 mL) and saturated aqueous $NaHCO_3$ (0.36 mL) was added to the flask. Solid $NaIO_4$, (1.6 g, 7.6 mmol, 1.9 eq) was subsequently added portion wise during a 20-min period while the reaction mixture was vigorously stirred. The reaction was allowed to proceed for 2 h while the temperature was kept below 30 °C by means of an ice bath. The white precipitate was filtered off and the solvent evaporated. The crude product was purified by bulb-to-bulb distillation (5 mbar, 100°C) to give aldehyde **34** as a colourless liquid (700 mg, 5.4 mmol, 67 %).
Analytical data were identical with the values reported in literature.[71]

Synthesis of 36 ((5-amino-2,2-dimethyl-1,3-dioxan-5-yl)methanol)[72]

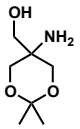

To a solution of tris(hy- droxymethyl)aminomethane hydrochloride (**35**) (20.0 g, 125 mmol, 1.0 eq.) in dry DMF (140 mL), PTSA (1.8 g, 6.0 mmol, 0.050 equiv) was added followed by 2,2-dimethoxypropane (16.9 mL, 138 mmol, 1.1 equiv) in one portion. After stirring the reaction mixture for 12 h, Et_3N (1.0 mL, 7.0 mmol, 0.060 equiv) was added. After 10 min, the mixture was concentrated and more Et_3N (13.7 mL, 98.0 mmol) and EtOAc (500 mL) was added. The white precipitate, which was formed after the addition of Et_3N was removed via filtration and the filtrate was purified by FC (ethylacetate/ MeOH 4:1) to afford the desired product as a white solid (17.4 g, 108 mmol, 86 %).
Analytical data were identical with the values reported in literature.[72]

Synthesis of 37 (2,2-dimethyl-1,3-dioxan-5-one)[72]

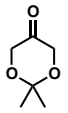

A solution of 5-amino-5-hydroxymethyl-2,2-dimethyl-1,3-dioxane (**36**) (9.7 g, 60 mmol, 1.0 eq) and KH_2PO_4 (8.2 g, 60 mmol, 1.0 eq) in water (200 mL) was cooled to 5°C and a solution of $NaIO_4$ (12.8 g, 60.0 mmol, 1.0 eq) in water (175 mL) was added via dropping funnel during a period of 30 min. After 3 h, the starting material was consumed and the reaction mixture was allowed to stir for another hour at 5 °C and 5 h at room temperature. Then $Na_2S_2O_3$ (14.8 g, 60.0 mmol, 1.0 equiv) was added, and the resulting solution was stirred for 15 min. The reaction mixture was extracted with CH_2Cl_2 (5 x 50 mL). The combined organic phases were dried over $MgSO_4$, filtered and concentrated. The crude product was purified by bulb-to-bulb distillation (5 mbar, 80°C) to afford the product as colorless oil (6.6 g, 51 mmol, 85 %).
Analytical data were identical with the values reported in literature.[72]

Synthesis of 39 (*D*-Glyceraldehyde 3-phosphate)[73]

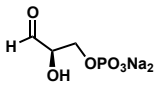

A solution of *D*-fructose 6-phosphate disodium salt (**38**) (5,0 g, 15.5 mmol, 1 eq) in water (150 mL) was cooled to 0°C and a solution of periodic acid (12.6 g, 109 mmol, 7 eq) in water (50 mL) was added dropwise. After 1 h, ethylene glycol (5 mL) was added and the solution stirred for 30 min, before the pH was adjusted to 3.5 using aqueous NaOH (2 M) and acetone (150 mL) was added, whereupon a white precipitate was formed, which was removed by filtration after 90 min. Subsequently, $Ca(OAc)_2$ (7.9 g, 43.5 mmol, 2.8 eq) in water (45 mL) was added. The suspension was stirred for 90 min at 0°C and the white solid was filtrated and washed with aceton, HCl (10 µM), HCl (1 mM) and again with acetone to obtain the product as white solid (1.8 g, 8.7 mmol, 56 %)
Analytical data were identical with the values reported in literature.[73]

Synthesis of aldehyde 4a

Synthesis of 41 (5-(1,3-dioxolan-2-yl)-2-nitrophenol)

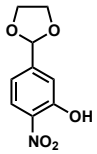

In a 50 mL round-bottom flask, 3-hydroxy-4-nitrobenzaldehyde (**40**) (1.49 g, 8.93 mmol, 1 eq) and ethylene glycol (0.75 mL 13.39 mmol, 1.5 eq) were dissolved in toluene (25 mL) and *p*TsOH (0.17 g, 0.89 mmol, 0.1 eq) was added. The apparatus was fitted with a Dean-Sark water trap and the solution heated to reflux. The solution was stirred under reflux overnight. After purification by column chromatography (9:1:1 cyclohexane/EtOAc/MeOH) the product was obtained in quantitative yield (1.85 g, 8.93 mmol). ^{1}H NMR (400 MHz, $CDCl_3$) δ 10.59 (s, 1H), 8.11 (d, *J* = 8.8 Hz, 1H), 7.27 (d, *J* = 6.5 Hz, 1H), 7.09 (d, *J* = 10.4 Hz, 1H), 5.82 (s, 1H), 4.07 (d, *J* = 38.4 Hz, 4H). ^{13}C NMR (101 MHz, $CDCl_3$) δ 155.06, 148.35, 133.67, 125.31, 118.14, 117.85, 101.87, 65.45. HRMS (ESI [M - H]$^-$) m/z: calcd for ($C_9H_8O_5N$) 210.04080, found 210.04059.

Synthesis of 42 (2-(5-(1,3-dioxolan-2-yl)-2-nitrophenoxy)ethanol (modified procedure of Lepore *et al.*[74])

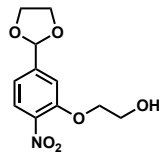

Acetal **41** (1.85 g, 8.76 mmol, 1 eq) and PPh_3 (2.98 g, 11.39 mmol, 1.3 eq) was dissolved in THF (20 ml). Upon dropwise addition of diisopropylazodicarboxylate (DIAD) (2.30, 2.24 ml, 11.39 mmol, 1.3 eq) a red precipitate was formed. Addition of ethylene glycol (0.70 g, 0.63 mL, 11.39 mmol, 1.3 eq) led to a red solution. The reaction mixture was heated to 55 °C and stirred for 3 h. The product was obtained after purification by column chromatography (cyclohexane/EtOAC 1:1) in 46 % yield (1.03 g, 4.04 mmol). ^{1}H NMR (400 MHz, $CDCl_3$) δ 7.87 (d, *J* = 8.3 Hz, 1H), 7.26 (s, 1H), 7.23 (d, *J* = 1.5 Hz, 1H), 7.16 (dd, 1H), 5.83 (s, 1H), 4.28 – 4.25 (m, 2H), 4.12 – 4.03 (m, 4H), 4.00 – 3.96 (m, 2H). ^{13}C NMR (101 MHz, $CDCl_3$) δ 152.29, 144.99, 139.93, 125.96, 118.88, 112.98, 102.06, 71.44, 65.40, 60.93. HRMS (ESI $[M + Na]^+$) m/z: calcd for ($C_{11}H_{13}O_6NNa$) 278.06351, found 278.06344.

Synthesis of 4a (3-(2-hydroxyethoxy)-4-nitrobenzaldehyde)

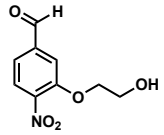

To a solution of **42** (427.0 mg, 1.68 mmol, 1 eq) in a mixture of acetone/water 9:1 (10 mL), *p*TsOH (63.5 mg, 0.34 mmol, 0.2 eq) was added. The reaction mixture was heated to 55 °C and stirred overnight. The mixture was diluted by addition of EtOAc (20 ml) and extracted with $NaHCO_3$ (3x20 mL). The combined organic phases were washed with brine (20 mL), dried over $MgSO_4$ and the solvent removed *in vacuo*. Aldehyde **4a** was obtained as a yellow solid in quantitative yield. ^{1}H NMR (400 MHz, $CDCl_3$) δ 10.05 (s, 1H), 7.97 (d, *J* = 8.1 Hz, 1H), 7.62 (d, *J* = 1.5 Hz, 1H), 7.58 (dd, 1H), 4.35 – 4.31 (m, 2H), 4.05 – 3.99 (m, *J* = 19.8 Hz, 2H). ^{13}C NMR (126 MHz, $CDCl_3$) δ 188.47, 150.84, 141.93, 138.29, 124.58, 121.32, 112.70, 70.19, 59.27. HRMS (EI $[M]^+$) m/z: calcd for ($C_9H_9O_5N$) 211.04752, found 211.04766.

Synthesis of 61 (2-(5-(1,3-dioxolan-2-yl)-2-nitrophenoxy)ethyl bis((9*H*-fluoren-9-yl)methyl) phosphate)

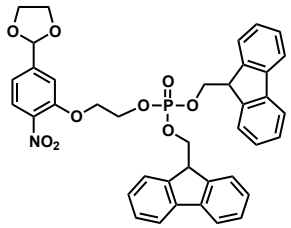

Fm-phosphoramidite (266 mg, 0.51 mol, 1.3 eq) was coevaporated with MeCN (3 x 1 mL). Pentafluorophenol (361 mg, 1.96 mmol, 5 eq) and MeCN (3 mL) was added and the mixture stirred at room temperature for 1 h. After complete acitivation, which was monitored by ^{31}P-NMR, the solvent was removed on high vacuum. A solution of **42** (100 mg, 0.39 mmol, 1 eq) in MeCN (3 mL) was added ant the reaction stirred over night at room temperature. Upon complete consumption of starting material (monitored by ^{31}P-NMR), the reaction mixture was cooled to 0°C and *m*CPBA (70 %, 125 mg, 0.51 mmol, 1.3 eq.) was added. The crude product was purified by column chromatography (EtOAc/Chex) and the product was obtained as slightly yellow oil (169 mg, 0.25 mmol, 62 %). ^{1}H NMR (400 MHz, $CDCl_3$) δ 7.83 – 6.99 (m, 1H), 5.68 (s, 1H), 4.32 – 4.12 (m, 1H), 4.10 – 4.02 (m, 1H), 3.98 – 3.86 (m, 1H), 1.96 (d, J = 8.0 Hz, 1H), 1.26 – 1.13 (m, 1H). ^{13}C NMR (101 MHz, $CDCl_3$) δ 170.04, 150.62, 143.66, 142.09, 142.05, 140.39, 140.38, 139.39, 134.03, 126.83, 126.12, 126.11, 124.61, 124.11, 124.08, 118.93, 118.92, 118.07, 112.04, 101.04, 70.52, 68.32, 68.27, 67.59, 67.53, 64.23, 64.19, 59.91, 59.33, 46.95, 46.89, 44.68, 28.68, 19.97, 13.18, 7.47. ^{31}P {^{1}H} NMR (162 MHz, $CDCl_3$) δ -0.71. HRMS (ESI [M + Na]$^{+}$) m/z: calcd for ($C_{39}H_{35}O_9N$) 692.20439, found 692.20475.

2.5.1.5 Towards substrates for intramolecular aldol reactions

Synthesis of 43 (3-bromo-6-nitroisobenzofuran-1(3*H*)-one)[76]

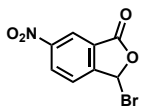

In a 50 mL round bottom flask, 6-nitroisobenzofuran-1(3*H*)-one (**42**) (896 mg, 5.0 mmol, 1.0 eq) was dissolved in benzene (20 mL). *N*-bromosuccinimide (890 mg, 5.0 mmol, 1.0 eq) and AIBN (41.0 mg, 0.25 mmol, 0.05 eq) were added and the reaction mixture was refluxed for 2 h. The reaction mixture was cooled to 0°C and stirred for 1 h before it was filtered and

the filtrate concentrated under reduced pressure. The crude product was purified by flash chromatography (cyclohexane/ ethylacetate 9:1) to give 3-bromo-6-nitroisobenzofuran-1(3H)-one as a colourless oil (839 mg, 3.25 mmol, 65 %).
Analytical data were identical with the values reported in literature.[76]

Synthesis of 44 (2-formyl-5-nitrobenzoic acid)[76]

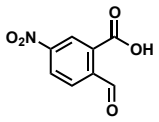

A round bottom flask with 3-bromo-6-nitroisobenzofuran-1(3H)-one (**43**) (100 mg, 0.4 mmol, 1.0 eq) and water (10 mL) was prepared and the suspension was stirred at reflux for 1 h. The resulting solution was cooled to room temperature and ethylacetate (10 ml) was added and the phases were separated. The aqueous phase was extracted with EtOAc (3 × 10 mL), the combined organic phases were dried over $MgSO_4$. The solvent was evaporated to give 2-formyl-5-nitrobenzoic acid (**44**) in quantitative yield.
Analytical data were identical with the values reported in literature.[76]

Synthesis of 55 (2-(1,3-dioxolan-2-yl)-5-nitrobenzoic acid)

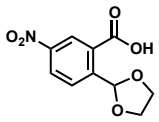

In a 50 mL round-bottom flask, 2-formyl-5-nitrobenzoic acid (**44**) (1.74 g, 8.93 mmol, 1 eq) and ethylene glycol (0.75 mL 13.39 mmol, 1.5 eq) were dissolved in toluene (25 mL) and *p*TsOH (0.17 g, 0.89 mmol, 0.1 eq) was added. The apparatus was fitted with a Dean-Sark water trap and the solution heated to reflux. The solution was stirred under reflux overnight. After purification by column chromatography (9:1 – 7:3 EtOAc/MeOH) the product was obtained in quantitative yield (2.13 g, 8.93 mmol). ^{1}H NMR (400 MHz, Chloroform-*d*) δ 8.65 (d, *J* = 2.0 Hz, 1H), 8.53 (dd, *J* = 8.3, 2.0 Hz, 1H), 7.76 (dt, *J* = 8.3, 0.5 Hz, 1H), 6.46 (s, 1H), 4.10 – 3.91 (m, 2H), 3.83 (dd, *J* = 5.1, 3.8 Hz, 2H).

2.5.1.6 Synthesis of nornicotine as reference catalyst

Synthesis of 55 (ethyl 5-bromonicotinate)[77]

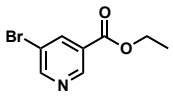

To a solution of acid **54** (2.0 g, 10 mmol, 1 eq), DCC (2.06 g, 10 mmol, 1 eq) followed by DMAP (1.22 g, 10 mmol, 1 eq.) at 0°C. The solution was stirred for 1 h and EtOH (0.92 g, 20 mmol, 2 eq) was added dropwise during a period of 10 min. The reaction mixture was stirred for 3 d at room temperature, then CH_2Cl_2 was added and the mixture was washed with a solution of saturated $NaHCO_3$. The organic phase was separated and the aqueous phase extracted with DCM and the combined organic phase was washed with brine and dried over MgSO4. The solvent was evaporated under vacuo and the crude product was purified by column chromatography (cyclohexane/EtOAc 8:2) to give pure ester **55** (1.7 g, 7.5 mmol, 75 %). ^{1}H NMR (400 MHz, $CDCl_3$) δ 9.12 (s, 1H), 8.83 (s, 1H), 8.43 (s, 1H), 4.44 (d, *J* = 7.1 Hz, 2H), 1.42 (d, *J* = 7.1 Hz, 3H). ^{13}C NMR (101 MHz, $CDCl_3$) δ 164.02, 154.42, 148.85, 139.48, 127.66, 120.58, 61.91, 14.23. HRMS (ESI [M + H]$^+$) m/z: calcd for ($C_8H_9O_2NBr$) 229.01583, found 229.01568.
Analytical data were identical with the values reported in literature.[77]

Synthesis of 56 (3-bromo-5-(3,4-dihydro-2*H*-pyrrol-5-yl)pyridine)[77]

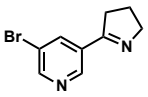

Sodium hydride (277 mg of a 60% dispersion in mineral oil, 6.92 mmol, 1.33 eq) in a 50 mL flask was washed with three portions of THF (10 mL). Then THF was added (25 mL) and a solution of ethyl 5- bromonicotinate (**fd**) (1.2 g, 5.2 mmol,1.0 eq.) and *N*-vinylpyrrolidinone (642 mg, 5.8 mmol, 1.1 eq.) in THF (10 mL) was added. After 10 min, an exothermic reaction started and gas formation was observed. The reaction mixture was allowed to stir for 1 h room temperature before it was heated up to reflux for 1 h and cooled to room temperature again. Conc. HCl (3 mL), diluted with H_2O (5 mL), was added and THF was evaporated. Additional HCl conc. (5 mL) and H_2O (10 mL) were added. The mixture was refluxed for 16 h. The solution was cooled to 0°C and concentrated aqueous NaOH (50 mL) was added. The crude product precipitated and the mixture was extracted with CH_2Cl_2 (3 x 50 mL). The combined organic phases were washed with H_2O (20 mL), the solvent evaporated and the crude product

purified by a bulb-to-bulb distillation (130°C, 3 mbar) to obtain the product as a yellow oil (772 mg, 3.43 mmol, 66 %). ^{1}H NMR (500 MHz, $CDCl_3$) δ 8.87 (s, 1H), 8.70 (s, 1H), 8.36 (s, 1H), 5.29 (s, 2H), 4.09 (t, *J* = 7.4 Hz, 2H), 2.93 (t, *J* = 8.2 Hz, 2H), 2.19 – 2.00 (m, 2H). ^{13}C NMR (126 MHz, $CDCl_3$) δ 169.97, 152.21, 147.04, 137.24, 131.61, 120.92, 61.62, 53.36, 34.82, 22.53. HRMS (ESI [M + H]$^{+}$) m/z: calcd for ($C_9H_{10}N_2Br$) 226.07127, found 226.07093. Analytical data were identical with the values reported in literature.[77]

Synthesis of 57 (3-bromo-5-(pyrrolidin-2-yl)pyridine)[77]

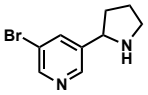

To a solution of 5-bromomyosmine (1.0 g, 4.4 mmol, 1 eq) in 10 mL methanol/acetic acid (8:2) at -40°C, $NaBH_4$ (0.38 g, 10.1 mmol, 2.3 eq) was added portionwise over a period of 10 min. The reaction temperature increased during the course of the addition to -20 °C. After the addition, the reaction mixture was allowed to warm to room temperature. The solvent was evaporated and aqueous NaOH (2 M, 25 mL) was added and extracted with CH_2Cl_2 (3 x 20 mL). The combined organic phases were washed with brine (20 mL) dried over $MgSO_4$ and the solvent evaporated. The crude product was purified by flash chromatography (pure ethylacetate) to obtain racemic bromo-nornicotine (**57**) as yellow oil (790 mg, 3.48 mmol, 79 %). ^{1}H NMR (500 MHz, $CDCl_3$) δ 8.42 (d, 1H), 8.39 (s, 1H), 7.81 (s, 1H), 4.08 (t, *J* = 7.6 Hz, 1H), 3.13 – 2.90 (m, 2H), 2.24 – 2.06 (m, *J* = 70.8 Hz, 1H), 1.93 (s, 1H), 1.88 – 1.70 (m, 2H), 1.60 – 1.48 (m, 1H). ^{13}C NMR (126 MHz, $CDCl_3$) δ 147.59, 145.20, 141.35, 135.17, 119.30, 57.74, 45.46, 33.12, 24.05. ESI [M + H]$^{+}$) m/z: calcd for ($C_9H_{12}N_2Br$) 227.01756, found 227.01785. Analytical data were identical with the values reported in literature.[77]

X-ray structure of 57a ((*R*)-3-bromo-5-(pyrrolidin-2-yl)pyridine)[77]

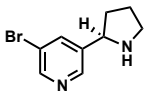

The racemic mixture of 3-bromo-5-(pyrrolidin-2-yl)pyridine) (**57**) was resolved according to a reported procedure to obtain (*R*)-3-bromo-5-(pyrrolidin-2-yl)pyridine (-)MTPA salt. After filtration and washing, the crystalline salt was obtained. The crystal was determined by single crystal X-ray diffraction. (*R*)-3-bromo-5-(pyrrolidin-2-yl)pyridine (**57a**) was liberated from

the (-) MTPAsalt with K_2CO_3 according to a reported procedure. $[\alpha]_D$: 31° (3.8 mM, EtOH, 20°C). Analytical data were identical with the values reported in literature.[77]

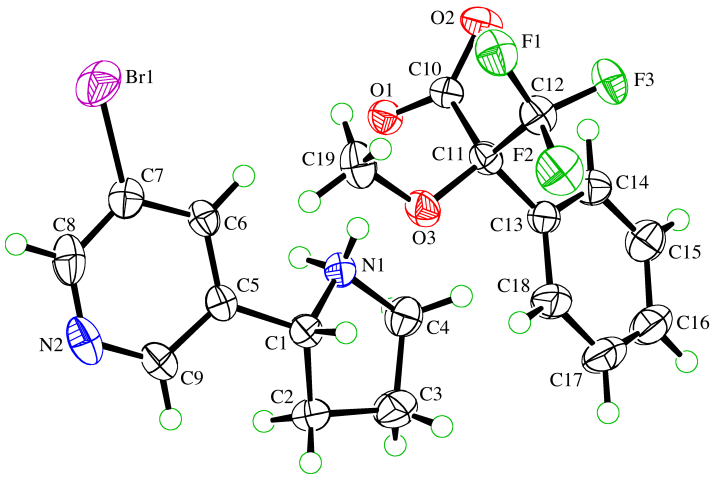

Figure 10: ORTEP representation of **57a** (50% probability ellipsoids; H-atoms given arbitrary displacement parameters for clarity).

The structure of **57a** has been solved and refined successfully with no unusual features. The compound in the crystal is enantiomerically pure and the absolute configuration of the ions has been determined independently by the diffraction experiment. The anion has the expected *S*-configuration and the cation has the *R*-configuration. The optical resolution of the cation has thus been successful. The ammonium group forms hydrogen bonds with a carboxylate O-atom from each of two neighboring anions.

A crystal of **57a**, obtained from EtOAc, was mounted on a glass fibre and used for a low-temperature X-ray structure determination. All measurements were made on a *Rigaku Oxford Diffraction SuperNova* area-detector diffractometer using Cu $K\alpha$ radiation (λ = 1.54184 Å) from a micro-focus X-ray source and an *Oxford Instruments Cryojet XL* cooler. The unit cell constants and an orientation matrix for data collection were obtained from a least-squares refinement of the setting angles of 12617 reflections in the range 9° < 2θ < 153°. A total of 1809 frames were collected using ω scans with κ offsets, 2.0-15.0 seconds exposure time and a rotation angle of 19.0° per frame, and a crystal-detector distance of 55.0 mm.

X-ray structure of 57b ((*S*)-3-bromo-5-(pyrrolidin-2-yl)pyridine)[77]

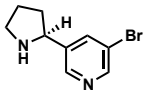

The racemic mixture of 3-bromo-5-(pyrrolidin-2-yl)pyridine) (**57**) was resolved according to a reported procedure to obtain (*R*)-3-bromo-5-(pyrrolidin-2-yl)pyridine (+)MTPA salt. After filtration and washing, the crystalline salt was obtained. The crystal was determined by single crystal X-ray diffraction. (*S*)-3-bromo-5-(pyrrolidin-2-yl)pyridine (**57a**) was liberated from the (+) MTPA salt with K_2CO_3 according to a reported procedure. $[\alpha]_D$: -67° (3.8 mM, EtOH, 20°C). Analytical data were identical with the values reported in literature.[77]

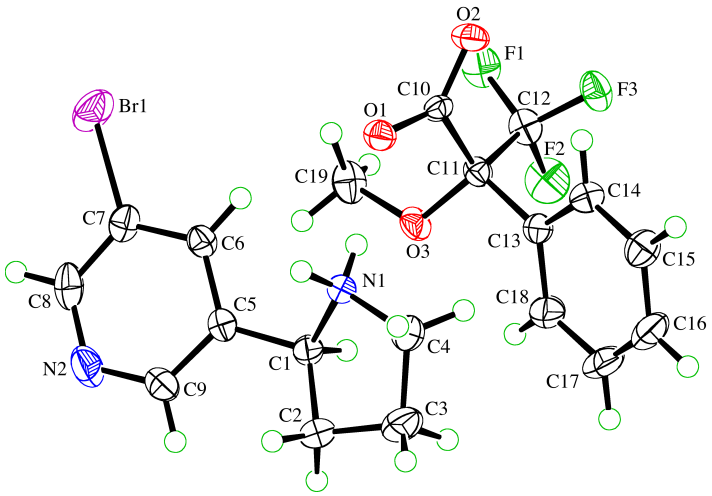

Figure 11: ORTEP representation of **57b** (50% probability ellipsoids; H-atoms given arbitrary displacement parameters for clarity).

The crystal structure of **57b** was obtained according to the above described procedure for **57a**.

Synthesis of 58a and 58b (*R*-nornicotine and *S*-nornicotine)

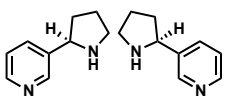

A solution of the corresponding bromo-nornicotine **57a** or **57b** (100 mg, 0.44 mmol, 1.0 eq) and THF (8 mL) was cooled to -78°C. By means of a syringe *n*-BuLi 2.5 M in hexane (0.35 mL, 0.88 mmol, 2.0 eq.) were added whereupon the color changed from brown to yellow. The solution was stirred for 5 min and water (0.1 mL) was added. The reaction mixture

was allowed to stir for 4 h at -78°C before it was quenched. The aqueous phase was extracted with DCM (3 x 30 mL), the combined organic phases were dried over $MgSO_4$, the solvent evaporated and the crude product was purified by flash chromatography (ethylacetate/hexane 1:1) to get pure nornicotine in quantitative yield.
Analytical data were identical with the values reported in literature.[77]

Synthesis of 59 (*tert*-butyl 2-(5-bromopyridin-3-yl)pyrrolidine-1-carboxylate)

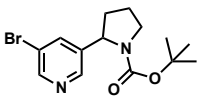

To a solution of **57** (1 g, 4.4 mmol, 1 eq) and TEA (1.24 mL, 8.93 mmol) in CH_2Cl_2 (20 mL) $(Boc)_2O$ (0.96 g, 4.4 mmol, 1 eq) was added. The reaction mixture was stirred overnight at room temperature. Water (20 mL) was added and extracted with CH_2Cl_2 (2 x 20 mL). The combined organic phases were washed with brine, dried over $MgSO_4$, and concentrated *in vacuo*. The crude product was purified by flash chromatography (pure ethylacetate and 1% NEt_3) to the pure product as a yellow oil. ^{1}H NMR (400 MHz, $CDCl_3$) δ 8.54 (s, 1H), 8.38 (d, *J* = 1.8 Hz, 1H), 7.63 (s, 1H), 4.99 – 4.84 (m, 1H), 4.83 – 4.66 (m, 1H), 3.70 – 3.51 (m, 2H), 2.48 – 2.24 (m, 1H), 1.97 – 1.76 (m, *J* = 23.9, 18.1 Hz, 3H), 1.44 (s, 4H), 1.25 (s, 8H). ^{1}H NMR (400 MHz, $CDCl_3$) δ 8.57 (s, 1H), 8.41 (d, *J* = 1.8 Hz, 1H), 7.66 (s, 1H), 4.94 (b-m, 1H), 4.77 (b-m, 1H), 3.72 – 3.52 (m, 2H), 2.46 – 2.33 (m, 1H), 2.01 – 1.80 (m, 3H), 1.47 (s, 4H), 1.25 (s, 6H). LRMS (ESI $[M + H]^+$) m/z: for ($C_{14}H_{20}O_2N_2Br$) 327.07.

2.5.1.7 Synthesis of aldol products using catalytic LCPs and cubosomes

Synthesis of 5a (*anti*-isomer) ((*S*)-2-((*R*)-hydroxy(3-(2-hydroxyethoxy)-4-nitrophenyl) methyl)cyclohexanone)

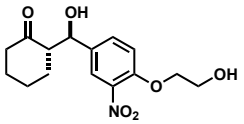

Synthesized according to the general procedure for the aldol reaction using catalytic LCPs or catalytic cubosomes. *Anti*-aldol product **5a** was obtained after purification by column chromatography (EtoAc). ^{1}H NMR (500 MHz, $CDCl_3$) δ 7.76 (dd, *J* = 10.3, 4.7 Hz, 1H), 7.04 (s, 1H), 6.87 (d, *J* = 8.3 Hz, 1H), 4.73 (d, *J* = 8.2 Hz, 1H), 4.24 – 4.09 (m, 2H), 4.06 – 3.81 (m, 2H), 2.56 – 2.19 (m, 3H), 2.09 – 1.96 (m, 1H), 1.75 (d, *J* = 12.9 Hz, 1H), 1.67 – 1.37 (m, 3H), 1.37 – 1.10 (m, 1H). ^{13}C NMR (126 MHz, $CDCl_3$) δ 214.67, 152.48, 148.50, 139.03, 125.73, 119.53, 113.48, 74.05, 71.41, 60.95, 57.20, 42.66, 30.76, 27.62, 24.69. HRMS (ESI [M + Na]$^+$) m/z: calcd for ($C_{15}H_{19}O_6NNa$) 332.11046, found 332.11037.

Synthesis of 5a (*syn*-isomer) ((*R*)-2-((*R*)-hydroxy(3-(2-hydroxyethoxy)-4-nitrophenyl)methyl)cyclohexanone and (*S*)-2-((*S*)-hydroxy(3-(2-hydroxyethoxy)-4-nitrophenyl)methyl)cyclohexanone)

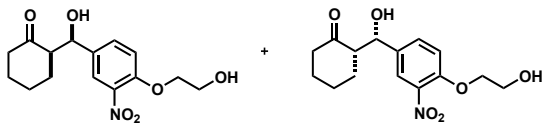

Synthesized according to the general procedure for the aldol reaction using catalytic LCPs or catalytic cubosomes. *Syn*-aldol product **5a** was obtained after purification by column chromatography (EtoAc). ^{1}H NMR (500 MHz, $CDCl_3$) δ 7.78 (d, *J* = 8.4 Hz, 1H), 7.07 (s, 1H), 6.82 (d, *J* = 8.4 Hz, 1H), 5.37 – 5.30 (m, 1H), 4.18 (t, *J* = 4.2 Hz, 2H), 3.96 – 3.87 (m, 2H), 3.08 (s br, OH), 2.56 – 2.46 (m, 1H), 2.43 – 2.37 (m, 1H), 2.35 – 2.27 (m, 1H), 2.07 – 1.99 (m, 1H), 1.82 – 1.75 (m, 1H), 1.68 – 1.40 (m, 4H). ^{13}C NMR (126 MHz, $CDCl_3$) δ 214.06, 152.51, 149.32, 138.04, 125.86, 117.81, 112.74, 71.39, 69.95, 60.96, 56.73, 42.60, 27.85, 25.95, 24.78. HRMS (ESI [M + Na]$^+$) m/z: calcd for ($C_{15}H_{19}O_6NNa$) 332.11046, found 332.11037.

Synthesis of 5b (*anti*-isomer) ((*S*)-2-((*R*)-hydroxy(phenyl)methyl)cyclohexanonen)

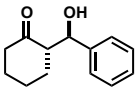

Synthesized according to the general procedure for the aldol reaction using catalytic LCPs or catalytic cubosomes. *Anti*-aldol product **5b** was obtained after purification by column chromatography (Chex/EtoAc 9:1). ^{1}H NMR (500 MHz, $CDCl_3$) δ 7.30 – 7.20 (m, 5H), 4.72 (dd, *J* = 8.8, 2.5 Hz, 1H), 3.87 (d, *J* = 2.7 Hz, 1H), 2.59 – 2.51 (m, 1H), 2.44 – 2.38 (m, 1H), 2.33 – 2.25 (m, 1H), 2.05 – 1.98 (m, 1H), 1.75 – 1.68 (m, 1H), 1.65 – 1.42 (m, 3H), 1.28 – 1.17 (m, 1H). ^{13}C NMR (126 MHz, $CDCl_3$) δ 215.52, 140.94, 128.37 (2C), 127.89, 127.02 (2C), 74.77, 57.45, 42.69, 30.86, 27.81, 24.75. HRMS (ESI $[M + Na]^+$) m/z: calcd for ($C_{13}H_{16}O_2Na$) 227.10425, found 227.10402.

Synthesis of 5b (syn-isomer) ((*R*)-2-((*R*)-hydroxy(phenyl)methyl)cyclohexanone and (*S*)-2-((*S*)-hydroxy(phenyl)methyl)cyclohexanone)

Synthesized according to the general procedure for the aldol reaction using catalytic LCPs or catalytic cubosomes. *Syn*-aldol product **5b** was obtained after purification by column chromatography (Chex/EtoAc 9:1). ^{1}H NMR (500 MHz, $CDCl_3$) δ 7.30 – 7.21 (m, 4H), 7.20 – 7.15 (m, 1H), 5.32 (s, 1H), 2.96 (d, *J* = 3.1 Hz, 1H), 2.57 – 2.49 (m, 1H), 2.41 – 2.35 (m, 1H), 2.35 – 2.25 (m, 1H), 2.05 - 197 (m, 1H), 1.81 – 1.72 (m, 1H), 1.71 – 1.54 (m, 3H), 1.49 – 1.38 (m, 1H). ^{13}C NMR (126 MHz, $CDCl_3$) δ 214.85, 141.42, 128.15 (2C), 126.97, 125.74 (2C), 70.61, 57.18, 42.68, 27.96, 26.00, 24.88. HRMS (ESI $[M + Na]^+$) m/z: calcd for ($C_{13}H_{16}O_2Na$) 227.10425, found 227.10402.

Synthesis of 5c (*anti*-isomer) ((*S*)-2-((*R*)-hydroxy(3-(2-hydroxyethoxy)phenyl)methyl)cyclohexanone)

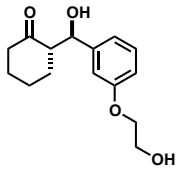

Synthesized according to the general procedure for the aldol reaction using catalytic LCPs or catalytic cubosomes. *Anti*-aldol product **5c** was obtained after purification by column chromatography (EtoAc). 1H NMR (500 MHz, $CDCl_3$) δ 7.21 – 7.15 (m, 1 H), 6.87 – 6.81 (m, 2H), 6.78 (dd, J = 8.2, 2.0 Hz, 1H), 4.69 (d, *J* = 8.7 Hz, 1H), 4.05 – 4.01 (m, 2H), 3.91 – 3.87 (m, 2H), 2.56 – 2.45 (m, 1H), 2.44 – 2.36 (m, 1H), 2.34 – 2.24 (m, 1H), 2.06 – 1.98 (m, 1H), 1.87 – 1.39 (m, 4H), 1.28 – 1.16 (m, 1H). ^{13}C NMR (126 MHz, $CDCl_3$) δ 215.44, 158.76, 142.70, 129.41, 119.99, 113.96, 113.15, 74.66, 69.15, 61.51, 57.40, 42.69, 30.86, 27.79, 24.75. HRMS (ESI $[M + Na]^+$) m/z: calcd for ($C_{15}H_{20}O_4Na$) 287.12538, found 287.12524.

Synthesis of 5c (*syn*-isomer) ((*R*)-2-((*R*)-hydroxy(3-(2-hydroxyethoxy)phenyl)methyl)cyclohexanone and (*S*)-2-((*S*)-hydroxy(3-(2-hydroxyethoxy)phenyl)methyl)cyclohexanone)

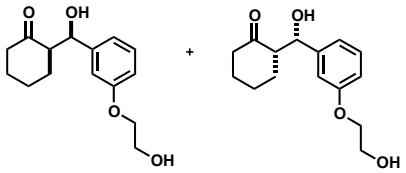

Synthesized according to the general procedure for the aldol reaction using catalytic LCPs or catalytic cubosomes. *Syn*-aldol product **5c** was obtained after purification by column chromatography (EtoAc). ^1H NMR (500 MHz, $CDCl_3$) δ 7.23 – 7.12 (m, 1H), 6.85 (s, 1H), 6.80 (d, *J* = 7.6 Hz, 1H), 6.73 (dd, *J* = 8.1, 2.2 Hz, 1H), 5.29 (s, 1H), 4.07 – 3.98 (m, 2H), 3.95 – 3.85 (m, 2H), 2.98 (d, *J* = 2.5 Hz, 1H), 2.55 – 2.49 (m, 1H), 2.41 – 2.35 (m, 1H), 2.34 – 2.26 (m, 1H), 2.15 – 1.95 (m, 2H), 1.81 – 1.74 (m, 1H), 1.72 – 1.54 (m, 2H), 1.50 – 1.39 (m, 1H), 1.25 – 1.08 (m, 1H). ^{13}C NMR (126 MHz, $CDCl_3$) δ 214.73, 158.63, 143.34, 129.23, 118.39, 112.92, 112.17, 70.38, 69.10, 61.47, 57.14, 42.64, 27.91, 26.01, 24.85. HRMS (ESI $[M + Na]^+$) m/z: calcd for ($C_{15}H_{20}O_4Na$) 287.12538, found 287.12524.

2.5.2 Preparation of catalytic LCPs

MO (and in case of LCP C cholesterol) was weight into a pyrex glass tube and the corresponding amount of a catalyst stock-solution (catalyst in CH_2Cl_2) was added to obtain a homogeneous lipid mixture. The solvent was evaporated (at high vacuum 10^{-2} mbar for 24 h) and the lipidic mixture subsequently hydrated by adding appropriate volumes of buffer and mixed. To obtain homogeneous catalytic LCPs, samples were centrifuged in a Heraeus Megafuge 16R centrifuge (at 5 000 rpm) for 1 h at 23 °C. Samples were finally stored and left to equilibrate for 48 h in tightly closed glass tubes.

LCP A: 0.0071 mmol catalyst (3.4 mg in case of catalyst **2**), 66.6 mg MO, 53 µl PBS 1X, pH 7.4.

LCP B: 0.0071 mmol catalyst (3.4 mg in case of catalyst **2**), 66.6 mg MO, 60 µl HEPES 20 mM, pH 7.4.

LCP C: 0.0071 mmol catalyst (3.4 mg in case of catalyst **2**), 50.0 mg MO, 10 mg Cholesterol, 63 µl HEPES 20 mM, pH 7.4.

PT LCPs: 0.0071 mmol catalyst (4.5 mg in case of catalyst **2**), 70 mg PT, 30 µl PBS 1X, pH 7.4.

2.5.3 Preparation of catalytic cubosomes

MO (and in case of LCP C cholesterol) was weight into a glass vial and the corresponding amount of a catalyst stock-solution (catalyst in CH_2Cl_2) was added to obtain a homogeneous lipid mixture. The solvent was evaporated (at high vacuum 10^{-2} mbar for 24 h) and the lipidic mixture subsequently hydrated by adding appropriate volumes of stabilizer containing buffer (PF108, 1.65 mg / mL) to obtain the cubosome sample with the desired lipid concentration. The sample was vortex-mixed and then dispersed using an ultrasonic processor Brenson digital 250 (cycle 0.9 s on/ 0.9 s off, amplitude 50%, for 3 x 5 min). Subsequently, the cubosome dispersion was filtered through Acrodisc 450 nm filters.

Cubosomes A: 0.0071 mmol catalyst (3.4 mg in case of catalyst **2**), 66.6 mg MO, 2 mL PBS 1X, pH 7.4.

Cubosomes B: 0.0071 mmol catalyst (3.4 mg in case of catalyst **2**), 66.6 mg MO, 2 mL HEPES 20 mM, pH 7.4.

Cubosomes C: 0.0071 mmol catalyst (3.4 mg in case of catalyst **2**), 50.0 mg MO, 10 mg Cholesterol, 2 mL HEPES 20 mM, pH 7.4.

Cubosomes D: 0.0071 mmol catalyst (3.4 mg in case of catalyst **2**), 66.6 mg MO, 2 mL PBS 0.1X, pH 7.4.

2.5.4 Dynamic Light Scattering (DLS)

Particle size of the cubosomes was performed after preparation, before the reaction was started, and after the reaction was terminated (1-2 d) with a Zeta Sizer Nano ZS (Malvern Instruments, Malvern, UK) at 25 ± 0.1 °C. The samples were measured in disposable polystyrene cuvettes of 1 cm optical path length with the corresponding buffer as solvent. Scattering angle was 90°. A triplicate of the samples was performed. The width of the DLS hydrodynamic diameter distribution is indicated by PDI (polydispersion index). The intensity size distribution of the cubosomes was typically unimodal; therefore the autocorrelation function was analyzed according to the cumulant method.

Table 6: DLS data before and after the aldol reaction.

Cubosomes	phase identity	size (nm) before reaction	PDI before reaction	size (nm) after reaction	PDI after reaction
A	Im3m	177 ± 2	0.19	161± 2	0.20
B	Pn3m	174.4 ± 2	0.17	246.1 ± 5	0.28
C	Pn3m/Im3m	133.2 ± 1	0.17	139.7±14	0.31
D	Pn3m	234.9 ± 3	0.20	244 ± 2	0.26

2.5.5 Small angle X-ray scattering (SAXS)

SAXS measurements were used to identify the symmetry of the catalytic LCPs and cubosomes and the fully hydration line of the catalytic LCPs. Experiments were performed on a Bruker AXS Micro, with a microfocused X-ray source, operating at voltage filament current of 50 kV and 1.000 μA, respectively. The Cu Kα radiation (λCu Kα =1.5418 Å) was collimated by a 2D Pilatus 100K detector. The scattering vector q = (4π/λ)sinθ, with 2θ being the scattering angle, was calibrated using silver behenate. Data were collected and azimuthally averaged using the Saxsgui software to yield one-dimensional intensity versus scattering vector *q*, with a *q* range from 0.004 – 0.5 $Å^{-1}$. For all bulk measurements, the samples were placed inside a stainless-steel cell between two thin replaceable mica sheets and sealed by an O-ring, with a sample volume of 10 μL and a thickness of ~1 mm. Measurements were performed at 23°C, and samples were equilibrated for 15 min before measurements, whereas scattered intensity was collected over 30 min. For the cubosomes samples, the sample-to-detector distance was 1 m, providing a q range from 0.005 to 0.77 $Å^{-1}$. Samples were loaded into a quartz glass capillary (Hiligenberg, length: 80 mm; outside: 2.0 mm; wall thickness: 0.01 mm). Measurements were performed at 23 °C, and samples were equilibrated for 10 min prior to measurements, while scattered intensity was collected over 4 hours.

Mesophase identification and calculation of the aqueous channels

Mesophases were identified by their specific Bragg peak positions. For the double diamond cubic phase (*Pn3m*) the relative positions in *q* of the Bragg reflections are at √2:√3:√4:√6:√8:√9…, whereas for the primitive cubic phase (*Im3m*) the Bragg peaks are at q = √2:√4:√6:√8:√10:√12:√14:√16:√18… The mean lattice parameter, a, was deduced from the corresponding set of observed interplanar distances, d (d = 2π/*q*), using the appropriate scattering law for the phase structure. For cubic phases:

$$a = d\sqrt{h^2 + k^2 + l^2} \qquad (1)$$

By knowing from SAXS measurements the geometry and the lattice parameter a, and knowing the lipid volume fraction of the sample ϕ, the length of the lipid tail, *l,* can be calculated by solving the following cubic equation[80]:

$$\Phi = 2A_0\left(\frac{L_{lip}}{a}\right) + \frac{4}{3}\pi\chi\left(\frac{L_{lip}}{a}\right)^3 \qquad (2)$$

where A_0 is the area of the surface in the unit cell in which the lattice parameter is equal to unity, and χ is the Euler-Poincare characteristic. Depending on the specific cubic phase they have the following values: $A_0 = 3.091$ and $\chi = -8$ for *Ia3d;* $A_0 = 1.919$ and $\chi = -2$ for *Pn3m;* and $A_0 = 2.345$ and $\chi = -4$ for *Im3m*. For the radius of the aqueous channels, *r* the following equations are valid for the *Ia3d*, *Pn3m* and *Im3m* phases, respectively[17]:

$$r = 0.248a - L_{lip} \qquad (3a)$$

$$r = 0.391a - L_{lip} \qquad (3b)$$

$$r = 0.3055a - L_{lip} \qquad (3c)$$

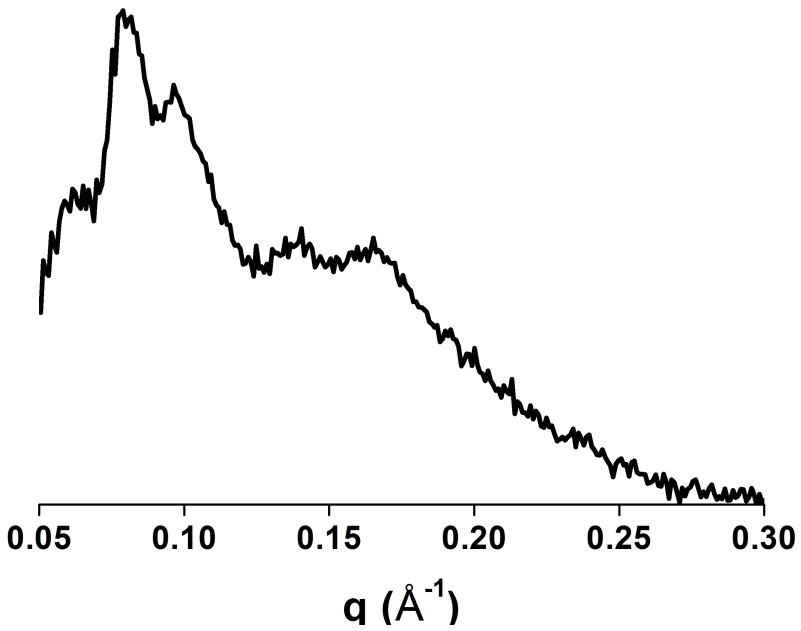

Figure 12: SAXS pattern of cubosomes C at 23°C: 3.4 mg catalyst **2**, 50.0 mg MO, 10 mg Cholesterol, 2 mL HEPES 20 mM, pH 7.4.

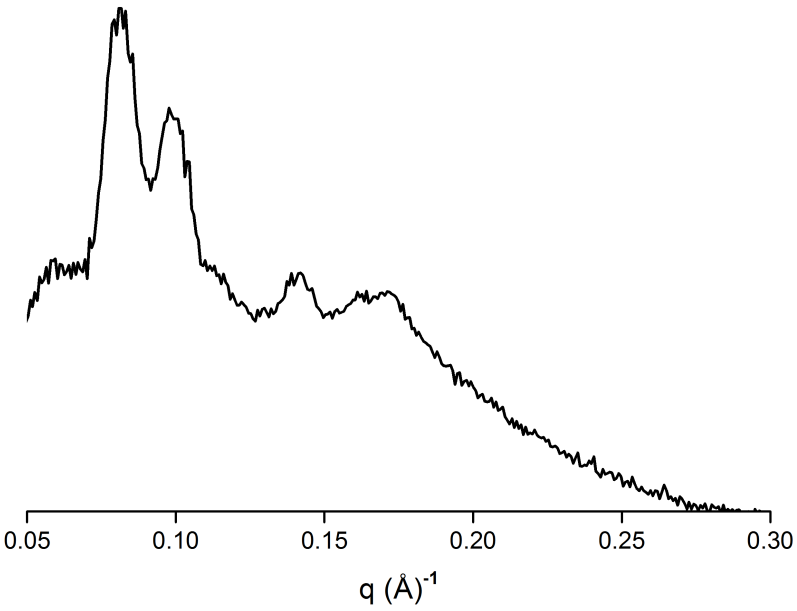

Figure 13: SAXS pattern of cubosomes D at 23°C: 3.4 mg in case of catalyst **2**, 66.6 mg MO, 2 mL PBS 0.1x, pH 7.4.

2.5.5.1 Control experiments: SAXS before and after catalysis

SAXS spectra of catalytic LCPs and cubosomes were acquired before and after catalysis. The cubic structure was maintained in all cases. In Figure 14, an exemplary SAXS spectrum of both, catalytic LCPs (LCP vc) and cubosomes (cubosomes xy) is depicted.

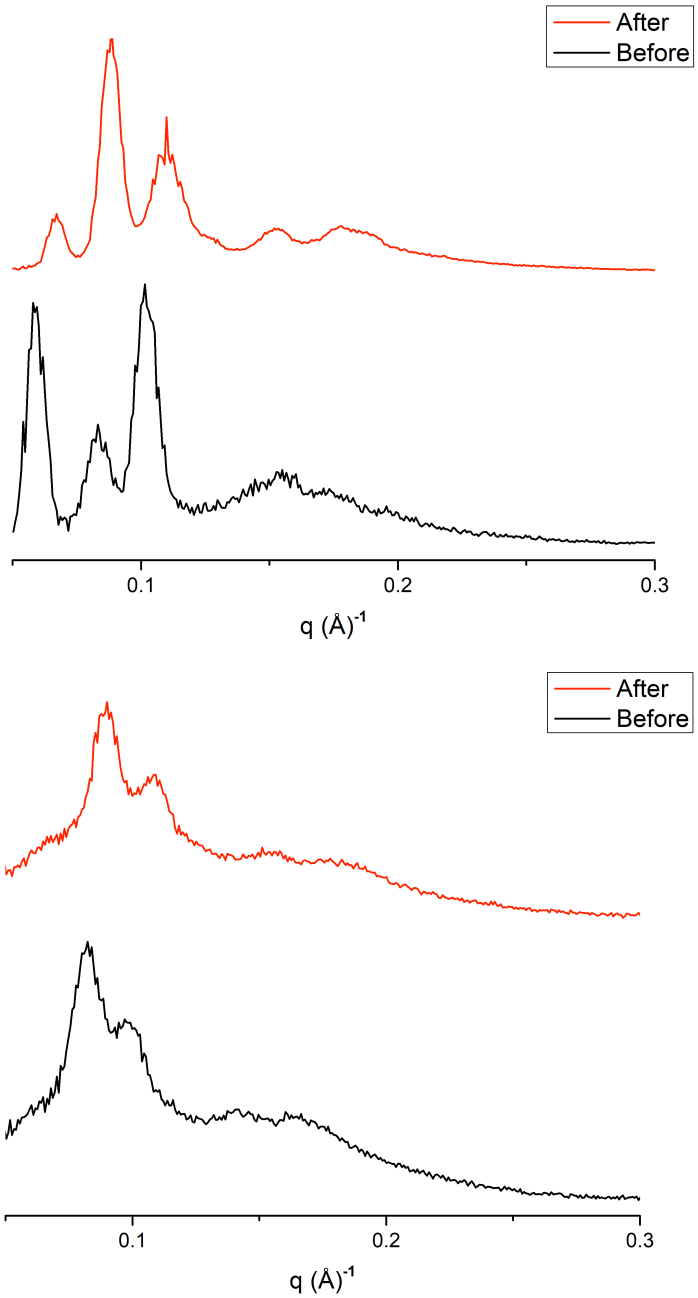

Figure 14: SAXS pattern of catalytic LCP C at 23 °C. 0.0071 mmol catalyst (3.4 mg in catalyst **2**, 50.0 mg MO, 10 mg Cholesterol, 63 µl HEPES 20 mM, pH 7.4 (top panel) and cubosomes C 0.0071 mmol catalyst (3.4 mg catalyst **2**), 50.0 mg MO, 10 mg Cholesterol, 2 mL HEPES 20 mM, pH 7.4 (bottom panel) before and after catalysis.

2.5.6 Chiral stationary phase HPLC

Reagents: Hexane (gradient HPLC grade from Honeywell (Art. No.65801)), EtOH (gradient grade from J.T. Baker (Art. No84462)).
Sample solvent: MeOH, 2.0 mg/mL, injection volume: 5 µL, column: Chiralpak AD-H, 250 x 4.6 mm, 5 µm (Daicel), flow rate: 0.6 mL/min, run time: 50.0 min, column temperature: 30°C, detection (DAD) at 214 nm (BW16nm), mobile phase: hexane/EtOH (8:2)

Table SI2: Retention times of the major and minor aldol products.

Nr.	Isomer	Retention (min)
5a	Anti, major enantiomer	41.739
	Anti, minor enantiomer	35.246
	Syn, major enantiomer	33.492
	Syn, minor enantiomer	29.664
5b	Anti, major enantiomer	18.320
	Anti, minor enantiomer	17.193
5c	Anti, major enantiomer	33.712
	Anti, minor enantiomer	28.056

2.5.7 Cryogenic transmission electron microscopy (cryo-TEM)

The microscopical characterization of the particles in their hydrated state was carried out in a Tecnai F20 cryo-TEM (FEI, USA). 300-mesh lacey carbon-coated copper grids (Quantifoil, Germany) were glow discharged (Emitech K100X, GB) for 30 s. 3 µl of sample solution were applied onto the grids in a Vitrobot Mark II (FEI, USA) and the excess of the dispersion was removed by controlled blotting. A mixture of liquid ethane/propane was used for sample vitrification. The grids were then transferred on a Gatan cryo-holder into the microscope and kept at -180°C during observation. Micrographs were recorded under low dose conditions ($<500e^{-}/nm^{2}$) using a 4k x 4k Gatan CCD camera, operating the microscope at 200 kV acceleration voltage in bright field mode.

Bibliography

(1) Yeh, C.; Sun, Y.; Huang, S.; Tsai, Y. Alternating Chiral Selectivity of Aldol Reactions under the Confined Space of Mesoporous Silica. *Chem. Commun.* **2015**, *51*, 17116–17119.

(2) Benaglia, M.; Puglisi, A.; Cozzi, F. Polymer-Supported Organic Catalysts. *Chem. Rev.* **2003**, *103*, 3401–3429.

(3) Lee, J.; Farha, O. K.; Roberts, J.; Scheidt, K. A.; Nguyen, S. T.; Hupp, J. T. Metal–organic Framework Materials as Catalysts. *Chem. Soc. Rev.* **2009**, *38*, 1450–1459.

(4) Xu, H.; Gao, J.; Jiang, D. Stable , Crystalline , Porous , Covalent Organic Frameworks as a Platform for Chiral Organocatalysts. *Nat. Chem.* **2015**, *7*, 905–912.

(5) Lee, J.; Mayer-Gall, T.; Opwis, K.; Song, C. E.; Gutmann, J. S.; List, B. Organotextile Catalysis. *Science* **2013**, *341*, 1225–1229.

(6) La Sorella, G.; Strukul, G.; Scarso, A. Recent Advances in Catalysis in Micellar Media. *Green Chem.* **2015**, *17*, 644–683.

(7) Lipshutz, B. H.; Abela, A. R. Micellar Catalysis of Suzuki-Miyaura Cross-Couplings with Heteroaromatics in Water. *Org. Lett.* **2008**, *10*, 5329–5332.

(8) Walde, P.; Ichikawa, S. Enzymes inside Lipid Vesicles: Preparation, Reactivity and Applications. *Biomol. Eng.* **2001**, *18*, 143–177.

(9) Küchler, A.; Yoshimoto, M.; Luginbühl, S.; Mavelli, F.; Walde, P. Enzymatic Reactions in Confined Environments. *Nat. Nanotechnol.* **2016**, *11*, 409–420.

(10) Monnard, P. A. Liposome-Entrapped Polymerases as Models for Microscale/nanoscale Bioreactors. *J. Membr. Biol.* **2003**, *191*, 87–97.

(11) Raynal, M.; Ballester, P.; Vidal-Ferran, A.; van Leeuwen, P. W. N. M. Supramolecular Catalysis. Part 2: Artificial Enzyme Mimics. *Chem. Soc. Rev.* **2014**, *43*, 1734–1787.

(12) Poznik, M.; Maitra, U.; König, B. The Interface Makes a Difference: Lanthanide Ion Coated Vesicles Hydrolyze Phosphodiesters. *Org. Biomol. Chem.* **2015**, *13*, 9789–9792.

(13) Gruber, B.; Kataev, E.; Aschenbrenner, J.; Stadlbauer, S.; König, B. Vesicles and Micelles from Amphiphilic Zinc(II)-Cyclen Complexes as Highly Potent Promoters of Hydrolytic DNA Cleavage. *J. Am. Chem. Soc.* **2011**, *133*, 20704–20707.

(14) Sun, W.; Vallooran, J. J.; Mezzenga, R. Enzyme Kinetics in Liquid Crystalline Mesophases: Size Matters, but Also Topology. *Langmuir* **2015**, *31*, 4558–4565.

(15) Sun, W.; Vallooran, J. J.; Zabara, A.; Mezzenga, R. Controlling Enzymatic Activity and Kinetics in Swollen Mesophases by Physical Nano-Confinement. *Nanoscale* **2014**, *6*, 6853–6859.

(16) Vauthey, S.; Milo, C.; Frossard, P.; Garti, N.; Leser, M. E.; Watzke, H. J. Structured Fluids as Microreactors for Flavor Formation by the Maillard Reaction. *J. Agric. Food Chem.* **2000**, *48*, 4808–4816.

(17) Briggs, J.; Chung, H.; Caffrey, M. The Temperature-Composition Phase Diagram and Mesophase Structure Characterization of the Monoolein / Water System. *J. Phys. II Fr.* **1996**, *6*, 723–751.

(18) Osornio, Y. M.; Uebelhart, P.; Bosshard, S.; Konrad, F.; Siegel, J. S.; Landau, E. M. Design and Synthesis of Lipids for the Fabrication of Functional Lipidic Cubic-Phase Biomaterials. *J. Org. Chem.* **2012**, *77*, 10583–10595.

(19) Fong, W.-K.; Hanley, T.; Boyd, B. J. Stimuli Responsive Liquid Crystals Provide “on-Demand” Drug Delivery in Vitro and in Vivo. *J. Control. Release* **2009**, *135*, 218–226.

(20) Negrini, R.; Mezzenga, R. pH-Responsive Lyotropic Liquid Crystals for Controlled Drug Delivery. *Langmuir* **2011**, *27*, 5296–5303.

(21) Landau, E. M.; Rosenbusch, J. P. Lipidic Cubic Phases : A Novel Concept for the Crystallization of Membrane Proteins. *Proc. Natl. Acad. Sci.* **1996**, *93*, 14532–14535.

(22) Cherezov, V.; Rosenbaum, D. M.; Hanson, M. A.; Rasmussen, S. G. F.; Thian, F. S.; Kobilka, T. S.; Choi, H.-J.; Kuhn, P.; Weis, W. I.; Kobilka, B. K.; Stevens, R. C. High-Resolution Crystal Structure of an Engineered Human beta2-Adrenergic G Protein-Coupled Receptor. *Science* **2007**, *318*, 1258–1265.

(23) Nazaruk, E.; Górecka, E.; Bilewicz, R. Enzymes and Mediators Hosted Together in Lipidic Mesophases for the Construction of Biodevices. *J. Colloid Interface Sci.* **2012**, *385*, 130–136.

(24) Mezzenga, R.; Schurtenberger, P.; Burbidge, A.; Michel, M. Understanding Foods as Soft Materials. *Nat. Mater.* **2005**, *4*, 729–740.

(25) Spicer, P.; Hayden, K.; Lynch, M. Novel Process for Producing Cubic Liquid Crystalline Nanoparticles (Cubosomes). *Langmuir* **2001**, *17*, 5748–5756.

(26) Lawrence, M. J. Surfactant Systems: Their Use in Drug Delivery. *Chem. Soc. Rev.* **1994**, *23*, 417–424.

(27) Rahanyan-Kägi, N.; Aleandri, S.; Speziale, C.; Mezzenga, R.; Landau, E. M. Stimuli-Responsive Lipidic Cubic Phase: Triggered Release and Sequestration of Guest Molecules. *Chem. - A Eur. J.* **2015**, *21*, 1873–1877.

(28) Liu, Q.; Dong, Y. Da; Hanley, T. L.; Boyd, B. J. Sensitivity of Nanostructure in Charged Cubosomes to Phase Changes Triggered by Ionic Species in Solution. *Langmuir* **2013**, *29*, 14265–14273.

(29) Komisarski, M.; Osornio, Y. M.; Siegel, J. S.; Landau, E. M. Tailored Host-Guest Lipidic Cubic Phases: A Protocell Model Exhibiting Nucleic Acid Recognition. *Chem. - A Eur. J.* **2013**, *19*, 1262–1267.

(30) Mlynarski, J.; Bas, S. Catalytic Asymmetric Aldol Reactions in Aqueous Media – a 5 Year Update. *Chem. Soc. Rev.* **2014**, *43*, 577–587.

(31) Trost, B. M.; Brindle, C. S. The Direct Catalytic Asymmetric Aldol Reaction. *Chem. Soc. Rev.* **2010**, *39*, 1600–1632.

(32) Bisai, V.; Bisai, A.; Singh, V. K. Enantioselective Organocatalytic Aldol Reaction Using Small Organic Molecules. *Tetrahedron* **2012**, *68*, 4541–4580.

(33) Dean, S. M.; Greenberg, W. A.; Wong, C.-H. Recent Advances in Aldolase-Catalyzed Asymmetric Synthesis. *Adv. Synth. Catal.* **2007**, *349*, 1308–1320.

(34) Brogan, A. P.; Dickerson, T. J.; Janda, K. D. Enamine-Based Aldol Organocatalysis in Water: Are They Really “all Wet”? *Angew. Chem. Int. Ed. Engl.* **2006**, *45*, 8100–8102.

(35) List, B.; Lerner, R. A.; Barbas III, C. F. Proline-Catalyzed Direct Asymmetric Aldol Reactions The Skaggs Institute for Chemical Biology and the Department of Molecular Biology The Scripps Research Institute Most Enzymatic Transformations Have a Synthetic Counterpart . Often Though , the Mechanism. *J. Am. Chem. Soc.* **2000**, *122*, 2395–2396.

(36) Dickerson, T. J.; Janda, K. D. Aqueous Aldol Catalysis by a Nicotine Metabolite. *J. Am. Chem. Soc.* **2002**, *124*, 3220–3221.

(37) Córdova, A.; Notz, W.; Barbas III, C. F. Direct Organocatalytic Aldol Reactions in Buffered Aqueous Media. *Chem. Commun.* **2002**, *0*, 3024–3025.

(38) Chowdari, N. S.; Ramachary, D. B.; Córdova, A.; Barbas III, C. F. Proline-Catalyzed Asymmetric Assembly Reactions: Enzyme-like Assembly of Carbohydrates and Polyketides from Three Aldehyde Substrates. *Tetrahedron Lett.* **2002**, *43*, 9591–9595.

(39) Mase, N.; Nakai, Y.; Ohara, N.; Yoda, H.; Takabe, K.; Tanaka, F.; Barbas III, C. F. Organocatalytic Direct Asymmetric Aldol Reactions in Water. *J. Am. Chem. Soc.* **2006**, *128*, 734–735.

(40) Hayashi, Y.; Aratake, S.; Okano, T.; Takahashi, J.; Sumiya, T.; Shoji, M. Combined Proline-Surfactant Organocatalyst for the Highly Diastereo- and Enantioselective Aqueous Direct Cross-Aldol Reaction of Aldehydes. *Angew. Chem. Int. Ed. Engl.* **2006**, *45*, 5527–5529.

(41) Hayashi, Y.; Sumiya, T.; Takahashi, J.; Gotoh, H.; Urushima, T.; Shoji, M. Highly Diastereo- and Enantioselective Direct Aldol Reactions in Water. *Angew. Chem. Int. Ed. Engl.* **2006**, *45*, 958–961.

(42) Lu, A.; Cotanda, P.; Patterson, J. P.; Longbottom, D. a; O’Reilly, R. K. Aldol Reactions Catalyzed by L-Proline Functionalized Polymeric Nanoreactors in Water. *Chem. Commun.* **2012**, *48*, 9699–9701.

(43) Tsutsui, A.; Takeda, H.; Kimura, M.; Fujimoto, T.; Machinami, T. Novel Enantiocontrol System with Aminoacyl Derivatives of Glucoside as Enamine-Based Organocatalysts for Aldol Reaction in Aqueous Media. *Tetrahedron Lett.* **2007**, *48*, 5213–5217.

(44) Miura, D.; Fujimoto, T.; Tsutsui, A.; Machinami, T. Stereoselective Synthesis of Ketoses by Aldol Reaction Using Water--Compatible Prolinamide Catalysts in Aqueous Media. *Synlett* **2013**, *24*, 1501–1504.

(45) Angelov, B.; Angelova, A.; Ollivon, M.; Bourgaux, C.; Campitelli, A. Diamond-Type Lipid Cubic Phase with Large Water Channels. *J. Am. Chem. Soc.* **2003**, *125*, 7188–7189.

(46) Yaghmur, A.; De Campo, L.; Sagalowicz, L.; Leser, M. E.; Glatter, O. Control of the Internal Structure of MLO-Based Isasomes by the Addition of Diglycerol Monooleate and Soybean Phosphatidylcholine. *Langmuir* **2006**, *22*, 9919–9927.

(47) Negrini, R.; Mezzenga, R. Diffusion, Molecular Separation, and Drug Delivery from Lipid Mesophases with Tunable Water Channels. *Langmuir* **2012**, *28*, 16455–16462.

(48) Bornaghi, L. F.; Poulsen, S. A. Microwave-Accelerated Fischer Glycosylation. *Tetrahedron Lett.* **2005**, *46*, 3485–3488.

(49) Angelin, M.; Hermansson, M.; Dong, H.; Ramström, O. Direct, Mild, and Selective Synthesis of Unprotected Dialdo-Glycosides. *European J. Org. Chem.* **2006**, *19*, 4323–4326.

(50) Xu, H.-S.; Ding, S.-Y.; An, W.-K.; Wu, H.; Wang, W. Constructing Crystalline Covalent Organic Frameworks from Chiral Building Blocks. *J. Am. Chem. Soc.* **2016**, *138*, 11489–11492.

(51) He, T.; Li, K.; Wu, M. Y.; Wu, M. B.; Wang, N.; Pu, L.; Yu, X. Q. Water Promoted Enantioselective Aldol Reaction by Proline-Cholesterol and -Diosgenin Based Amphiphilic Organocatalysts. *Tetrahedron* **2013**, *69*, 5136–5143.

(52) Lipshutz, B. H.; Ghorai, S. Organocatalysis in Water at Room Temperature with *In-Flask* Catalyst Recycling. *Org. Lett.* **2012**, *14*, 422–425.

(53) Lo, C. M.; Chow, H. F. Structural Effects on the Catalytic, Emulsifying, and Recycling Properties of Chiral Amphiphilic Dendritic Organocatalysts. *J. Org. Chem.* **2009**, *74*, 5181–5191.

(54) Arivalagan, P. R.; Zhao, Y. Interfacial Catalysis of Aldol Reactions by Prolinamide Surfactants in Reverse Micelles. *Org. Biomol. Chem.* **2015**, *13*, 770–775.

(55) Aleandri, S.; Speziale, C.; Mezzenga, R.; Landau, E. M. Design of Light-Triggered Lyotropic Liquid Crystal Mesophases and Their Application as Molecular Switches in “On Demand” Release. *Langmuir* **2015**, *31*, 6981–6987.

(56) Asami Masatoshi. Asymmetric Transformation of Symmetrical Epoxides to Allylic Alcohols by Lithium (S)-2-(N,N,-Disubstituted Aminomethyl)pyrrolidide. *Bull. Chem. Soc. Jpn* **1990**, *63*, 721–727.

(57) Appel, R. Tertiary Phosphane/Tetrachloromethane, a Versatile Reagent for Chlorination, Dehydration, and P-N Linkage. *Angew. Chemie Int. Ed.* **1975**, *14*, 801–811.

(58) Srivastava, S. K.; Chauhan, P. M. S.; Bhaduri, A. P. A Novel Strategy for N-Alkylation of Primary Amines. *Synth. Commun.* **1999**, *29*, 2085–2091.

(59) Agarwal, J.; Peddinti, R. K. Synthesis and Characterization of Monosaccharide Derivatives and Application of Sugar-Based Prolinamides in Asymmetric Synthesis. *European J. Org. Chem.* **2012**, *32*, 6390–6406.

(60) Cherezov, V.; Clogston, J.; Misquitta, Y.; Abdel-Gawad, W.; Caffrey, M. Membrane Protein Crystallization In Meso: Lipid Type-Tailoring of the Cubic Phase. *Biophys. J.* **2002**, *83*, 3393–3407.

(61) Dong, Y. D.; Larson, I.; Hanley, T.; Boyd, B. J. Bulk and Dispersed Aqueous Phase Behavior of Phytantriol: Effect of Vitamin E Acetate and F127 Polymer on Liquid Crystal Nanostructure. *Langmuir* **2006**, *22*, 9512–9518.

(62) Aleandri, S.; Bandera, D.; Mezzenga, R.; Landau, E. M. Biotinylated Cubosomes: A Versatile Tool for Active Targeting and Codelivery of Paclitaxel and a Fluorescein-Based Lipid Dye. *Langmuir* **2015**, *31*, 12770–12776.

(63) Chong, J. Y. T.; Mulet, X.; Waddington, L. J.; Boyd, B. J.; Drummond, C. J. Steric Stabilisation of Self-

Assembled Cubic Lyotropic Liquid Crystalline Nanoparticles: High Throughput Evaluation of Triblock Polyethylene Oxide-Polypropylene Oxide-Polyethylene Oxide Copolymers. *Soft Matter* **2011**, *7*, 4768–4777.

(64) Kaasgaard, T.; Drummond, C. J. Ordered 2-D and 3-D Nanostructured Amphiphile Self-Assembly Materials Stable in Excess Solvent. *Phys. Chem. Chem. Phys.* **2006**, *8*, 4957–4975.

(65) von Schnering, H. G.; Nesper, R. Nodal Surfaces of Fourier Series: Fundamental Invariants of Structured Matter. *Zeitschrift für Phys. B Condens. Matter* **1991**, *83*, 407–412.

(66) Larsson, K. Cubic Lipid-Water Phases : Structures and Biomembrane Aspects. *J. Phys. Chem.* **1989**, *93*, 7304–7314.

(67) Demurtas, D.; Guichard, P.; Martiel, I.; Mezzenga, R.; Hébert, C.; Sagalowicz, L. Direct Visualization of Dispersed Lipid Bicontinuous Cubic Phases by Cryo-Electron Tomography. *Nat. Commun.* **2015**, *6*, 1–8.

(68) Wu, Y. S.; Chen, Y.; Deng, D. S.; Cai, J. Proline-Catalyzed Asymmetric Direct Aldol Reaction Assisted by D-Camphorsulfonic Acid in Aqueous Media. *Synlett* **2005**, *10*, 1627–1629.

(69) Zhang, J.; Han, X.; Wu, X.; Liu, Y.; Cui, Y. Multivariate Chiral Covalent Organic Frameworks with Controlled Crystallinity and Stability for Asymmetric Catalysis. *J. Am. Chem. Soc.* **2017**, *139*, 8277–8285.

(70) Sun, W.; Vallooran, J. J.; Fong, W. K.; Mezzenga, R. Lyotropic Liquid Crystalline Cubic Phases as Versatile Host Matrices for Membrane-Bound Enzymes. *J. Phys. Chem. Lett.* **2016**, *7*, 1507–1512.

(71) Schmid, C. R.; Bryant, J. D.; Dowlatzedah, M.; Phillips, J. L.; Prather, D. E.; Schantz, R. D.; Sear, N. L.; Vianco, C. S. Synthesis of 2,3- 0-1sopropylidene-D-Glyceraldehydein High ChemicalandOpticalPurity: Observationson the Development of a Practical Bulk Process. *J. Org. Chem.* **1991**, *56*, 4056–4058.

(72) Forbes, D. C.; Ene, D. G.; Doyle, M. P. Stereoselective Synthesis of Substituted 5-Hydroxy-1 , 3-Dioxanes. *Synthesis.* **1998**, 5–8.

(73) Gauss, D.; Schoenenberger, B.; Wohlgemuth, R. Chemical and Enzymatic Methodologies for the Synthesis of Enantiomerically Pure Glyceraldehyde 3-Phosphates. *Carbohydr. Res.* **2014**, *389*, 18–24.

(74) Lepore, S. D.; He, Y. Use of Sonication for the Coupling of Sterically Hindered Substrates in the Phenolic Mitsunobu Reaction. *J. Org. Chem.* **2003**, *68*, 8261–8263.

(75) Fronert, J.; Bisschops, T.; Cassens-Sasse, E.; Atodiresei, I.; Enders, D. Asymmetric Organocatalytic Synthesis of Trans -3,4-Disubstituted Isochromanones via an Intramolecular Aldol Reaction. *Synth.* **2013**, *45*, 1708–1712.

(76) Zhang, H.; Zhang, S.; Liu, L.; Luo, G.; Duan, W.; Wang, W. Synthesis of Chiral 3-Substituted Phthalides by a Sequential Organocatalytic Enantioselective Aldol-Lactonization Reaction. Three-Step Synthesis of (S)-(-)-3-Butylphthalide. *J. Org. Chem.* **2010**, *75*, 368–374.

(77) Jacob, P. Resolution of 5-Bromonornicotine. Synthesis of (R) and (S)-Nornicotine of High Enantiomeric Purity. *J. Org. Chem.* **1982**,19, 4165–4167.

(78) Tyler, A. I. I.; Barriga, H. M. G.; Parsons, E. S.; McCarthy, N. L. C.; Ces, O.; Law, R. V; Seddon, J. M.; Brooks, N. J. Electrostatic Swelling of Bicontinuous Cubic Lipid Phases. *Soft Matter* **2015**, *11*, 3279–3286.

(79) Borch, R. F.; Bernstein, M. D.; Durst, H. D. The Cyanohydridoborate Anion as a Selective Reducing Agent. *J. Am. Chem. Soc.* **1971**, *93*, 2897–2904.

(80) Turner, D. C.; Wang, Z.-G.; Gruner, S. M.; Mannock, D. a.; McElhaney, R. N. Structural Study of the Inverted Cubic Phases of Di-Dodecyl Alkyl-β-D-Glucopyranosyl-Rac-Glycerol. *J. Phys. II* **1992**, *2*, 2039–2063.

Chapter 3

Lipidic mesophases as novel nanoreactor scaffolds for metal complex catalysts: Degradation of pesticides

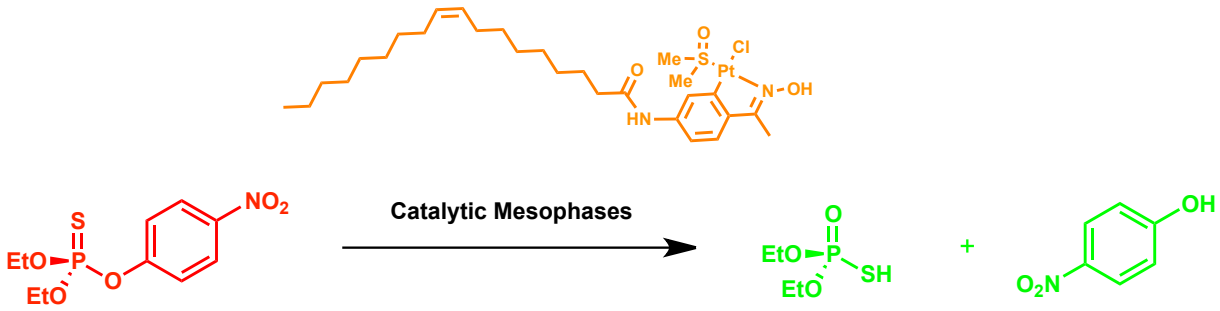

3.1 Introduction

Phosphate esters like paraoxon (**67**) or parathion (**68**) are pesticides with hundred thousands of tons annual world production.[1] Due to their toxicity and chemical stability, their accumulation in the environment is ecologically problematic. Some chemical warfare agents, also called G-type nerve agents, like sarin, soman and tabun are chemically related. Both classes possess phosphate ester bonds.[2] These compounds are highly potent acetylcholine esterase inhibitors. Acetylcholin is a neurotransmitter that triggers muscular response and its accumulation leads to asphyxiation.[3] Considerable efforts have been undertaken towards the safe, efficient and controlled decomposition of such compounds, usually through oxidation or hydrolysis.[4,5] Thermally robust and water-stable metal-organic-frameworks (MOFs) have been functionalized and used to hydrolyze such compounds very efficiently.[2] Katz *et al*., developed a zirconium(IV)-cluster containing MOF catalyst. The combination of the strong Lewis acid Zr(IV) and the bridging hydroxide anions leads to a highly efficient catalyst. The system is inspired by nature; the enzyme phosphotriesterase contains a hydroxyl-anion-bridged binuclear Zn(II) active site.[6] König *et al.* for example, used vesicles and micelles to catalyze hydrolytic cleavage of organophosphates with amphiphilic cyclen-zinc(II) complexes.[7,8] The same group used lanthanide coated liposomes to hydrolyze phosphodiesters and DNA.[7] Interestingly, these Eu(III) coated liposomes showed up to 17-fold hydrolysis activity as compared to the aqueous europium salt. Furthermore, methoxides of La(III) and Zn(II) have been successfully applied to the methanolysis of phosphateseter. Gunnlaugson *et al*. used cyclen based lanthanide complexes with pyridine as a cofactor for phosphodiester hydrolysis.[9] *Ryabov et al*. developed a platinum aryl oxime metallacycle that enables efficient degradation of thiophosphate pesticides like parathion (**68**).[1] Catalyst **69** hydrolyzes parathion (**68**) by a factor of 10^6-10^7 faster than hydroxide. Due to this remarkable catalytic performance and the potential possibility for lipidic modification, this catalyst was chosen for our model system. Added guest catalysts can affect significantly the structural and dynamic properties of the ensuing host mesophases, depending on the additives' molecular structure.[10–13]

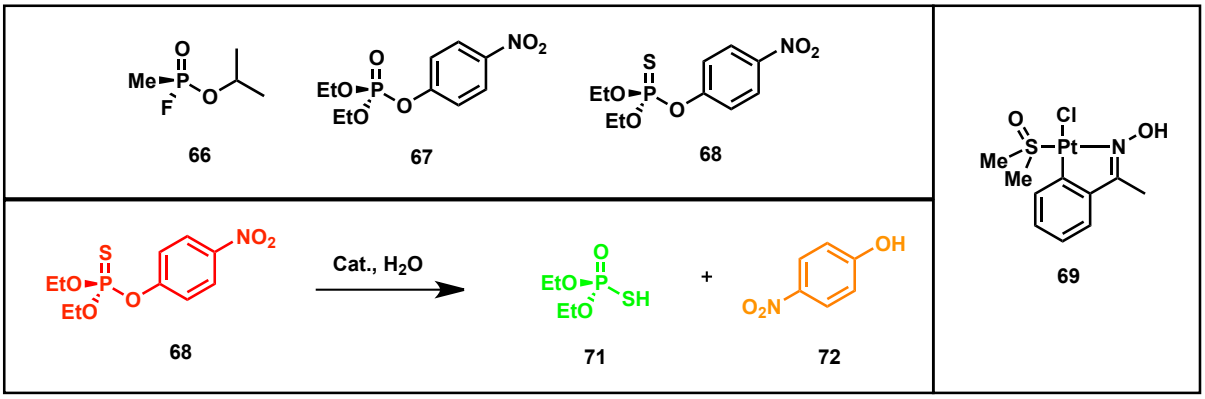

Figure 1: Top: Examples of acetylcholine esterase inhibitors. Sarin (**66**), is a chemical warfare agent, paraoxon (**67**) and parathion (**68**) are pesticides. Bottom: Hydrolysis reaction of parathion. Right: Pt-metallacycle **69**.

3.2 Results and discussion

3.2.1 Synthesis of Pt-complexes

To investigate the impact of the catalyst's structure on its catalytic performance, structural motifs were varied. To that end, three different lipidic platinum catalysts were designed and synthesized (Scheme 1). Modifications were introduced at the lipidic chain and at the linker that connects the Pt-metallacycle headgroup to the lipidic chain. Thus, catalysts with a stearyl, a lauryl and an oleyl (**75**, **81** and **82**), saturated (**75** and **81**) and unsaturated (**82**) lipidic chains, as well as catalysts in which the metallacycle is linked to the lipids via an amide (**81** and **82**), or to an amine (**75**) were synthesized. The lipidic chain of catalyst **75** was installed at commercially available 1-(4-bromophenyl)ethanone (**72**) via *Buchwald-Hartwig* amination using stearyl amine. The subsequent steps, oxime formation and cycloplatination, were performed analogous to the synthesis of the original catalyst **84** (Scheme 1). The lauryl and oleyl lipid chains of catalyst **81** and **82**, respectively were installed by coupling the corresponding acyl chlorides to commercially available 1-(4-aminophenyl)ethanone (**76**). The subsequent steps, oxime formation and cycloplatination were also performed analogous to the original catalyst **84**, which was synthesized as well and serves as a reference catalyst.

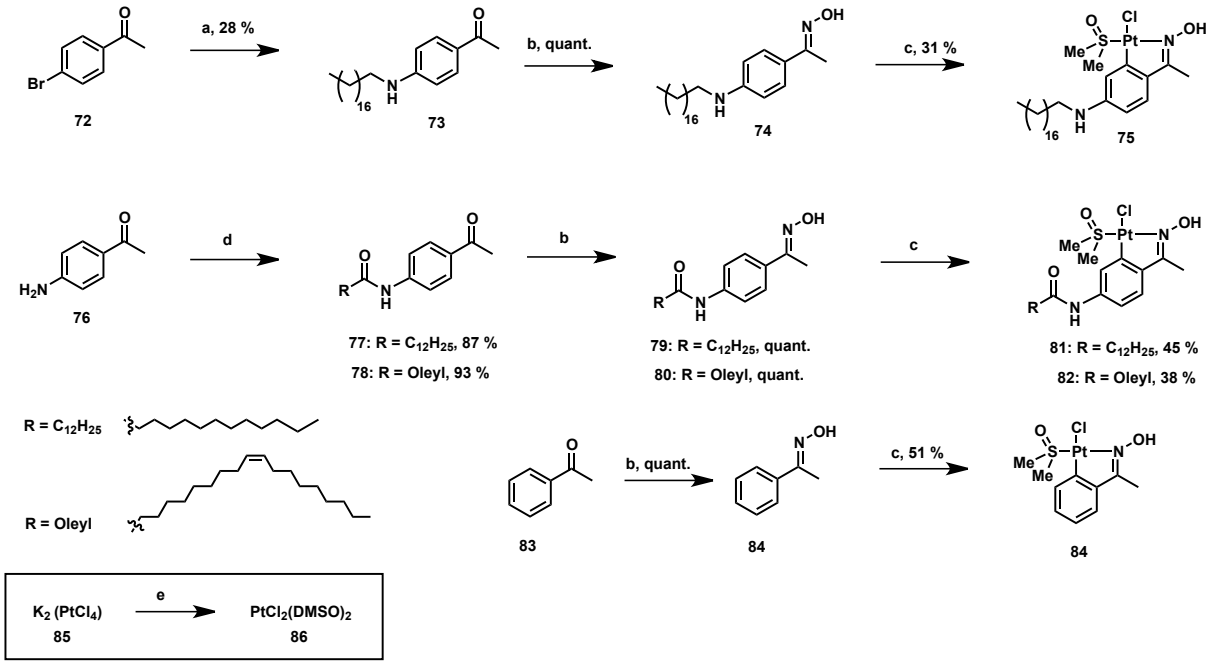

Scheme 1: Syntheses of different lipidically modified Pt-catalysts and Ryabov's catalyst which was used as reference. Conditions: a) $Pd(OAc)_2$ 0.05 eq, XPhos 0.1 eq, Na*t*BuO, toluene, 50°C. b) NH_2OH x HCl, EtOH/pyridine 2:1, reflux. c) $Pt(DMSO)_2Cl_2$ (**86**), MeOH, reflux. d) Lauroyl or oleoyl chloride, DIPEA, CH_2Cl_2, r.t.. e) DMSO, H_2O, r.t..

3.2.2 Parathion hydrolysis using Pt-catalyst 82 in LCPs

Having catalysts **75**, **81** and **82** successfully synthesized, first Pt-complex containing LCPs was prepared in order to test the stability of the mesophases and to determine the highest possible catalyst loading. Stable and transparent LCPs were obtained with catalyst **75** with a maximum catalyst loading of 3 % (w/w of the lipidic content). With catalyst **81** (stearyl) a similar additive loading could be achieved; 3.5 % (w/w of the lipidic content), whereas a significant higher loading of 7.0 % (w/w of the lipidic content) was achieved with catalyst **82**. The oleyl lipidic chain of catalyst **82** leads to a better packing of host- and guest-lipids due to the compatibility of the lipidic chains. Thus, LCPs containing catalyst **82** were used for initial hydrolysis experiments using parathion as the substrate (Figure 2).

The proposed mechanism of this platinum catalyst mediated P-ester hydrolysis is depicted in Scheme 2.[1] Once the catalyst is in aqueous environment, the chloro ligand is replaced by a water molecule. Subsequently, the water ligand is substituted by parathion, which coordinates to the platinum center via its sulfur atom. Intramolecular nucleophilic attack by the oximate leads to cleavage of the P-ester bond releasing a phenolate. Upon hydrolysis of the metallo-

phosphorus complex, the active species is recovered and the next catalytic cycle can be launched.

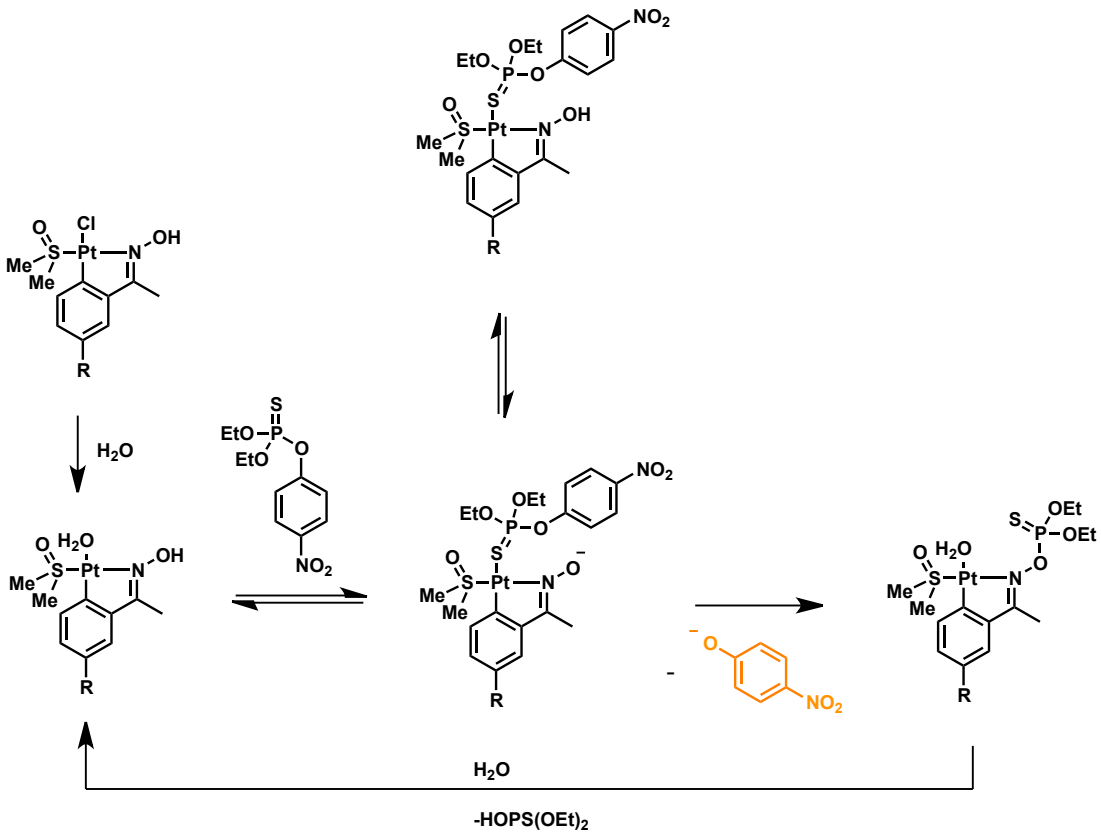

Scheme 2: Proposed hydrolysis mechanism of parathion with Pt-metallacycles. Adapted from Ref. (1).

Catalyst **82**-containing LCP was produced directly in an NMR-tube (with 3 % catalyst w/w of the lipidic content, 20 mol % relative to the substrate, 100 mg LCP total weight). To the NMR tube with the catalytic LCP at the bottom, a buffer solution (0.005 M $Na_2B_4O_7$/NaOH, pH 8.5, 0.01 M $NaClO_4$) with parathion (**68**) (6.5 mM) was added on top as an overlay. The reaction mixture was gently shaken and the reaction was monitored by ^{31}P-NMR. Figure 2 shows the ^{31}P-NMR spectra acquired during the reaction and photographs of the respective NMR tubes. The top panel is at the start just after addition of the parathion solution; only the signal of parathion is present: The spectrum in the middle, which was taken after 9 h, shows a significant amount of decomposition product (ca. 50%). The ^{31}-P-NMR on the bottom panel was acquired after 26 h and shows only the signal of the decomposition product. The color change from colorless to an intense yellow is a second indication for the formation of the decomposition product, since it arises from increasing phenolate concentration.

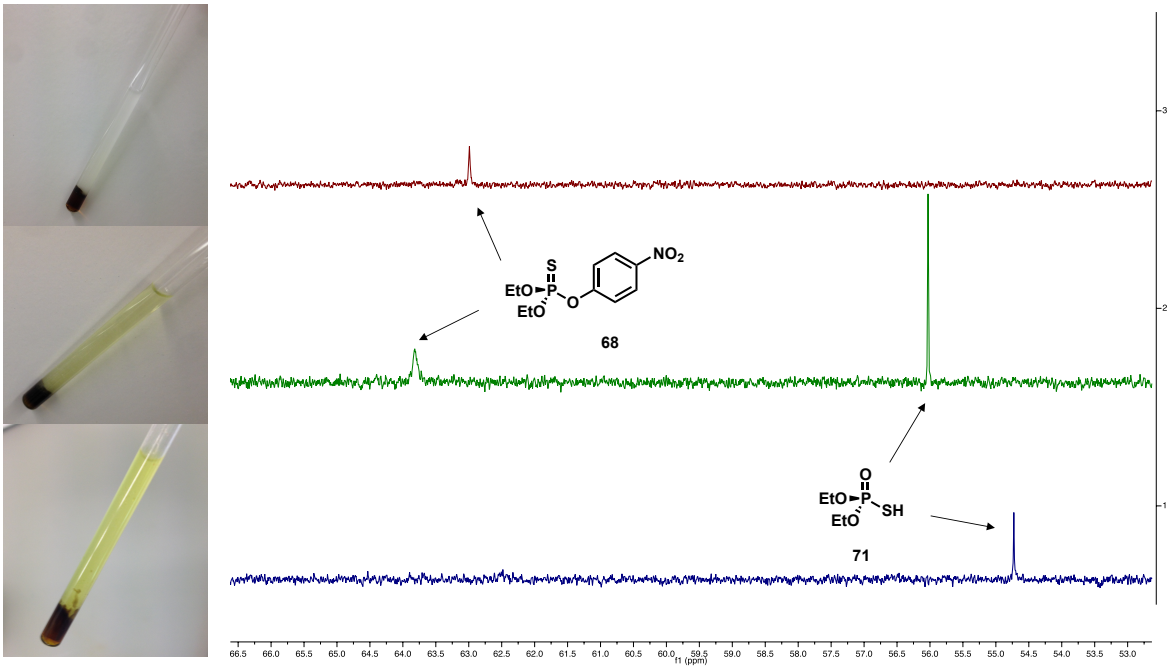

Figure 2: ^{31}P-NMR spectra of parathion hydrolysis using Pt-catalyst **82** in LCP. Top: Reaction start. Middle: After 9h. Bottom: after 26 h with the corresponding photographs of the experimental set-up. The yellow color intensifies with increasing phenolate concentration.

However, the system has a major drawback: Parathion (**68**) was found to accumulate in the lipidic compartment of the LCP, where the catalyst cannot reach it. After dissolving the LCP in EtOH, the total amount of parathion was determined to be 30 %. In addition, an NMR tube containing reference parathion solution, which did not contain any catalyst, was used as a control. As expected, no hydrolysis product was detected after 26 h by ^{31}P-NMR. Furthermore, a control experiment was carried out in which the same amounts of LCP-compatible catalyst **82** and parathion solution were mixed (and sonicated for 5 min) without LCP present. The resulting suspension was analyzed after 30 h and no significant amount of decomposition product was detected. This experiment shows the necessity of the LCP in this set up. This experiment proves the basic functionality of our concept: The catalyst, which is incorporated into LCP destroys parathion. However, the rate with which the substrate is destroyed is far too low as compared to our reference system.[1] Thus, optimization is needed. Several parameters can be changed to achieve this goal: Catalyst loading and surface area between LCP and overlay could be increased, and the aqueous channels of the mesophase could be swollen with additives like cholesterol and sucrose stearate. Additionally, the use of dispersed mesophase nanoparticles, i.e. cubosomes might increase the efficiency of our system. This approach is described in the next paragraph.

3.2.3 Parathion hydrolysis using Pt-catalyst 82 in cubosomes

In order to compare the catalytic performance of these two mesophase modes, the same model reaction and lipidic Pt-catalyst **82** as in the previously described LCP experiments were applied using cubosomes as the catalyst immobilization platform. In contrast to bulk LCPs, which are malleable and exhibit a gel-like consistency and adhesive properties, cubosome nanoparticles have a much lower viscosity.[14] Such self-assembled fluid dispersions allow therefore running reactions in classical reaction flasks applying stirring, and therefore potentially increase reaction rates. Cubosomes are obtained upon ultra-sonication of the parent bulk LCP and show identical packing arrangement and phase identity to those of the parent gel LCP (see chapter 1). Since bulk LCPs are thermodynamically favored, cubosomes need to be stabilized in order to prevent them from reassembling to bulk LCPs. Pluronics,[15] are the most frequently used stabilizers for such systems. The most efficient stabilizer was found to be Pluronic F108 (PF 108),[16] which was consequently used in this study. Cubosomes with a lipid concentration of 33 mg/mL in a buffer solution (0.005 M $Na_2B_4O_7$/NaOH, pH 8.5, 0.01 M $NaClO_4$) and uniform particle size of 210 ± 3 nm were prepared using a standard sonication process (see experimental section). Subsequently, parathion (6.5 mM) was added to the nanoparticle dispersion and the reaction mixture was stirred. The progress of the reaction was again monitored by ^{31}P-NMR. To this end, aliquots were removed, cubosomes filtered off and ^{31}P-NMR spectra were acquired. After 2 hours, no parathion could be detected and only the decomposition product was present according to ^{31}P-NMR. However, after destroying the cubosomes by dissolving them with EtOH after 20 h and subsequent analysis, it was found that parathion, like in the LCP case, was accumulated in the lipidic compartment of the cubosomes where it could not be hydrolyzed by the Pt-catalyst, which resides in the aqueous compartment. After 20 hours ca. 50% of the parathion is still present. The relatively high hydrophobicity of parathion (ClogP value: 3.648) is responsible for this accumulation effect.

Several attempts to overcome this problem were undertaken by lowering the parathion concentration in the buffer solution. A similar extent of accumulation occurred even at 0.325 mM and at 0.163 mM parathion. We expected that replacing parathion with more hydrophilic phosphate esters might solve this problem. Therefore, bis(4-nitrophenyl)phosphate (BNPP) (**86**), 4-nitrophenylphosphate (**87**) and paraoxon (**67**) (Figure 3) were tested as hydrolysis substrates with Pt-catalyst-containing cubosomes.

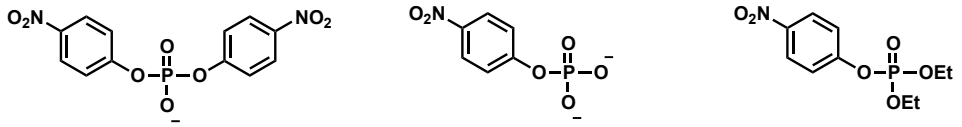

86 **87** **67**

Figure 3: Structures of bis(4-nitrophenyl)phosphate (BNPP, **86**), 4-nitrophenylphosphate (**87**) and paraoxon (**67**).

In the case of BNPP (**86**) and 4-nitrophenylphosphate (**87**), no decomposition product was detected by ^{31}P-NMR. A possible explanation might be the negative charges which interfere with the oxime-oxygen and makes intramolecular nucleophilic attack impossible (compare hydrolysis mechanism, Scheme 2). Hydrolysis using paraoxon (**67**), in which sulfur is replaced by oxygen, occurred, but significantly slower, thereby only 10 % of paraoxon (**67**) was hydrolyzed after 20 h.

3.3 Conclusion

Lipidic Pt-catalyst **75**, **81** and **82** were synthesized and successfully incorporated into LCPs and cubosomes. Especially catalyst **82**, with its oleyl chain enables a relatively high additive loading of 7 % (w/w lipid). The catalytic performance of LCPs and cubosomes containing catalyst **82** on the hydrolysis of paraoxon, a phosphate-ester derived pesticide that is structurally related to chemical warfare agents like sarin was compared: It was shown that cubosomes are more efficient, after 2 h parathion was destroyed, whereas it took 26 h to achieve the same with LCPs. However, in both systems parathion was accumulated within the lipidic compartment of the mesophase. Whereas in cubosomes 50 % of the parathion was found to be accumulated in the lipidic compartment, this value was lower in the case of LCPs (30 %). More hydrophilic substrates were tested to circumvent this problem. However, hydrolysis of BNPP (**86**) and 4-nitrophenylphosphate (**87**) did not occur. Hydrolysis of paraoxon (**67**) was inefficient, only 10 % was decomposed after 20 h. These results indicate that such Pt-metallacycles hydrolyze specifically parathion (**68**). Non-sulfur-containing or charged substrates cannot be hydrolyzed efficiently. In summary, parathion (**68**) can be destroyed with our detoxing mesophases. Cubosomes are preferable to LCPs for this purpose due to the higher reaction rate. However, due to its lipophilicity, parathion (**68**) tends to accumulate in the lipidic compartment of the mesophases, which constiturtes a major drawback in these experiments.

3.4 Outlook

The lipidic Pt-metallacycles seem to hydrolyze parathion (**68**) relative specifically, which turned out to be too lipophilic for our system. Therefore, catalysts that enable hydrolysis of a broad range of phosphate esters are needed, thereby providing a more general approach. Zinc(II)-cyclen complexes have been shown to hydrolyze BNPP (**86**) and DNA efficiently.[8] Lipidic modification of cyclen-derivatives is a promising approach. First precursors have already been synthesized by coupling one and four equivalents of oleyl chloride to Boc-protected cyclen **88** or cyclen (**91**), respectively (Scheme 3). The target catalysts can be obtained after three synthetic steps: After Boc-deprotection, the amide will be reduced using $LiAlH_4$ to the tertiary amines to allow coordination of Zinc(II), which will be achieved adding $Zn(ClO_4)_2$.

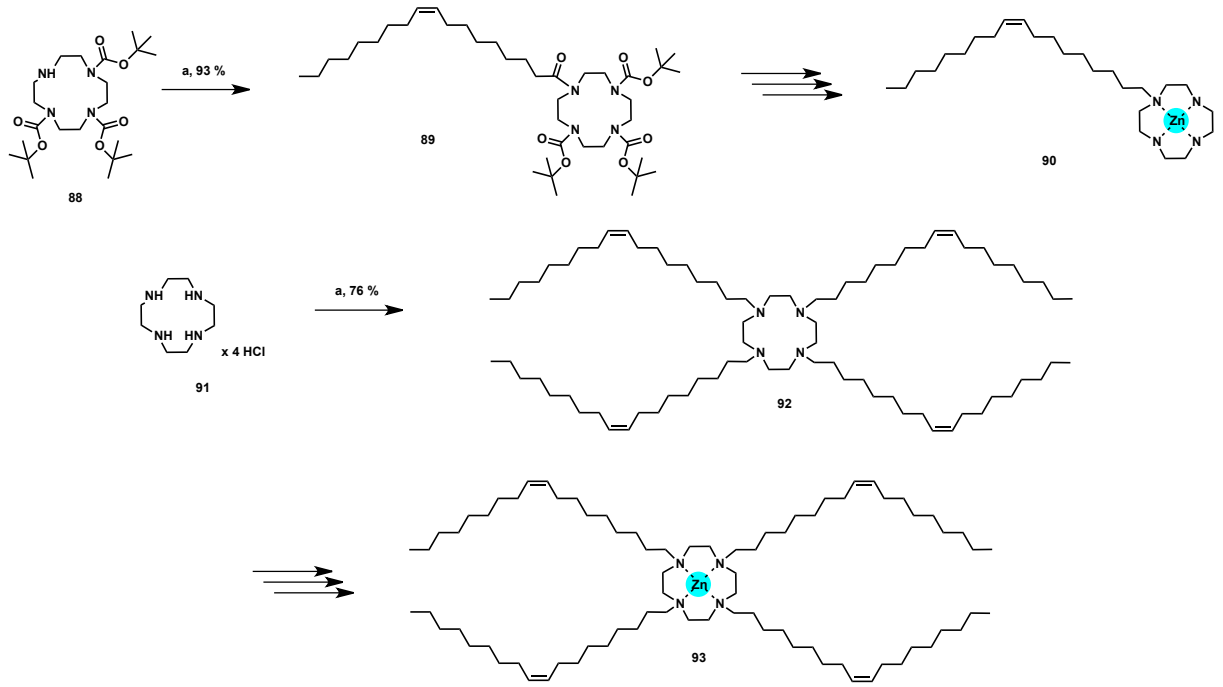

Scheme 3: Synthesis of lipidic cyclen precursor **89** and **92** as Zn(II)-ligands and the proposed synthesis of the lipidic Zn(II)-cyclen complexes. One and four oleyl chains, respectively have successfully been installed. Boc-deprotection, reduction of the amide to the tertiary amines followed by Zn(II) complex formation will lead to the target catalysts **90** and **93**. Conditions: a) Oleoyl chloride, DIPEA, CH_2Cl_2, r.t..

3.5 Experimental section

General Information

1-Monooleoyl-sn-glycerol C18:1 (monoolein, MO) was purchased from Nu-Chek Prep, Inc. (MN, USA), and phosphate buffer solution (PBS (1X) pH 7.4) was purchased from Invitrogen. N-(3- dimethylaminopropyl)-N′-ethylcarbodiimide hydrochloride (EDC) was purchased from TCI, and all other reagents and solvents were purchased from Sigma Aldrich. All chemicals and solvents were used as received, unless otherwise stated. Reactions were carried out under an inert atmosphere of argon in dry solvents. Dichloromethane was degassed with argon and purified by passage through activated alumina solvent column (MC Brown solvent system) prior to use. Column chromatography was performed using silica gel Merck 60 (particle size 0.040–0.063 mm). Analytical thin- layer chromatography (TLC) was performed using Merck pre-coated silica gel plates 60 F254; visualization by UV absorption and/or by dipping in a solution of KMnO4 (1 g), K2CO3 (2 g) in H2O (100 mL) and subsequent heating. 1H-NMR spectra were recorded on a Bruker AV2-500 (500MHz) spectrometer. Chemical shifts are given in parts per million (ppm) relative to the internal standard TMS (δ = 0 ppm). Coupling constants J are expressed in Hz and multiplicities are abbreviated as follows: s (singlet), br (broad), d (doublet), t (triplet), q (quadruplet), quint (quintet), m (multiplet). 13C-NMR chemical shifts are reported relative to the solvent residual peaks: $CDCl_3$ = 77.00 ppm. Mass spectra were recorded by the Mass Spectroscopy Service of UZH on Finnigan MAT95 MS, BrukerLC MS and Finnigan TSQ700 MS machines.

3.5.1 Synthesis

Synthesis of 86 ($PtCl_2(DMSO)_2$)

An aqueous solution (2.5 mL) of $K_2(PtCl_4)$ (100 mg, 0.24 mmol, 1 eq) was prepared and DMSO (56 mg, 0.72 mmol, 3 eq) was added with a syringe. The solution was allowed to stand at room temperature until yellow crystals precipitated (24 h). The precipitate was filtered, washed with water (1 mL), ethanol (1 mL), and ether (1 mL). After drying at high vacuum, the product was obtained as yellow crystals in quantitative yield. Analytical data were identical with the values reported in literature.[17]

Synthesis of 84 ((*E*)-acetophenone oxime)

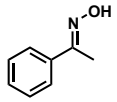

Acetophenone (22 mg, 0.18 mmol, 1 eq) and hydroxylamine hydrochloride (14 mg, 0.2 mmol, 1.1 eq) were dissolved in a mixture of ethanol absolute and pyridine (1:1, 5 mL). The solution was refluxed until the starting material was consumed (2 h). The solvent was evaporated to give a transparent oil, which was treated with distilled water and lyophilized. The crude product was purified by flash chromatography (ethylacetate/CH_2Cl_2) to give the desired pure product in quantitative yield. Analytical data were identical with the values reported in literature.[18]

Synthesis of catalyst 69

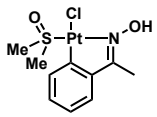

The platinum precursor **86** *cis*-Pt[(DMSO)Cl_2] (315 mg, 0.75 mmol, 1 eq) and MeOH (30 mL) were stirred at 40°C for 2.5 h. Acetophenone oxime **84** (90 mg, 0.75 mmol, 1 eq.) was added and the mixture was stirred for 2 h before it was heated up to reflux and stirred for another 20 h. The solvent was evaporated until a precipitate was formed, then the mixture was allowed to stand for 2 h at 5°C, filtrated and washed with cold MeOH. A second batch was isolated from

the mother liquor to get the product as a brown solid (170 mg, 0.383 mmol, 51 %). Analytical data were identical with the values reported in literature.[18]

Synthesis of 73 (1-(4-(octadecylamino)phenyl)ethan-1-one)[19]

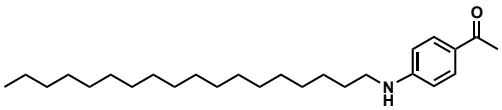

A round bottom flask with $Pd(OAC)_2$ (11.3 mg, 0.05 mmol, 0.05 eq), XPhos (95 mg, 0.1 mmol, 0.1 eq) and 4-bromoacetophenon (200 mg, 1 mmol, 1 eq), stearyl amine (320 mg, 1.5 mmol, 1.5 eq) and Na*t*BuO (190 mg, 2 mmol, 2 eq) was prepared and degased toluene (10 mL) was added. The yellow reaction mixture was heated up to 100°C whereupon the colour turned from brown to black. After 6 h, the oil bath was removed and the reaction mixture was allowed to cool to room temperature. Then the mixture was filtered over celite and the solvent evaporated. The crude product was purified by flash chromatography (ethylacetate/ hexane 2:8) to give the product as slightly yellow oil (280 mg, 0.72 mmol, 28 %). ^{1}H NMR (500 MHz, Chloroform-d) δ 7.81 (d, J = 8.7, 2H), 6.53 (d, J = 8.7, 2H), 4.14 (s, 1 H, NH), 3.17 (q, J = 5.5, 7.0, 2H) 2.48 (s, 3H), 1.61 (quint., J = 7.1, 7.4, 2H); 1.25 (m, 31H); 0.87 (t, J = 7.0, 3H). ^{13}C NMR (126 MHz, Chloroform-*d*) δ 196.27, 152.31, 130.83 (2C), 111.25 (2C), 43.35, 31.93, 29.69–29.33 (*m*, 14C), 27.06, 25.97, 22.69, 14.12. HRMS (ESI $[M + H]^+$) m/z: calcd for ($C_{26}H_{46}ON$) 388.35739, found 388.35691.

Synthesis of 74 ((E)-1-(4-(octadecylamino)phenyl)ethan-1-one oxime)[18]

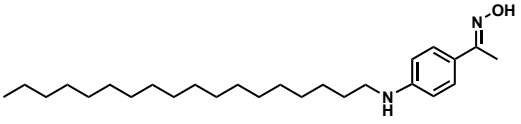

In a round bottom flask equipped with a reflux condenser, **73** (40 mg, 0.103 mmol, 1 eq) and NH_2OH x HCl (9.3 mg, 0.134 mmol, 1.3 eq) were added and dissolved in ethanol (5 mL). Pyridine (2.5 mL) was added and the solution was heated to reflux. After full conversion of **10**, which was monitored by TLC, the solvent was evaporated *in vacuo*. The crude solid was purified by column chromatography (EtOAc/ cyclohexane 15:85). The purified product **27** was obtained as a clear liquid (41 mg, 0.101 mmol, 98%).

^{1}H NMR (500 MHz, Chloroform-d) δ 7.48 (d, J = 8.7, 2H), 6.61 (d, J = 8.4, 2H), 3.13 (t, J = 5.5, 7.0, 2H), 2.23 (s, 3H), 1.63 (quint., J = 7.1, 7.4, 2H), 1.26 (m, 31H), 0.88 (t, J = 7.0, 3H). ^{13}C

NMR (126 MHz, Chloroform-*d*) δ 142.31, 127.28 (2C), 111.25 (2C), 43.35, 31.93, 29.67 - 29.31 (*m*, 14C), 27.08, 25.97, 22.69, 14.11. HRMS (ESI [M + H]$^+$) m/z: calcd for ($C_{26}H_{47}ON_2$) 403.36829, found 403.36858.

Synthesis of catalyst 75[18]

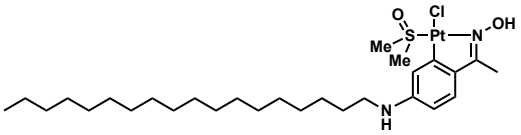

The platinum precursor *cis*-Pt[(DMSO)Cl_2] (31.5 mg, 0.075 mmol, 1 eq) and MeOH (3 mL) were stirred at 40°C for 2.5 h. The acetophenone oxime derivative (30 mg, 0.075 mmol, 1 eq) was added and the mixture stirred for 2 h at before it was heated up to reflux and stirred for another 20 h. The solvent was evaporated until precipitate was formed, then the mixture was allowed to stand for 2 h at 5°C, filtrated, washed with cold MeOH. A second batch was isolated from the mother liquor to get the product as a brown solid (yield: 31%). ^{1}H NMR (500 MHz, DMSO-d_6) δ 7.20 (s, 1H), 7.03 (d, *J* = 7.9 Hz, 1H), 6.29 (s, 1H), 2.98 (t, *J* = 6.6 Hz, 2H), 2.46 (s, 6H), 2.23 (s, 2H), 1.57 – 1.42 (m, 2H), 1.19 (s, 32H), 0.81 (t, *J* = 6.2 Hz, 3H). ^{13}C NMR (126 MHz, DMSO-d_6) δ 170.6, 141.7, 129.4, 110.3, 41.49, 32.35, 30.09 (15C), 29.91, 29.76, 27.62, 23.15, 15.02, 12.19. HRMS (ESI [M + H]$^+$) m/z: calcd for ($C_{28}H_{52}ClN_2O_2PtS$) 710.30805, found 710.30852.

Synthesis of 77 (N-(4-acetylphenyl)dodecanamide)

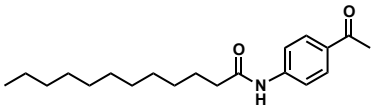

To a solution of 4-aminoacetophenone (0.506 g, 3.69 mmol, 1eq) in CH_2Cl_2 (15 mL) diisopropylethylamin (0.6 mL, 3.69 mmol, 1 eq) was added. The solution was cooled to 0 °C with an ice bath. Lauroylchloride (1.2 mL, 5.54 mmol, 1.5 eq.) was dissolved in CH_2Cl_2 (5 mL) and added dropwise to the reaction mixture. The solution was allowed to warm up to room temperature and stirred overnight. The solution was poured into brine and extracted three times with CH_2Cl_2 (3x 20 mL). The combined organic phases were washed with brine and dried over $MgSO_4$. After evaporation of the solvent, the crude product was purified by column chromatography (EtOAc/ cyclohexane 4:6). The desired product **77** was obtained as a white solid (1.02 g, 3.21 mmol, 87%). ^{1}H NMR (500 MHz, Chloroform-d) δ 7.93 (*d*, *J* = 8.5, 2H), 7.61

(*d*, *J* = 8.5, 2H), 2.57 (*s*, 3H); 2.38 (*t*, *J* = 7.7, 2H), 1.74 (*quint*, 2H), 1.36– 1.26 (*m*, 17H), 0.88 (*t*, *J* = 6.9, 3H). ^{13}C NMR (126 MHz, Chloroform-d) δ 196.99, 171.69, 142.39 (2C), 133.01, 129.92, 116.91 (2C), 60.52, 38.09, 32.05, 29.74–29.38 (6C), 26.56, 25.57, 22.82, 14.25. HRMS (ESI [M + H]$^+$) m/z: calcd for ($C_{20}H_{32}O_2N$) 318.24276, found 318.24247.

Synthesis of 79 ((E)-N-(4-(1-(hydroxyimino)ethyl)phenyl)dodecanamide)

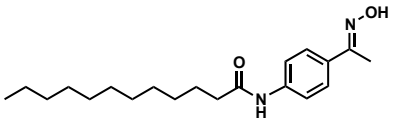

To a solution of ketone **77** (1.0 g, 3.15 mmol, 1 eq) in ethanol (70 mL) NH_2OH x HCl (0.291 g, 4.095 mmol, 1.3 eq) and pyridine (20 mL) was added and the solution was heated to reflux. After full conversion of **77**, which was monitored by TLC, the solvent was evaporated *in vacuo*. The crude solid was purified by column chromatography (EtOAc/ cyclohexane 3:7). The purified product **79** was obtained as a white solid (1.01 g, 3.01 mmol, quant.). ^{1}H NMR (500 MHz, Chloroform-d) δ 7.62 (d, J = 8.7, 2H), 7.55 (d, J = 8.9, 2H), 2.36 (t, J = 7.5, 2H), 2.28 (s, 3H), 1.71 (quint, 2H), 1.36–1.25 (m, 18H), 0.88 (t, J = 6.9, 3H). ^{13}C NMR (126 MHz, Chloroform-d) δ 171.79, 142.40, 129.92 (2C), 128.17, 127.22, 119.53 (2C), 38.05, 32.06, 29.75–29.41 (6C), 26.57, 25.58, 22.83, 14.26. HRMS (ESI [M + H]$^+$) m/z: calcd for ($C_{20}H_{33}O_2N_2$) 333.25365, found 333.25336.

Synthesis of catalyst 81

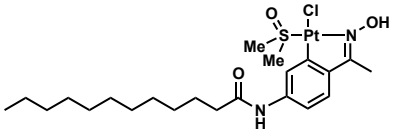

A solution of Pt(II)$(DMSO)_2Cl_2$ (161.7 mg, 0.383 mmol, 1 eq) in methanol (26 mL) was stirred at 40 °C for 2 hours. Oxime **79** (123.5 mg, 0.383 mmol, 1 eq) was dissolved in methanol (6 mL) and added to the reaction mixture, which was stirred for 2 h. The reaction mixture was refluxed for 36 h and the solvent was evaporated and the crude product was filtered and washed with cold methanol. The desired product **81** was obtained as yellow crystals (110.3 mg, 0.172 mmol, 45 %). ^{1}H NMR (500 MHz, Chloroform-d) δ 9.96 (s, 1H), 7.97 (d, J = 8.1, 1H), 7.64 (d, J =2.2, 1H), 7.19 (s, 1H), 7.15 (d, J = 8.8, 1H), 3.55 (s, 6H), 2.37 (s, 3H), 2.32 (t, J = 7.5, 2H), 1.71 (quint, 2 H); 1.39–1.25 (m, 17 H) 0.87 (t, J = 6.9, 3H). ^{13}C NMR (126

MHz, Chloroform-d) δ 171.59, 168.32, 139.78, 138.73, 127.22 (2C), 122.56, 115.47 (2C), 47.36, 38.02, 31.91, 29.47–29.28 (6C) 25.49, 22.69, 14.12, 11.42. HRMS (ESI $[M + H]^+$) m/z: calcd for ($C_{22}H_{38}O_3N_2ClPtS$) 640.19339, found 640.19337.

Synthesis of 78 (N-(4-acetylphenyl)oleamide)

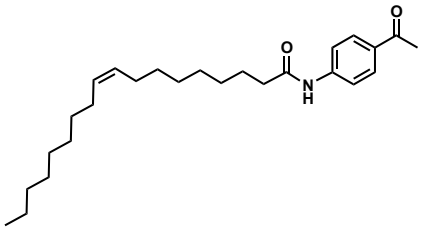

To a solution of 4-aminoacetophenone **76** (0.499 g, 3.69 mmol, 1 eq) in anhydrous CH_2Cl_2 (15 mL) diisopropylethylamin (0.6 mL, 3.69 mmol, 1 eq) was added. The reaction mixture was cooled to 0 °C with an ice bath and a solution of oleylchloride (1.82 mL, 5.54 mmol, 1.5 eq) in CH_2Cl_2 (5 mL) was added dropwise. The solution was allowed to warm to room temperature and stirred for 90 minutes. After complete conversion of the starting material the solution was poured into brine and extracted with CH_2Cl_2 (3x 20 mL). The combined organic phases were washed with brine and dried over $MgSO_4$. After evaporation of the solvent *in vacuo*, the crude product was purified by column chromatography (EtOAc/ cyclohexane 2:8). The desired product **78** was obtained as a white solid (1.37 g, 3.43 mmol, 93%). ^{1}H NMR (500 MHz, Chloroform-d) δ 7.93 (d, J = 8.9, 2H), 7.61 (d, J = 8.7, 2H), 7.24 (s, 1H), 5.34 (m, 2H), 2.57 (s, 3H), 2.38 (t, J = 7.7, 2H), 2.00 (m, 4H), 1.73 (quint, 2 H), 1.41-1.26 (m, 20H), 0.87 (t, J = 6.9, 3H). ^{13}C NMR (126 MHz, Chloroform-d) δ 196.93, 171.59, 142.30 (2C), 132.82, 130.07, 129.78, 129.70, 118.77 (2C), 37.92, 31.91, 29.77–29.11 (m, 8C); 27.24, 27.16, 26.44, 25.42, 22.69, 14.13. HRMS (ESI $[M + H]^+$) m/z: calcd for ($C_{26}H_{42}O_2N$) 400.32101, found 400.32064.

Synthesis of 80 (N-(4-((E)-1-(hydroxyimino)ethyl)phenyl)oleamide)

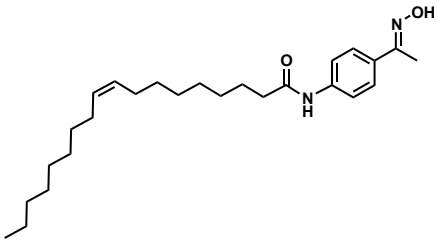

To a solution of ketone **78** (1.0 g, 2.502 mmol, 1 eq) in ethanol (40 mL), NH_2OH x HCl (0.23 g, 3.253 mmol, 1.3 eq) and pyridine (20 mL) was added and the solution was heated to reflux. After full conversion of **78**, which was monitored by TLC, the solvent was evaporated *in vacuo*. The crude solid was purified by column chromatography (EtOAc/ cyclohexane 3:7). The purified product **80** was obtained as a white solid (0.89 g, 2.146 mmol, 95%). ^{1}H NMR (500 MHz, Chloroform-d) δ 7.61 (d, J = 8.8, 2H), 7.54 (d, J = 8.8, 2H), 7.14 (s, 1H), 5.34 (m, 2H), 2.57 (s, 3H), 2.38 (t, J = 7.6, 2H), 2.00 (m, 4 H), 1.73 (quint, 2H), 1.41 - 1.26 (m, 20H), 0.87 (t, J = 6.9, 3H). ^{13}C NMR (126 MHz, Chloroform-d) δ 171.48, 155.77, 139.02, 132.19, 130.17, 129.85, 126.95 (2C), 119.47 (2C), 38.01, 32.03, 29.90–29.24 (10C); 27.36, 27.30, 25.66, 22.81, 14.24, 12.03. HRMS (ESI $[M + H]^+$) m/z: calcd for ($C_{26}H_{43}O_2N_2$) 415.33191, found 415.33221.

Synthesis of 82 (N-(4-((E)-1-(hydroxyimino)ethyl)phenyl)oleamide-Pt(II)(dimethylsulfoxid)chlorid)

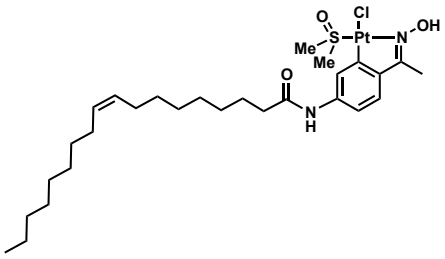

A solution of $Pt(II)(DMSO)_2Cl_2$ (277 mg, 0.65 mmol, 1 eq) in methanol (50 mL) was stirred at 40 °C for 2 hours. Oxime **80** (270 mg, 0.65 mmol, 1 eq) was dissolved in methanol (10 mL) and added to the reaction mixture, which was stirred for 2 h. The reaction mixture was refluxed for 36 h and the solvent was evaporated and the crude product was filtered and washed with cold methanol. The desired product **82** was obtained as a brown solid (178.15 mg, 0.247 mmol, 38 %). ^{1}H NMR (500 MHz, Chloroform-d) δ 9.95 (s, 1H), 7.96 (d, J = 8.8, 1H), 7.69 (d, J = 7.5, 1H) 7.20 (s, 1H), 7.14 (d, J = 8.8, 1H); 5.35 (m, 2H), 3.65 (s, 6H), 2.60 (s, 3H), 2.31 (m, 2H), 1.99 (m, 4H), 1.55 (m, 2H), 1.24 (m, 20H), 0.87 (t, J = 6.9, 3H). ^{13}C

NMR (126 MHz, Chloroform-d) δ 171.48, 155.77, 139.02, 132.19, 130.17, 129.85 (2C), 126.95, 119.47 (2C); 38.01, 32.03, 29.90–29.24 (10C), 27.36, 27.30, 25.66, 22.81, 14.24, 12.03. HRMS (ESI $[M + Na]^+$) m/z: calcd for ($C_{28}H_{47}O_3N_2NaPtS$) 744.25360, found 744.25342.

Synthesis of 89 (tri-tert-butyl(E)-10-(octadec-9-enoyl)-1,4,7,10-tetraazacyclododecane-1,4,7-tricarboxylate)

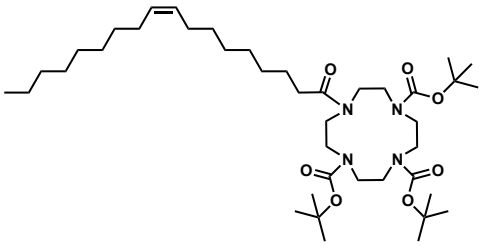

1,4,7-*tris*-Boc-1,4,7,10-tetraaza-cyclododecane **88** (128.8 mg, 0.27 mmol, 1eq) was dissolved in anhydrous CH_2Cl_2 (5 mL) and diisopropylethylamin (0.35 mL, 0.27 mmol, 1 eq.) was added. The solution was cooled to 0 °C and oleylchloride (0.2 mL, 0.408 mmol, 1.5 eq) was dissolved in CH_2Cl_2 (2 mL) was added dropwise. The solution was allowed to warm up to room temperature and was stirred for 90 minutes. The reaction mixture was poured into brine and extracted with CH_2Cl_2 (3 x 10 mL). The combined organic phases were washed with brine and dried over $MgSO_4$. After evaporation of the solvent in vacuo, the crude product was purified by column chromatography (EtOAc/ cyclohexane 2:8) to obtain the desired product **89** as a yellow oil (190 mg, 0.25 mmol, 93%). ^{1}H NMR (500 MHz, Chloroform-d) δ 5.29 (m, 2H), 3.47-3.35 (m, 14H), 2.27 (t, J = 7.6, 2H), 1.99 (m, 4 H), 1.60 (m, 2H), 1.46-1.44 (m, 22 H), 1.28-1.22 (m, 27H) 0.86 (t, J = 7.0, 3H). ^{13}C NMR (126 MHz, Chloroform-d) δ 173.69, 157.43 (2C), 155.49, 130.04, 129.84, 80.45, 80.28, 80.16, 51.49, 50.50 (2C), 49.62, 31.98, 29.85–29.27 (14C); 28.58 (9C), 27.30, 25.49 22.75, 14.19. HRMS (ESI $[M + H]^+$) m/z: calcd for ($C_{41}H_{77}O_7N_4$) 737.57868, found 737.57829.

Synthesis of 92 ((9Z,9'Z,9''Z,9'''Z)-1,1',1'',1'''-(1,4,7,10-tetraazacyclododecane-1,4,7,10-tetrayl)tetrakis - (octadec-9-en-1-one))

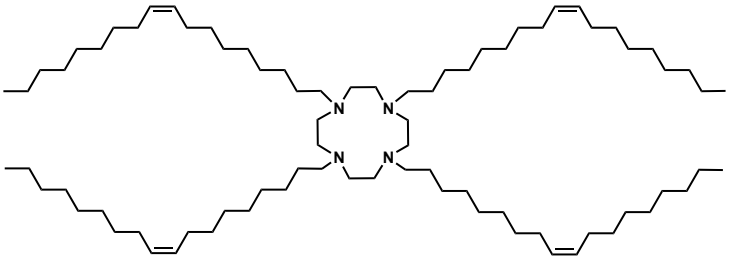

A solution of cyclen tetrahydrochloride **91** (250.2 mg, 0.79 mmol, 1eq) and diisopropylethylamin (0.7 mL, 3.0 mmol, 4 eq) in CH_2Cl_2 (15 mL) was cooled to 0 °C. Subsequently, a solution of oleylchloride (1.5 mL, 3.95 mmol, 5 eq.) in CH_2Cl_2 (5 mL) was added dropwise. The solution was warmed up to room temperature and stirred for 1.5 h. Brine (50 mL) was added and the mixture was extracted with ethylacetate (3 x 30 mL). The combined organic phases were washed with brine and dried over $MgSO_4$. After evaporation of the solvent *in vacuo*, the crude product was purified by column chromatography (EtOAc/ cyclohexane 4:6). The product **37** was obtained as a white solid (737 mg, 0.60 mmol, 76%). ^{1}H NMR (500 MHz, Chloroform-d) δ 5.33 (m, 8H), 3.51 (m, 16H); 2.32 (m, 7H), 2.00 (m, 14 H), 1.62 (m, 9H), 1.29-1.26 (m, 84H), 0.87 (t, J = 7.1, 12H). ^{13}C NMR (126 MHz, Chloroform-d) δ 176.86 (2Cs), 173.85 (2C), 130.11 (4C), 129.76 (4C), 50.31 (8C), 32.00 (4C), 29.86─29.28 (XC); 27.32 (4C); 22.77 (4C); 14.20 (4C). HRMS (ESI $[M + Na]^+$) m/z: calcd for ($C_{80}H_{148}O_4N_4Na$) 1252.13928, found 1252.13954.

3.5.2 Preparation of catalytic mesophases

Catalytic LCPs

MO was weight into a pyrex glass tube and the corresponding amount of a catalyst stock-solution (catalyst in CH_2Cl_2) was added to obtain a homogeneous lipid mixture. The solvent was evaporated (at high vacuum 10^{-2} mbar for 24 h) and the lipidic mixture subsequently hydrated by adding appropriate volumes of buffer and mixed. To obtain homogeneous catalytic LCPs, samples were centrifuged in a Heraeus Megafuge 16R centrifuge (at 5 000 rpm) for 1 h at 23 °C. Samples were finally stored and left to equilibrate for 48 h in tightly closed glass tubes.

3.5.3 Preparation of catalytic cubosomes

MO was weight into a glass vial and the corresponding amount of a catalyst stock-solution (catalyst in CH_2Cl_2) was added to obtain a homogeneous lipid mixture. The solvent was evaporated (at high vacuum 10^{-2} mbar for 24 h) and the lipidic mixture subsequently hydrated by adding appropriate volumes of stabilizer containing buffer (PF108, 1.65 mg / mL) to obtain the cubosome sample with the desired lipid concentration. The sample was vortex-mixed and then dispersed using an ultrasonic processor Brenson digital 250 (cycle 0.9 s on/ 0.9 s off, amplitude 50%, for 3 x 5 min). Subsequently, the cubosome dispersion was filtered through Acrodisc 450 nm filters.

3.5.4 Dynamic Light Scattering (DLS)

Particle size of the cubosomes was performed after preparation, before the reaction was started, and after the reaction was terminated (1-2 d) with a Zeta Sizer Nano ZS (Malvern Instruments, Malvern, UK) at 25 ± 0.1 °C. The samples were measured in disposable polystyrene cuvettes of 1 cm optical path length with the corresponding buffer as solvent. Scattering angle was 90°. A triplicate of the samples was performed. The width of the DLS hydrodynamic diameter distribution is indicated by PDI (polydispersion index). The intensity size distribution of the cubosomes was typically unimodal; therefore the autocorrelation function was analyzed according to the cumulant method.

Bibliography

(1) Kazankov, G. M.; Sergeeva, V. S.; Efremenko, E. N.; Alexandrova, L.; Varfolomeev, S. D.; Ryabov, A. D. Highly Efficient Degradation of Thiophosphate Pesticides Catalyzed by Platinum and Palladium Aryl Oxime Metallacycles. *Angew. Chemie Int. Ed.* **2000**, *112*, 3247–3249.

(2) Mondal, S. S.; Holdt, H.-J. Breaking Down Chemical Weapons by Metal-Organic Frameworks. *Angew. Chemie Int. Ed.* **2015**, 42-44.

(3) Bigley, A. N.; Raushel, F. M. Catalytic Mechanisms for Phosphotriesterases. *Biochim. Biophys. Acta* **2013**, *1834*, 443–453.

(4) Yang, Y.; Baker, J.; Ward, J. Decontamination of Chemical Warfare Agents. *Chem. Rev.* **1992**, No. 92, 1729–1743.

(5) Morales-Rojas, H.; Moss, R. A. Phosphorolytic Reactivity of O -Iodosylcarboxylates and Related Nucleophiles. *Chem. Rev.* **2002**, No. 102, 2497–2551.

(6) Katz, M. J.; Mondloch, J. E.; Totten, R. K.; Park, J. K.; Nguyen, S. T.; Farha, O. K.; Hupp, J. T. Simple and Compelling Biomimetic Metal-Organic Framework Catalyst for the Degradation of Nerve Agent Simulants. *Angew. Chemie Int. Ed.* **2013**, 507-511.

(7) Poznik, M.; Maitra, U.; König, B. The Interface Makes a Difference: Lanthanide Ion Coated Vesicles Hydrolyze Phosphodiesters. *Org. Biomol. Chem.* **2015**, *13*, 9789–9792.

(8) Gruber, B.; Kataev, E.; Aschenbrenner, J.; Stadlbauer, S.; König, B. Vesicles and Micelles from Amphiphilic Zinc(II)-Cyclen Complexes as Highly Potent Promoters of Hydrolytic DNA Cleavage. *J. Am. Chem. Soc.* **2011**, *133*, 20704–20707.

(9) Gunnlaugsson, T.; Davies, R. J. H.; Kruger, P. E.; Jensen, P.; McCabe, T.; Mulready, S.; O'Brien, J. E.; Stevenson, C. S.; Fanning, A. M. Cyclen Based Lanthanide Ion Ribonuclease Mimics: The Effect of Pyridine Cofactors upon Phosphodiester HPNP Hydrolysis. *Tetrahedron Lett.* **2005**, *46*, 3761–3766.

(10) Osornio, Y. M.; Uebelhart, P.; Bosshard, S.; Konrad, F.; Siegel, J. S.; Landau, E. M. Design and Synthesis of Lipids for the Fabrication of Functional Lipidic Cubic-Phase Biomaterials. *J. Org. Chem.* **2012**, *77*, 10583–10595.

(11) Komisarski, M.; Osornio, Y. M.; Siegel, J. S.; Landau, E. M. Tailored Host-Guest Lipidic Cubic Phases: A Protocell Model Exhibiting Nucleic Acid Recognition. *Chem. - A Eur. J.* **2013**, *19*, 1262–1267.

(12) Rahanyan-Kägi, N.; Aleandri, S.; Speziale, C.; Mezzenga, R.; Landau, E. M. Stimuli-Responsive Lipidic Cubic Phase: Triggered Release and Sequestration of Guest Molecules. *Chem. - A Eur. J.* **2015**, *21*, 1873–1877.

(13) Aleandri, S.; Speziale, C.; Mezzenga, R.; Landau, E. M. Design of Light-Triggered Lyotropic Liquid Crystal Mesophases and Their Application as Molecular Switches in "On Demand" Release. *Langmuir* **2015**, *31*, 6981–6987.

(14) Aleandri, S.; Bandera, D.; Mezzenga, R.; Landau, E. M. Biotinylated Cubosomes: A Versatile Tool for Active Targeting and Codelivery of Paclitaxel and a Fluorescein-Based Lipid Dye. *Langmuir* **2015**, *31*, 12770–12776.

(15) Kaasgaard, T.; Drummond, C. J. Ordered 2-D and 3-D Nanostructured Amphiphile Self-Assembly Materials Stable in Excess Solvent. *Phys. Chem. Chem. Phys.* **2006**, *8*, 4957–4975.

(16) Chong, J. Y. T.; Mulet, X.; Waddington, L. J.; Boyd, B. J.; Drummond, C. J. Steric Stabilisation of Self-Assembled Cubic Lyotropic Liquid Crystalline Nanoparticles: High Throughput Evaluation of Triblock Polyethylene Oxide-Polypropylene Oxide-Polyethylene Oxide Copolymers. *Soft Matter* **2011**, *7*, 4768–4777.

(17) Price, B. Y. J. H.; Williamson, A. N.; Schramm, R. F.; Wayland, B. B. Palladium(II) and Platinum(II) Alkyl Sulfoxide Complexes. Examples of Sulfur-Bonded, Mixed Sulfur- and Oxygen-Bonded, and Totally

Oxygen-Bonded Complexes. *Inorg. Chem.* **1972**, *11*, 1280–1284.

(18) Ryabov, A. D.; Kazankov, G. M.; Panyashkina, I. M.; Grozovsky, O. V; Dyachenko, O. G.; Polyakov, A.; Kuz, L. G. Cycloplatination of Aryl and Ferrocenyl Oximes by. *J. Chem. Soc., Dalt. Trans.* **1997**, *2*, 4385–4391.

(19) Altman, R. A.; Buchwald, S. L. Pd-Catalyzed Suzuki-Miyaura Reactions of Aryl Halides Using Bulky Biarylmonophosphine Ligands. *Nat. Protoc.* **2007**, *2*, 3115–3121.

Chapter 4

Palladium nanoparticles synthesized, templated and supported by lipidic cubic phases as catalysts of *Suzuki-Miyaura* cross coupling reactions

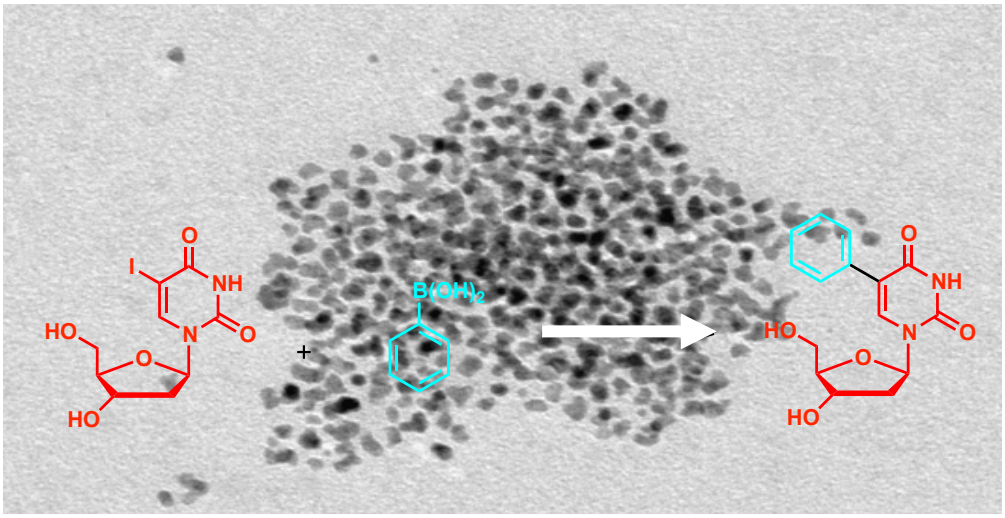

4.1 Introduction

4.1.1 *Suzuki-Miyaura* cross coupling reactions

Among other palladium catalyzed cross coupling reactions,[1–3] the discovery of the *Suzuki-Miyaura* cross coupling reaction in 1979 revolutionized the capabilities for building carbon-carbon bonds. [4,5] Further development of these cross coupling reactions allowed for their versatile application, including the coupling of sp^2-sp^3 and sp^3-sp^3 carbons.[6,7] The chemistry noble prize awarded in 2010 to the discoverer of the palladium catalyzed cross coupling reactions underlines the significance of the *Suzuki-Miyaura* reaction, which is an extensively used method to build-up complex molecules that finds broad application in industry as well as in academic research.

Breslow's discovery of the positive effect of water on the reaction rate and selectivity of *Diels-Alder* reactions in the 1980s led to a renaissance of water as reaction medium for chemical transformations.[8,9] This work has initiated widespread interest in the field of green chemistry, and the repertoire of chemical transformations that can efficiently be carried out in water is ever growing.[10] As early as 1990, a first example of a water tolerant *Suzuki-Miyaura* cross coupling catalyst has been reported.[11] Ever since, many examples of water soluble palladium catalysts have been developed[12,13] including systems using organic co-solvents[14,15], phase transfer catalysts and surfactants.[16–18]

The fact that commonly used phosphine-based ligands for homogeneous catalysis of these reactions are expensive and their recovery is tedious, led to the development of heterogeneously catalyzed systems. Furthermore, by developing heterogeneous catalytic systems that are more easily recyclable, the actual life-time is extended, which improves the efficiency of the catalysts.[19] The heterogenization of established catalysts to different supports is ineffective and many phosphine-free systems are known to leach catalytically active species to the solution.[20] Recent discoveries revealed the potential of palladium nanoparticles (PdNPs) in catalysis,[20,21] which might be a possible approach to overcome earlier mentioned difficulties. Various types of materials have been used for immobilization of PdNPs and their subsequent application in catalysis: Mesoporous silica, polymer supports, carbon nanotubes and metal organic frameworks, only to mention a few.[21] By tuning morphology, shape and size of PdNPs, tailored heteregeneous catalytic systems can be designed.[22,23] Therefore, the method for the synthesis of the PdNPs is a crucial step for the design of such heteregeneous catalytic systems. Not surprisingly, there is a myriad of procedures for the preparation of PdNPs described in literature, many of them require sophisticated reducing steps, are energy-inefficient, or do not allow control over the particle size distribution.[24]

4.1.2 Synthesis of PdNPs

Procedures for the preparation of PdNPs described in the literature will be shortly summarized (without being complete). They can be separated into physical and chemical methods. Physical methods include ion and electron beam deposition,[25,26] laser ablation[27,28] and sputtering.[29,30] They are based on molecular rearrangements; palladium metal precursors do not undergo any chemical transformation. The hydrothermal method is a chemical approach for the synthesis of PdNPs in which the alternated properties of water as solvent at high temperature and high pressure are exploited.[24] Often $PdCl_2$ is used as the palladium precursor, and ammonium formate, formaldehyde and ethylene glycol are used as reducing agents.[24] Electrochemical deposition is another efficient method. In general, the electrolyte serves as the palladium source in a three- or two-electrode cell set up,[24] and several techniques are described in the literature: cyclic voltammetry, square-wave voltammetry, chronoamperometry, chronopotentiometry, chronocoulometry to mention a few examples.[24] Whereas for these methods external current is applied, this is not the case for electroless deposition methods, which can be separated into two categories: displacement deposition (or galvanic replacement) and autocatalytic deposition. the latter requires chemical reducing agents like ethylene glycol, sodium borohydride, ascorbic or citric acid.[24] Additionally, there has been much effort recently to develop more sustainable methods for the synthesis of PdNPs, leading to an entirely new research field called biogenic synthesis of nanoparticles, in which the reductive properties of compounds which are present in plants (polyphenols, alkaloids and terpenoids) is exploited.[31] Liposomes have also been used as nanoreactors to synthesize ultra-small and mono-disperse PdNPs with glycerol as the reducing agents.[32]

4.1.3 Medical applications

Recently, palladium nanoparticles have attracted attention due to their use in the nanomedical field.[33] Weiss *et al*. showed that supported Pd(0) particles were able to bioorthogonally activate 5-fluoro-1-propargyluracil and N^4-propargyloxycarbonylgemcitabine, which in combination are cytotoxic to colorectal and pancreatic cancer cells.[34,35] Huang *et al*. used hexagonal palladium nanosheets for phototermal therapy: They were able to kill liver cancer cells after only 5 min irradiation time.[36] Furthermore, Balbin *et al.* treated four different human cancer cell lines with mesoporous silica supported PdNPs and reported high cytotoxicity of these PdNPs on these cell lines.[37] Additionally, the same particles were successfully applied in *Suzuki-Miyaura* cross coupling- thus a dual application was reported.

4.1.4 PdNP synthesis within LCPs

Puvvada et al.[38] used for the first time MO-based LCPs to synthesize PdNPs. The concept is based on a polyol type reduction of Pd^{2+} and allows PdNP synthesis at benign conditions - neither solvent, nor high temperature, high pressure and expensive equipment are needed. Furthermore, the size of the nanoparticles can be controlled as the LCP plays a dual role as reductant and template with controllable water pore sizes. However, this remains the only such report, and no further investigations with such PdNP-containing LCPs have been carried out. Due to the great potential of this method, we took up the concept and adapted it for our research: the investigation of mesophases as catalyst scaffolds.

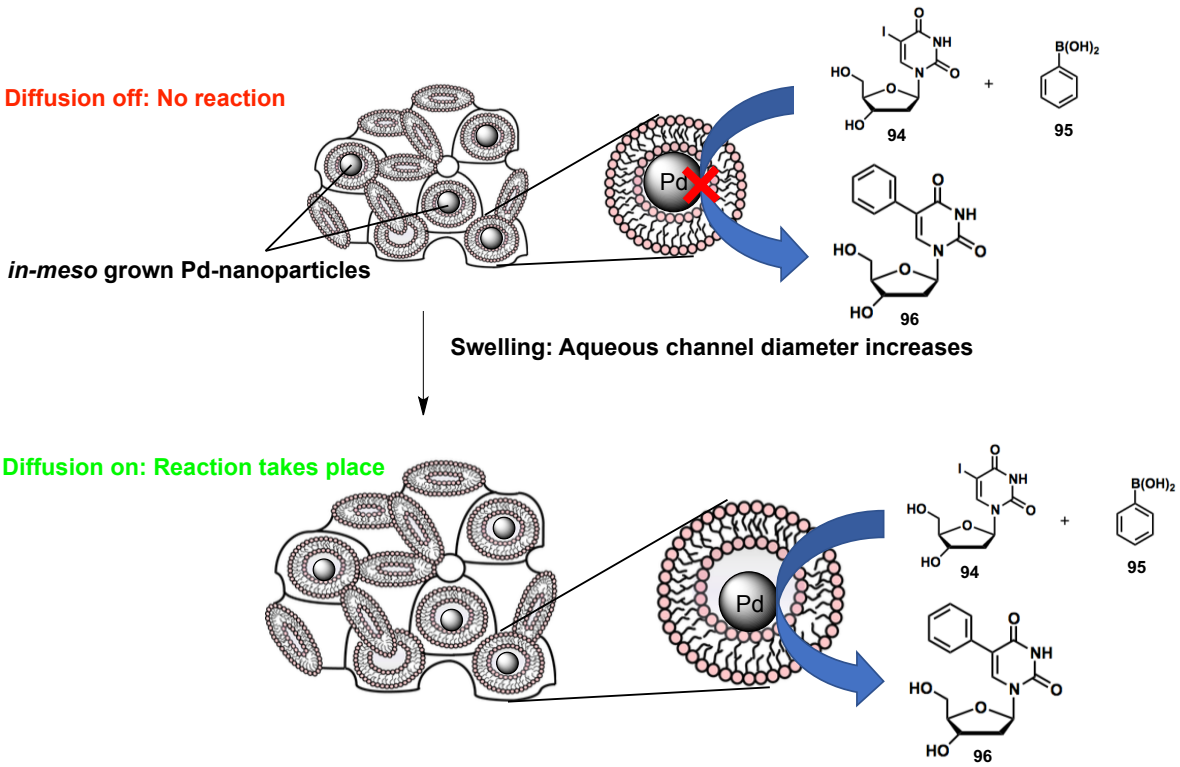

Figure 1: Schematic representation of the PdNPs formed in the aqueous channels of LCPs and subsequent swelling of the aqueous channels. Top panel: The growth of PdNPs is limited by the size of the aqueous channels. This prevents the substrates from diffusing efficiently into the LCP, and thus no product is formed. Bottom panel: The size of the aqueous channels increases upon adding a swelling agent, resulting in the entry of substrates into the LCP and enabling the reaction to take place.

We use this method to directly catalyze cross-coupling reactions in LCPs. Following nanoparticle formation as described by *Puvvada et al.*[38] the aqueous channels were found to be blocked, and diffusion is therefore "switched off". * To overcome this drawback, a "switching on" modification of the LCP is required in order to enable diffusion and allow the reaction to take place (Figure 1). The mesophases thus play a threefold role: they act as a reducing agent for Pd^{2+}, as a template for their growth, and as a support in one. The LCP modifications, material characterization and kinetics of the *Suzuki-Miyaura* cross couplings carried out in bulk LCP, as well as in dispersed palladium lipid hybrid nanoparticles are described herein. Catalyzing *Suzuki-Miyaura* cross couplings with PdNPs synthesized and stabilized in LCPs is a novel approach which is different from our previous work, in which we have developed catalytic LCPs and cubosomes with tunable activity for investigating aldol reactions,[39] demonstrating the broad applicability of these materials in aqueous catalysis.

* An assumption: It was found that the PdNPs size is controlled by the diameter of the aqoueus pores of the LCP. Furthermore, no product is formed applying the LCP before modification.

4.2 Results and discussion

4.2.1 Investigation of *in meso*-PdNP synthesis

The previously reported method to produce PdNP-containing lipidic cubic phases was successfully reproduced: Monoolein was hydrated with a 20 mM solution of K_2PdCl_4, mixed, centrifuged and equilibrated for 24 h.[38] The data of several analytical methods prove the formation of PdNPs within the LCP. The LCP undergoes color change from orange to black (Figure 2A) and the maximum at 420 nm of the UV spectrum of K_2PdCl_4 disappears after the PdNP synthesis. The lipid fraction of the LCP was isolated after PdNP synthesis and analyzed by ^{1}H-NMR. The signal at 9.66 ppm appeared after PdNP synthesis and might originate from an aldehyde formed during the redox process (Figure 2B and 2C). Puvvada *et al*. reported already the corresponding FTIR bands.[38]

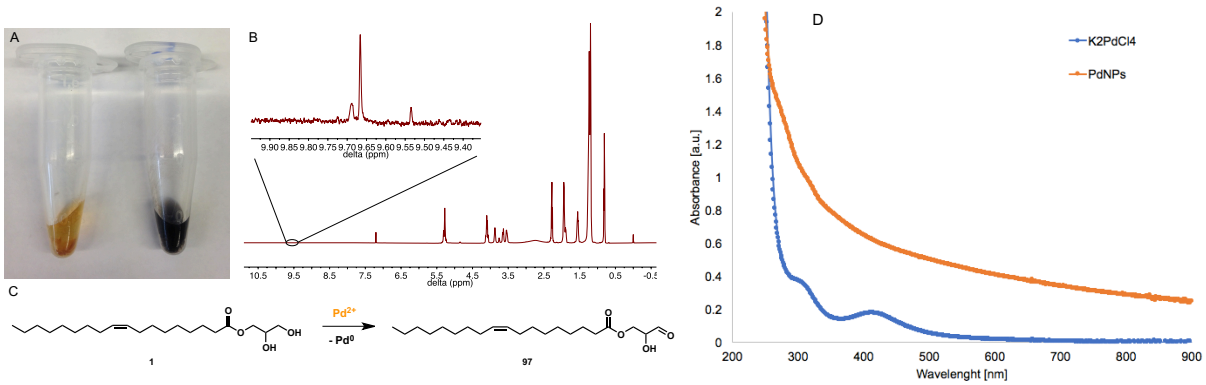

Figure 2: A) Pictures of a LCP directly after hydration with a K_2PdCl_4 solution (left), and after 24 h (right). The characteristic brown color of K_2PdCl_4 disappears and the LCP turns black. B) ^{1}H-NMR spectrum in $CDCl_3$ of the lipid fraction (MO) after PdNP synthesis; a signal which has a typical chemical shift (9.67 ppm) of an aldehyde proton, was detected. C) Proposed redox process leading to PdNP formation. D) UV/Vis spectra of K_2PdCl_4 (blue) and PdNPs (orange).

The kinetics of the PdNP formation was carefully analyzed using small angle X-ray scattering (Figure 3). The slope of the signal at low q value increases in the first 15 h (indicated by the blue arrow), indicating formation of smaller particles. Since the slope does not increase further, the PdNP synthesis is probably completed. Interestingly, shortly before the increase of the slope stagnates, the *Pn3m* LCP undergoes a phase transition to a *Ia3d* cubic phase. It is not clear whether the phase transition is induced, directly or indirectly, by the PdNPs since reduction of the Pd-precursor K_2PdCl_4 brings along the oxidation of MO to aldehyde **97** (Figure 2B and 2C), which might change the lipidic packing. However, the amount of K_2PdCl_4 present in the sample can oxidize no more than 0.47 % of to the aldehyde **97**.

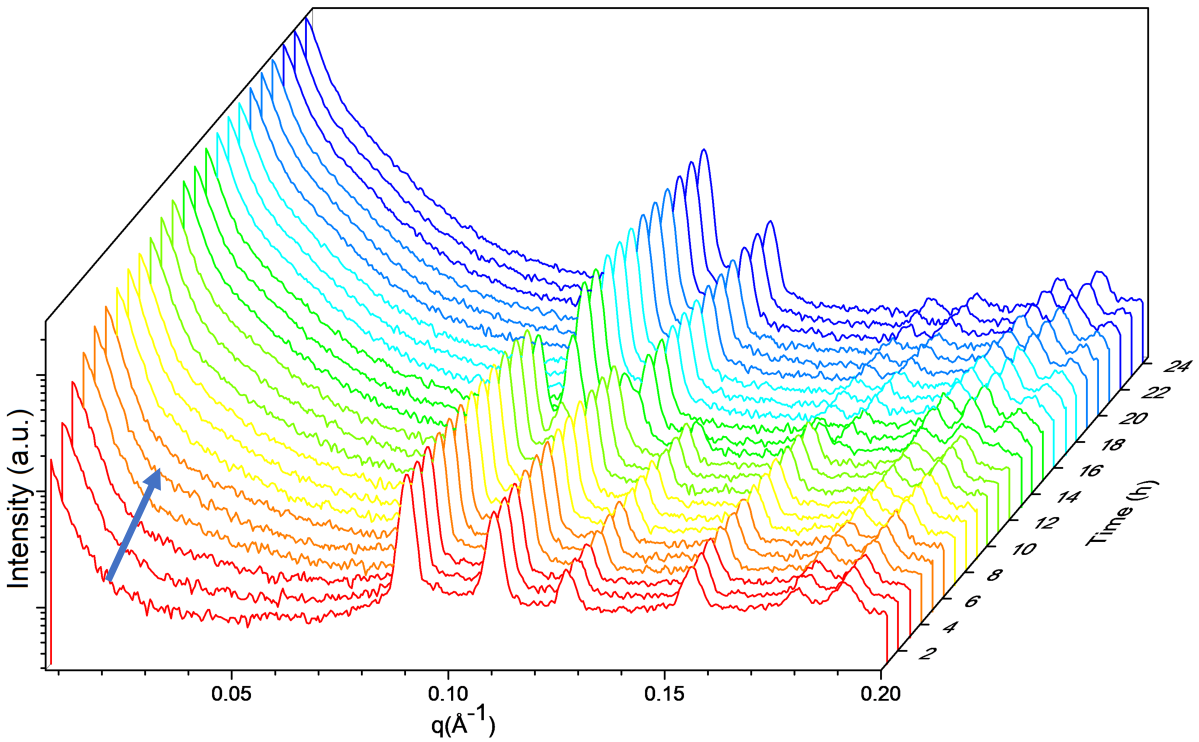

Figure 3: SAXS profile of the time-resolved intensity vs. scattering vector q during the PdNP synthesis in MO LCPs at room temperature.

In a next step, PdNPs were analyzed after lipid removal using transmission electron microscopy (TEM) and DLS. TEM micrographs were taken after adding Pd-LCP on a grid and removing the lipid by simply rinsing the grid with ethyl acetate. PdNPs of 5.3 ± 2.5 nm diameter were found (Figure 4B). For DLS measurements, dodecanethiol was added to the Pd-LCP and mixed. The lipid precipitate was removed by centrifugation, and ethanol was added to the supernatant, which contains PdNPs. This procedure was repeated three times before DLS was measured. Nanoparticles from 3 – 5 nm were detected (Figure 4C).

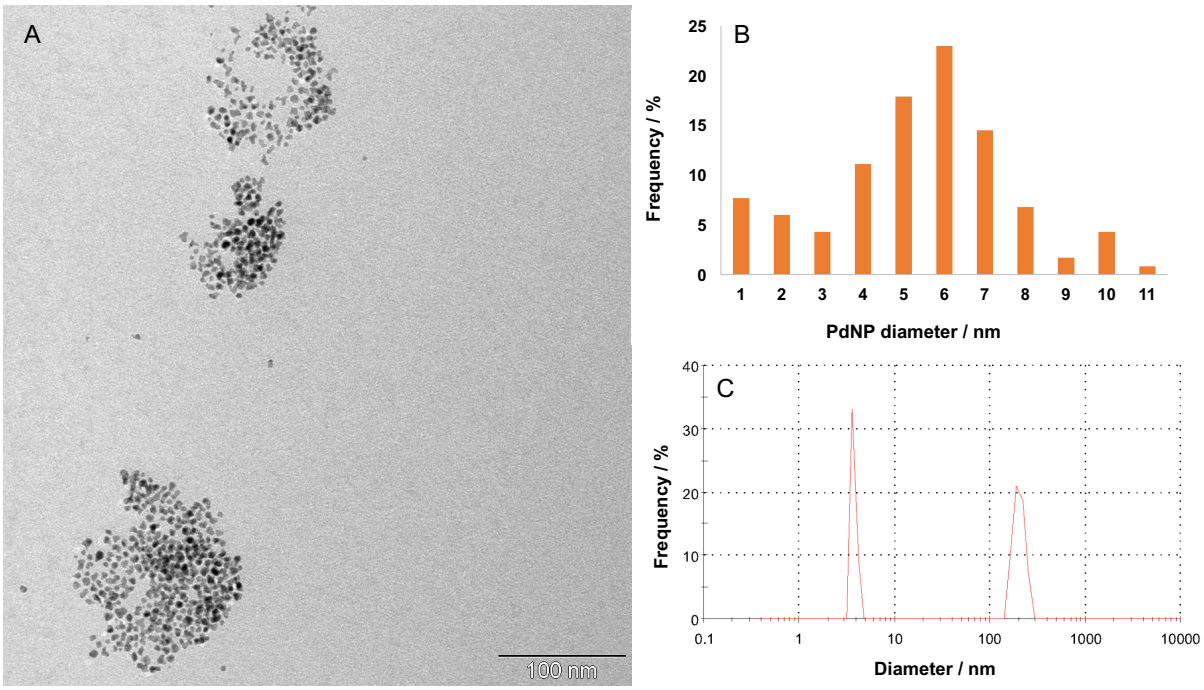

Figure 4: A) TEM micrograph of PdNPs after removal of lipid with ethyl acetate B) Size distribution of PdNPs in A, obtained using ImageJ. C) DLS analysis of PdNPs after removal of lipids with ethanol and PdNP stabilization with dodecanethiol.

Initially, we intended to apply these unmodified mesophases directly for the catalysis of *Suzuki-Miyaura* cross couplings. Catalysis in LCPs and cubosomes requires water-soluble substrates to enable diffusion of substrates from the bulk water into the aqueous channels of the LCPs. To this end, 5-iodo-2'-deoxyuridine (**95**) and phenylboronic acid (**94**) were chosen as substrates for the model reaction to be investigated (Figure 1). A maximum concentration of **95** of ca. 5 mM was identified to be the highest one tolerated by the LCP, as higher concentrations led to destruction of the cubic structure of the material. As already mentioned earlier, only traces (3 %) of the corresponding product was formed (Table 1, entry 5). Puvvada et al. suggested that the size of the PdNPs corresponds to the size of the aqueous channels of the LCPs which were used for their synthesis.[38] Hence, the aqueous channels are blocked by the PdNPs, which leads to strongly reduced diffusion, an thus the substrates do not get into contact with the catalyst and no product is formed.

4.2.2 Swelling of Pd-containing LCPs

We set out to address this problem by swelling the LCP following the PdNP synthesis, thereby "switching on" the diffusion and allowing for the formation of the corresponding cross coupling product (Figure 1). The swelling can be induced via modification of the lipidic compartment, or of the aqueous phase. Hence, our system has two different "switches" to turn on reactivity and to tune it, as has been shown in a previous paper of our group.[39] Cholesterol was chosen as a lipidic swelling agent. Following PdNP synthesis, cholesterol was added and the LCP was equilibrated for at least 4 days before being used for catalysis. The full hydration line with 4 % chlolesterol (w/w lipid) was reached at a hydration degree of 47 %. The diameter of this LCP was calculated to be 5.5 nm (see experimental part for equations and references). In comparison, Puvvada *et. al.* reported an aqueous channel diameter of 5 nm for pure MO LCPs containing PdNPs.[38] Polyethylene glycol (PEG 4000), on the other hand, was used to induce swelling via the aqueous phase and was added simultaneously with the substrates. Since PEG 4000 is water-soluble, it can be removed from the mesophase. This approach allows not only the "on-switching", but also the "off-switching" of the system.

4.2.3 Catalysis of Suzuki-Miyaura cross coupling reactions with PdNP-containing LCPs

Using this approach, LCPs can be applied for catalysis directly following PdNP synthesis. Both approaches led to successful conversion of the starting materials to the desired *Suzuki-Miyaura* product. When cholesterol was used to modify the LCP, 95 % of 5-iodo-2'-deoxyuridine (**94**) was converted to the product (**96**) in 24 h (Table 1, entry 1), whereas 87 % of 5-iodo-2'-deoxyuridine was transformed in 32 h when PEG 4000 was used (Table 1, entry 4). In a next step, the influence of the base on this PdNP-LCP catalysis was investigated. Three bases were tested; K_2CO_3, KOH and NEt_3. Beside the impact of the base on the reaction itself, the tolerance of the LCP toward the base needs to be considered. K_2CO_3 and KOH showed very similar results and allowed for efficient catalysis: after 24 h, 95 % and 98 %, respectively, of **94** was converted (Table 1, entry 1 and 2). When NEt_3 was used as a base, the reaction was significantly slower: after 72 h, 84 % of **94** was consumed (Table 1, entry 3). All these experiments were carried out with 3 mol % Pd with respect to 5-iodo-2'-deoxyuridine (**94**), and only entry 5 was carried out with 1 mol % Pd, which resulted in slower conversion (76 % after 48 h). The reaction progress of Pd-LCP with a catalyst loading of 3 mol % and with K_2CO_3 as base (Table 1, entry 1) is depicted in Figure 5.

Table 1: Comparison of the catalytic efficiencies of PdNP-containing LCPs with different bases, Pd concentrations and swelling approaches on the model *Suzuki-Miyaura* reaction of 5-iodo-2'-deoxyuridine (**94**) and phenylboronic acid (**95**).

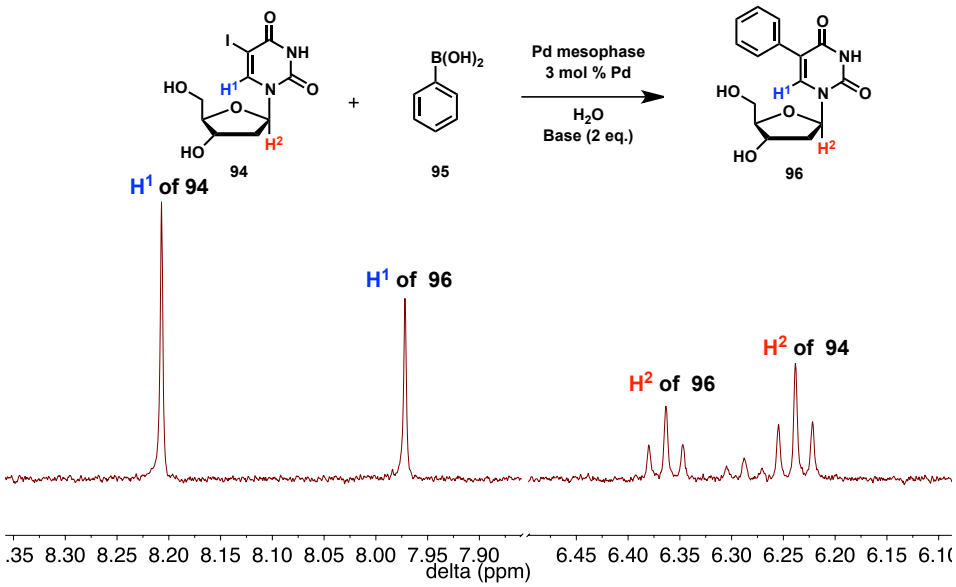

Entry	Swelling agent	Base	Time [h]	Conv.[a] [%]
1	Cholesterol, 4 %[b]	K_2CO_3	24	95
2	Cholesterol, 8 %[b]	K_2CO_3	19	97
3	Cholesterol, 4 %[b]	KOH	24	98
4	Cholesterol, 4 %[b]	Et_3N	72	84
5	Cholesterol, 4 %[c]	K_2CO_3	48	95
6	PEG 4000	K_2CO_3	32	87
7	-	K_2CO_3	24	3
8[d]	-	K_2CO_3	24	0

Conditions: Reactions were carried out in special, home built metal holders at room temperature in miliQ H_2O with 2 eq of base and 2 eq of phenyl boronic acid (**95**). [a]Determined by ^{1}H-NMR. The NMR shows the shift of H^1 (blue) and H^2 (red) when transformed from starting material to product. [b] % w/w of lipid content. [c] Reaction carried out with Pd-LCP containing 1 mol % Pd. [d]Control experiment: Aqueous phase was separated from PdNP-containing LCP and controlled for catalytic activity by ^{1}H-NMR.

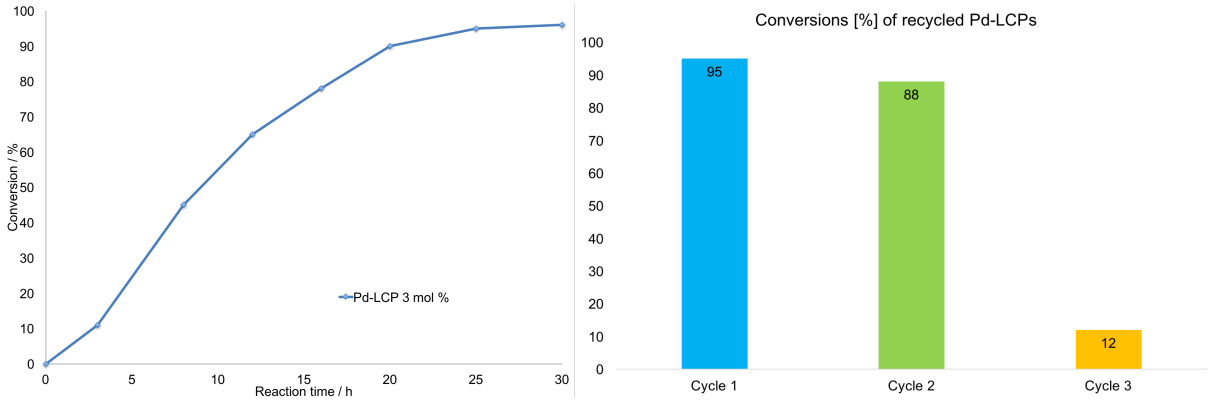

Figure 5: Left: Progress of the *Suzuki-Miyaura* cross coupling reaction of phenyl boronic acid (**95**) with 5-iodo-2'-deoxyuridine (**94**) in Pd-LCP with 3 mol % Pd. Right: Recycling efficiency of PdNP-containing LCPs. Conditions: Reactions were carried out in special, home built metal holders at room temperature in miliQ H_2O with 2 eq. of base and phenyl boronic acid (**95**). Conversions determined by ^{1}H-NMR.

Overall, the best results were obtained when K_2CO_3 was used as base with 3 mol % palladium (Table 1, entry 1). Therefore, this system was used for further investigations such as lowering Pd concentration (Table 1, entry 5), PEG-swelling and recycling of Pd-LCPs. K_2CO_3 is a weaker base compared KOH and nearly as efficient. Weaker bases are preferred due to the better tolerance towards LCPs (e.g. due to hydrolysis of ester group of monoolein).

To prove that the reaction takes place in the aqueous compartment of the LCP rather than in the aqueous overlay, the aqueous phase was checked for its catalytic activity by ^{1}H-NMR. However, no product was observed, indicating that PdNPs remain in the mesophase. ICP-MS analyses supported this finding. Only low Pd-concetrations of 75.2 ng/mL (less than 0.05 % of total Pd) were found in the aqueous phases.

In principle, PdNP-containing LCPs can easily be reused by just removing the crude product and by decanting the aqueous phase. After rinsing with water, a new substrate solution can be added to the LCP as an overlay. However, only two cycles could be achieved without significant loss of activity. The conversion drops slightly in the second cycle from 95 % to 88 % conversion and then drops dramatically to 12 % conversion during the third cycle. This is not consistent with comparable, previous reports on *in-meso* enzymatic and organocatlaytic reactions that are recyclable multiple times.[39,40] The assembly of PdNPs to bigger aggregates might be a reason for the loss of activity. A second reason might be the physical sinking of the PdNPs towards the bottom of the sample. The observation that the upper part of Pd-LCPs turn colorless after two weeks of storage in some cases, supports this hypothesis.

In the initial studies only one substrate pair (phenyl boronic acid (**95**) with 5-iodo-2'-deoxyuridine (**94**) was used. To enlarge the substrate scope of our system, several halogen derivatives were tested, coupling them with phenylboronic acid. The coupling of 4-iodo-benzoeic acid (**98**) and phenyl boronic acid (**3**) delivered the product in traces (Table 2, entry 1). However, the substrates in combination with the products dissolve the LCP, which made completion of the reaction impossible. Bisphospho 5-iodo-2'-deoxyuridine (**100**) is much more hydrophilic than 5-iodo-2'-deoxyuridine (**94**) but leads to similar results (Table 2, entry 2). Adding Boc-4-iodo-*L*-phenylanaline (**102**) to the Pd-LCP destroyed the latter, and no product was detected (Table 2, entry 3). A stable Pd-LCP was observed upon adding 5-bromo-2'-deoxyuridine (**104**) and phenylboronic acid, but also here no product was detected (Table 1, entry 4). To sum up, the substrate scope of Pd-LCPs is so far limited to deoxyuridine derivatives. Other nucleoside derivatives and small peptides are potential candidates to enlarge the scope.

Table 2: Attempts to enlarge the substrate scope for *Suzuki-Miyaura* cross coupling reaction catalyzed by Pd-LCPs by testing different halogen-aryls.

Entry	Halogen-derivatives	*Suzuki*- product	Outcome
1	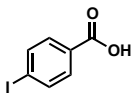 **98**	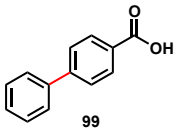 **99**	Traces of product detected[a], LCP is destroyed
2	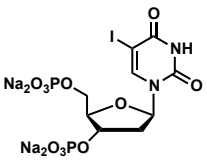 **100**	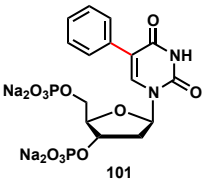 **101**	91 % conversion after 24 h[b]
3	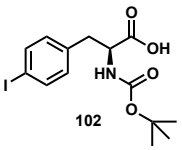 **102**	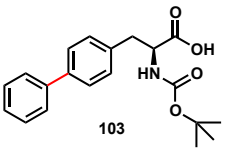 **103**	No product formed, LCP is destroyed already at low concentrations
4	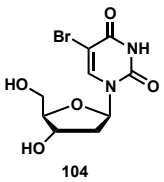 **104**	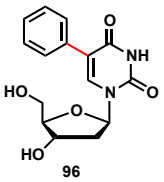 **96**	No product formed, LCP remains stable

Conditions: Reactions were carried out in special, home built metal holders (see experimental part) at room temperature in miliQ H_2O with 2 eq. of base and 2 eq. of phenyl boronic acid (**95**). [a] Determined by ESI-MS. [b] Determined by ^{1}H-NMR.

4.2.4 Preparation and characterization of PdNP/lipid nanoparticles

Since PdNPs need to be grown in bulk LCP, only a top down approach for the formation of lipidic dispersions can be applied. Attempts to synthesize PdNPs in cubosomes after their preparation failed. MO- and PT-based LCPs have been prepared and their aqueous channels were swollen using cholesterol or 1,2-distearoyl-*sn*-glycero-3-phospho-*rac*-(1-glycerol) (DGPG). Interestingly, by varying lipid composition, different Pd/lipidic hybrid nanoparticles can be obtained (Table 3).

Table 3: Formation of various Pd/lipidic hybrid nanoparticles as a function of lipid composition and their catalytic performance in the model reaction of 5-iodo-2'-deoxyuridine (**94**) and phenylboronic acid (**95**). (Cf. Table 1).

Entry	Lipid	Additive	Nanoparticle[a]	Conversion [%][b]
1	MO	Cholesterol	Liposomes	68
2	PT	Cholesterol	Hexosomes	51
3	PT	DGPG	Cubosomes[c]	35
4	PT	DGPG	Cubosomes[d]	54
5	-		-[e]	-

Conditions: Reactions were carried out in special, home built metal holders (see experimental part) at 40°C with 2 eq. of base and 2 eq. of phenyl boronic acid (**95**), and stopped after 72 h. [a] Determined by SAXS. [b] Determined by ^{1}H-NMR after 24 h. [c] Cubosomes underwent phase transition to hexosomes during the reaction [d]Substrate concentration: 1.1 mM (5-iodo-2'-deoxyuridine), Pd loading: 12 mol %. [e] Control experiment: Aqueous phase was separated from the lipid dispersion and controlled for catalytic activity by ^{1}H-NMR.

Dispersion of monoolein/cholesterol LCP, which form cubosomes in the absence of Pd,[39] led to liposomes (Figure 6A), probably due to interactions of the double bond of MO with PdNPs. These samples did not scatter when analyzed by SAXS, but the liposomal structure can be detected by TEM (Figure 6A). The Pd-liposomes are catalytically active and recyclable (3 cycles, Figure 7). The dispersion of phytantriol/cholesterol LCP led to hexosomes which are catalytically active (slightly less than liposomes, Table 2, entry 2). Cubosomes could be obtained upon dispersion of PT/DGPG LCPs (Figure 6B and 6C). Interestingly, a phase transition from the cubic *Pn3m* to H_{II} occurred (Figure 6C) when applied to *Suzuki-Miyaura* cross coupling reaction of phenyl boronic acid (**95**) with 5-iodo-2'-deoxyuridine (**94**) using our standard substrate concentrations (4.3 mM) (Table 2, entry 3). SAXS spectra of the resulting hexosomes were acquired at 22 °C, 40 °C, 50 °C and 60 °C, proving their stability up to 50-°C, while the lattice parameter shifts to higher q values. The sample loses its structure at 60 °C (Figure 6D). The cubic structure could only be retained if the substrate concentration (5-iodo-deoxyuridine) was substantially reduced from 4.3 to 1.1 mM.

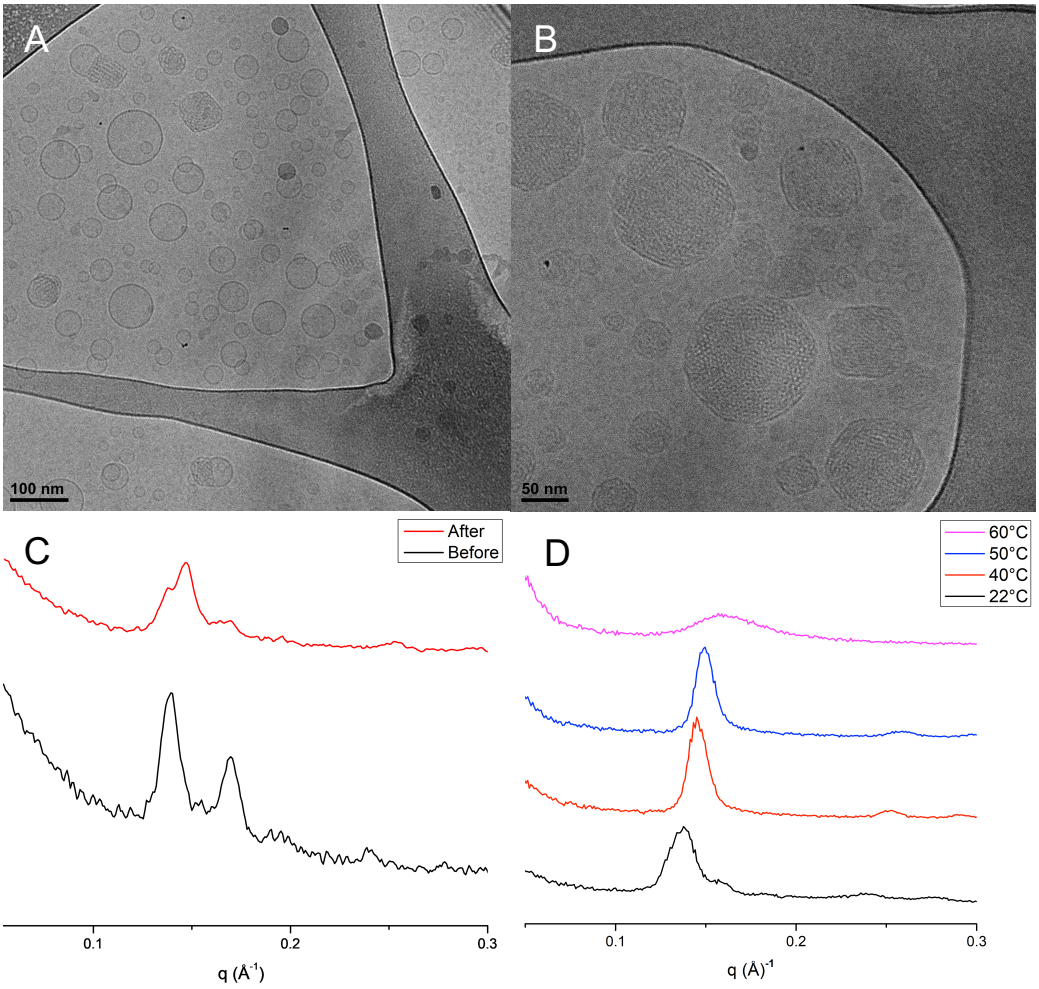

Figure 6: A) TEM micrograph of Pd-liposomes B) TEM micrograph of Pd-cubosomes C) SAXS pattern of Pd-cubosomes before and after reaction at 40 °C D) SAXS pattern of Pd-hexosomes at 22 °C, 40 °C, 50 °C and 60 °C, where the sample starts to lose its hexagonal structure.

4.2.5 Catalysis of Suzuki-Miyaura cross coupling reactions with PdNP/lipid hybrid-nanoparticles

The catalytic activity of Pd-liposomes, Pd-hexosomes and Pd-cubosomes hybrid-nanoparticles were compared using the model coupling reaction 5-iodo-2'-deoxyuridine (**94**) and phenylboronic acid (**95**). In contrast to bulk Pd-LCPs, which are catalytically active at ambient temperatures, the lipid dispersions require elevated temperatures (40 °C) to transform the substrates to the products. Pd-liposomes (Table 3, entry 1), exhibited the best catalytic activity after 48 h, whereby 68 % of the starting material was converted to the product (and 87 % after 78 h, see Figure 4). Using Pd-hexosomes, 51 % of 5-iodo-2'-deoxyuridine (**94**) was consumed (Table 3, entry 2). The lowest catalytic activity was observed with Pd-cubosomes, only 35 % of 5-iodo-2'-deoxyuridine (**94**) were transformed to

the product after 48 h (Table 3, entry 3). These cubosomes underwent phase transitions, resulting in hexosomes when applied to the *Suzuki-Miyaura* coupling of 5-iodo-2'-deoxyuridine (**94**) and phenylboronic acid (**95**). This problem could only be circumvented by reducing the substrate concentration to ca. 25 % of the usual concentration (from 4.3 to 1.1 mM). Since the cubosomes including Pd concentration were kept constant, this led to an increase of Pd to 12 mol % relative to the substrates 5-iodo-2'-deoxyuridine (**95**). After 72 h, 54 % of the substrate was transformed to the product (Table 3, entry 4). We proposed that this problem could be solved if a more hydrophilic substrate was used. To this end, bisphospo-5-iodo-2'-deoxyuridine (**100**) was synthesized (see 4.2.6). However, phase transitions to H_{II} was still observed when **100** was applied as a substrate.

To control if the PdNPs remain inside the lipidic particles, the catalytic activity of the aqueous phase was investigated by adding the substrates 5-iodo-2'-deoxyuridine (**94**) and phenylboronic acid (**95**) (including K_2CO_3). No product was formed after 24 h or after 48 h. ICP-MS analysis of the aqueous phase revealed that the Pd-concentration was 5.2 ng/mL, which corresponds to 0.00325 % of total Pd in the system. To recycle Pd-dispersions, the lipid is separated from the water by filtration, a new stabilizer solution is added, and the sonication process is repeated. Pd-liposomes could be recycled, albeit with a certain loss of catalytic activity after every cycle (Figure 7). Whereas in cycle 1 the conversion was 68 %, it dropped to 59 % in cycle 2 and finally to 45 % in cycle 3 (Figure 7). In general, the coupling reactions catalyzed by Pd/lipid dispersion are slower compared to bulk Pd LCPs and need to be performed at 40 °C. Noteworthy, this is the first report on PdNP-containing hexosomes and cubosomes.

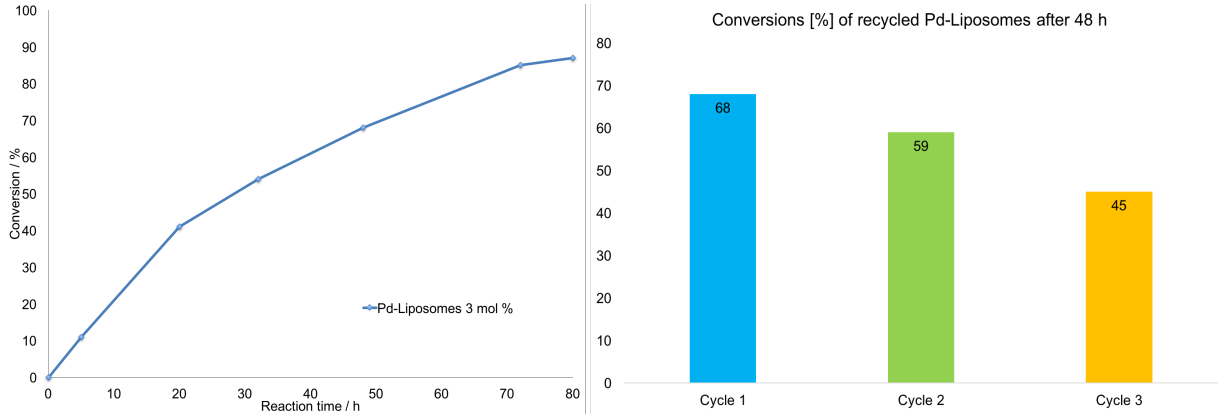

Figure 7: Left: Progress of the *Suzuki-Miyaura* cross coupling reaction of phenyl boronic acid (**95**) with 5-iodo-2'-deoxyuridine (**94**) using Pd-liposomes with 3 mol % Pd. Right: Recycling efficiency of PdNP-containing liposomes. Conditions: Reactions were carried at 40 °C with 2 eq. of base and phenyl boronic acid (**95**). Conversions determined by ^{1}H-NMR.

4.2.6 Synthesis of bisphospho 5-iodo-2'-deoxyuridine (100)

The initial substrates and the product of the model *Suzuki-Miyaura* cross coupling reaction are water-soluble. However, the product with its phenyl group bears a hydrophobic moiety that is introduced in this reaction. During the coupling reaction, an unexpected phase transition from the cubic *Pn3m* to the H_{II} phase was observed. This phase transition might be induced by the formation of this hydrophobic compound, which would interfere with the self-assembled architecture of the cubosomes. To test this assumption, more hydrophilic substrates are required, which were obtained by phosphorylation of 5-iodo-2'-deoxyuridine (**94**). Two different strategies were applied. In a first approach, 5-iodo-2'-deoxyuridine (**94**) was bis-phosphitylated using a Fm-phosphor-amidite, and subsequently oxidized with *t*BuOOH to obtain **105**. The Fm-protecting group was cleaved in a second step using piperidine (Scheme-1). The second approach includes only one step; 5-iodo-2'-deoxyuridine (**94**) was treated with phosphorus oxychloride to obtain bis-phosphorylated 5-iodo-2'-deoxyuridine (**100**). Initially, mono-phosphorylated 5-iodo-2'-deoxyuridine was targeted via phosphitylation of the primary alcohol with Fm-P-amidite. However, a non-separable mixture of mono- and bis-phosphorylated product was obtained. Since two phosphates are more favorable than one, no further attempts towards monophosphorylation have been undertaken.

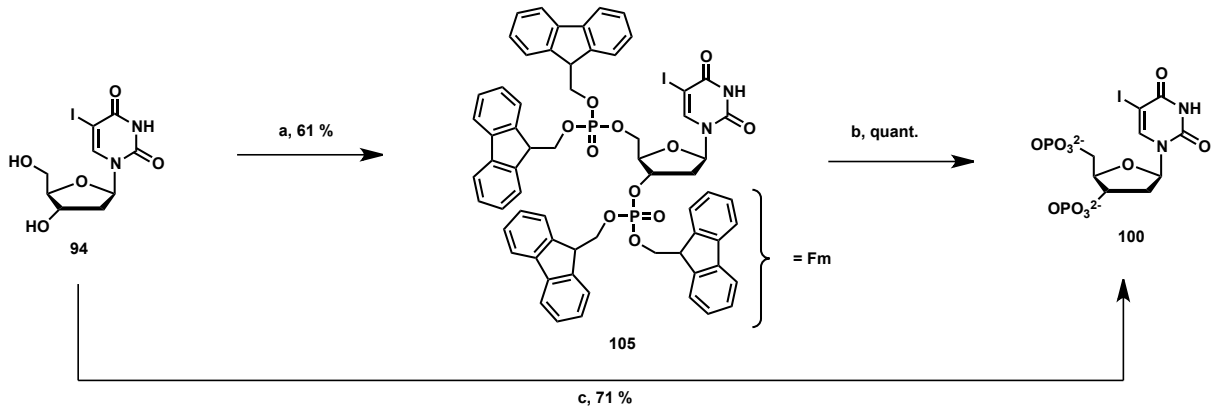

Scheme 1: Diphosphorylation of 5-iodo-2'-deoxyuridine (**94**) in two steps (upper scheme) using Fm-P-amidite followed by oxidation and deprotection, or in one step (procedure c) using phosphorus oxychloride. Conditions: a) Fm-P-amidite, tetrazole, MeCN, 0°C, *t*BuOOH. b) DMF/Piperidine 10:1, r.t. c) phosphorus oxychloride, water, pyridine, acetonitrile, 0°C.

4.2.7 Towards *Suzuki-Miyaura* cross coupling reactions with lipidic Pd-complexes immobilized in mesophases

In addition to the previously described approach using PdNP-containing LCPs to catalyze *Suzuki-Miyaura* cross coupling reactions, a lipidic Pd-catalyst was synthesized that can be incorporated into the mesophases. Gayakhe *et al*. and Kapdi *et. al.* developed water-soluble Pd-imidate complexes that enable chemical modification of nucleoside derivatives via *Suzuki-Miyaura* cross couplings in water as solvent.[41,42] This system served as orientation for the design of an LCP-compatible Pd-complex that can be incorporated into LCPs. In the above-mentioned work, 1,3,5-triaza-7-phosphaadamantane (PTA) served as hydrophilic phosphine ligand that, together with imidate ligands assures the water-solubility of the catalyst. Since for incorporation into LCPs a catalyst with amphiphilic character is required, a lipidic triphenylphosphine ligand **107** was prepared by coupling oleylamine to 4-(diphenylphosphino)benzoic acid (**106**) (Scheme 2). Phtalimidate Pd-complex **cv** was obtained upon treatment of $Pd(OAc)_2$ in dimethyl sulfide (SMe_2) with phthalimid.[43] The desired lipidic Pd-complex **110** was synthesized by treating the Pd-precursor **109** with phosphine ligand **107** in CH_2Cl_2 at reflux for 1 h.[41]

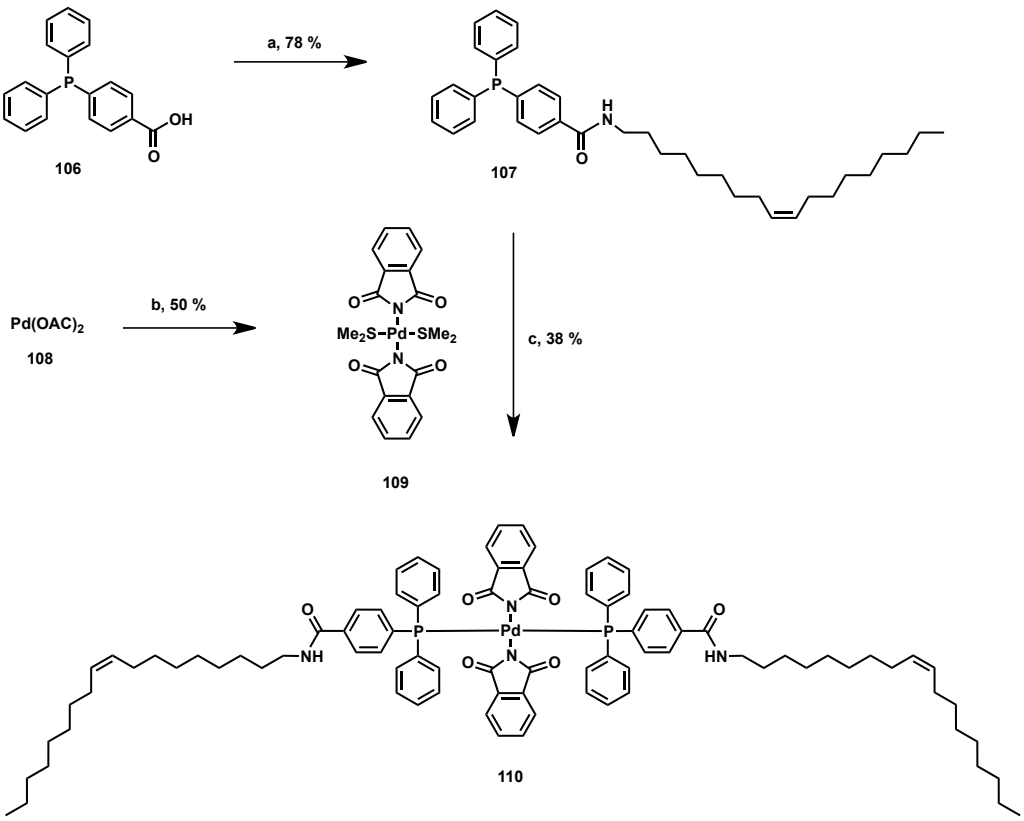

Scheme 2: Synthesis of LCP-compatible Pd-complex **110**. Conditions: a) Oleyl amine 1.2 eq, EDC/DMAP, 0°C, CH_2Cl_2/DMF. b) Phthalimid (2 eq.), Me_2S, r.t. c) **109** 1 eq, **107** 2 eq, CH_2Cl_2, reflux.

Lipidic catalyst **110** was incorporated into MO-based LCPs (3 % w/w lipid). The LCP was then tested in our model *Suzuki-Miyaura* cross coupling reaction. The product was formed very efficiently after 24 h, and no starting material was left. However, as the control experiments revealed that the aqueous phase was also catalytically active, research was focused in the PdNP approach.

4.3 Conclusion

Puvvada *et al*, who reported the only PdNP synthesis in LCPs so far, analyzed the mesophases after the PdNP synthesis with SAXS, and the PdNPs after lipid removal using solvents with TEM.[38] By carefully investigating the PdNP synthesis in LCPs, we were able to provide additional information on the kinetics of this process by using time resolved SAXS analysis, which revealed that the synthesis was completed after 14 h, and induced a phase transition of the LCP from the *Pn3m* to the *Ia3d* cubic phase. Furthermore, we could confirm the formation of aldehyde **97** by means of ^{1}H-NMR, which was proposed based on IR data.[38] In addition to the analysis of isolated PdNPs with TEM, we were able to perform DLS measurements on these particles. The Pd LCPs were used to catalyze a model *Suzuki-Miyaura* cross coupling reaction. The bulk Pd LCPs need to be activated to enable catalysis.

This was achieved by swelling the aqueous channels of the LCPs with a lipidic additive (cholesterol or DGPG) or with PEG 4000, thereby providing two different switches to initiate the reaction. The model cross coupling substrates were transformed to the product with yields as high as 98 % within 24 h, with Pd loading of 3 mol %. Pd-containing liposomes, hexosomes and cubosomes could be prepared from bulk LCPs. By carefully combining the host lipid MO and PT with cholesterol or DGPG as swelling agent, the desired lipidic nanoparticles can be obtained. To the best of our knowledge, PdNP hexosomes and cubosomes are novel, and have not yet been reported. Analogous the parent bulk phase, the dispersed lipid/Pd hybrid nanoparticles are catalytically active as well. However, they are less efficient than bulk Pd LCPs, and thus the reaction needs to be performed at 40 °C.

4.4 Outlook

The narrow substrate scope and the limited recycling are weak points of our approach, which need to be improved. The recycling might be improved by additional stabilization of the PdNPs, using thiols for example.[44] The substrate scope can be extended using small peptides or different nucleosides and nucleotides. Furthermore, these novel Pd/lipid hybrid nanoparticles have potential medical applications. PdNPs have been successfully tested against cancer cell lines.[34,35] Our Pd cubosomes and hexosomes are thus potential delivery vehicles for PdNPs. This would be a very elegant approach, since the PdNPs are *in-situ* synthesized by its drug delivery vehicle.

4.5 Experimental section

General Information

1-Monooleoyl-sn-glycerol C18:1 (monoolein, MO) was purchased from Nu-Chek Prep, Inc. (MN, USA), and phytantriol was purchased from DSM. All other reagents and solvents were purchased from Sigma Aldrich. All chemicals and solvents were used as received, unless otherwise stated. Reactions were carried out under an inert atmosphere of argon in dry solvents. Dichloromethane was degassed with argon and purified by passage through activated alumina solvent column (MC Brown solvent system) prior to use. Column chromatography was performed using silica gel Merck 60 (particle size 0.040–0.063 mm). Analytical thin- layer chromatography (TLC) was performed using Merck pre-coated silica gel plates 60 F_{254}; visualization by UV absorption and/or by dipping in a solution of $KMnO_4$ (1 g), K_2CO_3 (2 g) in H_2O (100 mL) and subsequent heating. ^{1}H-NMR spectra were recorded on a Bruker AV2-500 (500MHz) spectrometer. Chemical shifts are given in parts per million (ppm) relative to the internal standard TMS (δ = 0 ppm). Coupling constants J are expressed in Hz and multiplicities are abbreviated as follows: s (singlet), br (broad), d (doublet), t (triplet), q (quadruplet), quint (quintet), m (multiplet). ^{13}C-NMR chemical shifts are reported relative to the solvent residual peaks: $CDCl_3$ = 77.00 ppm. Mass spectra were recorded by the Mass Spectroscopy Service of UZH on Finnigan MAT95 MS, BrukerLC MS and Finnigan TSQ700 MS machines.

4.5.1 Dynamic Light Scattering (DLS)

Particle size of the cubosomes was performed after preparation, before the reaction was started, and after the reaction was terminated (1-2 d) with a Zeta Sizer Nano ZS (Malvern Instruments, Malvern, UK) at 25 ± 0.1 °C. The samples were measured in disposable polystyrene cuvettes of 1 cm optical path length with the corresponding buffer as solvent. Scattering angle was 90°. A triplicate of the samples was performed. The width of the DLS hydrodynamic diameter distribution is indicated by PDI (polydispersion index). The intensity size distribution of the cubosomes was typically unimodal; therefore the autocorrelation function was analyzed according to the cumulant method.

Table 4: DLS data before and after the aldol reaction.

Particles	SAXS	Size (nm)	PDI
Liposomes	-	226 ± 11	0.272
Hexosomes	H_{II}	176 ± 5	0.237
Cubosomes	*Pn3m*	210 ± 9	0.190

4.5.2 Small angle X-ray scattering (SAXS)

SAXS measurements were used to identify the symmetry of the catalytic LCPs and cubosomes and the fully hydration line of the catalytic LCPs. Experiments were performed on a Bruker AXS Micro, with a microfocused X-ray source, operating at voltage filament current of 50 kV and 1.000 μA, respectively. The Cu Kα radiation (λCu Kα =1.5418 Å) was collimated by a 2D Pilatus 100K detector. The scattering vector q = (4π/λ)sinθ, with 2θ being the scattering angle, was calibrated using silver behenate. Data were collected and azimuthally averaged using the Saxsgui software to yield one-dimensional intensity versus scattering vector *q*, with a *q* range from 0.004 – 0.5 $Å^{-1}$. For all bulk measurements, the samples were placed inside a stainless-steel cell between two thin replaceable mica sheets and sealed by an O-ring, with a sample volume of 10 μL and a thickness of ~1 mm. Measurements were performed at 23°C, and samples were equilibrated for 15 min before measurements, whereas scattered intensity was collected over 30 min. For the cubosomes samples, the sample-to-detector distance was 1 m, providing a q range from 0.005 to 0.77 $Å^{-1}$. Samples were loaded into a quartz glass capillary (Hiligenberg, length: 80 mm; outside: 2.0 mm; wall thickness: 0.01 mm). Measurements were performed at 23 °C, and samples were equilibrated for 10 min prior to measurements, while scattered intensity was collected over 4 hours.

Mesophase identification and calculation of the aqueous channels

Mesophases were identified by their specific Bragg peak positions. For the double diamond cubic phase (*Pn3m*) the relative positions in *q* of the Bragg reflections are at √2:√3:√4:√6:√8:√9…, whereas for the primitive cubic phase (*Im3m*) the Bragg peaks are at q = √2:√4:√6:√8:√10:√12:√14:√16:√18… The mean lattice parameter, a, was deduced from the corresponding set of observed interplanar distances, d (d = 2π/*q*), using the appropriate scattering law for the phase structure. For cubic phases:

$$a = d\sqrt{h^2 + k^2 + l^2} \qquad (1)$$

By knowing from SAXS measurements the geometry and the lattice parameter a, and knowing the lipid volume fraction of the sample ϕ, the length of the lipid tail, *l,* can be calculated by solving the following cubic equation[45]:

$$\Phi = 2A_0\left(\frac{L_{lip}}{a}\right) + \frac{4}{3}\pi\chi\left(\frac{L_{lip}}{a}\right)^3 \qquad (2)$$

where A_0 is the area of the surface in the unit cell in which the lattice parameter is equal to unity, and χ is the Euler-Poincare characteristic. Depending on the specific cubic phase they have the following values: $A_0 = 3.091$ and $\chi = -8$ for *Ia3d;* $A_0 = 1.919$ and $\chi = -2$ for *Pn3m;* and $A_0 = 2.345$ and $\chi = -4$ for *Im3m*. For the radius of the aqueous channels, *r* the following equations are valid for the *Ia3d*, *Pn3m* and *Im3m* phases, respectively[46]:

$$r = 0.248a - L_{lip} \qquad (3a)$$

$$r = 0.391a - L_{lip} \qquad (3b)$$

$$r = 0.3055a - L_{lip} \qquad (3c)$$

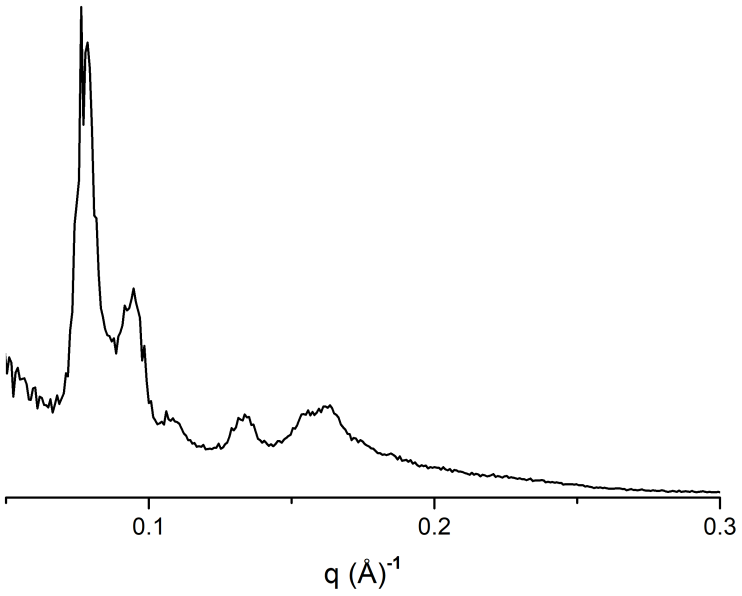

Figure 8: *Pn3m* SAXS pattern of fully hydrated Pd LCP with 47 % w/w water (10 mM K_2CO_3), 4 % cholesterol of the lipid content at 23°C.

4.5.3 General procedures for PdNP-mesophases synthesis

MO and PT LCPs

MO or PT (60 mg) was weight into an eppendorf tube and molten with a heating gun (40°C). The lipid was subsequently hydrated by adding appropriate volumes of a solution of K_2PdCl_4 (20 mM) and K_2CO_3 (10 mM) in miliQ H_2O (50 µL). To obtain homogeneous palladium particle containing LCPs, samples were centrifuged in an eppendorf 5415 R centrifuge for at least 1 h at 23 °C at 13'000 rpm. Samples were stored and left to equilibrate for at least 48 h in tightly closed eppendorf tubes. The color of the LCP changes during this time from brown to black. In order to swell the LCP, a suspension of cholesterol (2.5 mg or 1.25 mg) in 10 mM aqueous K_2CO_3 solution (50 µL) was added, stirred with a needle and centrifuged again in an eppendorf 5415 R centrifuge for at least 1 h at 23 °C at 13'000 rpm. Samples were finally stored and left to equilibrate for at least 5 days in tightly closed eppendorf tubes in the dark.

PT cubosomes

Cubosomes were prepared using a top down approach; after production of bulk PT LCP, a swelling agent (1,2-distearoyl-sn-glycero-3-phospho-rac-(1-glycerol) sodium salt) was added and the sample was dispersed in a stabilizer solution (PF-127) by ultra sonication. PT (60 mg) was weight into a eppendorf tube and the lipid was subsequently hydrated by adding appropriate volumes of a solution of K_2PdCl_4 (20 mM) in miliQ H_2O (50 µL). To obtain homogeneous palladium particle containing LCPs, the samples were centrifuged in an eppendorf 5415 R centrifuge for 1 h at 23 °C at 13'000 rpm. Samples were stored and left to equilibrate for 48 h in tightly closed eppendorf tubes. The color of the LCP changes during this time from brown to black. In order to swell the LCP, a suspension of 1,2-distearoyl-sn-glycero-3-phospho-rac-(1-glycerol) sodium salt (2.0 mg) in miliQ H_2O (50 µL) was added, stirred with a needle and centrifuged again in an eppendorf 5415 R centrifuge for at least 1 h at 23 °C at 13'000 rpm. After the sample was stirred and centrifuged a second time, they were finally stored and left to equilibrate for at least 5 days in tightly closed eppendorf tubes in the dark. The lipidic mixture was subsequently hydrated by adding appropriate volumes of stabilizer containing buffer (PF-127, 1% w/w) to obtain the cubosome sample with the desired lipid concentration. The sample was vortex-mixed and then dispersed using an ultrasonic processor Brenson digital 250 (cycle 0.9 s on/ 0.9 s off, amplitude 50%, for 3 x 5 min). Subsequently, the cubosome dispersion was filtered through Acrodisc 450 nm filters.

PT hexosomes

Hexosomes were prepared using a top down approach; after production of bulk LCP, a swelling agent (cholesterol) was added. The sample was dispersed in a stabilizer solution (PF-127) by ultra sonication. PT (60 mg) was weight into a eppendorf tube and the lipid was subsequently hydrated by adding appropriate volumes of a solution of K_2PdCl_4 (20 mM) in miliQ H_2O (50 µL). To obtain homogeneous palladium particle containing LCPs, the samples were centrifuged in an eppendorf 5415 R centrifuge for 1 h at 23 °C at 13'000 rpm. The samples were stored and left to equilibrate for 48 h in tightly closed eppendorf tubes. The color of the LCP changes during this time from brown to black. In order to swell the LCP, a suspension of cholesterol (5.0 mg) in miliQ H_2O (50 µL) was added, stirred with a needle and centrifuged again in an eppendorf 5415 R centrifuge for at least 1 h at 23 °C at 13'000 rpm. After the sample was stirred and centrifuged a second time, they were finally stored and left to equilibrate for at least 5 days in tightly closed eppendorf tubes in the dark. The lipidic mixture was subsequently hydrated by adding appropriate volumes of stabilizer containing buffer (PF-127, 1% w/w) to obtain the hexosome sample with the desired lipid concentration. The sample was vortex-mixed and then dispersed using an ultrasonic processor Brenson digital 250 (cycle

0.9 s on/ 0.9 s off, amplitude 50%, for 3 x 5 min). Subsequently, the hexosome dispersion was filtered through Acrodisc 450 nm filters.

MO liposomes

MO (60 mg) was weight into an eppendorf tube and molten with a heating gun (40°C). The lipid was subsequently hydrated by adding appropriate volumes of a solution of K_2PdCl_4 (20 mM) and K_2CO_3 (10 mM) in miliQ H_2O (50 µL). To obtain homogeneous palladium particle containing LCPs, samples were centrifuged in an eppendorf 5415 R centrifuge for at least 1 h at 23 °C at 13'000 rpm. Samples were stored and left to equilibrate for at least 48 h in tightly closed eppendorf tubes. The color of the LCP changes during this time from brown to black. In order to swell the LCP, a suspension of cholesterol (5.0 mg or 2.5 mg) in 10 mM aqueous K_2CO_3 solution (50 µL) was added, stirred with a needle and centrifuged again in an eppendorf 5415 R centrifuge for at least 1 h at 23 °C at 13'000 rpm. Samples were finally stored and left to equilibrate for at least 5 days in tightly closed eppendorf tubes in the dark. The lipidic mixture was subsequently hydrated by adding appropriate volumes of stabilizer containing buffer (PF-127, 1% w/w or PF-108, 1.65 mg / mL) to obtain the liposome sample with the desired lipid concentration. The sample was vortex-mixed and then dispersed using an ultrasonic processor Brenson digital 250 (cycle 0.9 s on/ 0.9 s off, amplitude 50%, for 3 x 5 min). Subsequently, the liposome dispersion was filtered through Acrodisc 450 nm filters.

4.5.4 General procedures for the Suzuki-Miyaura couplings in LCP

Previously prepared LCP (containing PdNPs, prepared as described above) was added on homemade metal holders and the plastic container for the aqueous phase was attached. Subsequently, a solution of the desired aryl halide (2 mL, 4.3 mM, 1 eq) and phenyl boronic acid (8.6 mM, 2eq) in 2 mL miliQ H_2O was carefully poured on top of the catalytic LCP. The set-up was gently shaken on a laboratory shaker. The reaction was monitored by ^{1}H-NMR. After completion of the reaction, the aqueous phase was removed and the LCP rinsed with 2-mL of miliQ H_2O. The aqueous phases were extracted with EtOAc (5 x 3 mL). The combined organic phases were washed with brine and dried over MgSO4. The solvent was removed and the crude product was purified by column chromatography (silica gel, cyclohexane/EtOAc) to obtain the pure Suzuki-Miyaura product.

4.5.5 General procedures for the Suzuki-Miyaura couplings in cubosomes, hexosomes and liposomes

The halogen derivative (3 mg, 0.0085 mmol, 1 eq) and phenyl boronic acid (2.1 mg, 0.017 mmol, 2 eq) were added to previously prepared lipidic nanoparticles (containing PdNPs, prepared as described above) and the reaction mixture was stirred at 40 °C. The reaction was monitored by ^{1}H-NMR. After completion of the reaction, the lipidic nanoparticles were separated from the aqueous phase by centrifugation with vivacon 500 filter. The lipidic part was rinsed with 2 mL miliQ H_2O. The aqueous phases were extracted with EtOAc (5 x 3 mL). The combined organic phases were washed with brine and dried over $MgSO_4$. The solvent was removed and the crude product was purified by column chromatography (silica gel, cyclohexane/EtOAc) to obtain the *Suzuki-Miyaura* products.

Synthesis of 96 (1-((2*R*,4*S*,5*R*)-4-hydroxy-5-(hydroxymethyl)tetrahydrofuran-2-yl)-5-phenylpyrimidine-2,4(1*H*,3*H*)-dione)

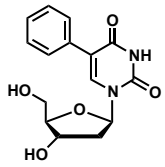

Synthesized using PdNP-containing LCPs and lipid/Pd hybrid nanoparticles.
^{1}H NMR (500 MHz, DMSO-d_6) δ 11.51 (s, 1H), 8.20 (s, 1H), 7.81 – 7.76 (m, 3H), 7.55 (d, *J* = 7.4 Hz, 3H), 7.34 (ddq, *J* = 29.0, 14.5, 7.3 Hz, 9H), 6.24 (t, *J* = 6.6 Hz, 1H), 5.26 (d, *J* = 3.8 Hz, 2H), 5.12 (t, *J* = 4.4 Hz, 2H), 3.82 (d, *J* = 3.1 Hz, 1H), 3.66 – 3.55 (m, 4H), 2.28 – 2.12 (m, 4H). ^{13}C NMR (126 MHz, DMSO-d_6) δ 162.09, 149.92, 138.01, 134.07, 130.02, 128.12 (2C), 127.90 (2C), 127.36 (2C), 113.46, 87.50, 84.47, 70.24, 60.98. HRMS (ESI $[M + Na]^+$) m/z: calcd for ($C_{15}H_{16}O_5N_2Na$) 327.09514, found 327.09503.

4.5.6 Synthesis of *Suzuki-Miyaura* substrates

Synthesis of 105 (Fm-protected bisphosphorylated iodo-deoxyuridine) modified from[47]

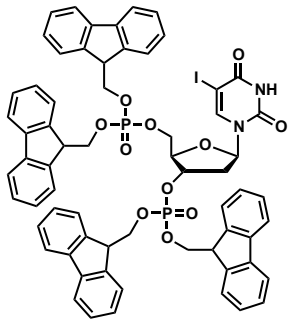

Fm-phosphoramidite (266 mg, 0.510 mmol, 2.6 eq) was coevaporated with MeCN (3 x 1 mL). Pentafluorophenol (380 mg, 2 mmol, 5 eq.) in MeCN (3 mL) were added and the mixture stirred at room temperature for one hour. The activation was checked by ^{31}P-NMR. Subsequently, the solvent was removed and a solution of 5-iodo-2'-deoxyuridine (**95**) (71 mg 0.2 mmol, 1 eq) in MeCN (3 mL) was added and the reaction stirred overnight at room temperature. As soon as the starting material was consumed, the reaction mixture was cooled in an ice/water bath and *m*CPBA (70 %, 65 mg, 0.510 mmol, 1.3 eq.) was added. The crude product was purified by column chromatography (cyclohexane/EtOAc) to obtain the desired product as a yellow oil (148 mg, 0.122 mmol, 61 %). ^{1}H NMR (500 MHz, Chloroform-*d*) δ 8.60 (s, 1H), 8.06 – 7.98 (m, 1H), 7.61 (m, 7.68 – 7.56, 8H), 7.48 – 7.02 (m, 24H), 5.88 (dd, *J* = 8.5, 5.6 Hz, 1H), 4.45 (t, *J* = 6.2 Hz, 1H), 4.30 – 4.11 (m, 10H), 4.04 – 3.94 (m, 4H), 3.76 (s, 1H), 3.67 – 3.47 (m, 2H). ^{13}C NMR (126 MHz, Chloroform-*d*) δ 171.21, 159.53 (2C), 149.27, 145.33, 143.69, 142.86 – 142.54 (m, 8C), 141.69 – 141.21 (m, 8C), 129.44, 129.37, 127.97 (2C), 127.31 – 126.99 (m, 8C), 124.97 (m, 8C), 124.90 – 124.77 (m, 8C), 120.28 – 119.84 (m, 8C), 116.46, 116.28, 86.02, 84.85, 83.21, 69.27, 68.84, 68.26, 66.04, 61.57, 60.42, 47.97 – 47.61 (m, 4C), 21.06, 14.19. ^{31}P NMR {^{1}H} (203 MHz, Chloroform-*d*) δ -1.46, -2.78. ^{31}P NMR (203 MHz, Chloroform-*d*) δ -1.46, -2.78 (q, *J* = 5.3 Hz). HRMS (ESI [M + H]$^{+}$) m/z: calcd for ($C_{65}H_{54}O_{11}N_2IP_2$) 1227.22420, found 1227.22592.

Synthesis of 100 (Diphosphorylated iodo-deoxyuridine)

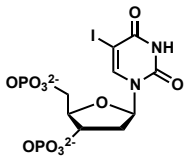

Method A

Fm-protected 5-iodo-2'-deoxyuridine bis-phosphate **105** (148 mg, 0.122 mmol) was dissolved in 5 mL of a mixture of DMF/piperidine (5:1) and stirred overnight. The solvent and excess piperidine was was removed at high vacuum to obtain the product as piperidine salt in quantitative yield.

Method B, modified procedure from Sowa *et al*.[48]

A mixture of phosphoroxy chloride (675 mg, 4.4 mmol, 4.4 eq.), water (500 mg, 2.8 mmol, 1.4-eq), pyridine (380 mg, 4.8 mmol, 4.8 eq) was cooled to 0°C and 5-iodo-2'-deoxyuridine (360 mg, 1.0 mmol, 1 eq) was added. The mixture was stirred for 4 h at 0 °C whereupon the reaction mixture was quenched with cold water and stirred for 1 h. The pH was adjusted to 9 with aq. NaOH (0.1 M) and the solvent was removed. The desired product was obtained as white solid (408 mg, 0.71 mmol, 71 %).

^{1}H NMR (400 MHz, Deuterium Oxide) δ 8.20 (s, 1H), 7.84 (s, 1H), 6.25 – 6.14 (m, 1H), 4.60 (s, 1H), 4.19 (s, 1H), 4.05 (d, *J* = 4.1 Hz, 1H), 3.94 – 3.68 (m, 1H), 2.52 – 2.20 (m, 2H). 13C NMR (126 MHz, DMSO-d6) δ 160.92, 150.58, 145.09, 85.02, 73.87, 70.39, 49.05. ^{31}P NMR {^{1}H} (162 MHz, Deuterium Oxide) δ 3.52, 3.02. ^{31}P NMR (162 MHz, Deuterium Oxide) δ 3.51, 3.02 (d, *J* = 7.6 Hz). HRMS (ESI [M + H]$^{+}$) m/z: calcd for ($C_9H_{12}O_{11}N_2IP_2$) 512.89665, found 512.89680.

4.5.7 Synthesis of lipidic Pd Complex

Synthesis of 107 ((*Z*)-4-(diphenylphosphino)-*N*-(octadec-9-en-1-yl)benzamide)

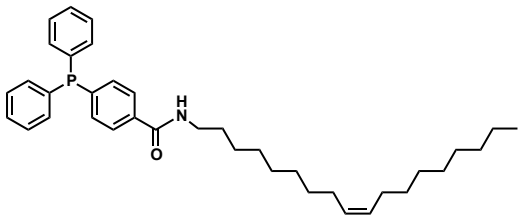

To a stirred solution of 4-(diphenylphosphino)benzoic acid (**106**) (710 mg mg, 2.32 mmol, 1-eq) in 50 mL of a mixture of dry CH_2Cl_2 and dry DMF (1:1) was added EDC (466 mg mg, 3.00 mmol, 1.3 eq) and DMAP (28 mg, 0.232 mmol, 0.1 eq) at 0 °C under an inert atmosphere. The solution was stirred for 1 h at 0 °C and then the oleylamine amine (930 mg, 3.48 mmol, 1.5 eq.) was added dropwise over a period of 10 min. The reaction mixture was stirred for 14 h at room temperature and then CH_2Cl_2 (50 mL) was added, the mixture was washed with a saturated solution of $NaHCO_3$. The organic phase was separated and the aqueous phase was extracted with CH_2Cl_2 (50 mL). The combined organic phases were washed with brine and dried over $MgSO_4$. The solvent was removed and the crude product was purified by column chromatography. After evaporated the solvent, the desired product was obtained as slightly yellow oil (1.01 g, 1.81 mmol, 78 %). ^{1}H NMR (400 MHz, Chloroform-*d*) δ 7.61 (d, *J* = 8.0 Hz, 2H), 7.32 – 7.20 (m, 12H), 6.06 (s, 1H), 3.36 (q, *J* = 6.7 Hz, 2H), 1.51 (q, *J* = 7.1 Hz, 2H), 1.33 – 1.11 (m, 30H), 0.80 (t, *J* = 6.7 Hz, 3H). ^{13}C NMR (126 MHz, Chloroform-*d*) δ 167.15, 141.70, 136.36, 136.28, 134.87, 133.91 (2C), 133.75 (2C), 133.60, 133.45, 129.03 (2C), 128.65 (2C), 128.59, 126.74, 126.66, 31.91, 29.68 (5C), 29.65 (5C), 29.58, 29.54, 29.35, 26.99, 22.68, 14.11. ^{31}P {^{1}H} NMR (203 MHz, Chloroform-d) δ -5.60. ^{31}P NMR (203 MHz, Chloroform-*d*) δ -5.40 – -5.80 (m). HRMS (ESI [M + H]$^+$) m/z: calcd for ($C_{37}H_{53}ONP$) 558.38593, found 558.38604.

Synthesis of 109 (trans-[Pd(Succinimidate)$_2$(DMSO)$_2$])[43]

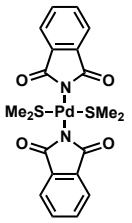

To a mixture of SMe_2 (20 mL) and $Pd(OAc)_2$ (0.5 g, 2.23 mmol, 1 eq), phthalimide (0.66 g, 4.46 mmol, 2 eq) was added and stirred at room temperature. The resulting yellow suspension was filtered and the precipitate washed with a mixture of MeOH and Et_2O. After drying at high vacuum, Pd-complex **109** was obtained (0.74 g, 1.36 mmol, 61 %).
Analytical data were identical with the values reported in literature.[43]

Synthesis of 110[41]

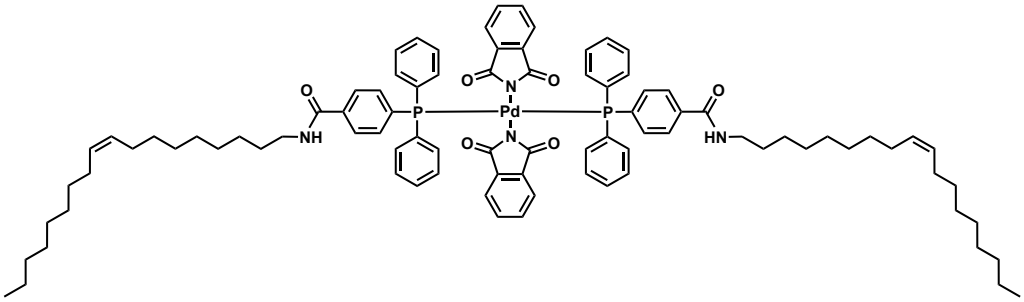

Pd-complex **109** (74 mg, 0.136 mmol, 1 eq) was dissolved in CH_2Cl_2 (10 mL) and phosphine ligand **107** (152 mg, 0.272 mmol, 2 eq) was added. The reaction mixture was then refluxed for 1 h, the solvent removed under vacuum and the resulting crude product washed with Et_2O (3 x 5 mL) and dried at high vacuum to obtain the Pd-complex **110** (76 mg, 0.052 mmol 38 %). ^{1}H NMR (400 MHz, Benzene-d_6) δ 8.36 – 8.28 (m, 4H), 8.14 (q, *J* = 5.8 Hz, 10H), 7.75 (d, *J* = 7.6 Hz, 4H), 7.09 (t, *J* = 7.5 Hz, 10H), 7.02 – 6.95 (m, 8H), 5.79 – 5.64 (m, 4H), 3.43 (q, *J* = 7.0 Hz, 4H), 2.30 (p, *J* = 8.9, 7.4 Hz, 4H), 1.68 – 1.35 (m, 54H), 1.14 – 0.99 (m, 6H). ^{31}P-NMR-{^{1}H} (162 MHz, Benzene-d_6) δ 32.74. ESI-MS (ESI $[M + H]^+$) m/z: 1509.68824 ($C_{90}H_{109}O_6N_4P_2Pd$).

4.5.8 Inductively coupled plasma mass spectrometry (ICP MS)

ICP-MS measurements were performed with an Agilent QQQ 8800 Triple quad ICP-MS spectrometer, equipped with a standard x-lens setting, nickel cones and a “micro-mist” quartz nebulizer.

All solutions were prepared from 60% HNO_3 (Merck 1.1518.1000 ultrapur) and 18.2 MΩ Millipore water. Palladium was measured against a serial dilutions of single element standard (Palladium: Merck 1.70339.0100 2% HNO3). Antimony (100 ppb in 2% HNO3) was used as internal standard.

Tune settings were based on the Agilent General Purpose method and only slightly modified by an autotune procedure using an Agilent 1 ppb tuning solution containing Li, Y, Ce and Tl.

Palladium was determined as m/z 105 Pd^+ in a “no gas” mode, where the instrument is set to a single quadrupole setting.

The feed was 0.1 ml/min, the RF power 1550 W. Values are reported as the average of 10 sweeps x 3 replicates.

Bibliography

(1) Heck, K. F.; Nolley, J. P. Palladium-Catalyzed Vinylic Hydrogen Substitution Reactions with Aryl, Benzyl, and Styryl Halides. *J. Org. Chem.* **1972**, *37*, 2320–2322.

(2) Sonogashira, K.; Tohda, Y.; Hagihara, N. A Convenient Synthesis of Acetylenes: Catalytic Substitutions of Acetylenic Hydrogen with Bromoalkenes, Iodoarenes and Bromopyridines. *Tetrahedron Lett.* **1975**, *16*, 4467–4470.

(3) King, A. O.; Okukado, N.; Negishi, E. Highly General Stereo-, Regio-, and Chemo-Selective Synthesis of Terminal and Internal Conjugated Enynes by the Pd-Catalysed Reaction of Alkynylzinc Reagents with Alkenyl Halides. *J. Chem. Soc. Chem. Commun.* **1977**, No. 19, 683.

(4) Miyaura, N.; Yamada, K.; Suzuki, A. A New Stereospecific Cross-Coupling by the Palladium-Catalyzed Reaction of 1-Alkenylboranes with 1-Alkenyl or 1-Alkenyl Halides. *Tetrahedron Lett.* **1979**, No. 36, 3437–3440.

(5) Miyaura, N.; Suzuki, A. Stereoselective Synthesis of Arylated (E)-Alkenes by the Reaction of Alk-1-Enylboranes with Aryl Halides in the Presence of Palladium Catalyst. *J. C. S. Chem. Comm.* **1979**, No. 866, 866–867.

(6) Budagumpi, S.; Haque, R. A.; Salman, A. W. Stereochemical and Structural Characteristics of Single- and Double-Site Pd(II)-N-Heterocyclic Carbene Complexes: Promising Catalysts in Organic Syntheses Ranging from C-C Coupling to Olefin Polymerizations. *Coord. Chem. Rev.* **2012**, *256*, 1787–1830.

(7) Kantchev, E. A. B.; O'Brien, C. J.; Organ, M. G. Palladium Complexes of N-Heterocyclic Carbenes as Catalysts for Cross-Coupling Reactions - A Synthetic Chemist's Perspective. *Angew. Chemie - Int. Ed.* **2007**, *46*, 2768–2813.

(8) Rideout, D. C.; Breslow, R. Hydrophobic Acceleration of Diels-Alder Reactions. *J. Am. Chem. Soc.* **1980**, *102*, 7816–7817.

(9) Breslow, R.; Maitra, U.; Rideout, D. Selective Diels-Alder Reactions in Aqueous Solutions and Suspensions. *Tetrahedron Lett.* **1983**, *24*, 1901–1904.

(10) Lindström, U. M. Stereoselective Organic Reactions in Water. *Chem. Rev.* **2002**, *102*, 2751–2772.

(11) Casalnuovo, A. L.; Calabrese, J. C. Palladium-Catalyzed Alkylations in Aqueous Media. *J. Am. Chem. Soc.* **1990**, *112*, 4324–4330.

(12) Carril, M.; SanMartin, R.; Domínguez, E. Palladium and Copper-Catalysed Arylation Reactions in the Presence of Water, with a Focus on Carbon–heteroatom Bond Formation. *Chem. Soc. Rev.* **2008**, *37*, 639-647.

(13) Shaughnessy, K. H. Beyond TPPTS: New Approaches to the Development of Efficient Palladium-Catalyzed Aqueous-Phase Cross-Coupling Reactions. *European J. Org. Chem.* **2006**, *8*, 1827–1835.

(14) Mondal, M.; Bora, U. An Efficient Protocol for Palladium-Catalyzed Ligand-Free Suzuki–Miyaura Coupling in Water. *Green Chem.* **2012**, *14*, 1873.

(15) Qiu, J.; Wang, L.; Liu, M.; Shen, Q.; Tang, J. An Efficient and Simple Protocol for a PdCl2-Ligandless and Additive-Free Suzuki Coupling Reaction of Aryl Bromides. *Tetrahedron Lett.* **2011**, *52*, 6489–6491.

(16) Zhi, J.; Song, D.; Li, Z.; Lei, X.; Hu, A. Palladium Nanoparticles in Carbon Thin Film-Lined SBA-15 Nanoreactors: Efficient Heterogeneous Catalysts for Suzuki–Miyaura Cross Coupling Reaction in Aqueous Media. *Chem. Commun.* **2011**, *47*, 10707.

(17) Lipshutz, B. H.; Ghorai, S.; Abela, A. R.; Moser, R.; Nishikata, T.; Duplais, C.; Krasovskiy, A.; Gaston, R. D.; Gadwood, R. C. TPGS-750-M: A Second-Generation Amphiphile for Metal-Catalyzed Cross-Couplings in Water at Room Temperature. *J. Org. Chem.* **2011**, *76*, 4379–4391.

(18) Krasovskiy, A.; Thomé, I.; Graff, J.; Krasovskaya, V.; Konopelski, P.; Duplais, C.; Lipshutz, B. H. Cross-Couplings of Alkyl Halides with Heteroaromatic Halides, in Water at Room Temperature. *Tetrahedron Lett.*

2011, *52*, 2203–2205.

(19) Astruc, D.; Lu, F.; Aranzaes, J. R. Nanoparticles as Recyclable Catalysts: The Frontier between Homogeneous and Heterogeneous Catalysis. *Angew. Chemie - Int. Ed.* **2005**, *44*, 7852–7872.

(20) Kashin, A. N.; Ganina, O. G.; Cheprakov, A. V.; Beletskaya, I. P. The Direct Non-Perturbing Leaching Test in the Phosphine-Free Suzuki-Miyaura Reaction Catalyzed by Palladium Nanoparticles. *ChemCatChem* **2015**, *7*, 2113–2121.

(21) Fihri, A.; Bouhrara, M.; Nekoueishahraki, B.; Basset, J.-M.; Polshettiwar, V. Nanocatalysts for Suzuki Cross-Coupling Reactions. *Chem. Soc. Rev.* **2011**, *40*, 5181–5203.

(22) Polshettiwar, V.; Nadagouda, M. N.; Varma, R. S. The Synthesis and Applications of a Micro-Pine-Structured Nanocatalyst W. **2008**, 6318–6320.

(23) Polshettiwar, V.; Cha, D.; Zhang, X.; Basset, J. M. High-Surface-Area Silica Nanospheres (KCC-1) with a Fibrous Morphology. *Angew. Chemie - Int. Ed.* **2010**, *49*, 9652–9656.

(24) Chen, A.; Ostrom, C. Palladium-Based Nanomaterials: Synthesis and Electrochemical Applications. *Chem. Rev.* **2015**, *115*, 11999–12044.

(25) Farella, I.; Valentini, A.; Cioffi, N.; Torsi, L. Dual Ion-Beam Sputtering Deposition of Palladium-Fluoropolymer Nano-Composites. *Appl. Phys. A Mater. Sci. Process.* **2005**, *80*, 791–795.

(26) Wang, M.; Feng, Y. Palladium-Silver Thin Film for Hydrogen Sensing. *Sensors Actuators, B Chem.* **2007**, *123*, 101–106.

(27) Mortazavi, S. Z.; Parvin, P.; Reyhani, A.; Golikand, A. N.; Mirershadi, S. Effect of Laser Wavelength at IR (1064 nm) and UV (193 nm) on the Structural Formation of Palladium Nanoparticles in Deionized Water. *J. Phys. Chem. C* **2011**, *115*, 5049–5057.

(28) Nishi, T.; Takeichi, A.; Azuma, H.; Suzuki, N.; Hioki, T.; Motohiro, T. Fabrication of Palladium Nanoparticles by Laser Ablation in Liquid. *J. Laser Micro Nanoeng.* **2010**, *5*, 192–196.

(29) Savadogo, O.; Lee, K.; Oishi, K.; Mitsushima, S.; Kamiya, N.; Ota, K. I. New Palladium Alloys Catalyst for the Oxygen Reduction Reaction in an Acid Medium. *Electrochem. commun.* **2004**, *6*, 105–109.

(30) Jukk, K.; Alexeyeva, N.; Sarapuu, A.; Ritslaid, P.; Kozlova, J.; Sammelselg, V.; Tammeveski, K. Electroreduction of Oxygen on Sputter-Deposited Pd Nanolayers on Multi-Walled Carbon Nanotubes. *Int. J. Hydrogen Energy* **2013**, *38*, 3614–3620.

(31) Qazi, F.; Hussain, Z.; Tahir, M. N. Advances in Biogenic Synthesis of Palladium Nanoparticles. *RSC Adv.* **2016**, *6*, 60277–60286.

(32) Clergeaud, G.; Genç, R.; Ortiz, M.; O'Sullivan, C. K. Liposomal Nanoreactors for the Synthesis of Monodisperse Palladium Nanoparticles Using Glycerol. *Langmuir* **2013**, *29*, 15405–15413.

(33) Dumas, A.; Couvreur, P. Palladium: A Future Key Player in the Nanomedical Field? *Chem. Sci.* **2015**, *6*, 2153–2157.

(34) Weiss, J. T.; Dawson, J. C.; Fraser, C.; Rybski, W.; Torres-Sánchez, C.; Bradley, M.; Patton, E. E.; Carragher, N. O.; Unciti-Broceta, A. Development and Bioorthogonal Activation of Palladium-Labile Prodrugs of Gemcitabine. *J. Med. Chem.* **2014**, *57*, 5395–5404.

(35) Weiss, J. T.; Dawson, J. C.; Macleod, K. G.; Rybski, W.; Fraser, C.; Torres-Sánchez, C.; Patton, E. E.; Bradley, M.; Carragher, N. O.; Unciti-Broceta, A. Extracellular Palladium-Catalysed Dealkylation of 5-Fluoro-1-Propargyl-Uracil as a Bioorthogonally Activated Prodrug Approach. *Nat. Commun.* **2014**, *5,* 1–9.

(36) Huang, X.; Tang, S.; Mu, X.; Dai, Y.; Chen, G.; Zhou, Z.; Ruan, F.; Yang, Z.; Zheng, N. Freestanding Palladium Nanosheets with Plasmonic and Catalytic Properties. *Nat. Nanotechnol.* **2011**, *6*, 28–32.

(37) Balbín, A.; Gaballo, F.; Ceballos-Torres, J.; Prashar, S.; Fajardo, M.; Kaluđerović, G. N.; Gómez-Ruiz, S. Dual Application of Pd Nanoparticles Supported on Mesoporous Silica SBA-15 and MSU-2: Supported Catalysts for C–C Coupling Reactions and Cytotoxic Agents against Human Cancer Cell Lines. *RSC Adv.* **2014**, *4*, 54775–54787.

(38) Puvvada, S.; Baral, S.; Chow, G. M.; Qadri, S. B.; Ratna, B. R. Synthesis of Palladium Nanoparticles In the

Bicontinious Cubic Phase of Glycerol Monooleate. *J. Am. Chem. Soc.* **1994**, *116*, 2135–2136.

(39) Duss, M.; Salvati Manni, L.; Moser, L.; Handschin, S.; Mezzenga, R.; Jessen, H. J.; Landau, E. M. Lipidic Mesophases as Novel Nanoreactor Scaffolds for Organocatalysts: Heterogeneously Catalyzed Asymmetric Aldol Reactions in Confined Water. *ACS Appl. Mater. Interfaces* **2018**, *10*, 5114–5124.

(40) Sun, W.; Vallooran, J. J.; Fong, W. K.; Mezzenga, R. Lyotropic Liquid Crystalline Cubic Phases as Versatile Host Matrices for Membrane-Bound Enzymes. *J. Phys. Chem. Lett.* **2016**, *7*, 1507–1512.

(41) Kapdi, A.; Gayakhe, V.; Sanghvi, Y. S.; Garcia, J.; Lozano, P.; da Silva, I.; Perez, J.; Serrano, J. L. New Water Soluble Pd-Imidate Complexes as Highly Efficient Catalysts for the Synthesis of C5-Arylated Pyrimidine Nucleosides. *Rsc Adv.* **2014**, *4*, 17567–17572.

(42) Gayakhe, V.; Ardhapure, A.; Kapdi, A. R.; Sanghvi, Y. S.; Serrano, J. L.; García, L.; Perez, J.; Garcia, J.; Sanchez, G.; Fischer, C.; Schulzke, C. Water-Soluble Pd-Imidate Complexes: Broadly Applicable Catalysts for the Synthesis of Chemically Modified Nucleosides via Pd-Catalysed Cross-Coupling. *J. Org. Chem.* **2016**, *81*, 2713–2729.

(43) Sánchez, G.; García, J.; Martínez, M.; Kapdi, A. R.; Pérez, J.; García, L.; Luis Serrano, J. Bis(imidate)palladium(II) Complexes with Labile Ligands. Mimics of Classical Precursors? *Dalton Transactions*. **2011**, *40*, 12676–12689.

(44) Battocchio, C.; Porcaro, F.; Mukherjee, S.; Magnano, E.; Nappini, S.; Fratoddi, I.; Quintiliani, M.; Russo, M. V.; Polzonetti, G. Gold Nanoparticles Stabilized with Aromatic Thiols: Interaction at the Molecule-Metal Interface and Ligand Arrangement in the Molecular Shell Investigated by SR-XPS and NEXAFS. *J. Phys. Chem. C* **2014**, *118*, 8159–8168.

(45) Turner, D. C.; Wang, Z.-G.; Gruner, S. M.; Mannock, D. a.; McElhaney, R. N. Structural Study of the Inverted Cubic Phases of Di-Dodecyl Alkyl-β-D-Glucopyranosyl-Rac-Glycerol. *J. Phys. II* **1992**, *2*, 2039–2063.

(46) Briggs, J.; Chung, H.; Caffrey, M. The Temperature-Composition Phase Diagram and Mesophase Structure Characterization of the Monoolein / Water System. *J. Phys. II Fr.* **1996**, *6*, 723–751.

(47) Duss, M.; Capolicchio, S.; Linden, A.; Ahmed, N.; Jessen, H. J. Desymmetrization of Myo-Inositol Derivatives by Lanthanide Catalyzed Phosphitylation with C2-Symmetric Phosphites. *Bioorganic Med. Chem.* **2015**, *23*, 2854–2861.

(48) Sowa, T.; Ouchi, S. The Facile Synthesis of 5'-Nucleotides by the Selective Phosphorylation of a Primary Hydroxyl Group of Nucleosides with Phosphoryl Chloride. *Bull. Chem. Soc. Jpn* **1975**, *48*, 2084–2090.

Chapter 5

Enzyme immobilization in lipidic mesophases by ionic interactions and lipidic modification

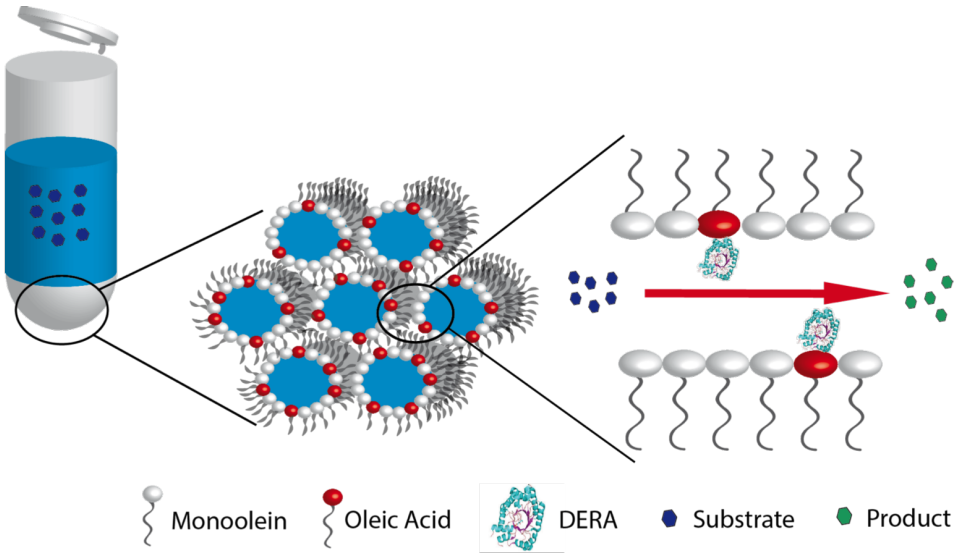

5.1 Introduction

Enzymes are versatile and sophisiticated catalysts that perform chemical reactions with high substrate specificity and stereoselectivity under benign conditions. Thus, enzymes find applications in research laboratories as well as in industry. Immobilizing enzymes facilitates their recovery and enables efficient recycling. Additionally, immobilization often increases the stability and prevents hydrophobic enzymes from aggregation.[1] In general, potential immobilization platforms should have a large surface area. This can be achieved by using porous materials or small particles. The most common immobilization approaches use one of the following approaches:[1]

- Noncovalent adsorption such as van der Waals interaction or hydrogen bonding
- Ionic interactions via deprotonated carboxylic acids or protonated lysins
- Covalent fixation using activated linkers
- Cross-linking of enzymes
- Entrapment in capsules

LCPs show a plethora of properties that render these materials suitable as immobilization matrices for enzymes. The large surface area of *ca.* 400 m^2 g^{-1} lipid[2] between the well-defined aqueous channels and the lipidic bilayer in these structures promises efficient catalysis. The feasibility of doping LCPs with tailored additives enables a broad variety of potential anchoring approaches. Furthermore, the diameter of the aqueous channels can be modified, which allows tuning of the enzyme kinetics, not only before but even while catalysis is ongoing. Sun *et al*., for example, used LCPs to encapsulate horseradish peroxidase (HRP) and investigated enzyme kinetics in LCPs with different aqueous channel diameters. They could show that HRP encapsulated in swollen LCPs can achieve up to 92.1 % of its native activity.[3] In another study, the same group showed that not only the diameter of the aqueous channels is an important parameter for efficient enzyme catalysis, but also the topology of the mesophases.[4] In this work, HRP was encapsulated and thus immobilized in LCPs to some extent. However, HRP was not fixed to the lipidic bilayer and could diffuse to an excess water reservoir, if present. We plan to circumvent this issue by fixing enzymes permanently to the lipidic bilayer of the mesophases. Two different approaches with two different enzymes have been applied. The first is deoxyribose-5-phosphate aldolase (DERA, EC 4.1.2.4, 259 amino acids, 27.7 kDa)[5], which reversibly transforms *D*-glyceraldehyde 3-phosphate and acetaldehyde to 2-deoxyribose 5-phosphate.[6] DERA is an unusual aldolase, being the only one known to condense two aldehydes, as opposed to other aldolases that have a ketone and an aldehyde as substrates.[7] DERA has been used as a catalyst for asymmetric aldol condensation of a

broad range of aliphatic aldehydes.[7,8] It possesses several solvent-exposed lysins, whose amino groups are protonated at physiological pH, and are therefore positively charged. By using an additive that bears a negative charge, DERA can be bound to the LCP based on ionic interactions.

The second enzyme, tobacco etch virus (TEV) protease has been chemically modified with lipid chains, which should anchor the enzyme at the lipidic bilayer of the mesophase, leading to a supramolecular enzyme-LCP-complex. Proteases, among them also TEV protease, are being used to remove affinity tags of recombinant proteins. TEV protease is highly specific and remains active in a broad range of conditions.[9] With these enzyme-containing LCPs, a novel class of biocatalytic material is being introduced.

5.2 Results and discussion

5.2.1 Deoxyribose-5-phosphate aldolase

5.2.1.1 Immobilization by ionic interactions

As already mentioned in Chapter 2, the aldol reaction is a powerful method to form new carbon-carbon bonds by forming ß-hydroxy carbonyl moieties. Whereas in Chapter 2 aldol reactions catalyzed by proline-derived lipids were described, we report herein the same reaction type performed enzymatically, using DERA-containing LCPs. The solvent exposed lysins present at the surface of DERA constitute an ideal opportunity for the immobilization of the enzyme by ionic interactions. The amino groups of these lysins are positively charged since they are protonated at pH 7.4. We hypothesized that mesophases doped with an additive bearing a negative charge will enable efficient immobilization of the enzyme by virtue of electrostatic attraction. According to the pKa of oleic acid (OA, **6**), which is 4.8,[10] the carboxylic acid is mostly deprotonated at pH 7.4 and constitutes therefore a suitable ionic counterpart to the lysins of DERA for binding to the mesophase bilayer by ionic interactions. Reversed hexagonal phases (H_{II}) and *Pn3m* cubic phases based on mixtures MO and OA (**6**) have been described previously.[11,12] The immobilization principle and the experimental set-up are illustrated in Figure 1. Substrates from an excess water reservoir diffuse into the aqueous channels of the mesophase and are transformed to the corresponding aldol products, which then can diffuse back to the bulk water. The product can then easily be separated from the catalyst by simply removing the overlaid water.

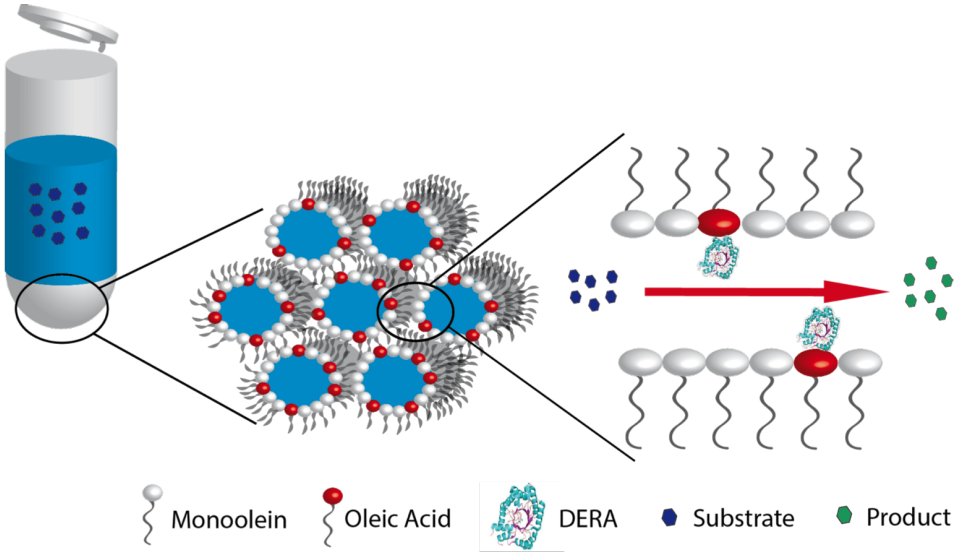

Figure 1: Schematic representation of the immobilization principle and the experimental set up including the structure of the host-guest $H_{(II)}$ phase. The $H_{(II)}$ phase, composed of host MO lipids (white), guest lipid oleic acid (red), water (blue) and DERA, is placed in an Eppendorf tube, and is overlaid with an aqueous substrate solution. The substrates (dark blue) are transformed by the enzyme DERA to the products (green). The reaction takes place at the lipid-water interface of the catalytic mesophase. The proportions of lipids and enzyme do not match reality.

The immobilization efficiency of the MO/OA reverse hexagonal phase was tested by determining the DERA release to the overlaid excess water. As a control, a H_{II} phase with the uncharged additive tetradecane was used, which has been described previously.[13] Due to the lack of charges of this additive, the enzyme should be released from the control H_{II} phase much faster. The two H_{II} phases were overlaid with buffer solution. The DERA-release of the H_{II} phase to the excess water reservoir was measured by UV/Vis spectroscopy over four days, and the results are shown in Figure 2. A concentration of 100 % in the overlaid buffer solution corresponds to release of the all the enzyme molecules from the H_{II} phase to the excess water reservoir. The oleic acid-doped H_{II} phase is depleted by ca. 10 % of its DERA within the first 24 h, and the enzyme concentration remains almost constant thereafter- this value only slightly increasing to 13 % after 96 h. The tetradecane-doped H_{II} phase, on the other hand, loses 18 % of its DERA within the first 24 h and the release rate is subsequently only slightly reduced and reaches 37 % after 96 h. The significantly different release rates are the basis for further experiments and proves our immobilization hypothesis.

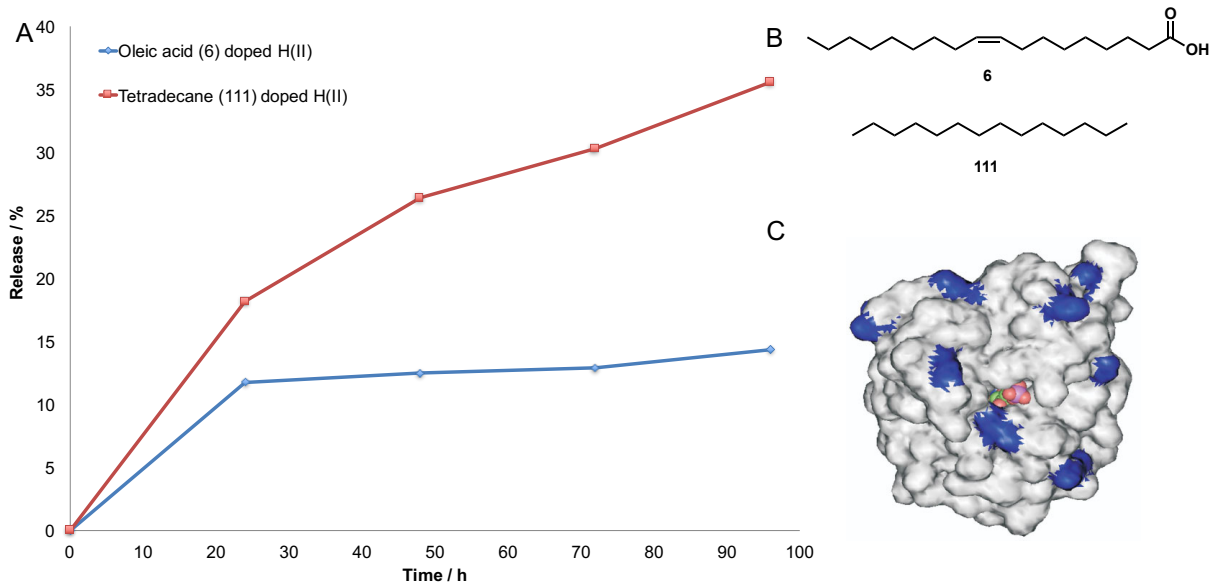

Figure 2: A) DERA immobilization study of oleic acid- and tetradecane-doped $H_{(II)}$ phases. Uncharged, tetradecane-doped $H_{(II)}$ phase (red curve) releases DERA much faster and to a greater extent than oleic acid-doped $H_{(II)}$ phase (blue curve). B) Molecular structures of oleic acid (top) and tetradecane (bottom). C) X-ray surface structure of DERA with solvent exposed lysine residues shown in blue. DERA crystal structure reprinted with permission from Ref. 5.

5.2.1.2 Activity assays of immobilized DERA

The activity of native and immobilized DERA was determined using a previously reported coupled enzymatic assay which allows to follow the oxidation of nicotinamide adenine dinucleotide (NADH) by UV/Vis spectroscopy.[14] After cleaving 2-deoxy-*D*-ribose 5-phosphate (DRP) to glyceraldehyde 3-phosphate (G-3-P) and acetaldehyde (ACH) with DERA, G-3-P is transformed to dihydroxy acetone phosphate (DHAP) by a triose-phosphate isomerase (TPI) and further reduced to glycerol 3-phosphate with glycerol 3-phosphate isomerase (GDH). The oxidation of NADH can be monitored by UV/Vis spectroscopy at 340 nm and serves as the read-out of this assay.

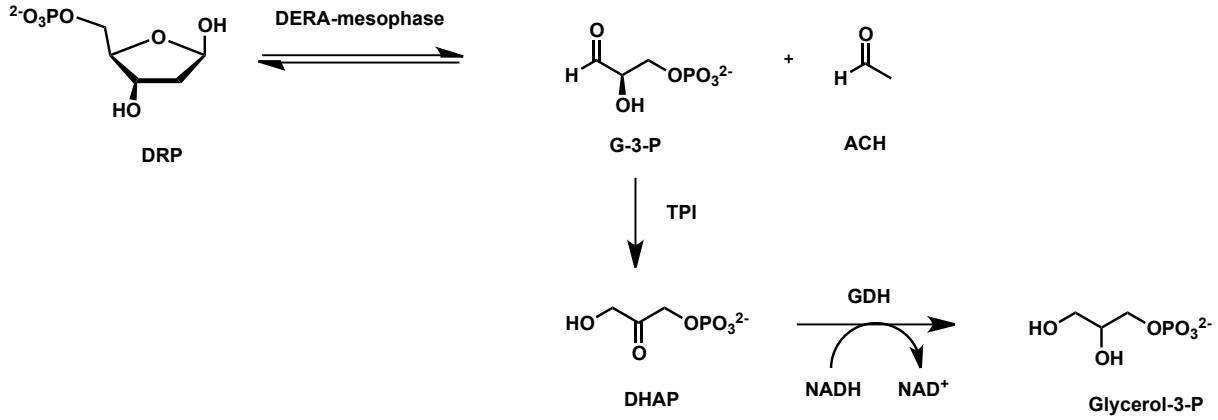

Scheme 1: Coupled enzymatic assay to determine DERA-activity. The consumption of NADH is directly related to the activity of DERA and can be monitored by UV/Vis spectroscopy at 340 nm.[14] Abbreviations: 2-deoxy-*D*-ribose 5-phosphate (DRP), glyceraldehyde 3-phosphate (G-3-P), acetaldehyde (ACH), deoxyribose-5-phosphate aldolase DERA, dihydroxy acetone phosphate (DHAP), triose-phosphate isomerase (TPI), glycerol 3-phosphate (glycerol-3-P), glycerol 3-phosphate isomerase (GDH). Adapted from Ref. 22.

Despite several optimization attempts, e.g. varying oleic acid and DERA concentration in LCPs or changing their ratio, enzyme leaking was observed in all DERA-LCPs that were prepared. However, the *in-meso* enzyme activity of DERA-LCP could be determined be subtracting the activity of the proportion of released enzyme from the total enzyme activity. The enzyme activity arising from released DERA was determined by removing the overlay and repeating the assay without DERA-LCP. The actual DERA-LCP activity was found to be 22 % relative to the native DERA activity (Table 1, entry 1 and 2). The activity of DERA-H_{II} was with 3 % relative to native DERA significantly lower (Table 1, entry 3). This can be explained by the smaller lattice parameter and the different mesophase topology as compared to LCPs.[4] Whereas DERA was found to leak from all LCPs that were prepared, this was not the case for H_{II} phases when a washing step was conducted.

Table 1: Catalytic activity of native DERA, DERA-LCP and DERA-H_{II}.

Entry	Catalyst	OA[a]	Activity [%][b]
1	Native DERA	-	100
2	DERA-LCP	2 %	22
3	DERA-H_{II}	20 %	3

Conditions: Reactions were carried out in special, home built metal holders in UV/Vis cuvettes at 25°C. [a] Oleic acid concentration in the mesophase in w/w % of the lipid fraction. [b] The activity was normalized for native DERA to 100 %. 1 mg native DERA consumes 6 mmol DRP/min.

Lipidic modification of enzymes for immobilization in mesophases

Chemical modification of proteins after translation is a ubiquitous process that is responsible for the broad protein chemodiversity present in nature. These post-translational modifications play important roles in cellular processes such as signaling, trafficking or differentiation, and include among others acylation, methylation, phosphorylation, sulfation, farnesylation, ubiquitination, and glycosylation. Together with the possibility of unnatural biorthogonal modifications developed by chemists, a broad range of chemical modifications are available which allow to study proteins and to control their properties by design.[15,16]

5.2.2 TEV protease

5.2.2.1 Synthesis of lipidic linkers 114 and 115

Attaching lipidic chains to water-soluble enzymes will render these enzymes more hydrophobic and might enable their immobilization by anchoring them at the lipidic bilayer of the mesophase. To this end, two differently functionalized lipidic linkers (**114** and **115**, Scheme 2) have been synthesized. Although procedures to couple such compounds to enzymes have been reported earlier,[17,18] the linker had to be customized for our purposes, *i.e.* incorporating oleyl residues to allow anchoring of the enzyme to the lipidic bilayer. Linker **114** was obtained by coupling commercially available 2-(2-bromoethyl)-1,3-dioxolane (**112**) and oleic chloride (**10**) via *Grignard* reaction. In a subsequent step, the acetal was cleaved with acetic acid to obtain linker **114**, which forms a pyrrole ring upon coupling to a lysine amine via Paal-Knoor synthesis.[17,19] Linker **115** was obtained by simply activating oleic acid with *N*-hydroxysuccinimide to obtain the NHS-ester thereof. The modification of enzymes occurs at the exposed lysines as well. Initially, several attempts were undertaken to modify HRP. However, the coupling that was performed according to reported procedures[17,18] was not successful, and we decided to exchange the enzyme and to work with a TEV protease instead. Linker **vc** was coupled in a mixture DMF and PBS buffer (1:4) in the presence of

DBU as a base.[17] NHS-activated linker **115** was coupled under similar conditions, but without DBU.

We have some evidence for the successful lipidic modification of a TEV protease for both linkers. For linkers **115** MALDI-MS data indicates that a mixture of TEV protease with several modifications was obtained, whereas the coupling of **114** to TEV protease was only proven indirectly by comparing the release of modified and unmodified TEV protease from LCPs. Unmodified TEV protease was released significantly faster from a LCP than its modified analogue.[20]

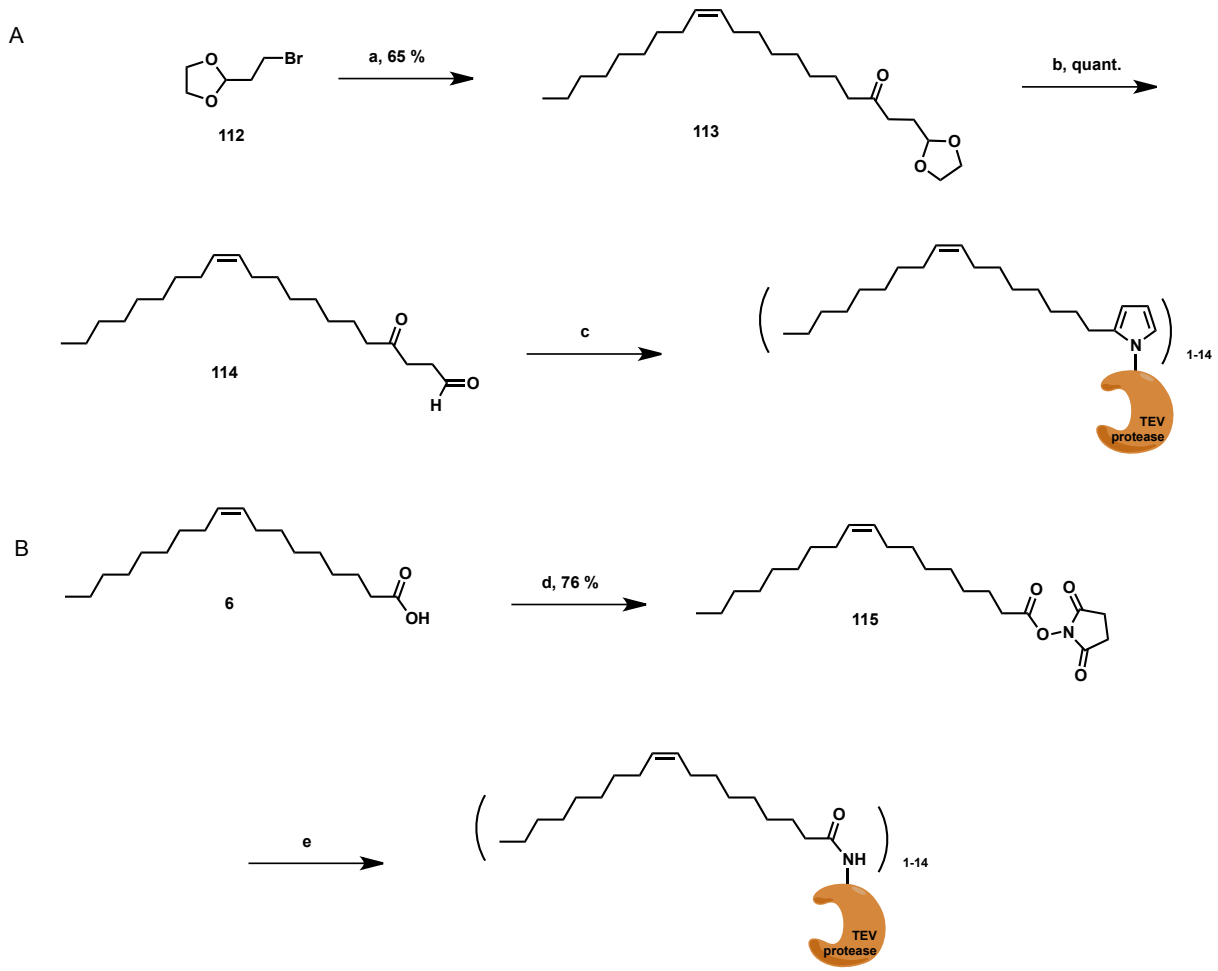

Scheme 2: Synthesis of three different lipidic linkers and their coupling to a TEV protease. Conditions: a) Oleylchloride, Mg, THF, - 78°C. b) AcOH/H_2O, r.t.. c) TEV protease, DMF/PBS (1:4), DBU, d) DCC, NHS, EtOAc/dioxane 1:1, r.t e) TEV protease, DMF/PBS 1:4, pH 7.4.

5.3 Conclusions

The immobilization of DERA within H_{II} phases based on ionic interactions was shown, albeit with a strongly reduced activity of the enzyme as compared to the native form (3 % vs. 100 %, Table 1, entries 1 and 3). In contrast, using LCPs to immobilize DERA only works partially using the same approach, as a fraction of the enzyme content was released to the excess water reservoir. The activity of 22 % relative to the native enzyme is reasonable (Table 1, entry 2). Thus, even though the principle was shown to work, both cases have a strong drawback and optimization is necessary in order to obtain a robust and reliable catalytic system that can be used to study aldol reactions.

Finally, two different linkers to modify enzymes chemically with a lipidic chain have been successfully synthesized. Both linker **114** and **115** enable modifications at lysins residues. There is evidence for the successful lipidic modification of a TEV protease with both linkers.[20]

5.4 Outlook

Optimal conditions at which DERA is immobilized in the mesophase but still shows high activity need to be established. Therefore, a comprehensive screening of conditions is needed. Varying systematically the oleic acid, monoolein and DERA concentration might be a successful approach. The aqueous channel diameter is an important parameter that might be crucial and could be varied as well.

Marco Etter and Philipp Ansorge from our group are continuing the project and are currently investigating the immobilization of TEV protease and its *in-meso* activity.

5.5 Experimental section

General Information

1-Monooleoyl-sn-glycerol C18:1 (monoolein, MO) was purchased from Nu-Chek Prep, Inc. (MN, USA). All other reagents and solvents were purchased from Sigma Aldrich. All chemicals and solvents were used as received, unless otherwise stated. Reactions were carried out under an inert atmosphere of argon in dry solvents. Dichloromethane was degassed with argon and purified by passage through activated alumina solvent column (MC Brown solvent system) prior to use. Column chromatography was performed using silica gel Merck 60 (particle size 0.040–0.063 mm). Analytical thin- layer chromatography (TLC) was performed using Merck pre-coated silica gel plates 60 F_{254}; visualization by UV absorption and/or by dipping in a solution of $KMnO_4$ (1 g), K_2CO_3 (2 g) in H_2O (100 mL) and subsequent heating. ^{1}H-NMR spectra were recorded on a Bruker AV2-500 (500MHz) spectrometer. Chemical shifts are given in parts per million (ppm) relative to the internal standard TMS (δ = 0 ppm). Coupling constants J are expressed in Hz and multiplicities are abbreviated as follows: s (singlet), br (broad), d (doublet), t (triplet), q (quadruplet), quint (quintet), m (multiplet). ^{13}C-NMR chemical shifts are reported relative to the solvent residual peaks: $CDCl_3$ = 77.00 ppm. Mass spectra were recorded by the Mass Spectroscopy Service of UZH on Finnigan MAT95 MS, BrukerLC MS and Finnigan TSQ700 MS machines.

5.5.1 Preparation of DERA mesophases

MO was weight into an *Eppendorf* vial and a corresponding amount of additive was added to obtain a homogeneous lipidic mixture. The lipidic mixture was subsequently hydrated by adding appropriate volumes of PBS buffer (pH = 7.4) and mixed. To obtain homogeneous LCPs, the samples were centrifuged at 5000 rpm for 85 minutes at 23 °C. The samples were finally stored to equilibrate for at least 24 h in a closed *Eppendorf* tube. The ratio of components was chosen on the basis of the reported phase diagrams.[11,21]

5.5.2 DERA Activity assay

The catalytic assay was conducted as described by Dean *et al*.[14] and Subrizi *et al*.[22] The phase with 8.4 µg DERA was transferred to a metal holder inside a glass cuvette and PBS buffer (2 mL) was added. DR-5-P (39.5 µL, 1.97 µmol), α-GPD (2 µL, 3.2 µmol) and NADH (39.75 µL, 0.59 µmol) were added to start the reaction. The assay was monitored by UV-Vis spectroscopy. Therefore, the absorbance of NADH at λ = 340 nm was measured. The overlay of this assay was drained to another glass cuvette and measured with the same reagents. This procedure was repeated two to five times.

5.5.3 Synthesis

Synthesis of 113 ((*Z*)-1-(1,3-dioxolan-2-yl)icos-11-en-3-one)[17]

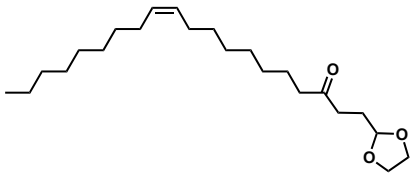

To a flask with Magnesium turnings (150 mg, 6.25 mmol, 1.33 eq.) and dry THF (4 mL) a solution of 2-(2-bromoethyl)-1,3-dioxolane (1 g, 5.5 mmol, 1.17 eq.) in dry THF (2 mL) was added dropwise. A small amount of iodine was used to initiate the reaction. Subsequently, THF (5 mL) was added and as soon as the reaction was completed, more THF (15 mL) was added. The reaction mixture stirred for 1 h and then cooled to -78 °C. A solution of oleyl chloride (1.41 g, 4.7 mmol, 1 eq.) in dry THF (5 mL) was then added slowly via dropping funnel. The reaction mixture was stirred for 40 min before it was quenched with saturated aqueous NH_4Cl (30 mL). The phases were separated and the aqueous phase was extracted with ethylacetate (4 x 15 mL) and the combined organic phases were washed with brine, dried over $MgSO_4$, and the solvents removed *in vacuo*. The resulting crude product was purified by flash chromatography (hexane/ethylacetate 8:2) to obtain the product as colourless oil (1.12 g, 3.06 mmol, 65%). ^{1}H NMR (500 MHz, Chloroform-*d*) δ 5.49 – 5.19 (m, 2H), 4.84 (t, *J* = 4.4 Hz, 1H), 3.92 – 3.84 (m, 2H), 3.81 – 3.74 (m, 2H) 2.44 (t, *J* = 6.9 Hz, 2H), 2.35 (t, *J* = 6.9 Hz, 2H), 2.12 – 1.75 (m, 6H), 1.57 – 1.44 (m, 2H), 1.42 – 0.98 (m, 20H), 0.81 (t, *J* = 6.9 Hz, 3H). ^{13}C NMR (126 MHz, Chloroform-*d*) δ 210.25, 129.96, 129.74, 103.36, 64.95 (2C), 42.81, 36.43, 31.89, 29.76, 29.69, 29.51, 29.31 (2C), 29.20, 29.11, 27.58, 27.20, 27.16, 23.86, 22.67, 14.11. HRMS (ESI [M + Na]$^+$) m/z: calcd for ($C_{23}H_{42}O_3Na$) 389.30262, found 389.30200.

Synthesis of 114 ((*Z*)-4-oxohenicos-12-enal)[17]

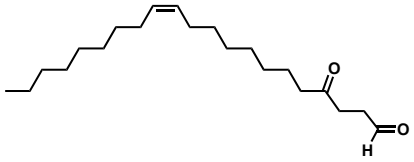

Acetal (100 mg, 0.27 mmol, 1 eq.) was dissolved in a mixture of AcOH and H_2O (3:1, v/v) and stirred for 5 h at 50 °C when TLC showed completion of the reaction. The solvent was removed and the desired product was obtained without further purification in quantitative yield. ^{1}H NMR (500 MHz, Chloroform-*d*) δ 9.73 (s, 1H), 5.38 – 5.19 (m, 2H), 2.71 – 2.61 (m, 4H), 2.39 (t, *J* = 7.5 Hz, 2H), 2.02 – 1.85 (m, 4H), 1.57 – 1.44 (m, 2H), 1.30 – 1.14 (m, 20H), 0.81 (t, *J* = 6.9 Hz, 3H). ^{13}C NMR (126 MHz, Chloroform-*d*) δ 208.83, 200.47, 129.91, 129.67, 42.68, 37.39, 34.54, 31.84, 29.70, 29.63, 29.46, 29.26 (2C), 29.23, 29.10, 29.04, 27.15, 27.10, 23.79, 22.62, 14.05. HRMS (ESI [M + Na]$^+$) m/z: calcd for ($C_{21}H_{38}O_2Na$) 345.27640, found 345.27633.

Synthesis of 115 (2,5-dioxopyrrolidin-1-yl oleate)[18]

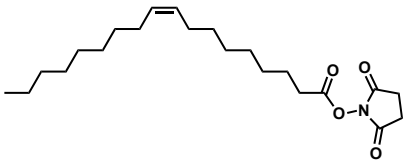

Oleic acid (1.0 g, 3.4 mmol, 1 eq.) was dissolved in a mixture of ethyl acetate/dioxane (1:1, 10 mL) and cooled to 0°C. Subsequently, *N*-hydroxysuccinimide (0.424 g, 3.68 mmol, 1.04 eq) and DCC (0.76 g, 3.68 mmol, 1.04 eq.) was added. The mixture was stirred at room temperature for 5 h and the precipitate was filtered off and the solvent was evaporated *in vacuo*. The resulting oil was dissolved in ethyl acetate (35 mL) and washed with aqueous $NaHCO_3$ 5% (3 × 5 mL) and brine (10 mL). The combined organic phases were dried over $MgSO_4$ and the solvent removed. The crude product was purified by flash chromatography (cyclohexane/ethylacetate 5:1) to give the product as slightly yellow oil (981 mg, 2.58 mmol, 76%). ^{1}H NMR (400 MHz, Chloroform-*d*) δ 5.64 – 4.94 (m, 2H), 2.76 (s, 4H), 2.53 (t, *J* = 7.5 Hz, 2H), 1.98 – 1.88 (m, 4H), 1.68 (p, *J* = 7.5 Hz, 2H), 1.42 – 1.08 (m, 20H), 0.87 – 0.74 (m, 3H). ^{13}C NMR (126 MHz, Chloroform-*d*) δ 169.20 (2C), 168.67, 130.02, 129.68, 31.89, 30.92, 29.75, 29.62, 29.50, 29.30 (2C), 28.98 (2C), 28.75, 27.20, 27.13, 25.57 (2C), 24.54, 22.66, 14.10. HRMS (ESI [M + Na]$^+$) m/z: calcd for ($C_{22}H_{37}O_4NNa$) 402.26153, found 402.26106.

5.5.4 Protein modifications

Enzyme modification with linker 114

(Procedure adapted from Lu *et al.*[17])

Oleyl linker **114** (2 mg, 0.006 mmol) was dissolved in DMF (0.5 mL) and added to 1.5 mL to a 0.08 mM solution of HRP or TEV protease. The reaction mixture was stirred under argon for 4 days. DBU (0.2 mL) was then added and the mixture was stirred overnight. The reaction mixture was submitted to MALDI-MS after dialysis (12 h, *Mr* cutoff 14'000, against 500 mL 20 % DMF in 10 mM PBS, pH 7.4).

Enzyme modification with linker 115

NHS-activated oleyl linker **115** (2 mg, 0.005 mmol) was dissolved in DMF (0.5 mL) and added to 1.5 mL to a 0.08 mM solution of HRP or TEV protease. The reaction mixture was stirred for 4 days. The reaction mixture was submitted to MALDI-MS after dialysis (12 h, *Mr* cutoff 14'000, against 500 mL 20 % DMF in 10 mM PBS, pH 7.4).

TEV protease was expressed and purified by Philipp Ansorge according to the procedure described in his PhD thesis.[23]

Bibliography

(1) Hanefeld, U.; Gardossi, L.; Magner, E. Understanding Enzyme Immobilisation. *Chem. Soc. Rev.* **2009**, *38*, 453–468.

(2) Lawrence, M. J. Surfactant Systems: Their Use in Drug Delivery. *Chem. Soc. Rev.* **1994**, *23*, 417–424.

(3) Sun, W.; Vallooran, J. J.; Zabara, A.; Mezzenga, R. Controlling Enzymatic Activity and Kinetics in Swollen Mesophases by Physical Nano-Confinement. *Nanoscale* **2014**, *6*, 6853–6859.

(4) Sun, W.; Vallooran, J. J.; Mezzenga, R. Enzyme Kinetics in Liquid Crystalline Mesophases: Size Matters, but Also Topology. *Langmuir* **2015**, *31*, 4558–4565.

(5) Jennewein, S.; Schürmann, M.; Wolberg, M.; Hilker, I.; Luiten, R.; Wubbolts, M.; Mink, D. Directed Evolution of an Industrial Biocatalyst: 2-Deoxy-D-Ribose 5-Phosphate Aldolase. *Biotechnol. J.* **2006**, *1*, 537–548.

(6) Racker, E. Enzymatic Synthesis and Breakdown of Desoxyribose Phosphate. *J. Biol. Chem.* **1952**, *196*, 347–366.

(7) Barbas, C. F.; Wang, Y.; Wong, C.; Force, A.; Command, S. Deoxyribose-5-phosphateAldolase as a Synthetic Catalyst. *J. Am. Chem. Soc.* **1990**, 2013–2014.

(8) Chen, L.; Dumas, D. P.; Wong, C. Deoxyribose-5-Phosphate Aldolase as a Catalyst in Asymmetric Aldol Condensation. *J. Am. Chem. Soc.* **1992**, *114*, 741–748.

(9) Vergis, J. M.; Wiener, M. C. The Variable Detergent Sensitivity of Proteases That Are Utilized for Recombinant Protein Affinity Tag Removal. *Protein Expr. Purif.* **2011**, *78*, 139–142.

(10) Cistola, D. P.; Small, D. M.; Hamilton, J. a. Carbon 13 NMR Studies of Saturated Fatty Acids Bound to Bovine Serum Albumin. *J. Biol. Chem.* **1987**, *262*, 10980–10985.

(11) Lopes, L. B.; Ferreira, D. a.; De Paula, D.; Garcia, M. T. J.; Thomazini, J. a.; Fantini, M. C. a; Bentley, M. V. L. B. Reverse Hexagonal Phase Nanodispersion of Monoolein and Oleic Acid for Topical Delivery of Peptides: In Vitro and in Vivo Skin Penetration of Cyclosporin A. *Pharm. Res.* **2006**, *23*, 1332–1342.

(12) Aleandri, S.; Speziale, C.; Mezzenga, R.; Landau, E. M. Design of Light-Triggered Lyotropic Liquid Crystal Mesophases and Their Application as Molecular Switches in “On Demand” Release. *Langmuir* **2015**, *31*, 6981–6987.

(13) Li, S. J.; Yamashita, Y.; Yamazaki, M. Effect of Electrostatic Interactions on Phase Stability of Cubic Phases of Membranes of Monoolein/dioleoylphosphatidic Acid Mixtures. *Biophys. J.* **2001**, *81*, 983–993.

(14) Dean, S. M.; Greenberg, W. A.; Wong, C.-H. Recent Advances in Aldolase-Catalyzed Asymmetric Synthesis. *Adv. Synth. Catal.* **2007**, *349*, 1308–1320.

(15) Boutureira, O.; Bernardes, G. J. L. Advances in Chemical Protein Modification. *Chem. Rev.* **2015**, *115*, 2174–2195.

(16) Walsh, C. T.; Garneau-Tsodikova, S.; Gatto, G. J. Protein Posttranslational Modifications: The Chemistry of Proteome Diversifications. *Angew. Chemie - Int. Ed.* **2005**, *44*, 7342–7372.

(17) Lu, L.; Gu, X.; Hong, L.; Laird, J.; Jaffe, K.; Choi, J.; Crabb, J.; Salomon, R. G. Synthesis and Structural Characterization of Carboxyethylpyrrole-Modified Proteins: Mediators of Age-Related Macular Degeneration. *Bioorg. Med. Chem.* **2009**, *17*, 7548–7561.

(18) Foillard, S.; Rasmussen, M. O.; Razkin, J.; Boturyn, D.; Dumy, P. 1-Ethoxyethylidene, a New Group for the Stepwise SPPS of Aminooxyacetic Acid Containing Peptides. *J. Org. Chem.* **2008**, *73*, 983–991.

(19) Kaur, K.; Salomon, R. G.; O’Neil, J.; Hoff, H. F. (Carboxyalkyl)pyrroles in Human Plasma and Oxidized Low-Density Lipoproteins. *Chem. Res. Toxicol.* **1997**, *10*, 1387–1396.

(20) Etter, M.; Ansorge, P. Unpublished Results. **2018**, University of Zurich.

(21) Zabara, A.; Negrini, R.; Baumann, P.; Onaca-Fischer, O.; Mezzenga, R. Reconstitution of OmpF Membrane Protein on Bended Lipid Bilayers: Perforated Hexagonal Mesophases. *Chem. Commun.* **2014**,

50, 2642–2645.

(22) Subrizi, F.; Crucianelli, M.; Grossi, V.; Passacantando, M.; Botta, G.; Antiochia, R.; Saladino, R. Versatile and Efficient Immobilization of 2‑Deoxyribose-5-Phosphate Aldolase (DERA) on Multiwalled Carbon Nanotubes. *ACS Catal.* **2014**, *4*, 2–11.

(23) Ansorge, P. Solution NMR Studies on Membrane Proteins in Lipid Bilayers. **2017**, Doctoral Thesis, University of Zurich.

Chapter 6

Towards catalytic LCP polymers

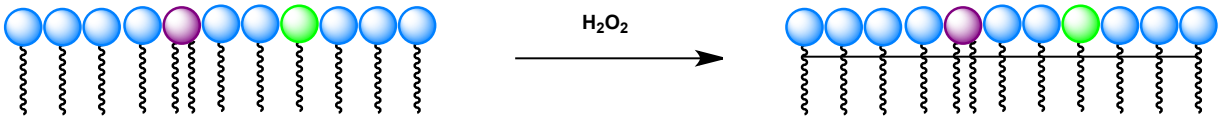

6.1 Introduction - Polymerization of LCPs

The development of catalytic LCPs and cubosomes during this thesis revealed both the huge potential of this approach, as well as its limitations and drawbacks. For example, the major drawback of the aldol LCPs and cubosomes described in Chapter 2 is the limitation to water-soluble substrates. Similarly, the detoxifying hydrolysis of parathion in Chapter 3 suffered from substrate accumulation in the lipidic compartment, which seems to be too hydrophobic. The recycling of PdNP-containing LCPs described in Chaper 4 is restricted to few cycles. A possible explanation is the gravity-induced migration of the PdNPs over time, leading to the loss of substrate-accessible PdNPs in the aqueous compartment. However, these complications can potentially be overcome by polymerizing LCPs. In an ideal case, LCPs can be designed with customized properties, which can then be "frozen" to obtain more stable LCPs that are even compatible with organic solvents. To address these possibilities, a polymerizable catalytic LCP based on reported technology[1,2] was designed, and its lipid building blocks synthesized.

Generally, two strategies to achieve polymerization of three-dimensional, supramolecular structures such as LCPs are available: First by hydrating lipids that contain polymerizable moieties to form the corresponding mesophases and subsequent linear or cross-linked polymerization. Second, the inverse approach by pre-polymerization in organic solvents, subsequent evaporation of the solvent and purification of the polymer followed by hydration.[3] The research using the first approach is briefly introduced herein. The overall objective is to develop more stable LCPs (and H_{II} phases) with enhanced temperature and concentration ranges, and therefore achieve a much broader application area of these biomaterials.[3] A very crucial part for the success of this research is the rational design of lipid monomers. Polymerizable moieties which allow photo or redox initiation, such as dienes, styrenes and acryloyls are favored over thermal inducible groups, since temperature affects the phase behavior. The position of the polymerizable moiety in the lipid needs to be considered; linking lipids between the tail and head groups should interfere the least with the forces required for self-assembly.[3,4] Lee *et al*. polymerized a pre-formed LCP and H_{II} phase using a mixture of mono-dienoyl-substituted phosphoethanolamine and bis-dienoyl-substituted phosphocholine, which exhibited a *Pn3m* cubic phase at 60 °C. The polymer was insoluble in several organic solvents.[4] Srisiri *et al*. synthesized polymerizable monoacylglycerols and 1,2-diacyl-*sn*-glycerols and studied their mesophases. A mixture of 9/1 molar ratio of polymerizable monoacylglycerol **116** and 1,2-diacyl-*sn*-glycerol **117** formed an *Ia3d* cubic phase which was found to be stable from 5 – 45 °C. A similar 1,2-diacyl-*sn*-glycerol lipid was used to prepare polymerized cubosomes.[5]

6.2 Results and discussion

The work of Srisiri *et al.*[1,2] serves as the basis for our polymerized catalytic LCPs. These lipids bear the polymerizable moiety just below the head group (Figure 1). This prevents hydrophobic substrates from accumulation in the lipidic compartment and does not interfere with the forces required for self-assembly. To functionalize, i.e. render the LCP catalytically active, polymerizable proline-derived lipid **118** was designed and synthesized, with the aim of using it as an additive that should co-polymerize with **116** and **117**. The polymerization process is schematically illustrated in Figure 1, together with the molecular structures of the three required polymerizable lipids.

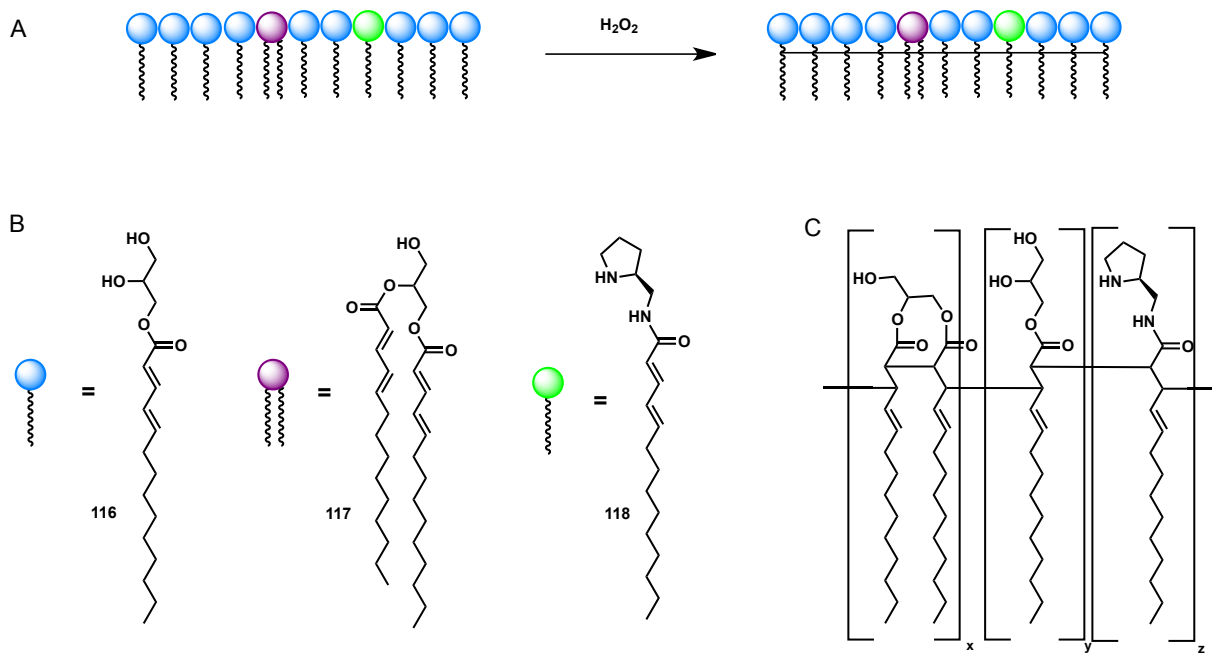

Figure 1: A) Schematic representation of the polymerization process. B) Molecular structure of the three polymerizable lipids **116**, **117** and **118**. C) Schematic representation of the resulting polymer.

6.2.1 Synthesis of polymerizable lipids

Fatty acid **122** is the key compound and is required in the synthesis of all three lipids **116**, **117** and **118**, it introduces the polymerizable moiety. Fatty acid **122** was obtained in two synthetic steps. Commercially available decanal (**119**) was transformed to methyl 2,4-tetradecadienoate (**121**) in a *Wittig-Horner* reaction using trimethyl 4-phosphocrotonate (**120**) (Scheme 1).[6] Methylester **121** was obtained as a mixture of the (*E,E*)-isomer (80 %) and the (*E,Z*)-isomer (20 %) according to ^{1}H-NMR. Methyl ester hydrolysis was carried out in a KOH solution in methanol at reflux to obtain a mixture of the (*E,E*)- and (*E,Z*)-acids **122**.[2] Separation of the (*E,E*)- and (*E,Z*)-acids was accomplished using urea inclusion in methanol (Scheme 1). Urea crystallizes in methanol in a helical lattice with a narrow cylindrical channel of 5.3 Å due to hydrogen bonding.[2,7] Whereas the (*E,E*)-isomer is included in this crystals, the (*E,Z*)-isomer remains outside.

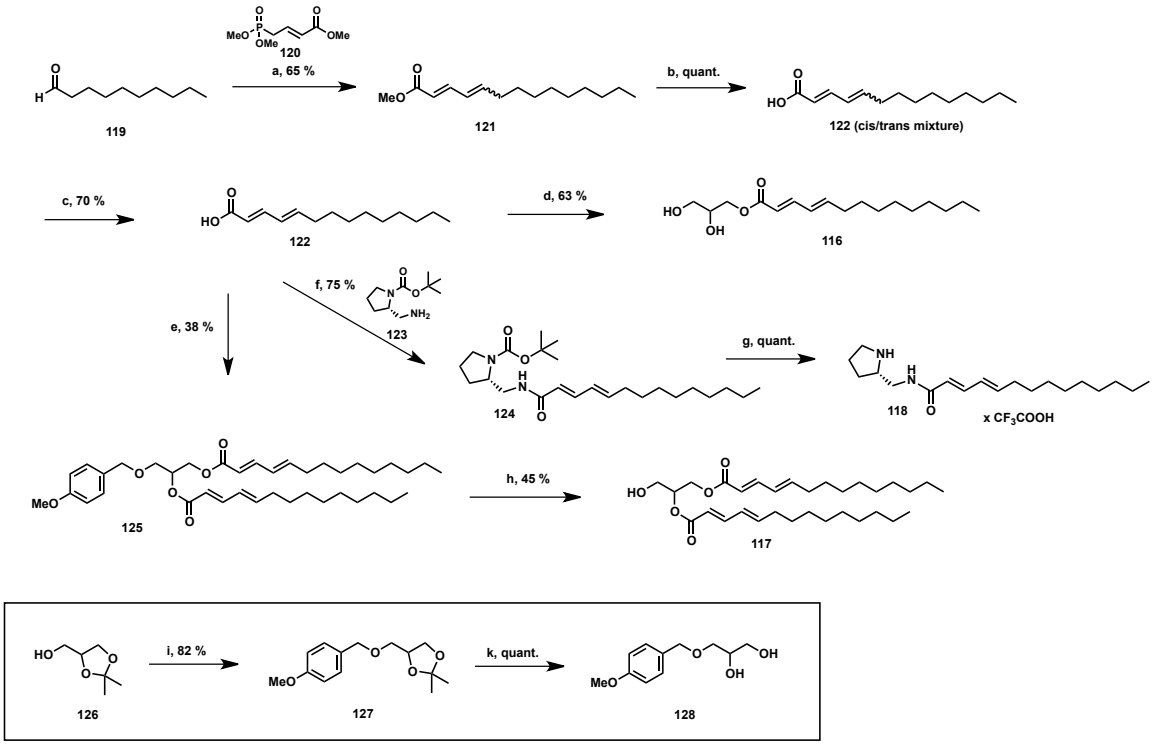

Scheme 1: Synthesis of the polymerizable building blocks for catalytic LCPs. Lipids **116** and **117** are known to form LCPs when mixed 9:1 and hydrated (25 %). Catalyst **118** is planned to be incorporated as an additive to the LCP. Conditions: a) **120** (1.2 eq), NaH (1.5 eq), THF, 0 °C. b) KOH (1.5 eq), MeOH, reflux. c) Urea (8.5 eq), MeOH, 0 °C. d) EDC (1.1 eq), DMAP (0.1 eq), glycerol (6 eq), CH_2Cl_2/DMF (1:1), 0 °C. e) **122** (2 eq.), EDC (2.2 eq), DMAP (0.2 eq), **128** (1 eq), CH_2Cl_2, 0 °C. f) **122** (1 eq), EDC (1.1 eq), DMAP (0.1 eq), **123** (1.1 eq), CH_2Cl_2, 0 °C. g) TFA/CH_2Cl_2 (1:9), 0 °C. h) HCl (1 M), MeOH, r.t. i) 4-methoxybenzyl chloride (1 eq), NaH (1.7 eq), DMF, reflux. k) HCl (0.1 M), MeOH, r.t..

Polymerizable monoacylglycerol **116** was obtained by esterification with an excess of glycerol (Scheme 1). The synthesis of 1,2-diacyl-*sn*-glycerol **117** including a specific glycerol protecting strategy and was achieved in four steps. The free hydroxyl group of acetal-protected glycerol (**126**) was reacted with para-methoxy-benzyl (PMB) chloride to obtain **127**. After cleaving the acetal, PMB-protected 1,2-diacyl-*sn*-glycerol was obtained upon esterification with fatty acid **122**. In a final step, the PMB group was removed to obtain **117** (Scheme 1). Polymerizable proline catalyst was available after coupling fatty acid **122** to (*S*)-2-(Aminomethyl)-1-Boc-pyrrolidine (**123**) using EDC/DMAP followed by BOC deprotection with trifluoro acetic acid (Scheme 1).

6.2.2 Polymerization experiments

In a first experiment, the polymerization of a 9:1 hydrated mixture of **116** and **117** in 25 % H_2O_2/H_2O according to the procedure of Srisiri *et al*. was reproduced.[1] To this end, a lipid film consisting of polymerizable lipids **116** and **117** in a molar ratio of 9:1 was prepared and hydrated with 25 % (w/w) aqueous H_2O_2 30 % (w/w). The sample was centrifuged and equilibrated at 5 °C in the dark, and subsequently polymerized at 45 °C. comparison of the ^{1}H-NMR spectra of **116** (Figure 2, top panel) and the hydrated lipid mixture of **116** and **117** (Figure 2, bottom panel) indicates that the polymerization took place. The ^{1}H-NMR signals of the protons at the two trans carbon-carbon double bonds of **116** (Figure 2, top panel) are absent after incubation of the sample at 45 °C (Figure 2, bottom panel). However, attempts to verify this by ESI-MS and MALDI-TOF-MS failed. As an alternative, determination of the polymerization degree using size exclusion chromatography is planned. Since the obtained mesophase was not transparent, SAXS analysis was not carried out. The LCP preparation procedure thus requires optimization.

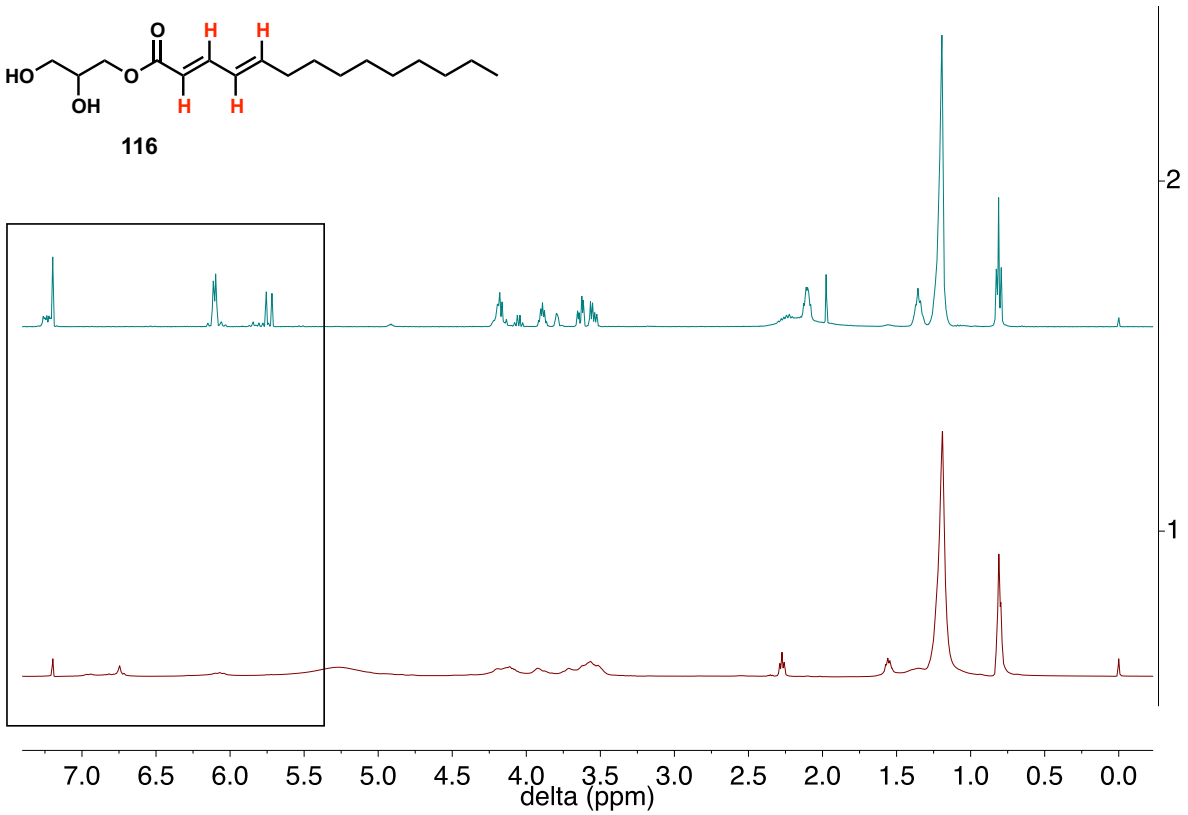

Figure 2: ^{1}H-NMR spectra in $CDCl_3$ of polymerizable lipid **116** (top panel, blue) and of the hydrated (25 % H_2O_2/H_2O) mixture of polymerizable lipids **116** and **117** (9:1) after incubation at 45 °C for 48 h and subsequent lyophylization (bottom panel, red). The hydrogen atoms attached to the two carbon-carbon double bonds of **116** (colored in red) in the ppm range of 5.5 – 7.5 (top panel, box) disappear after incubation at 45 °C (bottom panel, box), which suggests that polymerization occurred.

6.3 Conclusions and Outlook

The polymerizable lipid reported by Srisiri *et al.*[2] were successfully resynthesized. Acid **122** is available in gram scale for future polymerization experiments. Additionally, polymerizable proline-derived catalyst **118** was synthesized, which is used as an additive and allows to test the polymerized LCP for aldol reactions. ^{1}H-NMR data indicate that polymerization of a 9:1 mixture of **116** and **117** took place. However, the mesophase was not transparent and was therefore not analyzed by SAXS. This experiment needs to be repeated and optimized. If the reported *Pn3m* LCP can be reproduced, catalyst **118** can be incorporated to the LCP as an additive and aldol organocatalysis will be investigated. Finally, we plan to prepare cubosomes consisting of polymerizable lipids and to apply them to catalysis as well.

6.4 Experimental section

General Information

N-(3- dimethylaminopropyl)-N′-ethylcarbodiimide hydrochloride (EDC) was purchased from TCI, and all other reagents and solvents were purchased from Sigma Aldrich. All chemicals and solvents were used as received, unless otherwise stated. Reactions were carried out under an inert atmosphere of argon in dry solvents. Dichloromethane was degassed with argon and purified by passage through activated alumina solvent column (MC Brown solvent system) prior to use. Column chromatography was performed using silica gel Merck 60 (particle size 0.040–0.063 mm). Analytical thin- layer chromatography (TLC) was performed using Merck pre-coated silica gel plates 60 F_{254}; visualization by UV absorption and/or by dipping in a solution of $KMnO_4$ (1 g), K_2CO_3 (2 g) in H_2O (100 mL) and subsequent heating. ^{1}H-NMR spectra were recorded on a Bruker AV2-500 (500MHz) spectrometer. Chemical shifts are given in parts per million (ppm) relative to the internal standard TMS (δ = 0 ppm). Coupling constants J are expressed in Hz and multiplicities are abbreviated as follows: s (singlet), br (broad), d (doublet), t (triplet), q (quadruplet), quint (quintet), m (multiplet). ^{13}C-NMR chemical shifts are reported relative to the solvent residual peaks: $CDCl_3$ = 77.00 ppm. Mass spectra were recorded by the Mass Spectroscopy Service of UZH on Finnigan MAT95 MS, BrukerLC MS and Finnigan TSQ700 MS machines.

6.4.1 Synthesis of polymerizable lipids

Synthesis of 121 (methyl tetradeca-2,4-dienoate)[2]

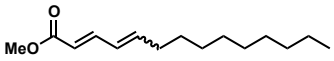

A solution of NaH 60% in mineral oil (0.8 g, 22.5 mmol, 1.4 eq) in THF (50 mL) was cooled to 0°C and a solution of trimethyl 4-phosphonocrotonate (4 g, 19 mmol, 1.2 eq) in THF (50 mL) was added dropwise. The reaction mixture was then stirred for 1 h at 0°C before a solution of decanal (2.5 g, 16 mmol, 1 eq) was added slowly via dropping funnel. The cooling bath was removed and the reaction was monitored by TLC. After completion of the reaction, excess NaH was quenched using cold water. The reaction mixture was concentrated *in vacuo*, diluted with ethyl acetate and extracted with water (1x 100 mL) and brine (1x 100 mL) and dried over $MgSO_4$. After removal of the solvent *in vacuo*, the crude product was purified by column chromatography (cyclohexane/ethyl acetate 10:0 – 9:1) to obtain the desired product as a yellow oil as an isomeric mixture (3.34 g, 14.63 mmol, 65 %). ^{1}H NMR (500 MHz, Chloroform-

d) δ 7.62 – 7.45 (m, 1H), 7.28 – 7.01 (m, 1H), 6.57 – 6.28 (m, 1H), 6.16 – 5.23 (m, 2H), 3.79 – 3.46 (m, 3H), 2.78 – 2.47 (m, 1H), 2.30 – 1.84 (m, 2H), 1.45 – 0.95 (m, 14H), 0.81 (t, *J* = 6.7 Hz, 3H). ^{13}C NMR (126 MHz, Chloroform-*d*) δ 172.77 (d, *J* = 11.4 Hz), 168.35 – 166.19 (m), 145.37, 145.10, 145.06, 144.97, 141.85, 139.72 (2 C), 126.33, 125.19, 120.60, 118.58, 52.27 – 50.52 (4C), 32.46 – 31.56 (2C), 30.16 – 28.90 (5C), 22.65, 14.07. HRMS (ESI $[M + H]^+$) m/z: calcd for ($C_{15}H_{27}O_2$) 229.20056, found 229.20038.

Synthesis of 122 ((2*E*,4*E*)-tetradeca-2,4-dienoic acid) modified procedure[2]

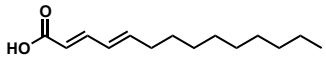

To a solution of methyl ester (2.5 g, 10 mmol, 1 eq) in methanol (50 mL) an aqueous solution of KOH (85 %, 1.5 eq) was added. The solution was then stirred at reflux until the methyl ester was disappeared (ca. 3 h). Methanol was removed and water (30 mL) was added, the solution was acidified to pH 3 with aqueous HCl 10 % and extracted with ethyl acetate (5 x 50 mL). The combined organic phases were washed with brine and dried over $MgSO_4$. The solvent evaporated *in vacuo* to get the crude product. A solution of acid (1.35 g, 6 mmol) in methanol (50 mL) was treated with a solution of urea (3 g, 50 mmol) and stored in the fridge (4°C) for 3 days. The precipitated crystals were filtered off and washed with ethyl acetate. The filtrate was then concentrated and stored in the fridge (4 °C) for 3 days. The procedure was repeated 3 times. The pure product (tran-trans isomer) was obtained as a urea adduct (0.3 g), which was treated with HCl (5 %, 30 mL). The solution was extracted with ethyl acetate (3x 50 mL), dried over $MgSO_4$ and the solvent evaporated *in vacuo* to get the pure product (1.6 g, 7 mmol, 70 %). ^{1}H NMR (400 MHz, Chloroform-*d*) δ 7.36 – 7.21 (m, 1H), 6.17 – 6.06 (m, 2H), 5.71 (d, *J* = 15.3 Hz, 1H), 2.11 (q, *J* = 7.1 Hz, 2H), 1.43 – 1.27 (m, 1H), 1.20 (s, 13H), 0.81 (t, *J* = 6.7 Hz, 3H). ^{13}C NMR (126 MHz, Chloroform-*d*) δ 173.22, 148.59, 147.26, 128.12, 117.53, 33.11, 31.86, 29.49, 29.41, 29.28, 29.18, 28.57, 22.66, 14.09. HRMS (ESI $[M + H]^+$) m/z: calcd for ($C_{14}H_{25}O_2$) 225.18491, found 225.18522.

Synthesis of 122B (2*E*,4*Z*)-pentadeca-2,4-dienoic acid (not reported by Srisiri *et al.*)[2]

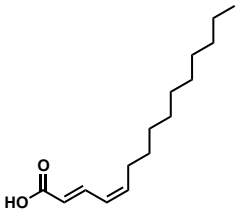

The trans-cis isomer was obtained after evaporating the filtrate after three crystallization cycles. The product was treated with aqueous HCl (5 %, 30 mL). The solution was extracted with ethyl acetate (3x 50 mL), dried over $MgSO_4$ and the solvent evaporated *in vacuo* to obtain the free acid (0.23 g, 1 mmol, 70 %). ^{1}H NMR (500 MHz, Chloroform-*d*) δ 7.63 (dd, *J* = 15.2, 11.8 Hz, 1H), 6.18 – 6.04 (m), 5.91 – 5.82 (m), 5.79 (d, *J* = 15.2 Hz, 1H), 3.44 – 3.16 (m, impurity), 2.24 (q, *J* = 7.6, 6.9 Hz, 1H), 1.44 – 1.00 (m, 13H), 0.81 (t, *J* = 6.9 Hz, 3H). ^{13}C NMR (126 MHz, Chloroform-*d*) δ 172.54, 143.09, 141.81, 126.23, 120.17, 31.86, 29.50, 29.43, 29.30, 29.27, 29.18, 28.34, 22.65, 14.09. HRMS (ESI $[M + H]^+$) m/z: calcd for ($C_{14}H_{25}O_2$) 225.18491, found 225.18522.

Synthesis of 116 ((2*E*,4*E*)-2,3-dihydroxypropyl tetradeca-2,4-dienoate) (modified procedure of Ref. 9)

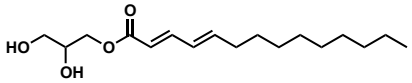

To a stirred solution of acid (100 mg, 0.45 mmol, 1 eq) in 50 mL of a mixture of dry CH_2Cl_2/DMF (3:1) was added EDC (250 mg, 0.59 mmol, 1.3 eq) followed by DMAP (15 mg, 0.045 mmol, 0.01 eq) at 0 °C under argon. The solution was stirred for 1 h at 0 °C and then was added dropwise over a period of 30 min to a solution of glycerol (250 mg, 2.7 mmol, 6 eq.) in 50 mL of dry DMF at 0 °C. The mixture was stirred for 12 h at room temperature and then washed with a saturated solution of $NaHCO_3$. The organic phase was separated and the aqueous phase was extracted with CH_2Cl_2 (3 x 100 mL). The combined organic phases were washed with brine and dried over $MgSO_4$. The solvent was removed under reduced pressure and the residue was purified by column chromatography on silica gel and eluted with a mixture of cyclohexane/ethylacetate 8:2 to 4:6. The solvent was removed to give colorless solid product (84 mg, 0.28 mmol, 63 %). ^{1}H NMR (400 MHz, Chloroform-*d*) δ 7.29 – 7.20 (m, 1H), 6.11 (d, *J* = 6.4 Hz, 2H), 5.74 (d, *J* = 15.3 Hz, 1H), 4.25 – 4.12 (m, 2H), 4.05 (q, *J* = 7.2 Hz, 1H), 3.89 (p, *J* = 5.2 Hz, 1H), 3.80 (s, 1H), 3.66 – 3.61 (m, 1H), 3.58 – 3.52 (m, 1H), 2.33

– 2.07 (m, 3H), 1.35 (d, *J* = 7.0 Hz, 1H), 1.19 (s, 12H), 0.81 (t, *J* = 6.6 Hz, 3H). ^{13}C NMR (126 MHz, Chloroform-*d*) δ 167.74, 146.46, 145.95, 128.11, 117.96, 70.34, 65.08, 63.31, 33.03, 31.84, 29.48, 29.39, 29.26, 29.16, 28.62, 22.64, 14.08. HRMS (ESI [M + Na]$^+$) m/z: calcd for ($C_{17}H_{30}O_4Na$) 321.20363, found 321.20351.

Synthesis of 127 (4-(((4-methoxybenzyl)oxy)methyl)-2,2-dimethyl-1,3-dioxolane)[2]

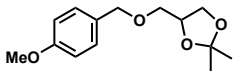

To a suspension of NaH 60 % in mineral oil (1.0 g, 25 mmol, 1.66 eq) in DMF (100 mL) a solution of 1,2-*O*-isopropylidene glycerol (2.0 g, 15 mmol, 1 eq) in DMF (50 mL). The reaction mixture was heated to reflux and after 30 min, 4-methoxybenzyl chloride (2.4 g, 15 mmol, 1 eq) was added dropwise. After completion of the reaction, the mixture was allowed to warm up to room temperature and the excess NaH was quenched with cold water. The mixture was concentrated and the residue dissolved in ethyl acetate. The organic phase was washed with water (3x 50 mL) and brine (50 mL), dried over $MgSO_4$ and the solvent was evaporated *in vacuo* to obtain the crude product, which was purified by column chromatography (cyclohexane/ethyl acetate 3:1) to obtain the desired product (5.17 g, 20.5 mmol, 82 %).
Analytical data were identical with the values reported in literature.

Synthesis of 128 (3-((4-methoxybenzyl)oxy)propane-1,2-diol)[2]

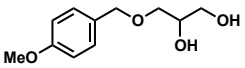

PMB protected 1,2-*O*-isopropylidene glycerol (0.5 g, 1.98 mmol) was dissolved in methanol (50 mL) and an aqueous solution of 10% HCl was added and the reaction mixture stirred for 3 h. The solvent was evaporated *in vacuo* to obtain the crude product, which was purified by column chromatography (cyclohexane/ethyl acetate 3:1) to obtain the desired product in quantitative yield (0.42 mmol, 1.98 mmol). ^{1}H NMR (400 MHz, $CDCl_3$) δ 7.28 – 7.22 (m, 2H), 6.93 – 6.86 (m, 2H), 4.49 (s, 2H), 3.88 (s, 1H), 3.82 (s, 3H), 3.74 – 3.58 (m, 2H), 3.57 – 3.47 (m, 2H). ^{13}C NMR (75 MHz, CDCl3) δ 159.35, 129.73 (2C), 129.53 (2C), 113.87, 73.22, 71.44, 70.70, 64.05, 55.30. Analytical data were identical with the values reported in literature.

Synthesis of 125 ((2*E*,2'*E*,4*E*,4'*E*)-3-((4-methoxybenzyl)oxy)propane-1,2-diyl bis(tetradeca-2,4-dienoate))[2]

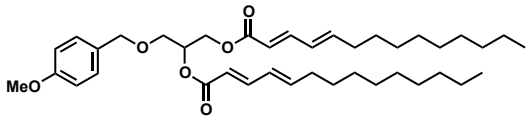

To a stirred solution of acid (100 mg, 0.45 mmol, 1 eq) in 50 mL of a mixture of dry CH_2Cl_2/DMF (3:1) was added EDC (250 mg, 0.59 mmol, 1.3 eq.) followed by DMAP (15 mg, 0.045 mmol, 0.01 eq.) at 0 °C under argon. The solution was stirred for 1 h at 0 °C and then was added dropwise over a period of 30 min to a solution of PMB-protected glycerol **128** (113-mg, 0.45 mmol, 1 eq.) in 50 mL of dry DMF at 0 °C. The mixture was stirred for 12 h at room temperature and then washed with a saturated solution of $NaHCO_3$. The organic phase was separated and the aqueous phase was extracted with CH_2Cl_2 (3 x 100 mL). The combined organic phases were washed with brine and dried over $MgSO_4$. The solvent was removed under reduced pressure and the residue was purified by column chromatography on silica gel and eluted with a mixture of cyclohexane/ethylacetate 8:2 to 4:6. The solvent was removed to give the product (106 mg, 0.17 mmol 38 %) as a slightly yellowish oil. ^{1}H NMR (300 MHz, $CDCl_3$) δ 7.41 – 7.18 (m, 4H), 6.94 – 6.85 (m, 2H), 6.29 – 6.03 (m, 4H), 5.87 – 5.71 (m, 2H), 5.39 – 5.28 (m, 1H), 4.58 – 4.27 (m, 4H), 3.81 (s, 3H), 3.71 – 3.55 (m, 2H), 2.18 (dd, *J* = 12.1, 5.8 Hz, 4H), 1.53 – 1.19 (m, 28H), 0.90 (t, *J* = 6.7 Hz, 6H). ^{13}C NMR (75 MHz, $CDCl_3$) δ 166.86, 166.52, 159.27, 146.01, 145.79, 145.41, 145.30, 129.85, 129.33 (2C), 128.27 (2C), 118.58, 118.44, 113.82 (2C), 72.96, 70.18, 67.89, 62.77, 55.24, 33.03 (2C), 31.88 (2C), 29.52 (2C), 29.43 (2C), 29.30 (2C), 29.19 (2C), 28.69 (2C), 22.67 (2C), 14.11 (2C). HRMS (ESI [M + Na]$^+$) m/z: calcd for ($C_{39}H_{60}O_6Na$) 647.52821, found 647.42765. Analytical data were identical with the values reported in literature.

Synthesis of 117 ((2*E*,2'*E*,4*E*,4'*E*)-3-hydroxypropane-1,2-diyl bis(tetradeca-2,4-dienoate))[2]

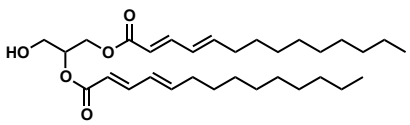

A solution of PMB-protected glycerol **125** (100 mg, 0.16 mmol) in CH_2Cl_2 (5 mL) was cooled to -0 °C and TFA (0.25 mL) was added. The reaction mixture was stirred for 4 h at 0 °C before the solvent was evaporated. In order to remove residual TFA, CH_2Cl_2 (3 x 3 mL) was added

and evaporated. The product was obtained as colorless oil (36 mg, 0.072 mmol, 45 %) Analytical data were identical with the values reported in literature.

Synthesis of 124 ((*S*)-*tert*-butyl 2-((2*E*,4*E*)-tetradeca-2,4-dienamidomethyl)pyrrolidine-1-carboxylate)

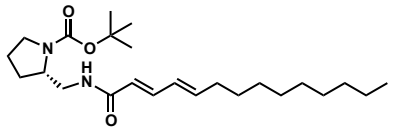

To a stirred solution of acid **122** (63 mg, 0.27 mmol, 1 eq) in 10 mL of a mixture of dry CH_2Cl_2 and dry DMF (1:1) was added EDC (165 mg, 0.35 mmol, 1.3 eq) and DMAP (3.3 mg, 0.027-mmol 0.1 eq) at 0 °C under an inert atmosphere. The solution was stirred for 1 h at 0 °C and then **123** (64 mg, 0.32 mmol,1.2 eq.) was added dropwise over a period of 10 min. The reaction mixture was stirred for 14 h at room temperature and then CH_2Cl_2 (50 mL) was added, the mixture was washed with a saturated solution of $NaHCO_3$. The organic phase was separated and the aqueous phase was extracted with CH_2Cl_2 (50 mL). The combined organic phases were washed with brine and dried over $MgSO_4$. The solvent was removed and the crude product was purified by column chromatography to obtain the product (81 mg, 0.20-mmol,75 %) ^{1}H NMR (500 MHz, Chloroform-*d*) δ 7.42 (s, 1H), 7.15 – 7.00 (m, 1H), 6.09 – 5.91 (m, 2H), 5.70 (d, *J* = 15.1 Hz, 1H), 3.44 – 3.15 (m, 4H), 2.06 (q, *J* = 7.0 Hz, 2H), 1.97 – 1.58 (m, 4H), 1.40 (s, 9H) 1.32 (q, *J* = 6.9 Hz, 2H), 1.21 (s, 14H), 0.81 (t, *J* = 6.9 Hz, 3H). ^{13}C NMR (126 MHz, Chloroform-*d*) δ 166.72, 156.65, 142.43, 140.37, 128.34, 122.26, 79.90, 56.25, 46.98, 46.01, 32.83, 31.79, 29.43, 29.35 (2C), 29.20, 29.07, 28.74, 28.36 (3C), 23.78, 22.57, 14.02. HRMS (ESI $[M + H]^+$) m/z: calcd for ($C_{24}H_{43}O_3N_2$) 407.32682, found 407.32684.

Synthesis of 118 ((2*E*,4*E*)-*N*-((*S*)-pyrrolidin-2-ylmethyl)tetradeca-2,4-dienamide)

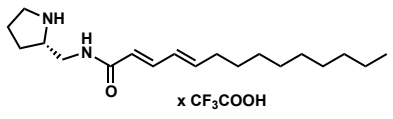

Boc-protected catalysts **124** (89 mg, 0.22 mmol) were dissolved in CH_2Cl_2 (5 mL), cooled to 0-°C and trifluoro acetic acid (TFA) (3 mL) was added slowly. The solution was stirred for 3 h at 0 °C while the reaction was monitored by TLC. Upon completion of the reaction, the solvent was evaporated *in vacuo*. In order to remove residual TFA, CH_2Cl_2 (3 x 3 mL) was added and

evaporated to obtain the product quantitatively (67 mg, 0.22 mmol). ^{1}H NMR (500 MHz, Chloroform-*d*) δ 7.03 (dd, *J* = 15.1, 9.7 Hz, 1H), 6.11 – 5.91 (m, 2H), 5.76 (d, *J* = 15.1 Hz, 1H), 3.86 – 3.11 (m, 6H), 2.08 – 1.86 (m, 4H), 1.75 – 1.60 (m, 1H), 1.36 – 1.25 (m, 2H), 1.16 (s, 14H), 0.78 (t, *J* = 6.8 Hz, 3H). ^{13}C NMR (126 MHz, Chloroform-*d*) δ 169.29, 144.84, 142.80, 128.02, 120.27, 60.57, 45.25, 41.05, 33.00, 31.85, 29.50, 29.42, 29.28, 29.20, 28.73, 27.52, 24.10, 22.64, 14.07. HRMS (ESI $[M + H]^+$) m/z: calcd for ($C_{19}H_{35}ON_2$) 307.27439, found 307.27456.

6.4.2 Polymerization of lipidic cubic phases[1]

Polymerizable lipids **116** and **117** were mixed in a molar ratio of 9:1. The lipids were dissolved in CH_2Cl_2 to obtain a homogeneous mixture. After removal of the solvent at high vacuum, the lipid mixture was hydrated with a degassed aqueous solution of H_2O_2 (30 % w/w) at a concentration of 25 % w/w. The mixture was centrifuged at room temperature and subsequently stored for 24 hours at 5 °C in the dark to equilibrate. Polymerization was carried out at 45 °C for 48 hours.

Bibliography

(1) Srisiri, W.; Benedicto, A.; O'Brien, D. F.; Trouard, T. P.; Orädd, G.; Persson, S.; Lindblom, G. Stabilization of a Bicontinuous Cubic Phase from Polymerizable Monoacylglycerol and Diacylglycerol. *Langmuir* **1998**, *14*, 1921–1926.

(2) Srisiri, W.; Lamparski, H. G.; O'Brien, D. F. Syntheses of Polymerizable Monoacylglycerols and 1,2-Diacyl-Sn -Glycerols. *J. Org. Chem.* **1996**, *61*, 5911–5915.

(3) Mueller, A.; O'Brien, D. F. Supramolecular Materials via Polymerization of Mesophases of Hydrated Amphiphiles. *Chem. Rev.* **2002**, *102*, 727–757.

(4) Lee, Y. S.; Gleeson, J. T.; Yang, J. Z.; Sisson, T. M.; Frankel, D. A.; O'Brien, D. F.; Keller, S. L.; Aksay, E.; Gruner, S. M. Polymerization of Nonlamellar Lipid Assemblies. *J. Am. Chem. Soc.* **1995**, *117*, 5573–5578.

(5) Yang, D.; O'Brien, D. F.; Marder, S. R. Polymerized Bicontinuous Cubic Nanoparticles (Cubosomes) from a Reactive Monoacylglycerol. *J. Am. Chem. Soc.* **2002**, *124*, 13388–13389.

(6) Dorn, K.; Klingbiel, R. T.; Specht, D. P.; Tyminski, P. N.; Ringsdorf, H.; O'Brien, D. F. Permeability Characteristics of Polymeric Bilayer Membranes from Methacryloyl and Butadiene Lipids. *J. Am. Chem. Soc.* **1984**, *106*, 1627–1633.

(7) Smith, A. E. The Crystal Structure of the Urea–hydrocarbon Complexes. *Acta Crystallogr.* **1952**, *5*, 224–235.

Chapter 7

Homochiral lipidic cubic phases

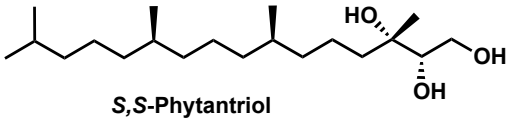

***S,S*-Phytantriol**

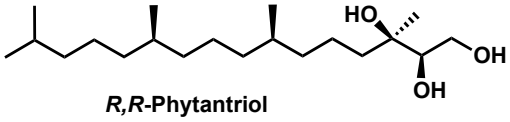

***R,R*-Phytantriol**

7.1 Introduction

Our world is full of objects that are incongruent with their mirror images. These objects are called chiral. Examples are hands, snails, shoes and most significantly, many molecules. In the living world, chirality is unbalanced and molecules of life such as proteins and their amino acid building blocks, sugars, and nucleic acids appear in only one handed form. This has profound consequences, since two enantiomers interact differently with the human body, for example. The pharmaceutical properties of one enantiomer can be different from the other, and in some cases the enantiomer of a drug can be highly toxic, demonstrating the importance of chirality and hence stereoselective synthesis. Enantioselective heterogeneous catalysis has initiated widespread interest in chirality at solid surfaces. For example, achiral compounds were aligned and pre-organized on a chiral surface so that hydrogenation of carbon-carbon or carbon-oxygen bonds occurred selectively.[1,2] Mesoporous organosilica materials (PMO),[3] or metal organic frameworks (MOF) have been applied for asymmetric heterogeneous catalysis as well.[4] Catalytic LCPs and cubosomes based on lipidic proline catalysts have been developed in our group and are described in Chapter 2 of this thesis.[5] However, in this case, the chiral information originates from the chiral lipidic proline catalysts. A chiral surface within pure lipid-water LCPs can be obtained by preparing these mesophases from chiral lipid building blocks, leading to novel chiral materials which have, to the best of our knowledge, not yet been described. In contrast, chiral lipid monolayers[6] and chiral thermotropic cubic phases have been reported.[7,8] MO, the most common lipid that forms LCPs is in principle chiral. However, once in contact with water MO, which is an ester, is in a transesterification equilibrium which leads to loss of chiral information. Commercial MO is available as a racemic mixture. Phytantriol (PT) (Scheme 1) lacks the ester moiety and is therefore a more suitable chiral target lipid. PT is often used as additive in the cosmetic industry, and its binary phase behavior upon hydration is very similar to that of hydrated MO. However, it is based on a mixture of diastereoisomers. A major difference between these phase diagrams is the lower hydration degree, and smaller lattice parameter of the *Pn3m* cubic phase of PT at excess water conditions as compared to MO.[9] The absence of the ester group renders PT chemically more stable, as compared to MO, since ester groups are prone to hydrolysis. The same is true for *in vivo* applications in the presence of digestive enzymes. The goal of this project is to synthesize two different PT diastereoisomers and to study their mesophases. Furthermore, their impact on catalysis and has been investigated and experiments towards chiral recognition and separation were performed.

7.2 Results and discussion

7.2.1 Synthesis of two different phytantriol diastereoisomers

Commercially available phytol is a suitable precursor to obtain two pure phytantriol diastereoisomers via *Sharpless* asymmetric dihydroxylation (Scheme 1).[10] With this approach, using the corresponding *AD*-Mix-α or *AD*-Mix-ß, (2*S*,3*S*,7*R*,11*R*)-3,7,11,15-tetramethylhexadecane-1,2,3-triol (**130**), denoted herein *R,R*-PT, and (2*R*,3*R*,7*R*,11*R*)-3,7,11,15-tetramethylhexadecane-1,2,3-triol (**131**), denoted herein *S,S*-PT, can be obtained in one synthetic step with *ca*. 70 % yield in each case.

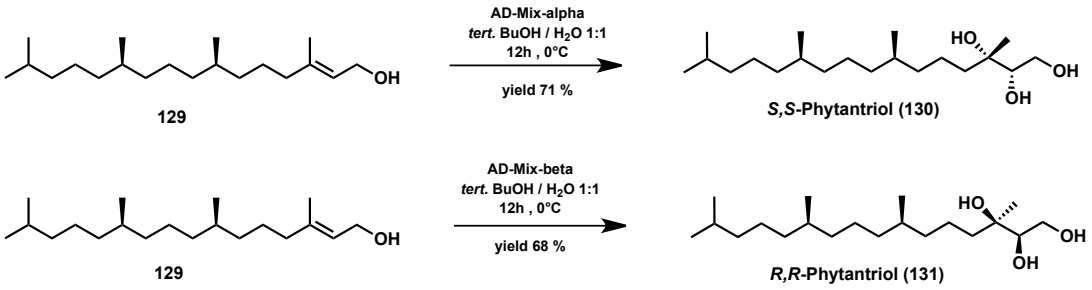

Scheme 1: Synthesis of *S,S*-PT (**130**) and *R,R*-PT (**131**) from commercial phytol using *AD*-Mix-α or *AD*-Mix-ß, respectively.

The ^{1}H-NMR spectra of commercially available PT (blue), *R,R*-PT (brown) and *S,S*-PT (green) are compared in Figure 1. A closer look at the proton at position 2 indicates that commercial PT consist of four diastereoisimers, two of them are *R,R*-PT and *S,S*-PT (Figure 1C). The other two are (2*R*,3*S*,7*R*,11*R*)-3,7,11,15-tetramethylhexadecane-1,2,3-triol and (2*S*,3*R*,7*R*,11*R*)-3,7,11,15-tetramethylhexadecane-1,2,3-triol, which would be referred to *S,R*-PT and *R,S*-PT in the nomenclature used before.

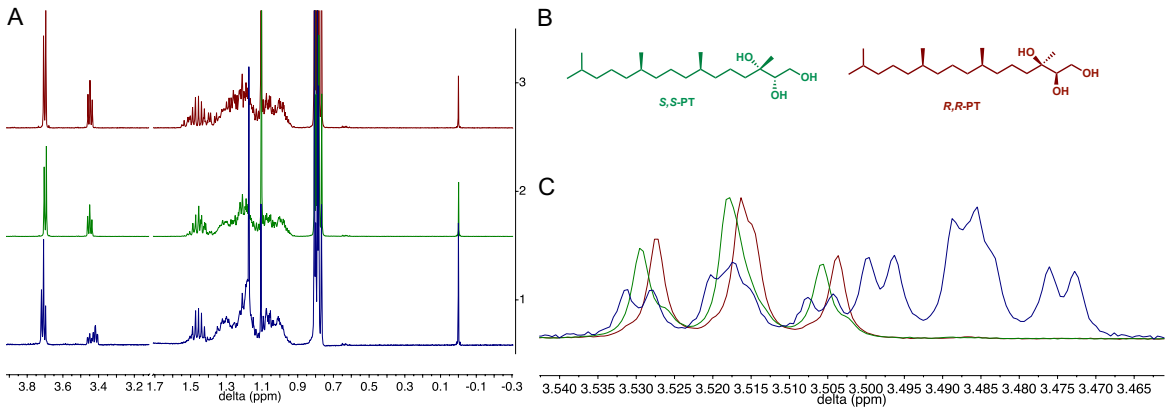

Figure 1: A) Stacked ^{1}H-NMR spectra of commercially available PT (blue), *S,S*-PT (green) and *R,R*-PT (brown). B) Structures of *S,S*-PT (green) and *R,R*-PT (brown). C) Superimposed sections of ^{1}H-NMR spectra of commercial PT (blue), *S,S*-PT (green) and *R,R*-PT (brown) showing the triplet arising from the hydrogen at position 2.

With these two diastereomeric moldecules *R,R*-PT and *S,S*-PT in hand, novel chiral LCPs can be produced and potentially applied for catalysis and chiral recognition. As a model system, the aldol reaction described in Chapter 2 will be used. Two important questions will be addressed: Firstly, can stereochemical information be induced to the aldol reaction applying a nonchiral catalyst but a chiral supporting LCP? And secondly, is it possible to enhance the stereoselectivity of a chiral catalyst with a chiral LCP?

7.2.2 Applications of chiral LCPs

7.2.2.1 Catalysis

LCPs based on *S,S*-PT, *R,R*-PT, and commercially available PT, each containing lipidic aldol catalyst **2** (40 mol % relative to aldehyde **4a**) were prepared and used to catalyze the model aldol reaction described in Chapter 2. The goal of these experiments was to determine whether the chiral surfaces of the ensuing *S,S*-PT and *R,R*-PT LCPs, respectively, would support the catalyst by preorganizing the substrates specifically and thus affecting the stereochemical outcome of the reaction. Furthermore, the kintics of these were compared, as preliminary data suggest that the phase diagrams of the individual PT diastereomers are different from the mixture, which is reported in literature.[11] However, neither the reaction rates nor the stereochemistry were found to be significantly different for one of the three PT-based LCPs, as shown in Figure 2, which has already been shown in Chapter 2.

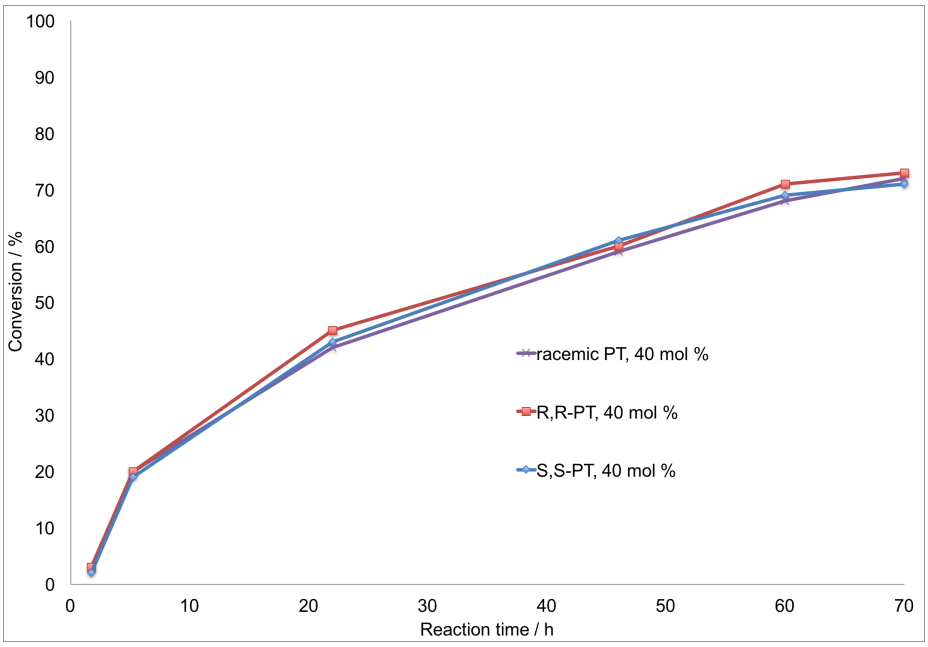

Figure 2: Progress of the aldol reaction of cyclohexanone **3** with aldehyde **4a in** three different phytantriol LCP systems (determined by ^{1}H-NMR). Comparison of LCP media consisting of racemic PT, *S,S*-PT and *R,R*-PT with 40 mol % cat. loading.

7.2.2.2 Characterization of *S,S*-PT and *R,R*-PT monolayers and mesophases

Monolayers of commercially available PT, *S,S*-PT, and *R,R*-PT were prepared in a trough at at the air-water interface, and their Langmuir-Blodgett isotherms and Brewster-angle-microscopic images compared. No significant differences were found between the three systems (results not shown). However, initial comparison of the phase behavior indicates differences between that of the single diastereoisomers with the one of commercially available PT. In the pure form at room temperature, the single diastereoisomers *S,S*-PT and *R,R*-PT form white crystals, whereas commercial PT appears as a viscous liquid. Polarized light micrographs and SAXS analysis of *S,S*-PT (Figure 3A and 3C) reveal the presence of a L_c phase, which gives rise to anisotropy, whereas polarized light micrographs and SAXS analysis of commercial PT show an isotropic sample (Figure 3B and 3D). The detailed phase diagram of the hydrated *S,S*-PT and *R,R*-PT systems are currently being elucidated in our group.

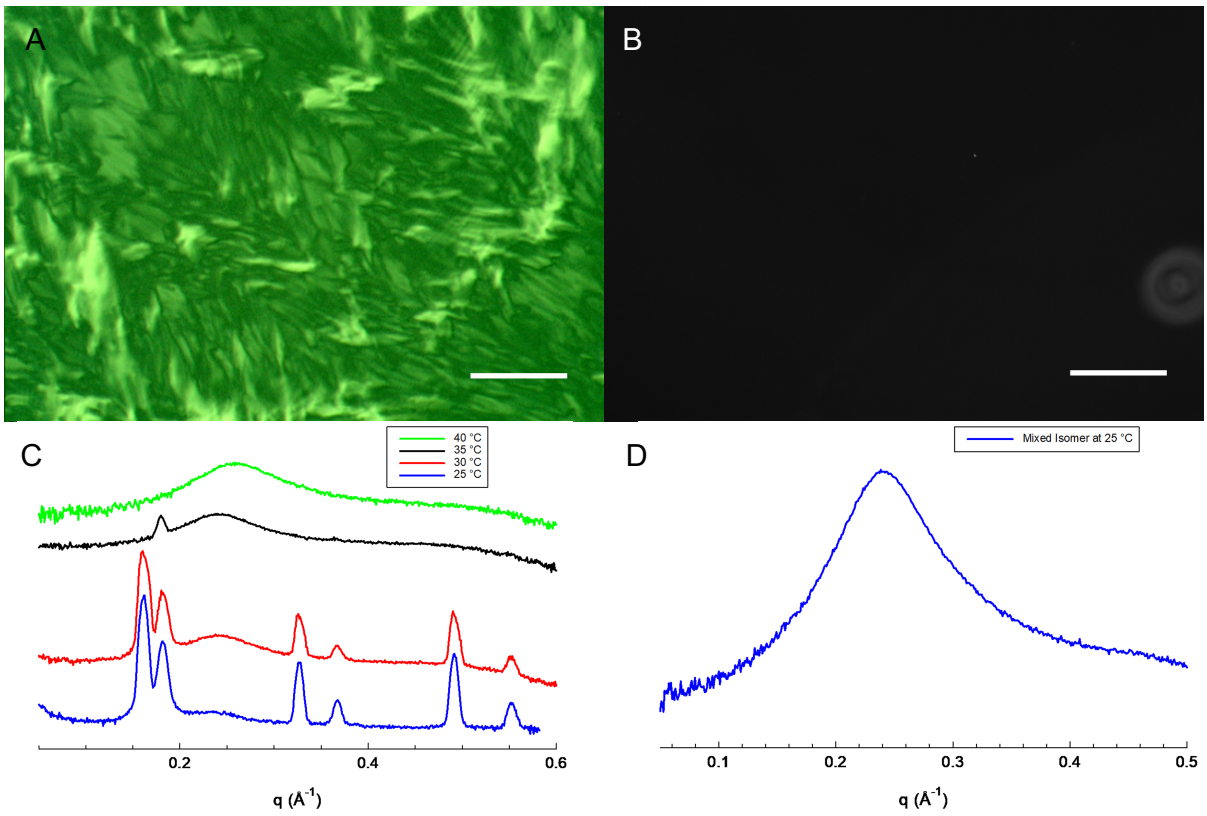

Figure 3: A) Polarized light micrograph of *S,S*-PT. B) Polarized light micrograph of commercially available PT. C) SAXS pattern of *S,S*-PT. D) SAXS pattern of commercially available PT.

7.3 Conclusions

The two diastereoisomers of phytantriol, *S,S*-PT and *R,R*-PT were synthesized from commercially available phytol within one synthetic step using *Sharpless* asymmetric dihydroxylation. With these lipids in hand, homochiral LCPs are accessible. Such materials are potentially interesting for catalysis or for chiral recognition. Homochiral LCPs of both *S,S*-PT and *R,R*-PT have been prepared and used for catalysis of a model aldol reaction. However, neither kinetic nor stereochemical differences have been found in preliminary experiments. Whereas the Langmuir monolayers of commercially available PT, *S,S*-PT, and *R,R*-PT show identical behavior, differences in their hydrated phase behavior was observed using SAXS and light microscopy.

7.4 Outlook

A project in our group was started to investigate the properties of such homochiral LCPs. Elucidation of the phase diagrams of the single diastereoisomers is in progress. Furthermore, experiments towards chiral recognition/separation will be performed. In order to exploit the chiral surface of these LCPs, metals could be coordinated to the lipids. The resulting catalytic LCP complex can then be used for asymmetric catalysis.

7.5 Experimental section

General information

Phytantriol was purchased from DSM. All other reagents and solvents were purchased from Sigma Aldrich. All chemicals and solvents were used as received, unless otherwise stated. Reactions were carried out under an inert atmosphere of argon in dry solvents. Dichloromethane was degassed with argon and purified by passage through activated alumina solvent column (MC Brown solvent system) prior to use. Column chromatography was performed using silica gel Merck 60 (particle size 0.040–0.063 mm). Analytical thin- layer chromatography (TLC) was performed using Merck pre-coated silica gel plates 60 F_{254}; visualization by UV absorption and/or by dipping in a solution of $KMnO_4$ (1 g), K_2CO_3 (2 g) in H_2O (100 mL) and subsequent heating. ^{1}H-NMR spectra were recorded on a Bruker AV2-500 (500MHz) spectrometer. Chemical shifts are given in parts per million (ppm) relative to the internal standard TMS (δ = 0 ppm). Coupling constants J are expressed in Hz and multiplicities are abbreviated as follows: s (singlet), br (broad), d (doublet), t (triplet), q (quadruplet), quint (quintet), m (multiplet). ^{13}C-NMR chemical shifts are reported relative to the solvent residual peaks: $CDCl_3$ = 77.00 ppm. Mass spectra were recorded by the Mass Spectroscopy Service of UZH on Finnigan MAT95 MS, BrukerLC MS and Finnigan TSQ700 MS machines.

7.5.1 Synthesis

Synthesis of 130 ((2*S*,3*S*,7*R*,11*R*)-3,7,11,15-tetramethylhexadecane-1,2,3-triol)[12]

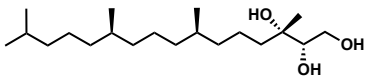

To a round-bottomed flask, *tert*-butyl alcohol (5 mL), water (5 mL), and 1.4 g of AD-mix-α were added. The yellow mixture was allowed to stir at room temperature whereupon two clear phases were obtained. Methanesulfonamide (95 mg, 1 mmol, 1eq) was added. The reaction mixture was cooled to 0 °C which led to the precipitation of salts. Phytol (296 mg, 1 mmol, 1 eq) was added and the reaction mixture was stirred for 22 h. Sodium sulfite (1.5 g) was added and the mixture was allowed to warm to room temperature. After 60 min, DCM (20 mL) was added and the phases were separated. The aqueous phase was extracted with DCM (3 x 20 mL) and the combined organic phases were washed with aqueous KOH 2 M (30 mL), dried over $MgSO_4$ concentrated. The crude product was purified by flash chromatography (cyclohexane/ethylacetate 9:1) to give the product as colourless oil (235 mg, 0.71 mmol, 71%). ^{1}H NMR (400 MHz, Chloroform-*d*) δ 3.70 (d, *J* = 4.9 Hz, 2H), 3.46 (t, *J* = 4.3 Hz, 1H), 2.07 (s, br, OH), 1.55 – 0.93 (m, 24H), 0.82 – 0.75 (m, 12H). ^{13}C NMR (101 MHz, Chloroform-*d*) δ 75.12, 70.55, 63.43, 39.81, 39.36, 37.53, 37.42, 37.39, 37.27, 32.79, 27.98, 24.79, 24.48, 22.72, 22.62, 22.35, 21.05, 19.74, 19.68. HRMS (ESI [M + Na]$^+$) m/z: calcd for ($C_{20}H_{42}O_3$) 353.30262, found 353.30224.

Synthesis of 131 ((2*R*,3*R*,7*R*,11*R*)-3,7,11,15-tetramethylhexadecane-1,2,3-triol)[12]

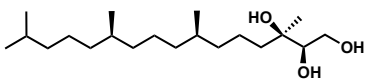

To a round-bottomed flask, *tert*-butyl alcohol (5 mL), water (5 mL), and 1.4 g of AD-mix-β were added. The yellow mixture was allowed to stir at room temperature whereupon two clear phases were obtained. Methanesulfonamide (95 mg, 1 mmol, 1eq) was added. The reaction mixture was cooled to 0 °C which led to the precipitation of salts. Phytol (296 mg, 1 mmol, 1 eq) was added and the reaction mixture was stirred for 22 h. Sodium sulfite (1.5 g) was added and the mixture was allowed to warm to room temperature. After 60 min, DCM (20 mL) was added and the phases were separated. The aqueous phase was extracted with DCM (3 x 20 mL) and the combined organic phases were washed with aqueous KOH 2 M (30 mL),

dried over $MgSO_4$ concentrated. The crude product was purified by flash chromatography (cyclohexane/ethylacetate 9:1) to give the product as colourless oil (225 mg, 0.68 mmol, 68%) ^{1}H NMR (400 MHz, Chloroform-*d*) δ 3.70 (d, *J* = 4.9 Hz, 2H), 3.45 (t, *J* = 4.3 Hz, 1H), 2.07 (s, br, OH), 1.55 – 0.93 (m, 24H), 0.82 – 0.75 (m, 12H). ^{13}C NMR (101 MHz, Chloroform-*d*) δ 75.18, 74.58, 63.43, 39.80, 39.37, 37.53, 37.43 (2C), 37.28, 32.79 (2C), 27.97, 24.79, 24.49, 22.71, 22.62, 22.34, 21.04, 19.74, 19.66. HRMS (ESI [M + Na]$^+$) m/z: calcd for ($C_{20}H_{42}O_3$) 353.30262, found 353.30318.

Commercial phytantriol (mixture of diastereoisomers)

^{1}H NMR (400 MHz, Chloroform-*d*) δ 3.70 (d, *J* = 4.9 Hz, 2H), 3.47 – 3.40 (m, 1H), 2.07 (s, br, OH), 1.55 – 0.93 (m, 24H), 0.82 – 0.75 (m, 12H). ^{13}C NMR (126 MHz, Chloroform-*d*) δ 76.53, 76.51, 75.67, 75.64, 74.69, 74.68, 74.52, 74.51, 63.34, 63.19, 39.61, 39.64, 39.35, 38.32, 38.36, 37.81, 37.72, 37.62, 37.44, 37.41, 37.38, 37.27, 32.78, 27.95, 24.79, 24.78, 24.49, 23.47, 23.44, 22.70, 22.61, 22.19, 22.16, 20.99, 20.95, 19.72, 19.67, 19.64, 19.61, 19.57, 19.55. HRMS (ESI [M + Na]$^+$) m/z: calcd for ($C_{20}H_{42}O_3$) 353.30318.

7.5.2 Langmuir Blodgett

Surface pressure versus molecular area isotherms were recorded using the KSV LB through 5000 equipped hydrophilic barriers. The experiment was controlled with software version KSV 5000. A Wilhelmy balance was used as a surface pressure sensor. Surface pressure was recorded as function of molecular area. The accuracy of measurements of area per molecule was 1 Å^2 and that of surface pressure was 1 mN/m. After the solution was spread, it was left for 15 min for solvent evaporation. Compression was accomplished with a barrier speed of 7.5 cm^2/min. Temperature was kept at 22 ± 1 °C.

7.5.3 Brewster Angle Microscopy

Brewster angle microscopy experiments were performed using a Nanofilm Ep3 instrument (Accurion GmbH, Germany) equipped with an UltraBam objective (10 x magnification), 50 mW solid-state laser emitting p-polarized light at a wavelength of 658 nm and a CCD camera. The lateral resolution of the UltraBam objective is 2 μm. Images were captured during the compression of the monolayers at the air-water interface and each picture represents the area of 320 μm x 410 μm.

7.5.4 Small angle X-ray scattering (SAXS)

Experiments were performed on a Bruker AXS Micro, with a microfocused X-ray source, operating at voltage filament current of 50 kV and 1.000 μA, respectively. The Cu Kα radiation (λCu Kα =1.5418 Å) was collimated by a 2D Pilatus 100K detector. The scattering vector $q = (4\pi/\lambda)\sin\theta$, with 2θ being the scattering angle, was calibrated using silver behenate. Data were collected and azimuthally averaged using the Saxsgui software to yield one-dimensional intensity versus scattering vector *q*, with a *q* range from 0.004 – 0.5 $Å^{-1}$. The samples were placed inside a stainless-steel cell between two thin replaceable mica sheets and sealed by an O-ring, with a sample volume of 10 μL and a thickness of ~1 mm. Measurements were performed at 23°C, and samples were equilibrated for 15 min before measurements, whereas scattered intensity was collected over 30 min.

7.5.5 Light microscopy

Images were taken under cross-polarized light using a Zeiss Axioskop 2 mot microscope.

Bibliography

(1) Blaser, H.-U. Enantioselective Synthesis Using Chiral Heterogeneous. *Tetrahedron: Asymmetry* **1991**, *2*, 843–866.

(2) McFadden, C. F.; Cremer, P. S.; Gellman, A. J. Adsorption of Chiral Alcohols on “Chiral” Metal Surfaces. *Langmuir* **1996**, *12*, 2483–2487.

(3) Kuschel, A.; Polarz, S. Effects of Primary and Secondary Surface Groups in Enantioselective Catalysis Using Nanoporous Materials with Chiral Walls. *J. Am. Chem. Soc.* **2010**, No. 8, 6558–6565.

(4) Yoon, M.; Srirambalaji, R.; Kim, K. Homochiral Metal-Organic Frameworks for Asymmetric Heterogeneous Catalysis. *Chem. Rev.* **2012**, *112*, 1196–1231.

(5) Duss, M.; Salvati Manni, L.; Moser, L.; Handschin, S.; Mezzenga, R.; Jessen, H. J.; Landau, E. M. Lipidic Mesophases as Novel Nanoreactor Scaffolds for Organocatalysts: Heterogeneously Catalyzed Asymmetric Aldol Reactions in Confined Water. *ACS Appl. Mater. Interfaces* **2018**, *10*, 5114–5124.

(6) Basnet, P. B.; Mandal, P.; Malcolm, D. W.; Mann, E. K.; Chaieb, S. Chiral Hierarchical Self-Assembly in Langmuir Monolayers of Diacetylenic Lipids. *Soft Matter* **2013**, *9*, 1437–1446.

(7) Yamamoto, T.; Nishiyama, I.; Yoneya, M.; Yokoyama, H. Novel Chiral Effect That Produces the Anisotropy in 3D Structured Soft Material: Chirality-Driven Cubic-Tetragonal Liquid Crystal Phase Transition. *J. Phys. Chem. B* **2009**, *113*, 11564–11567.

(8) Kamikawa, Y.; Nishii, M.; Kato, T. Supramolecular Chiral Cubic Phases Formed by Folic Acid Derivatives. *Mol. Cryst. Liq. Cryst.* **2005**, *435*, 95-105.

(9) Dong, Y. D.; Larson, I.; Hanley, T.; Boyd, B. J. Bulk and Dispersed Aqueous Phase Behavior of Phytantriol: Effect of Vitamin E Acetate and F127 Polymer on Liquid Crystal Nanostructure. *Langmuir* **2006**, *22*, 9512–9518.

(10) Jacobsen, E.; Marko, I.; Mungall, W.; Schröder, G.; Sharpless, K. Asymmetric Dihydroxylation via Ligand-Accelerated Catalysis. *J. Am. Chem. Soc.* **1988**, No. 110, 1968–1970.

(11) Barauskas, J.; Landh, T. Phase Behavior of the Phytantriol/water System. *Langmuir* **2003**, *19*, 9562–9565.

(12) Sharpless, K. B.; Amberg, W.; Bennani, Y. L.; Crispino, G. a; Hartung, J.; Jeong, K. S.; Kwong, H. L.; Morikawa, K.; Wang, Z. M.; Xu, D. Q.; Zhang, X. L. The Osmium-Catalyzed Asymmetric Dihydroxylation - a New Ligand Class and a Process Improvement. *J. Org. Chem.* **1992**, *57*, 2768–2771.

Chapter 8

Cyclopropanated lipids: Synthesis and mesophases

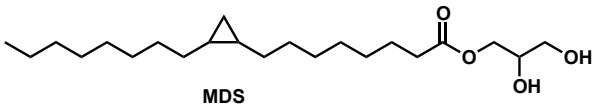

MDS

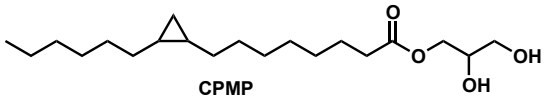

CPMP

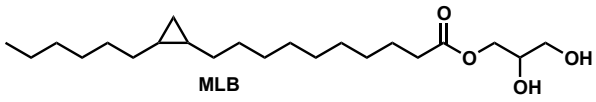

MLB

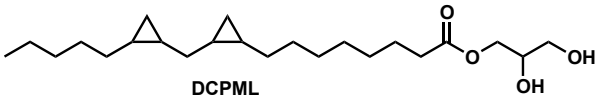

DCPML

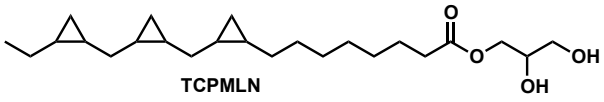

TCPMLN

8.1 Introduction

Due to their unique properties, LCPs find applications in a wide range of fundamental and applied fields. Landau and Rosenbusch introduced the concept of LCPs for the solubilization, stabilization, and crystallization of membrane proteins.[1] Ca. 31% of all X-ray structures of membrane proteins currently available were obtained with this method.[2] However, many membrane proteins are unstable at ambient temperature and should preferentially be studied at low temperatures. Available LCPs are inapplicable in such cases, as they undergo phase transitions at low temperatures. A research program to address this problem was launched in our group, yielding to MDS, a first cyclopropanated lipid which showed extended cubic phase boundary to lower temperature and enabled crystallization of bacteriorhodopsin at 4 °C.[3] Lipid polymorphism is a complex phenomenon based on a variety of parameters. Correlating molecular structures of lipids with the ensuing mesophase is therefore a major challenge.[4] Phase transitions are strongly governed by the lipid's molecular structure, i.e. on the nature of the head group and the length and curvature of the chain. It has been shown that the chain splay plays a pivotal role affecting the phase behavior of monoacylglycerols.[5] Varying systematically structural elements of the lipids might allow to gain information on how such changes affect phase behavior. To this end, a series of naturally occurring *cis*-monoacylglycerols that are known to form LCPs have been modified by replacing the *cis*-double bond with a cyclopropyl ring to obtain a small library of novel designer lipids (Figure 1).

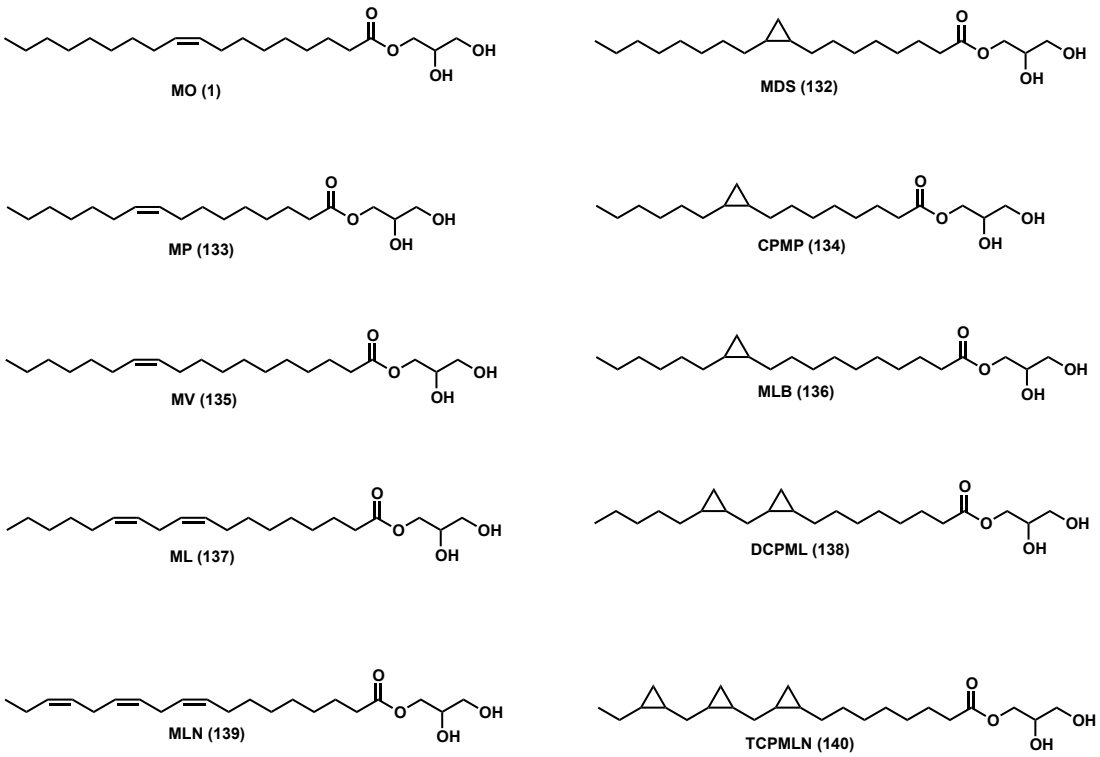

Figure 1: The most common monoacylglycerols (left column) and their cyclopropyl-analogues (right column).

Olefins and cyclopropanes have some characteristics in common; their chemical properties and the curvature of the *cis*-monoacylglycerols and their cyclopropyl analogues are similar, since the two functional groups have their residues attached in similar angles. However, the main difference is the change from sp^2 to sp^3 hybridized carbon atoms at the corresponding functional group. In contrast to classical *cis*-monoacylglycerols, our designer lipids protrude out of the plane of the molecule due to the tetrahedral geometry of the sp^3 carbon atoms at the cyclopropyl ring, resulting in a kink in the molecule that locks the *cis* geometry.
The cyclopropane modification is naturally inspired; cyclopropanated phospholipids are prevailed among the realm of bacteria. Their presence improves survival of bacterial pathogens like *M. tuberculosis*[6] and leads to resistance of the *E. coli* cell membrane against acid and cold shock.[7] Furthemore, cyclopropanated phospholipids seem to play an important role in membrane property regulation.[7]

8.2 Results and discussion

We hypothesized that the rigidity of the lipidic chain of the target compounds can be modified by varying the position and the number of the cyclopropyl moiety as well as the length of the lipidic tail. Cyclopropanated analogues of *cis*-monoacylglycerols that are known to exhibit lipidic cubic phases were targeted. By systematically substituting the carbon-carbon double bond with a cyclopropyl ring, a library of cyclopropanated lipids with variying lipidic tail length, location of cyclopropanation and number of cycloproanation have been prepared (Figure 1): monodihydrosterculin (MDS, **132**),[3] cyclopropyl monopalmitolein (CPMP, **134**), monolactobacillin (MLB, **136**), dicyclopropyl monolinolein (DCPML, **138**) and tricyclopropyl monolinolenin (TCPMLN, **140**). In summary, these comprise:

- Lipids with with modification at C_9 position and C_{16} and C_{18} chains (CPMP, C_{16}) and (MDS, C_{18}).

- The location of the cyclopropyl ring of lipids with a C_{18} was shifted from position C_9 (MDS) to position C_{11} (MLB).

- Lipids with one (MDS, CPMP, MLB), two (DCPML) and three cyclopropyl groups (TCPMLN).

8.2.1 Synthesis of cyclopropanated lipids

Cyclopropanation of olefins **1**, **133**, **135**, **137** and **139** was performed using diethyl zinc and diiodomethane in the presence of 2,4,6-trichlorophenol according to a reported procedure[8] to afford the corresponding cyclopropanated acids **141** - **145** with yields ranging from 61 to 73 %. Due to safety concerns, this procedure was not scaled up, although a great quantity of lipid was required. The maximum amount of lipid that was cyclopropanated was 3 g in one batch to ensure efficient cooling. However, up to three batches were conducted in parallel.

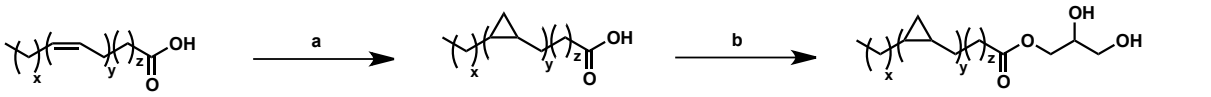

x = 7, y = 1, z = 6: **1**
x = 5, y = 1, z = 6: **133**
x = 5, y = 1, z = 8: **135**
x = 4, y = 2, z = 6: **137**
x = 1, y = 3, z = 6: **139**

x = 7, y = 1, z = 6: **141,** 65 %
x = 5, y = 1, z = 6: **142**, 73 %
x = 5, y = 1, z = 8: **143**, 71 %
x = 4, y = 2, z = 6: **144**, 69 %
x = 1, y = 3, z = 6: **145**, 61 %

x = 7, y = 1, z = 6: MDS (**132**), 69 %
x = 5, y = 1, z = 6: CPMP (**134**), 55 %
x = 5, y = 1, z = 8: MLB (**136**), 58 %
x = 4, y = 2, z = 6: DCPML (**138**), 71 %
x = 1, y = 3, z = 6: TCPMLN (**140**), 78 %

Scheme 1: Two step synthesis of cyclopropanated lipids MDS, CPMP, MLB, DCPML and TCPMLN from commercially available olefins. Conditons: a) 2,4,6-Trichlorophenol, CH_2I_2, $ZnEt_2$, CH_2Cl_2, -40 °C. b) EDC/DMAP, DMF/ CH_2Cl_2 (1:1), r.t..

The esterification underwent an optimization process, since initial yields below 50 % were obtained when using EDC/DMAP in CH_2Cl_2. Transesterification was tried starting from methylesters of **141** using P1-phosphazen. However, the high reported yields could not be reproduced.[9] Therefore, the initially applied method using EDC/DMAP was modified. First, a mixture of DMF and CH_2Cl_2 was used instead of pure CH_2Cl_2, since glycerol is only moderately soluble in CH_2Cl_2. The rate of glycerol addition to the activated acid is crucial; the formation of di-esterified product (Figure 2) was almost completely prevented when glycerol is added over a period of 2 h, leading to better yields between 55 and 78 %.

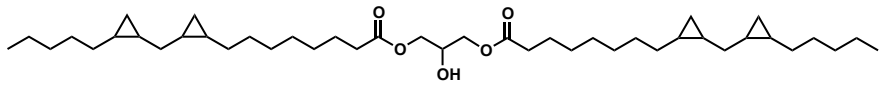

DCPDL (146)

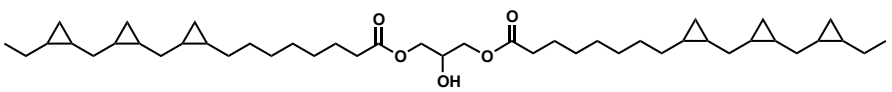

TCPDLN, (147)

Figure 2: Structures of di-esterified side products DCPDL (**146**) and TCPDLN (**147**).

Since mesophases of multiple cyclopropanated lipids DCPML and TCPLN show highly interesting properties (see page 196), the di-esterified side products were isolated as well and characterized for future investigations (Figure 2).

The final products also contain the 2-substituted products that are formed upon transesterification. In equilibrium, these amount to 6 – 10 % of the 1-substituted products.

8.2.2 Phase behavior of the designer cyclopropyl lipids

The following paragraph summarizes the data obtained from investigations of the mesophases of cyclopropanated lipids. This work was performed in collaboration with the group of Prof. Raffaele Mezzenga.[10] After successfully synthesizing the five designed cyclopropyl analogues MDS (**132**),[3] CPMP (**134**), MLB (**136**), DCPML (**138**) and TCPMLN (**140**), their phase behavior was investigated using small angle X-ray scattering (SAXS). The phase diagrams were built by systematically varying temperature and hydration degree of the water/lipid system. The MDS/water phase diagram, together with a first membrane protein crystallization therein, has been published by Salvati Manni *et al*.[3] The most important results are briefly summarized: The MDS/water phase diagram shows some important differences to its MO/water analogue, which arise from the structural difference of the lipids. The cubic phases appear in a broader range, *i.e.* to a higher water content and can therefore accommodate more water. Remarkably, MDS was shown to form cubic phases at lower temperatures than MO. A comparable effect was found for the corresponding phosphatidylethanolamines.[11,12] The fact that the installation of a cyclopropyl moiety has a profound effect on the phase behavior of the lipid reinforced our hypothesis and led to a further investigation of this phenomenon by studying the phase diagrams of the remaining cyclopropylated lipids CPMP (**134**), MLB (**136**), DCPML (**138**) and TCPMLN (**140**). CPMP and MLB show similar phase diagrams like the corresponding monoacylglycerols. DCPML, on the other hand, exhibits an unusual and highly remarkable phase behavior. The typical sequence of phase transitions at ambient temperatures for most hydrated monoacylglycerols, including unmodified ML is L_α, *Ia3d*, *Pn3m*. However, DCPML showed a phase transition from *Ia3d* to H_{II} instead. A stable H_{II} phase at room temperature and 37 °C is a novelty, and can usually only obtained by adding hydrophobic molecules like tetradecane or oleic acid to other monoacylglycerols[13,14] or if the ester group of the lipid is replaced with an ether linkage.[15] Moreover, the release of hydrophilic molecules from H_{II} phases is slower as compared to LCPs, which makes this phase interesting for several applications. H_{II} phases have been used as membrane protein reconstitution[16] matrix and for drug delivery.[17,18] Thus, with our DCPML H_{II} phases a simpler binary system is introduced, thereby avoiding the difficulties of available ternary systems. Having a stable H_{II} phases present at room temperature indicates that the entire phase diagram is shifted to lower temperatures and hydration. Therefore, low temperature phase behavior was investigated as well.

8.2.3 Low temperature phase behavior of DCPML

Investigating the phase behavior of DCPML yielded highly interesting results; a cubic phase was observed at lower temperature than expected. A DCPML sample with 12 % w/w of water was analyzed by SAXS at low temperature. The sample was slowly cooled to -20 °C (1 °C/min) and kept there for 3 h. Subsequently, the temperature was slowly increased from -20 to 22 °C while SAXS spectra were acquired. The phase transition from L_α to *Ia3d* phase at -15 °C and -10 °C when heating and cooling the sample, proves the presence of a stable cubic phase at sub-zero temperatures. This observation is remarkable, as all other known synthetic or natural monoacylglycerols crystallize in a lamellar crystalline (L_c) phase at low temperatures. MO, the most common monoacylglycerol exhibits a L_c phase below 10 °C and coexists at any water concentration below 0 °C as a L_c and ice.[19]

A possible explanation for this phenomenon is the presence of bound water that is formed within the confined aqueous channels of this mesophase. To test this hypothesis, differential scanning calorimetry (DSC) was performed. This technique allows to resolve the first-order transitions of confined and free water, which usually differ from each other. In a reference sample of pure water, a sharp first-order peak appears at 0 °C, when heated up from -70 °C. The water in this DCPML mesophases is confined in planes (L_α) or channels (*Ia3d*, H_{II}) which change their thickness and radii, respectively, while altering the lipid/water composition. Using DSC, the changes of the freezing temperature can be monitored depending on the lipid/water composition. Remarkably, the first-order peak is completely absent in DCPML samples with 5 and 10 % w/w of water while a sharp peak appears in the sample of 20 and 25 % w/w water. When the water content is lowered, a peak broadening occurs, indicating the presence of confined water which is of a different nature. The absence of the first order peak at low hydration degrees of 5 and 10 % w/w in *Ia3d* and L_α mesophases suggests that the water is confined, which prevents it from freezing. The fact that water confined in space from 1 to 100 nm might not freeze has been reported.[20] In confined space, the orientation of water molecules is restricted, and they are prevented from forming a tetrahedral ice structure. Freezing is thus hindered, which leads to a state of super-cooled water.[20] Control experiments were carried out on commercial monolinolein (ML), the natural analogue of DCPML. A first order transition at all water/lipid compositions was observed. This phenomenon was further confirmed by temperature dependent neutron elastic and inelastic scattering on a sample with 7.5 % w/w water, in which no phase transition was observed at 0 °C. Wide angle X-ray scattering (WAXS) measurements showed that the ice is present in hexagonal structure in the samples with higher hydrations (20 and 25 % w/w of water), while there is absence of crystalline structures for the other samples. Furthermore, diffusion NMR on a DCPML sample with 10 % w/w water revealed water mobility down to -11 °C.

8.3 Conclusions

In addition to the previously reported MDS, four new cyclopropanated monoacylglycerol derivatives have been synthesized. Both steps of the synthesis of these compounds - cyclopropanation and esterification - could be optimized, and disubstituted side products **146** and **147** were isolated and characterized. The phase diagrams of MLB and DCPML have been completed. DCPML shows a highly interesting and unusual phase behavior, especially at sub-zero temperatures, where confined liquid water was found. This is an extremely important property, not only from a fundamental science perspective but also for applications in various fields such as membrane protein crystallization. Furthermore, such mesophases, in which water is liquid until -11 °C constitute unprecedented matrices to study the kinetics of chemical or biochemical reactions.

8.4 Outlook

Increasing the number of cyclopropane rings at the C_{18} carbon chain from one (MDS) to two (DCPML) led to significantly different phase behavior of the corresponding mesophases. Therefore, threefold cyclopropanate TCPMLN (**140**) was synthesized and its phase behavior will be studied. Furthermore, the cyclopropanation of arachidonic acid to obtain a fourfold cyclopropanated C_{20} lipid is planned.

8.5 Experimental Section

General Information

Natural fatty acids were purchased from Nu-Chek Prep, Inc. (MN, USA). N-(3-dimethylaminopropyl)-N′-ethylcarbodiimide hydrochloride (EDC) was purchased from TCI, and all other reagents and solvents were purchased from Sigma Aldrich. All chemicals and solvents were used as received, unless otherwise stated. Reactions were carried out under an inert atmosphere of argon in dry solvents. Dichloromethane was degassed with argon and purified by passage through activated alumina solvent column (MC Brown solvent system) prior to use. Column chromatography was performed using silica gel Merck 60 (particle size 0.040–0.063 mm). Analytical thin- layer chromatography (TLC) was performed using Merck pre-coated silica gel plates 60 F_{254}; visualization by UV absorption and/or by dipping in a solution of $KMnO_4$ (1 g), K_2CO_3 (2 g) in H_2O (100 mL) and subsequent heating. ^{1}H-NMR spectra were recorded on a Bruker AV2-500 (500MHz) spectrometer. Chemical shifts are given in parts per million (ppm) relative to the internal standard TMS (δ = 0 ppm). Coupling constants J are expressed in Hz and multiplicities are abbreviated as follows: s (singlet), br (broad), d (doublet), t (triplet), q (quadruplet), quint (quintet), m (multiplet). ^{13}C-NMR chemical shifts are reported relative to the solvent residual peaks: $CDCl_3$ = 77.00 ppm. Mass spectra were recorded by the Mass Spectroscopy Service of UZH on Finnigan MAT95 MS, BrukerLC MS and Finnigan TSQ700 MS machines.

Synthesis of 141 (8-(2-octylcyclopropyl)octanoic acid, Cp-oleic acid)[3]

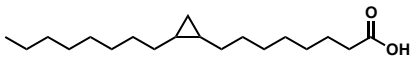

To a stirred solution of 2,4,6-trichlorophenol (8.60 g, 43.5 mmol, 4 eq) in 200 mL of dry CH_2Cl_2 at -40 °C under argon was added a 0.9 M hexane solution of diethyl zinc (49 mL, 44 mmol, 4.04 eq). The solution was stirred for 15 min at -40 °C and then diiodomethane (11.66 g, 3.50 mL, 43.5 mmol, 4 eq) was slowly added over a period of 10 min. After stirring for 15 min at the same temperature oleic acid (3.07 g, 3.46 mL, 10.88 mmol, 1 eq) was added. The reaction mixture was stirred at -40 ºC for an additional 1 h and then allowed to warm to r.t. and stirred overnight. The mixture was washed with 300 mL of 10 % HCl. The organic phase was separated and the aqueous phase was extracted with CH_2Cl_2 (3 x 150 mL). The combined organic phases were washed with a saturated solution of NaCl and dried over $MgSO_4$. The solvent was removed under reduced pressure and the residue was purified by column chromatography on silica gel, starting with CH_2Cl_2, and after elution of excess 2,4,6-trichlorophenol with CH_2Cl_2/MeOH 95:5 to get the product as colourless solid (2.11 g, 7.1 mmol, 65 %). Analytical data were identical with the values reported in literature.[3]

Synthesis of 132 (2,3-dihydroxypropyl 8-(2-octylcyclopropyl)octanoate, MDS)

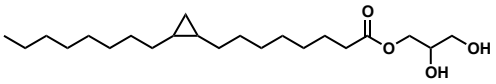

To a stirred solution of acid (660 mg, 2.23 mmol, 1 eq) in 50 mL of a mixture of dry CH_2Cl_2/DMF (3:1) was added EDC (556 mg, 2.90 mmol, 1.3 eq) followed by DMAP (27 mg, 0.223 mmol, 0.01 eq) at 0 °C under argon. The solution was stirred for 1 h at 0 °C and then was added dropwise over a period of 30 min to a solution of glycerol (1.23 g, 13.38 mmol, 6 eq) in 50 mL of dry DMF at 0 °C. The mixture was stirred for 12 h at room temperature and then washed with a saturated solution of $NaHCO_3$. The organic phase was separated and the aqueous phase was extracted with CH_2Cl_2 (3 x 100 mL). The combined organic phases were washed with brine and dried over $MgSO_4$. The solvent was removed under reduced pressure and the residue was purified by column chromatography on silica gel and eluted with a mixture of cyclohexane/ethylacetate 8:2 to 4:6. The solvent was removed to give the product (571 mg, 1.54 mmol 69 %) as a slightly yellowish oil. Analytical data were identical with the values reported in literature.[3]

Synthesis of 142 (8-(2-hexylcyclopropyl)octanoic acid, Cp-palmitoleic acid)[3]

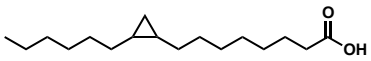

To a stirred solution of 2,4,6-trichlorophenol (8.60 g, 43.5 mmol, 4 eq) in 250 mL of dry CH_2Cl_2 at -40 °C under argon was added a 0.9 M hexane solution of diethyl zinc (49 mL, 44 mmol, 4.04 eq). The solution was stirred for 15 min at -40 °C and then diiodomethane (11.66 g, 3.50 mL, 43.5 mmol, 4 eq) was slowly added over a period of 10 min. After stirring for 15 min at the same temperature, palmitoleic acid (2.77 g, 3.10 mL 10.88 mmol, 1 eq) was added. The reaction mixture was stirred at -40 ºC for an additional 1 h and then allowed to warm to r.t. and stirred overnight. The mixture was washed with 300 mL of 10 % HCl. The organic phase was separated and the aqueous phase was extracted with CH_2Cl_2 (3 x 150 mL). The combined organic phases were washed with a saturated solution of NaCl and dried over $MgSO_4$. The solvent was removed under reduced pressure and the residue was purified by column chromatography on silica gel, starting with CH_2Cl_2, and after elution of excess 2,4,6-trichlorophenol with CH_2Cl_2/MeOH 95:5 to get the product as a slightly yellow oil (2.13 g, 7.94 mmol, 73 %). ^{1}H NMR (500 MHz, $CDCl_3$) δ 2.28 (t, *J* = 7.5 Hz, 2H), 1.57 (q, *J* = 7.5 Hz, 2H), 1.14 – 1.36 (m, 18H), 1.01 – 1.12 (m, 2H), 0.82 (t, *J* = 7.0 Hz, 3H), 0.46 – 0.62 (m, 3H), - 0.39 - -0.42 (m, 1H). ^{13}C-NMR (125 MHz, $CDCl_3$) 179.22, 33.91, 31.95, 30.18, 30.12, 29.42, 29.34, 29.28, 29.07, 28.72, 28.66, 24.70, 22.69, 15.77, 15.73, 14.11, 10.91. HRMS (ESI [M - H]$^-$) m/z: calcd for ($C_{17}H_{31}O_2$) 267.23295, found 267.23271.

Synthesis of 134 (2,3-dihydroxypropyl 8-(2-hexylcyclopropyl)octanoate, CPMP)

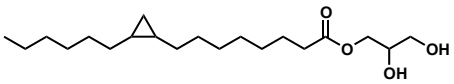

To a stirred solution of acid (600 mg, 2.23 mmol, 1 eq) in 50 mL of a mixture of dry CH_2Cl_2/DMF (3:1) was added EDC (556 mg, 2.90 mmol, 1.3 eq) followed by DMAP (27 mg, 0.223 mmol, 0.01 eq) at 0 °C under argon. The solution was stirred for 1 h at 0 °C and then was added dropwise over a period of 30 min to a solution of glycerol (1.23 g, 13.38 mmol, 6 eq) in 50 mL of dry DMF at 0 °C. The mixture was stirred for 12 h at room temperature and then washed with a saturated solution of $NaHCO_3$. The organic phase was separated and the aqueous phase was extracted with CH_2Cl_2 (3 x 100 mL). The combined organic phases were washed with brine and dried over $MgSO_4$. The solvent was removed under reduced pressure and the residue was purified by column chromatography on silica gel and eluted with a mixture of cyclohexane/ethylacetate 8:2 to 4:6. The solvent was removed to give colourless

solid product (420 mg, 1.23 mmol, 55 %). ^{1}H-NMR (500 MHz, $CDCl_3$) δ 4.86 (quint, *J* = 4.7 Hz, 1H of 2-NMH), 4.13 (dd, *J* = 11.7, 4.6 Hz, 1H), 4.08 (dd, *J* = 11.6, 6.2 Hz, 1H), 3.84 – 3.89 (m, 1H), 3.76 (t, *J* = 5.2 Hz, 4H of 2-NMH), 3.59 – 3.68 (m, 1H), 3.50 – 3.56 (m, 1H), 2.64 (br d, OH), 2.26 – 2.34 (m, 2H), 2.18 – 2.25 (m, 1 H), 1.52 – 1.60 (m, 2H), 1.14 – 1.35 (m, 18H), 1.01 – 1.12 (m, 2H), 0.82 (t, *J* = 6.8 Hz, 3H), 0.46 – 0.62 (m, 3H), -0.40 (q, *J* = 5.1 Hz, 1H). ^{13}C-NMR (125 MHz, $CDCl_3$) δ 174.34, 70.27, 65.16, 63.35, 34.15, 31.94, 30.16, 30.11, 29.42, 29.33, 29.28, 29.13, 28.71, 28.65, 24.91, 22.68, 15.76, 15.71, 14.10, 10.91. HRMS (ESI [M + Na]$^{+}$) m/z: calcd for ($C_{20}H_{38}O_4Na$) 365.26623, found 365.26647

Synthesis of 143 (10-(2-hexylcyclopropyl)decanoic acid, Cp-vaccenic acid)[3]

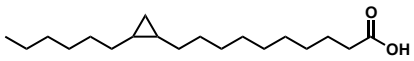

To a stirred solution of 2,4,6-trichlorophenol (8.60 g, 43.5 mmol, 4 eq) in 200 mL of dry CH_2Cl_2 at -40 °C under argon was added a 0.9 M hexane solution of diethyl zinc (49 mL, 44 mmol, 4.04 eq). The solution was stirred for 15 min at -40 °C and then diiodomethane (11.66 g, 3.50 mL, 43.5 mmol, 4 eq) was slowly added over a period of 10 min. After stirring for 15 min at the same temperature vaccenic acid (3.07 g, 3.46 mL, 10.88 mmol, 1 eq) was added. The reaction mixture was stirred at -40 °C for an additional 1 h and then allowed to warm to r.t. and stirred overnight. The mixture was washed with 300 mL of 10 % HCl. The organic phase was separated and the aqueous phase was extracted with CH_2Cl_2 (3 x 150 mL). The combined organic phases were washed with a saturated solution of NaCl and dried over $MgSO_4$. The solvent was removed under reduced pressure and the residue was purified by column chromatography on silica gel, starting with CH_2Cl_2, and after elution of excess 2,4,6-trichlorophenol with CH_2Cl_2/MeOH 95:5 to get the product as colourless solid (2.29 g, 7.72 mmol, 71 %). ^{1}H-NMR (500 MHz, $CDCl_3$) δ 2.28 (t, *J* = 7.5 Hz, 2H), 1.56 (quint, *J* = 7.4 Hz, 2H), 1.14 – 1.37 (m, 22H), 1.01 – 1.15 (m, 2H), 0.82 (t, *J* = 6.9 Hz, 3H), 0.47 – 0.61 (m, 3H), -0.40 (q, *J* = 5.1 Hz, 1H). ^{13}C-NMR (125 MHz, $CDCl_3$) δ 179.63, 33.97, 31.95, 30.19 (2C), 29.63 (2C), 29.44, 29.36, 29.25, 29.07, 28.73, 28.71, 24.69, 22.70, 15.77, 15.76, 14.12, 10.91. HRMS (ESI [M - H]$^{-}$) m/z: calcd for ($C_{19}H_{35}O_2$) 295.26425, found 295.26394.

Synthesis of 136 (2,3-dihydroxypropyl 10-(2-hexylcyclopropyl)decanoate, MLB)

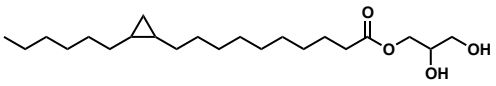

To a stirred solution of acid (660 mg, 2.23 mmol, 1 eq) in 50 mL of a mixture of dry CH_2Cl_2/DMF (3:1) was added EDC (556 mg, 2.90 mmol, 1.3 eq) followed by DMAP (27 mg, 0.223 mmol, 0.01 eq) at 0 °C under argon. The solution was stirred for 1 h at 0 °C and then was added dropwise over a period of 30 min to a solution of glycerol (1.23 g, 13.38 mmol, 6 eq) in 50 mL of dry DMF at 0 °C. The mixture was stirred for 12 h at room temperature and then washed with a saturated solution of $NaHCO_3$. The organic phase was separated and the aqueous phase was extracted with CH_2Cl_2 (3 x 100 mL). The combined organic phases were washed with brine and dried over $MgSO_4$. The solvent was removed under reduced pressure and the residue was purified by column chromatography on silica gel and eluted with a mixture of cyclohexane/ethylacetate 8:2 to 4:6. The solvent was removed to give the product (480 mg, 1.29 mmol, 58 %) as a slightly yellowish oil. ^{1}H-NMR (500 MHz, $CDCl_3$) δ 4.86 (quint, 1H of 2-MLB), 4.13 (dd, *J* = 11.7, 4.7 Hz, 1H), 4.09 (dd, *J* = 11.7, 6.1 Hz, 1H), 3.83 – 3.89 (m, 1H), 3.75 – 3.78 (m, 4H of 2-MLB), 3.62 (dd, *J* = 11.4, 4.0 Hz, 1H), 3.53 (dd, *J* = 11.5, 5.8 Hz, 1H), 2.24 – 2.35 (m, 2H), 2.04 (br s, 2H, OH), 1.52 – 1.61 (m, 2H), 1.15 – 1.37 (m, 22H), 1.01 – 1.12 (m, 2H), 0.82 (t, *J* = 7.8 Hz, 3H), 0.45 – 0.67 (m, 3H), -0.35 – -0.46 (m, 1H). ^{13}C-NMR (125 MHz, $CDCl_3$) δ 174.34, 70.26, 65.16, 63.32, 34.15, 31.94, 30.19, 30.17, 29.62 (2C), 29.45, 29.34, 29.24, 29.13, 28.71, 28.70, 24.91, 22.69, 15.76, 15.74, 14.12, 10.90. HRMS (ESI $[M + Na]^+$) m/z: calcd for ($C_{22}H_{42}O_4Na$) 393.29753, found 393.29757.

Synthesis of 144 (8-(2-((2-pentylcyclopropyl)methyl)cyclopropyl)octanoic) acid, 2-Cp-linoleic acid)[3]

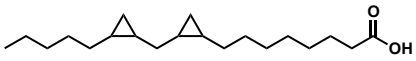

To a stirred solution of 2,4,6-trichlorophenol (8.60 g, 43.5 mmol, 4 eq) in 200 mL of dry CH_2Cl_2 at -40 °C under argon was added a 0.9 M hexane solution of diethyl zinc (49 mL, 44 mmol, 4.04 eq). The solution was stirred for 15 min at -40 °C and then diiodomethane (11.66 g, 3.50 mL, 43.5 mmol, 4 eq) was slowly added over a period of 10 min. After stirring for 15 min at the same temperature linoleic acid (1.53 g, 1.70 mL, 5.44 mmol, 0.5 eq) was added. The reaction mixture was stirred at -40 ºC for an additional 1 h and then allowed to warm to r.t. and stirred overnight. The mixture was washed with 300 mL of 10 % HCl. The organic phase was separated and the aqueous phase was extracted with CH_2Cl_2 (3 x 150 mL). The combined organic phases were washed with a saturated solution of NaCl and dried over $MgSO_4$. The solvent was removed under reduced pressure and the residue was purified by column chromatography on silica gel eluted, starting with CH_2Cl_2, and after elution of excess 2,4,6-trichlorophenol with CH_2Cl_2/MeOH 95:5 to get the product as a slightly yellow oil as a mixture of diastereoisomers (1.16 g, 3.75 mmol, 69 %). ^{1}H-NMR (500 MHz, $CDCl_3$) δ 2.28 (t, *J* = 7.5 Hz, 1H), 1.51 – 1.62 (m, 2H), 1.17 – 1.46 (m, 17H), 0.91 – 1.15 (m, 3H), 0.82 (t, *J* = 6.8 Hz, 3H), 0.67 – 0.75 (m, 2H), 0.51 – 0.66 (m, 4H), -0.30 – -0.40 (m, 2H). ^{13}C-NMR (125 MHz, $CDCl_3$) δ 179.90, 34.06, 31.90, 30.13, 29.89, 29.42, 29.30, 29.08, 28.88, 28.87, 28.72, 28.70, 28.02, 27.87, 24.70, 22.72, 16.05, 15.93, 15.91, 15.88, 15.66, 15.61, 14.12, 11.02, 10.84. HRMS (ESI [M - H]$^-$) m/z: calcd for ($C_{20}H_{35}O_2$) 307.26425, found 307.26407.

Synthesis of 138 (2,3-dihydroxypropyl 8-(2-((2-pentylcyclopropyl)methyl)cyclopropyl)octanoate, DCPML)

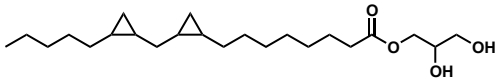

To a stirred solution of acid (688 mg, 2.23 mmol, 1 eq) in 50 mL of a mixture of dry CH_2Cl_2/DMF (3:1) was added EDC (556 mg, 2.90 mmol, 1.3 eq.) followed by DMAP (27 mg, 0.223 mmol, 0.01 eq) at 0 °C under argon. The solution was stirred for 1 h at 0 °C and then was added dropwise over a period of 30 min to a solution of glycerol (1.23 g, 13.38 mmol, 6 eq) in 50 mL of dry DMF at 0 °C. The mixture was stirred for 12 h at room temperature and then washed with a saturated solution of $NaHCO_3$. The organic phase was separated and the

aqueous phase was extracted with CH_2Cl_2 (3 x 100 mL). The combined organic phases were washed with brine and dried over $MgSO_4$. The solvent was removed under reduced pressure and the residue was purified by column chromatography on silica gel and eluted with a mixture of cyclohexane/ethylacetate 8:2 to 4:6. The solvent was removed to give the product (605 mg, 1.58 mmol, 71 %) as a slightly yellowish oil. ^{1}H NMR (400 MHz, $CDCl_3$) δ 4.86 (quint, *J* = 4.8 Hz, 1H of 2-subst), 4.13 (dd, *J* = 11.7, 4.7 Hz, 1H), 4.09 (dd, *J* = 11.6, 6.1 Hz, 1H), 3.83 – 3.90 (m, 1H), 3.75 – 3.78 (m, 4H of 2-subst), 3.62 (dd, *J* = 11.5, 4.0 Hz, 1H), 3.54 (dd, *J* = 11.5, 5.8 Hz, 1H), 2.25 – 2.34 (m, 2H), 2.18 (br s, 2H, OH), 1.52 – 1.61 (m, 2H), 1.17 – 1.47 (m, 17H), 0.91 – 1.13 (m, 3H), 0.82 (t, *J* = 7.0 Hz, 3H), 0.68 – 0.77 (m, 2H), 0.51 – 0.65 (m. 4H) -0.29 – -0.39 (m, 2H). ^{13}C-NMR (125 MHz, $CDCl_3$) δ 174.34, 70.25, 65.13, 63.32, 34.14, 31.88, 30.11, 29.87, 29.41, 29.28, 29.12, 28.86, 28.84, 28.69, 28.68, 28.01, 27.85, 24.90, 22.70, 16.03, 15.91, 15.91, 15.89, 15.85, 15.64, 15.58, 14.10, 11.01, 10.82. HRMS (ESI $[M + Na]^+$) m/z: calcd for ($C_{23}H_{42}O_4Na$) 405.29753, found 405.29715.

Synthesis of 146 (2-hydroxypropane-1,3-diyl bis(8-(2-((2-pentylcyclopropyl)methyl)cyclopropyl)octanoate), DCPDL)

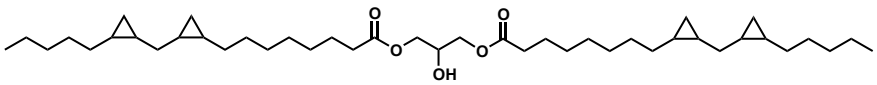

Isolated as a side product of **138**.

^{1}H NMR (500 MHz, Chloroform-*d*) δ 4.19 – 3.93 (m, 5H), 2.28 (t, *J* = 7.6 Hz, 4H), 1.60 – 1.52 (m, 4H), 1.46 – 1.38 (m, 1H), 1.37 – 1.16 (m, 32H), 1.13 – 1.01 (m, 4H), 0.96 (dt, *J* = 14.3, 7.9 Hz, 1H), 0.82 (t, *J* = 6.8 Hz, 6H), 0.76 – 0.67 (m, 4H), 0.66 – 0.57 (m, 4H), 0.56 – 0.51 (m, 4H), -0.31 – -0.38 (m, 4H). ^{13}C NMR (126 MHz, Chloroform-*d*) δ 173.89 (2C), 68.42, 65.04 (2C), 34.10 (2C), 31.89 (2C), 30.13 (2C), 29.89 (2C), 29.43 (2C), 29.30 (2C), 29.14 (2C), 28.87 (2C), 28.70 (2C), 28.03 (2C), 27.87 (2C), 16.05 (2C), 15.91 (2C), 15.87 (2C), 15.66 (2C), 15.60 (2C), 14.12 (2C), 11.02 (2C), 10.84 (2C). HRMS (ESI $[M + H]^+$) m/z: calcd for ($C_{43}H_{77}O_5$) 673.57655, found 673.57643.

Synthesis of 145 (8-(2-((2-((2-ethylcyclopropyl)methyl)cyclopropyl)methyl)cyclopropyl)octanoic acid, (3-Cp-linolenic acid)[3]

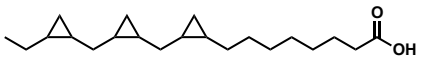

To a stirred solution of 2,4,6-trichlorophenol (8.60 g, 43.5 mmol, 4 eq) in 200 mL of dry CH_2Cl_2 at -40 °C under argon was added a 0.9 M hexane solution of diethyl zinc (49 mL, 44 mmol, 4.04 eq). The solution was stirred for 15 min at -40 °C and then diiodomethane (11.66 g, 3.50 mL, 43.5 mmol, 4 eq) was slowly added over a period of 10 min. After stirring for 15 min at the same temperature α-linolenic acid (1.01 g, 1.10 mL, 3.63 mmol) was added. The reaction mixture was stirred at -40 ºC for an additional 1 h and then allowed to warm to r.t. and stirred overnight. The mixture was washed with 300 mL of 10 % HCl. The organic phase was separated and the aqueous phase was extracted with CH_2Cl_2 (3 x 150 mL). The combined organic phases were washed with a saturated solution of NaCl and dried over $MgSO_4$. The solvent was removed under reduced pressure and the residue was purified by column chromatography on silica gel, starting with CH_2Cl_2, and after elution of excess 2,4,6-trichlorophenol with CH_2Cl_2/MeOH 95:5 to get the product as a mixture of diastereoisomers as a slightly yellow oil (0.71 g, 2.21 mmol, 61 %). ^{1}H NMR (500 MHz, Chloroform-*d*) δ 2.27 (t, *J* = 7.5 Hz, 2H), 1.56 (p, *J* = 7.4 Hz, 2H), 1.50 – 1.40 (m, 1H), 1.39 – 1.02 (m, 15H), 1.02 – 0.95 (m, 1H), 0.92 (td, *J* = 7.2, 2.1 Hz, 3H), 0.83 – 0.66 (m, 4H), 0.65 – 0.50 (m, 4H), -0.24 – 0.39 (m, 3H). ^{13}C NMR (126 MHz, Chloroform-*d*) δ 180.61, 34.12, 30.11, 29.40, 29.27, 29.06, 28.85, 28.69, 28.21, 28.11, 28.05, 27.97, 27.95, 27.90, 27.79, 24.65, 22.12, 21.96, 17.85, 17.57, 16.25, 16.17, 16.09, 16.05, 15.92, 15.88, 15.82, 15.62, 14.46, 11.11, 11.02, 10.91, 10.84, 10.76, 10.72, 10.60. HRMS (ESI [M - H]$^-$) m/z: calcd for ($C_{21}H_{35}O_2$) 319.26425, found 319.26403.

Synthesis of 140 (2,3-dihydroxypropyl 8-(2-((2-((2-ethylcyclopropyl)methyl)cyclopropyl)methyl)cyclopropyl)octanoate, TCPMLN)

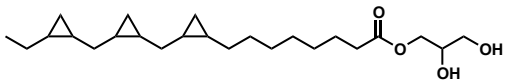

To a stirred solution of acid (688 mg, 2.23 mmol, 1 eq) in 50 mL of a mixture of dry CH_2Cl_2/DMF (3:1) was added EDC (556 mg, 2.90 mmol, 1.3 eq) followed by DMAP (27 mg, 0.223 mmol, 0.01 eq) at 0 °C under argon. The solution was stirred for 1 h at 0 °C and then was added dropwise over a period of 30 min to a solution of glycerol (1.23 g, 13.38 mmol, 6 eq) in 50 mL of dry DMF at 0 °C. The mixture was stirred for 12 h at room temperature and then washed with a saturated solution of $NaHCO_3$. The organic phase was separated and the aqueous phase was extracted with CH_2Cl_2 (3 x 100 mL). The combined organic phases were washed with brine and dried over $MgSO_4$. The solvent was removed under reduced pressure and the residue was purified by column chromatography on silica gel and eluted with a mixture of cyclohexane/ethylacetate 8:2 to 4:6. The solvent was removed to give the product as a mixture of diastereoisomers (687 mg, 1.74 mmol, 78 %) as a slightly yellowish oil. ^{1}H NMR (500 MHz, Chloroform-*d*) δ 4.14 (dd, *J* = 11.7, 4.6 Hz, 1H), 4.08 (dd, *J* = 11.7, 6.2 Hz, 2H), 3.87 (s, 1H), 3.80 – 3.75 (m, 1H), 3.67 – 3.60 (m, 1H), 3.65 – 3.60 (m, 1H), 2.32 – 2.26 (m, 2H), 1.61 – 0.95 (m, 18H), 0.92 (td, *J* = 7.4, 2.1 Hz, 3H), 0.82 – 0.69 (m, 4H), 0.67 – 0.49 (m, 4H), -0.15 – -0.29 (m, 3H). ^{13}C NMR (126 MHz, Chloroform-*d*) δ 174.34, 70.27, 65.17, 63.32, 34.15, 30.12, 29.42, 29.28, 29.13, 28.85, 28.69, 28.22, 28.11, 28.09, 28.06, 27.97, 27.95, 27.91, 27.79, 24.91, 22.04, 17.86, 17.58, 16.26, 16.18, 16.10, 16.05, 15.92, 15.88, 15.84, 15.80, 15.62, 14.50, 11.12, 11.02, 10.92, 10.85, 10.77, 10.73, 10.61. HRMS (ESI [M + Na]$^+$) m/z: calcd for ($C_{24}H_{42}O_4Na$) 417.29753, found 417.29748.

Synthesis of 147 (2-hydroxypropane-1,3-diyl bis(8-(2-((2-((2-ethylcyclopropyl)methyl)cyclopropyl)methyl)cyclopropyl)octanoate)) (TCDPLN)

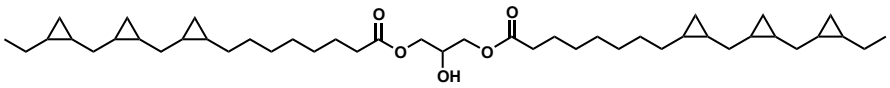

Isolated as a side product of **140**.

^{1}H NMR (500 MHz, Chloroform-*d*) δ 5.01 (p, *J* = 5.0 Hz, 1H, 2-subst.), 4.25 (dd, *J* = 11.9, 4.5 Hz, 1H, 2-subst), 4.20 – 3.97 (m, 4H), 3.71 – 3.62 (m, 1H), 2.27 (dt, *J* = 12.0, 7.6 Hz, 4H), 1.55 (q, *J* = 7.0 Hz, 4H), 1.50 – 1.40 (m, 2H), 1.39 – 0.95 (m, 32H), 0.92 (td, *J* = 7.3, 2.2 Hz, 6H), 0.82 – 0.67 (m, 8H), 0.66 – 0.49 (m, 8H), -0.24 – -0.38 (m, 6H). ^{13}C NMR (126 MHz, Chloroform-*d*) δ 173.88, 173.75, 173.39, 72.08, 68.33, 65.01, 61.99, 61.49, 34.26, 34.08, 30.11 (2C), 29.42 (2C), 29.28 (2C), 29.10 (2C), 28.84, 28.67, 28.20, 28.07, 28.04, 27.93, 27.89, 27.77, 24.86 (2C), 22.11, 21.94, 17.84, 17.56, 16.24 (2C), 16.17, 16.15, 16.08 (2C), 16.05, 16.03, 15.94, 15.90 (2C), 15.86 (2C), 15.82, 15.78, 15.61 (2C), 14.47 (2C), 11.10, 11.01 (2C), 10.90, 10.83, 10.75, 10.71, 10.59. HRMS (ESI $[M + NH_4]^+$) m/z: calcd for ($C_{45}H_{80}O_5N$) 714.60310, found 714.60311.

Bibliography

(1) Landau, E. M.; Rosenbusch, J. P. Lipidic Cubic Phases : A Novel Concept for the Crystallization of Membrane Proteins. *Proc. Natl. Acad. Sci.* **1996**, *93*, 14532–14535.

(2) Cherezov, V. (2018, April 10), *The Cherezov Lab*, Retrieved from http://cherezov.usc.edu.

(3) Salvati Manni, L.; Zabara, A.; Osornio, Y. M.; Schöppe, J.; Batyuk, A.; Plückthun, A.; Siegel, J. S.; Mezzenga, R.; Landau, E. M. Phase Behavior of a Designed Cyclopropyl Analogue of Monoolein: Implications for Low-Temperature Membrane Protein Crystallization. *Angew. Chem. Int. Ed. Engl.* **2014**, 1–6.

(4) Fong, C.; Le, T.; Drummond, C. J. Lyotropic Liquid Crystal Engineering-Ordered Nanostructured Small Molecule Amphiphile Self-Assembly Materials by Design. *Chem. Soc. Rev.* **2012**, *41*, 1297–1322.

(5) Kulkarni, C. V.; Tang, T.-Y.; Seddon, A. M.; Seddon, J. M.; Ces, O.; Templer, R. H. Engineering Bicontinuous Cubic Structures at the Nanoscale—the Role of Chain Splay. *Soft Matter* **2010**, *6*, 3191.

(6) Rao, V.; Fujiwara, N.; Porcelli, S. A.; Glickman, M. S. Mycobacterium Tuberculosis Controls Host Innate Immune Activation through Cyclopropane Modification of a Glycolipid Effector Molecule. **2005**, *201*, 535–543.

(7) Chang, Y.; Cronan, J. E. Membrane Cyclopropane Fatty Acid Content Is a Major Factor in Acid Resistance of Escherichia Coli. **1999**, *33*, 249–259.

(8) Charette, A.; Francour, S.; Martel, J.; Wilb, N. New Family of Cyclopropanating Reagents : Synthesis , Reactivity, and Stability Studies of Iodomethylzinc Phenoxides. *Angew. Chemie Int. Ed.* **2000**, *466*, 4539–4542.

(9) Fu, Y.; Weng, Y.; Hong, W. X.; Zhang, Q. Efficient Synthesis of Unsaturated 1-Monoacyl Glycerols for in Meso Crystallization of Membrane Proteins. *Synlett* **2011**, No. 6, 809–812.

(10) Salvati Manni, L. Unpublished Results. **2018**, ETH Zurich.

(11) Perly, B.; Smith, I. C. P.; Jarrell, H. C. Acyl Chain Dynamics of Phosphatidylethanolamines Containing Oleic Acid and Dihydrosterculic Acid: 2H NMR Relaxation Studies. *Biochemistry* **1985**, *24*, 4659–4665.

(12) Dufourc, E. J.; Smith, P.; Jarrell, H. A 2H-NMR Analysis of Dihydrosterculoyl - Containing Lipids in Model Membranes: Structural Effects of a Cyclopropane Ring. *Chem. Phys. Lipids* **1983**, *33*, 153–177.

(13) Li, S. J.; Yamashita, Y.; Yamazaki, M. Effect of Electrostatic Interactions on Phase Stability of Cubic Phases of Membranes of Monoolein/dioleoylphosphatidic Acid Mixtures. *Biophys. J.* **2001**, *81*, 983–993.

(14) Nakano, M.; Teshigawara, T.; Sugita, A.; Leesajakul, W.; Taniguchi, A.; Kamo, T.; Matsuoka, H.; Handa, T. Dispersions of Liquid Crystalline Phases of the Monoolein/oleic Acid/pluronic F127 System. *Langmuir* **2002**, *18*, 9283–9288.

(15) Engström, S.; Wadsten-Hindrichsen, P.; Hernius, B. Cubic, Sponge, and Lamellar Phases in the Glyceryl Monooleyl Ether-Propylene Glycol-Water System. *Langmuir* **2007**, *23*, 10020–10025.

(16) Zabara, A.; Negrini, R.; Baumann, P.; Onaca-Fischer, O.; Mezzenga, R. Reconstitution of OmpF Membrane Protein on Bended Lipid Bilayers: Perforated Hexagonal Mesophases. *Chem. Commun.* **2014**, *50*, 2642–2645.

(17) Phan, S.; Fong, W. K.; Kirby, N.; Hanley, T.; Boyd, B. J. Evaluating the Link between Self-Assembled Mesophase Structure and Drug Release. *Int. J. Pharm.* **2011**, *421*, 176–182.

(18) Nguyen, T. H.; Hanley, T.; Porter, C. J. H.; Boyd, B. J. Nanostructured Reverse Hexagonal Liquid Crystals Sustain Plasma Concentrations for a Poorly Water-Soluble Drug after Oral Administration. *Drug Deliv. Transl. Res.* **2011**, *1*, 429–438.

(19) Qiu, H.; Caffrey, M. The Phase Diagram of the Monoolein/water System: Metastability and Equilibrium Aspects. *Biomaterials* **2000**, *21*, 223–234.

(20) Bergman, R.; Swenson, J. Dynamics of Supercooled Water in Confined Geometry. *Nature* **2000**, *403*, 283–

286.

Chapter 9

Endoperoxide doped cubosomes for intracellular oxygen delivery

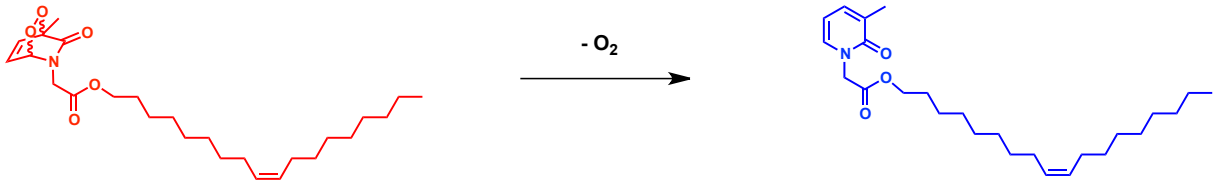

9.1 Introduction

9.1.1 Tissue engineering

Tissue engineering is an important medical field in which significant progress was made in the last three decades.[1] The replacement or regeneration of damaged tissue using artificially grown grafts is a powerful approach. The method is based on the isolation of donor cells, often from the patient, which then are proliferated *in vitro*. These cells are then seeded on a matrix to form a graft, which subsequently is implanted into the patient. A bottleneck in current cell-based transplantation therapies is the poor donor cell survival.[2,3] The implanted tissue is not connected to the blood vessel system of the patient's body, leading to oxygen and nutrition deficiencies. Since vascularization, *i.e.* the development of new blood vessels is a slow process, the cells often suffer from necrosis,[4] caused by insufficient oxygen supply.[5,6] Several studies on different tissues have revealed that most cells die within the first 24 h after transplantation.[7,8] Some studies show that 70-80 % of injected cells die within three days; 93 % of skeletal myoblasts were lost after 2 days.[9] Pathological processes or local immune and inflammatory responses causes early donor cell death.[10] Several approaches have been reported to address the problem of insufficient oxygen supply by delivering oxygen artificially to the cells. For example, the biodegradable polymer poly(lactic-co-glycolic acid) (PLGA) was loaded with sodium percarbonate. The application of the sodium percarbonate system led to a decrease of necrosis and enhanced cell viability for several days.[11] A hydrogen peroxide/catalase system as oxygen source has been introduced as well.[12] Pedreza *et al*. developed a system that generates oxygen from calcium peroxide encapsulated in polydimethylsiloxane.[13] However, these methods suffer from drawbacks such as generation of cytotoxic reactive oxygen species (ROS) and uncontrolled oxygen release.[14,15] Benz *et al*. treated fibroblasts and rat smooth muscle cells (SMCs) under hypoxic conditions with pyridone endoperoxides and could show that cell survival was improved.[16] These water-soluble methylated pyridone-derived endoperoxides undergo a *retro-Diels-Alder* reaction when exposed to aqueous environment, thereby releasing oxygen. Lipid-based cubosomes have attracted considerable attention in the field of nanomedicine as tunable drug-nanocarriers. The nanoparticles protect their cargo from digestion by enzymes, thereby improving their bioavailability, and can enter cells very efficiently.[17] Combining this elegant approach of producing oxygen via *retro-Diels-Alder* reaction of pyridone endoperoxides, with its efficient delivery into cells using cubosome nanoparticles, results in a novel and promising concept addressing the issue of oxygen deficiency in freshly transplanted cells, which is introduced herein.

9.1.2 Drug delivery and cubosomes

An ideal drug delivery system should be biodegradable, biocompatible and should be able to incorporate a variety of different cargo molecules, may they be proteins, nucleic acids or small molecules that are positively charged, negatively charged or neutral. It should deliver the incorporated active agents without loss of activity to the specific location *in vivo* in an efficient and controlled manner. Lipidic mesophases, specifically lipidic cubic phases (LCPs) constitute an attractive delivery system that can be triggered by external stimuli.[18]

To exploit the large potential of nano-medicinal techniques, the development and investigation of state-of-the-art drug delivery nanoparticles is required. These nanoparticles need to be tunable for distinct applications and need to consist of non-toxic and biocompatible compounds.[19] Whereas polymers and liposomes are well established drug delivery systems, the application of cubosomes is still at its infancy. Cubosomes, introduced in Chapter 1 of this thesis in more detail, are dispersions of LCPs which are formed by ultra sonication of the bulk parent phase. Undesirable biological responses such as opsonization of the colloidal lipidic cubic phases and subsequent clearance are reduced due to the polyethylene glycol layer around the particles, the so-called stealth corona. The resulting increase of the biological half-life depends on both the thickness and density of the stealth corona which mask the cubosomes.[20]

Innovation in the field of nanomedicine can be achieved by developing drug delivery systems which are rationally designed, with features like side-effect reduction, targeting, continuous drug release and imaging tools.[20] The application of a self-assembly approach to generate these drug-delivery vehicles allows to combine the required elements from toolboxes, for example fluorescently labelled lipids, to create tailored nanoparticles for specific applications.[20]

Whereas progress in the field of bioactive cubosomes and their *in-vitro* applications is quite advanced, transfer to clinics is still at an early stage.[21] Thus, the huge potential of cubosomes has not yet been fully exploited. Their application as multifunctional delivery vehicles for hydrophobic, hydrophilic, and amphiphilic drugs or imaging agents, as well as their tunable drug release properties and potential surface functionalization for targeted drug delivery provide great promise for their clinical applications.[21]

9.1.3 Pyridone endoperoxides

The fact that 2-pyridones can reversibly bind singlet oxygen[22,23] is the underlying principle of our oxygen supply strategy to engineered tissue.[14,16] Pyridone endoperoxides are obtained upon [4+2] cycloaddition of $^1O_2$ acting as dienophile and the 2-pyridone derivative as diene (Scheme 1). This type II photooxigenation requires the more reactive singlet oxygen for the *Diels-Alder* reaction to occur. A photosensitizer (ps) is excited by photons to the excited state (ps^*). Upon energy transfer from the excited photosensitizer to triplet oxygen ($^3O_2$), singlet oxygen ($^1O_2$) is formed, which undergoes [4+2] cycloaddition with the 2-pyridone derivative to form the corresponding pyridone endoperoxide.[24]

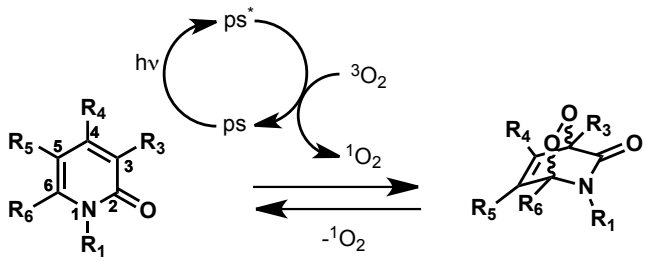

Scheme 1: General mechanism of type II photooxygenation using the example of a 2-pyridone derivative resulting in a 2-pyridone endoperoxide. Abbreviations: photosensitizer in the ground state (ps) and in the excited state (ps^*), photons (hν).

This [4+2] cycloaddition is a reversible process. Pyridone endoperoxides can therefore release singlet oxygen via *retro-Diels-Alder* reaction when in contact with water. However, singlet oxygen is cytotoxic and cannot be delivered to cells in this form. The use of vitamin C, among others, is a known method to physically quench singlet oxygen to obtain triplet oxygen[25] and was thus previously used to quench singlet oxygen released from pyridone endoperoxides.[16]

9.2 Results and discussion

Benz *et al*. showed that the stability and thus the $^1O_2$-release of such pyridone endoperoxides is tunable by varying the substitution pattern of the pyridone core, especially at position 1 and 3 (Scheme 1), leading to half-lives ($t_{1/2}$) on different time scales. Since vascularization of transplanted tissue is a lengthy process, taking up to weeks, artificial oxygen supply should ideally proceed on a similar time scale.[5,16] The development of compounds with very long half-lives remains a challenge, and the best available pyridone-based candidate shows a half-life of 8.5 h at 37 °C in water.[16]

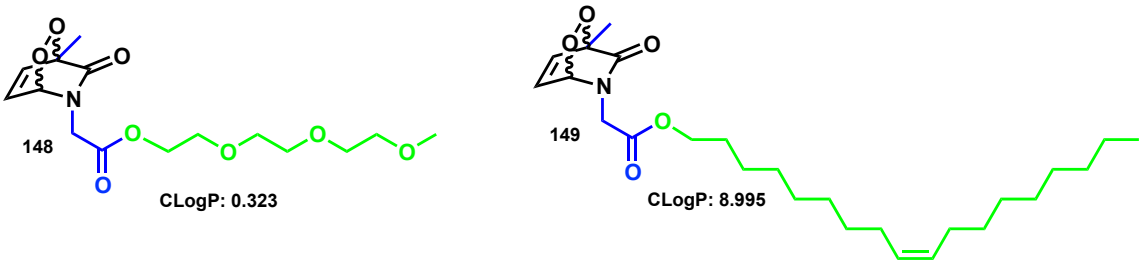

Figure 1: Structures of water-soluble pyridone endoperoxide **148** used by Benz *et al*.[16] (left), and lipidic pyridone endoperoxide **149** that allows incorporation into MO-cubosomes upon self-assembly (right). The relevant substitutions at positions 1 and 3 for the stability (in blue) were not altered, whereas the triethyleneglycol residue in the water-soluble molecule was replaced by an oleyl chain (in green), leading to significant increase of the CLogP value.

9.2.1 Synthesis of lipidic pyridone endoperoxides

The beneficial effects on survival of anoxic 3T3 fibroblasts and rat SMCs achieved by Benz *et al.* using water-soluble pyridone endoperoxides[16] might even be more efficient if the oxygen bearing precursors were delivered into the cells using cubosomes as nanocarriers. To this end, pyridone endoperoxides were lipidated to enable their incorporation via self-assembly into lipid-based cubosomes. Two lipidic pyridone endoperoxides bearing a saturated and an unsaturated lipidic chain were synthesized (Scheme 2), with the aim of optimal incorporation of these additives into cubosomes that are based on the saturated lipid PT, and on the unsaturated lipid MO, thereby enabling the use of both phytantriol (PT)- and MO-based cubosomes. In a first step, 2-bromoacetate (**150**) was coupled to dodecanol or oleyl alcohol, respectively, at -78 °C to obtain the required linker **151** and **152** bearing the corresponding lipidic tails. The synthesis was performed according to the procedure of Morrissey *et al*.[26] Alkylation of pyridones can occur at the nitrogen or the oxygen atom, depending on the conditions. Selective *N*-alkylation of commercially available 2-

methylpyridone was achieved using K_2CO_3 as a base in DMF and yielded the lipidated pyridone dienes **154** and **155**. [27] *O*-alkylation was not observed. Lipidated pyridone dienes **154** and **155** were subsequently photooxigenized using compressed air in the presence of *meso*-tetraphenylporphyrin as photosensitizer in CH_2Cl_2 and under irradiation with an LED at 627 nm.[22] Lipidic pyridone endoperoxides **156** and **157** were obtained in good yields in three synthetic steps each.

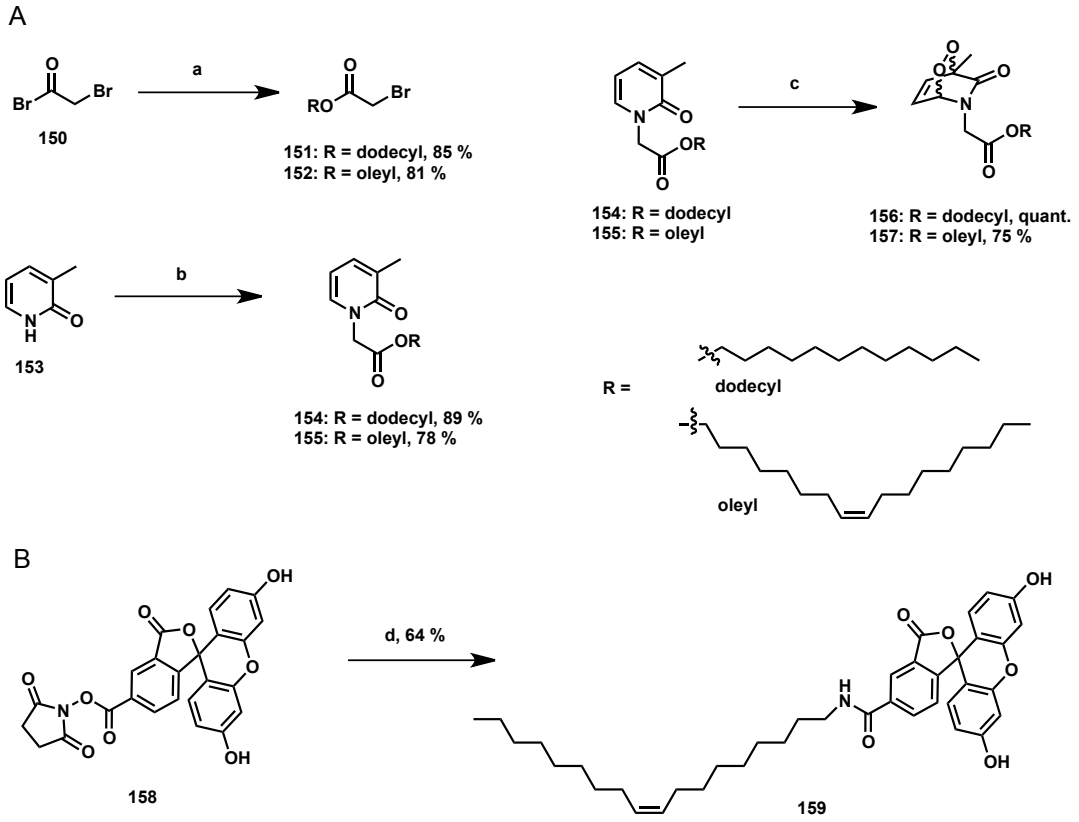

Scheme 2: A) Syntheses of the two lipidic pyridone endoperoxides. The saturated derivative was designed to be incorporated into PT-based cubosomes, the unsaturated derivative for MO-based cubosomes. B) Synthesis of a fluorescently labelled lipid from commercially available NHS-fluorescein and oleylamine. Conditions: a) Dodecanol or oleyl alcohol in CH_2Cl_2, -78 °C. b) **151** or **152**, K_2CO_3, DMF, -78 °C. c) compressed air, cat. *meso*-tetraphenylporphyrin, CH_2Cl_2, hν (LED, 627 nm), 0 °C. d) Oleylamine, 1.5 eq., NEt_3, 1.5 eq, DMF, r.t.

Several studies on the uptake mechanism and the intracellular fate of the nanoparticles have been published.[28–32] The results are, however restricted to the system under investigation.[33] In order to allow *in vitro* tracking of the cubosomes and to gain knowledge about the uptake mechanism and the intracellular fate of the nanoparticles in our study, a fluorescently labelled lipid was synthesized which can be incorporated as an additive into the cubosomes. Commercially available NHS-fluorescein **158**, was coupled to oleylamine to obtain fluorescently labelled lipid **159** in one step (Scheme 2 B).

9.2.2 Cubosome preparation, characterization and O_2-release kinetics

Cubosomes were prepared by evaporating dichloromethane from a solution with the corresponding lipid and additive in the required ratio. The lipidic was subsequently hydrated and ultrasonicated. The particle size and the polydispersion index (PDI) of the cubosomes were determined by DLS. Monoolein-based cubosomes were found to be 238 ± 4 nm with a PDI of 0.33, whereas phytantriol-based cubosomes were 218 ± 3 with a PDI of 0.21.

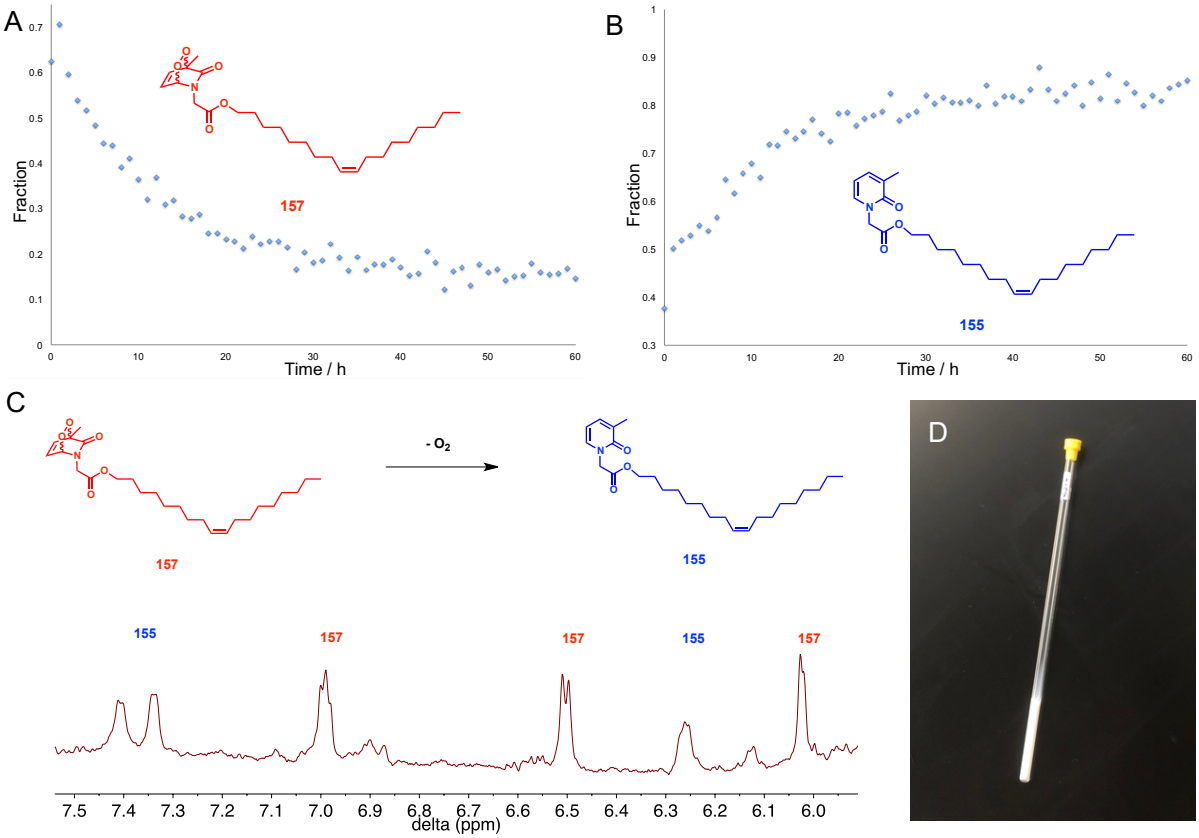

Figure 2: Kinetic measurements of O_2-release from cubosomes: A) Decay of lipidic pyridone endoperoxide **157** upon release of O_2 over time. B) Evolution of the retro-Diels-Alder product **2** over time. C) Relevant section of the ^{1}H-NMR spectrum of a cubosome dispersion during the reaction. D) NMR tube with O_2-releasing cubosome dispersion.

Following their preparation, the cubosomes were added to a NMR tube (Figure 2D) and their O_2-release was monitored directly by ^{1}H-NMR to prove the function of the system and to determine the half-lives of the O_2-releasing compound, which was found to be ca. 7 h, whereas the O_2-release is completed after ca. 30 h. Decay of the lipidic pyridone endoperoxide **157** and generation of the retro-Diels-Alder product **155** was plotted versus time (Figure 2 A and B) by integration of the corresponding signals in the NMR spectra (an example: Figure 2, C) at 37°C. One of the challenges with such compound is the fact that oxygen release is induced once the pyridone endoperoxides are in contact with water.

Hence, the cubosome preparation step needs to be done as fast as possible. However, some oxygen release will take place before the cubosomes can be used for kinetic measurements or actual applications. This can be seen in Figure 2A, 37 % of **157** underwent already *retro-Diels-Alder* reaction at the time the measurement was started. By accelerating the cubosome preparation process and reducing the sonication power, this loss might be reduced.

9.2.3 In vitro toxicity assessment and development of working concentration

Previous experiments by Prange, Aleandri *et al*.[17] served as orientation for the preparation of safe and non-toxic cubosome concentrations for *in vitro* studies. Therefore, we started with similar concentrations (0.1-0.2 mg/mL) to those used in these previous experiments. Surprisingly, it was found that empty MO- and PT-based cubosomes prepared in growth medium of the cells negatively influence the cell proliferation (Figure 4A left panel). However, when prepared in PBS and diluted in cell growth medium just before use for incubation, cell proliferation does not seem to be affected (Figure 3A right panel). Additionally, optimal vitamin C concentrations had to be found (Figure 3B/C). Vitamin C is required as a quencher of singlet oxygen ($^1O_2$) which is formed during the *retro-Diels-Alder* reaction, thereby obtaining non-cytotoxic triplet oxygen ($^3O_2$). It was also observed that higher vitamin C concentrations (Figure 3B) did not lead to better cell viability.

To find an optimal ratio between vitamin C and cubosomes, vitamin C concentrations of 25, 50 and 75 µg/mL were tested on 0.05, 0.1 and 0.2 mg/mL cubosomes (Figures 3C). The most stable cell proliferation was reached with either 25 or 50 µg/mL vitamin C for all tested cubosome concentrations. Hence, the working concentration for the *in vitro* tests was set to be 50 µg/mL vitamin C with 0.1 mg/mL cubosomes.

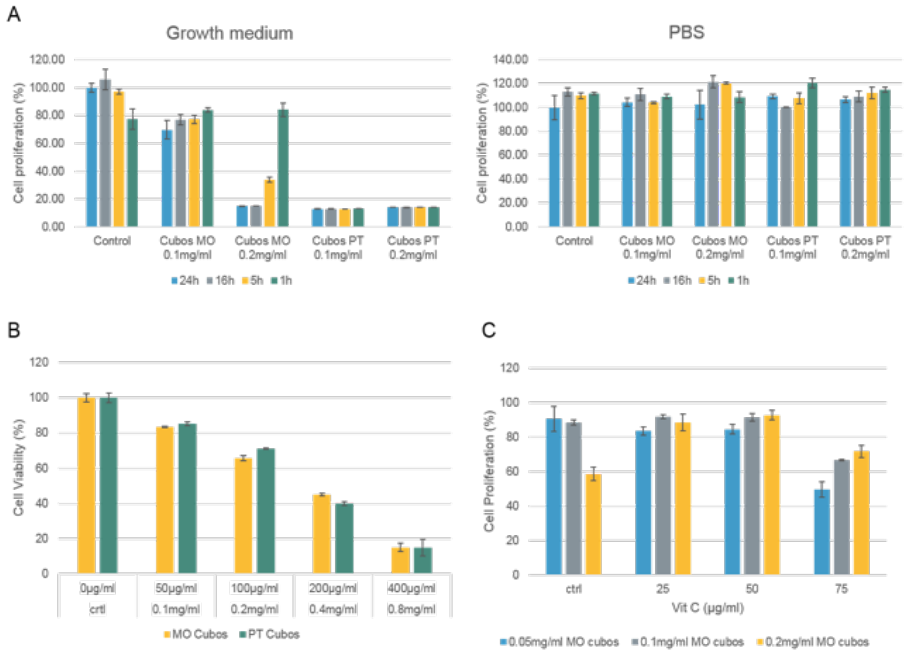

Figure 3: Toxicity determination of empty cubosomes (A), endoperoxide-loaded cubosomes (B), and vitamin C concentrations for non-toxic cubosome concentrations (C): MPCs were seeded 4 h prior to cubosomes treatment. Cubosomes were incubated on the cells for indicated times (A) or 24 h (B/C) and a routine cell proliferation assay (WST) was performed thereafter. (A) Preparation of empty cubosomes in PBS seems to affect cell proliferation less, independent of their lipidic basis, than preparation directly in growth medium. (B) Endoperoxide-loaded cubosomes need to be co-incubated with vitamin C as oxygen radical scavenger. Higher cubosome concentration leads to increased cell death despite parallel vitamin C increase. (C) Non-toxic concentrations of endoperoxide-loaded cubosomes could not be further expanded using different vitamin C concentrations.

9.2.4 The effect of endoperoxide-loaded cubosomes under hypoxic conditions *in vitro*

Preliminary test runs were performed with the muscle precursor cells (MPCs) under normal and reduced oxygen conditions. Following the observation with basic culture that hypoxic conditions affect the proliferation of the MPCs, cubosome samples were added under hypoxic and normoxic conditions to compare their potential effect on the Hypoxia-inducible factor-1a (Hif1a) protein expression. Hif1a is induced under hypoxia and is a key transcription factor which is regulated by a proline hydroxylase.[34] Proline hydroxylase requires 2-oxoglutarate, iron and oxygen for its activity, and it modifies Hif1a post-translationally by hydroxylation.[35] The post-translationally modified Hif1a interacts with the Von Hippel-Lindau protein which then leads to degradation of Hif1a.[34] However, this post-

translational modification does not occur under hypoxic conditions, which leads to accumulation of Hif1a. [34]

As can be seen in Figure 6C, Hif1a expression was reduced after cubosome treatment compared to its expression under untreated hypoxic conditions. Normoxia conditions did not show any Hif1a expression. These first results support our hypothesis that cubosomes loaded with endoperoxide could influence cellular reactivity to hypoxia by delivering oxygen.

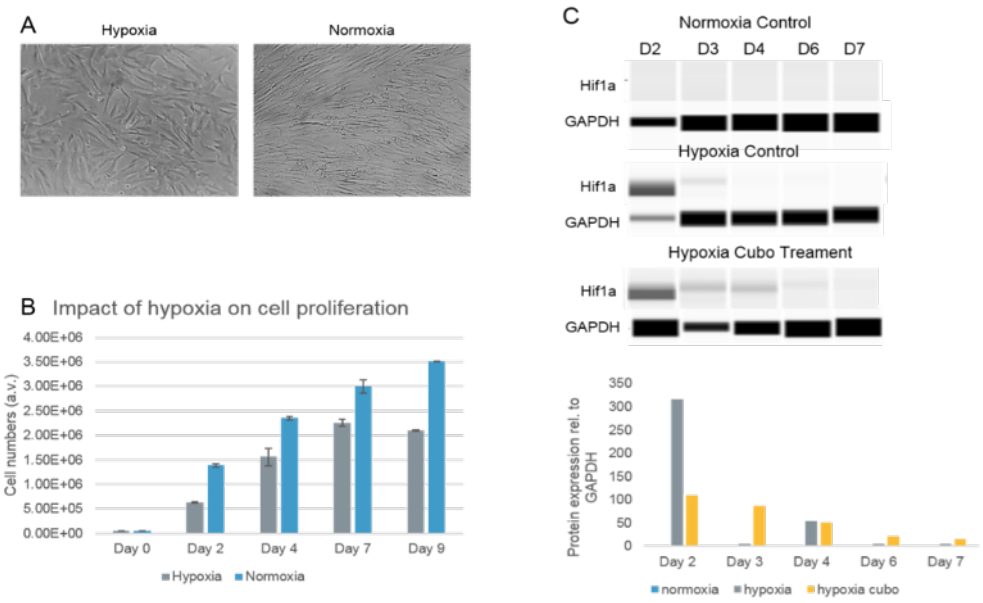

Figure 4: The impact of cubosome treatment on MPCs under hypoxic conditions: MPCs were cultured under normoxic and hypoxic conditions (representative images shown in A) and their proliferation was monitored (B). Protein analysis of these samples showed a reduced relative Hif1a expression after cubosome treatment under hypoxic conditions compared to untreated hypoxia samples (C).

9.3 Conclusions

Lipidic pyridone endoperoxides **156** and **157** have been prepared in good yields in three synthetic steps. In addition, fluorescein-derived lipid (**159**) was synthesized that allows *in vitro* tracking of the cubosome, thereby gaining information about the uptake mechanism and the intracellular fate of the nanoparticles. Cubosomes with lipidic pyridone endoperoxides **156** and **157** have been prepared and characterized using SAXS and DLS. Non-toxic cubosome concentrations were found to be up to 0.2 mg/mL with vitamin C concentrations of 25 or 50 µg/mL. The O_2-release kinetics of lipidic pyridone endoperoxide **157** in cubosomes at 37 °C was investigated by ^{1}H-NMR, and the half-live time of lipidic pyridone endoperoxide **157** was found to be *ca*. 7 h. Preliminary data on the effect of the O_2-releasing cubosomes on MPCs are available. Hif1a expression was reduced after cubosome treatment compared to its expression under untreated hypoxic conditions. This indicates that cubosomes loaded with endoperoxides could affect cellular reactivity to hypoxia by providing oxygen.

9.4 Outlook

Lipidic endoperoxides with prolonged half-lives are required to bridge oxygen supply until vascularization has taken place. Naphthalene-based endoperoxides seem to be a suitable compound class to achieve this goal.[36] Furthermore, novel lipids with several endoperoxide groups (two or three) within the same molecule will be developed to enable a maximal O_2-release potential. Moreover, the fluorescently labelled lipid **159** will be incorporated into cubosomes and used to investigate the cubosome uptake mechanism microscopically. In order to proceed with the first step towards clinical application of cubosomes in human trials, the cubosome effect has to be tested in animal models. For this purpose, we plan to apply cubosomes and MPCs after cubosome treatment *in vivo* into a mouse model to evaluate the potential toxic effect and to find proof on its positive effect on muscle regeneration. Preliminary data were already collected while injecting albumin-loaded cubosomes into the blood stream of endocytosis deficient mice.[17]

9.5 Experimental section

General Information

1-Monooleoyl-sn-glycerol C18:1 (monoolein, MO) was purchased from Nu-Chek Prep, Inc. (MN, USA), and phytantriol was purchased from DSM. Phosphate buffer solution (PBS (1X) pH 7.4) was purchased from Invitrogen. N-(3- dimethylaminopropyl)-N′-ethylcarbodiimide hydrochloride (EDC) and 3-methyl pyridone was purchased from TCI, and all other reagents and solvents were purchased from Sigma Aldrich. All chemicals and solvents were used as received, unless otherwise stated. Reactions were carried out under an inert atmosphere of argon in dry solvents. Dichloromethane was degassed with argon and purified by passage through activated alumina solvent column (MC Brown solvent system) prior to use. Column chromatography was performed using silica gel Merck 60 (particle size 0.040–0.063 mm). Analytical thin- layer chromatography (TLC) was performed using Merck pre-coated silica gel plates 60 F_{254}; visualization by UV absorption and/or by dipping in a solution of $KMnO_4$ (1 g), K_2CO_3 (2 g) in H_2O (100 mL) and subsequent heating. ^{1}H-NMR spectra were recorded on a Bruker AV2-500 (500MHz) spectrometer. Chemical shifts are given in parts per million (ppm) relative to the internal standard TMS (δ = 0 ppm). Coupling constants J are expressed in Hz and multiplicities are abbreviated as follows: s (singlet), br (broad), d (doublet), t (triplet), q (quadruplet), quint (quintet), m (multiplet). ^{13}C-NMR chemical shifts are reported relative to the solvent residual peaks: $CDCl_3$ = 77.00 ppm. Mass spectra were recorded by the Mass Spectroscopy Service of UZH on Finnigan MAT95 MS, BrukerLC MS and Finnigan TSQ700 MS machines.

9.5.1 Synthesis

Synthesis of 151 ((dodecyl 2-bromoacetate))[26]

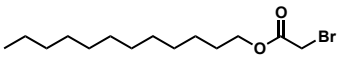

A stirred solution of dodecanol (2 g, 12.63 mmol, 1 eq) and triethylamine (1.4 g, 1.9 mL, 13.9 mmol, 1.1 eq) in CH_2Cl_2 (20 mL) was cooled to -78°C whereupon bromoacetyl bromide (2.5 g (1.08 mL), 1 eq) was added dropwise. The reaction mixture was stirred for 3 h and reaction mixture was allowed to warm up to -20°C and carefully quenched with water (5 mL). The organic phase was extracted with water (2 x 10 mL), ammonium chloride sat. (2 x 10 mL), sodium bicarbonate sat. (2 x 10 mL) and brine (2 x 10 mL) and dried over $MgSO_4$, filtered and the solvent removed by rotary evaporation. The crude product was purified by column chromatography (95:5 cyclohexane/ethylacetate) to yield the product as a colorless oil (3.3 g, 10.74 mmol 85 %). ^{1}H NMR (500 MHz, Chloroform-*d*) δ 4.10 (t, *J* = 6.7 Hz, 2H), 3.76 (2, 1H), 1.59 (p, *J* = 6.8 Hz, 2H), 1.40 – 1.05 (d, *J* = 11.4 Hz, 18H), 0.81 (t, *J* = 6.8 Hz, 3H). ^{13}C NMR (126 MHz, Chloroform-*d*) δ 167.30, 66.45 (2C), 29.60 (2C), 29.53, 29.46, 29.32, 29.16, 28.39, 25.92, 25.72, 22.67, 14.10. HRMS (ESI $[M + Na]^+$) m/z: calcd for ($C_{14}H_{27}BrO_2$) 329.10866, found 329.10849.

Synthesis of 154 (dodecyl 2-(3-methyl-2-oxopyridin-1(2*H*)-yl)acetate)[16]

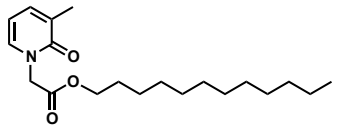

A solution of 3-methyl-2-pyridone (**153**) (160 mg, 1.46 mmol, 1.0 eq), dodecyl 2-bromoacetate (**151**) (600 mg, 1.95 mmol, 1.5 eq), and potassium carbonate (600 mg, 4.4 mmol, 3 eq) in DMF (20 mL) was stirred at room temperature for 16 h. The reaction mixture was concentrated *in vacuo,* the residue was dissolved in ethyl acetate and extracted with water (30 mL) and brine (30 mL). The organic phases were dried over $MgSO_4$ and concentrated *in vacuo*. The product was obtained after purification by column chromatography (cyclohexane/ethyl acetate 9:1) as a colorless oil (462 mg, 1.3 mmol, 89 %). ^{1}H NMR (500 MHz, Chloroform-*d*) δ 7.16 (d, *J* = 6.7 Hz, 1H), 7.02 (d, *J* = 6.7 Hz, 1H), 6.05 (t, *J* = 6.8 Hz, 1H), 4.56 (s, 2H), 4.10 (t, *J* = 6.7 Hz, 2H), 2.08 (s, 3H), 1.56 (q, *J* = 7.4, 6.8 Hz, 2H), 1.30 – 1.11 (m, 18H), 0.81 (t, *J* = 6.8 Hz, 3H). ^{13}C NMR (126 MHz, Chloroform-*d*) δ

167.93, 162.85, 137.23, 135.16, 130.05, 105.79, 65.90, 50.75, 31.90, 29.63, 29.61, 29.54, 29.47, 29.33, 29.18, 28.44, 25.76, 22.67, 17.10, 14.11. HRMS (ESI $[M + H]^+$) m/z: calcd for ($C_{20}H_{34}O_3N$) 336.25332, found 336.25302.

Synthesis of 156 (dodecyl 2-(1-methyl-6-oxo-2,3-dioxa-5-azabicyclo[2.2.2]oct-7-en-5-yl)acetate)

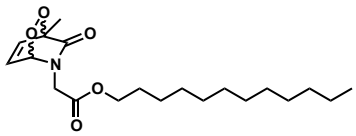

Dodecyl 2-((3-methyl-1,2-dihydropyridin-2-yl)oxy) acetate (**154**) (30 mg, 0.09 mmol) and meso-tetraphenylporphyrin (1 mg) were dissolved in CH_2Cl_2 (10 mL) and stirred vigorously. Compressed air (or oxygen) were bubbled through the reaction mixture, which was cooled to 0°C. The reaction mixture was kept under oxygen atmosphere and irradiated with an LED lamp at 627 nm for 1.5 h. The solvent was removed *in vacuo* and the crude product purified by column chromatography (cyclohexane/ethyl acetate 9:1) to obtain the product in quantitative yield (33 mg, 0.09 mmol). ^{1}H NMR (500 MHz, Chloroform-*d*) δ 6.85 (dd, *J* = 7.8, 5.4 Hz, 1H), 6.39 (dd, *J* = 7.8, 1.5 Hz, 1H), 5.66 (dd, *J* = 5.2, 1.5 Hz, 1H), 4.61 (d, *J* = 18.0 Hz, 1H), 4.13 – 4.00 (m, 2H), 3.80 (d, *J* = 18.0 Hz, 1H), 1.60 – 1.52 (s, 4H), 1.30 – 0.94 (m, 19 H), 0.81 (t, *J* = 6.8 Hz, 3H. ^{13}C NMR (126 MHz, Chloroform-*d*) δ 169.57, 168.99, 134.31, 132.80, 84.73, 81.43, 65.92, 44.21, 31.89, 29.61, 29.57, 29.54, 29.47, 29.33, 29.17, 28.45, 25.78, 22.67, 14.54, 14.11. HRMS (ESI $[M + Na]^+$) m/z: calcd for ($C_{20}H_{33}O_5NNa$) 390.22509, found 390.22534.

Synthesis of 152 ((*Z*)-octadec-9-en-1-yl 2-bromoacetate)[26]

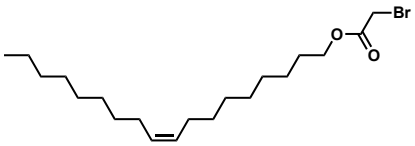

A stirred solution of oleyl alcohol (3.4 g, 12.63 mmol, 1 eq) and triethylamine (1.4 g, 1.9 mL, 13.9 mmol, 1.1 eq) in CH_2Cl_2 (20 mL) was cooled to -78°C whereupon bromoacetyl bromide (2.5 g (1.08 mL), 1 eq) was added dropwise. The reaction mixture was stirred for 3 h and reaction mixture was allowed to warm up to -20°C and carefully quenched with water (5 mL). The organic phase was extracted with water (2 x 10 mL), ammonium chloride sat. (2 x 10 mL), sodium bicarbonate sat. (2 x 10 mL) and brine (2 x 10 mL) and dried over $MgSO_4$, filtered and the solvent removed by rotary evaporation. The crude product was purified by column chromatography (95:5 cyclohexane/ethylacetate) to yield the product as a colorless oil (3.98 g, 10.23 mmol, 81%). ^{1}H NMR (500 MHz, Chloroform-*d*) δ 5.42 – 5.21 (m, 2H), 4.10 (t, *J* = 6.7 Hz, 2H), 3.76 (s, 2H), 1.97 – 1.86 (m, 4H), 1.59 (p, *J* = 6.8 Hz, 2H), 1.38 – 1.09 (m, 22H), 0.81 (t, *J* = 6.9 Hz, 3H). ^{13}C NMR (126 MHz, Chloroform-*d*) δ 166.29, 128.97, 128.73, 65.43, 30.89, 28.75, 28.70, 28.51, 28.35, 28.31, 28.16, 28.13 (2C), 27.39, 26.20, 26.16, 24.91, 24.72, 21.67, 13.10. HRMS (ESI [M + Na]$^+$) m/z: calcd for ($C_{20}H_{37}BrO_2$) 411.18691, found 411.18663.

Synthesis of 155 ((*Z*)-octadec-9-en-1-yl 2-(3-methyl-2-oxopyridin-1(2*H*)-yl)acetate)[16]

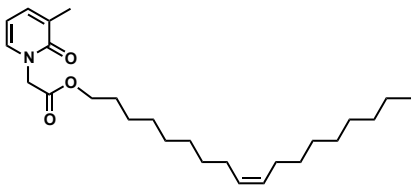

A solution of 3-methyl-2-pyridone (**153**) (200 mg, 1.83 mmol, 1.0 eq), (*Z*)-octadec-9-en-1-yl 2-bromoacetate (**152**) (1.07 g, 2.75 mmol, 1.5 eq), and potassium carbonate (760 mg, 5.5 mmol, 3 eq) in DMF (20 mL) was stirred at room temperature for 16 h. The reaction mixture was concentrated *in vacuo,* the residue was dissolved in ethyl acetate and extracted with water (30 mL) and brine (30 mL). The organic phases were dried over $MgSO_4$ and concentrated *in vacuo*. The product was obtained after purification by column chromatography (cyclohexane/ethyl acetate 9:1) as a colorless oil (597 mg, 1.43 mmol, 78 %). ^{1}H NMR (500 MHz, Chloroform-*d*) δ 7.15 (d, *J* = 6.8 Hz, 1H), 7.03 (d, *J* = 6.8 Hz, 1H),

6.05 (t, *J* = 6.8 Hz, 1H), 5.38 – 5.22 (m, 2H), 4.56 (s, 2H), 4.09 (t, *J* = 6.7 Hz, 2H), 2.08 (s, 3H), 1.97 – 1.86 (m, 4H), 1.57 (p, *J* = 6.6 Hz, 2H), 1.38 – 1.09 (m, 22H), 0.81 (t, *J* = 6.8 Hz, 3H). ^{13}C NMR (126 MHz, Chloroform-*d*) δ 167.88, 162.80, 137.19, 135.15, 129.97, 129.91, 129.71, 105.74, 65.82, 50.72, 31.85, 29.71, 29.69, 29.47, 29.33, 29.26 (2C), 29.14, 29.11, 28.40, 27.16, 27.14, 25.71, 22.63, 17.05, 14.06. HRMS (ESI $[M + H]^+$) m/z: calcd for ($C_{26}H_{44}O_3N$) 418.33157, found 418.33164.

Synthesis of 157 ((*Z*)-octadec-9-en-1-yl 2-(1-methyl-6-oxo-2,3-dioxa-5-azabicyclo[2.2.2]oct-7-en-5-yl)acetate)

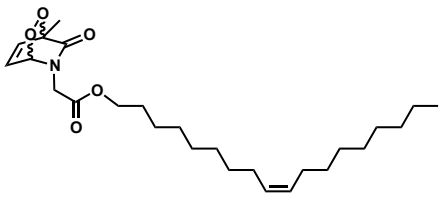

(*Z*)-octadec-9-en-1-yl 2-(3-methyl-2-oxopyridin-1(2*H*)-yl)acetate (30 mg, 0.072 mmol) and meso-tetraphenylporphyrin (1 mg) were dissolved in CH_2Cl_2 (10 mL) and stirred vigorously. Compressed air (or oxygen) were bubbled through the reaction mixture, which was cooled to 0°C. The reaction mixture was kept under oxygen athmoesphere and irradiated with an LED lamp at 627 nm for 4 h. The solvent was removed *in vacuo* and the crude product purified by column chromatography (cyclohexane/ethyl acetate 9:1) to obtain the product as colorless oil (24 mg, 0.054 mmol, 75 %). ^{1}H NMR (500 MHz, Chloroform-*d*) δ 6.96 – 6.79 (m, 1H), 6.39 (d, *J* = 7.8 Hz, 1H), 5.66 (d, *J* = 5.2 Hz, 1H), 5.33 – 5.23 (m, 2H), 4.61 (d, *J* = 18.0 Hz, 1H), 4.11 – 4.01 (m, 2H), 3.80 (d, *J* = 18.0 Hz, 1H), 1.99 – 1.86 (m, 4H), 1.59 – 1.47 (s, 5H), 1.34 – 1.07 (m, 22H), 0.81 (t, *J* = 6.5 Hz, 3H). ^{13}C NMR (126 MHz, Chloroform-*d*) δ 169.57, 134.31, 129.99, 129.72, 84.72, 81.43, 65.89, 44.20, 31.89, 29.75, 29.71, 29.53, 29.51, 29.37, 29.31 (2C), 29.18 (2C), 29.15, 28.45, 27.19, 27.14, 25.78, 22.67, 14.55, 14.11. HRMS (ESI $[M + Na]^+$) m/z: calcd for ($C_{26}H_{43}O_5NNa$) 472.30334, found 472.30340.

Synthesis of 159 ((*Z*)-3',6'-dihydroxy-*N*-(octadec-9-en-1-yl)-3-oxo-3*H*-spiro[isobenzofuran-1,9'-xanthene]-5-carboxamide)

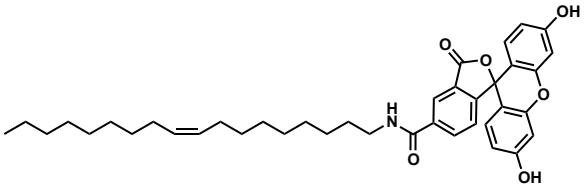

Commercially available NHS-fluorescein (**158**) (20 mg, 0.422 mmol, 1 eq) oleylamine (17 mg, 0.633 mmol, 1.5 eq), and triethylamine (39 mg, 3.8 mmol, 9 eq) in CH_2Cl_2 (5 mL). The reaction mixture was let to stir overnight at room temperature. The solvent was removed *in vacuo* and the crude product purified by column chromatography (cyclohexane/ethyl acetate 1:9) to obtain the product as a mixture of isomers (41 mg, 0.659 mmol, 64 %). ^{1}H NMR (500 MHz, DMSO-d_6) δ 10.15 (s, 1H??), 8.78 (t, *J* = 5.3 Hz, 1H), 8.64 (t, *J* = 5.4 Hz, 1H), 8.45 (s, 1H), 8.23 (d, *J* = 8.1 Hz, 1H), 8.16 (d, *J* = 8.1 Hz, 1H), 8.06 (d, *J* = 8.0 Hz, 1H), 7.66 (s, 1H), 7.36 (d, *J* = 8.0 Hz, 1H), 6.77 – 6.65 (m, 2H), 6.61 – 6.51 (m, 2H), 5.48 – 5.18 (m, 2H), 2.07 – 1.84 (m, 2H), 1.61 – 1.12 (m, 4H), 0.91 – 0.76 (m, 1H). ^{13}C NMR (126 MHz, DMSO-d_6) δ 168.20, 168.05, 164.42, 164.27, 159.60, 154.56, 152.66, 151.83, 140.84, 136.41, 134.66, 129.65, 129.62, 129.21, 129.12, 128.11, 126.43, 124.81, 124.18, 123.18, 122.19, 112.71, 112.64, 109.16, 109.10, 102.27, 102.24, 83.28, 83.24, 28.4 – 29.1 (m, 10C), 26.51, 26.55, 26.45, 22.09, 13.94. HRMS (ESI [M + H]$^+$) m/z: calcd for ($C_{39}H_{48}O_6N$) 626.34706, found 626.34687.

9.5.2 Cubosome preparation

MO or PT was weight into a glass vial and the corresponding amount of a lipidic pyridone endoperoxide stock-solution (in CH_2Cl_2) was added to obtain a homogeneous lipid mixture. The solvent was evaporated (at high vacuum 10^{-2} mbar for 24 h) and the lipidic mixture subsequently hydrated by adding appropriate volumes of stabilizer containing buffer (PF108, 1.65 mg / mL, and required vitamin C concentration) to obtain the cubosome sample with the desired lipid concentration. The sample was vortex-mixed and then dispersed using an ultrasonic processor Brenson digital 250 (cycle 0.9 s on/ 0.9 s off, amplitude 50%, for 3 x 5 min). Subsequently, the cubosome dispersion was filtered through Acrodisc 450 nm filters and directly used.

9.5.3 Dynamic light scattering (DLS)

Particle size of the cubosomes was performed after preparation, before the reaction was started, and after the reaction was terminated (1-2 d) with a Zeta Sizer Nano ZS (Malvern Instruments, Malvern, UK) at 25 ± 0.1 °C. The samples were measured in disposable polystyrene cuvettes of 1 cm optical path length with the corresponding buffer as solvent. Scattering angle was 90°. A triplicate of the samples was performed. The width of the DLS hydrodynamic diameter distribution is indicated by PDI (polydispersion index). The intensity size distribution of the cubosomes was typically unimodal; therefore the autocorrelation function was analyzed according to the cumulant method.

9.5.4 Small angle X-ray scattering (SAXS)

SAXS measurements were used to identify the symmetry of the cubosomes. Experiments were performed on a Bruker AXS Micro, with a microfocused X-ray source, operating at voltage filament current of 50 kV and 1.000 μA, respectively. The Cu Kα radiation (λCu Kα =1.5418 Å) was collimated by a 2D Pilatus 100K detector. The scattering vector q = $(4\pi/\lambda)\sin\theta$, with 2θ being the scattering angle, was calibrated using silver behenate. Data were collected and azimuthally averaged using the Saxsgui software to yield one-dimensional intensity versus scattering vector *q*, with a *q* range from 0.004 – 0.5 $Å^{-1}$. The sample-to-detector distance was 1 m, providing a q range from 0.005 to 0.77 $Å^{-1}$. Samples were loaded into a quartz glass capillary (Hiligenberg, length: 80 mm; outside: 2.0 mm; wall thickness: 0.01 mm). Measurements were performed at 23 °C, and samples were equilibrated for 10 min prior to measurements, while scattered intensity was collected over 4 hours.

SAXS spectrum of MO-cubosomes containing pyridone endoperoxide 157

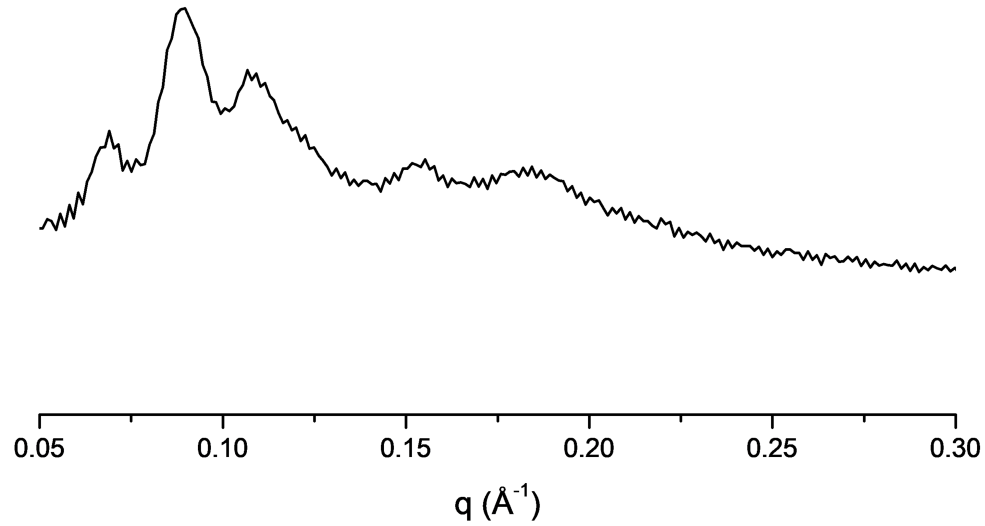

Figure 5: Pn3m SAXS pattern of cubosomes containing pyridone endoperoxide **157** (2 mg vc, 31 mg MO/ mL PBS 1X containing 1.65 mg/mL PF-108).

The experiments described in the following paragraphs have been performed by Jenny Prange at the University Hospital of Zurich.

9.5.5 Toxicity assessment and development of optimal *ex vivo* application conditions

hMPCs were isolated and expanded until passage 2/3 and frozen as stock. hMPCs were then thawed for each cubosome experiment, seeded in a cellular density of 3000-5000 cells/cm^2 and performed always in the same passage to avoid passaging effects. Cells were seeded at least 4h prior to cubosome treatment under both, normoxic and hypoxic conditions, to allow settling. Cubosome treatment was performed for 24 h, as the target treatment would be a slow release of the load, and hMPCs were cultured after cubosome treatment for maximum one week, which represents the time needed by the blood vessels to re-vascularize transplanted tissue. Analysis of the cubosome effect will be performed visually (light microscopy images), by cell proliferation assay (WST) and by cell counting.

Cell culture: single cells were isolated from human muscle biopsies (> 0.2 g) from patients (different sex and age) undergoing abdominal surgery. Ethical approval was achieved and inform consent will be obtained from each patient. Cells will be isolated for research purposes only and not used for cell therapy afterwards. All muscle biopsies were transported in PBS + 1 % penicillin/streptomycin at 2-8 °C and processed immediately after removal. Human MPC isolation procedure is as follows: the biopsy is clean from other tissues, such as tendons or fat, weighed and disinfected with 100% and 50% betadine solution for 5 min. After three times washing, the muscle tissue is minced and cut into a viscous mix which is then mixed with collagenase/ dispase enzymatic solution and incubated for about 1 h at 37 °C. After stopping the digestion, the tissue suspension is centrifuged, filtered and distributed on collagen-coated 6-well plates for 24 h. After 1 day, the suspension is transferred into the neighboring well to remove fibroblasts which have been settled already. In the following days, medium is changed every two to three days and growing hMPCs will be split and expanded when confluency reaches 80 %.

The growth medium is based on DMEM/F12 Nutirent Mix (1:1) supplemented with 1 % Penicillin/ streptomycin, 18 % FBS, 10 ng/mL hEGF, 1 ng/mL hbFGF, 10 µg/mL human Insulin, and 0.4 µg/mL dexamethasone and changed every two to three days. If confluency reaches 80 % hMPCs are split using 0.25 % trypsin (Gibco) and reseeded on new culture supports.

Differentiation medium contains DMEM/F12 Nutrient Mix (1:1), 10 % FBS, 1 % Penicillin/ Streptomycin and is changed every two to three days. If not directly used, hMPCs are stored

in 50 % FBS (Sigma), 40 % DMEM/F12 Nutrient Mix (Gibco) and 10 % Dimethylsulfoxide (Sigma) in liquid nitrogen.

Cubosome treatment: For the cubosome treatment, passage 2-5 hMPCs are seeded 4 h prior to the cubosome treatment to allow the cells to settle. Then various concentrations of cubosomes will be tested and incubated for 24 h before removal and replacement with fresh medium.

Hypoxia experiments: hMPCs were prepared in suspension (40.000±10.000 cells/mL) and seeded directly under hypoxic conditions, at least 4 h prior to cubosome treatment. Medium will be stored already 1 day prior to use under hypoxic conditions to ensure the lack of oxygen during the procedure. All materials and substances used under hypoxic conditions have to pass through the air lock system of the hypoxic chamber.

Cell proliferation assay: hMPCs were pre-seeded, treated and after treatment suspension is removed and replaced with a 1:10 dilution of the WST reagent (Roche) in DMEM/F12 Nutrient Mix (1:1). WST reagent is incubated for 1-4 h. After incubation, the supernatant was removed from the cells and transferred into a 96-well plate (flat bottom) and measured with an Epoch2 plate reader (Biotek) at 450 nm.

Mitochondria assessments: hMPCs treated with/ without cubosomes under hypoxic and normoxic conditions were stained for mitochondria morphology using immunofluorescence staining with Mitotracker or similar protocols (according to the manufacturers protocol). Cell Counting: For automated cell counting 10 µL of cell suspension was mixed with 10µl of trypan blue and loaded in the two chambers of a counting chamber for the Countess (Invitrogen). Cell number were reported directly from the machine. Countings were performed in triplicates to reduce intra-sampling variability.

9.5.6 Application and assessment of cubosome effect on hMPC morphology, survival and muscle-specific protein expression under hypoxic conditions

Protein Simple WES Analysis

Cells with different treatments were lysed with modified lysis buffer plus protease inhibitor-cocktail (Sigma-Aldrich). Samples were centrifuged for 20 min at 13'000 rpm, and the supernatant was taken for protein determination. Total protein will be measured using BCA protein assay kit (Thermo Scientific, Lausanne, Switzerland). 1 mg/mL of protein will be used for the WES sample preparation using 12-230 KDa cartridge kit and the proteins will be separated in WES with a capillary cartridge according to the manufacturer protocols (Protein Simple WES, Germany). The primary antibodies will be HIf1a (1:100), PHD2 (1:100), GAPDH (1:100), Desmin (1:50), Pax7 (1:100), MyoD (1:20), Actinin (1:10). Mouse anti-GAPDH (1:100, Novus Biologicals Europe) served as internal control.

Real time PCR: Cells will be mixed with RNA lysis buffer provided in the kit (SV Total RNA isolation system, Promega, Dübendorf, Switzerland). Total RNA will be isolated using a kit according to the manufacturer's protocol, which includes DNase digestion. RNA will be reverse transcribed using random primers (Retro- transcription RNA to cDNA, Applied Biosystem). Predesigned primers for EGLN1, Hif3A, Hif1A, ERO1A, DDIT3, MyHC1, desmin and human cytochrome c will be purchased from Applied Biosystem. The GAPDH was used to normalize cDNA concentrations. For quantification, expression in untreated control cells for each gene was taken as a 100% reference value. Negative controls were included as no template control and RNA control to check for genomic DNA contamination.

Fiber formation assay: The formation of muscle fibers was evaluated after 10 days, differentiation of hMPCs, seeded in a density of 3000-5000 cells/cm^2, in differentiation medium which was changed every two to three days. At day 10, culture supports were fixed in methanol for 7 min, air dried and stained with Giemsa (Sigma, 1:20 dilution) for 1 h at room temperature. After washing, samples were air dried and pictures taken with a Zeiss Axio imager M1 microscope. Five high power fields (HPF) were analyzed to calculate the average number of fiber per HPF. The data were expressed as fused cells per high power field, number of fibers per HPF and number of nuclei per fiber.

FACS: 500.000 cells will be fixed for 10 min with 2 % paraformaldehyde, permeabilized for 7 min with 0.5 % Triton X-100, blocked for 20 min with 5 % BSA + 0.1 Triton X-100 and each time washed with PBS in between. Samples were then immunolabelled with anti- Annexin V (apoptosis marker), anti- PI (necrosis marker), anti-desmin, anti-myosin heavy chain, anti-MyoD, anti-PAX7 and anti-sarcomeric actinin (hMPC markers, Sigma) at 4 °C before secondary labelling were done with a PE- (or equivalent) secondary antibody. Samples were

measured using a Becton FACS Calibur flow cytometer of the FACS Core Facility and analyzed with FlowJo software. **Cell apoptosis/ Necrosis assays:** Cell pellet were resuspended in cold PBS and pelleted by centrifugation at 1400 rpm for 7 min. Cell pellet were gently resuspended in 100 µL of 1x binding buffer (1 x 105 cells/100 µL Binding buffer). 1 µL of FITC / Annexin V (BD Pharmingen) were added and tubes were incubated for 15 min in the dark at room temperature. 350 µL 1 x binding buffer were added to each tube. Just before analyzing, 10 µL probidium iodide (100 µg/ml) was added and samples were analyzed by flow cytometry within 1 h.

Bibliography

(1) Vacanti, C. A. The History of Tissue Engineering. *J. Cell. Mol. Med.* **2006**, *10* (3), 569–576.

(2) Müller-Ehmsen, J.; Whittaker, P.; Kloner, R. A.; Dow, J. S.; Sakoda, T.; Long, T. I.; Laird, P. W.; Kedes, L. Survival and Development of Neonatal Rat Cardiomyocytes Transplanted into Adult Myocardium. *J. Mol. Cell. Cardiol.* **2002**, *34* (2), 107–116.

(3) Haider, H. K.; Ashraf, M. Strategies to Promote Donor Cell Survival: Combining Preconditioning Approach with Stem Cell Transplantation. *J. Mol. Cell. Cardiol.* **2008**, *45* (4), 554–566.

(4) Rivron, N. C.; Liu, J.; Rouwkema, J.; De Boer, J.; Van Blitterswijk, C. A. Engineering Vascularised Tissues in Vitro. *Eur. Cells Mater.* **2008**, *15*, 27–40.

(5) Tremblay, P. L.; Hudon, V.; Berthod, F.; Germain, L.; Auger, F. A. Inosculation of Tissue-Engineered Capillaries with the Host's Vasculature in a Reconstructed Skin Transplanted on Mice. *Am. J. Transplant.* **2005**, *5* (5), 1002–1010.

(6) Auger, F. A.; Gibot, L.; Lacroix, D. The Pivotal Role of Vascularization in Tissue Engineering. *Annu. Rev. Biomed. Eng.* **2013**, *15* (1), 177–200.

(7) Guérette, B.; Skuk, D.; Célestin, F.; Huard, C.; Tardif, F.; Asselin, I.; Roy, B.; Goulet, M.; Roy, R.; Entman, M.; Tremblay, J. P. Prevention by Anti-LFA-1 of Acute Myoblast Death Following Transplantation. *J. Immunol.* **1997**, *159* (5), 2522–2531.

(8) Snyder, B. R.; Chiu, A. M.; Prockop, D. J.; Chan, A. W. S. Human Multipotent Stromal Cells (MSCs) Increase Neurogenesis and Decrease Atrophy of the Striatum in a Transgenic Mouse Model for Huntington's Disease. *PLoS One* **2010**, *5* (2).

(9) Qu, Z.; Balkir, L.; Van Deutekom, J. C. T.; Robbins, P. D.; Pruchnic, R.; Huard, J. Development of Approaches to Improve Cell Survival in Myoblast Transfer Therapy. *J. Cell Biol.* **1998**, *142* (5), 1257–1267.

(10) Hodgetts, S. I.; Beilharz, M. W.; Scalzo, A. A.; Grounds, M. D. Why Do Cultured Transplanted Myoblasts Die in Vivo? DNA Quantification Shows Enhanced Survival of Donor Male Myoblasts in Host Mice Depleted of CD4+ and CD8+ Cells or NK1.1+ Cells. *Cell Transplant.* **2000**, *9* (4), 489–502.

(11) Harrison, B. S.; Eberli, D.; Lee, S. J.; Atala, A.; Yoo, J. J. Oxygen Producing Biomaterials for Tissue Regeneration. *Biomaterials* **2007**, *28* (31), 4628–4634.

(12) Li, Z.; Guo, X.; Guan, J. An Oxygen Release System to Augment Cardiac Progenitor Cell Survival and Differentiation under Hypoxic Condition. *Biomaterials* **2012**, *33* (25), 5914–5923.

(13) Pedraza, E.; Coronel, M. M.; Fraker, C. A.; Ricordi, C.; Stabler, C. L. Preventing Hypoxia-Induced Cell Death in Beta Cells and Islets via Hydrolytically Activated, Oxygen-Generating Biomaterials. *Proc. Natl. Acad. Sci.* **2012**, *109* (11), 4245–4250.

(14) Jaimes, E. A.; Sweeney, C.; Raij, L. Effects of the Reactive Oxygen Species Hydrogen Peroxide and Hypochlorite on Endothelial Nitric Oxide Production. **2001**, 877–883.

(15) Yang, L.; Zhu, L.; Dong, W.; Cao, Y.; Rong, Z. Oxygen-Generating Scaffolds: A New Strategy for Bone Tissue Engineering. *Bone* **2013**, *57* (1), 322–323.

(16) Benz, S.; Nötzli, S.; Siegel, J. S.; Eberli, D.; Jessen, H. J. Controlled Oxygen Release from Pyridone Endoperoxides Promotes Cell Survival under Anoxic Conditions. *J. Med. Chem.*

2013, *56* (24), 10171–10182.

(17) Aleandri, S.; Prange, J. Unpublished Results. **2018**.

(18) Rahanyan-Kägi, N.; Aleandri, S.; Speziale, C.; Mezzenga, R.; Landau, E. M. Stimuli-Responsive Lipidic Cubic Phase: Triggered Release and Sequestration of Guest Molecules. *Chem. - A Eur. J.* **2015**, *21* (5), 1873–1877.

(19) Farokhzad, O. C.; Langer, R. Impact of Nanotechnology on Drug\nDelivery. *ACS Nano* **2009**, *3* (1), 16–20.

(20) Mulet, X.; Boyd, B. J.; Drummond, C. J. Journal of Colloid and Interface Science Advances in Drug Delivery and Medical Imaging Using Colloidal Lyotropic Liquid Crystalline Dispersions. **2013**, *393*, 1–20.

(21) Zhang, L.; Gu, F. X.; Chan, J. M.; Wang, A. Z.; Langer, R. S.; Farokhzad, O. C. Nanoparticles in Medicine: Therapeutic Applications and Developments. *Clin. Pharmacol. Ther.* **2008**, *83* (5), 761–769.

(22) Sato, E.; Ikeda, Y.; Kanaoka, Y. Photochemistry of Conjugated Nitrogen-Carbonyl Systems. III Photosensitized Oxygenation of 3- and 6-Substituted 2-Pyridones. *Chem. Pharm. Bull.* **1987**, *35* (2), 507–513.

(23) Matsumoto, M.; Yamada, M.; Watanabe, N. Reversible 1,4-Cycloaddition of Singlet Oxygen to N-Substituted 2-Pyridones: 1,4-Endoperoxide as a Versatile Chemical Source of Singlet Oxygen. *Chem. Commun.* **2005**, No. 4, 483.

(24) DeRosa, M. C.; Crutchley, R. J. Photosensitized Singlet Oxygen and Its Applications. *Coord. Chem. Rev.* **2002**, *233–234*, 351–371.

(25) Chou, P. T.; Khan, A. U. L-Ascorbic Acid Quenching of Singlet Delta Molecular Oxygen in Aqueous Media: Generalized Antioxidant Property of Vitamin C. *Biochem. Biophys. Res. Commun.* **1983**, *115* (3), 932–937.

(26) Morrissey, S.; Pegot, B.; Coleman, D.; Garcia, M. T.; Ferguson, D.; Quilty, B.; Gathergood, N. Biodegradable, Non-Bactericidal Oxygen-Functionalised Imidazolium Esters: A Step towards “greener” Ionic Liquids. *Green Chem.* **2009**, *11* (4), 475.

(27) Liu, H.; Ko, S. B.; Josien, H.; Curran, D. P. Selective N-Functionalization of 6-Substituted-2-Pyridones. *Tetrahedron Lett.* **1995**, *36* (49), 8917–8920.

(28) Chithrani, B. D.; Ghazani, A. A.; Chan, W. C. W. Determining the Size and Shape Dependence of Gold Nanoparticle Uptake into Mammalian Cells. *Nano Lett.* **2006**, *6* (4), 662–668.

(29) Dausend, J.; Musyanovych, A.; Dass, M.; Walther, P.; Schrezenmeier, H.; Landfester, K.; Mailänder, V. Uptake Mechanism of Oppositely Charged Fluorescent Nanoparticles in Hela Cells. *Macromol. Biosci.* **2008**, *8* (12), 1135–1143.

(30) Banquy, X.; Suarez, F.; Argaw, A.; Rabanel, J.-M.; Grutter, P.; Bouchard, J.-F.; Hildgen, P.; Giasson, S. Effect of Mechanical Properties of Hydrogel Nanoparticles on Macrophage Cell Uptake. *Soft Matter* **2009**, *5* (20), 3984.

(31) Saha, K.; Kim, S. T.; Yan, B.; Miranda, O. R.; Alfonso, F. S.; Shlosman, D.; Rotello, V. M. Surface Functionality of Nanoparticles Determines Cellular Uptake Mechanisms in Mammalian Cells. *Small* **2013**, *9* (2), 300–305.

(32) Verma, A.; Uzun, O.; Hu, Y.; Hu, Y.; Han, H. S.; Watson, N.; Chen, S.; Irvine, D. J.; Stellacci, F.

Surface-Structure-Regulated Cell-Membrane Penetration by Monolayer-Protected Nanoparticles. *Nat. Mater.* **2008**, *7* (7), 588–595.

(33) Deshpande, S.; Singh, N. Influence of Cubosome Surface Architecture on Its Cellular Uptake Mechanism. *Langmuir* **2017**, *33* (14), 3509–3516.

(34) Harris, A. L. Hypoxia — a Key Regulatory Factor in Tumour Growth. *Nat. Rev. Cancer* **2002**, *2* (1), 38–47.

(35) Masson, N.; Willam, C.; Maxwell, P. H.; Pugh, C. W.; Ratcliffe, P. J. Independent Function of Two Destruction Domains in Hypoxia-Inducible Factor-?? Chains Activated by Prolyl Hydroxylation. *EMBO J.* **2001**, *20* (18), 5197–5206.

(36) Klaper, M.; Linker, T. New Singlet Oxygen Donors Based on Naphthalenes: Synthesis, Physical Chemical Data, and Improved Stability. *Chem. - A Eur. J.* **2015**, *21* (23), 8569–8577.

Acknowledgements

I would like to express my appreciation to Prof. Dr. Ehud M. Landau, for giving me the chance to pursue my PhD in his group and for his support during this time. He was a very encouraging advisor, especially when things did not work according to plan. I really appreciate his openness to new ideas and projects and to collaborations with groups from different fields. This made my PhD extremely interesting and interdisciplinary.
I want to thank Prof. Dr. Henning J. Jessen for mentoring this project and for his help to find my PhD position. Henning gave very important inputs for this project to work out. He still supported me after his move to Freiburg, which I appreciate very much.
I also thank Prof. Dr. Oliver Zerbe for being a part of my PhD committee.

I would like to thank all the present members of the Landau Group:
Marco Etter, who is the social and organizational heart of our group. I thank him for his help with the polymerizable lipids, a project that we started together and for his help with the enzyme catalysis project, that he is continuing together with Philipp. We went together through almost the whole PhD time and became true friends.
Nicole Kieliger, who is a very friendly colleague. I thank her for the help with the Pd-complexes.
Dr. Jijo Vallooran, he brought a lot of mesophase-related know-how into the group. I want to thank him for his contributions to the PdNP- and the chiral PT-project.
Dr. Philipp Ansorge, our biochemistry expert, thanks for your help in the enzyme catalysis project.
We had a wonderful working athmosphere in the group and I will miss the coffee breaks with you.
The former members of the Landau Group:
Dr. Livia Salvati Manni, with whom I have inspiring scientific, and private discussions. I thank her for the contributions on the aldol paper and the PdNP project.
Dr. Simone Aleandri for introducing me into the lipidic mesophase field.
Dr. Marek Komisarski and Dr. Yazmin Osornio
I want to thank the students whose Master or Bachelor theses I supervised:
Laurent Moser for his work on nornicotine organocatalysts, Giann Wieprächtiger for his work on phosphate ester hydrolysis, Daria Dällenbach for her contributions to the enzyme catalysis project. It was a pleasure to have you in the lab.

I want to thank Prof. Dr. Raffaele Mezzenga, who allowed us to use his facilities. Stephan Handschin for patiently taking TEM images of cubosomes and palladium nanoparticles.

Chiara Speziale for measuring SAXS and Dr. Salvatore Assenza for his help with some figures.

I want to thank Dr. Jenny Prange and Prof. Dr. Dr. med. Daniel Eberli for the collaboration on the oxygen-delivery project.
And I would like to thank Dr. Esther Gottwald and Prof Dr. Andrew Hall for the collaboration on kidney diseases. It was a pleasure to work with Esther.
These collaborations truly enriched my PhD thesis. I am very glad that I could work with people from the ETH, from the University Hospital of Zurich and from other groups here at UZH. Zurich is an amazing research city.

I would like to thank PD Laurent Bigler and Yvonne Forster for the MS service and Irene Lehmann for her analytical help.
And the people from the NMR facilities: Nadja Bross and especially Simon Jurt, who acquired NMR spectra of our Cp-mesophases and of our endoperoxide cubosomes

I would like to thank the Graduate School of Chemical and Molecular Science and to the Forschungskredit UZH for their financial support.

This PhD thesis would not have been possible without a very strong private support.
I want to thank the most important people in my life. Steffi, you are a wonderful woman, I am very happy to have you by my side. I admire you for how you are caring for Sebastian, how you handle the work load in your office and how you finish your MAS. All at the same time. I want to thank Sebastian, who reveals the important things in life.
My parents Rita and Niklaus, for their support in so many ways, and to my brothers David and Alexander, to Lotti and Thomas, who became a second pair of parents to me, and to Adi and Mary.

Universität Zürich[UZH]

CMSZH
CHEMICAL MOLECULAR SCIENCES ZURICH
GRADUATE SCHOOL

Curriculum Vitae

Personal information

First Name, Name	Michael DUSS
Address	Scheuchzerstrasse 223
	8057 Zurich
Mobile Phone	+41 79 565 84 14
Email	michael.duss@chem.uzh.ch
Date of Birth	05/29/1985
Place of Origin	Entlebuch LU

Education

PhD, Chemistry, University of Zurich, Department of Chemistry — 11/2013 – 06/2018
Supervisor: Prof. Ehud M. Landau
Thesis title: Design of Novel Functionalized Lipidic Mesophases and their Applications in Catalysis, Water Confinement and Cellular Oxygen Delivery

MSc, Chemistry, University of Zurich, Department of Chemistry — 09/2011 – 09/2013
Supervisor: Prof. Henning J. Jessen
Thesis title: Novel Applications of Phosphoramidites: Desymmetrization of *meso*-Compounds and Enrichment of Phosphorylated Proteins

BSc, Chemistry, ZHAW Zurich University of Applied Sciences — 09/2007 – 09/2010
Bachelor Thesis at Givaudan Suisse SA
Thesis title: Synthese von Benzophenondiethern und Benzophenondiacetalen als UV-Präkursoren für die Riechstoffindustrie

Preparatory course for the entrance examination — 10/2006 – 07/2007
at ZHAW Zurich University of Applied Sciences

Apprenticeship as Chemical Laboratory Technician, — 08/2002 – 08/2005
Dottikon Exclusive Synthesis AG

Professional experience

PhD, Chemistry, University of Zurich, Department of Chemistry — 11/2013 – 06/2018 (expected)
Supervisor: Prof. Ehud M. Landau

Chemical Laboratory Technician, Dottikon Exclusive Synthesis AG — 09/2005 – 09/2006
Supervisor: Dr. Frank Wierschem

Apprenticeship as Chemical Laboratory Technician, — 08/2002 – 08/2005
Dottikon Exclusive Synthesis AG, Supervisor: Peter Huber

Teaching activities and supervision of students

Practical Organic chemistry, synthesis course for 2nd year chemistry students (4 semesters, 600 hours). Students: Anaïs Troude (Internship), Laurent Moser (Master thesis), Giann Wiprächtiger (Bachelor thesis), Daria Dellenbach (Bachelor thesis).

Membership in scientific societies

Swiss Chemical Society

Awards and honors

- Nomination for an Albert Hofmann PhD Award for Excellence in Research, 2017
- Forschungskredit Candoc UZH, 2015, (FK-15-083)

Languages and software

German (native speaker), English (working language, C1/C2), French (good knowledge, B2)
MS Office, ChemDraw Ultra, Mestrenova, SciFinder

Contributions to conferences and scientific schools

- Swiss Summer School in Chemical Biology, September 1-5, 2014, Villars, Switzerland (poster presentation)
- SCS Fall Meeting, September 11, 2014, Zurich, Switzerland (poster presentation)
- 16th Tetrahedron Symposium, June 16-19, 2015, Berlin, Germany (poster presentation)
- 18th Tetrahedron Symposium, June 27-30, 2017, Budapest, Hungary (poster presentation)

Publications in peer-reviewed scientific journals

- Michael Duss, Samanta Capolicchio, Anthony Linden, Nisar Ahmed, Henning J. Jessen, Desymmetrization of *myo*-inositol derivatives by lanthanide catalyzed phosphitylation with C_2-symmetric phosphites*,* **2015** *Bioorganic & Medicinal Chemistry*, 23, 12, 2854 – 2861.
- Michael Duss, Livia Salvati Manni, Laurent Moser, Stephan Handschin, Raffaele Mezzenga, Henning J. Jessen, Ehud M. Landau, Lipidic mesophases as novel nanoreactor scaffolds for organocatalysts: Heterogeneously catalyzed asymmetric aldol reactions in confined water, *ACS Applied Materials & Surfaces*, **2018**, 10, 5114 **–** 5124.
- Esther M. Gottwald, Michael Duss, Milica Bugarski, Dominik Haenni, Claus D. Schuh, Ehud M. Landau, Andrew M. Hall. The targeted anti-oxidant MitoQ causes mitochondrial swelling and depolarization in kidney tissue, *Physiological Reports,* **2018**, 1 – 9.

Appendix: ^{1}H-and ^{13}C-NMR spectra

Table of contents

Chapter 2

Compound **2**, ^{1}H

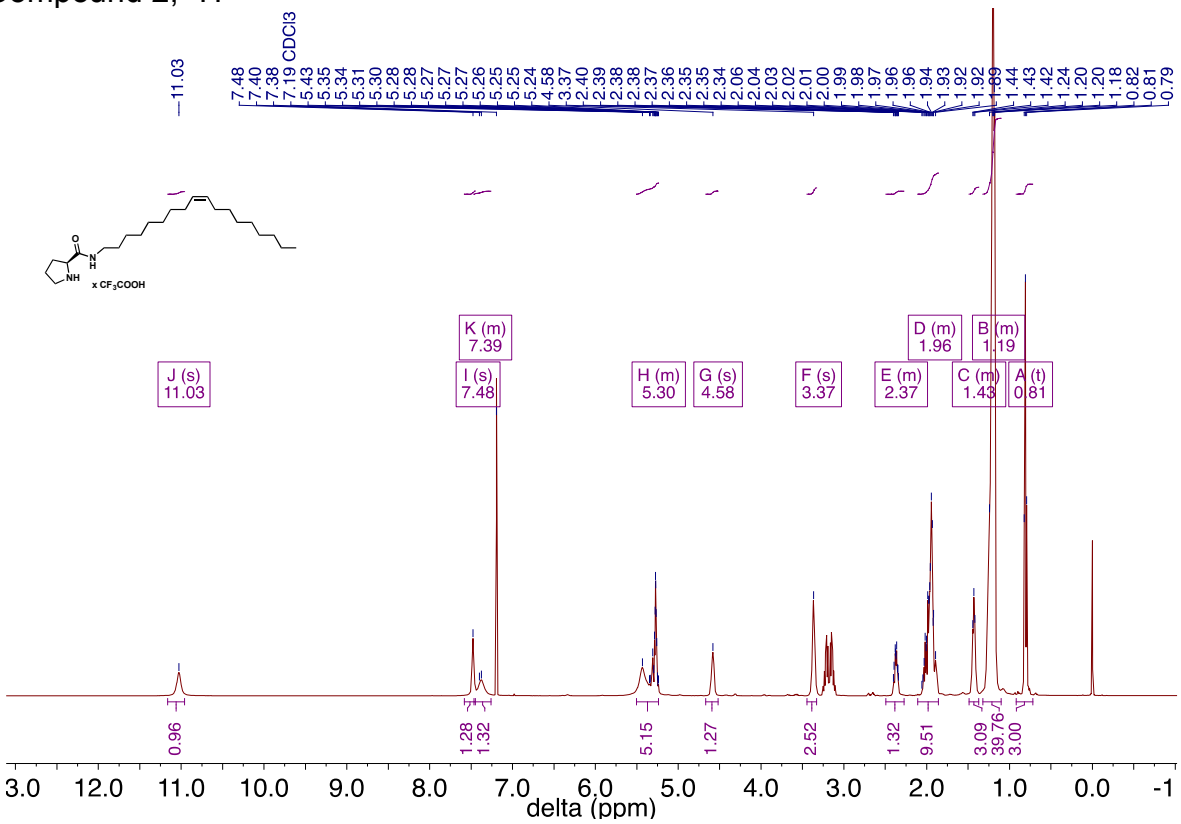

Compound **2**, ^{13}C

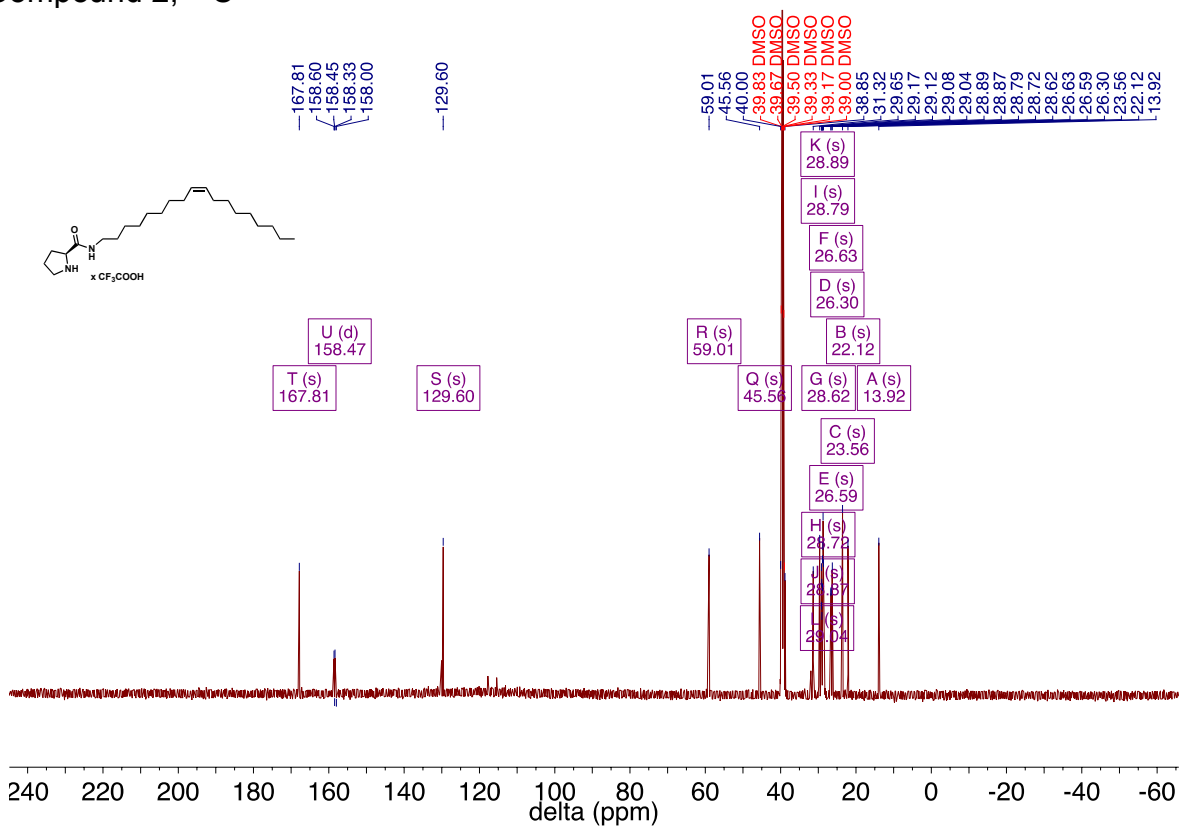

Compound **5a**, *anti*-isomer, ^{1}H

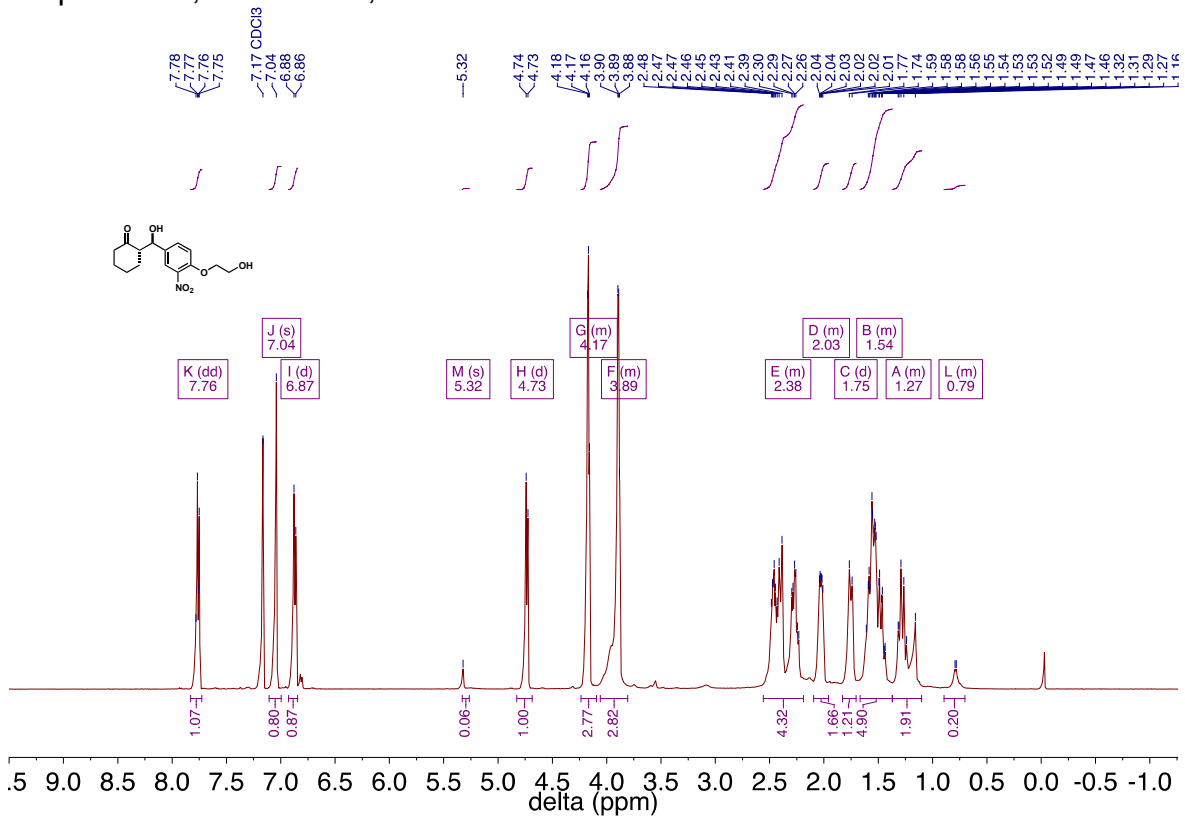

Compound **5a**, *anti*-isomer, ^{13}C

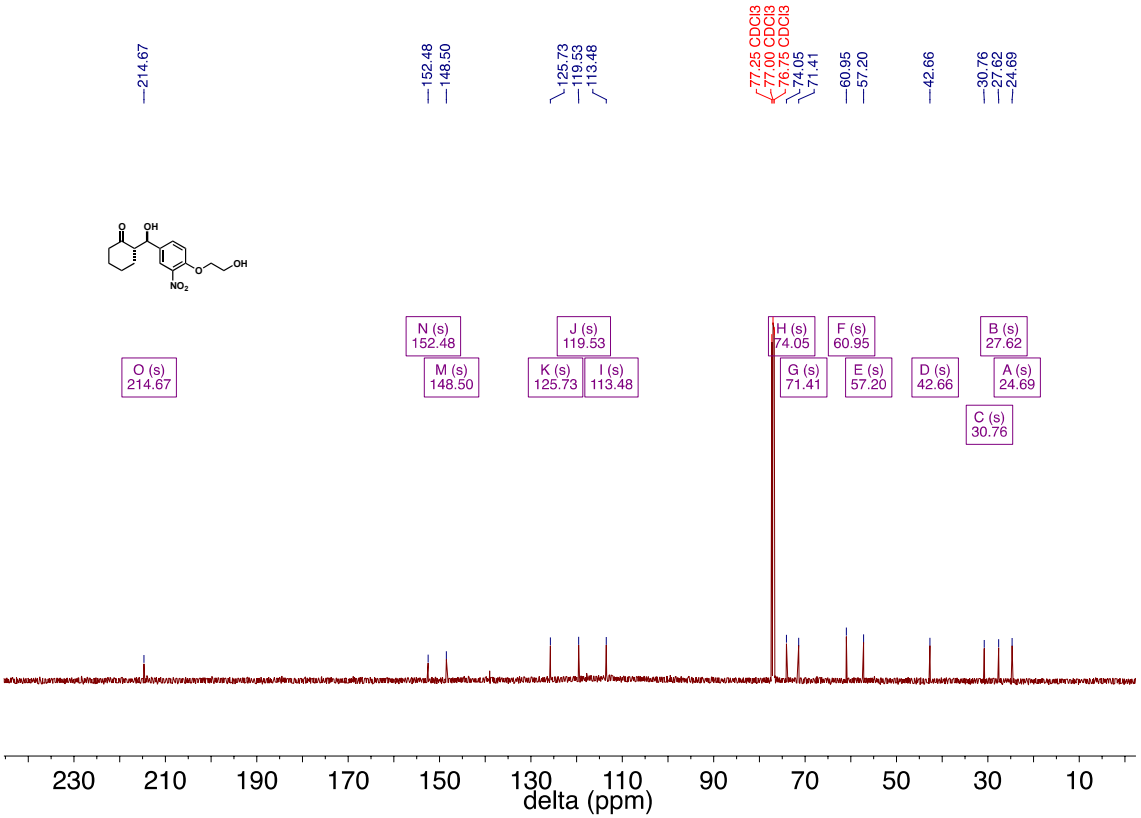

Compound **5a**, *syn*-isomer, ^{1}H

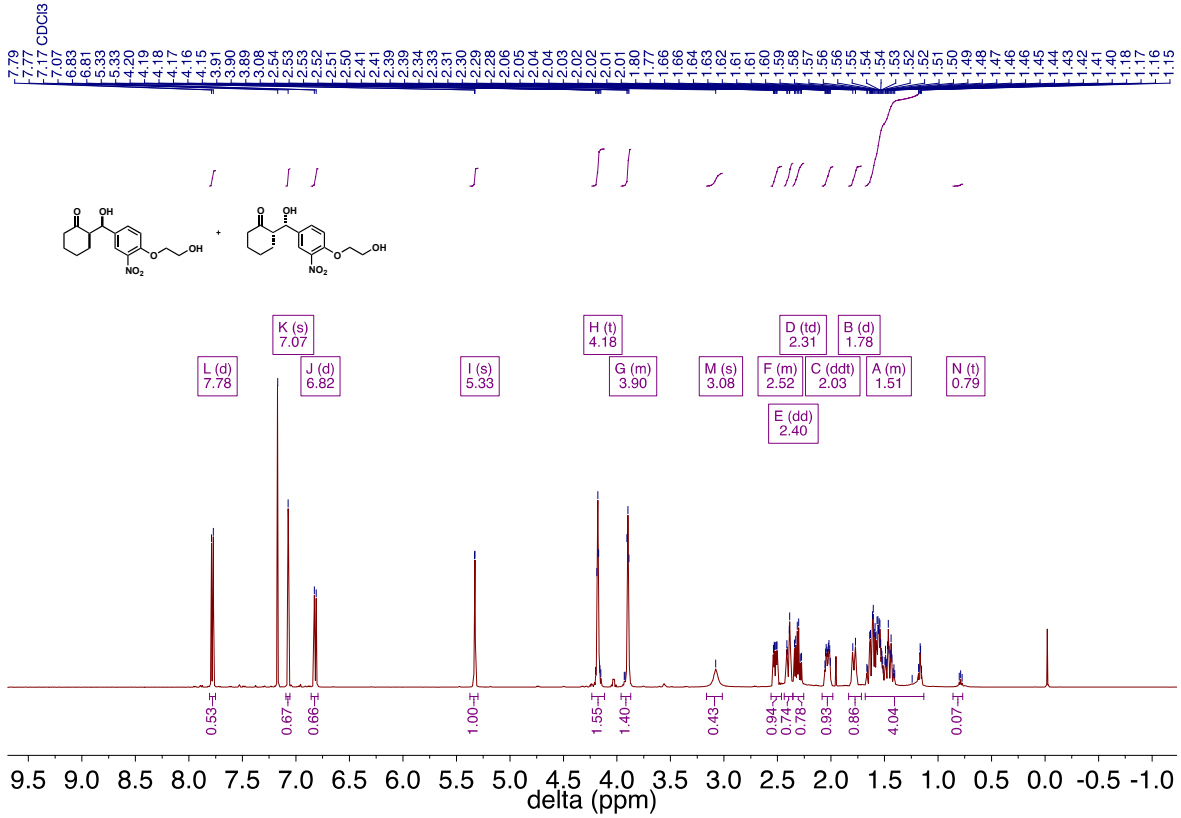

Compound **5a**, *syn*-isomer, ^{13}C

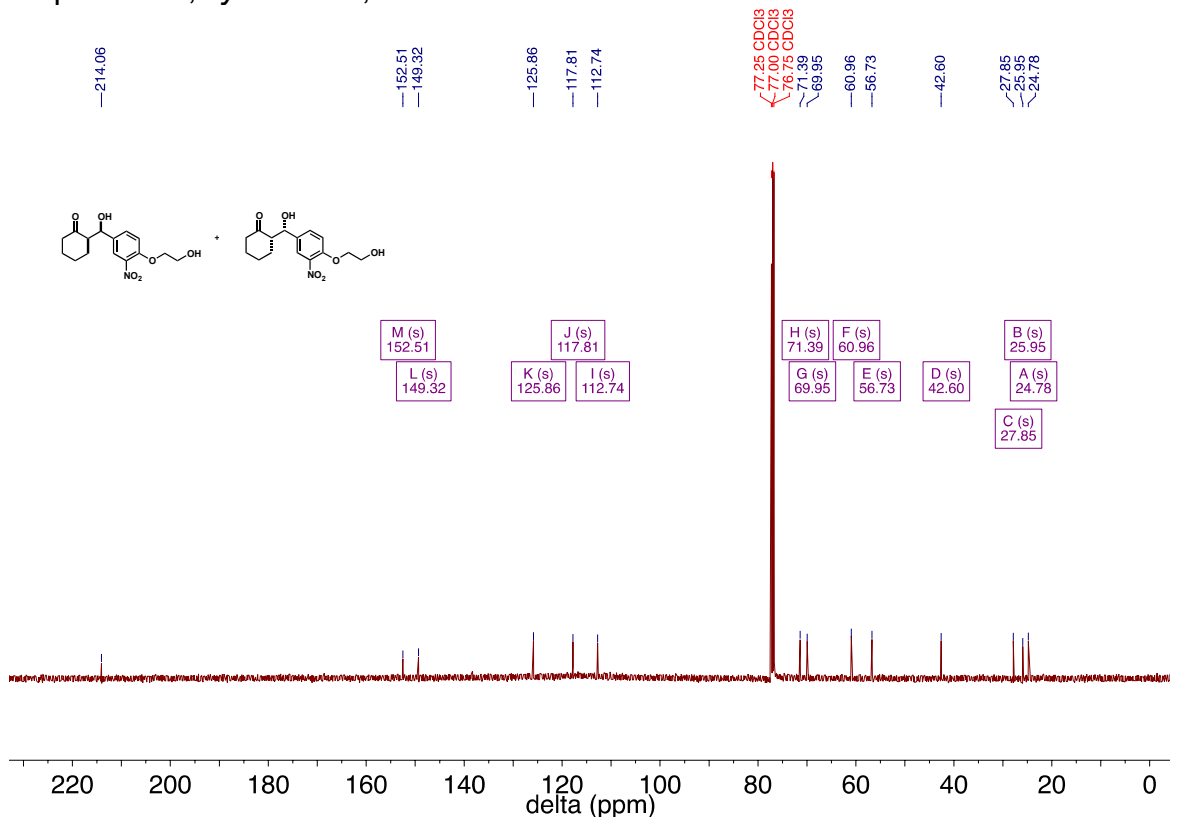

Compound **5b**, *anti*-isomer, ^{1}H

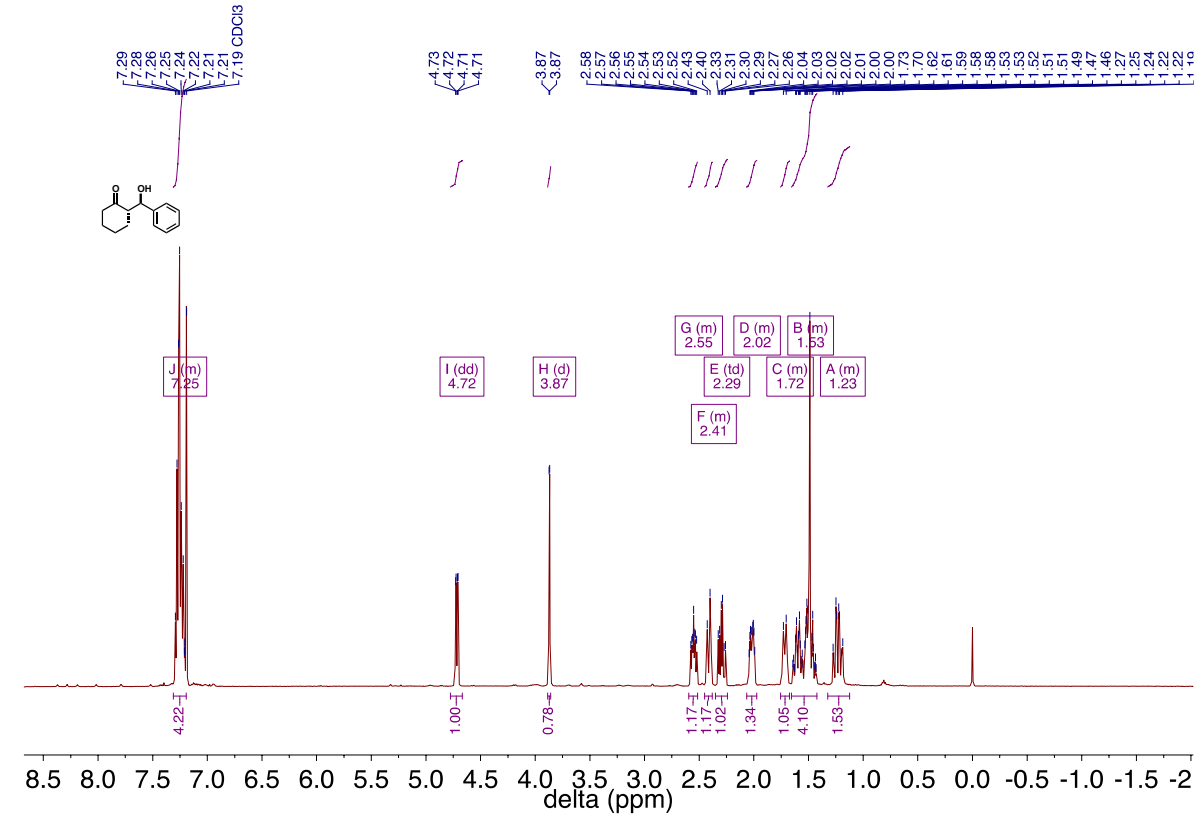

Compound **5b**, *anti*-isomer, ^{13}C

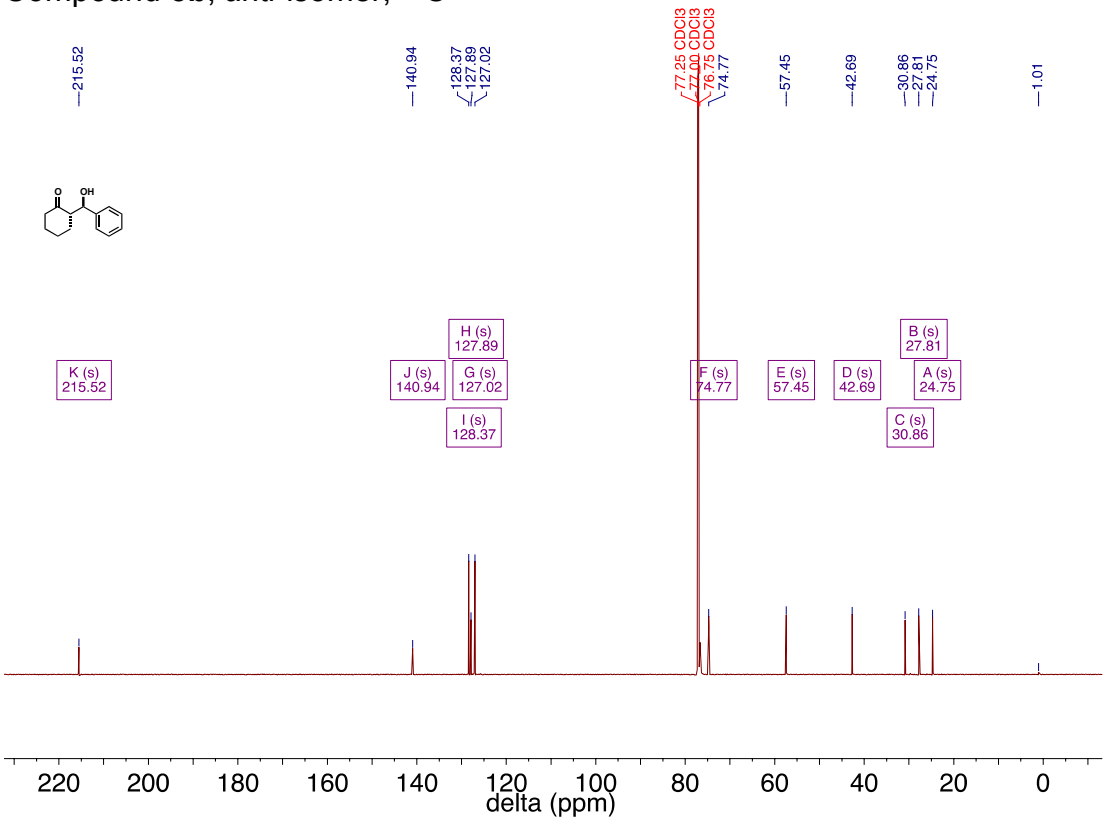

Compound **5b**, *syn*-isomer, ^{1}H

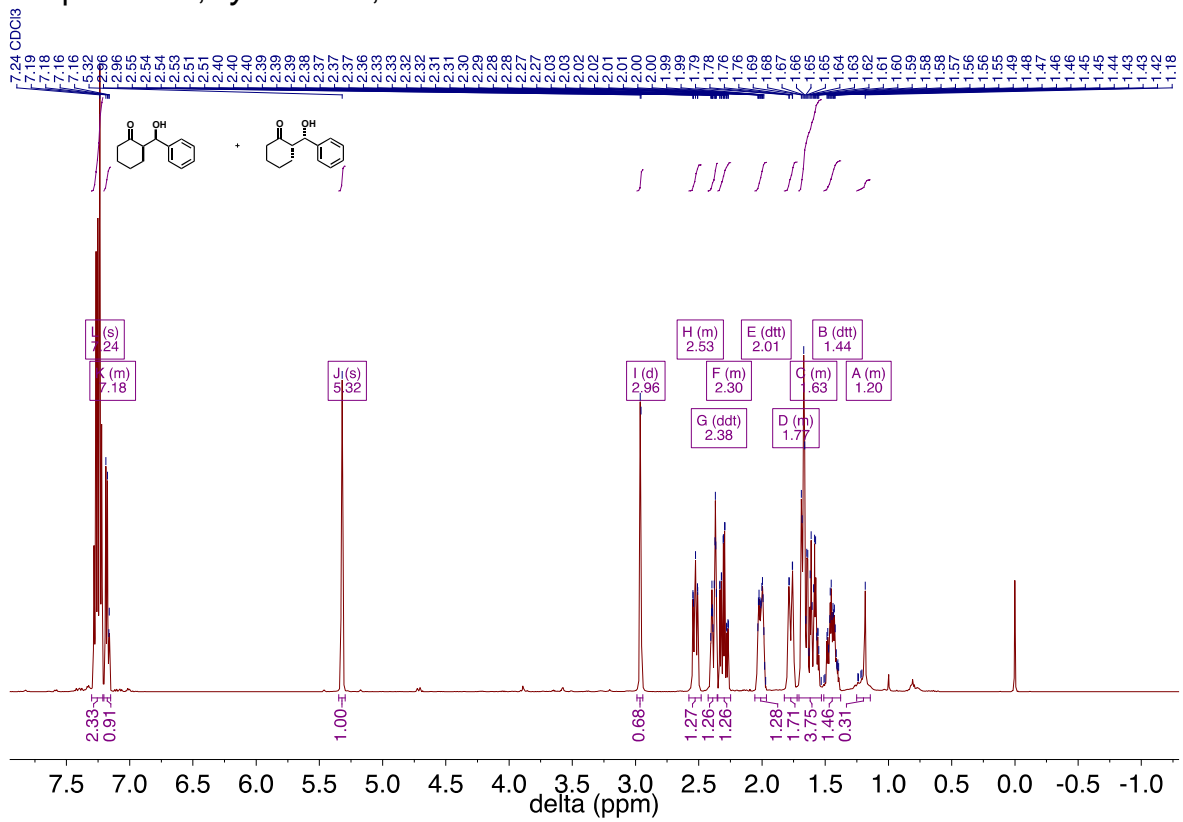

Compound **5b**, *syn*-isomer, ^{13}C

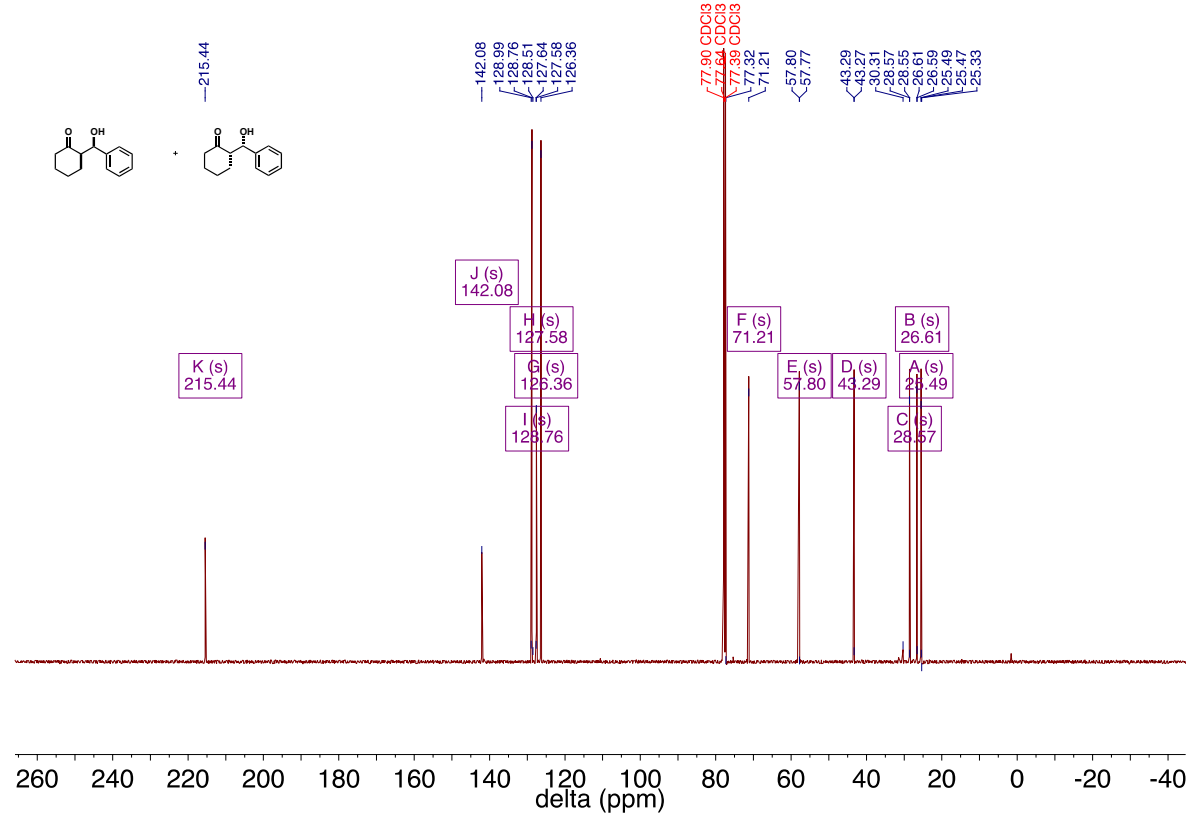

Compound **5c**, *anti*-isomer, ^{1}H

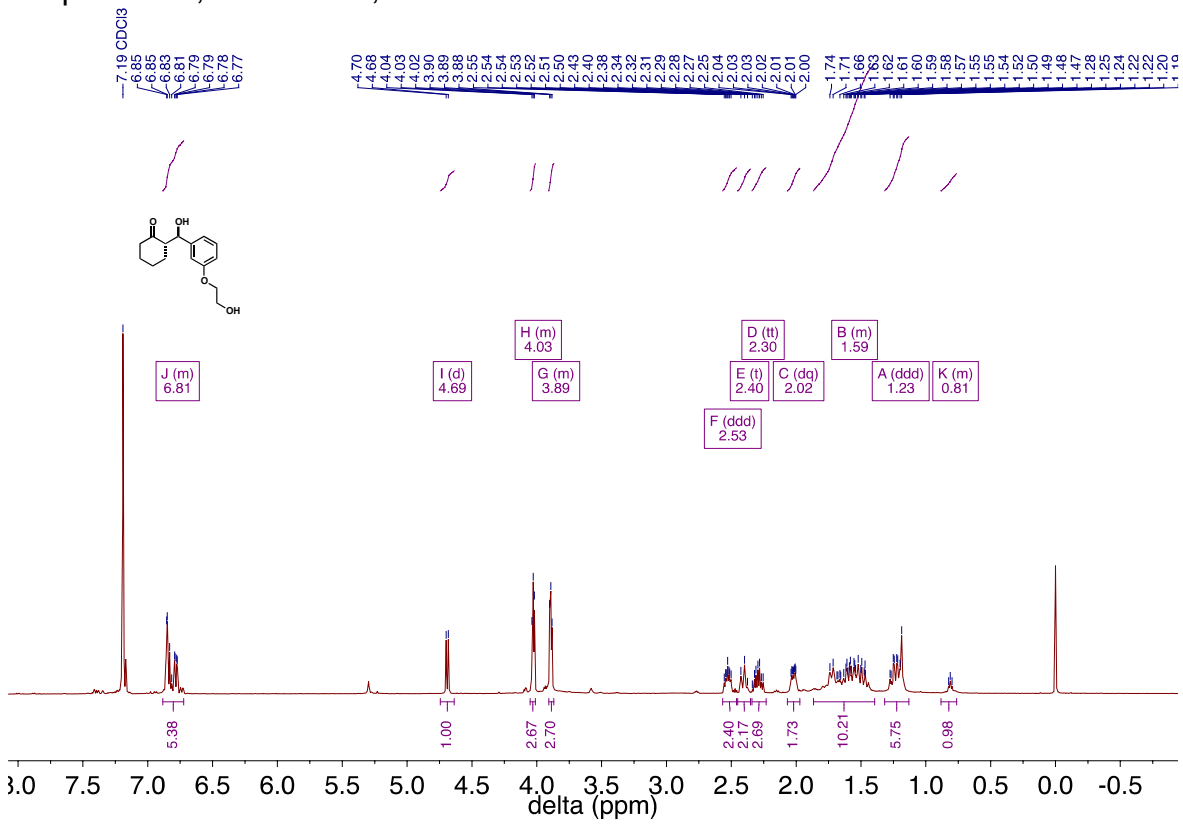

Compound **5c**, *anti*-isomer, ^{13}C

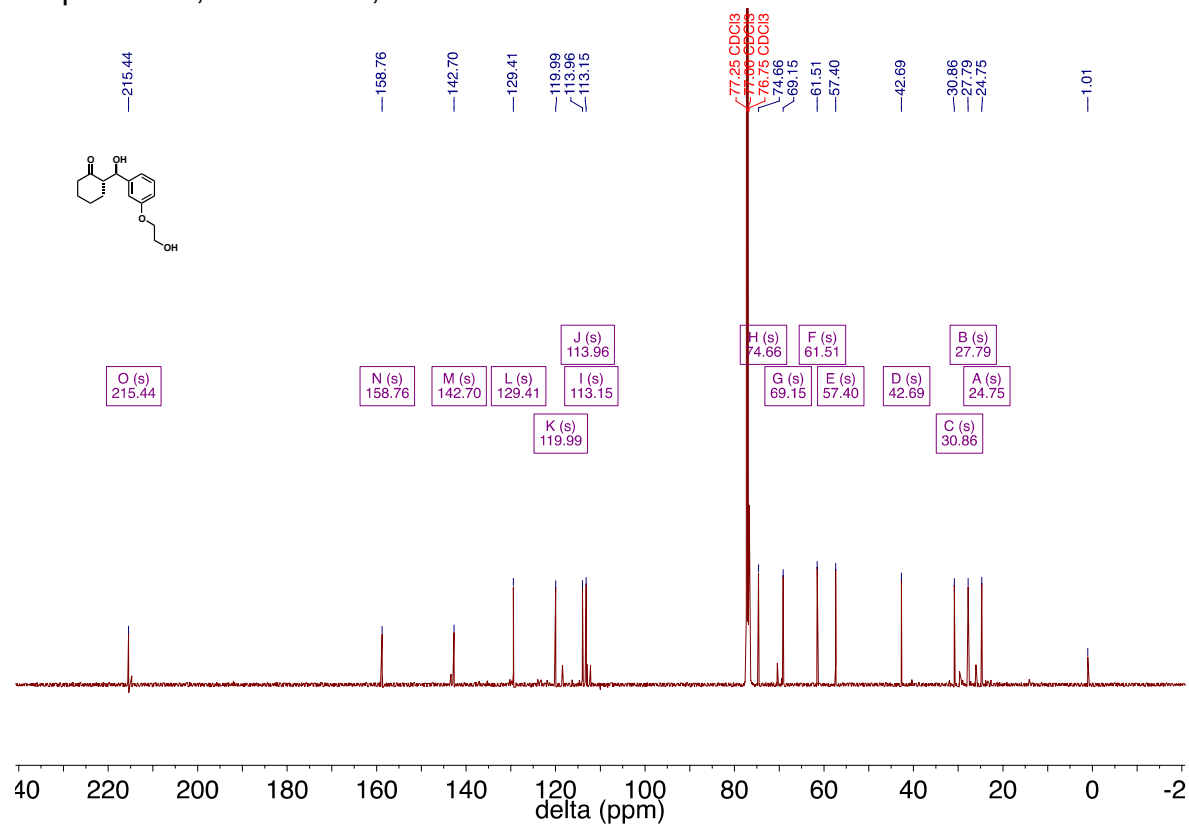

Compound **5c**, *syn*-isomer, ^{1}H

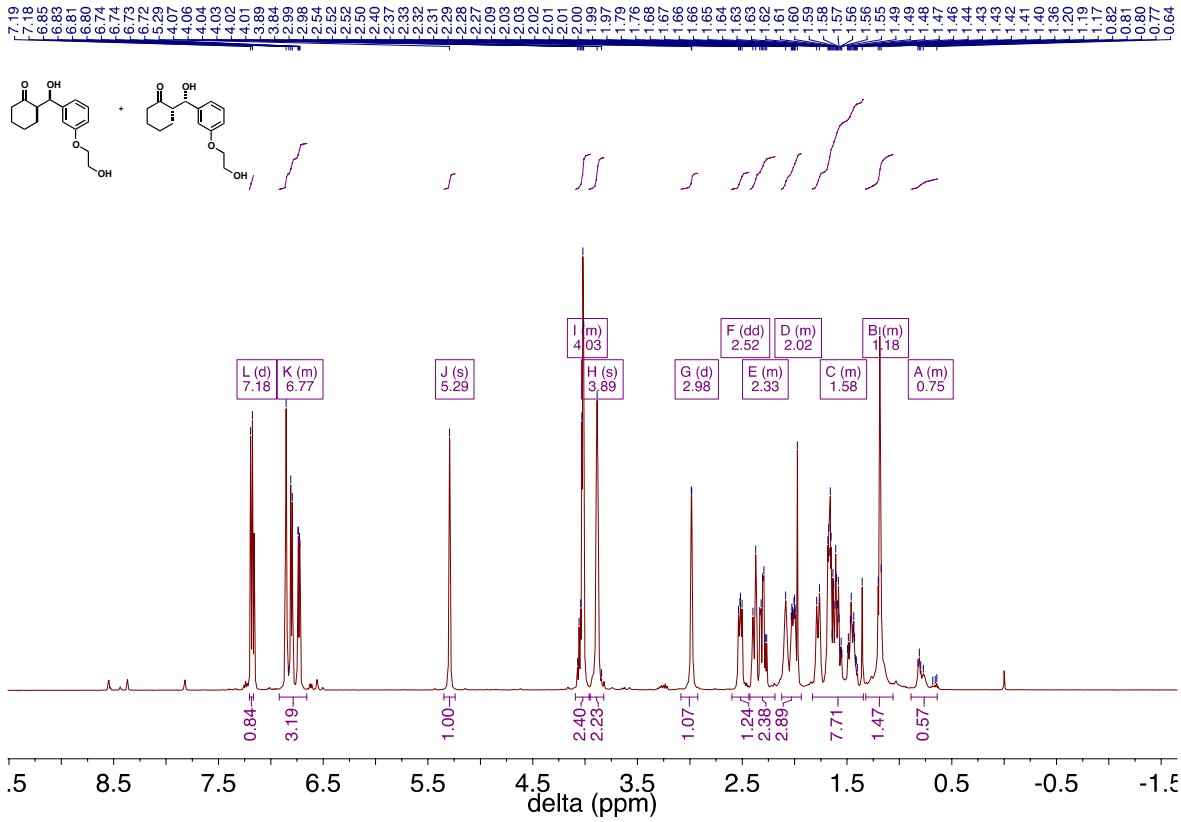

Compound **5c**, *syn*-isomer, ^{13}C

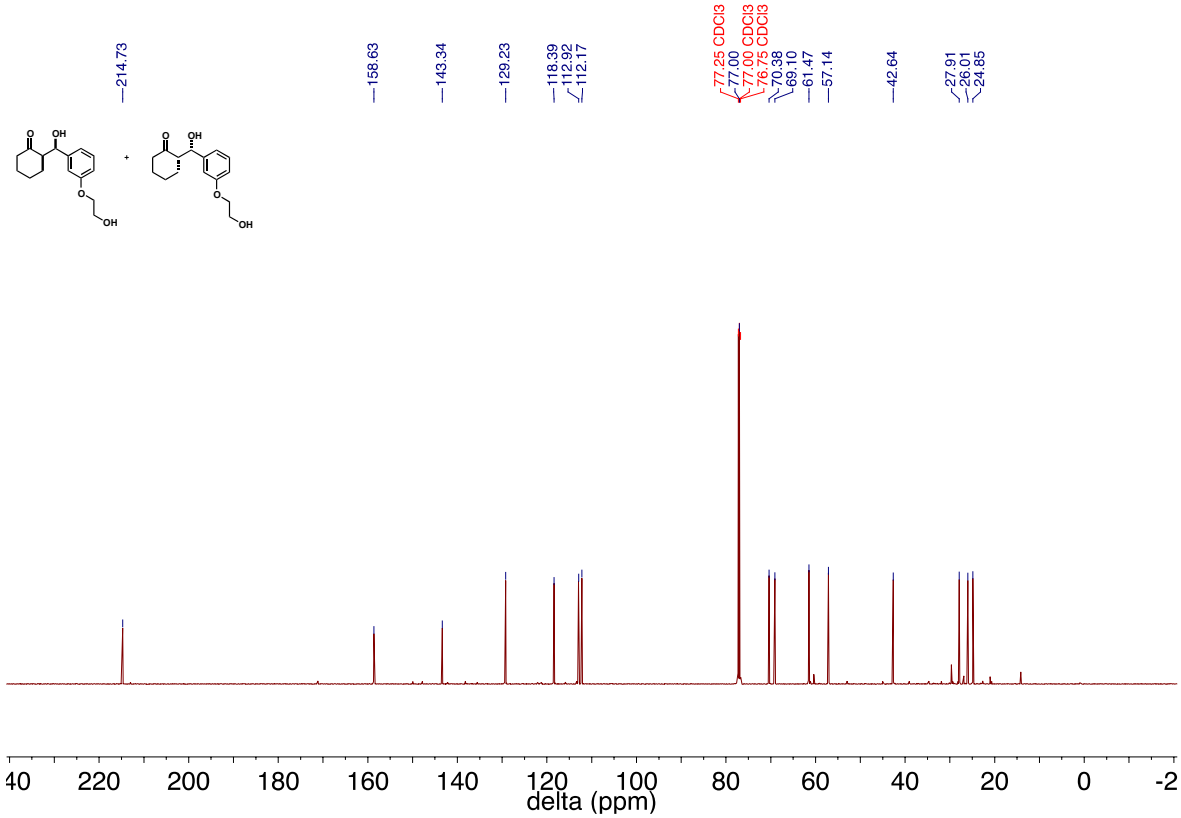

Compound **22**, ^{1}H

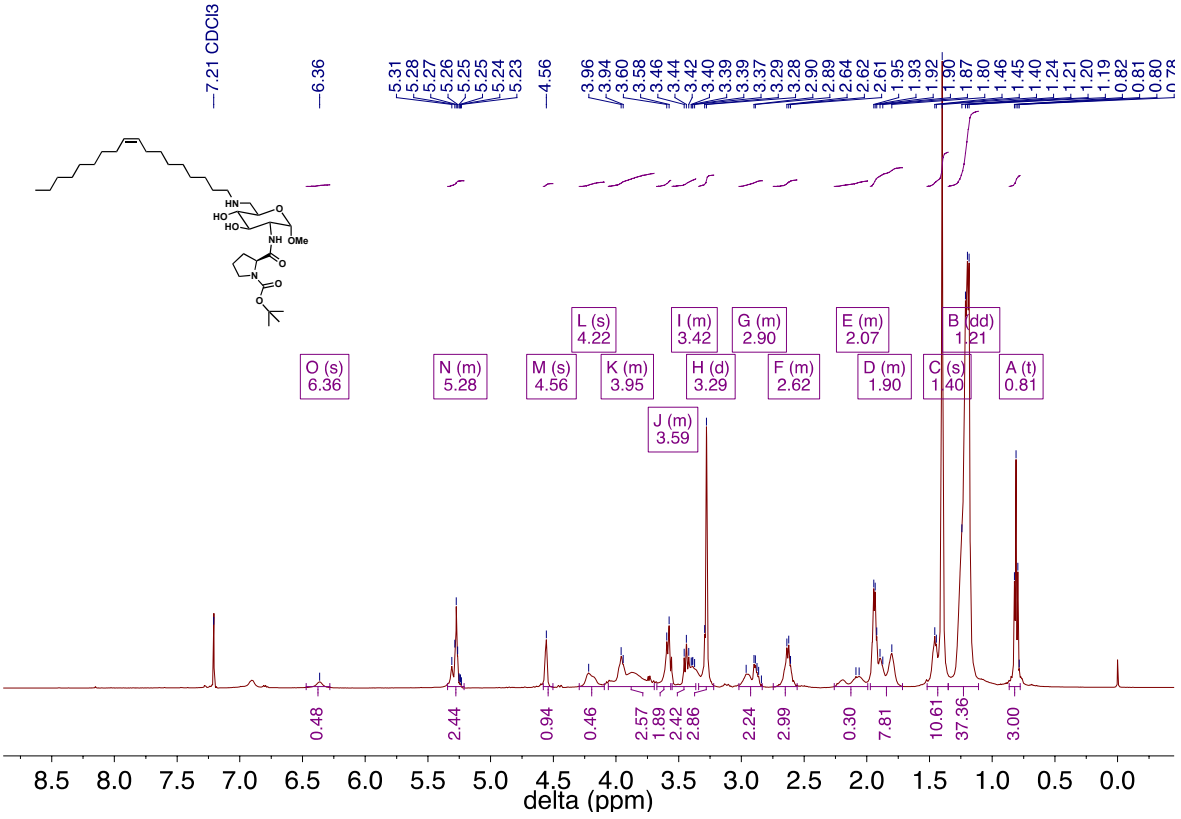

Compound **22**, ^{13}C

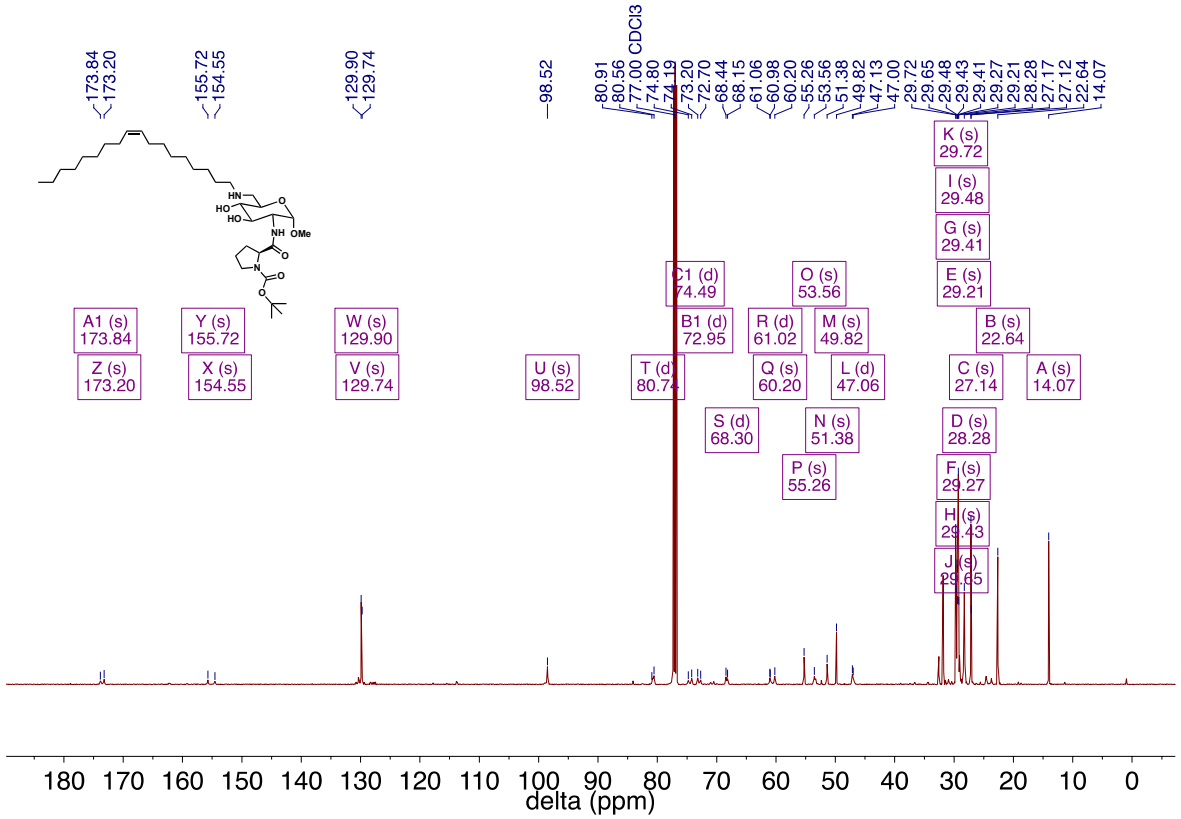

Compound **23**, ^{1}H

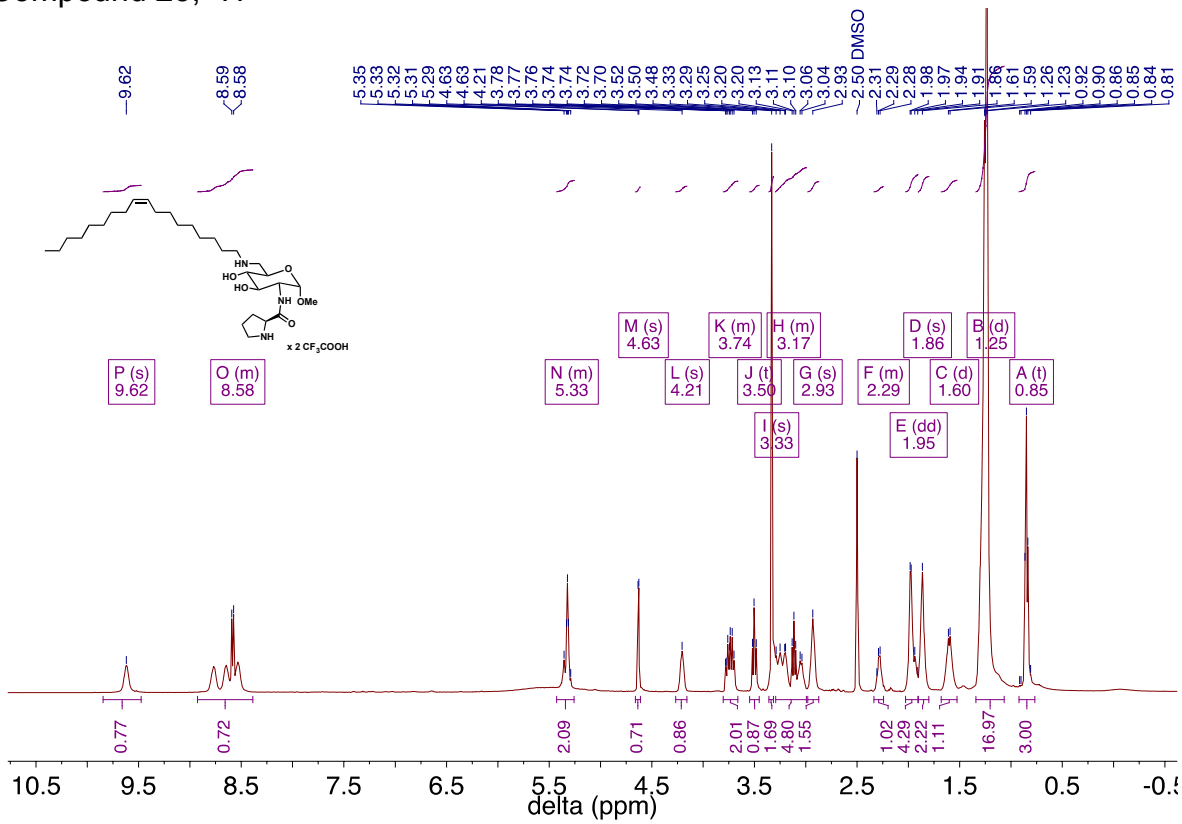

Compound **23**, ^{13}C

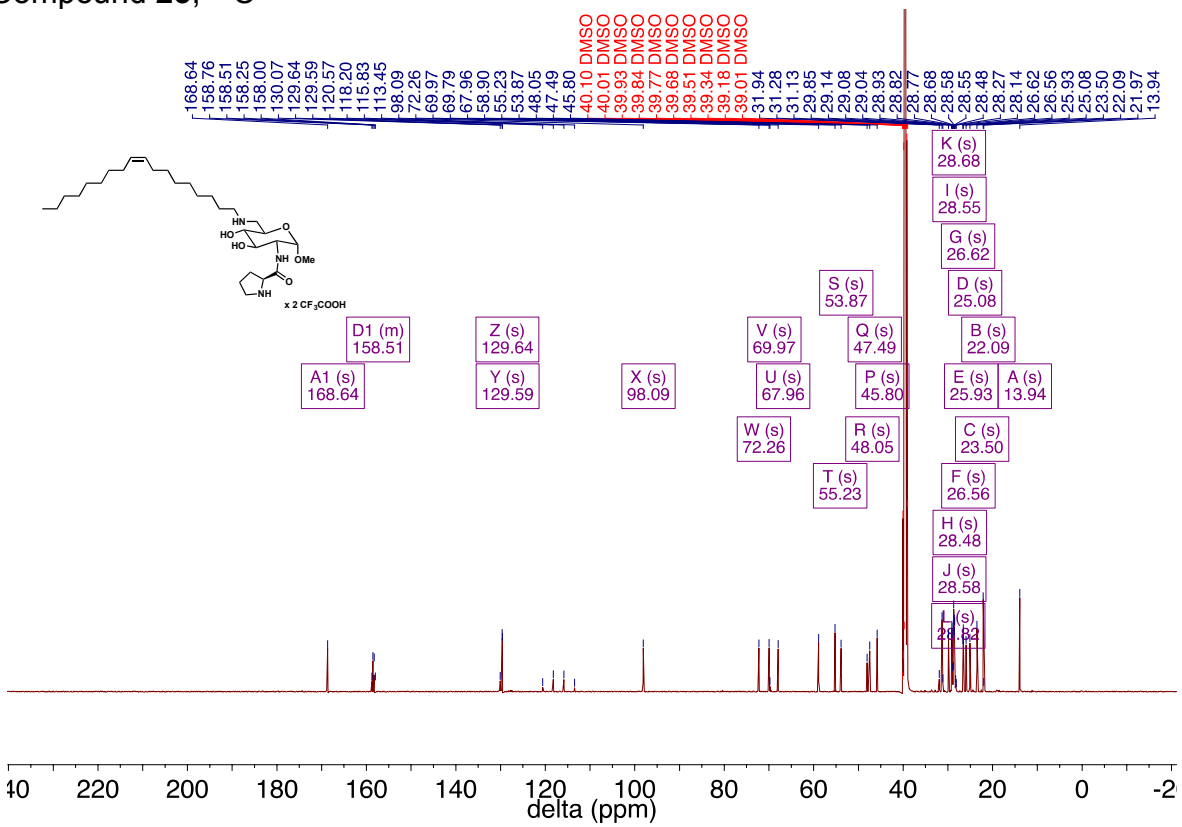

Compound **26**, ^{1}H

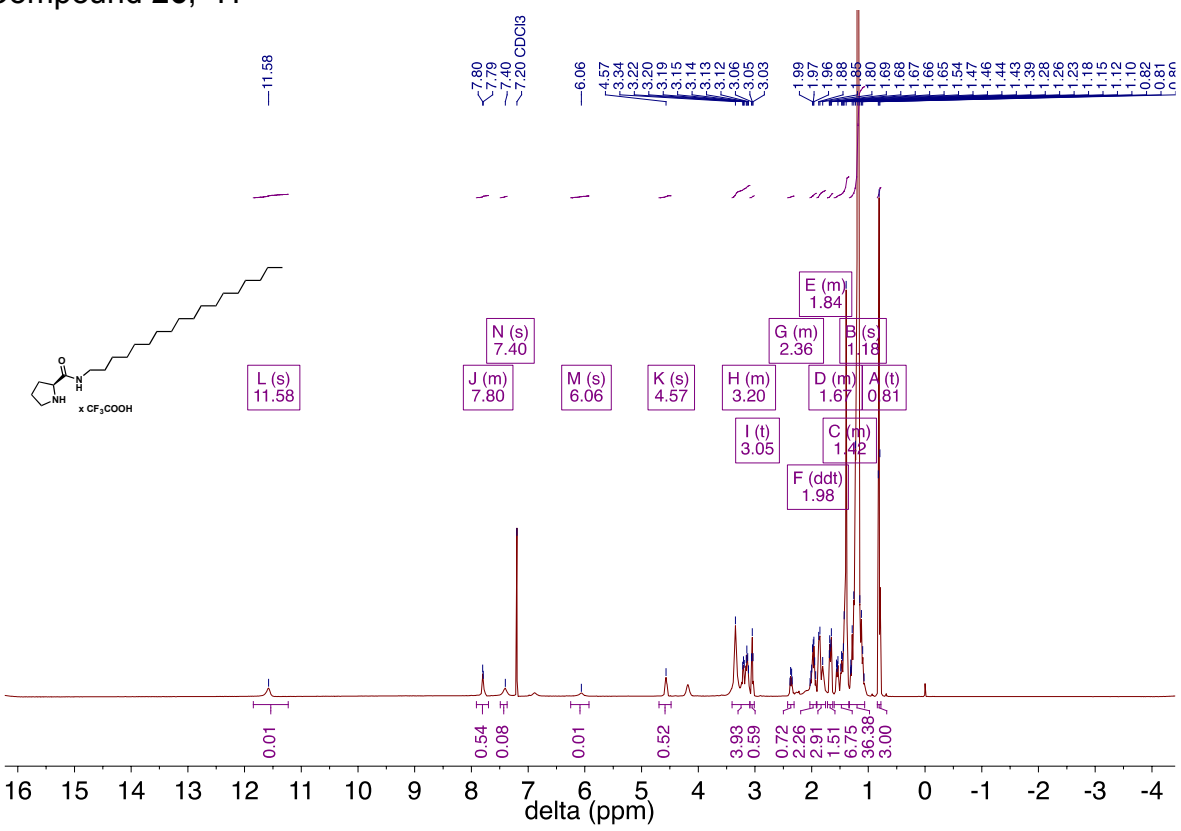

Compound **26**, ^{13}C

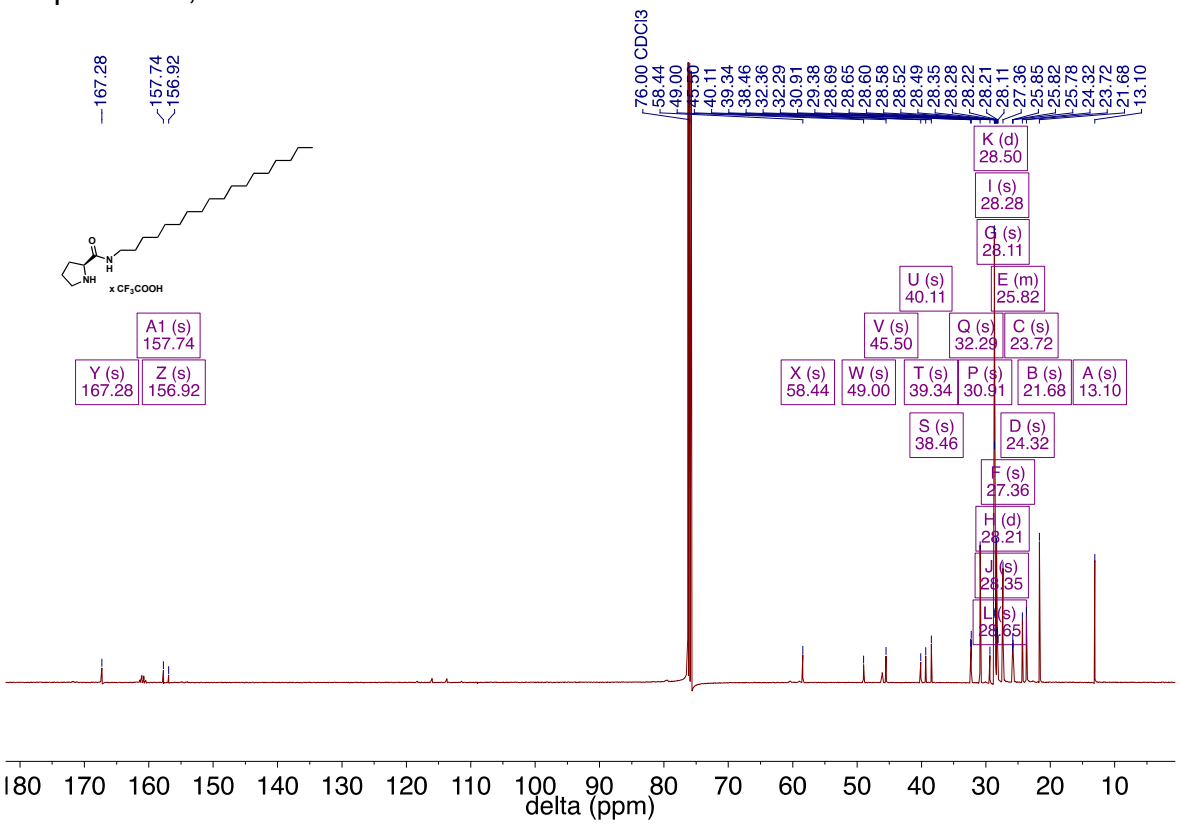

Compound **27**, ^{1}H

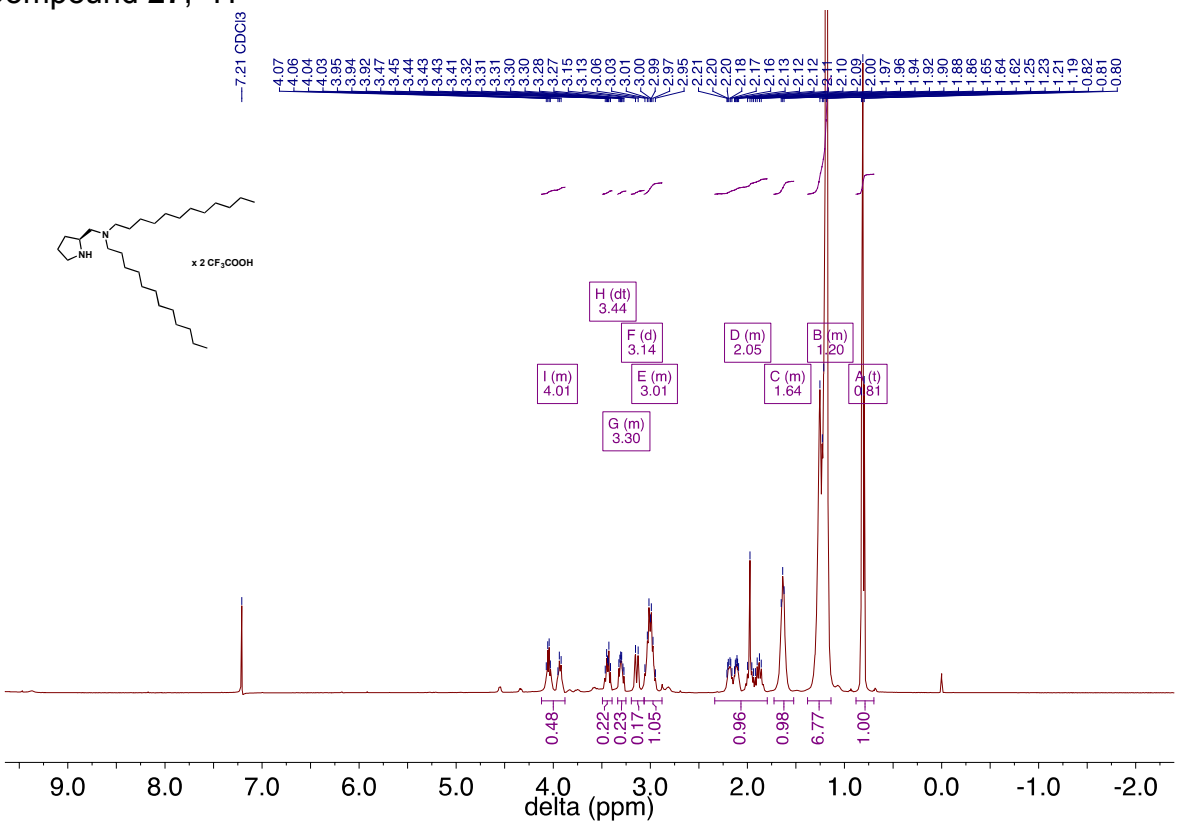

Compound **27**, ^{13}C

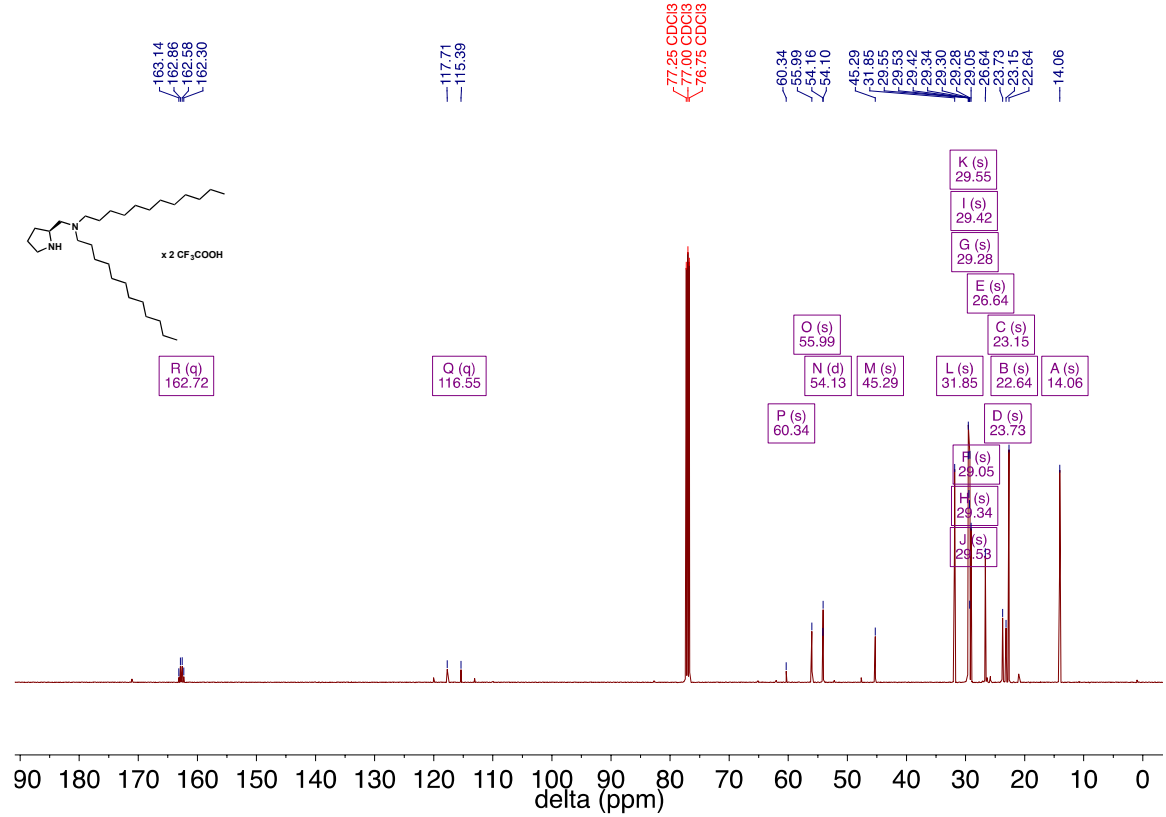

Compound **28**, ^{1}H

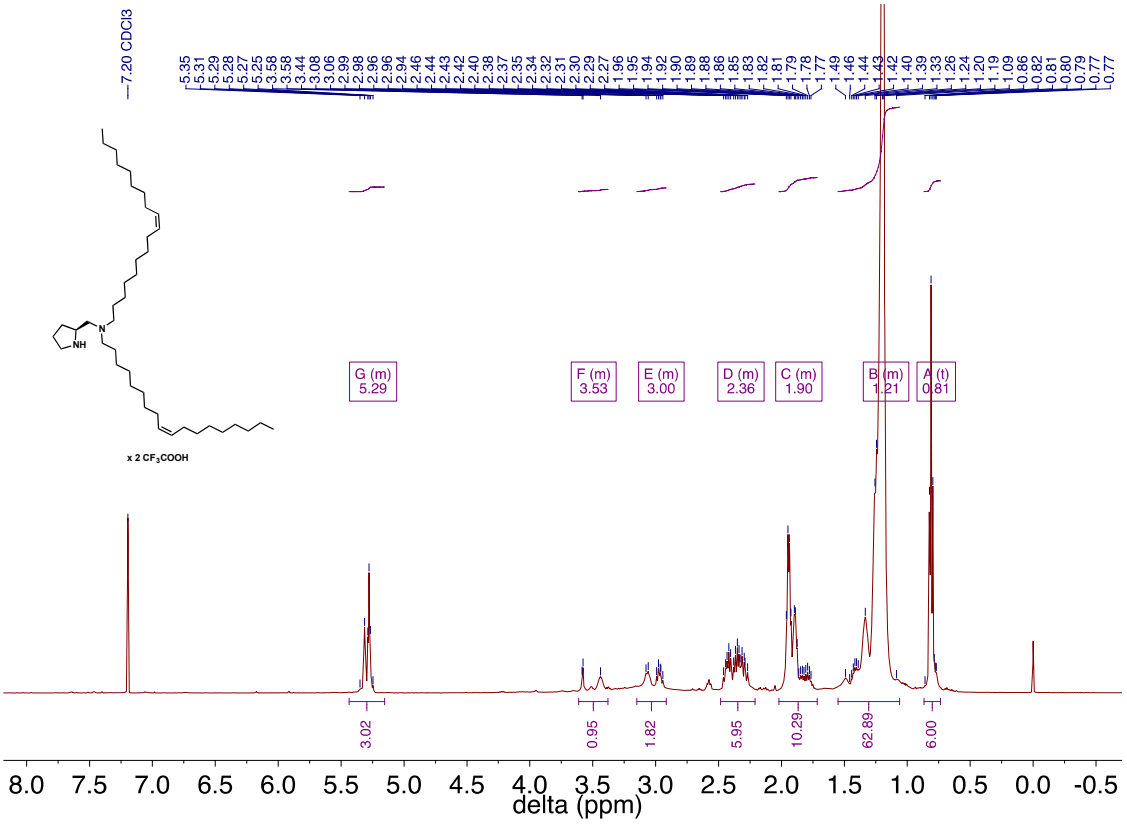

Compound **28**, ^{13}C

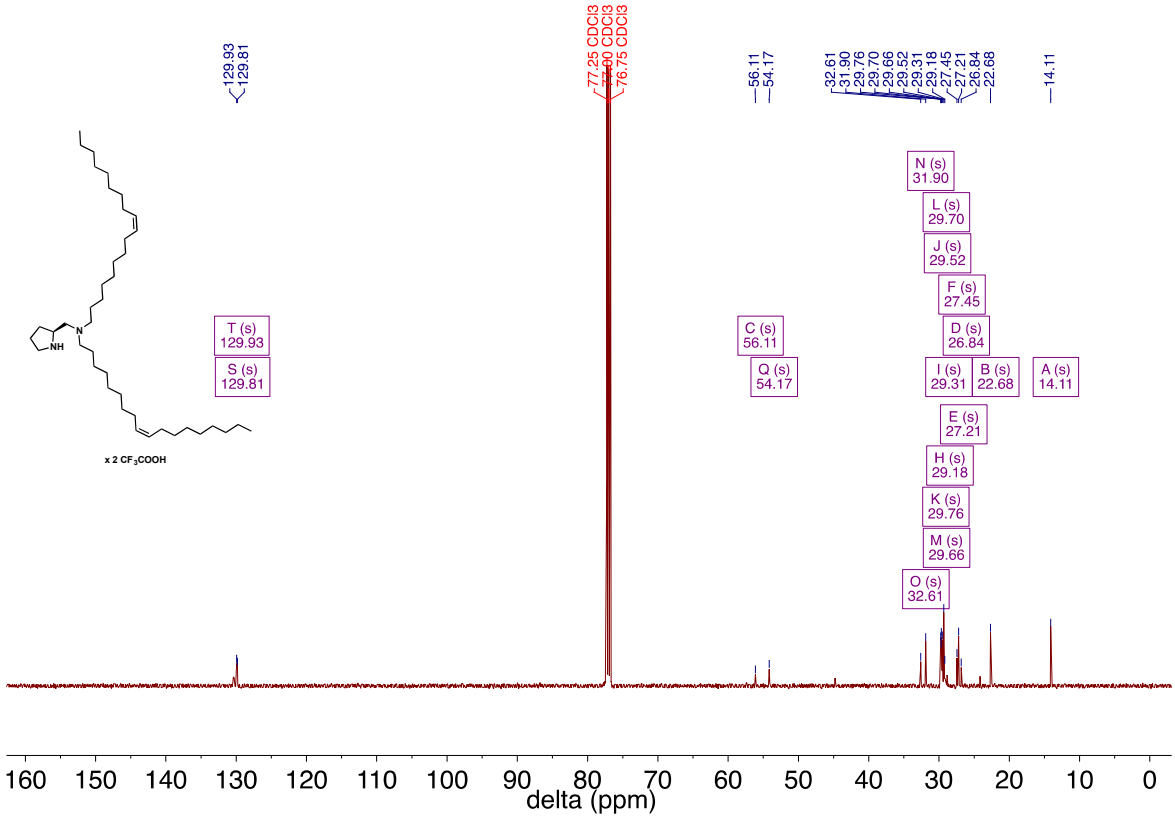

Compound **29**, ^{1}H

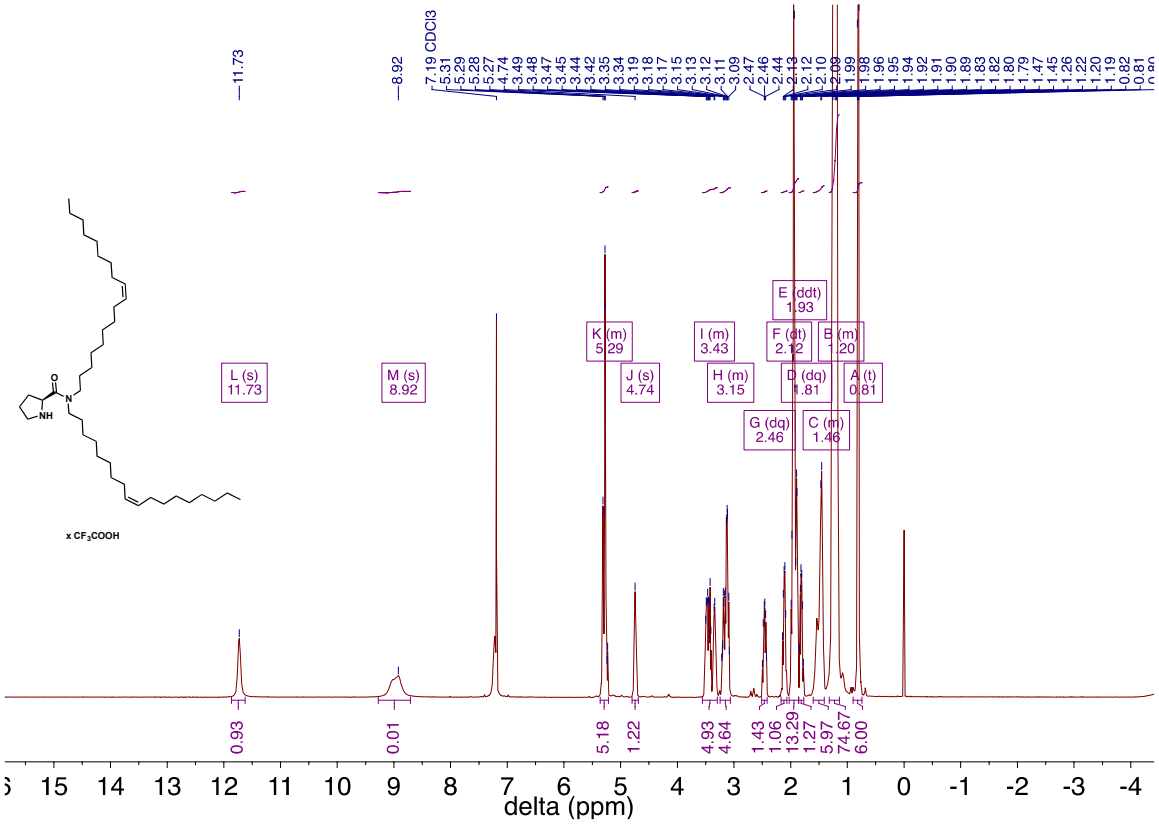

Compound **29**, ^{13}C

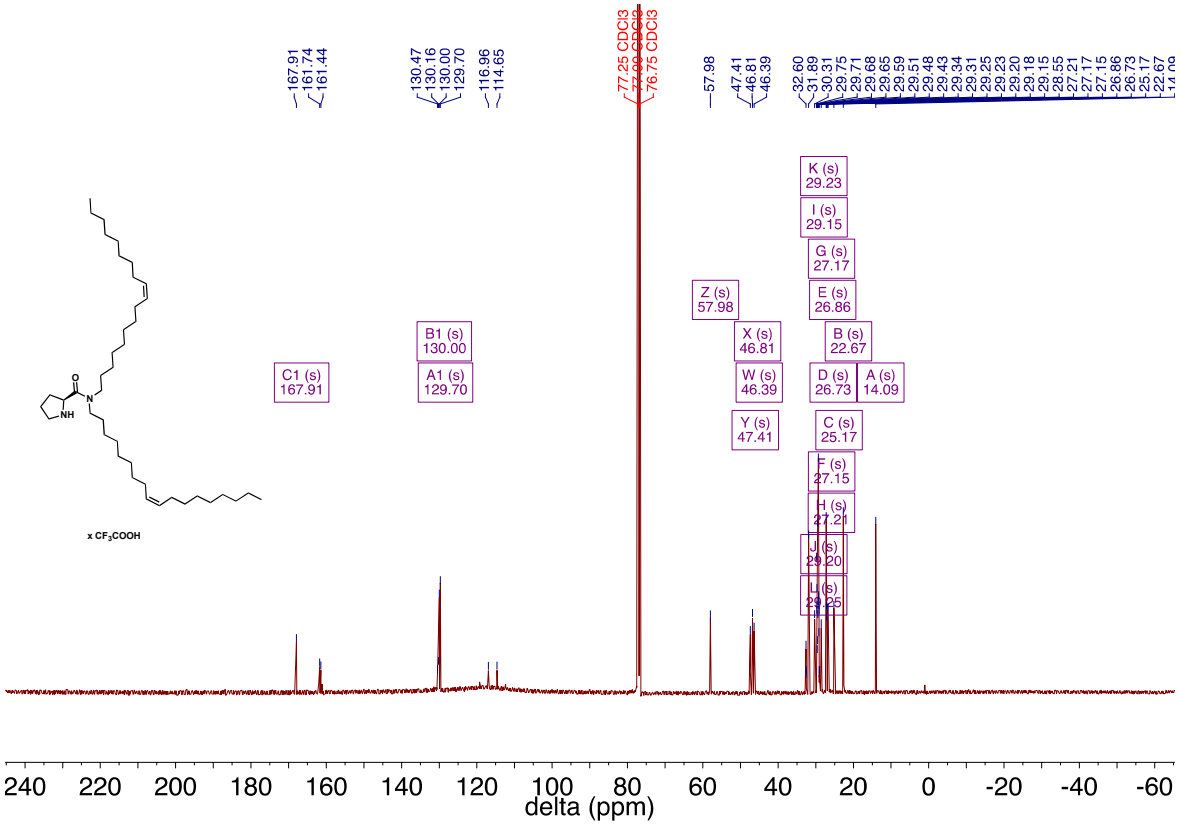

Compound **31**, ^{1}H

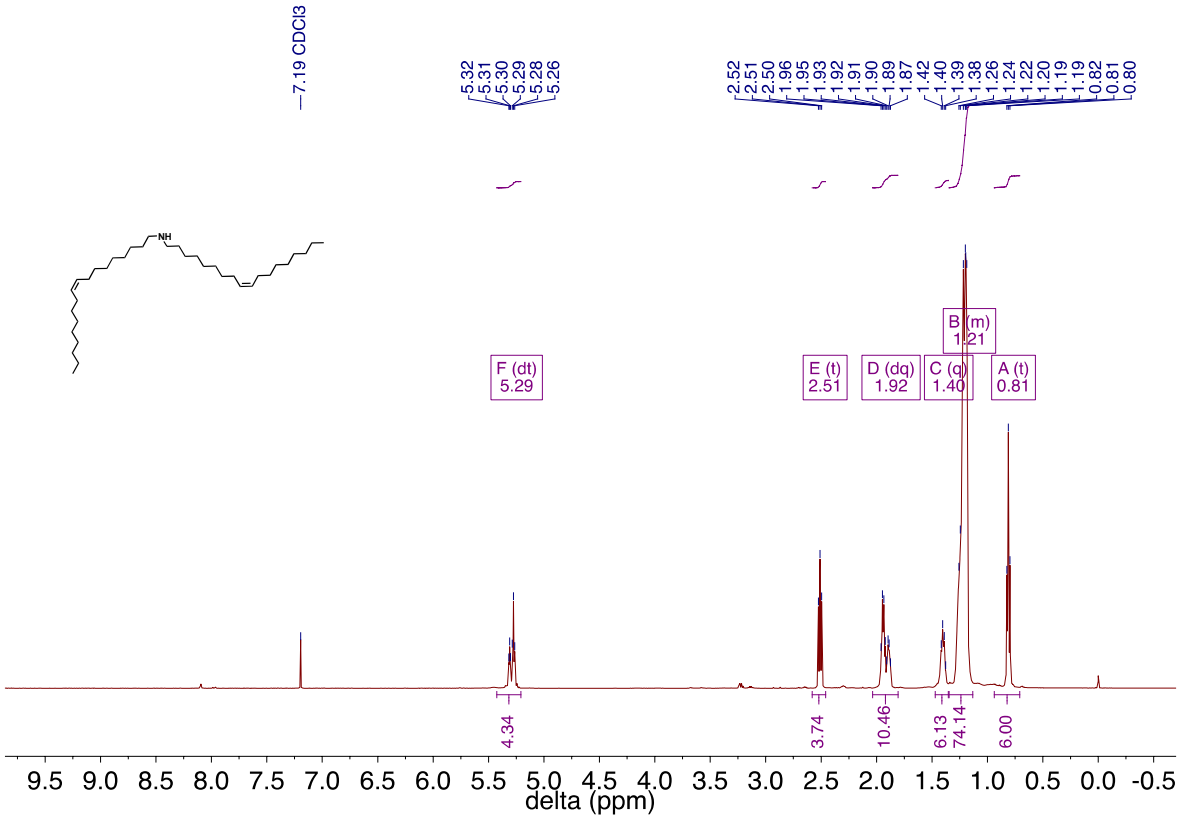

Compound **31**, ^{13}C

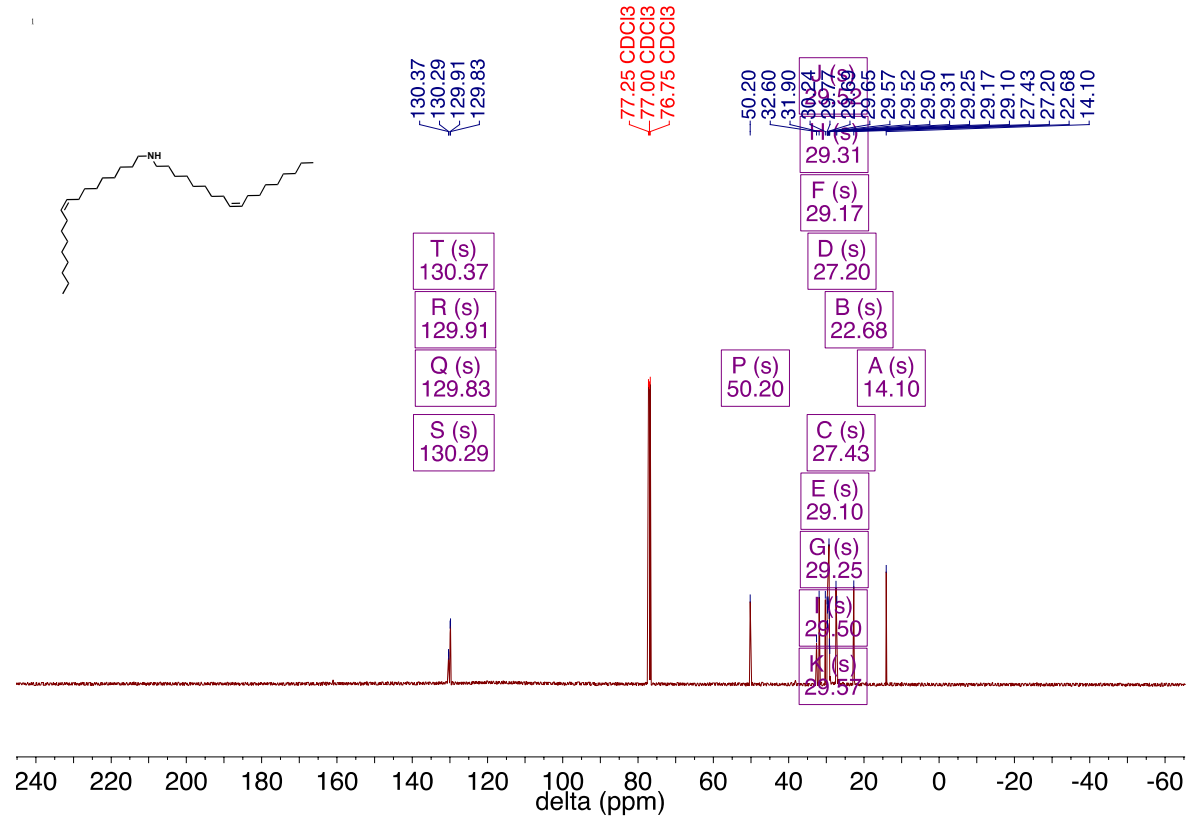

Compound **60**, ^{1}H

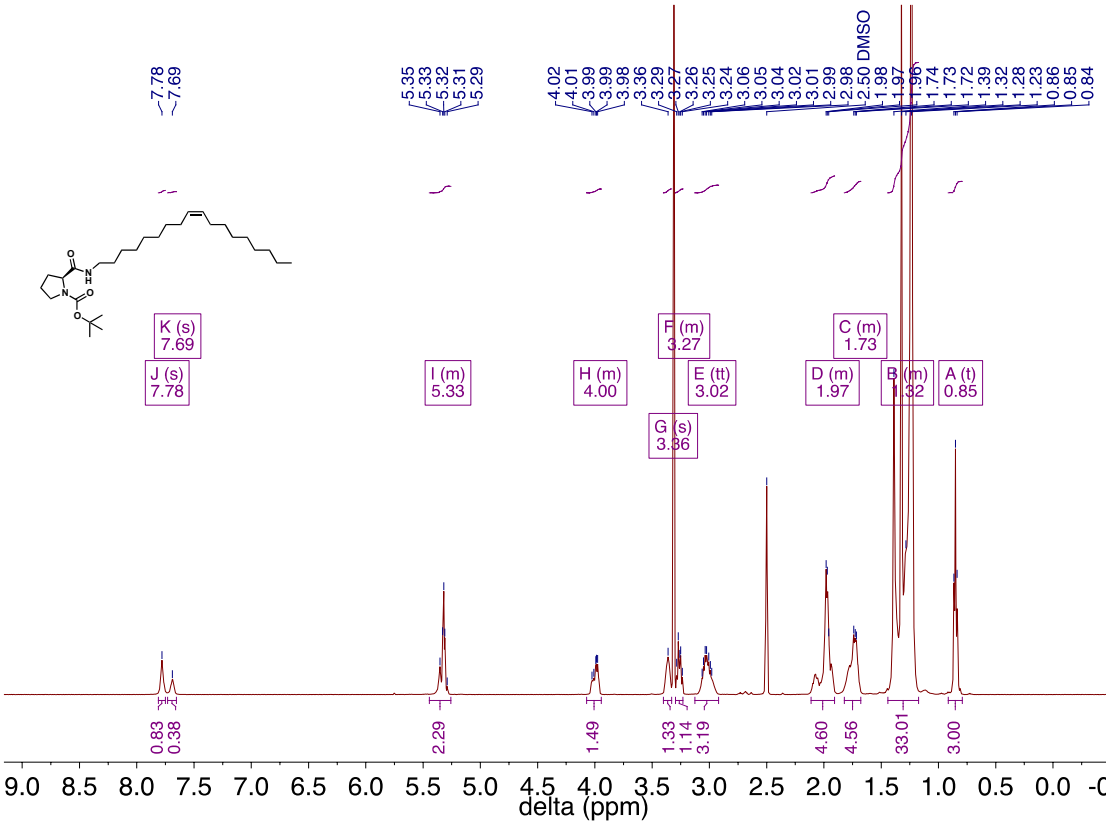

Compound **60**, ^{13}C

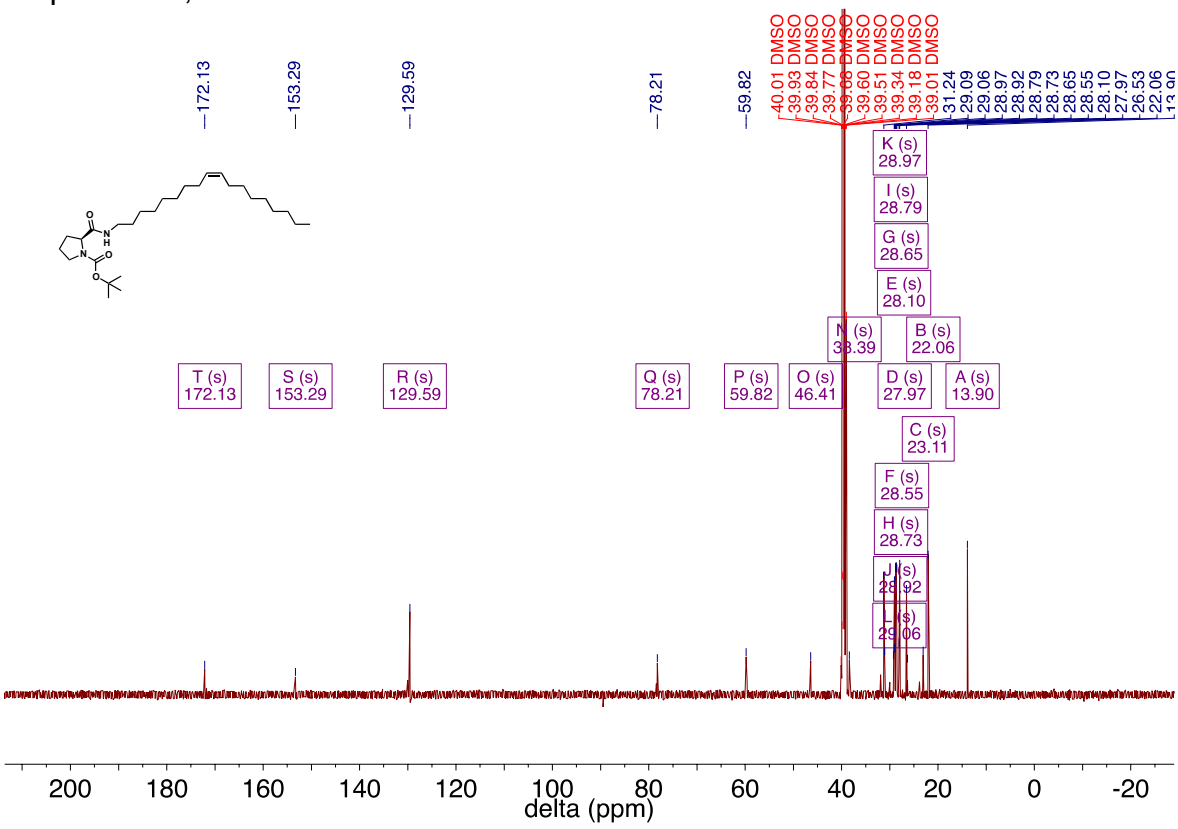

Compound **61**, ^{1}H

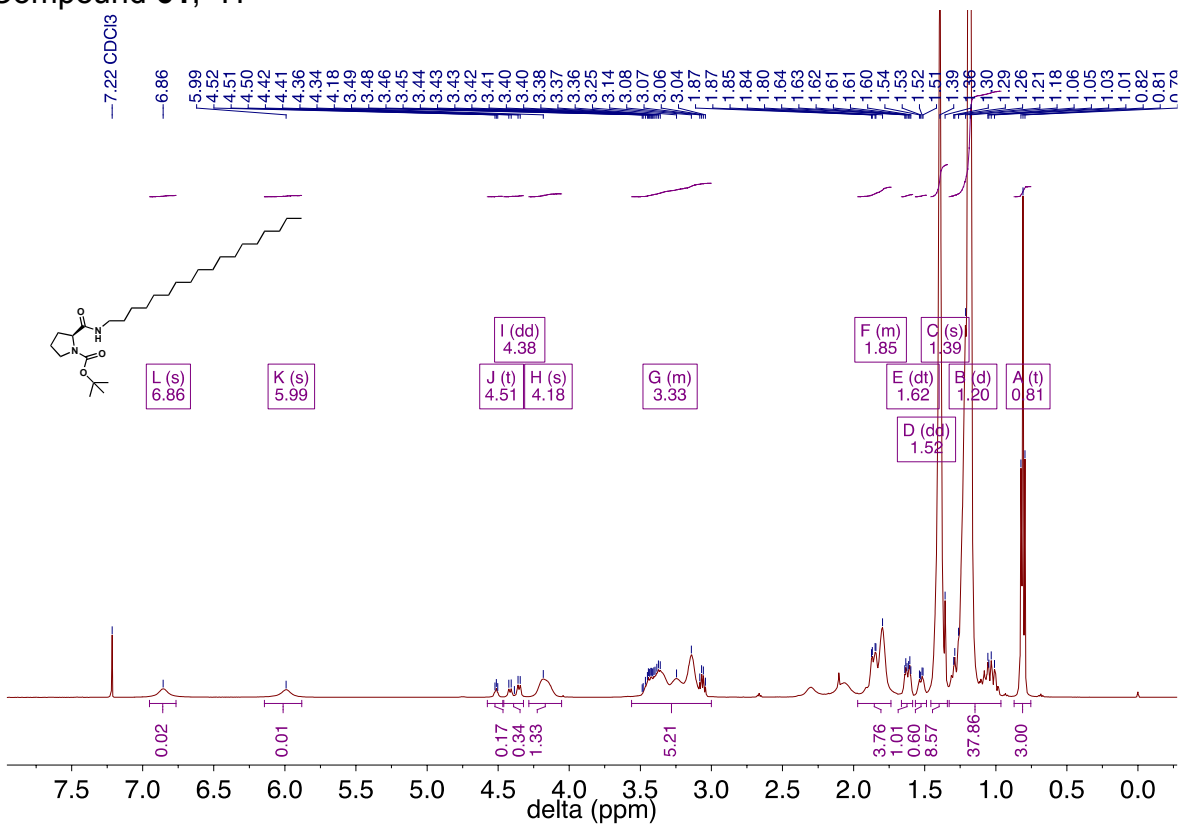

Compound **61**, ^{13}C

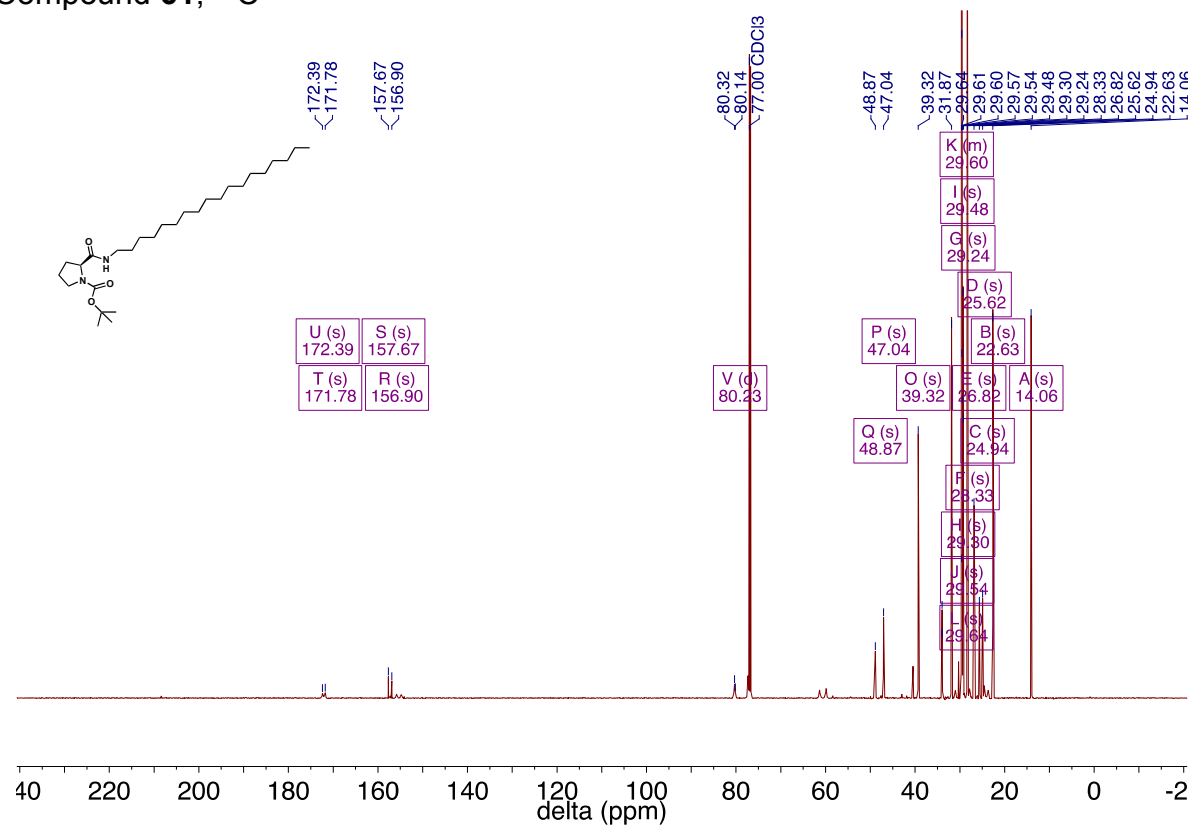

Compound **62**, ^{1}H

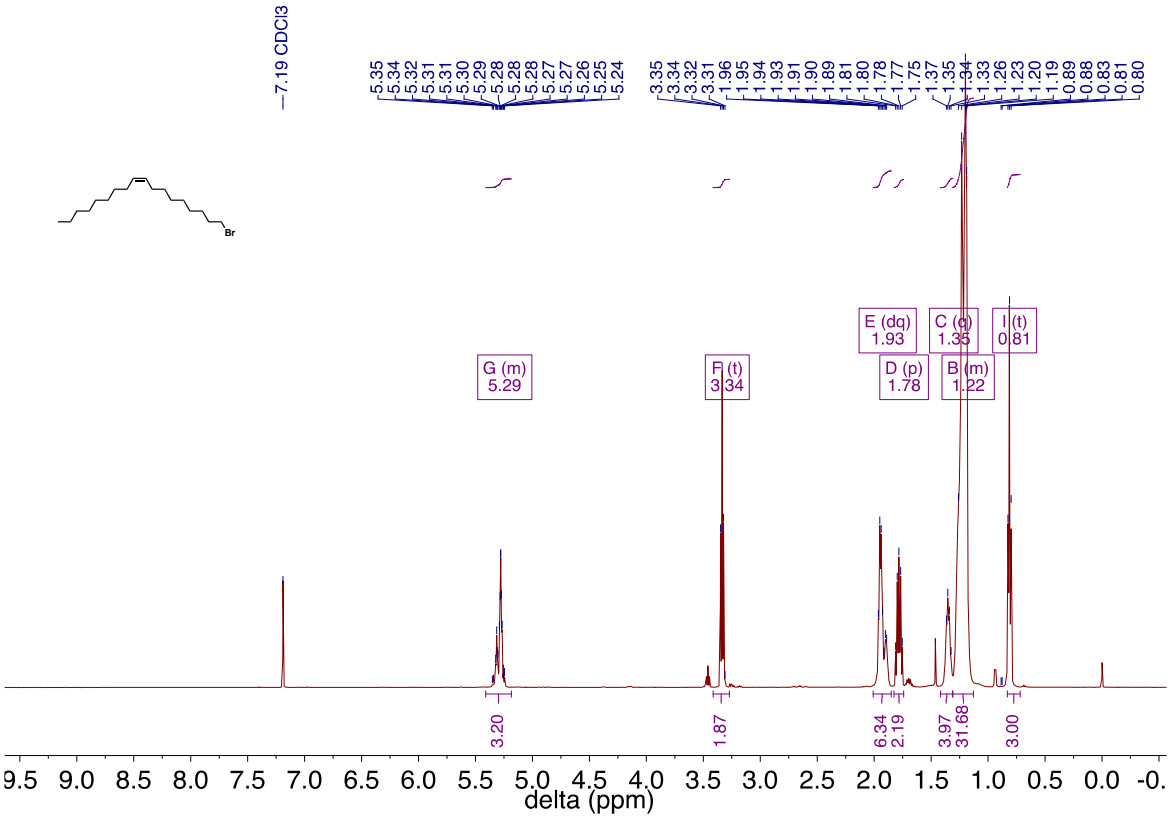

Compound **62**, ^{13}C

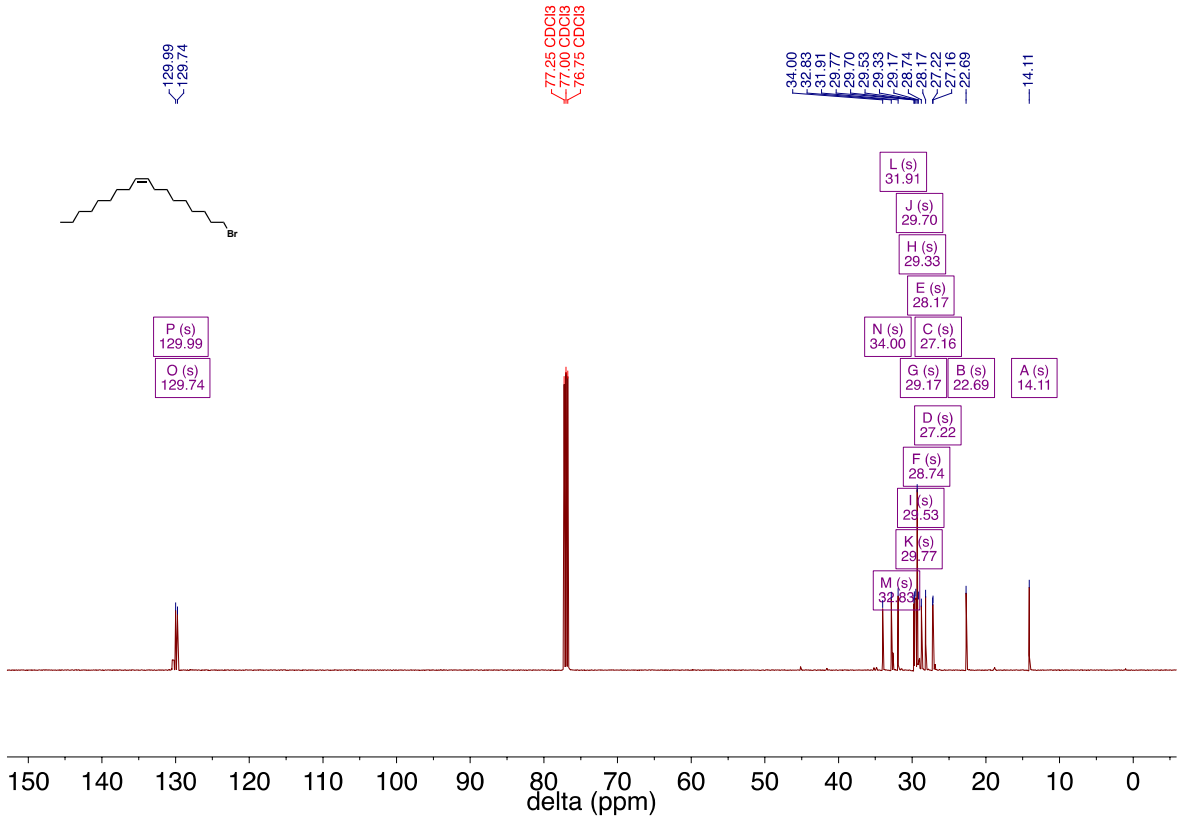

Compound **63**, ^{1}H

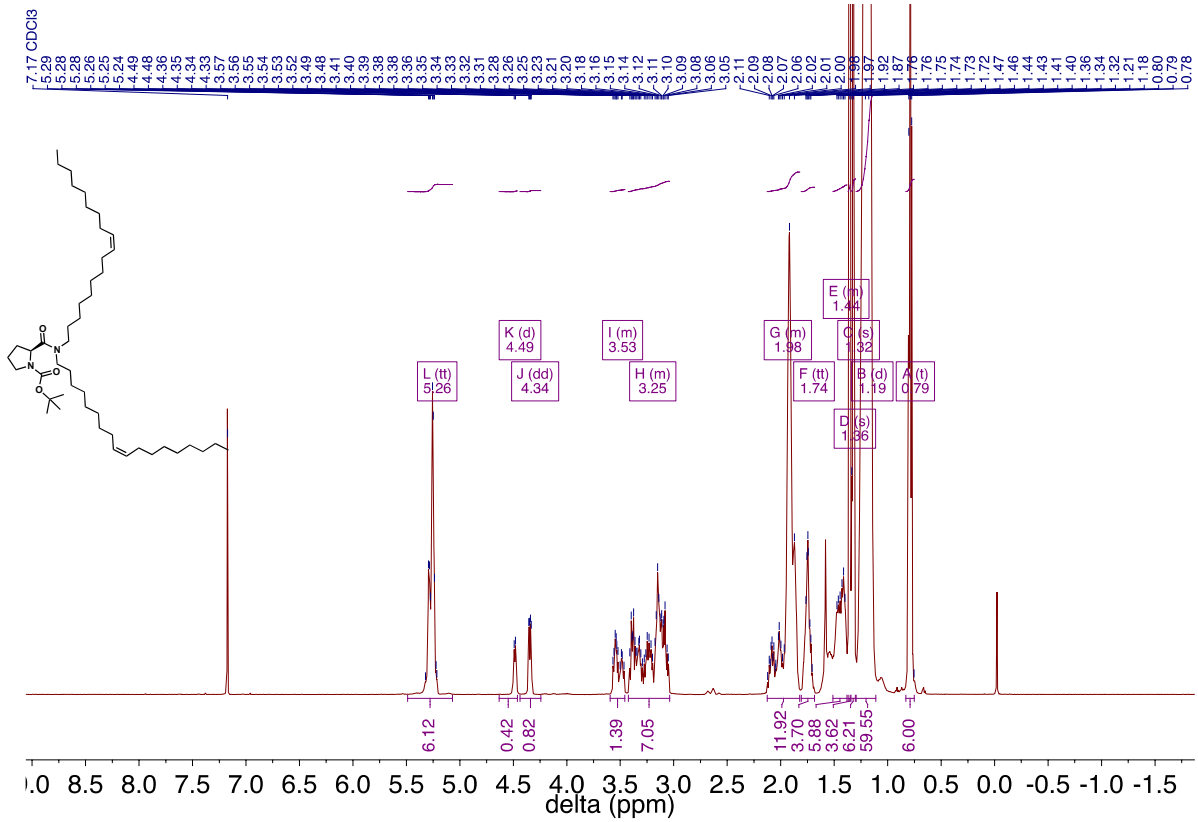

Compound **63**, ^{13}C

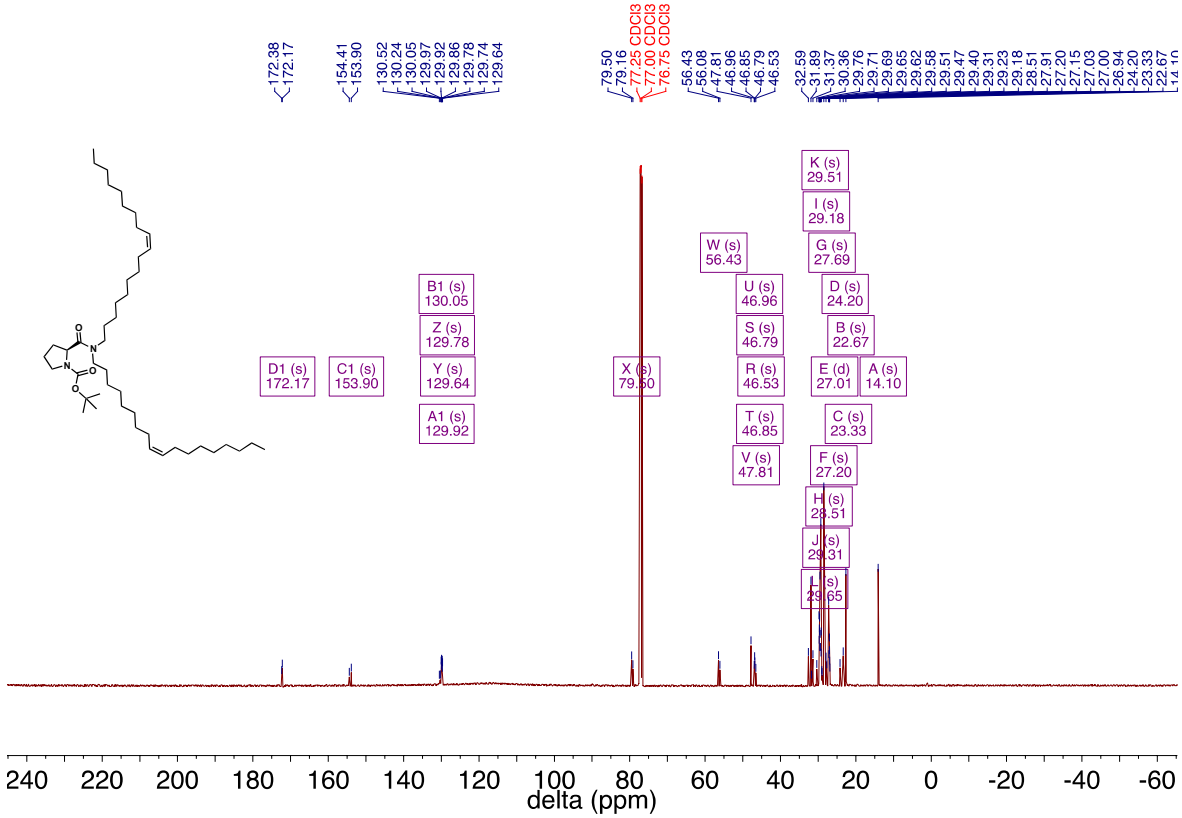

Compound **64**, ^{1}H

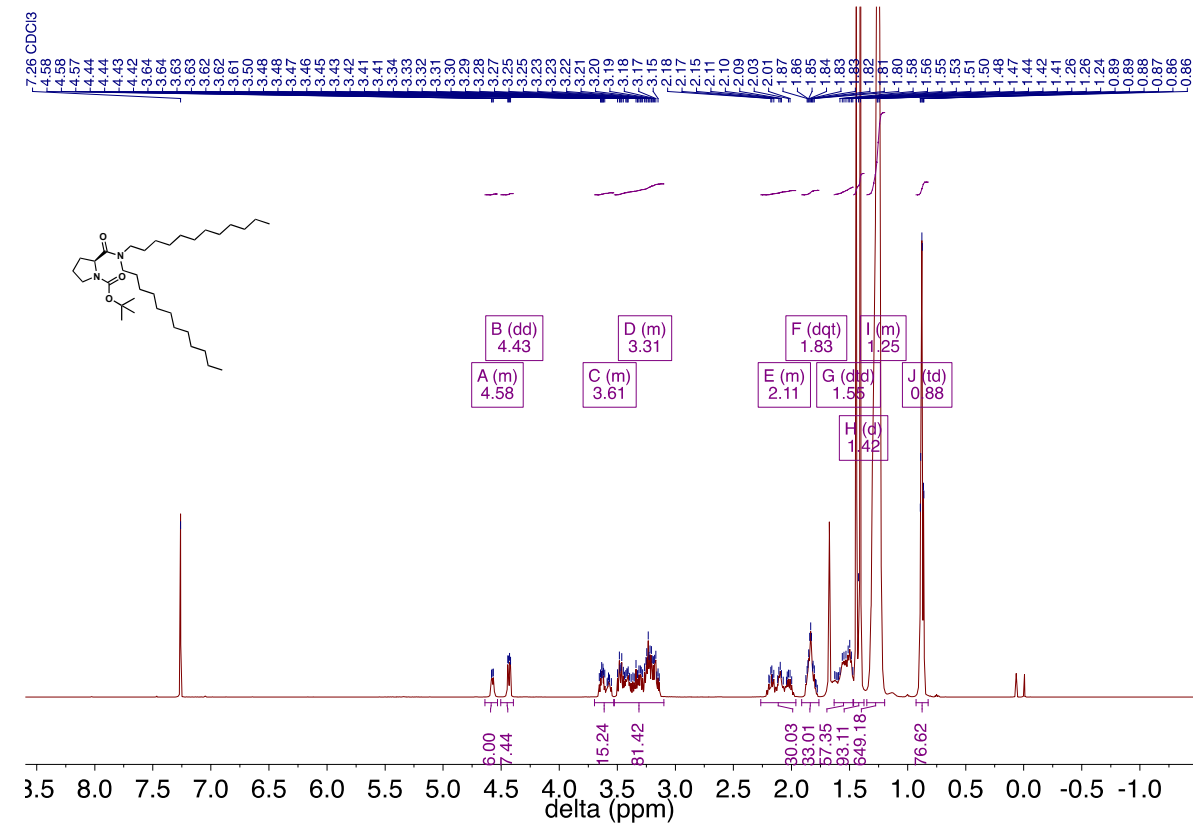

Compound **64**, ^{13}C

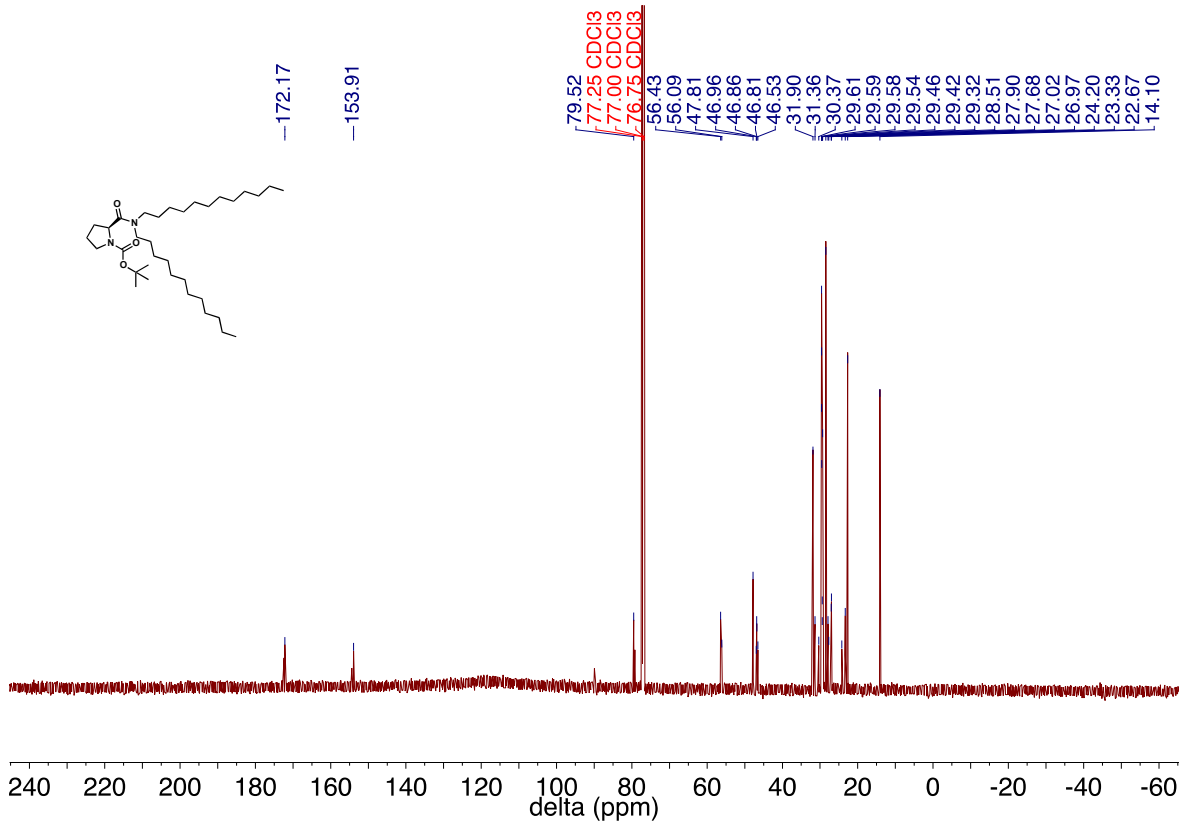

Chapter 3

Compound **78**, ^{1}H

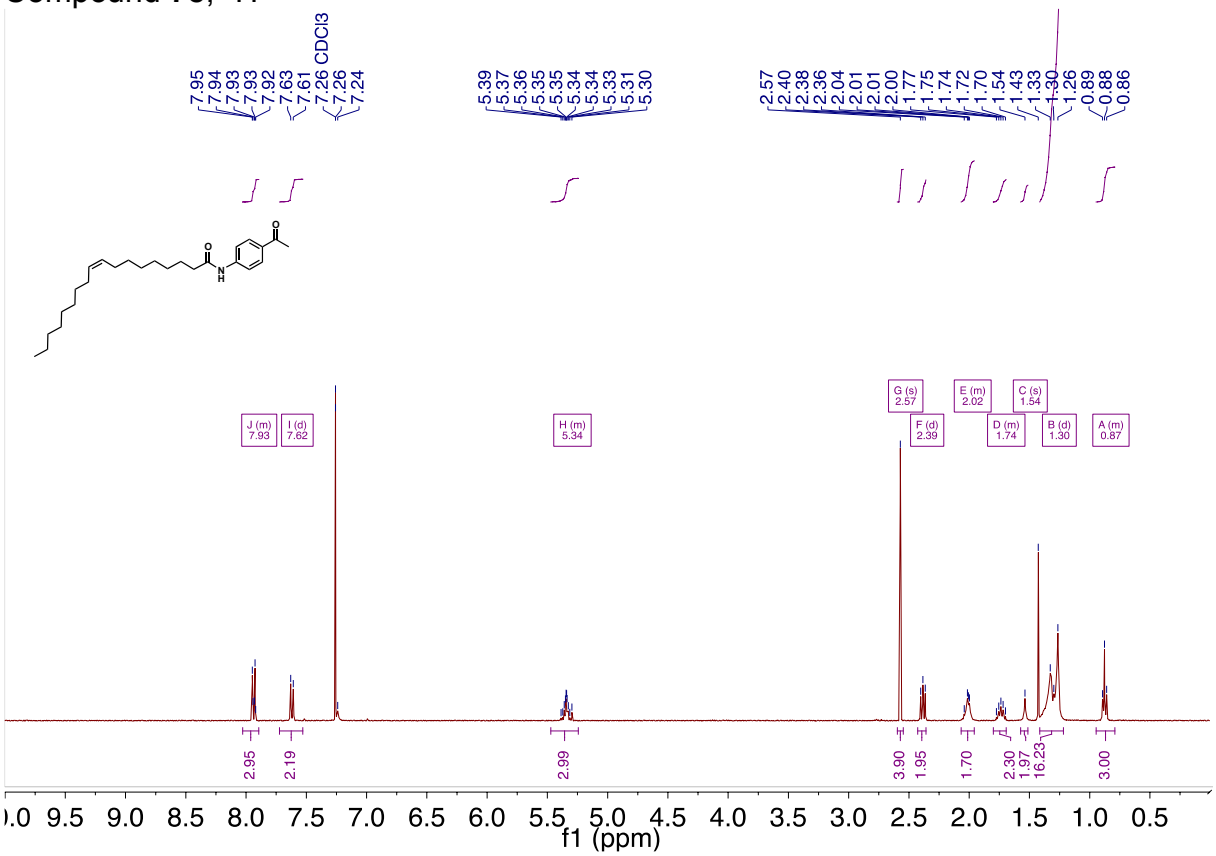

Compound **78**, ^{13}C

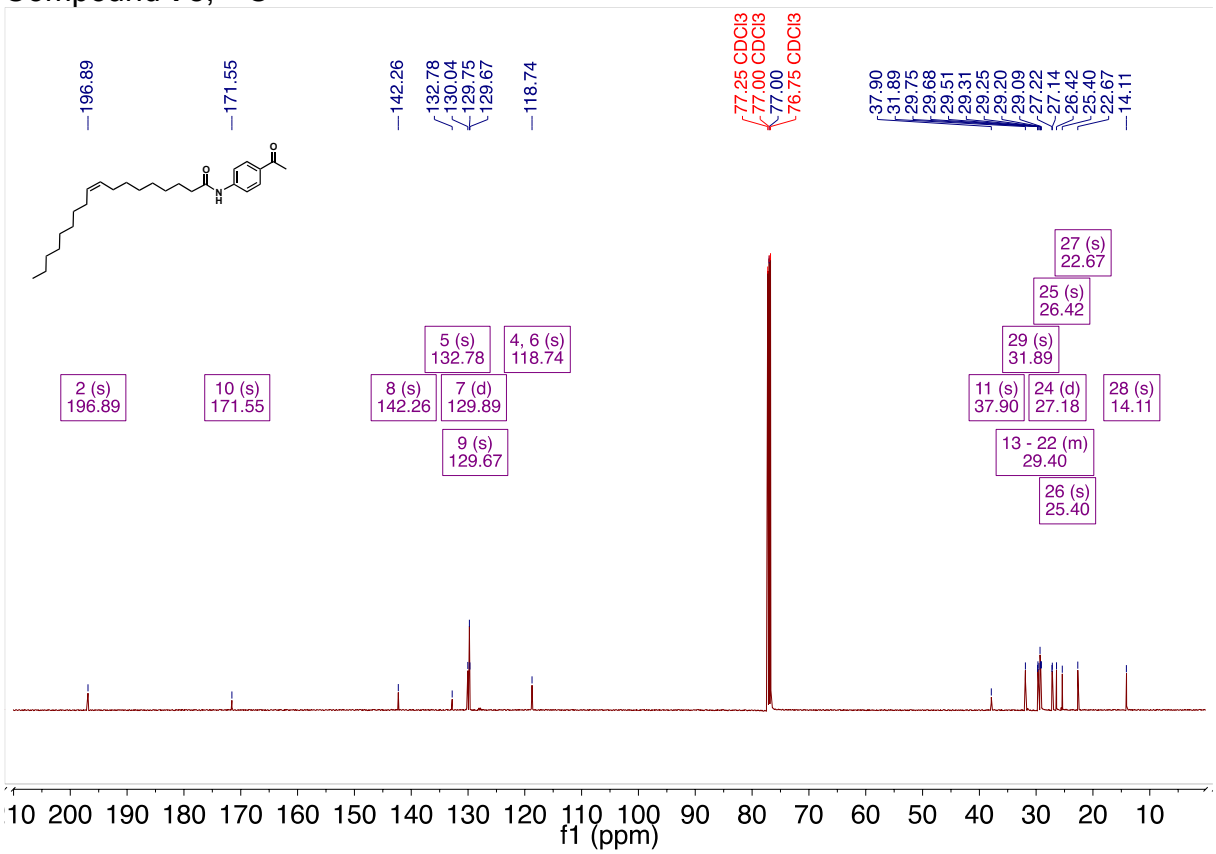

Compound **80**, ^{1}H

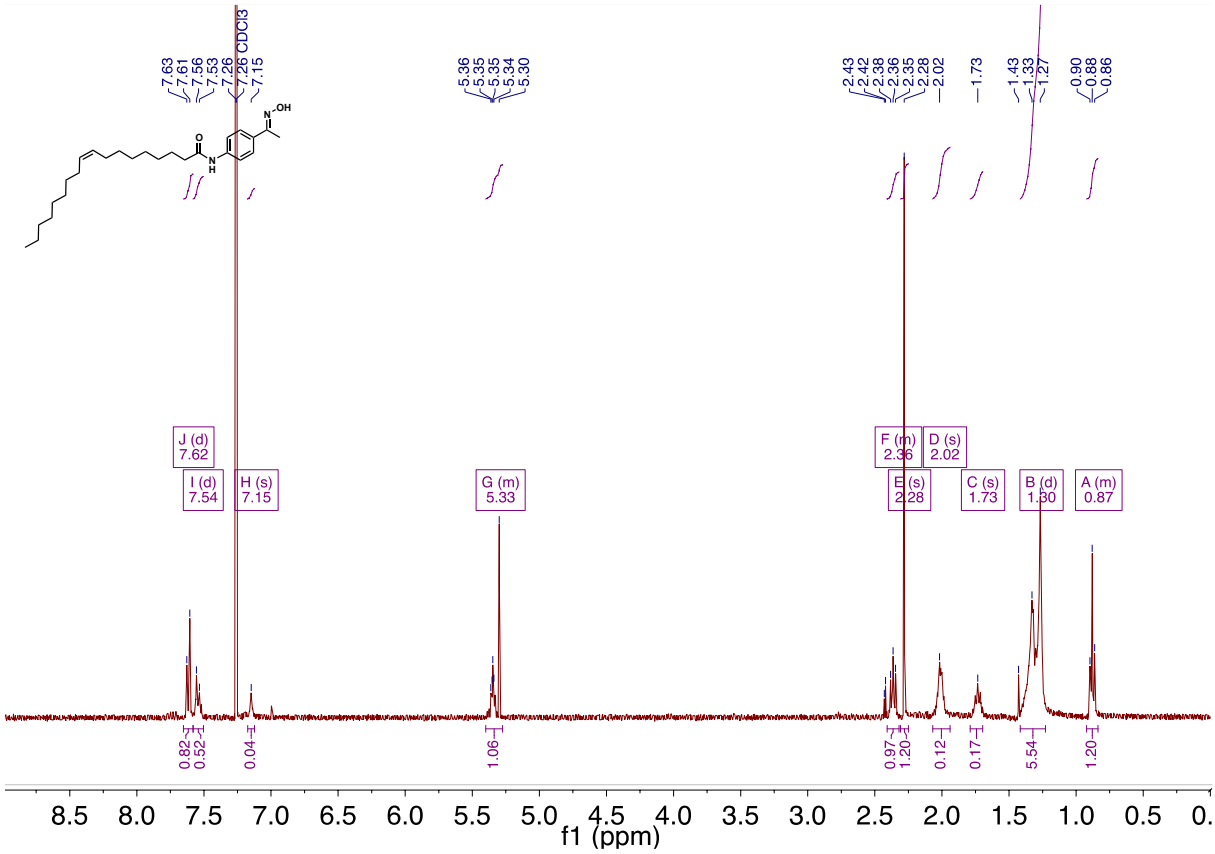

Compound **80**, ^{13}C

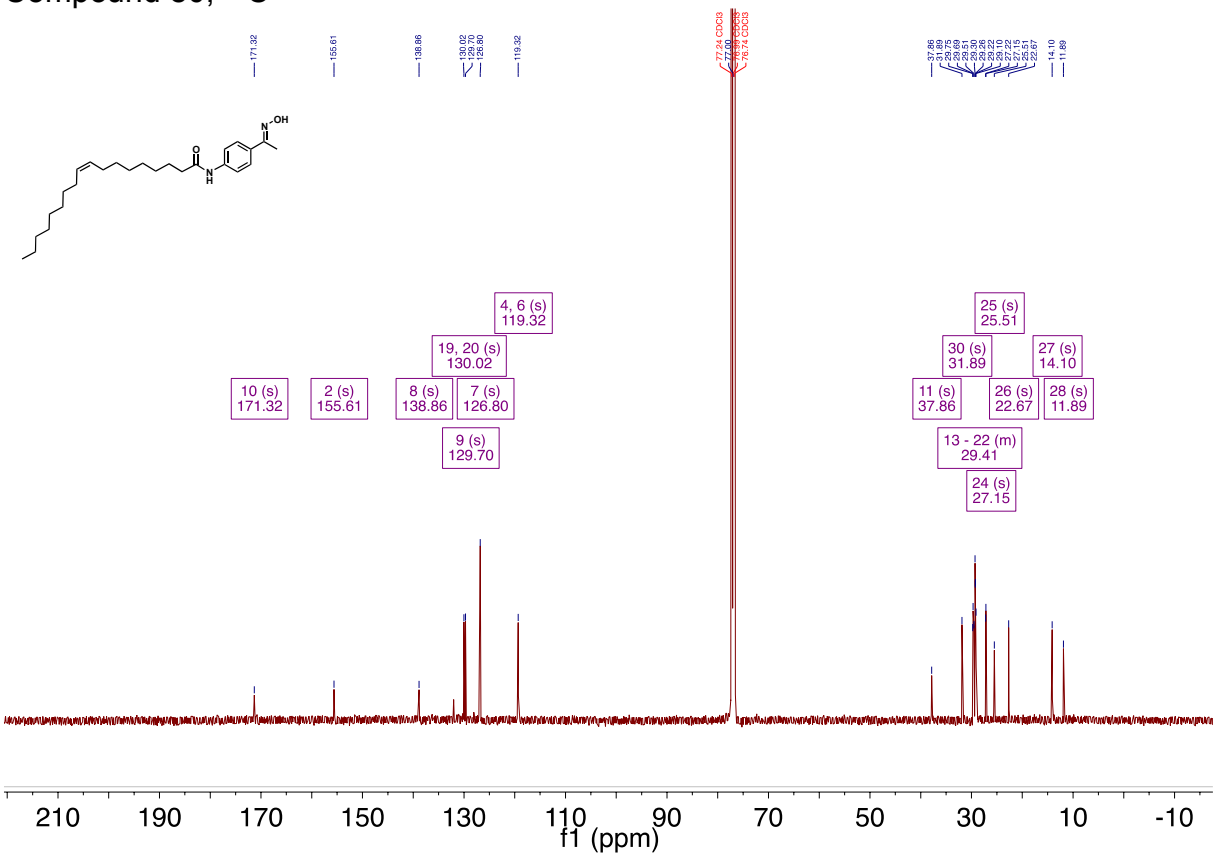

Compound **82**, ^{1}H

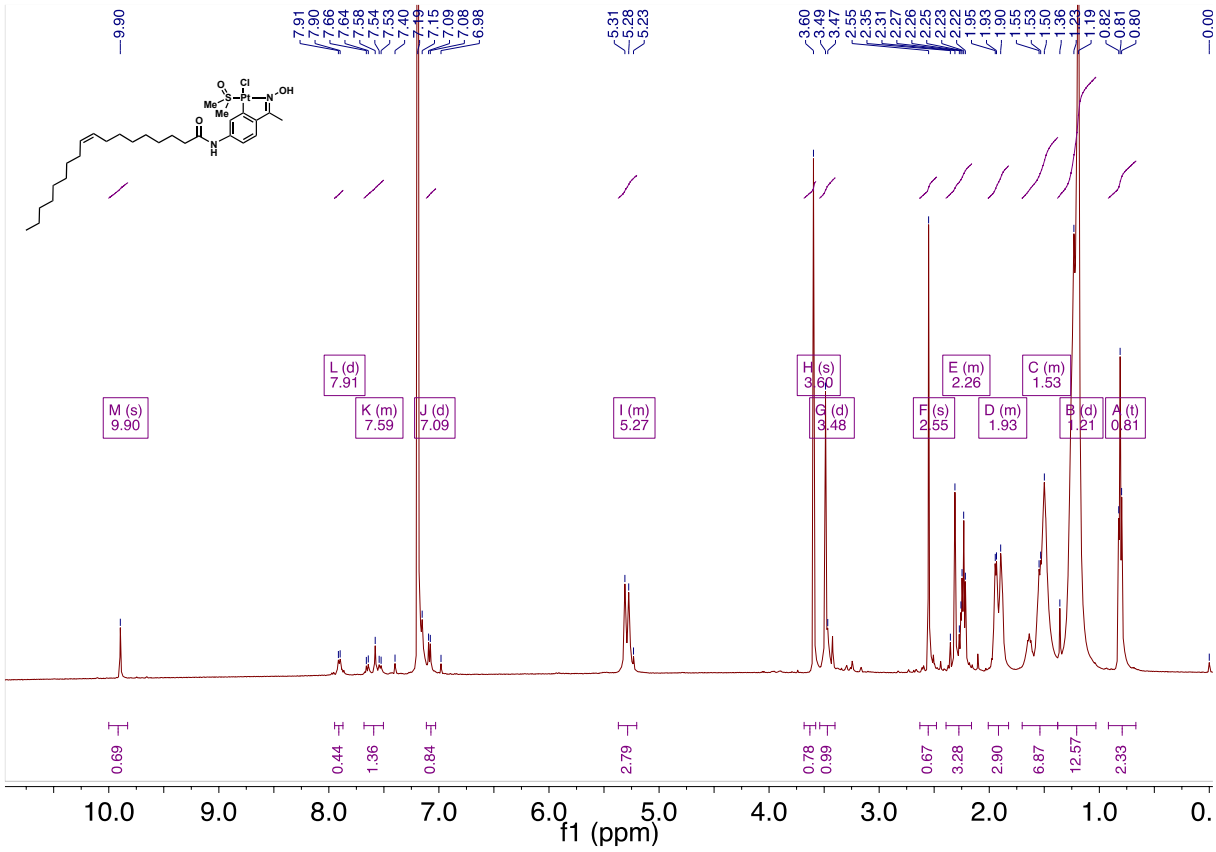

Compound **82**, ^{13}C

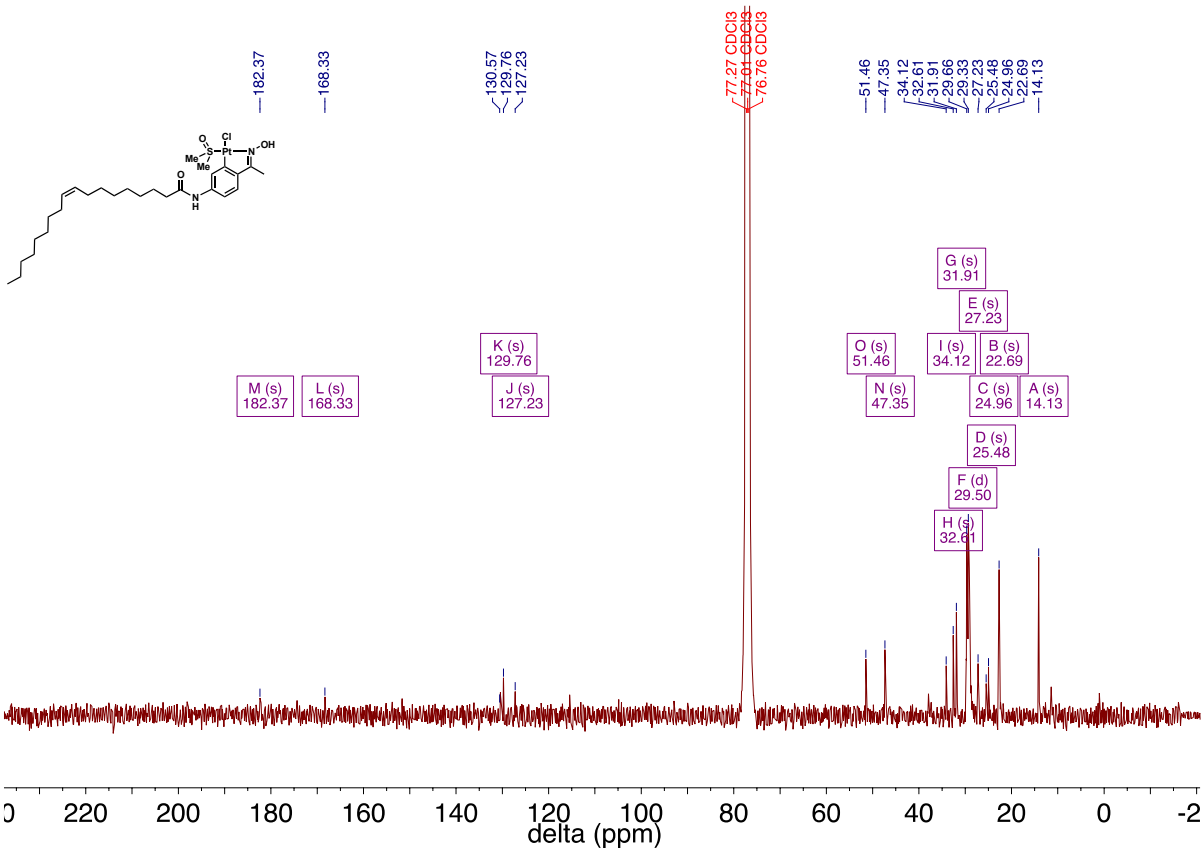

Chapter 4

Compound **96**, ^{1}H

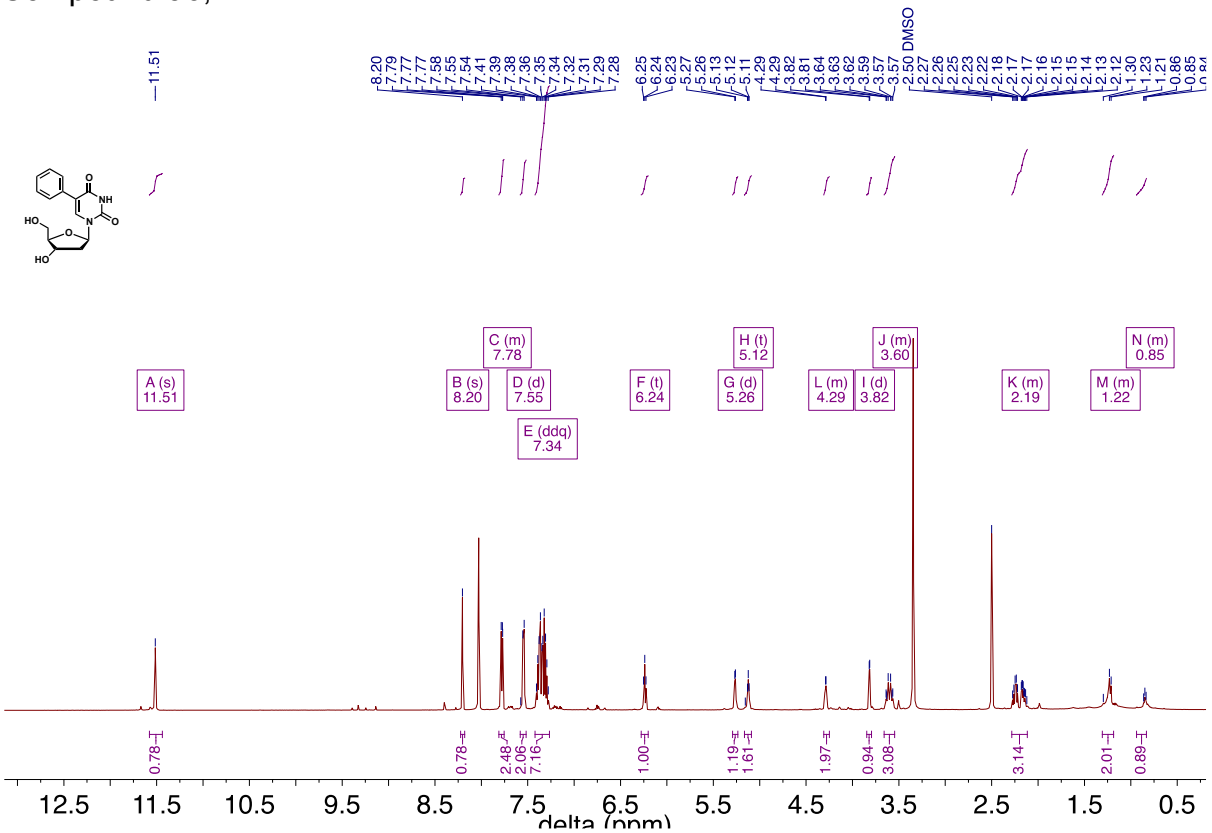

Compound **96**, ^{13}C

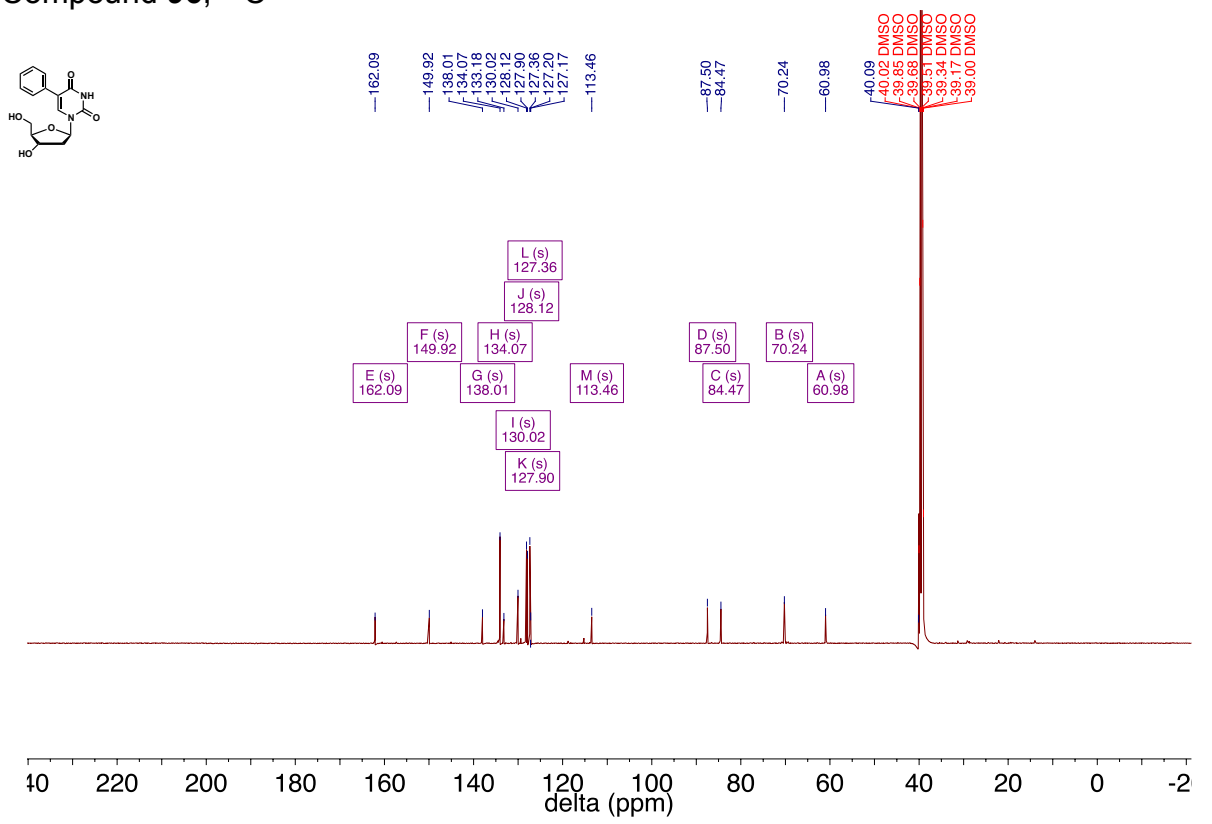

Chapter 5

Compound **113**, ^{1}H

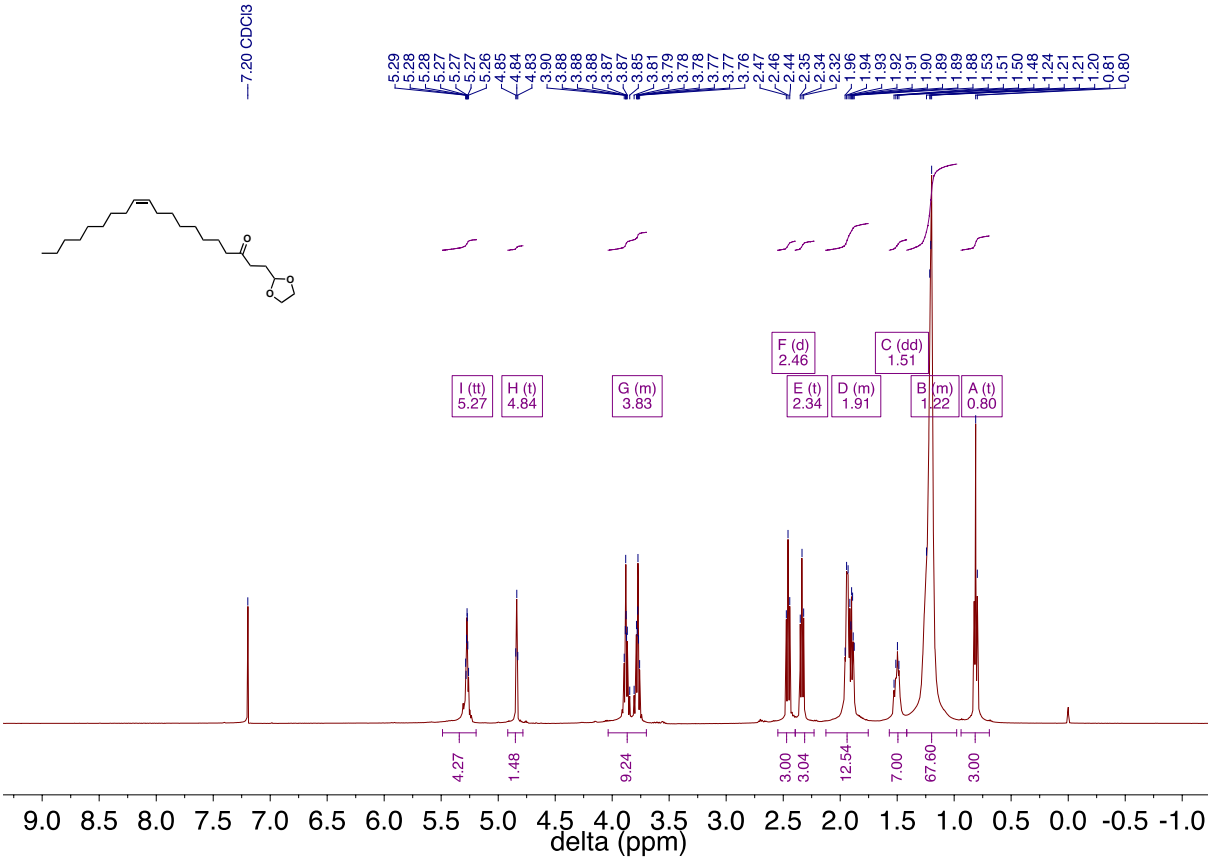

Compound **113**, ^{13}C

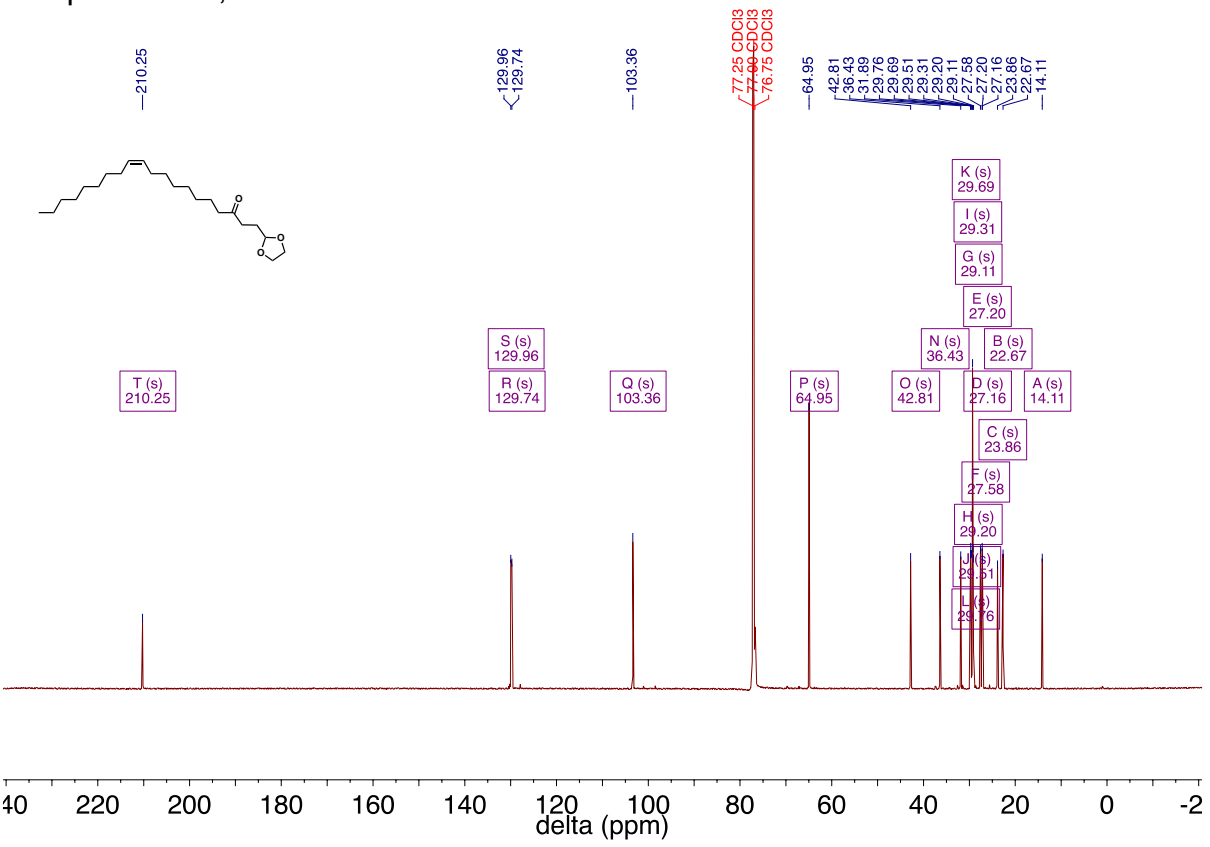

Compound **114**, ^{1}H

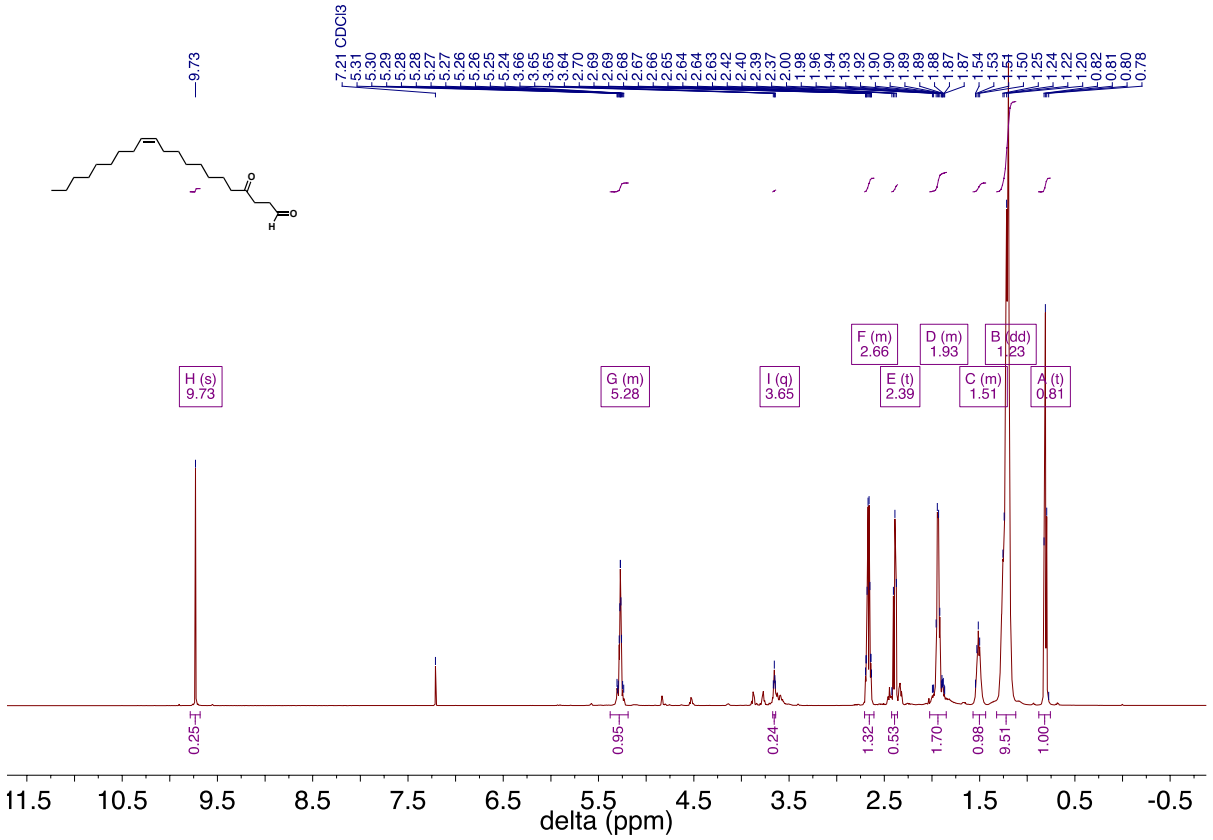

Compound **114**, ^{13}C

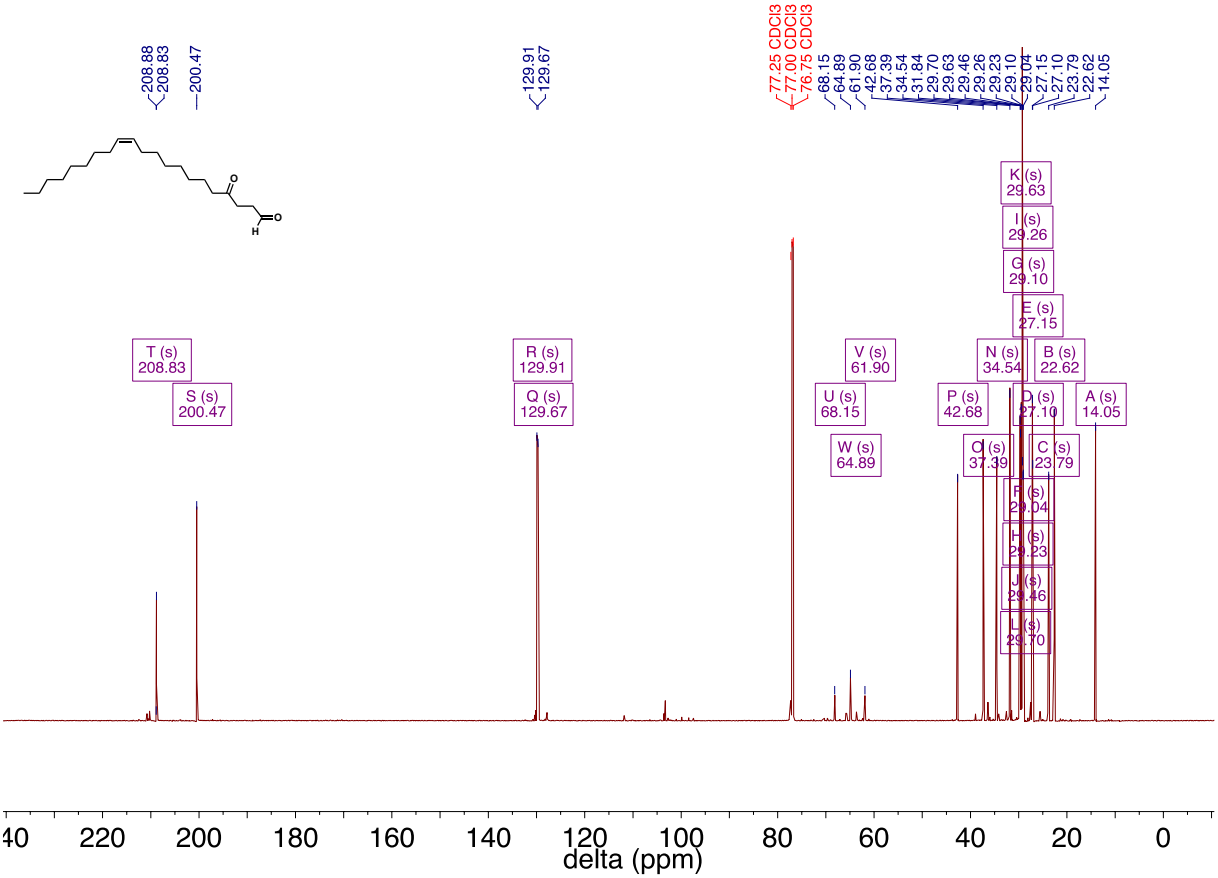

Compound **115**, ^{1}H

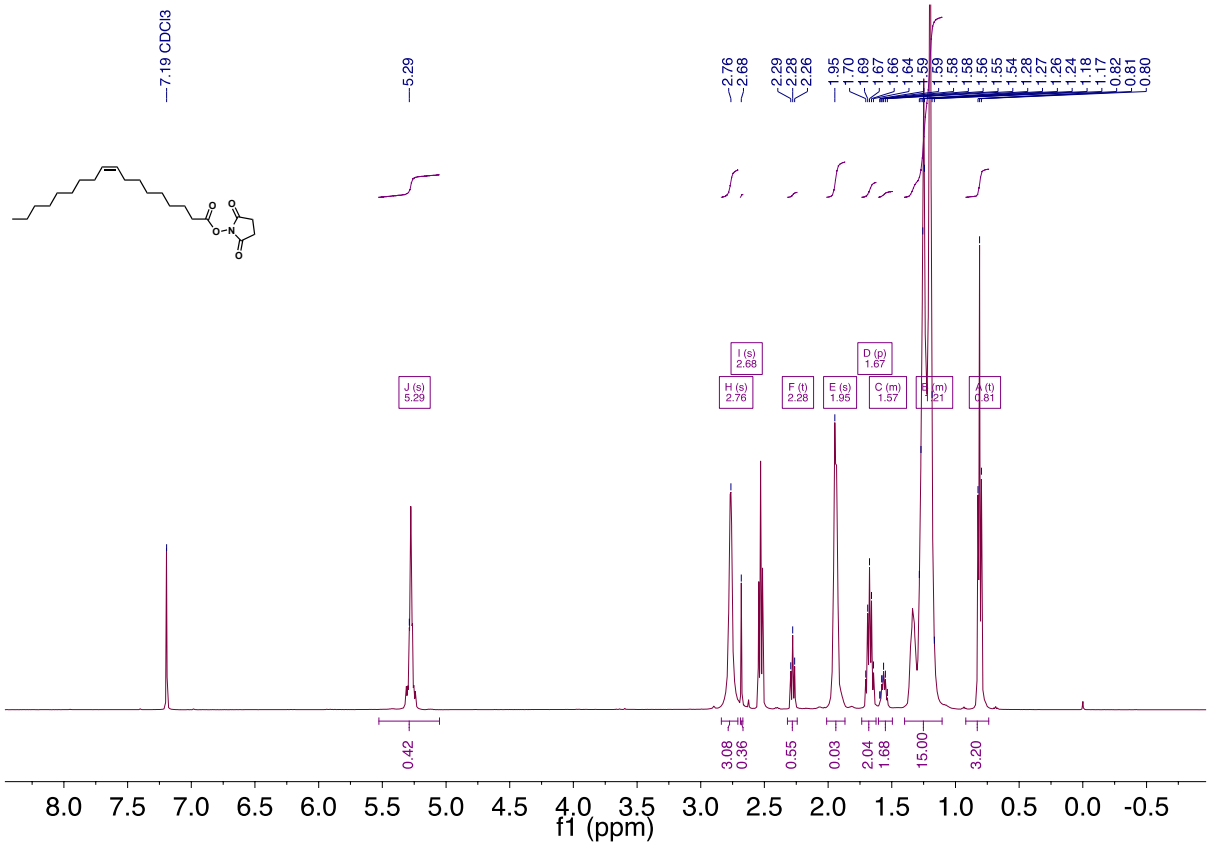

Compound **115**, ^{13}C

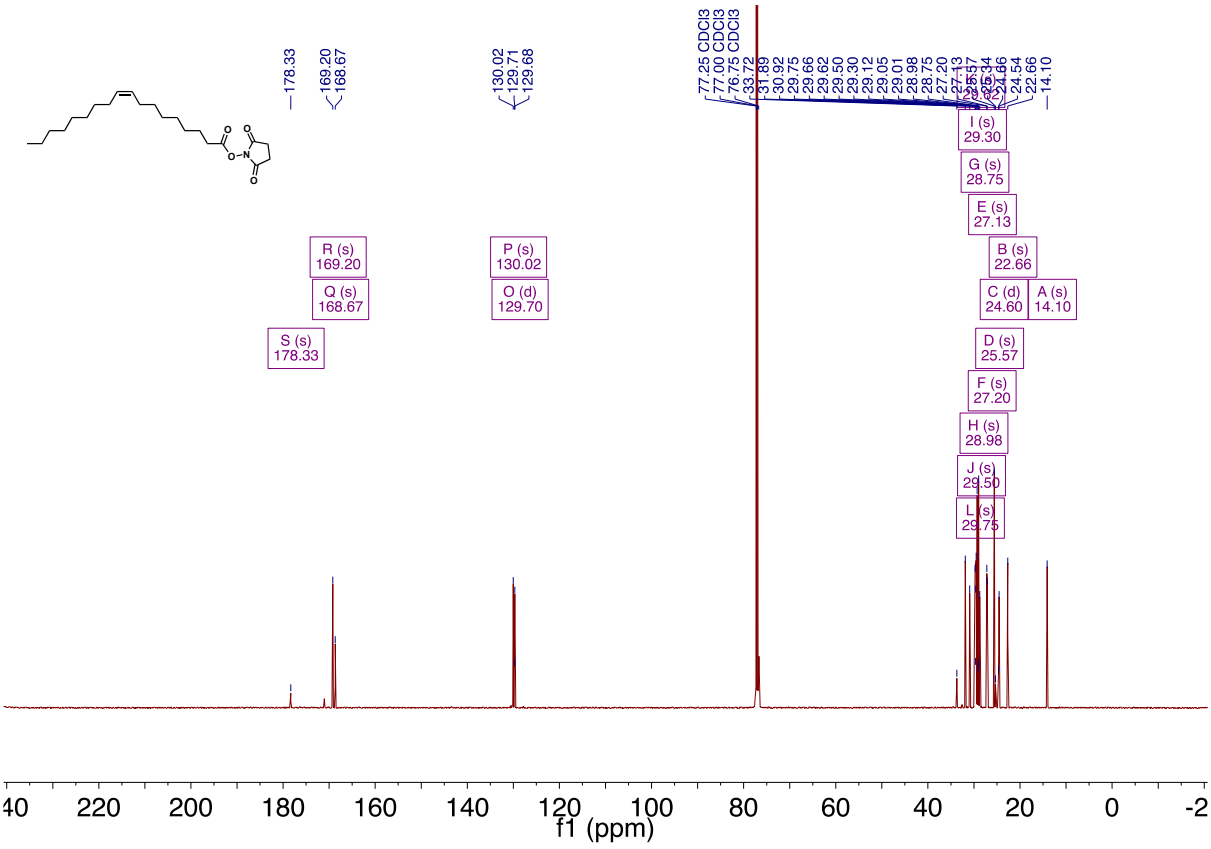

Chapter 6

Compound **124**, ^{1}H

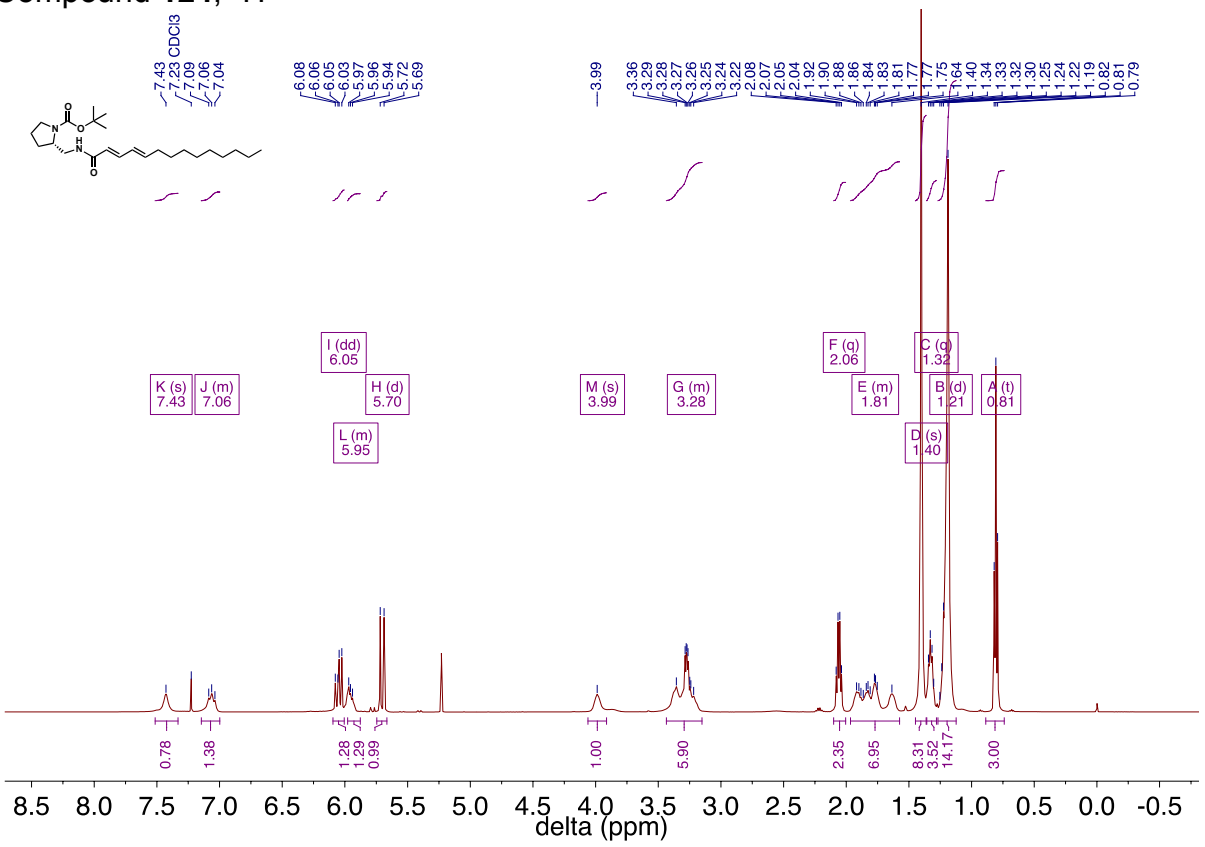

Compound **124**, ^{13}C

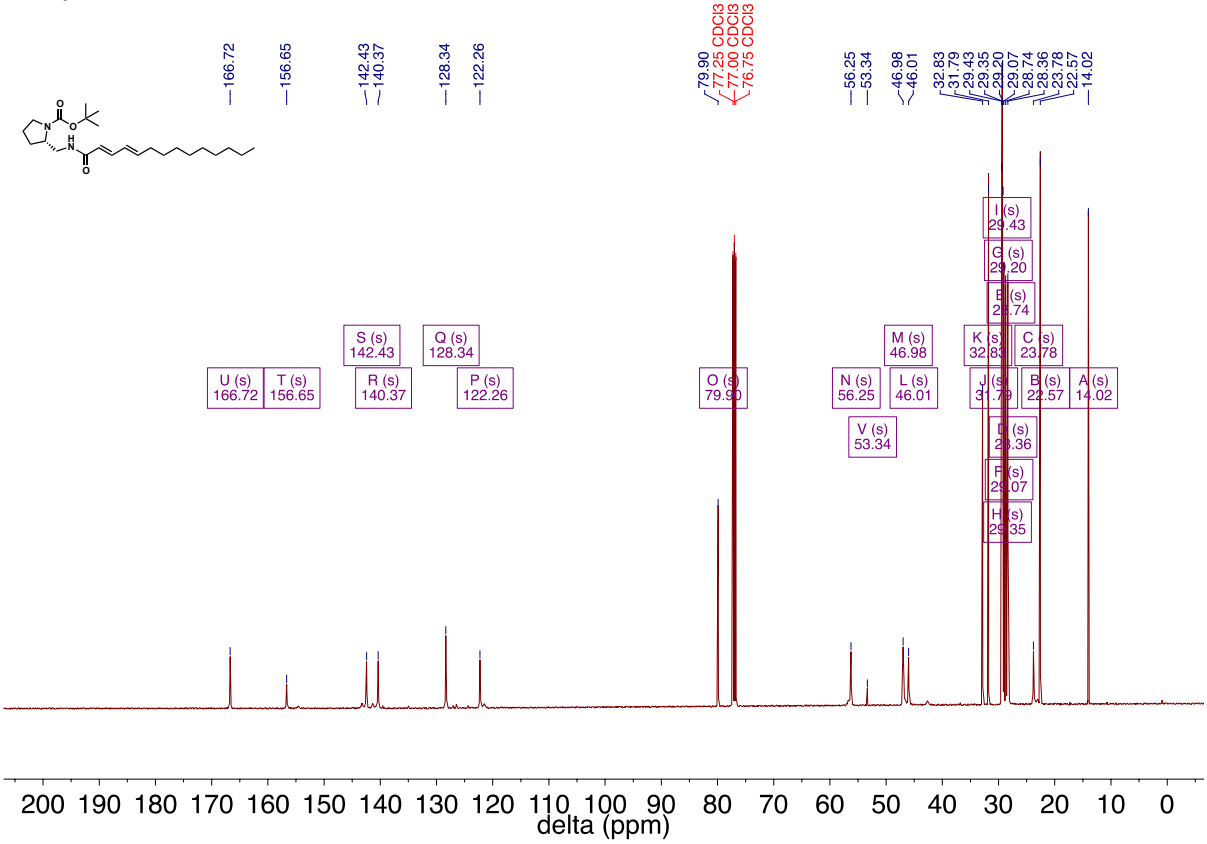

Compound **118**, ^{1}H

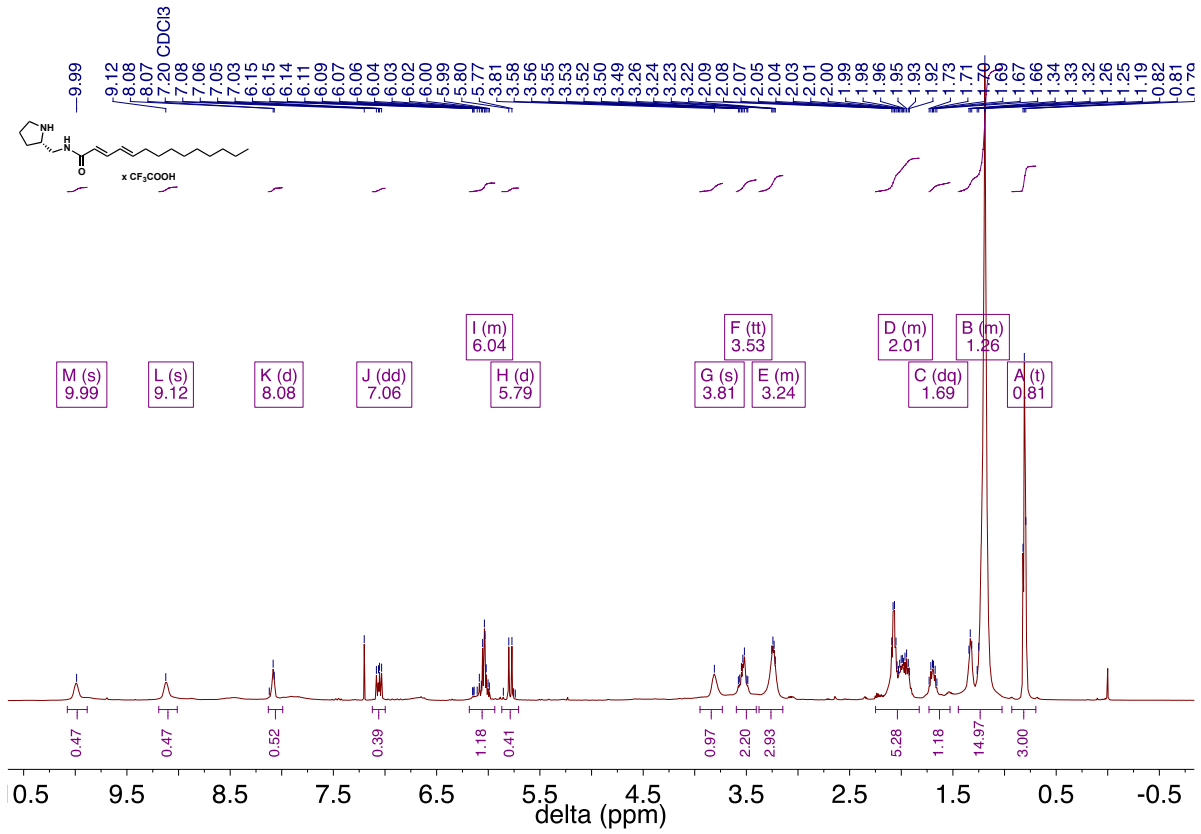

Compound **118**, ^{13}C

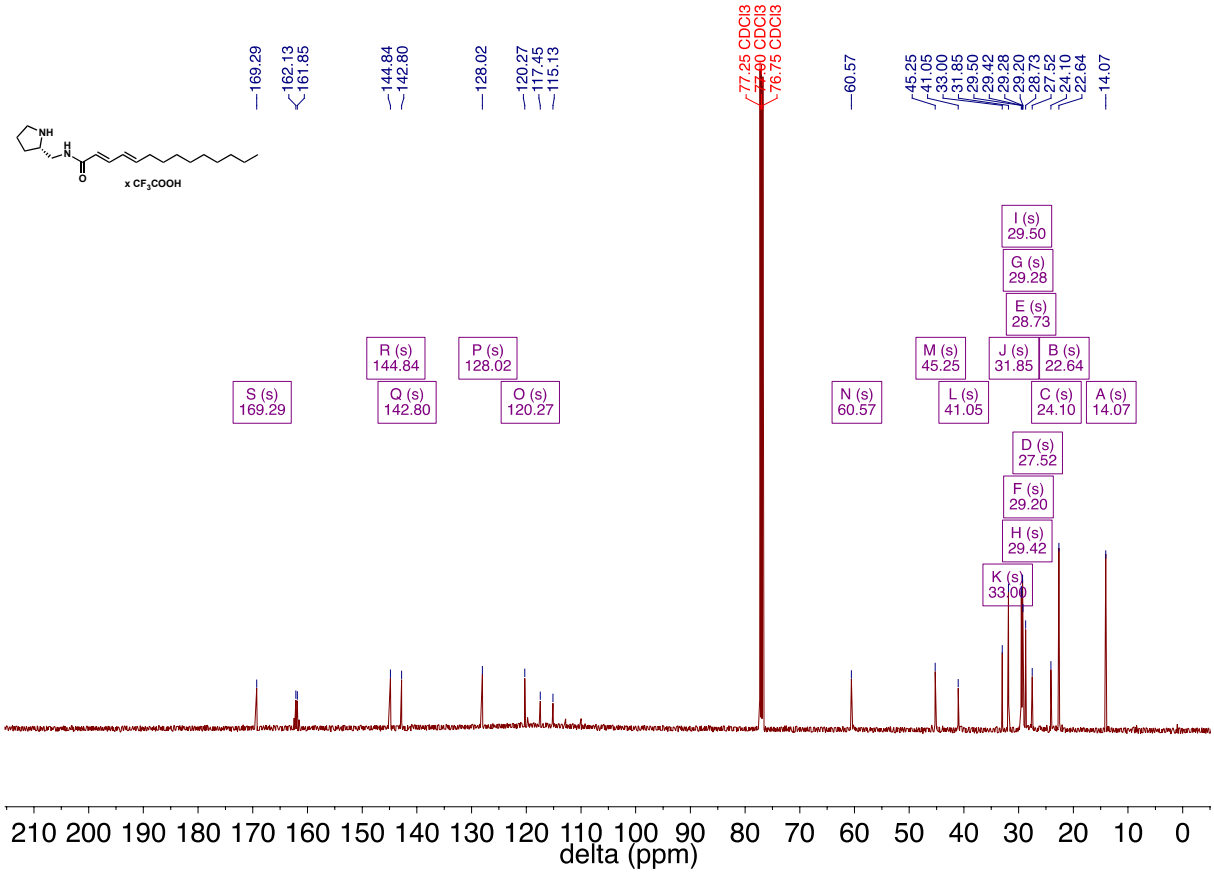

Chapter 7

Compound **130**, ^{1}H

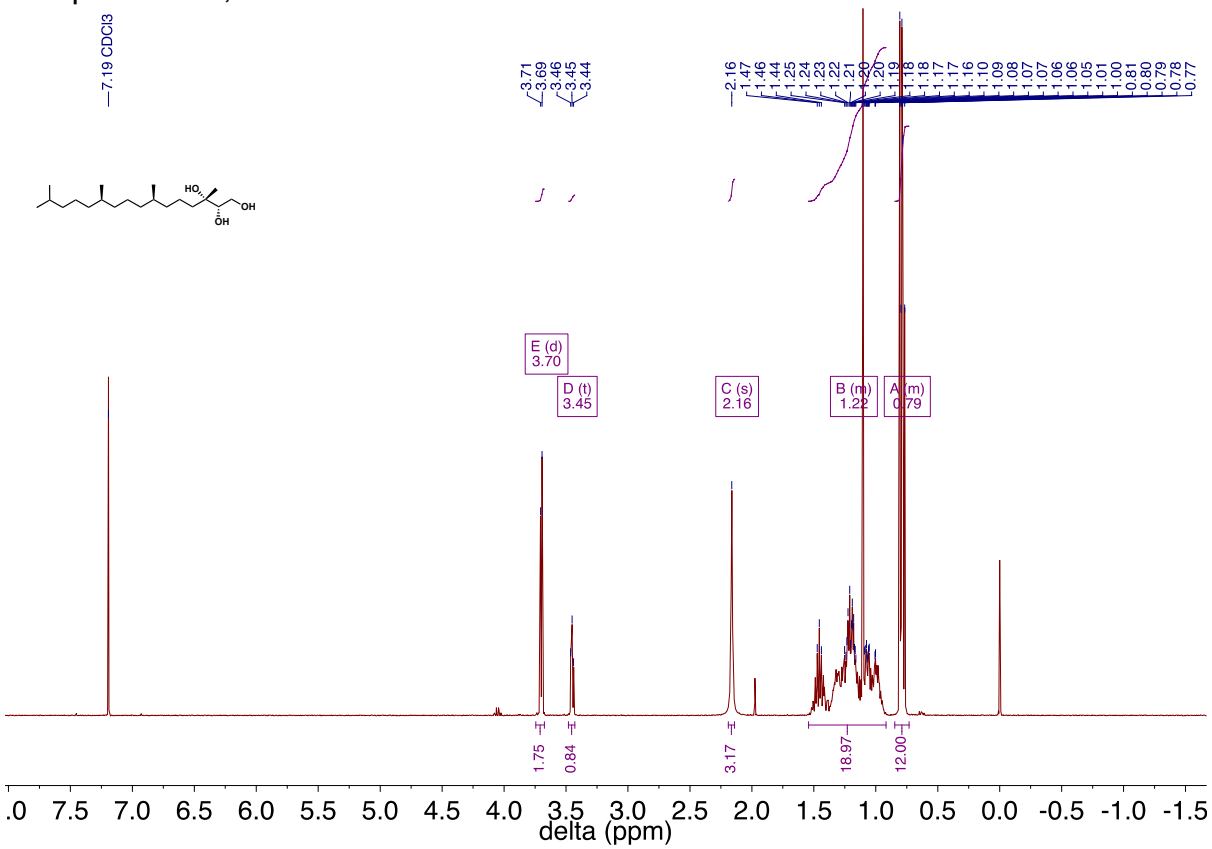

Compound **130**, ^{13}C

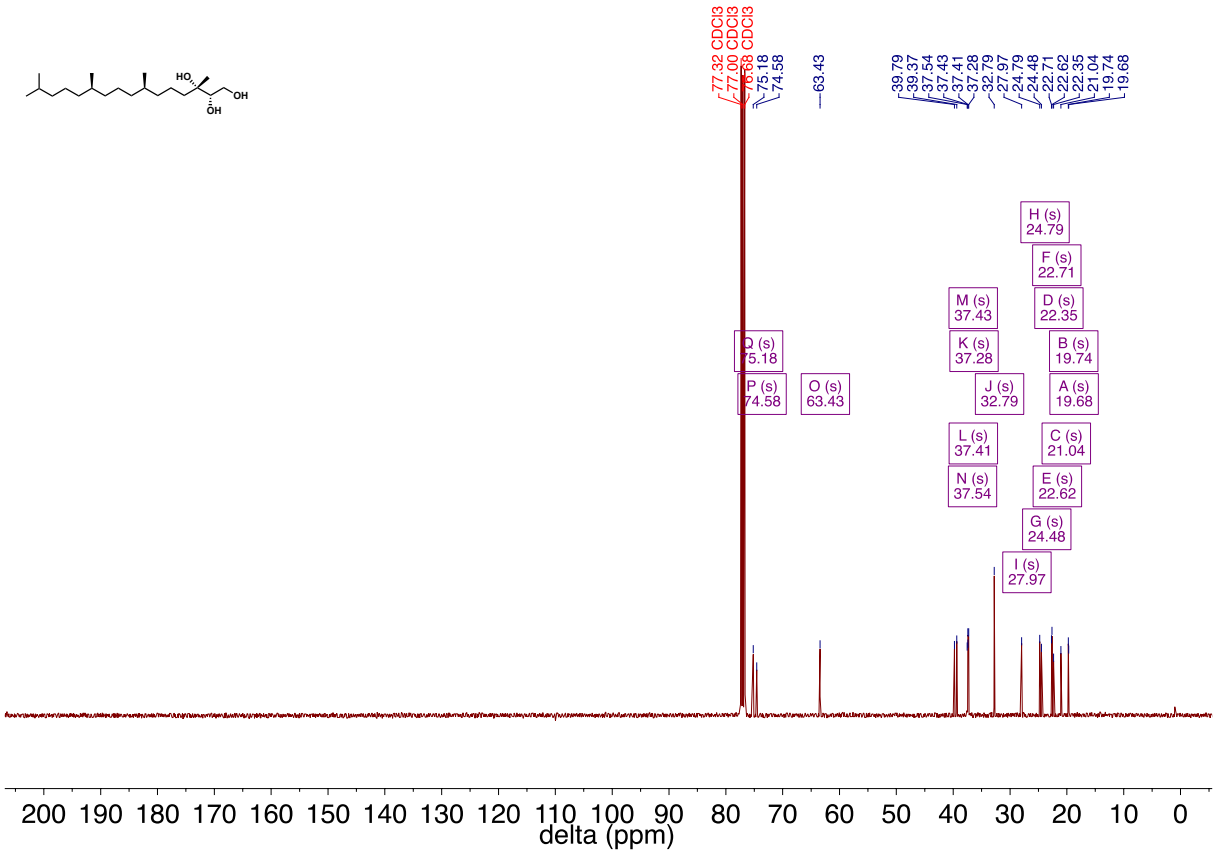

Compound **131**, ^{1}H

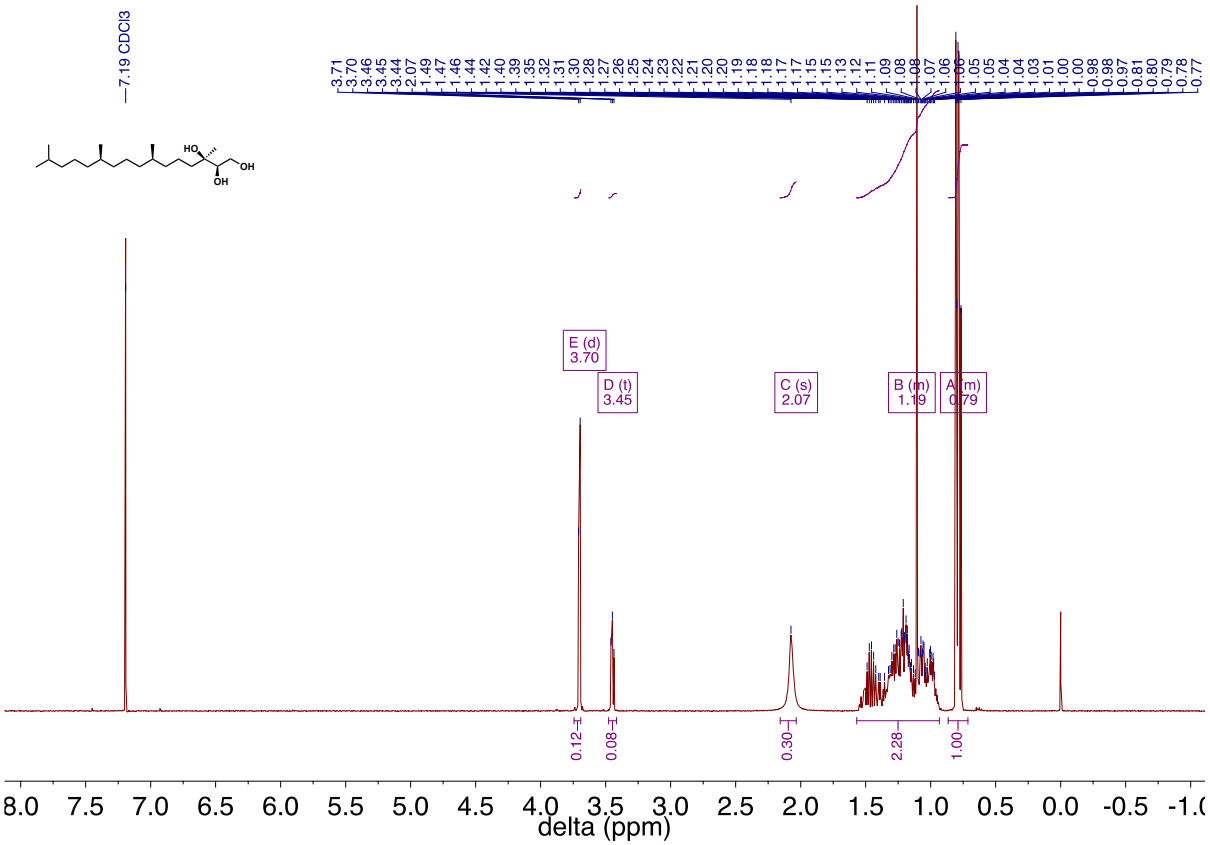

Compound **131**, ^{13}C

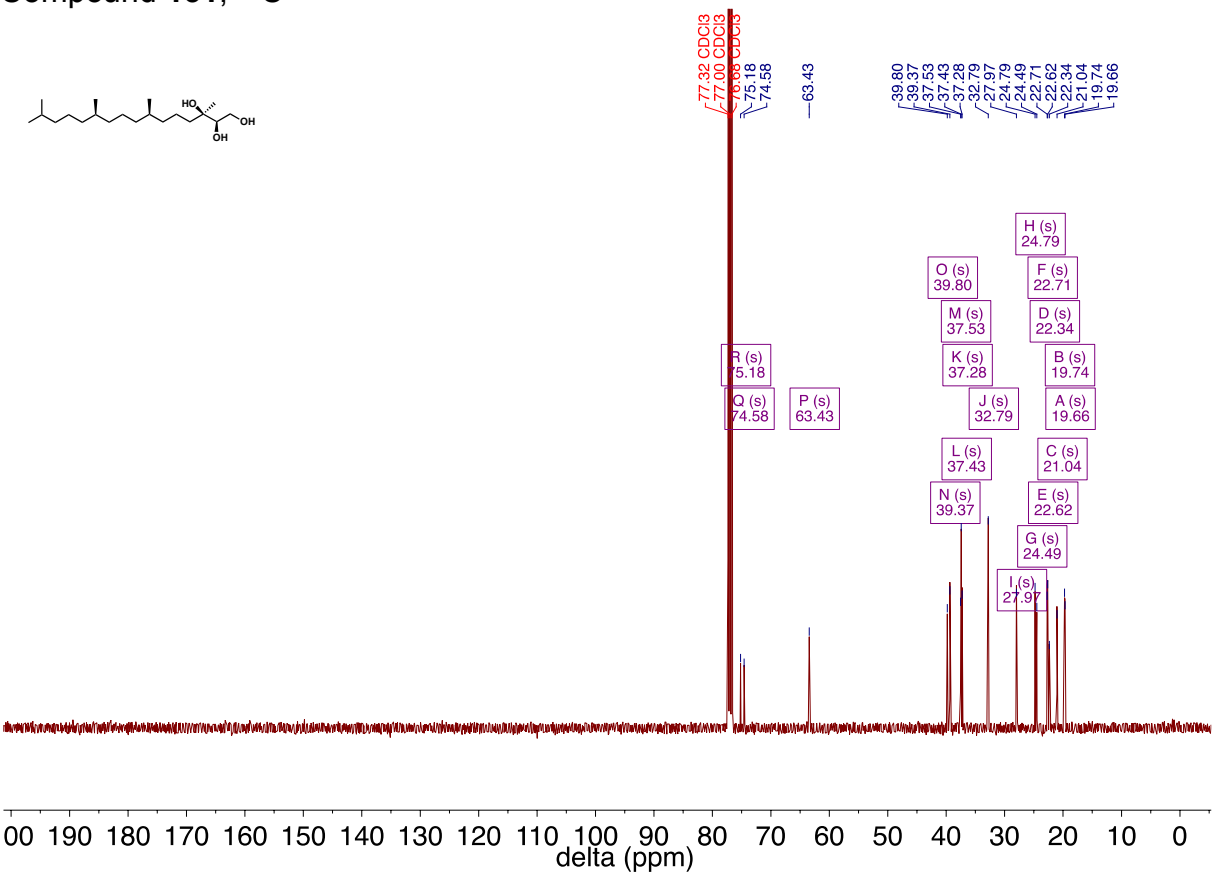

Commercial phytantriol (purchased from DSM), ^{1}H

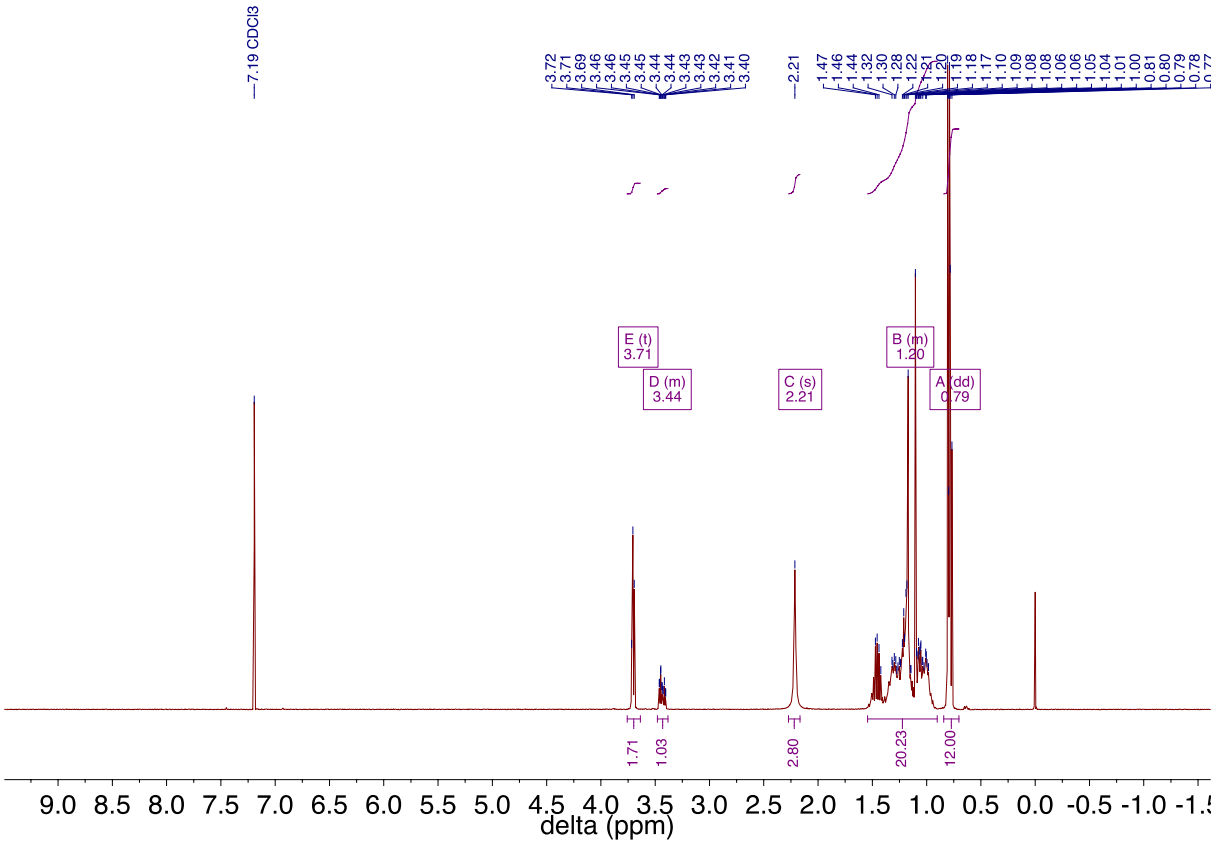

Commercial phytantriol (purchased from DSM), ^{13}C

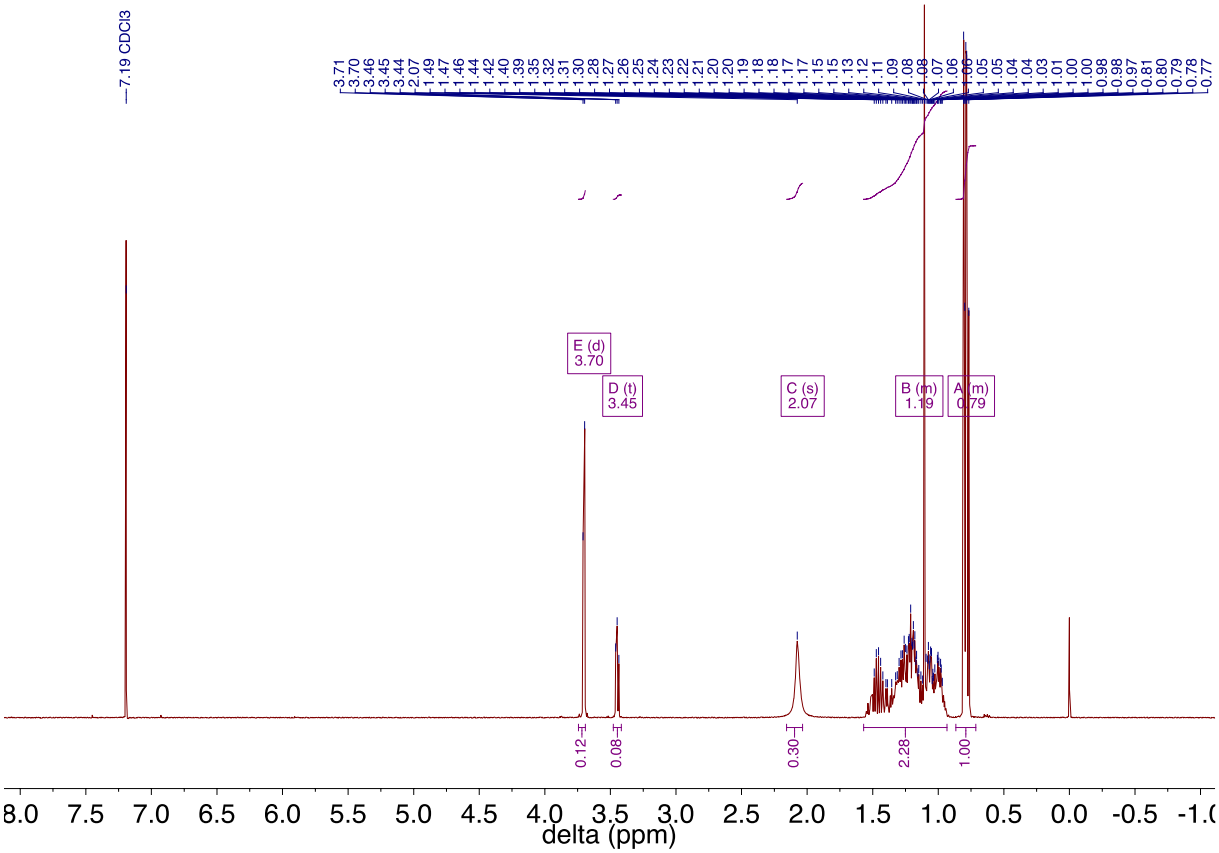

Chapter 8

Compound **142**, ^{1}H

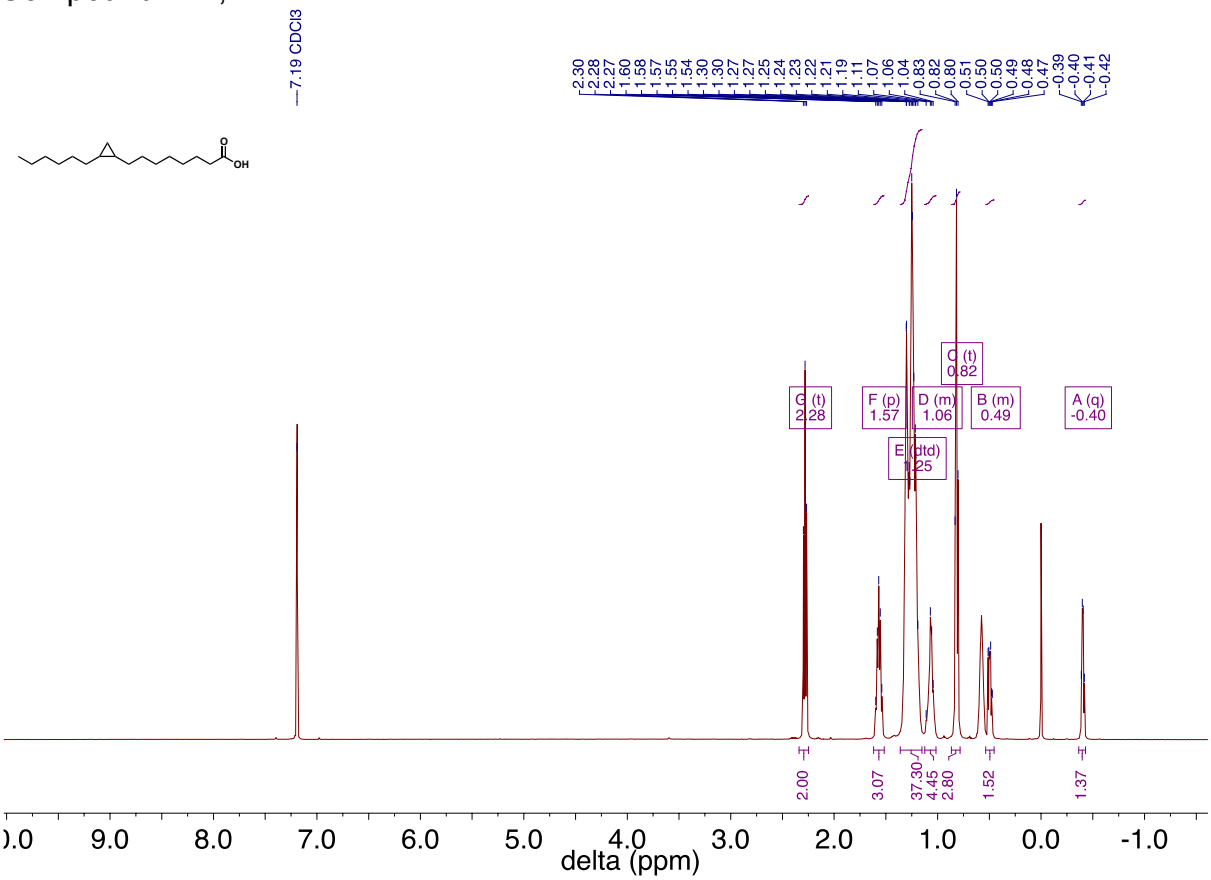

Compound **142**, ^{13}C

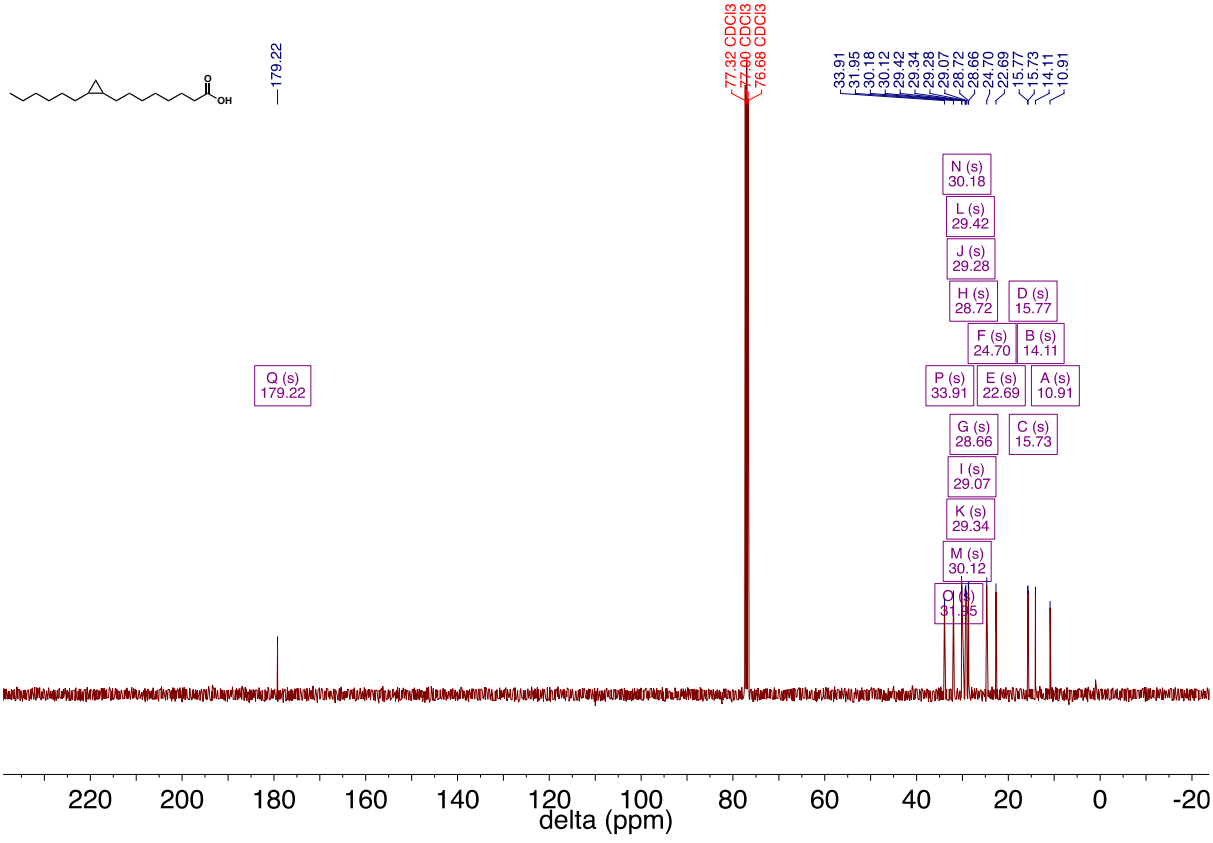

Compound **134**, ^{1}H

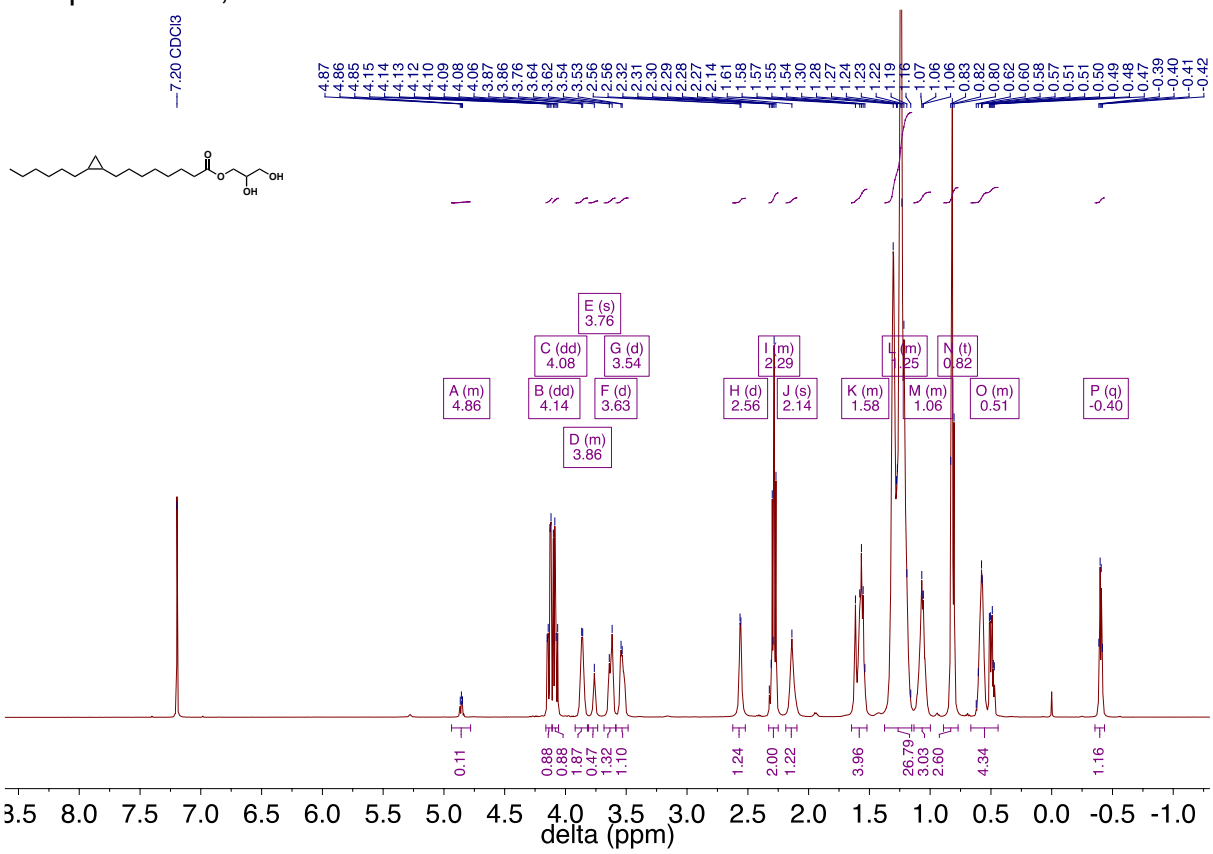

Compound **134**, ^{13}C

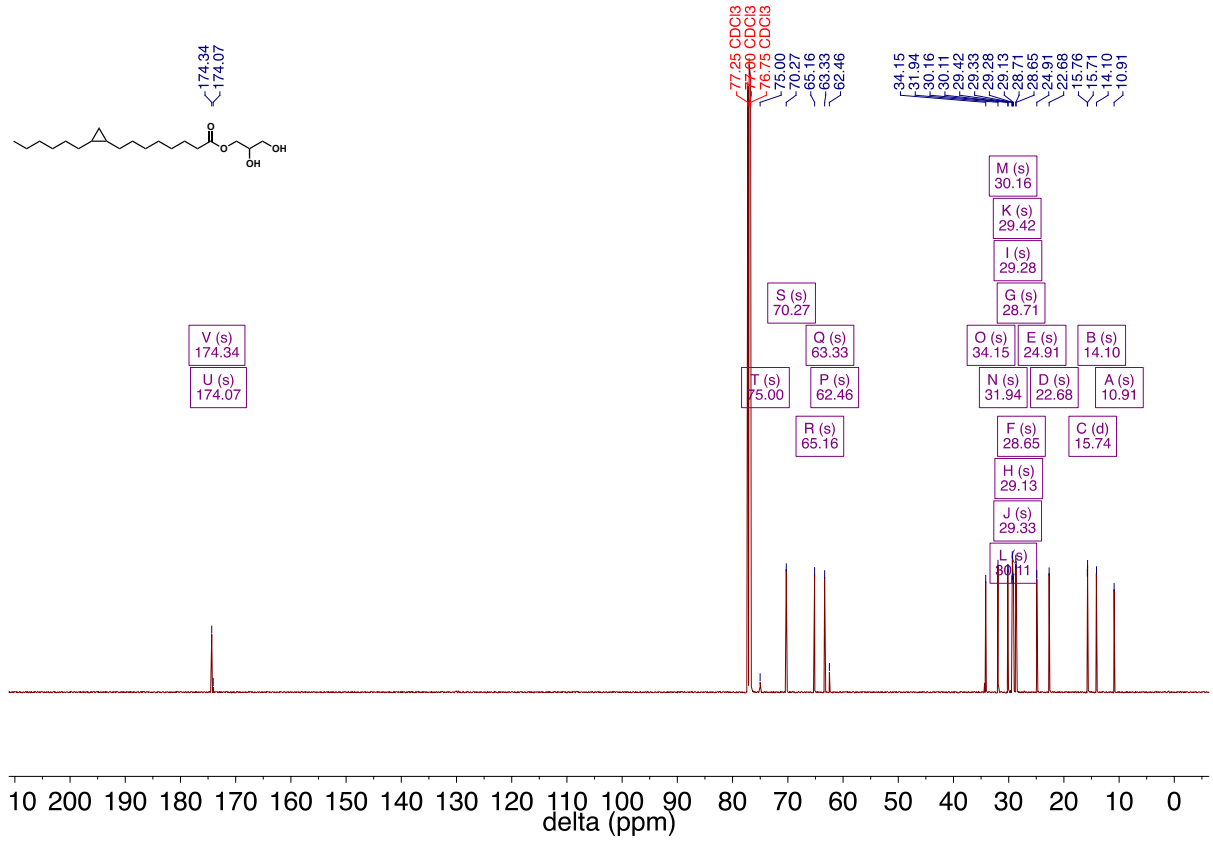

Compound **143**, ^{1}H

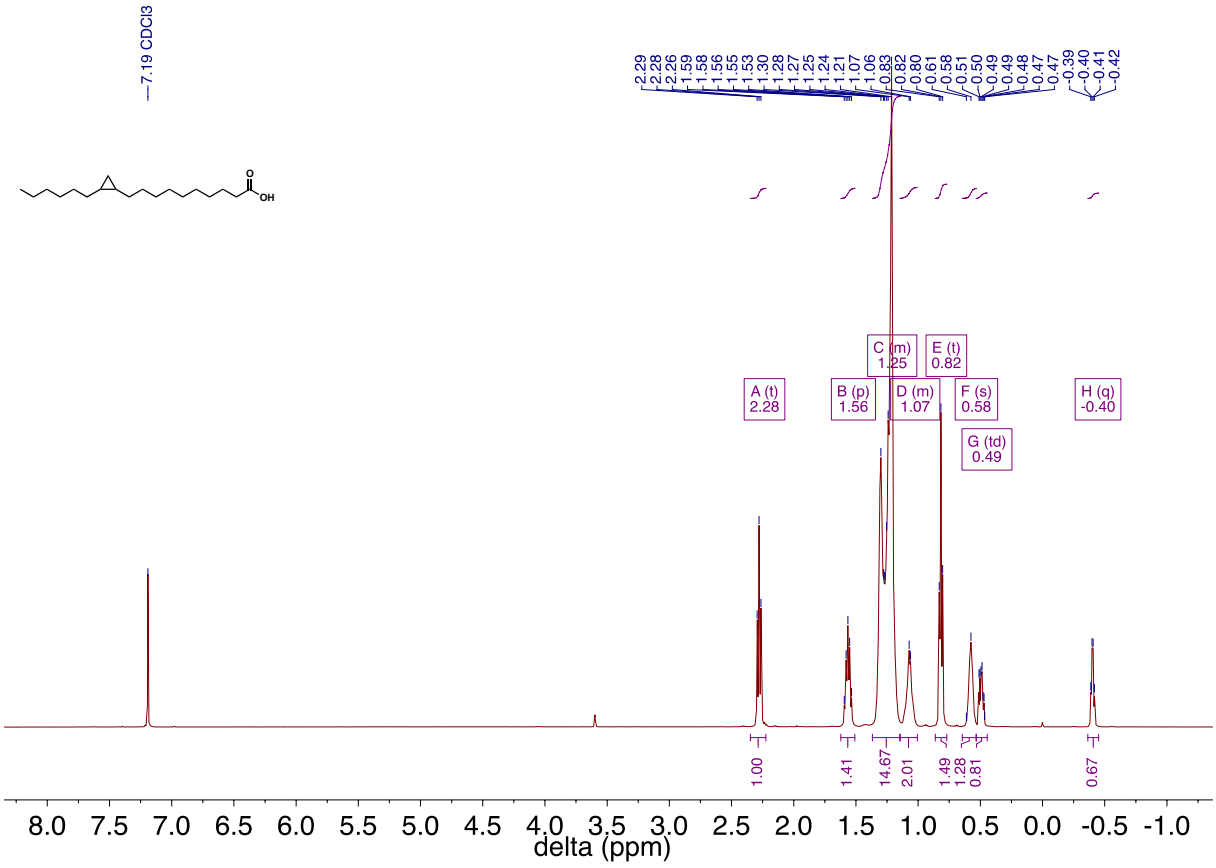

Compound **143**, ^{13}C

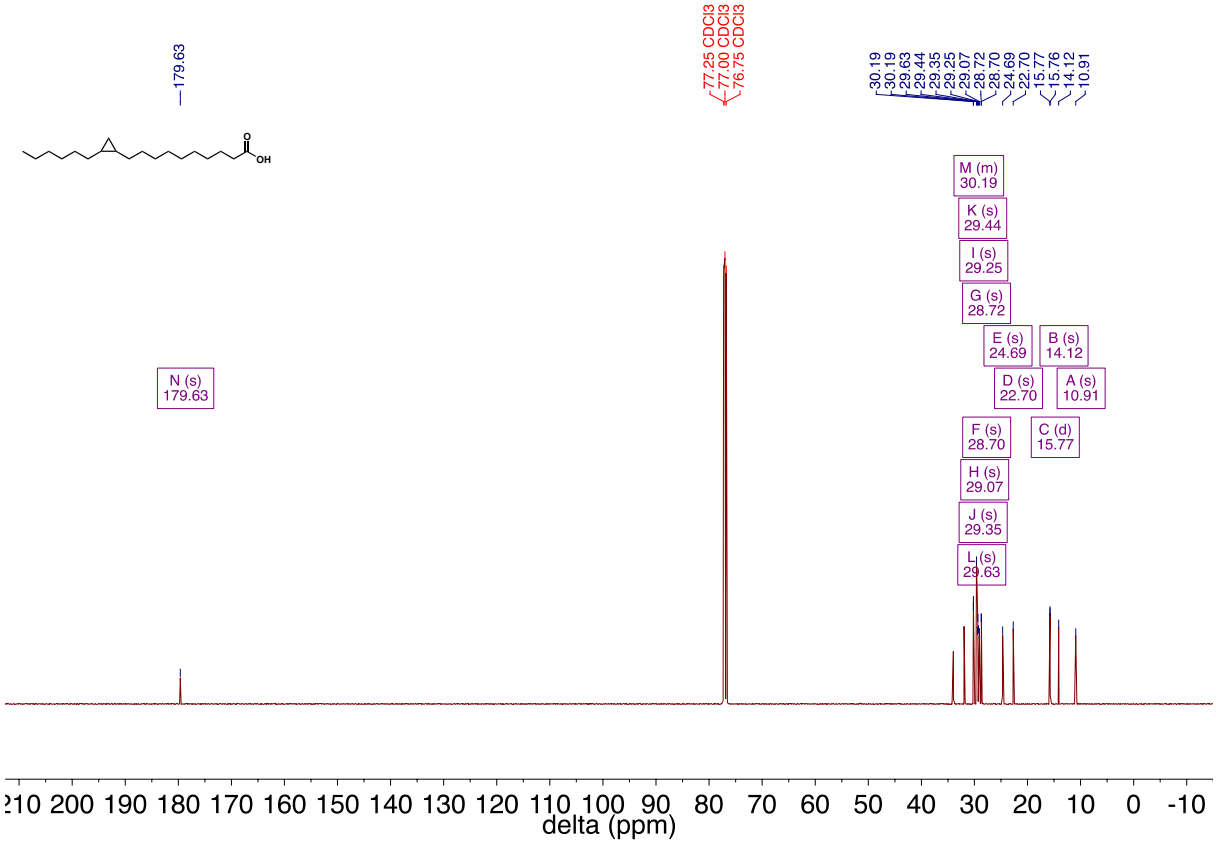

Compound **136**, ^{1}H

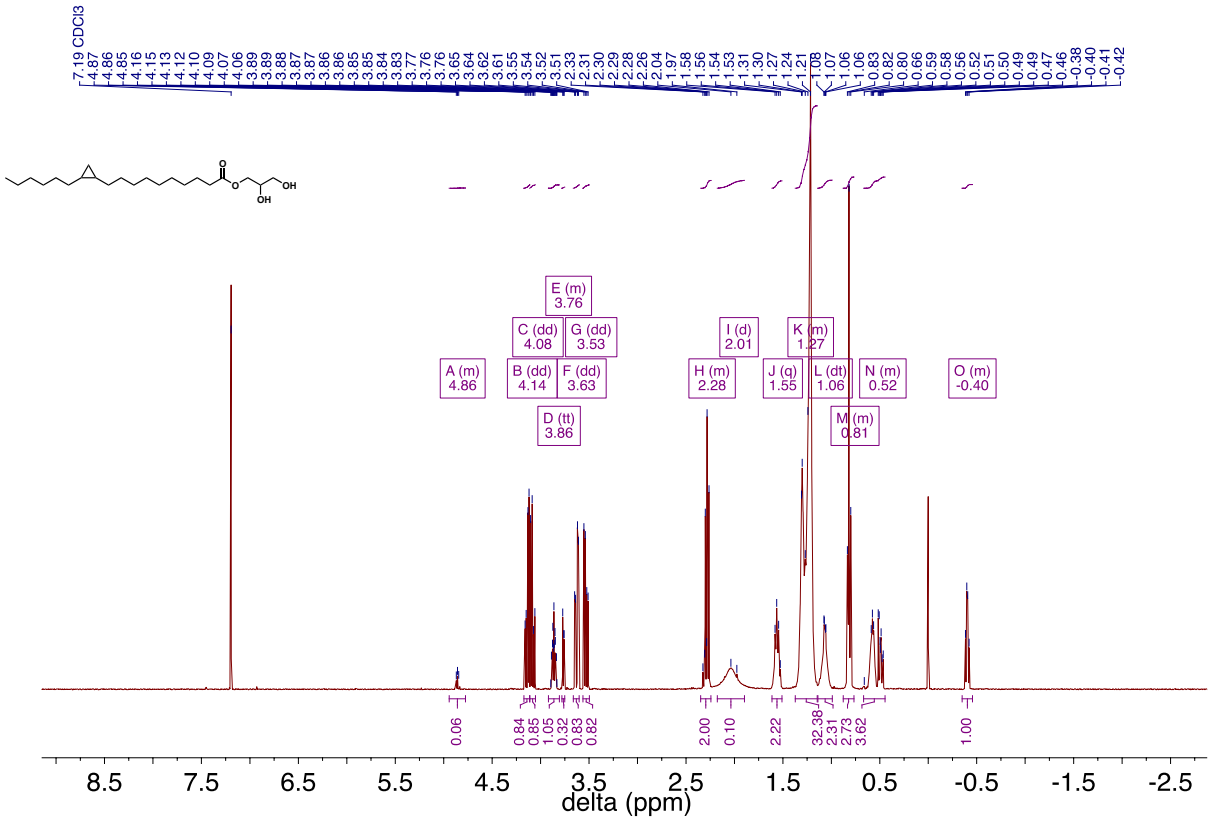

Compound **136**, ^{13}C

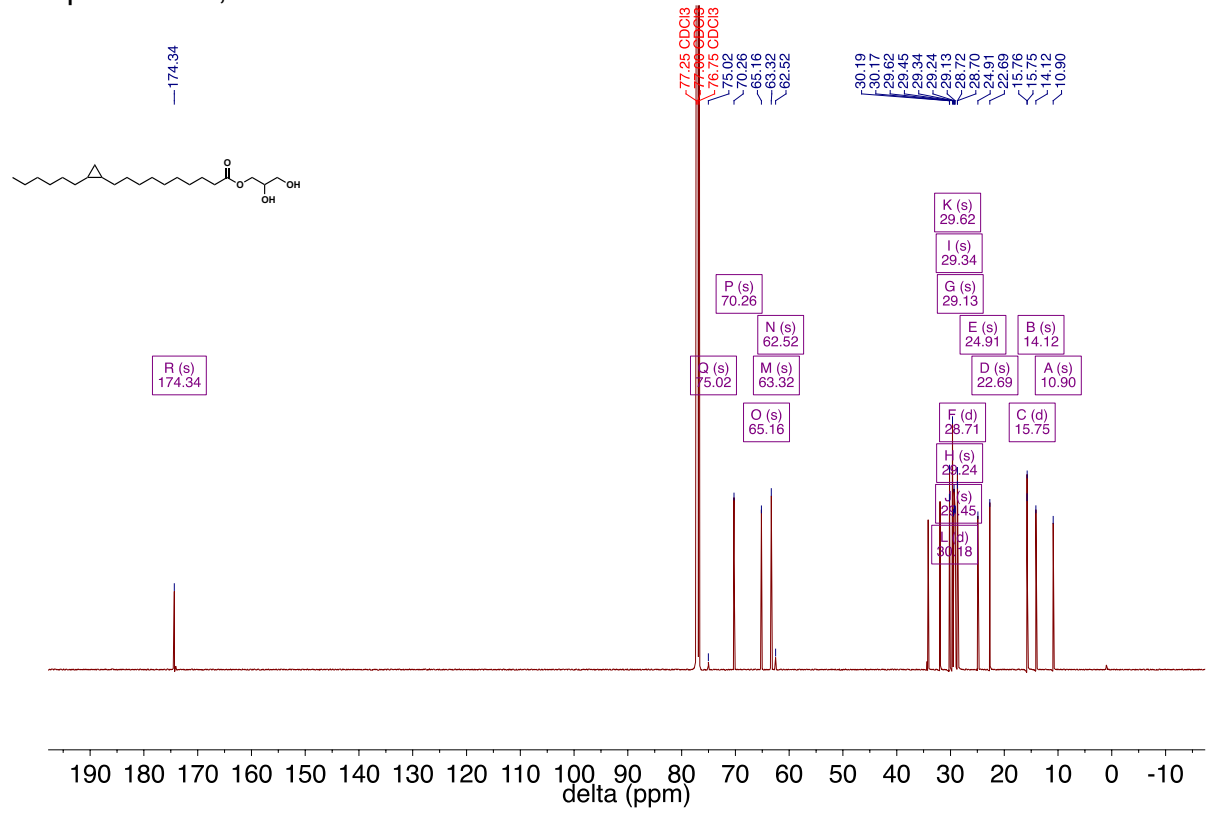

Compound **144**, ^{1}H

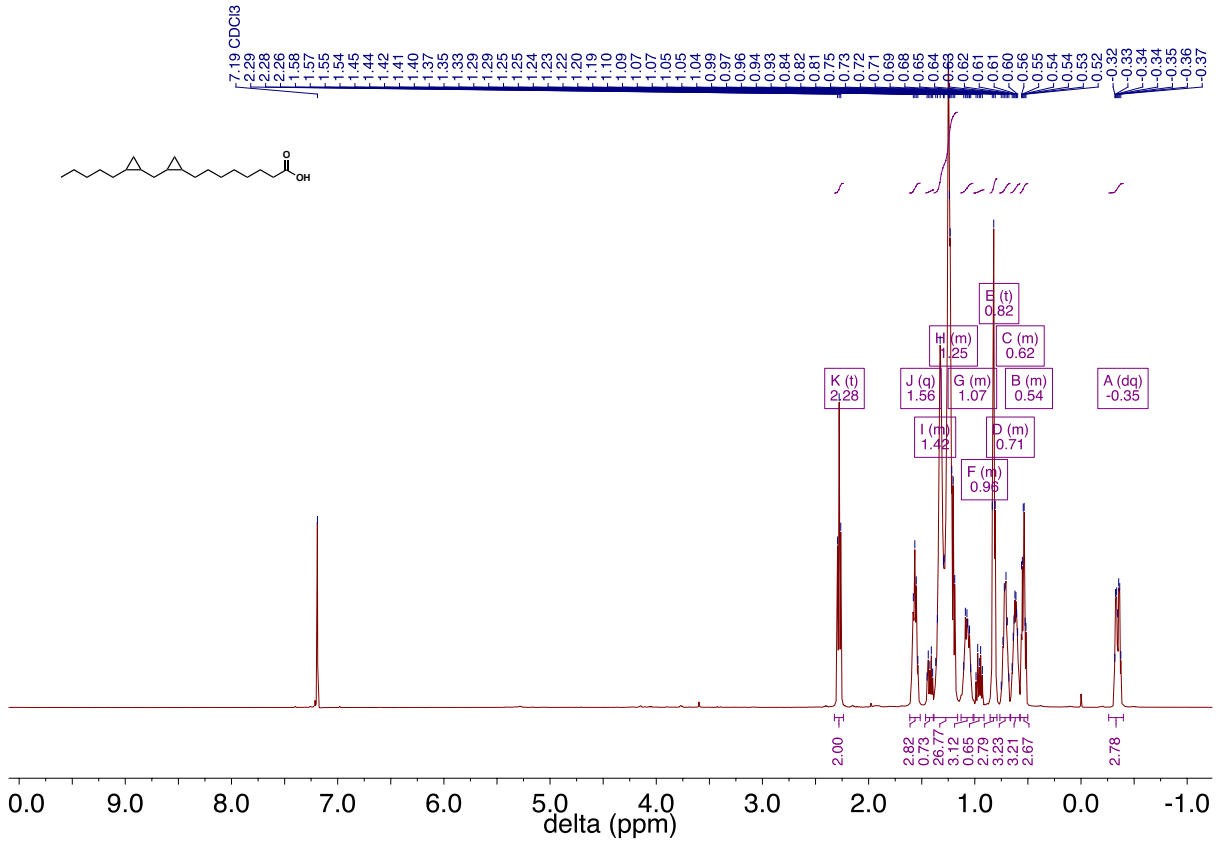

Compound **144**, ^{13}C

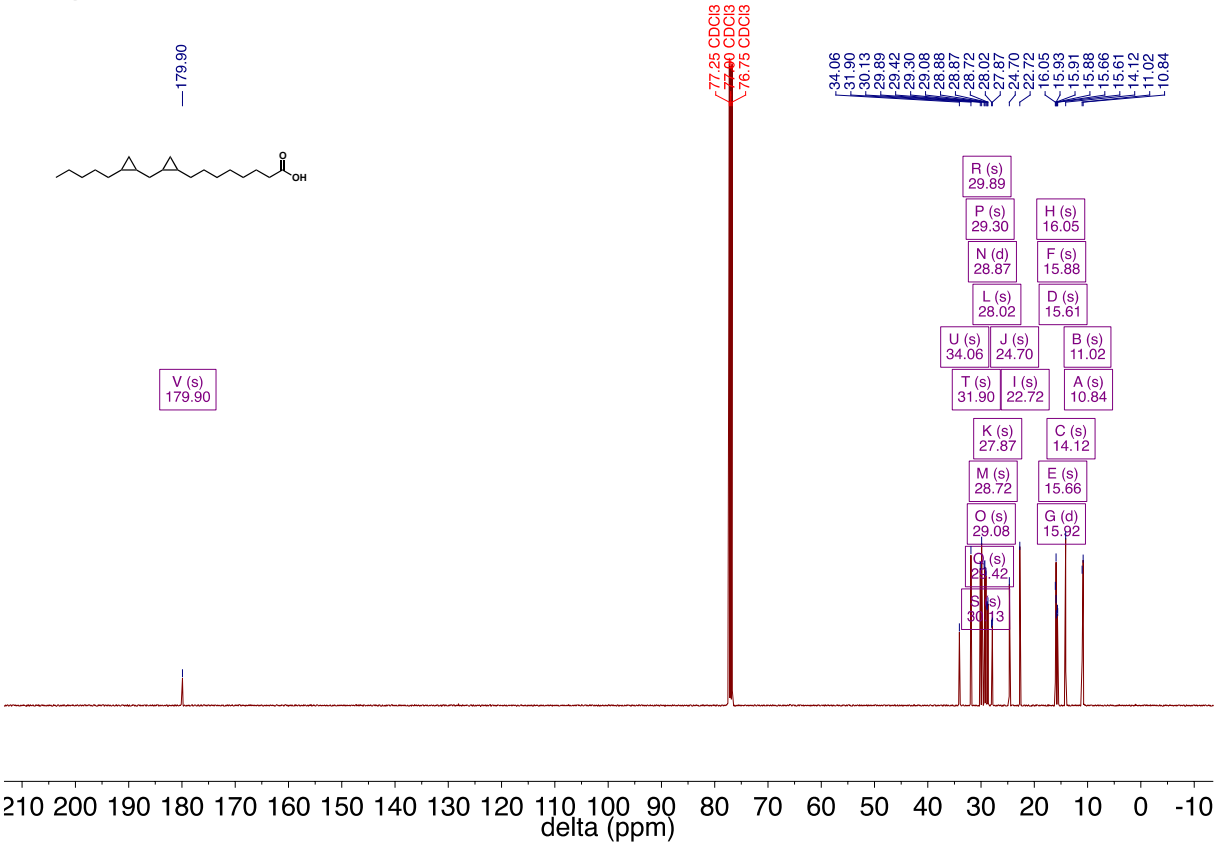

Compound **138**, ^{1}H

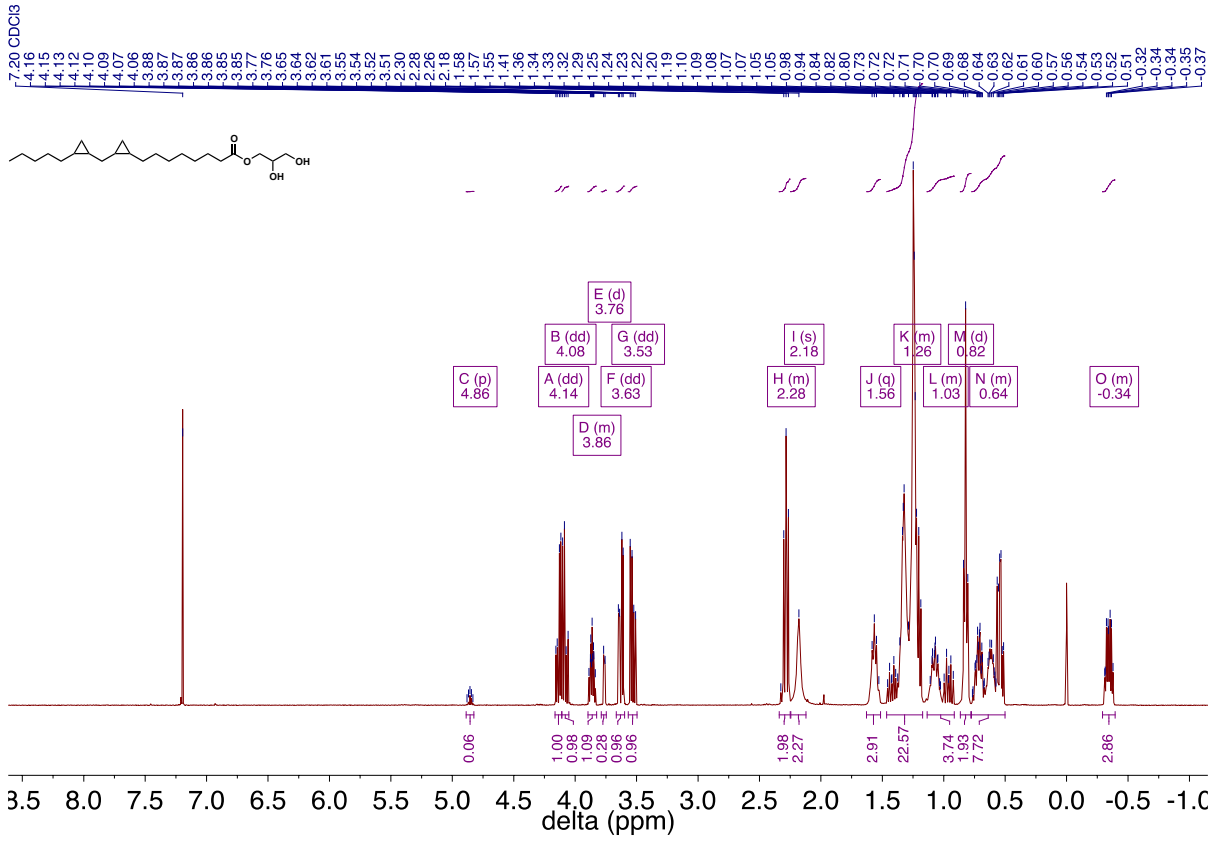

Compound **138**, ^{13}C

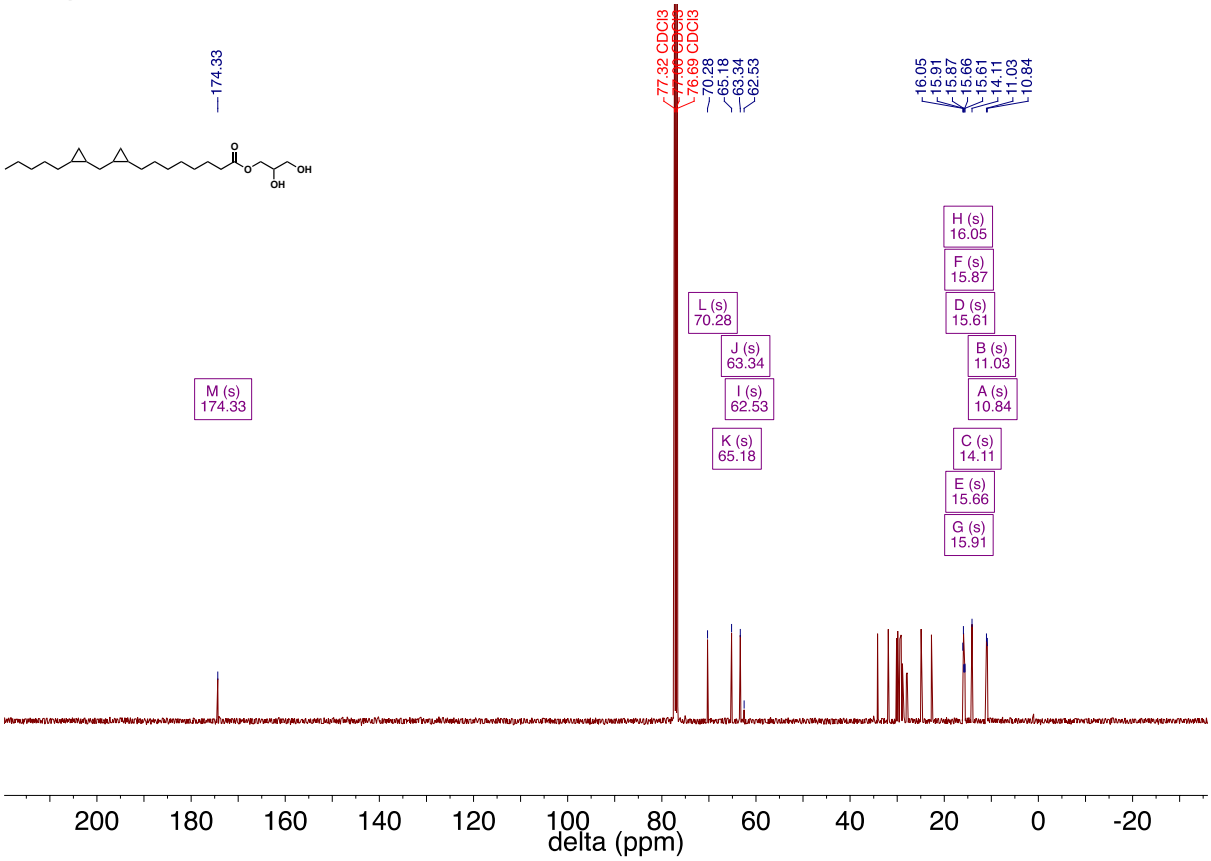

Compound **146**, ^{13}C

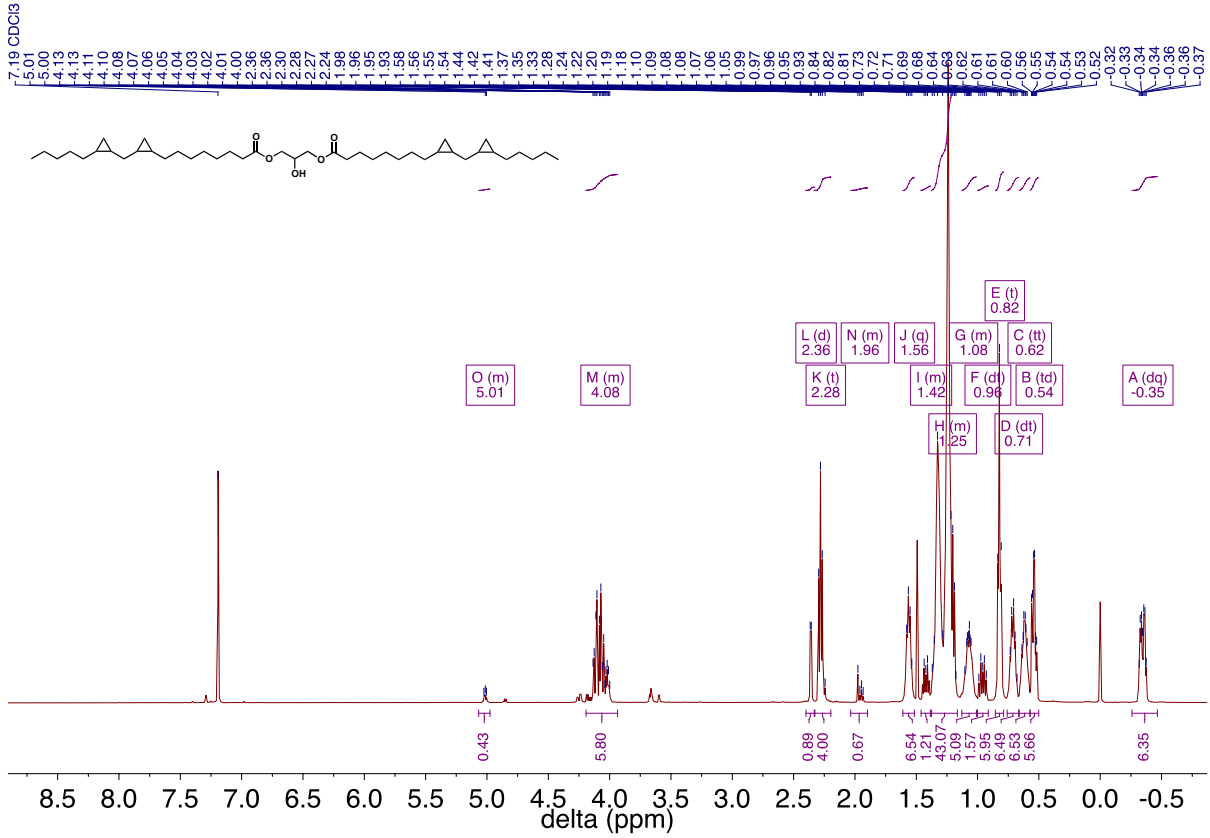

Compound **146**, ^{13}C

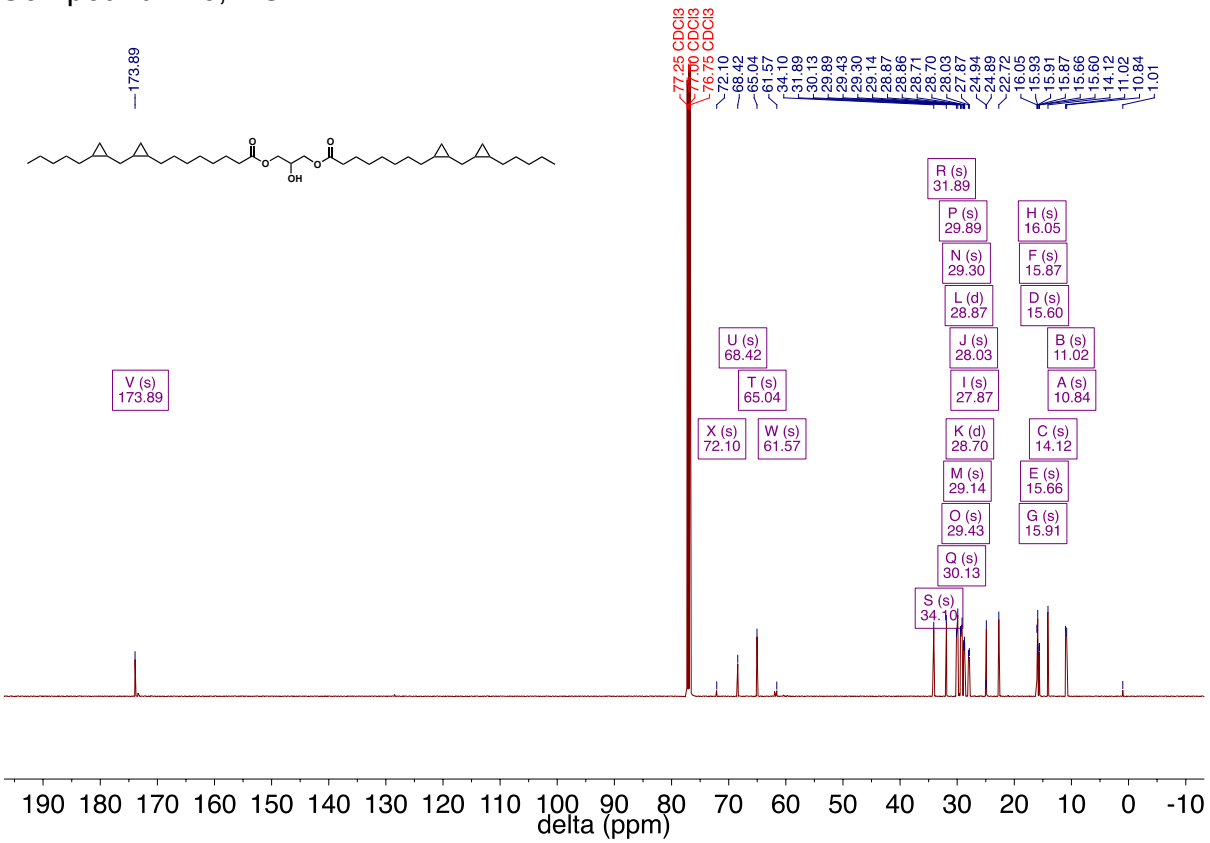

Compound **145**, ^{1}H

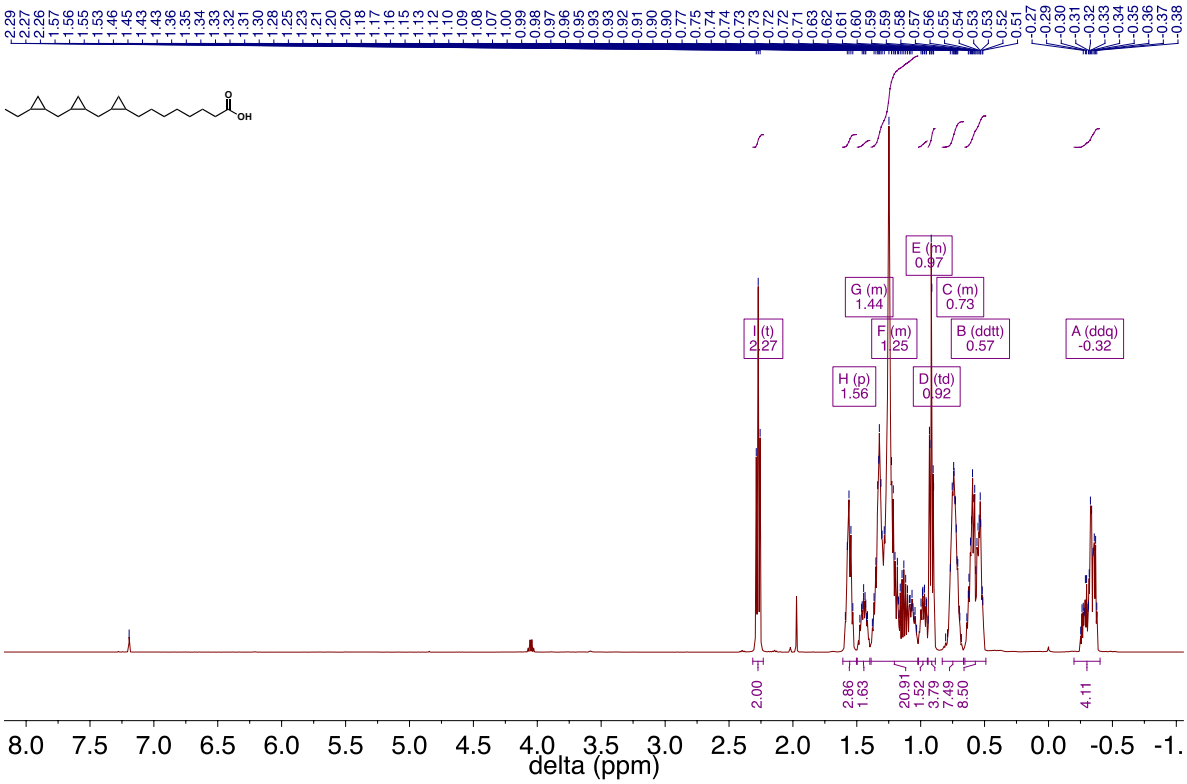

Compound **145**, ^{13}C

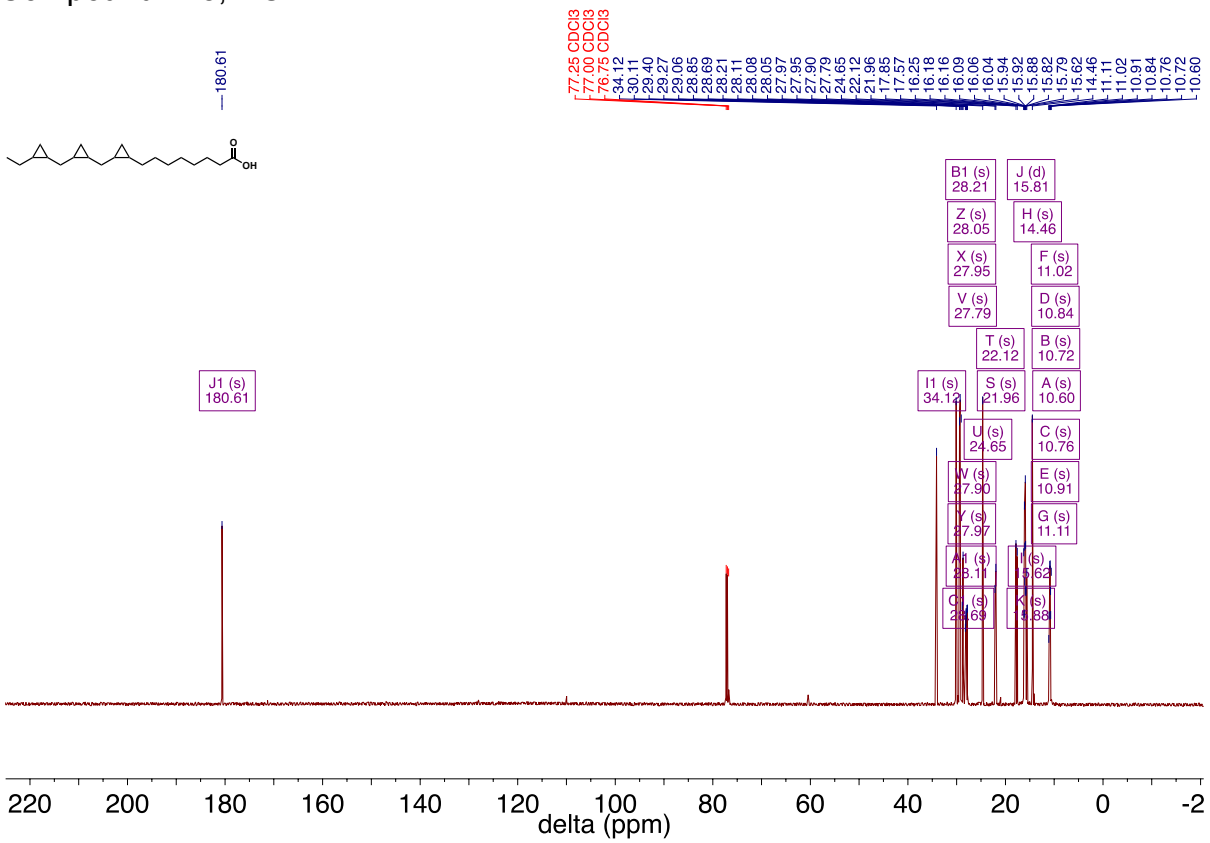

Compound **140**, ^{1}H

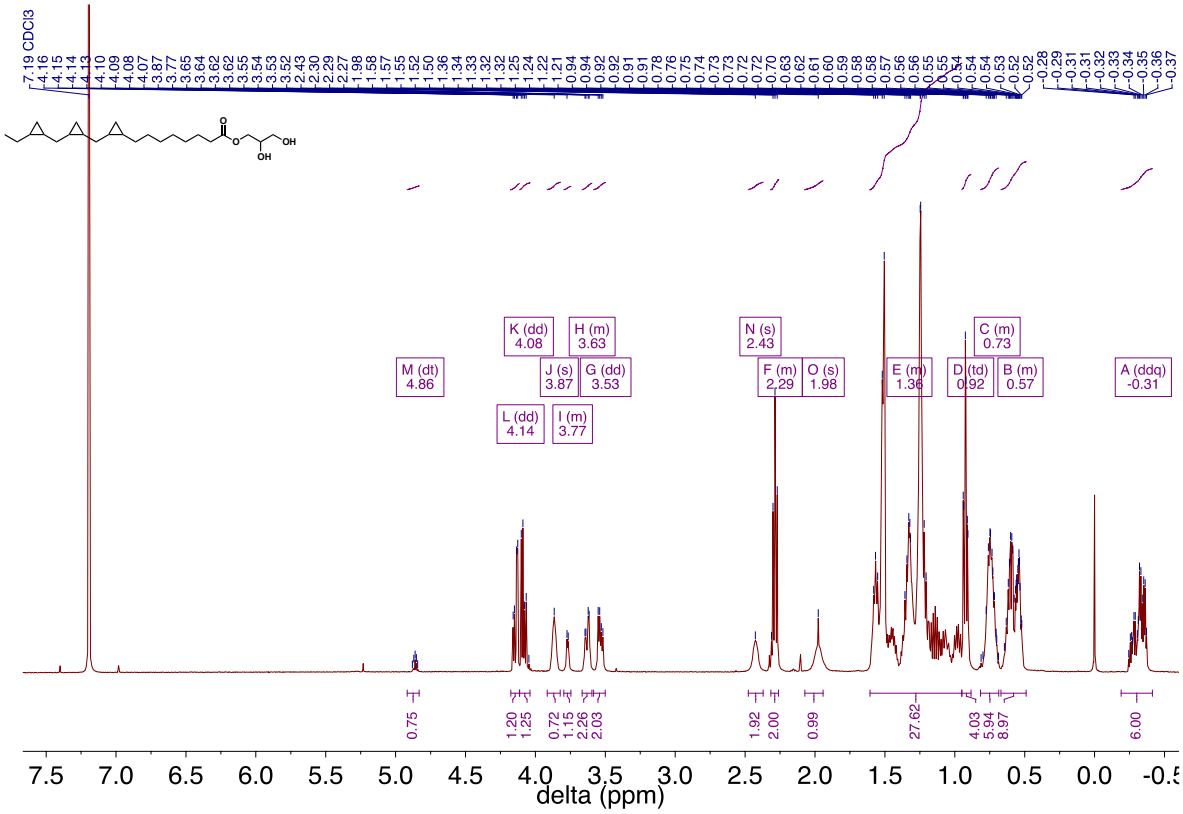

Compound **140**, ^{13}C

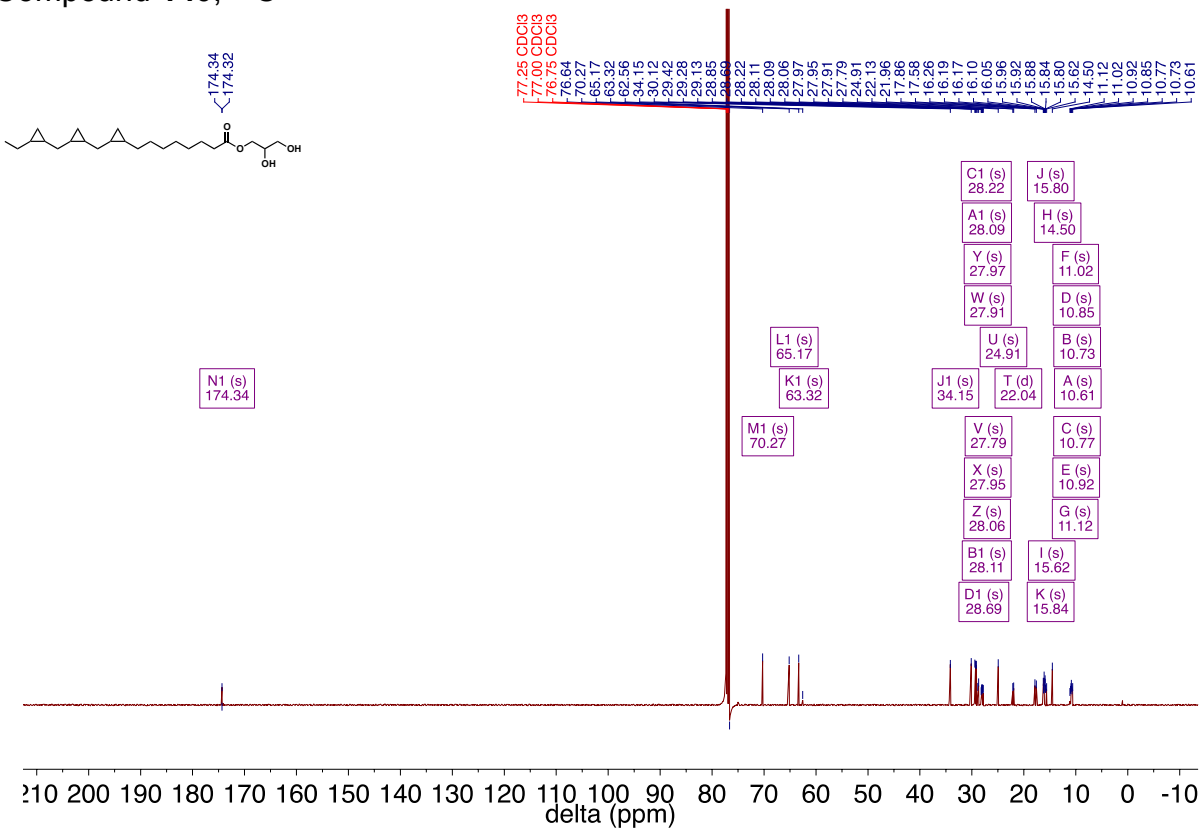

Compound **147**, ^{1}H

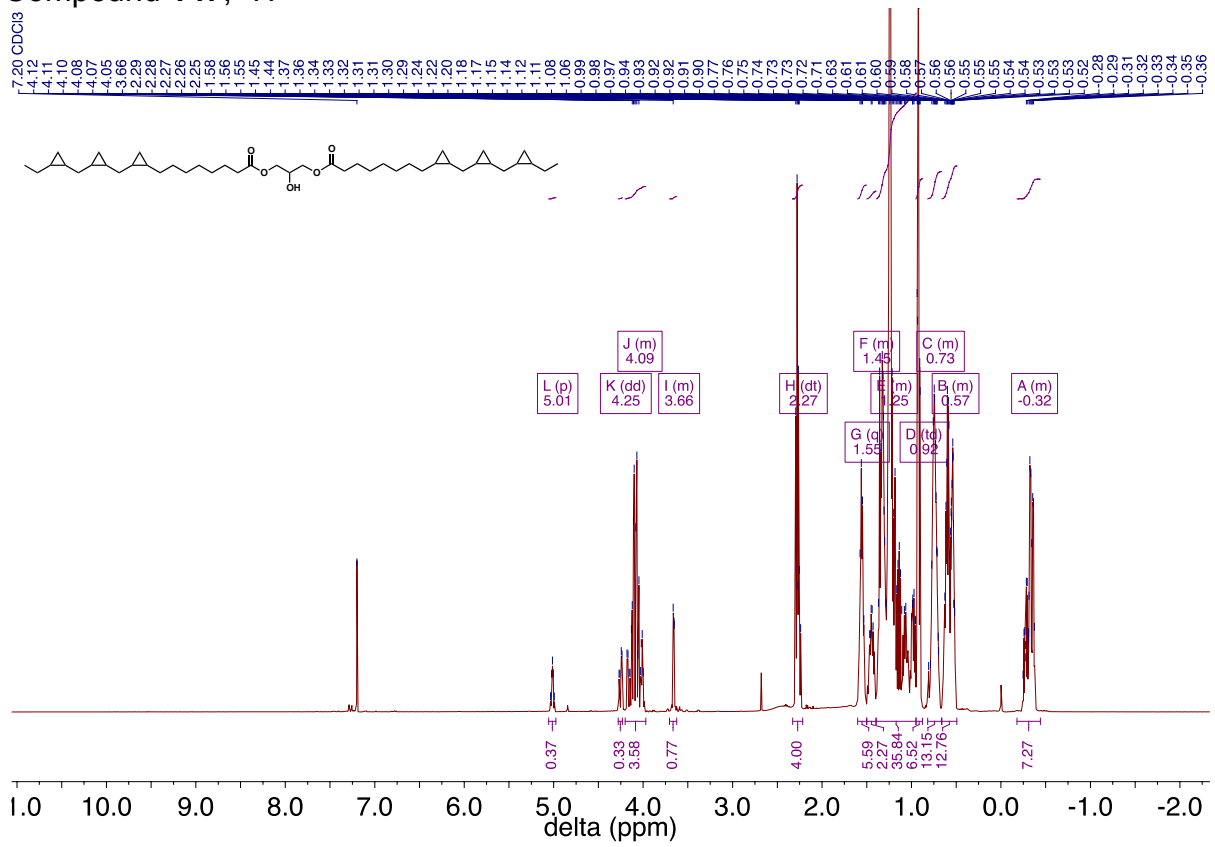

Compound **147**, ^{13}C

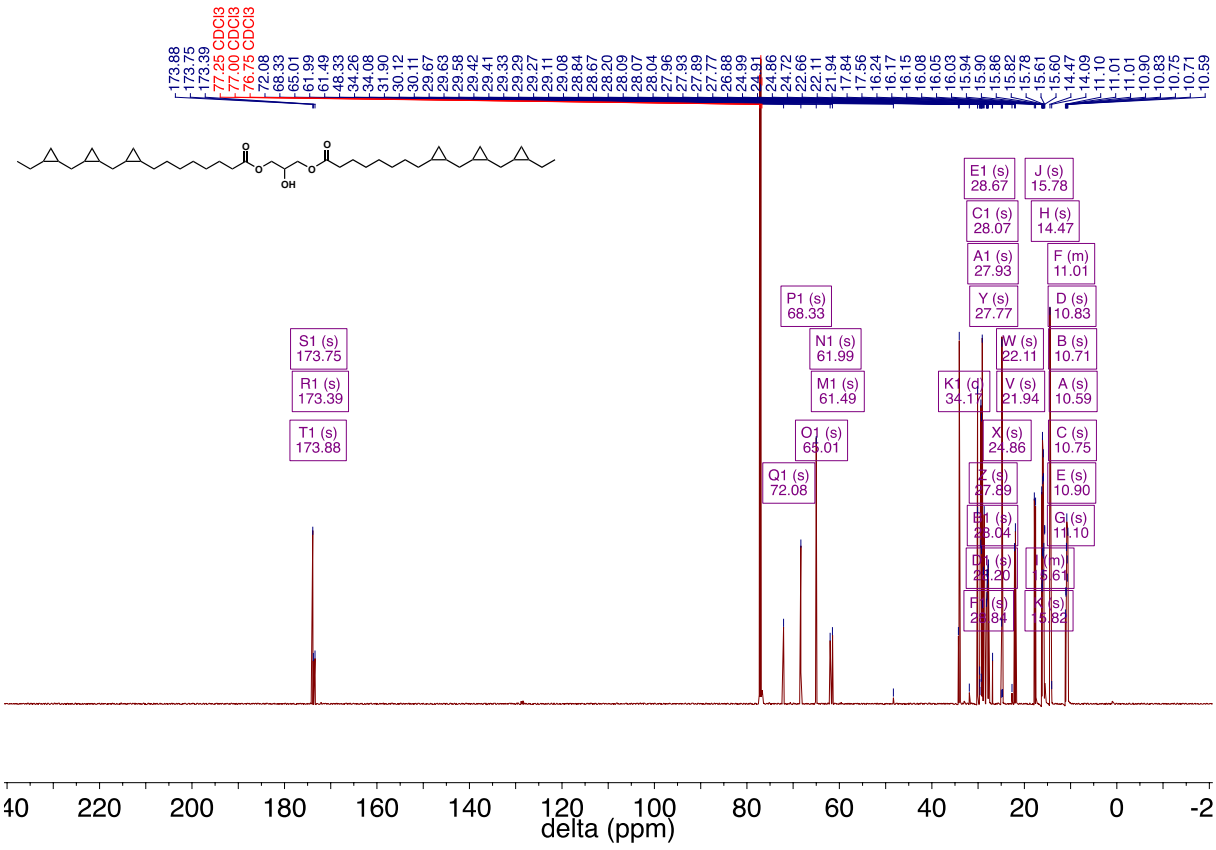

Chapter 9

Compound **151**, ^{1}H

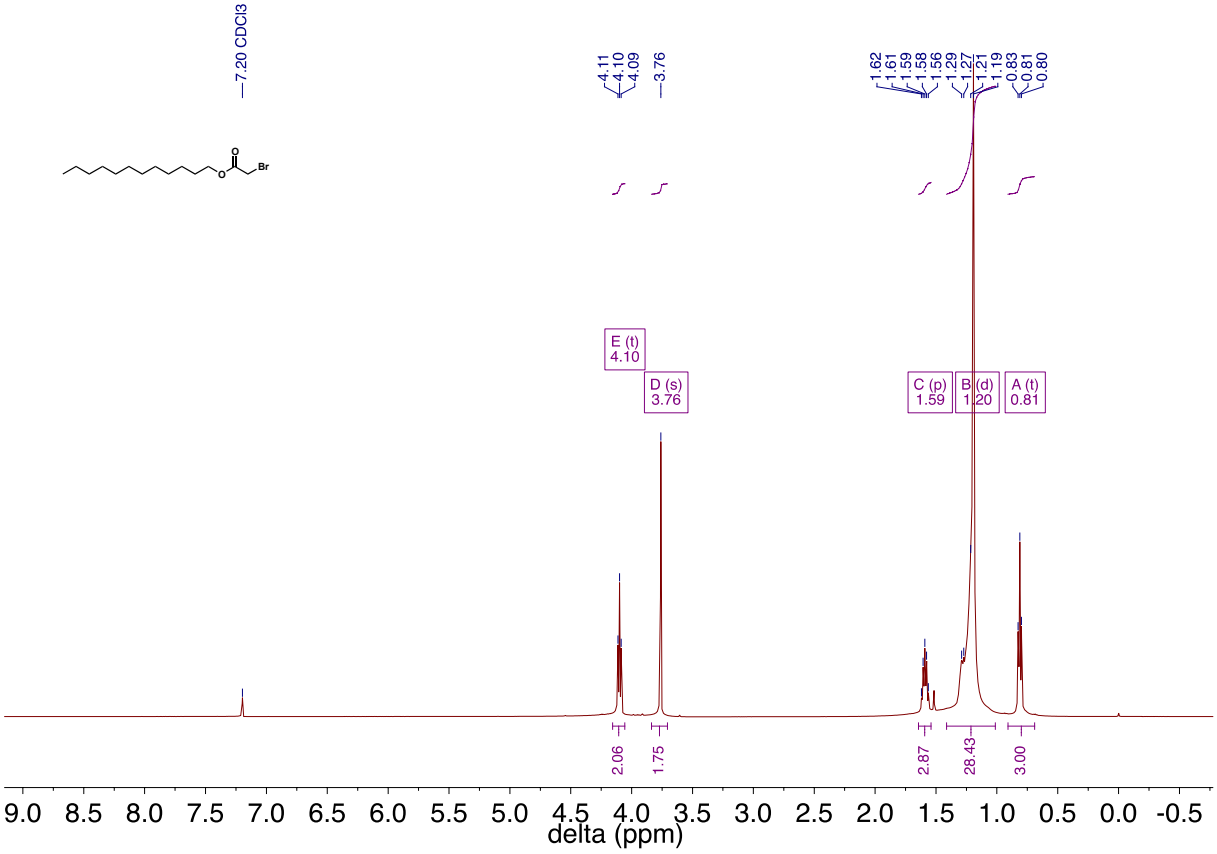

Compound **151**, ^{13}C

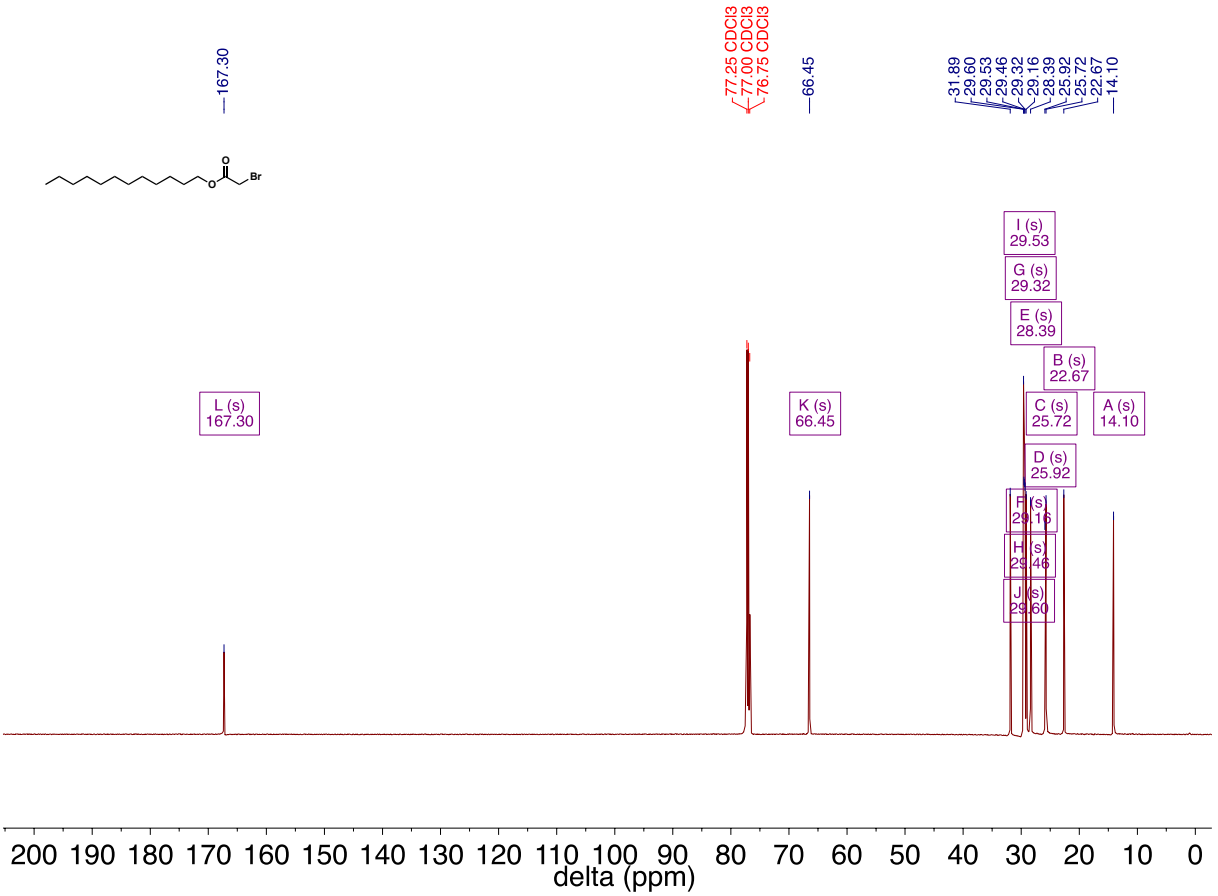

Compound **154**, ^{1}H

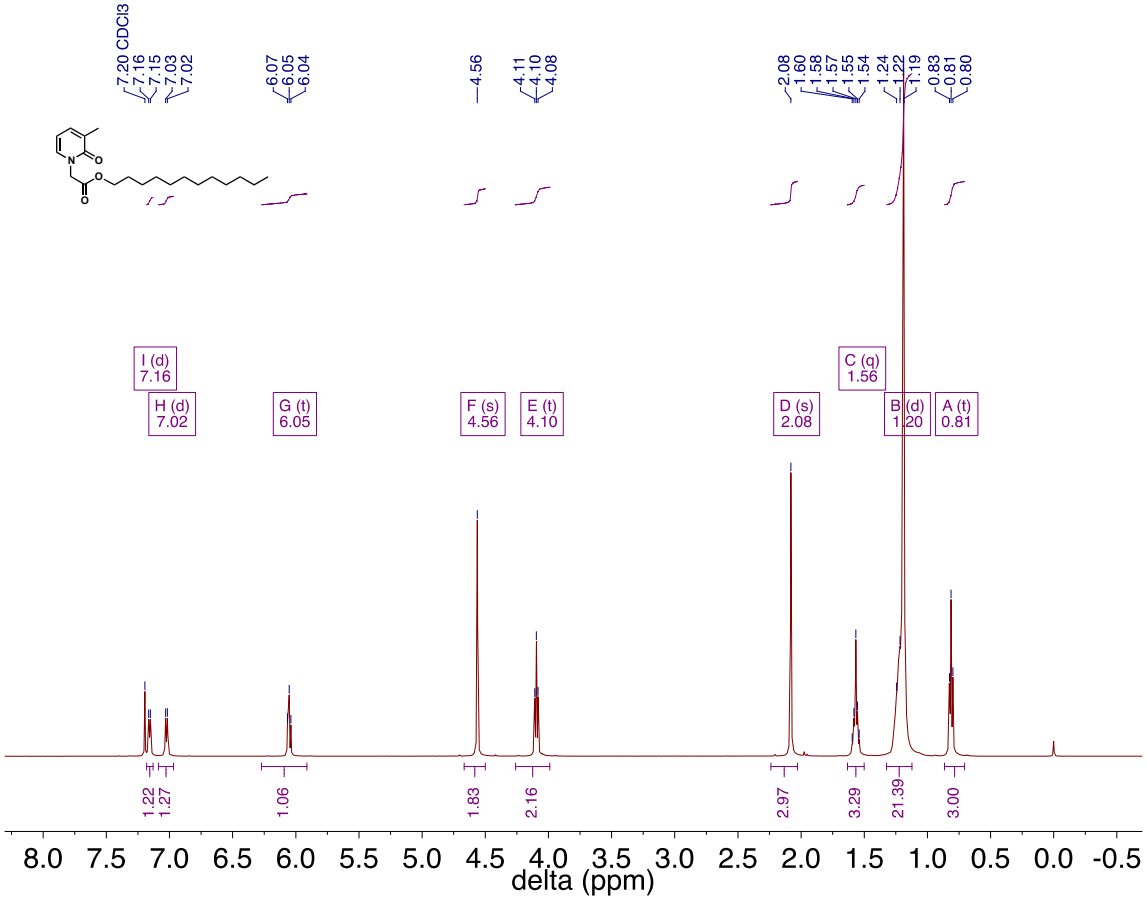

Compound **154**, ^{13}C

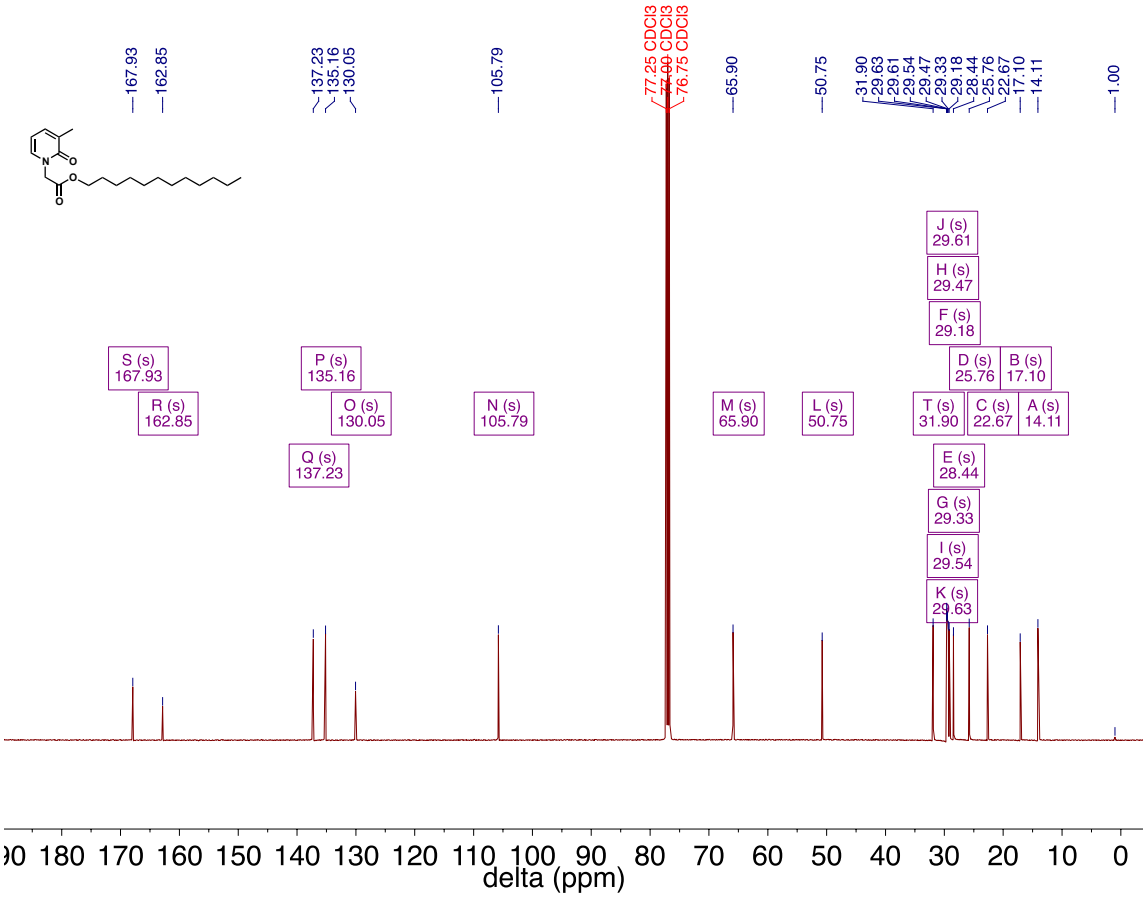

Compound **156**, ^{1}H

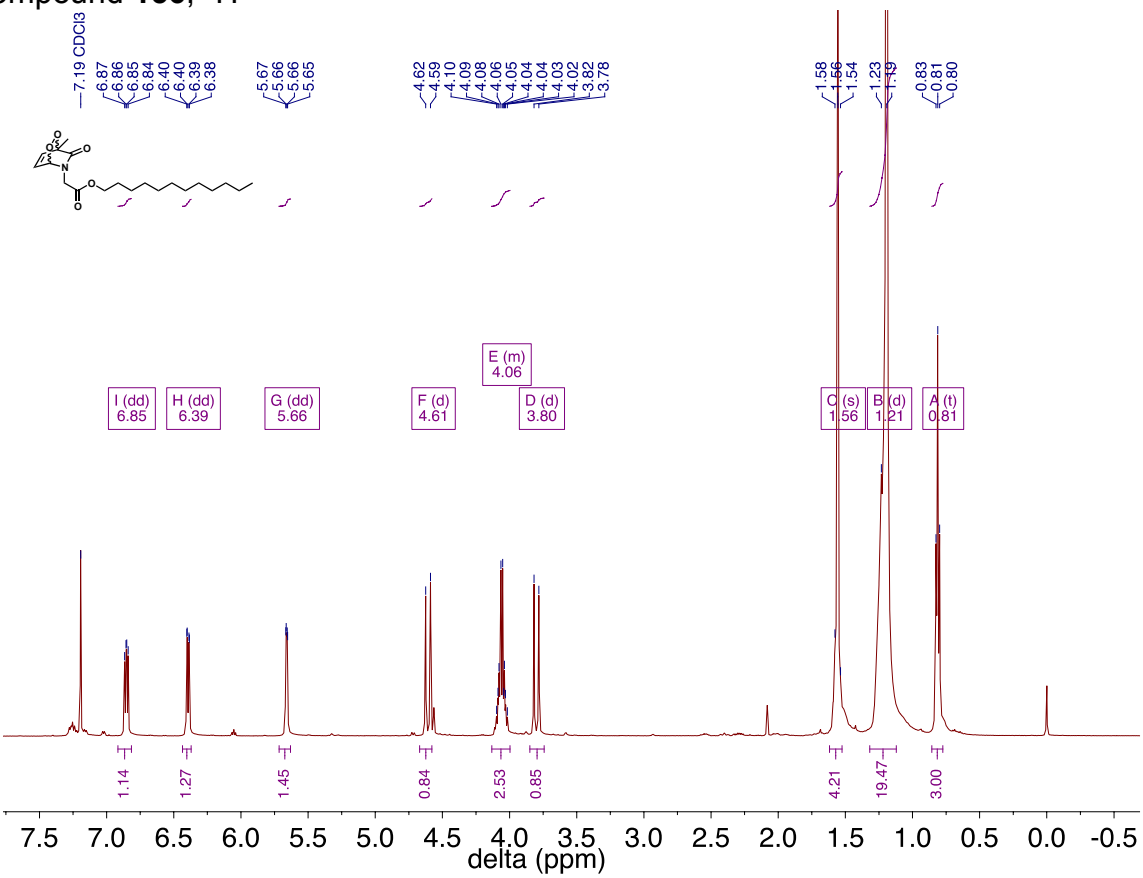

Compound **156**, ^{13}C

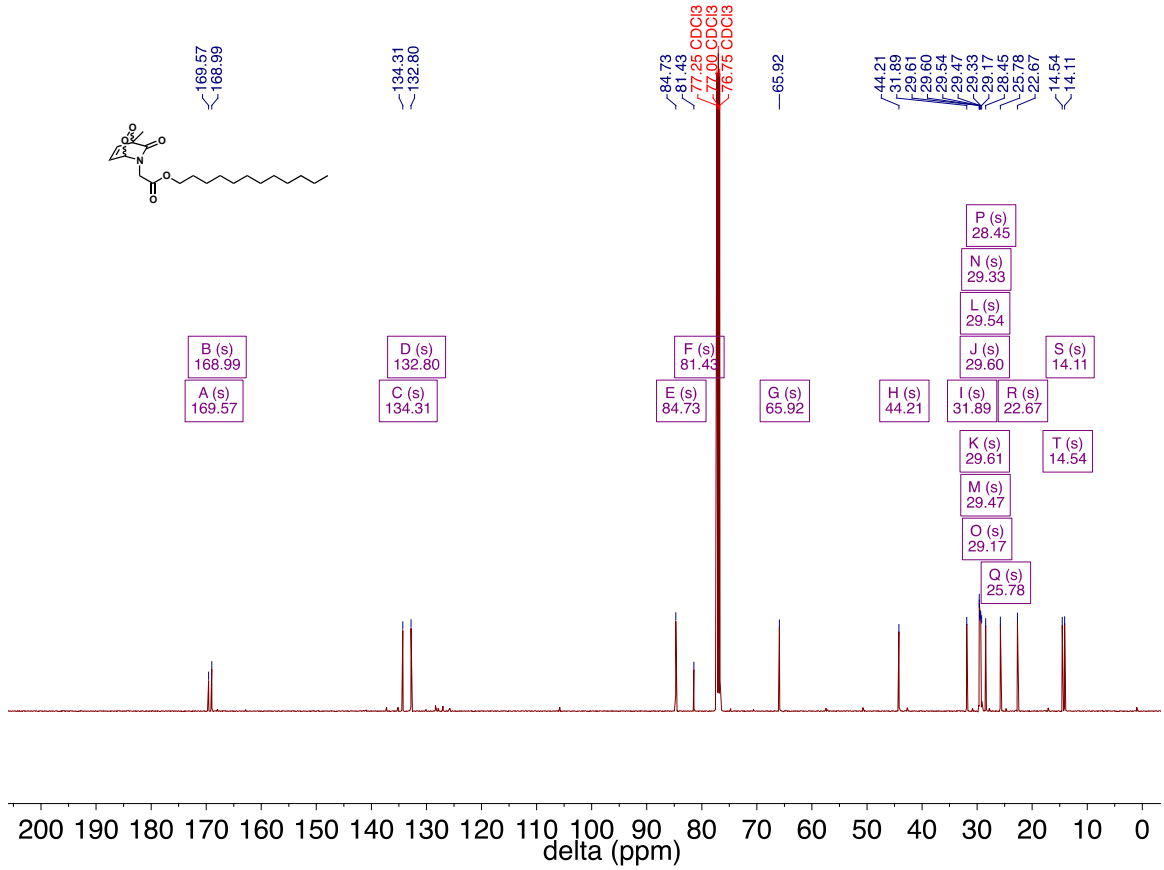

Compound **152**, ^{1}H

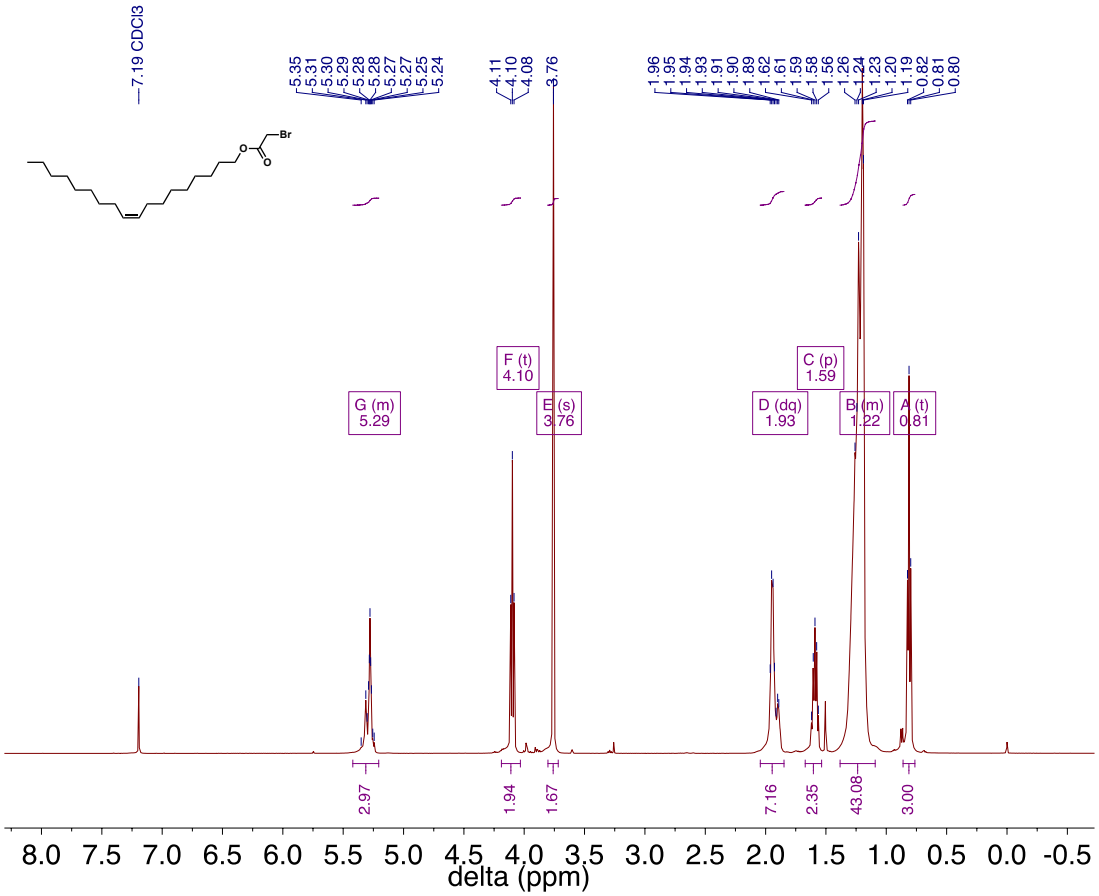

Compound **152**, ^{13}C

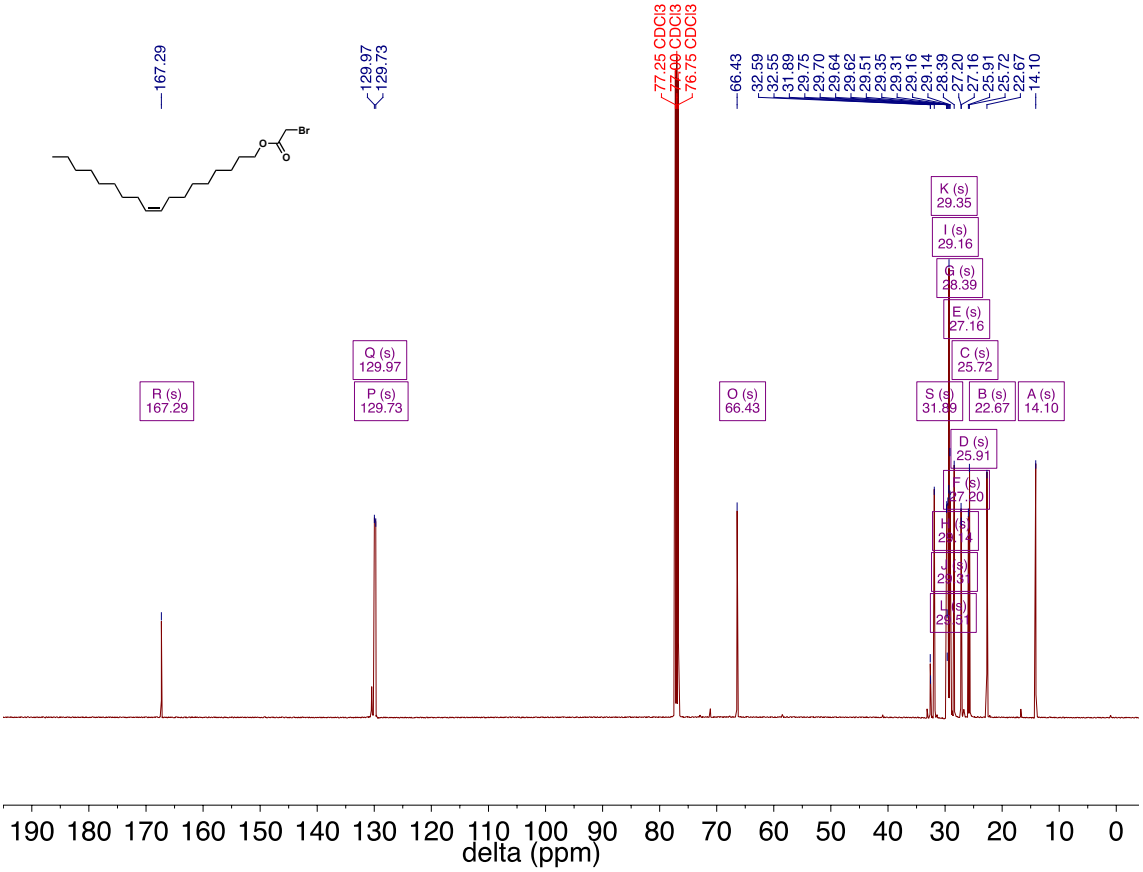

Compound **155**, ^{1}H

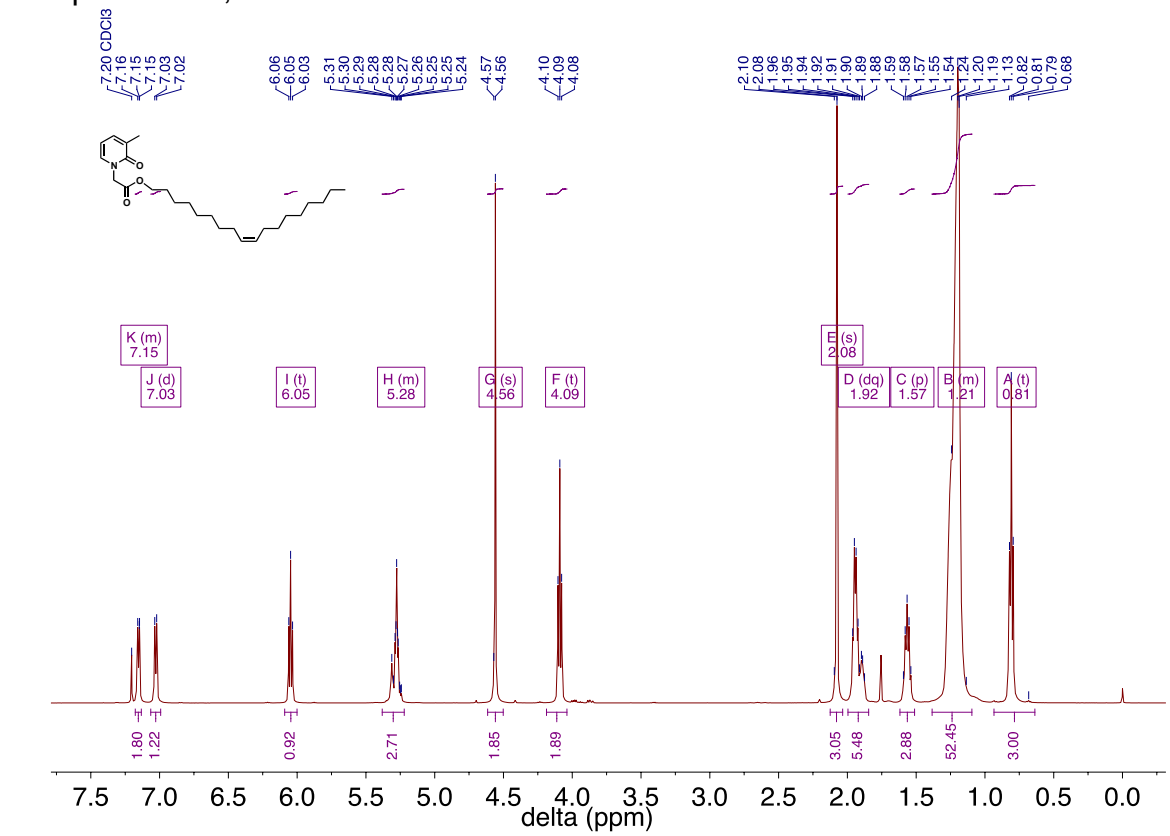

Compound **155**, ^{13}C

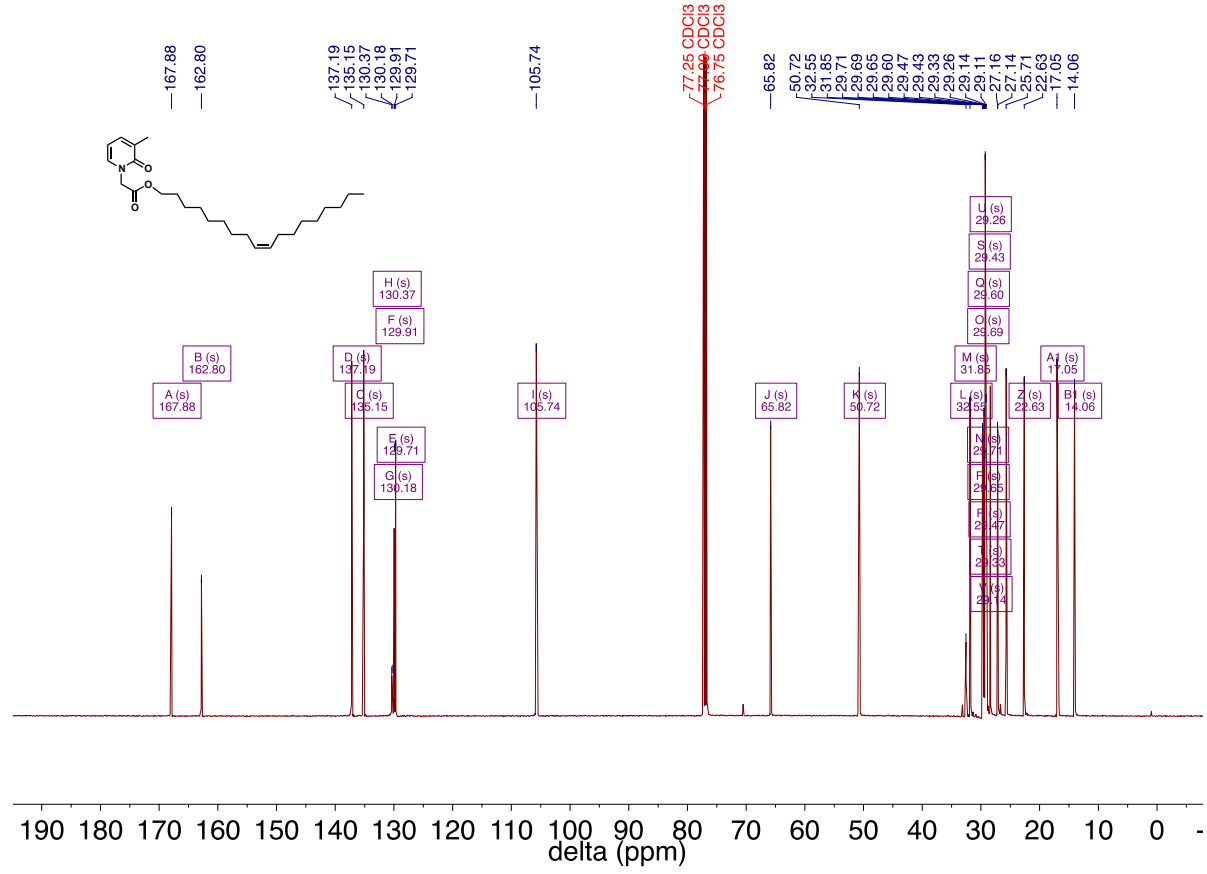

Compound **157**, ^{1}H

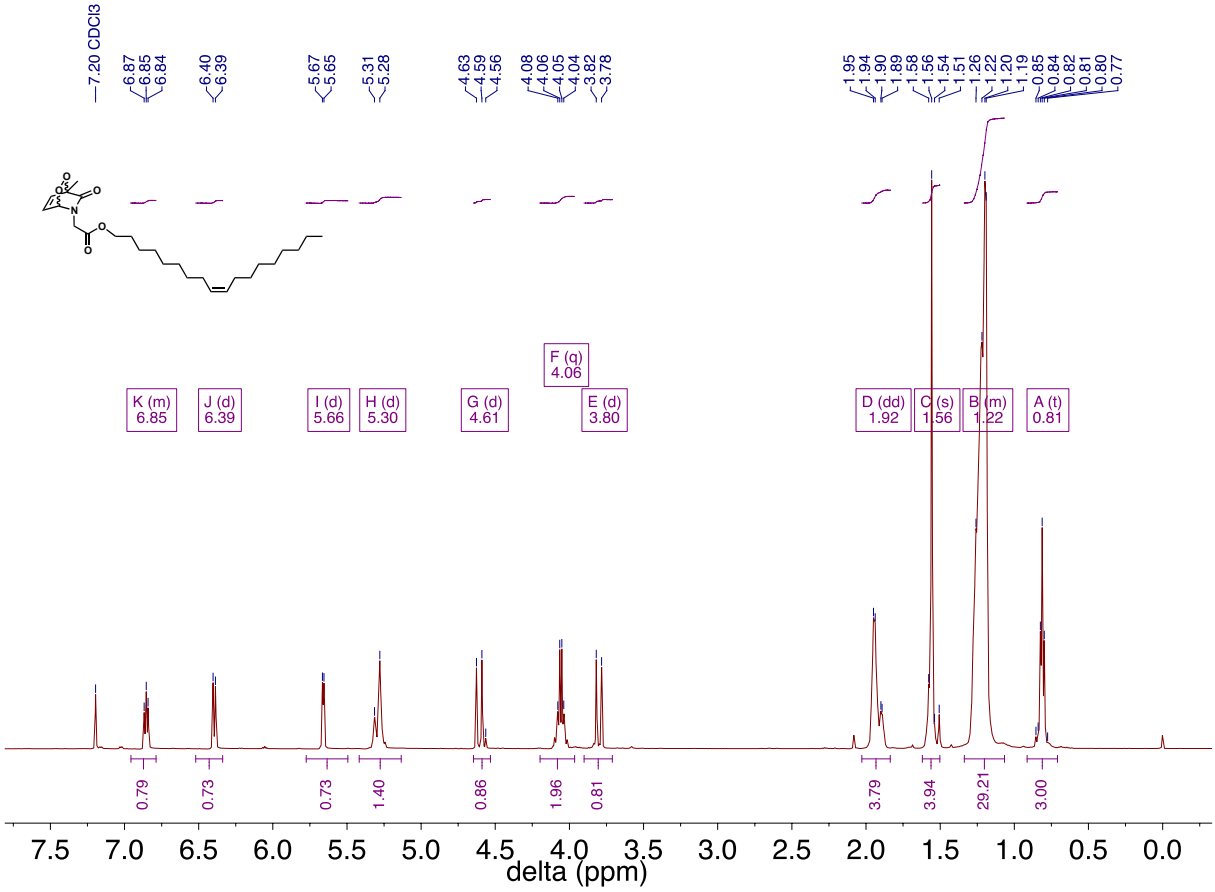

Compound **157**, ^{13}C

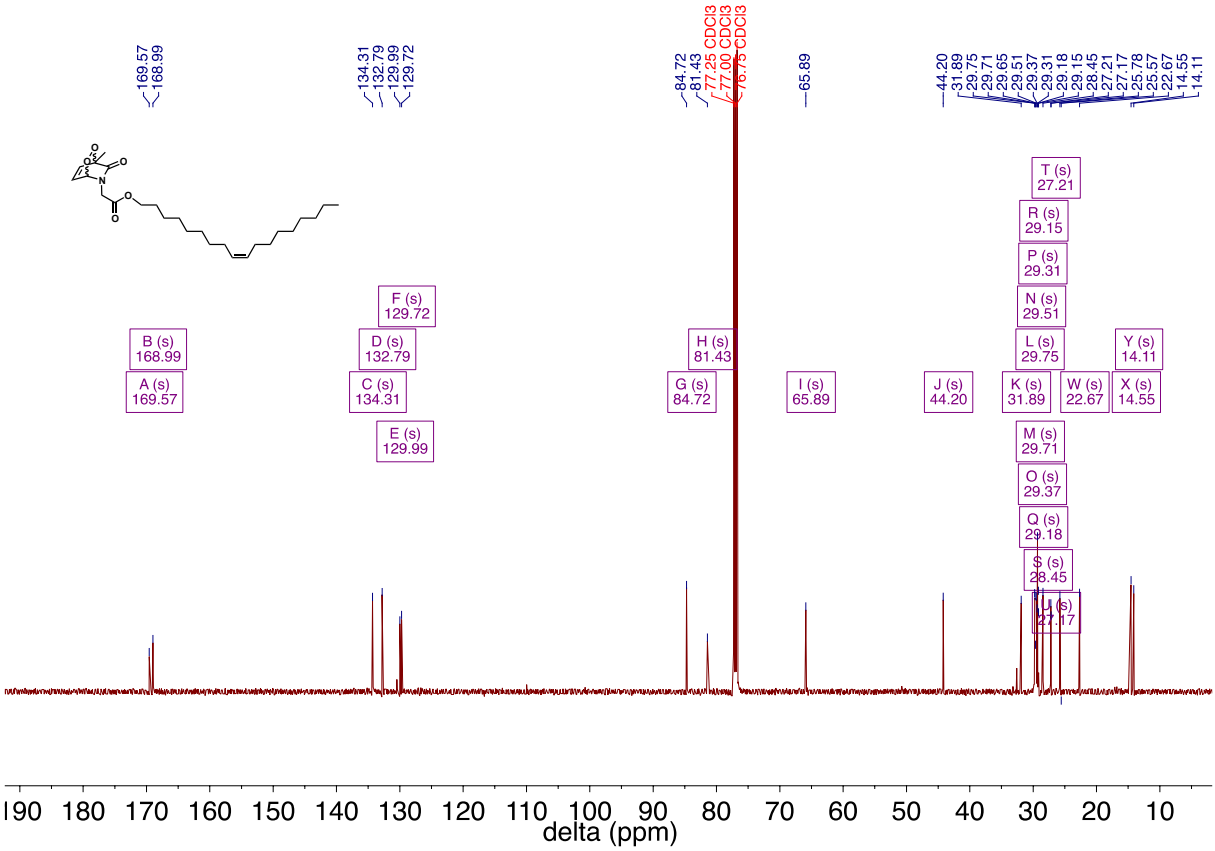

Compound **159**, ^{1}H

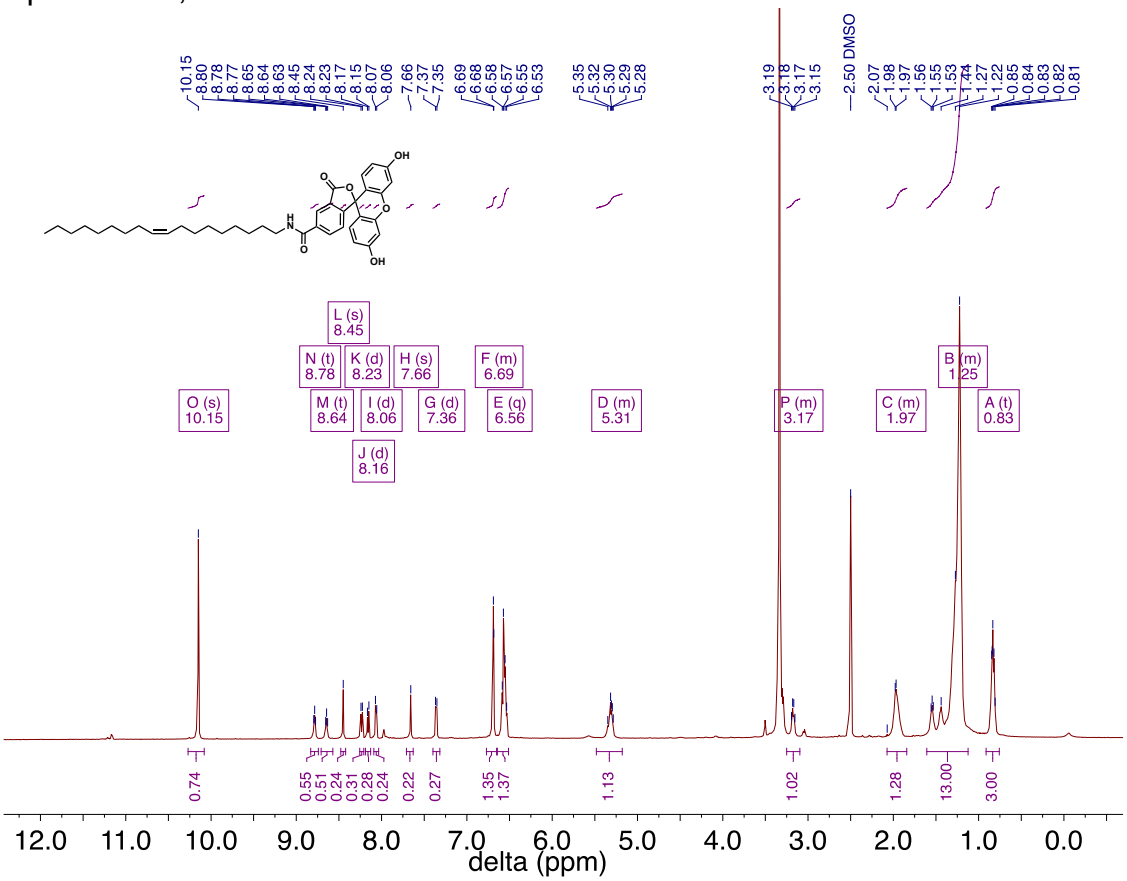

Compound **159**, ^{13}C